Origin of Darwin glass

by

Kieren Torres Howard

B.Sc. Hons. (University of Tasmania)

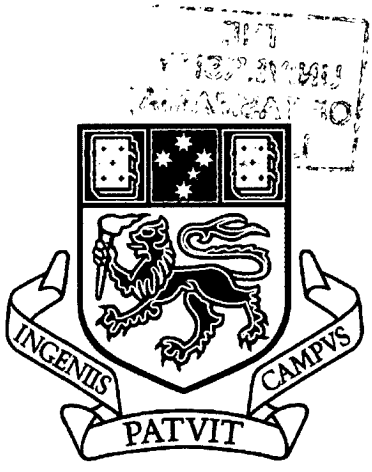

Submitted in fulfilment of the requirements for
the degree of Doctor of Philosophy

University of Tasmania
Australia

June, 2004

Statement and Authority of Access

This thesis contains no material which has been accepted for a degree or diploma by the University or any other institution and, to the best of my knowledge and belief, no material previously published or written by another person except where due acknowledgement is made in the text of this thesis.

This thesis may be made available for loan and limited copying in accordance with the *Copyright Act* 1968.

Kieren T. Howard

June 2004

Abstract

Darwin glass is an impact glass found in a strewn field near Mt Darwin, western Tasmania, Australia. It has been dated at 816 ± 7 ka by Ar-Ar methods. A 1.2 km circular depression, named Darwin Crater (42°18.39'S, 145°39.41'E), has previously been suggested as the source crater for the glass. The structure sits in a remote valley in Siluro-Devonian (Eldon Group) quartzite and slate. Earlier geophysical investigations demonstrated that the structure is an almost circular sediment-filled basin. The origin of this structure and its relationship to Darwin glass has long been a subject of controversy.

Drill core intersected fine grained lacustrine sediments (~60m thick) overlying poorly sorted crater-fill deposits. The pre-lacustrine crater-fill stratigraphy comprises an uppermost polymict breccia (~40m thick) of angular quartz and country rock, which contains very rare (<<1%) glass fragments (Crater-fill Facies A). Beneath the polymict breccia facies, the drill core intersected monomict sandy breccias of angular quartz (Crater-fill Facies B), and a complicated package of deformed slates (Crater-fill Facies C). One core penetrated to a maximum depth of ~230m, at which point coherent slate was encountered. Quartz grains in the crater-fill samples contain abundant irregular fractures. In some of the most deformed quartz grains, sub-planar fractures define zones of alternating extinction. Kinked micas are also present. The deformation observed in the crater-fill facies is far greater than in rocks cropping out around the crater. However, diagnostic shock indicators (eg. planar deformation features in quartz) are absent, preventing confirmation of an impact origin by petrographic analysis of crater-fill samples alone.

Geochemical analyses of the glass reveal two compositional groups. Group 1 is close to bulk average Darwin glass and is highly variable in composition. Its major element compositional range is: SiO_2 (80.6–93.9%), Al_2O_3 (3.1–10.6%), TiO_2 (0.2–0.7%), FeO (0.8–4.2%), MgO (0.25–2.3%) and K_2O (0.7– 2.7%). Group 1 glass is predominantly light green to dark green or white. Group 2 glass is almost always black. Group 2 has a lower average SiO_2 (81.1%) content, and a decreased range in SiO_2 (76.4–84.4) concentrations. Average Al_2O_3 (8.2%) is also greater than in Group 1. Group 2 glass is also significantly enriched in FeO (+1.5%), MgO (+1.3 %) and Ni, Co and Cr relative to Group 1. Average Ni (416ppm), Co (31ppm), and Cr (162ppm) concentrations in Group 2 glass are beyond the range expected in average sedimentary rocks. The remaining trace element data show affinity with typical upper crustal sediments including pronounced negative Eu anomalies (Eu/Eu*= 0.48– 0.66) and LREE enrichment (La/Lu* = 5.8 – 8.87).

Sr and Nd isotope data indicate that a mixture of the Eldon Group lithologies (suspected target rocks) can form Darwin glass. Mixing calculations using average Eldon Group compositions also successfully model the glass composition. Such models result in significant errors only for Ni, and to lesser extents Co, MgO, Cr and FeO in some Group 2 glass samples. Enrichments in these elements require an ultramafic contribution. However, mixing models using a component of Tasmanian dunite, pyroxenite, or lamprophyre fail to produce the required glass compositions, and can thus be ruled out as significant components of the target rock stratigraphy. The observed composition of Group 2 glass samples can only be explained by mixing with up to 9% of a chondrite or chondrite-like projectile. The distribution of projectile material in the glass is extremely heterogenous, and the amount of this contribution is varied. Only the transition metals are enriched, with no simultaneous enrichment in the highly siderophile elements (HSE) that are present in crustal abundances.

Physical trends in glass distribution relative to distance from the crater can also be used to test the supposed genetic relationship between the glass and crater. More than 4000 fragments of glass were recovered *in situ* from residual gravel deposits. These collection sites define the known extents of the strewn field, and show that the ejected melt cooled and rained down as glass fragments over more than 410km^2 of western Tasmania. In rare cases glass fragments exceeded 1kg, but typically were only a few grams in size. In a 50km^2 area surrounding the crater (~1/8th of the strewn field), it is estimated that the total glass volume is at least 11 250m^3, and relative to the size of the suspected source crater, Darwin glass is the most abundant impact glass on Earth. Analyses of glass recovered *in situ* show: **1)** the largest recovered fragments are found closest to the crater; **2)** a decrease in the proportion of fine glass fragments away from the crater; **3)** size distribution data for the recovered glass specimens are strongly skewed towards outlying large fragments; **4)** an increase in the proportion of black glass away from the crater; **5)** an increase in the proportion of splashform, relative to irregular or ropy shapes away from the crater; and **6)** splashform shapes are preferentially black in colour.

The geochemical and isotopic data presented in this study are considered to be consistent with Darwin Crater being the sole source of the glass. The crater-fill facies are also interpreted as consistent with impact processes. The argument for a genetic connection is strengthened by the observed trends in the distribution of glass relative to the crater. In the proposed model of the impact event, the polymict matrix supported breccia of Crater-fill Facies A is interpreted to have formed from non-melted angular quartz and country rock fragments that were blasted outwards and upward along the

cavity floor, before collapsing inwards and mixing. Crater-fill Facies B and C are interpreted as representing shattered quartzite and plastically deformed slate (<5GPa), sourced from slumping of the cavity walls.

In the impact model, impact glass size distribution data are considered to be consistent with ballistic ejection of melt. The poor size sorting is interpreted to indicate that the ballistic ejection of melt from the crater was as a highly turbulent plume, and that large and small fragments were deposited together, on the break down of turbulent cells. The increase in the proportion of black glass fragments with increasing distance from the crater is related to the depth of excavation. Black glass is interpreted to form from melting of pelitic layers in the Keel Quartzite, that is the upper most target formation, and it is the upper most target rocks that will be theoretically ejected farthest during impact cratering. The chemistry of the black Group 2 glass is also explained as a mixture of quartzite and pelite. Because the splashform shapes are formed by surface tension during aerial transport, increasing the distance of melt ejection will promote development of such shapes, and this is in turn consistent with the preference for splashform shapes to be black. The expected lower viscosity of the black melt (based on SiO_2 content) is also interpreted to have promoted the development of splashform shapes. Deriving of black glass from the upper-most target rocks, close to the target-projectile interface, also aids in explaining the evidence for preferential projectile contamination of some black Group 2 glass specimens. A vapour phase transfer of projectile materials into the silicate melt may explain the apparent transition metal/HSE paradox.

The wide distribution and anomalously high abundance of glass in the strewn field is explained as relating to ground water infiltration of the target rocks along fractures and faults prior to impact. Surface swamps are interpreted to have been present in the study area throughout the Pleistocene, and thus were a likely feature of the pre-impact environment. The abundance of water would have produced a highly volatile-charged target stratigraphy. This volatile enhancement is interpreted to have increased the explosiveness of the impact, and the efficiency of melt dispersal and ejection.

Analysed palynomorphs show that Huon pine dominated the first rainforest to recover after the impact, and that the crater was a lake until about 30ka. For more than 20ka, Tasmanian Aborigines collected glass from around the crater. The glass was prized by some tribes, who worked and transported it to trade outside of the strewn field and across much of Tasmania.

Acknowledgments

Clive Burrett instigated and supervised this project. Peter Haines was involved in field investigations and provided critical input to all aspects of the research, along with timely reviews of the thesis. Ron Berry provided expert advice on the statistical analyses and interpretation of geochemical data. David Steele provided assistance in the SEM analyses and Leonid Danyushevksy the laser ablation analyses. Marc Norman (Research School of Earth Science, Australian National University) provided expertise in laser ablation analyses of highly siderophile elements in Darwin glass. Ching-Hua Lo (Department of Geosciences, National Taiwan University) conducted Ar/Ar age determinations on the glass. Simon Stevens was responsible for the preparation of all thin sections and for many useful discussions about early investigations at the crater. June Pongratz provided assistance with preparation of the thesis. The Barringer Crater Company generously provided funds for the Sr and Nd isotopic analyses, along with funds to attend the Meteoritical Society Conference in 2003. The late Ramsay J. Ford's earlier investigations into the glass and Darwin Crater paved the way for this investigation. This research was carried out on the traditional lands of the Tasmanian Aboriginal people.

Table of Contents

List of Figures

Figure

Figure

Figure

List of Tables

Table

Table

Chapter 1

Introduction

1.1 Scope of this study

The aim of this study is to investigate in detail the *Origin of Darwin glass*. This has involved detailed collection of glass across the strewn field in western Tasmania and investigations at the suspected source crater. This has been carried out in order to determine if Darwin Crater is the source of Darwin glass and to further explore the geology of simple impact craters and the genesis of ejected impact glass. Therefore, the objectives of this thesis that will allow for fulfilment of the aim are to describe and interpret:

1. The physical properties and distribution of Darwin glass;

2. The geochemistry of Darwin glass;

3. The geology of the strewn field and Darwin Crater, including the detailed petrography of rocks sampled from drill core;

4. The geochemistry of rocks cropping out at Darwin Crater and sampled from the drill cores;

5. The relationship between Darwin glass and crater from a variety of physical, chemical and isotopic perspectives;

6. The origin of Darwin Crater; and

7. The nature of the projectile involved.

1.1.1 Note on the structure of this thesis

This chapter will first introduce the reader to the subject of terrestrial impact events. Darwin glass is then described briefly and the findings of previous investigations into its origin are summarised. The location, geomorphology, climate and flora of the strewn field, as well as access considerations are then outlined, and the pre-impact environment at ca. 800ka is described. Following this introductory chapter, the first part of the thesis describes the petrography (Chapter 2) and chemistry (Chapter 3) of Darwin glass, and rocks from Darwin Crater and the drill cores (Chapter 4). This is largely a descriptive process and only limited interpretations are presented at this stage. The later part of the thesis then focuses on describing and interpreting the relationship between Darwin glass and Darwin Crater from a variety of chemical and isotopic perspectives (Chapter 5), and in terms of variations in the properties of recovered glass samples relative to distance from the crater (Chapter 6). In this interpretation, discussion will attempt to falsify the hypothesis that there is a non-random or genetic relationship between the glass and crater. These relationships demonstrate the origin of the glass and crater that is summarised in the final chapter (Chapter 7). At this point relationships are integrated into a description of the impact event and the potential implications of these interpretations to our understanding of impact glass/tektite genesis are also discussed

1.2 Impact primer

In the following brief review of the current state of our understanding of impact events much information has been drawn from several key papers (e.g. Gault et al. 1968; Ahrens & O'Keefe 1977; Grieve et al. 1977; Kieffer & Simonds 1980; Grieve 1987; Grieve & Cintala 1992; Melosh & Vickery 1991; Vickery 1993; Stöffler & Langenhorst 1994; Koeberl 1994), a thesis (Albin 1997), and excellent books by Melosh (1989) and French (1998), along with many other works. These form the basis of knowledge for understanding the *origin of Darwin glass.*

1.2.1 Impact cratering

The term "impact crater" in this and most studies is used interchangeably with "hypervelocity impact crater". These are the structures formed by the impact of extraterrestrial projectiles that are large and coherent enough to penetrate the Earth-Atmosphere system, with virtually no deceleration, and to strike the ground at near to cosmic velocities (>11km/s) (Melosh 1989). Generally these projectiles are required to be relatively large, between at least 20-50 metres in diameter, depending on the type of projectile (Melosh 1989). Being comparatively more coherent, the minimum size of an iron impactor that may result in hypervelocity impact crater excavation is smaller than for the stony meteorites.

Projectiles that are smaller than a few metres in diameter behave very differently to compositionally equivalent bodies of a larger size. These lose almost all of their original velocity and kinetic energy by atmospheric friction and consequent disintegration and ablation during passage through the atmosphere. Subsequently, small bodies impact the Earth's surface at speeds of less than a few hundred m/s (French 1998). At such comparatively low velocities the impacting projectile will penetrate into the target only a very short distance, depending on the projectile's velocity and the nature of the target material. In the most extreme cases, this results in the excavation of a pit that is only slightly larger than the projectile and in most cases the projectile is preserved at the bottom of this pit (French 1998).

Hypervelocity impact craters are formed by the intense shock waves that result from projectile impacts at velocities much greater than the speed of sound through the target rocks. These shock waves are generated at the point of impact and radiate outwards through the target rocks (Gault et al. 1968; O'Keefe & Ahrens 1993; Melosh 1989). The shock waves being referred to are intense, transient, high-pressure stress waves that cannot be produced by endogenic geologic processes (Gault et al. 1968; O'Keefe & Ahrens 1993; Melosh 1989). To illustrate this, in typical hypervelocity impacts, peak shock pressures may reach several hundred GPa. Obviously, this far exceeds the stress levels (≅1 GPa) experienced as terrestrial rocks undergo normal elastic and plastic deformation, and these shock waves produce permanent deformation effects in the rocks that they encounter (Gault et al. 1968; O'Keefe & Ahrens 1993; Melosh 1989; Stöffler 1994; Stöffler & Langenhorst 1994). Many of these effects are unique to, and hence are diagnostic of, meteorite impacts, as is discussed in section 1.2.2.

As the shock waves radiate outwards and expand they interact with the target surface and the motion triggered in the target rocks results in the violent excavation of an impact crater. The process of crater formation can be divided into three main stages: 1) contact and compression; 2) excavation; and 3) modification (Gault et al. 1968; Melosh 1989; see French 1998 for review). However, it must be realised that this is an arbitrary subdivision and the processes involved in crater excavation and modification are both complex and continuous.

Stage 1) Contact and compression

The contact and compression stage of impact crater formation commences at the point where the rapidly advancing projectile strikes the target ground surface. The effects of this stage are controlled by the nature of the target. If the target surface is solid rock the projectile is very rapidly stopped in only a fraction of a second (Melosh 1989); ending a journey that may have started several billion years ago in the early Solar System. In an impact onto solid rock, the projectile will penetrate into the target stratigraphy to a maximum depth of between 1-2 times its own diameter before its immense kinetic energy is transferred to the target rocks by the shock waves described above (Gault et al. 1968; Kieffer & Simonds 1980; O'Keefe & Ahrens 1975; O'Keefe & Ahrens 1993; Melosh 1989). This conversion of kinetic energy into shock waves is poorly understood but it is clear that as one set of shock waves emanates outwards from the interface of the projectile with the ground surface into the target rocks, a complementary shock wave reflects back into the projectile (Melosh 1989; O'Keefe & Ahrens 1975; O'Keefe & Ahrens 1993, Fig. 1.1).

The time taken in the contact and compression stage is controlled by the complementary shock wave that is reflected back into the projectile (Melosh 1989). The point at which this shock wave reaches the back edge of the projectile sees the wave again reflected forward into the projectile as a rarefaction, tensional, or a release wave (Melosh 1989; O'Keefe & Ahrens 1993). The passing of this release wave through the projectile from back to front unloads the projectile from the extremely high shock pressures (Melosh 1989). These shock pressures induce extreme temperatures and the release results in virtually complete melting and vaporisation of the projectile (Melosh 1989; Artemieva 2003; Fig. 1.2). In the instant that the release wave reaches the front edge of the projectile the whole impacting body is unloaded and the advancing release wave continues into the target and begins to also decompress the target stratigraphy (Melosh 1989; O'Keefe & Ahrens 1975; O'Keefe & Ahrens 1993; Fig. 1.2). The moment that the release wave enters

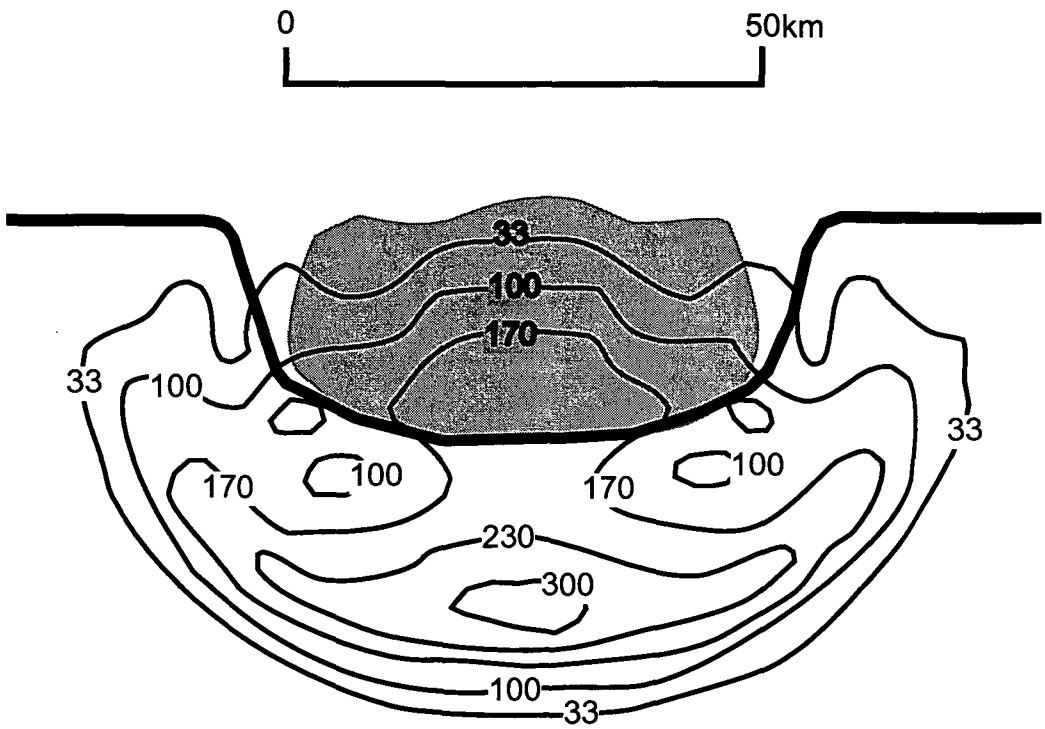

Figure 1.1 Stage 1) Contact/Compression: showing shock-wave generation and projectile deformation (pressures in GPa). The projectile has penetrated into the target to a depth close to half of its own diameter. Intense shock waves are radiating outwards from the interface of the projectile and target surface. The shock-wave too is being compressed and shock waves from the projectile/target interface are also travelling towards the rear of the projectile. Once this shock wave reaches the back of the projectile it is reflected forward as a release/tensional wave or rarefaction. This release will unload the projectile causing its immediate and complete melting and vaporisation.

Originally this model was developed for large lunar impacts (O Keefe & Ahrens 1975) and the conditions represented by the model are around 1s after a 15km/s impact of a 46km diameter anorthosite projectile onto a gabbroic anorthosite target. Diagram Based on Melosh (1989, Fig. 4.1a, p.47), re-drawn from the version in French (1998).

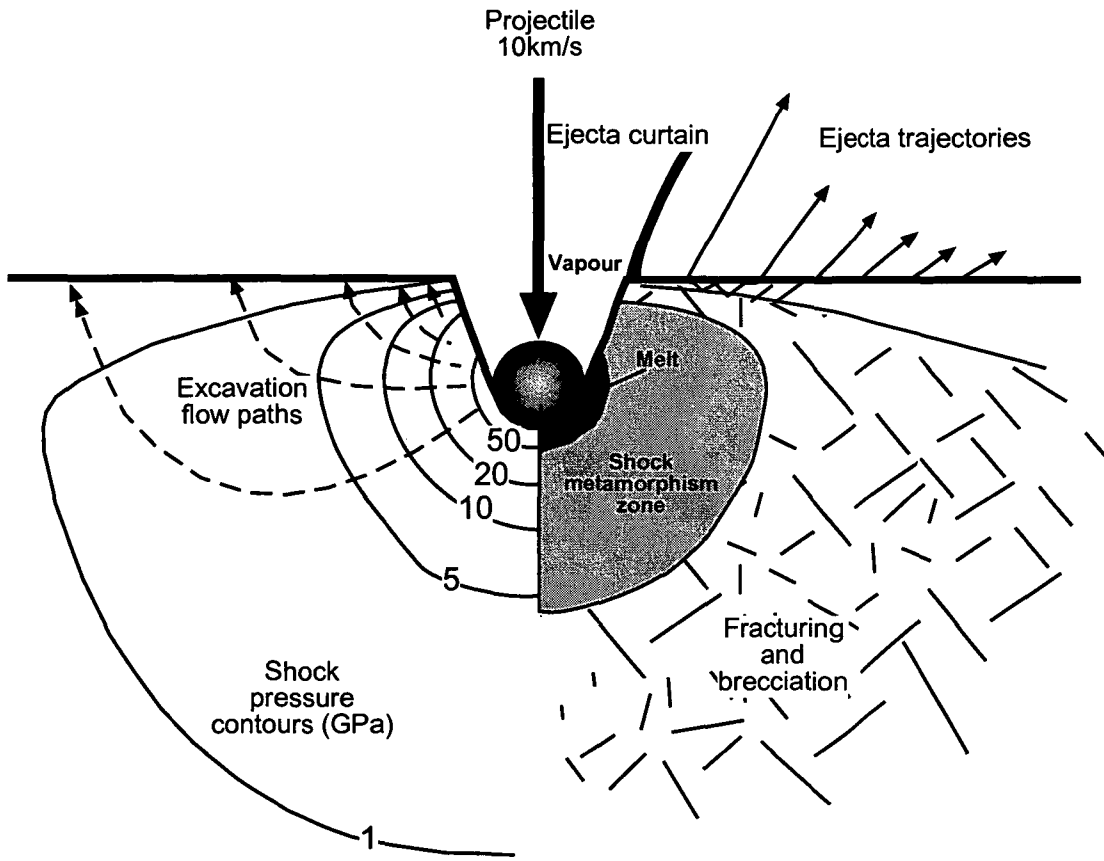

Figure 1.2 Stage 1) Contact/Compression: showing shock-wave pressures and excavation flow paths around the point of impact (pressures in GPa). The projectile is nearly completely destroyed and converted to melt + vapour. The shock waves radiating out from the projectile form a hemispherical zone in which the observed pressures and shock effects decrease outwards. At pressures: >50GPa = melting and formation of a large melt unit; 5-50GPa = shock deformation effects; 1-5GPa = fracturing and brecciation without diagnostic impact shock deformation effects. The excavation stage is divided into 2 processes: 1)vertical to near vertical ejection of near surface fragments and smaller ejecta in an ejecta curtain. 2) Sub-surface flow of target rocks downwards (excavation flow lines, left of diagram) to form the *transient cavity.*

Diagram Based on Melosh (1989, Fig. 5.4, p.64), re-drawn from the version in French (1998).

the target stratigraphy is taken to be the end of the compact and compression stage. From this point onwards the projectile itself is no longer involved in the crater formation that is now controlled by the passage of expanding shock waves through the target rocks (Melosh 1989; Fig. 1.2). Vaporised projectile may exit the crater cavity as part of an expanding vapor plume and the remaining projectile, that is now almost all melt, may be heterogeneously mixed into silicate melt produced by fusion of the target rocks, or incorporated into a melt component within brecciated target rocks (Melosh 1989; Artemieva 2003; Fig. 1.2). The compact and compression stage lasts only a few seconds, regardless of the size of the impact. Essentially, the time taken for the shock wave to travel from the projectile/target interface to the back edge of the projectile (allowing onset of the release wave) is approximately equal to the time required for the projectile to travel a distance equal to its diameter, at its original cosmic velocity! (French 1998).

Stage 2) Excavation stage

The contact compression stage progresses to a longer excavation stage where the actual impact crater cavity is blasted open by the interaction of the expanding shock waves with the original ground surface (Melosh 1989, Grieve 1987). At the end of the contact/compression a hemispherical envelope of shock waves that are rapidly expanding out into the target stratigraphy surrounds the buried projectile (Melosh 1989; Grieve 1987; Fig. 1.3). Critical to note is that, because the projectile has penetrated into the target stratigraphy, the centre of this shock wave hemisphere is within the original target rock package at some point below the pre-impact ground surface (Fig. 1.3).

Waves that travel upwards in the shock envelope to intersect the original ground surface are reflected downwards in rarefactions (release waves) (Melosh 1989, O'Keefe & Ahrens 1993). Near to the surface, where the stresses in these tensional release waves exceed the mechanical strength of the target rocks, these rocks are fractured and shattered (Gault et al. 1968; Kieffer & Simonds 1980; Melosh 1989). In this reflection process some of the shock-wave energy is converted to kinetic energy and the shattered rock is rapidly accelerated outwards, largely as discrete fragments (Grieve et al. 1977; Kieffer & Simonds 1980; Melosh 1989, Fig. 1.3). As the hemispherical shock envelope initiates from a central point, the processes that blast target rocks outwards result in a roughly symmetric excavation flow around the

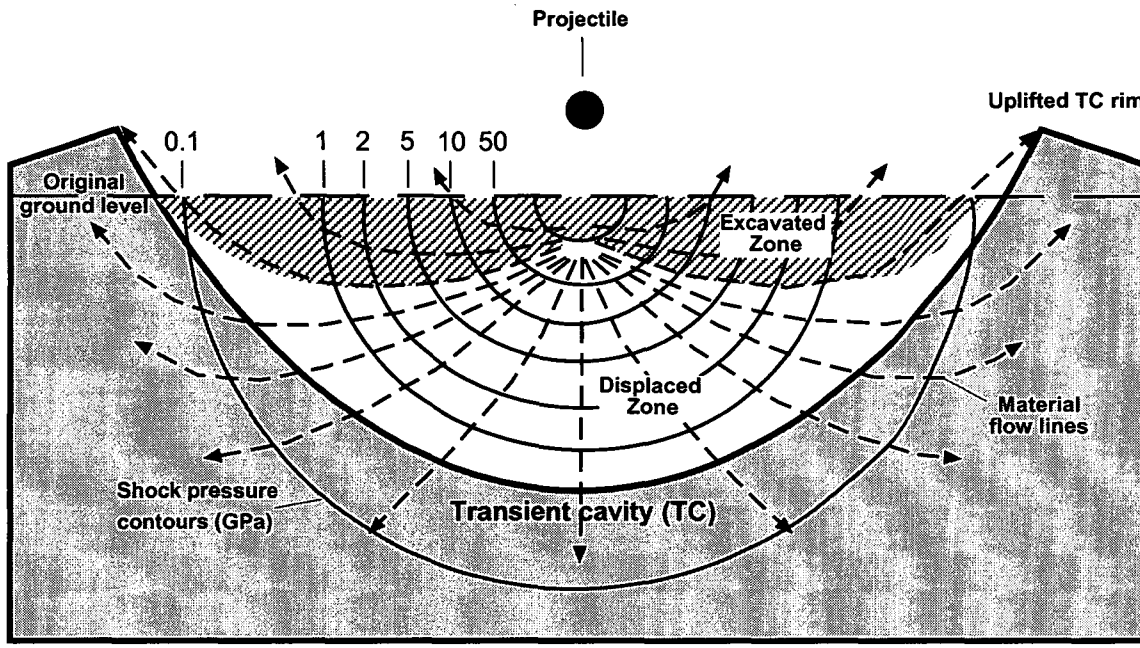

Fig. 1.3 Stage 2) Excavation of the transient cavity (pressures in GPa). original shock pressures are eminating from the point of impact in a hemispherical shape. Interactions between the original shock wave, the ground surface and the secondary release wave from unloading of the projectile and target stratigraphy, creates an outward excavation flow that opens the transient cavity. In the upper part of the expanding cavity the fractured target material is excavated and ejected to beyond the crater rim (excavation zone). Lower down in the transient cavity target materials are driven downwards and outwards but remain relatively coherent and are not ejected beyond the cavity rim. Clearly, the bulk of ejected material is derived from only the upper 1/3-1/2 of the transient cavity.

Diagram Based on Grieve (1987, Fig.5) and Horz et al. (1980, Fig. 4.3a), re-drawn from the version in French (1998).

centre of the expanding structure (Melosh 1989, Fig. 1.3). In the upper levels of the growing cavity the movement of target materials is largely upward and outward (Grieve et al. 1977; Kieffer & Simonds 1980; Melosh 1989; Fig. 1.3). Lower in the target stratigraphy shattered target material is moved predominantly downwards and outwards (Grieve et al. 1977; Kieffer & Simonds 1980; Grieve 1987; Melosh 1989; Fig. 1.3). The effect of these movements is the rapid production of a bowl-shaped cavity in the target rocks – the transient cavity or transient crater (Melosh 1989).

The upper zone is the ejection zone and here velocities imparted to the target rocks can be as great as several km/s (Grieve et al. 1977, Fig. 1.3). These velocities are great enough to excavate and eject fragments of the target rock to distances beyond the rim of the final crater structure (Grieve et al. 1977). The final crater structure can be up to 20-30 times the diameter of the projectile because shock pressures and ejection velocities still remain high enough to eject material from the cavity at large distances from the point of impact (French 1998). A fundamental principle of target rock ejection of the pre-impact stratigraphy is that as a crater is approached, ejected deposits become more representative of target rocks excavated from greater depths (Melosh 1989).

Lower down in the transient cavity stratigraphy is a displaced zone where material is driven downward and outward and remains more or less coherent (Grieve 1987; Melosh 1989; Fig. 1.3). Here the tensional stresses in the release waves are less and fracturing of the target rocks is less developed (Grieve 1987, Melosh 1989). The ejection velocities are low and the excavation flow lines are oriented such that the fragmented rock material is not ejected beyond the craters rim (Grieve 1987, Melosh 1989).

The upper and lower zones in the transient crater cavity expand, and if the expanding shock and release waves are strong enough to eject material from the expanding cavity, there is an associated uplift of the near surface rocks that develop the transient crater rim (Melosh 1989, Fig. 1.3). As these waves continue to pass through and deform and eject the fractured target rocks, energy is lost until the point where no more material can be ejected or displaced. At the critical point where the shock wave energies cease, but before forces of gravity and rock mechanics begin to dominate, the transient cavity has reached its maximum size and the excavation stage has ended (Melosh 1989). The shock waves are now present only as low-pressure elastic waves well beyond the crater rim in the surrounding country rocks. For a 1km diameter crater the excavation stage is predicted to be over in just 6

seconds, and at the instant excavation ends the modification stage begins (Melosh 1989).

Stage 3) Modification of the transient cavity

After excavation ceases, conventional geologic forces of gravity and rock mechanics immediately modify the transient crater cavity. The bulk of this modification takes only slightly longer than the excavation stage and simply put, this stage ends when materials "stop falling" but this stage merges into and is difficult to distinguish from later modification by normal processes of mass movement, erosion and sedimentation (Melosh 1989). The degree of morphological change to the transient cavity during the modification stage is controlled largely by the size of the structure, but the composition of the target material can also be of influence (Melosh 1989). For small transient cavities less than a few km in diameter, modification of the transient cavity is predominantly the result of the collapse of the upper walls that simply slump into the cavity and as such the shape of the modified structure, before later erosion or tectonic deformation, is little changed from the shape of the original transient cavity (Melosh 1989). In lager structures the modification stage involves major structural changes and deformation, this sees uplift of the central part of the cavity floor and major collapses around the rim (Melosh 1989). Subsequently the final shape of the structure is significantly different from the transient cavity. The extent of transient cavity modification determines the type of crater that results and there are 3 main forms; simple craters; complex craters; and multi ringed basins (Fig. 1.4A-C). Despite some claims, no confirmed examples of multi-ringed basins are known on Earth. Darwin is a suspected simple impact crater.

1.2.2 Shock metamorphic effects

The passage of impact-induced shock waves through the target stratigraphy produces a range of unique metamorphic effects summarised in table 1.1 and described below. The nature of these effects depends both on the amount of shock energy and the nature of the target materials involved (Stöffler & Langenhorst 1994). Lower shock pressures (~2-10GPa) are associated with the development of macro scale shatter cones in the target rocks (Stöffler & Langenhorst 1994). Shatter cones are developed from a conical fracture pattern in the target rocks and the cone surfaces show fine, shock-induced stria that diverge away from the cone apex. Higher shock pressures (>10 – 45GPa) produce a range of unusual microscopic deformation features in mineral grains such as quartz and feldspar, as well as

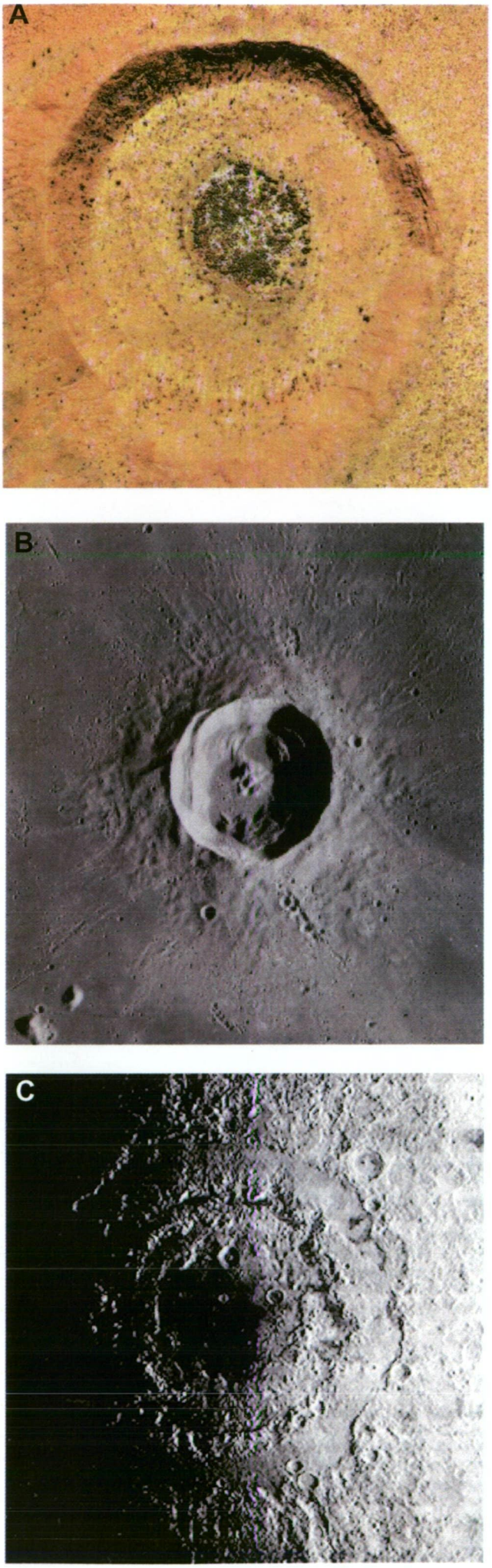

Figure 1.4 Types of impact crater

A) Simple crater:
Wolf Creek (D=0.87km; <0.3Ma).
Note the well preserved
hemisperical crater form.

B) Complex lunar crater:
Euler Crater (D= 28km).
Note the central uplift,
terraced walls and hummocky
ejecta deposits surrounding the crater.

C) Multi ringed lunar crater:
Mare Orientale (D=900km). Note the
circular rings that characterise these very
large crater forms. No multi-ringed basins
are currently recognised on Earth.

Approximate Shock Pressure (GPa)	Estimated Postshock Temperature (°C)*	Effects
2-6	<100	Rock fracturing; breccia formation; shatter cones
5-7	100	Mineral fracturing: (0001) and {1011} n quartz
8-10	100	Quartz with basal Brazil Twins (0001)
10	100*	Quartz with PDFs {1013}
12-15	150	Quartz – stishovite
13	150	Graphite – cubic diamond
20	170*	Quartz with Planar Deformation Features (PDF's) s {1012}; Quartz, feldspar with reduced refractive indexes, lowered birefringence
>30	275	Quartz - coesite
35	300	Diapelectic quartz, feldspar glasses
45	900	Normal (melted) feldspar glass (vesiculated)
60	>1500	Rock glasses, crystallised melt rocks (quenched from liquids)
80-100	>2500	Rock glasses (condensed from vapour)

Table 1.1Shock pressures and expected effects*This calibration is for dense nonpourous (eg. crystalline) rocks. For porous rocks (eg. sandstone), postshock temperatures = 700°C @ P = 10 GPa; and 1560 °C @ P = 20GPa. Based on Stöffler (1984); Melosh (1989); Stöffler & Langenhorst (1994); and French (1998).

distinctive high-pressure mineral polymorphs such as coesite that is formed from the conversion of quartz under impact conditions (>30GPa) (Stöffler & Langenhorst 1994). At even higher pressures (>50GPa) large volumes of the target rocks are molten and even vaporised (>100GPa) (Melosh 1989, Stöffler & Langenhorst 1994).

In most studies (e.g. Koeberl et al. 1995, Haines & Rawlings 2002) convincing evidence for the impact origin of a structure is found in the suite of unique microscopic deformation features produced in individual minerals by the passage of higher-pressure (~10-45GPa) shock waves during an impact event. Such pressures develop in target rocks near to the centre of the crater that are mostly fractured and incorporated in the excavation flow produced by the release waves expansion (Grieve 1987; Melosh 1989; Fig. 1.3.) Therefore, these shock effects are most commonly found in individual target rock fragments from crater-fill breccias or ejecta deposited beyond the craters rim. The main forms of mineral deformation features observed in shock-metamorphosed rocks (Stöffler & Langenhorst 1994; Grieve et al. 1977; French 1998) are:

1) kink bands, mostly in micas and sometimes in olivine and pyroxene;

2) planar microstructures and other deformation fabrics in quartz, feldspar and other minerals;

3) isotropic mineral glasses (diaplectic glass), these are produced preferentially from quartz and feldspar without actual melting; and

4) selective melting of individual minerals.

Kink bands can also be produced by tectonic processes and are not diagnostic evidence for impact-induced shock. The remaining deformation features, especially the planar microstructures in quartz and diaplectic glasses, are now generally accepted as diagnostic evidence for impact induced shock deformation (Stöffler & Langenhorst 1994; Grieve et al. 1996; French 1998). The main types of planar microstructures observed in quartz grains from shock-metamorphosed rocks are planar fractures (PF's), and planar deformation features (PDF's) (Stöffler & Langenhorst 1994).

1.2.2a Planar fractures (PF's)

These are parallel sets of planar fractures or cleavages formed at shock-pressures between ~5-8GPa (Stöffler & Langenhorst 1994). The fractures are typically 5-10μm wide and are usually spaced more than 15-20μm apart in an individual quartz grain (Stöffler & Langenhorst 1994). Tectonic processes can also produce such fractures and hence alone PF's cannot be used as diagnostic evidence for meteorite impact. However, the development of intense wide and closely spaced PF's, especially when abundant in quartz grains from a sample, is strongly suggestive of impact processes. Figure 1.5A shows a typical set of PF's in quartz.

1.2.2b Planar Deformation Features (PDF's)

PDF's are not simply open fractures as for PF's. PDF's occur as multiple sets of closed, extremely narrow, parallel planar regions in quartz or feldspar (Stöffler & Langenhorst 1994). The closure of the fractures reflects generation of diaplectic glass in the PDF planes during the shock-waves passage (Stöffler & Langenhorst 1994). PDF's are typically 2-3μm wide, <10μm apart, always straight and are generally orientated parallel to specific crystallographic planes in the quartz grain, especially to the base c(0001) (Stöffler & Langenhorst 1994). In ancient impact structures, the originally amorphous material filling the PDF planes may be recrystallised back to quartz, and in the process lines of small (1-2μm) fluid inclusions develop along the original fracture planes, such PDF's are said to be 'decorated' (Stöffler & Langenhorst 1994). Figure 1.5B shows typical PDF's in quartz.

1.2.3 Crater-fill breccias

During the short-lived modification stage, craters are rapidly partly filled by redeposited ejecta and debris slumped from the crater walls and rims (Stöffler et al. 1979; Melosh 1989; French 1998). This chaotic mixture is generally termed crater-fill breccia and may be associated with discrete units of impact melt rocks. Materials from four main sources form these allogenic crater fill breccias (French 1998): 1) material ejected ballistically at very steep, near to vertical trajectories that fall back to impact within the final cavity; 2) fragments of melt that are not ejected past the rim of the crater; 3) fragments of shocked and non-shocked target rocks that collapse inwards from the steep cavity walls. These fragments may range in size from

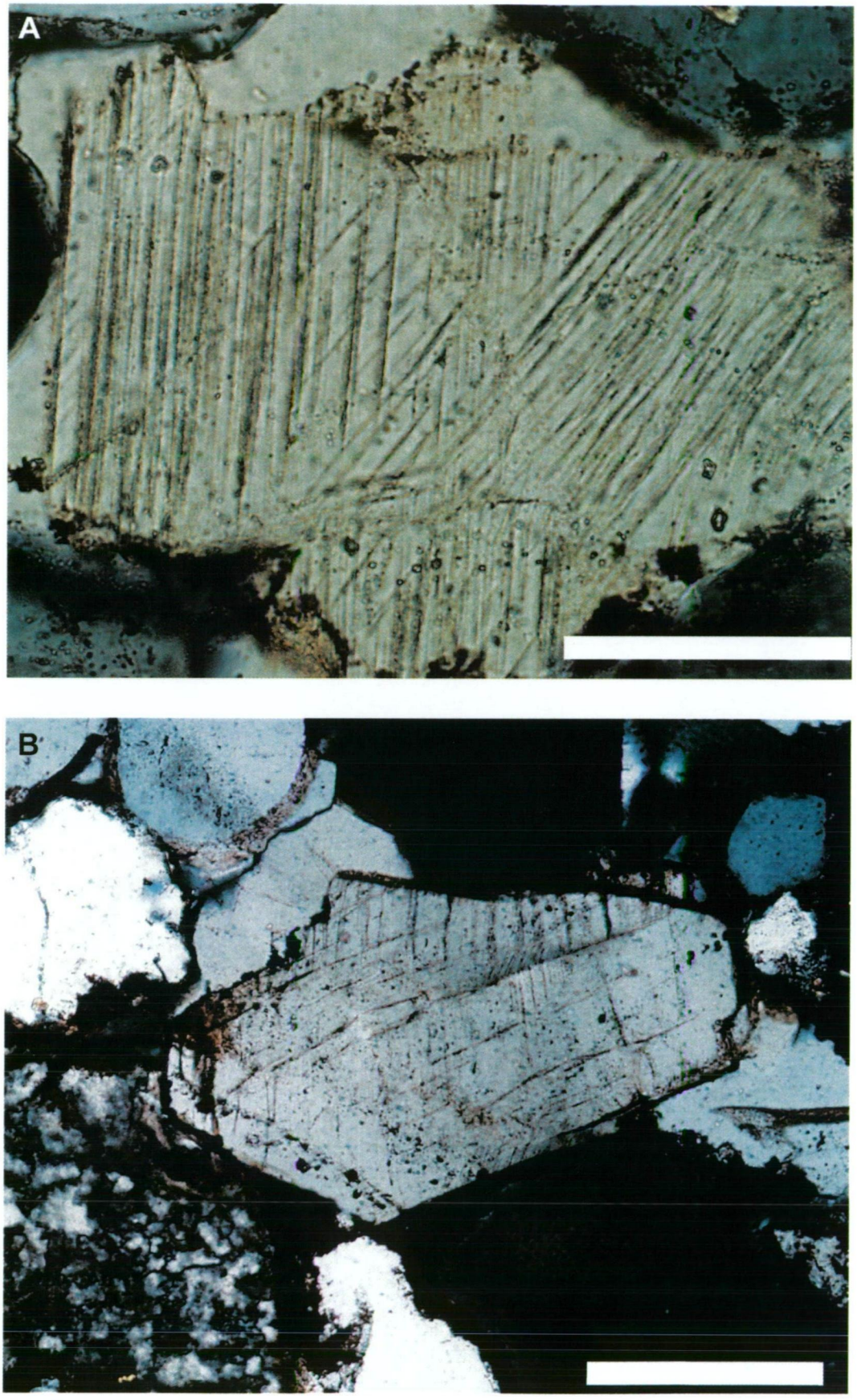

Figure 1.5 Planar microstructures in quartz grains from the Foelsche Structure, Northern Territory, Australia.
A) two prominent intersecting sets of fresh PDF s.
Scale bar =100um (Haines & Rawlings 2002, Fig.5A).
B) planar fractures (PF s). Scale bar =100um (Haines & Rawlings 2002, Fig.5D).

massive house sized blocks to small clasts; and 4) ejecta that was originally deposited near to or on the transient crater rim that is caught up in the subsequent collapse. The types of crater fill breccias that may be found are described below and this is based largely on the simplified classification scheme in French (1998).

1.2.3a Lithic Breccias

Melt-free or lithic breccias are the most common lithology in both large and simple craters. Lithic breccias consist of fragments of the target rocks and minerals in a finer clastic matrix of identical materials (French 1998). These breccias are always poorly sorted and fragments range in size from <1mm to many tens of metres. Typically the fragments are angular with sharp fractures. Allogenic lithic breccias are commonly polymict as materials are sourced from across a wide region of the excavated target rocks (French 1998). Most of the fragments in lithic breccias are sourced from low shock zones around the walls and rim of the transient crater and as such distinctive shock effects are rare (French 1998).

1.2.3b Melt breccias

Lithic breccias are often associated with units that contain a melt component present as discrete fragments or as a matrix for angular rock fragments (French 1998). When the melt component represents more than a few percent of a breccia these are regarded as melt-bearing breccias (French 1998) but the transition from lithic breccia to melt breccia is a continuum with no formal boundary. The maximum melt component in a melt breccia may be more than 90 vol% (e.g. Hörz 1982). The classification scheme of French (1998) effectively defines two end member melt breccia types; 1) melt fragment breccias (suevites), where the melt exists as large, centimetre sized, discrete clasts; and 2) melt-matrix breccias (impact melt breccias), where the melt component forms the matrix material for the target rock fragments.

1) Melt fragment breccia (Suevite)

The type example and origin of the term suevite comes from the melt fragment breccias at the Ries Crater, Germany (Engelhardt et al. 1969). Suevites consist of angular rock fragments and discrete clasts of melt in an identical matrix (French 1998, Claeys et al. 2003). Often the rock and mineral fragments in suevites are highly shocked and contain diagnostic evidence of an impact origin (e.g. PDF bearing quartz grains) (French 1998). Typically, suevites contain glassy bodies up to a few centimetres in size and these tend to comprise around 5-15 vol% of the

breccia, but glassy suevites are known that contain >50vol% glass fragments (Masaitis 1994). These suevite breccias are found both in the crater cavity (fallback suevite) and are also sometimes preserved as ejecta (fallout suevite). Around the Ries Crater, suevite is found out to 40km from the centre of the structure (Stöffler et al. 2003).

2) Melt-Matrix Breccias

Inside of the crater cavity, suevites can be intimately associated with melt-matrix breccias. Here the melt forms the matrix supporting the angular rock and mineral fragments and typically makes up 25-75 vol% of the rock that may appear obviously glassy or as a crystalline igneous rock (French 1998). Often the target rock fragments and minerals are partially molten or contain impact diagnostic shock effects (French 1998). These impact melt breccias exist at a variety of scales from small glassy inclusions in suevites to distinct dykes and sills from centimetres to hundreds of metres thick.

1.2.4 Simple craters

These are the smallest hypervelocity impact structures (other than pits on the surface of glassy ejecta) and are always less than a few kilometres across, the largest being Brent Crater, Canada (D=4km). Essentially, simple craters preserve the shape and dimensions of the original transient cavity. The modification stage in the development of a simple crater is confined to minor collapse of the steep upper walls of the transient cavity. This collapse is capable of increasing the final crater diameter by up to 20% relative to the initial transient crater, but the initial cavity depth remains unchanged but for minor re-deposition of the slumped materials (Melosh 1989). During the short-lived modification stage simple craters are rapidly filled, to around half the original cavity depth, by crater fill breccias as described above (Melosh 1989).

The idealised distribution of breccias and melt units in the crater fill stratigraphy of a simple crater is shown in Fig. 1.6. Clearly the crater fill units overlie the parautochtonous rocks of the crater floor and fill the structure to about half its original depth. These crater floor rocks may be brecciated and fractured, but are typically free of diagnostic shock effects except for a small zone at the crater's centre, and this can complicate any attempt to recognise a craters true floor during drilling operations.

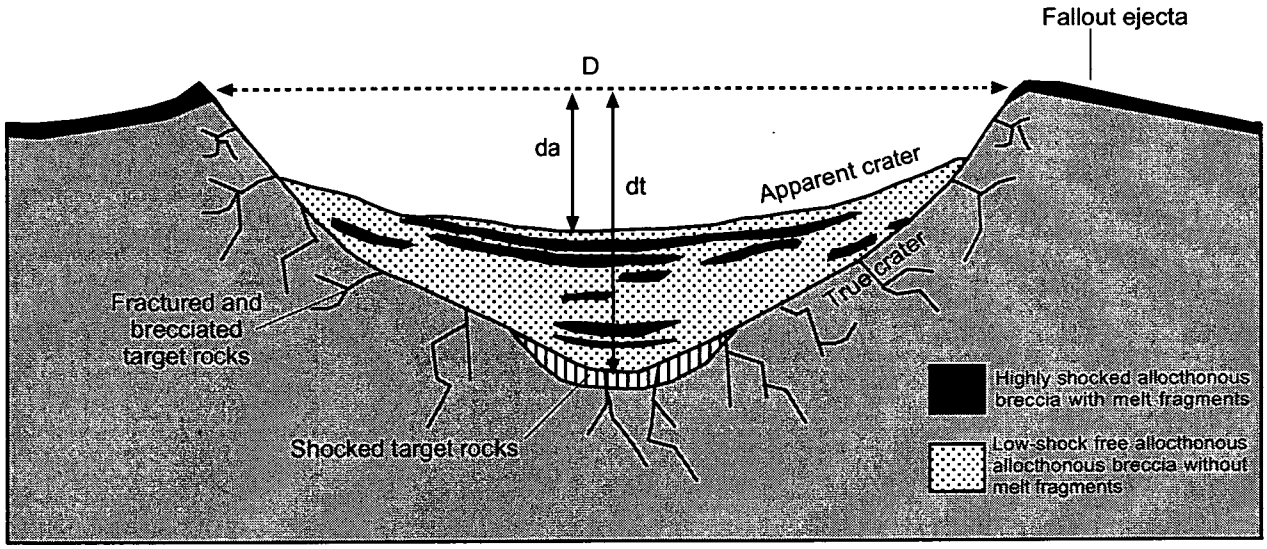

Figure 1.6 Simple crater stratigraphy. The crater is filled to about 1/2 of its original depth by a variety of allogenic breccias that may or may not be associated with a melt component- the crater fill or breccia lens. Outside of the crater a thin unit of ejected material blankets the uplifted crater rim (fallout ejecta). The parautochtonous rocks from below the true crater floor are fractured and brecciated but rarely contain impact diagnostic shock effects. If shock effects are present in rocks below the crater floor these are generally located over a small zone in the centre of the structure.

D = final crater diameter (10-20% > original transient cavity prior to the modification stage); **dt = true depth** of the final crater (approximately the same as the original transient cavity depth); **da = apparent depth** of the crater (the depth from the craters rim to the top of the crater fill sediments.

Diagram based on Grieve (1987, Fig.1), re-drawn from the version in French (1998).

1.2.5 Impact melt production

In the initial stages of a hypervelocity impact, post shock temperatures far exceed the normal melting point of the target rocks. In large impacts these post shock temperatures typically exceed 2000°C throughout a large volume of the target stratigraphy closest to the point of impact (Grieve et al. 1977; Ahrens & O'Keefe 1977; Melosh 1989; Fig. 1.7). Once the shock wave has passed through the target rocks and pressures return to normal, spontaneous and complete melting and even vaporisation of rocks takes place instantly across a large approximately spherical volume of the target material (Grieve et al. 1977; Ahrens & O'Keefe 1977; Melosh 1989; Artemieva 2003, Fig. 1.7).

The factors that control melt production remain poorly understood, but critically the amount of melt and vapor produced can be approximately scaled by the energy of the impactor (crater size) (Grieve & Cintala 1992; Pierazzo et al. 1997; equation 1.1; table 1.2). However, theoretical estimates of melt volume based on energy scaling relations tend to exceed volume estimates based in field observations in most cases, but this is particularly pronounced for craters in sedimentary rocks (Grieve & Cintala 1992), as discussed below.

$$\mathbf{V_m} = cDtc^d$$

Equation 1.1: melt production relative to crater size (Grieve & Cintala 1992)

Where: $\mathbf{V_m}$ = Melt volume (km^3); **Dtc** = Diameter of transient cavity; and **c** and **d** are constants derived from the regression of crater sizes vs. melt volume both modelled experimentally and known for terrestrial craters

Melt production also appears to be related to the nature of the target material involved, and some authors (e.g. Wasson & Heins 1993) suggest this is the dominant control on melt production. Theoretical and field studies indicate that the volumes of target material shocked to pressures sufficient for melting do not differ significantly between sedimentary and crystalline rocks (Kieffer & Simonds 1980). Huginot curves suggest more melt should be produced by an impact into sedimentary rocks than into crystalline rocks (Kieffer & Simonds 1980), and this is attributed to the higher porosity of sedimentary rocks that is predicted to promote

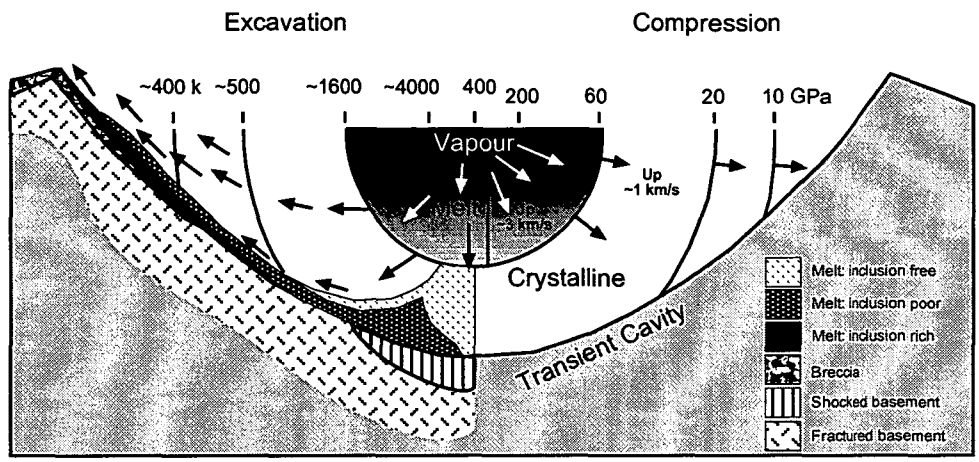

Figure 1.7 Impact melt formation and transport in the transient crater. The right hand side of the section shows peak shock pressure contours radiating from the point of impact during compression. The left hand side shows postshock temperatures during excavation. In the zone close to the point of impact shock pressures exceed 200 GPa and produce a short-lived zone of mixed projectile-target rock vapour. The melt body forms first immediately outwards of this zone where pressures are >60GPa. Kinetic energy that is imparted on the intial melt by the passage of the shock waves drives the hemispherical melt body downwards and outwards with particle velocites (Up) >1 km/s. On reaching the floor of the excavation zone the melt is ramped upwards along the expanding transient cavity floor. Here the melt can incorporate shocked and unshocked rock fragments from the craters floor and walls and may separate into inclusion free, inclusion poor and inclusion rich facies. During the crater modification stage, melt from high levels in the tranisent cavity, near to the rim, may slump back into to cavity to form disseminated small bodies and potentially large layers of melt towards or at the top of the crater fill breccias. Diagram based on Grieve et al. (1977, fig 5), modified from French (1998).

Crater	D_{rim} (km)	D_{tc} (km)	V_{melt} (km^3)	Comment
Brent	3.8	3.8	0.02	fairly reliable
Zapadnaya	4.5	4.42 ± 0.02	0.1	minimum estimate
Il'inets	8	7.21 ± 0.2	0.7	minimum estimate
Kahuga	15	12.3 ± 0.6	8	could be 8.5
Logoisk	17	13.7 ± 0.8	0.07	fairly reliable
Lappajarvi	17	13.7 ± 0.8	8	quite uncertain; minimum estimate
Ries	24	18.3 ± 1.3	0.2	up to 4-5
Boltysh	25	19.0 ± 1.4	11	fairly reliable
Mistasin	28	20.9 ± 1.6	20	uncertain by at least a factor of 2
W. Clearwater	35	25.3 ± 2.2	80	uncertain by at least a factor of 2
Kara	65	42.8 ± 4.8	480	minimum estimate
Manicouagan	100	61.7 ± 8.0	1200	minimum estimate
Popigai	100	61.7 ± 8.0	1750	fairly reliable; minimum estimate
Sudbury	200	111.2±17.5	8000	quite uncertain; minimum estimate

Table 1.2 Original impact melt volumes estimated in terrestrial craters. From Grieve & Cintala (1992).

melting (Kieffer & Simonds 1980, Melosh 1989). However, this does not appear to be the case in most field investigations that show craters formed in thick sedimentary sequences appear to be associated with less melt than craters in crystalline targets (Grieve & Cintala 1992). For example, the Ries Crater, which is the largest well preserved complex crater on Earth, and formed in sedimentary rocks, is remarkably depleted in melt relative to similar sized craters in crystalline targets (Grieve & Cintala 1992,). In their study, Kieffer & Simonds (1980) found that the proportion of recognizable impact melt rocks at craters in sedimentary rocks is two orders of magnitude less than for similar sized craters in crystalline target rocks. They explain this as relating to the increased volatile contents of typical sedimentary rocks, relative to crystalline rocks, that they suggest promotes the unusually wide dispersal of melt and inhibits the development of coherent in-crater melt bodies.

The passage of the shock wave also imparts kinetic energy that rapidly accelerates the melt along with the shattered target rocks during the excavation of the transient cavity (Grieve et al. 1977; Fig. 1.7). The bulk of the melt is produced near to the centre of the structure and is blasted, at velocities of a few km/s, downwards and outwards towards the floor of the expanding transient cavity (Grieve et al. 1977; Fig. 1.7). On reaching the transient cavity floor, the flowing melt travels outwards and upwards along the curved floor (Grieve et al. 1977; Fig. 1.7). Here the slowing melt incorporates and is mixed with shattered country rock and mineral fragments thereby developing into the melt breccias described above (Grieve et al. 1977; Fig. 1.7). Kinetic energies remain great enough to eject some melt fragment breccias (suevites) from low in the transient cavity late in the excavation stage (Grieve et al. 1977; Fig. 1.7).

In the earliest stages of the impact, before breccia formation, a unique type of melting occurs in the region nearest to the interface of the projectile and the target stratigraphy. In these regions extremely high shock pressures and temperatures >5000°C result in the production of melt + vapour, and critically this melt may be ejected in high-velocity jets at speeds potentially even greater than the initial impact velocity and without mixing with cooler inclusions of shattered target rocks and minerals (Grieve et al. 1977; Melosh 1989; Koeberl 1994; Fig. 1.7). Generally, ejected melt represents less than 1% of the total melt produced in an impact event, and the resulting ejecta are known as impact glasses or tektites, as described below. A fundamental principle of crater excavation is that the uppermost units in the target stratigraphy are ejected furthest from the source crater (Melosh 1989).

1.2.5a Ejected melt: Impact glasses and tektites

The term impact glass refers to target rock materials that are completely melted then quenched to form glass as they are ejected from the transient cavity during hypervelocity meteorite impacts. The diagnostic and characteristic features of impact glasses that distinguish them from volcanic glass are: 1) the presence of flow structure accompanied by strain birefringence; 2) the presence of siliceous (lechatelierite) inclusions; and 3) the complete absence of microlites or phenocrysts (O'Keefe 1976).

The most enigmatic impact glasses are tektites (Greek: tektos, "melted") that are naturally occurring, centimetre to decimetre sized siliceous glasses that Faul lamented are *"probably the most frustrating stones ever found on earth"* (Faul 1966, p.1341). In traditional cultures, particularly in Asia, tektites are also one of the most sacred stones on Earth as is evident from their naming of these glasses (Australian Aboriginal: mana, *"magic"*; Chinese: Lei-gong-mo, *"inkstones of the thunder god"*; Hindi: Saimantakimani, the *"Sacred Gem of Krishna"*; Sanskrit: Agni Mani *"fire pearl"*). Tektites occur in four strewn fields with unique ages: 1) North American, 35.4Ma; 2) Central European, 15.1Ma; 3) Ivory Coast, 1.07Ma and 4) Australasian, 0.8Ma (Koeberl 1994; Koeberl et al. 1997; Yamei et al. 2000; Laurenzi et al. 2001; Fig. 1.8). The North American, Ivory Coast and Australasian tektites are associated with microtektites (diameter (D) = <1mm) that are found in abundance only in deep-sea sediment cores. The distributions of the microtektites are critical in defining the outer limits of the geographic extent of each strewn field. The Australasian strewn field is the youngest, best preserved and largest. It extends from continental Southeast Asia to the Southern Ocean south of Tasmania, Australia and contains three morphological groups of macro-tektites: 1) "normal" or splashform, 2) aerodynamically shaped or ablated, and 3) layered or Muong-Nong type (Fig. 1.9). All three groups have a basic chemical and isotopic similarity and this suggests that they all formed from a single source material (Koeberl 1994). The North American, Ivory Coast and Central European strewn fields are now linked to the Chesapeake Bay (diameter (D=90km), Bosumtwi (D=11km) and Ries (D= 24km) impact craters, respectively (Koeberl 1994). The source crater for the Australasian tektite strewn field remains elusive despite over 40 years of work.

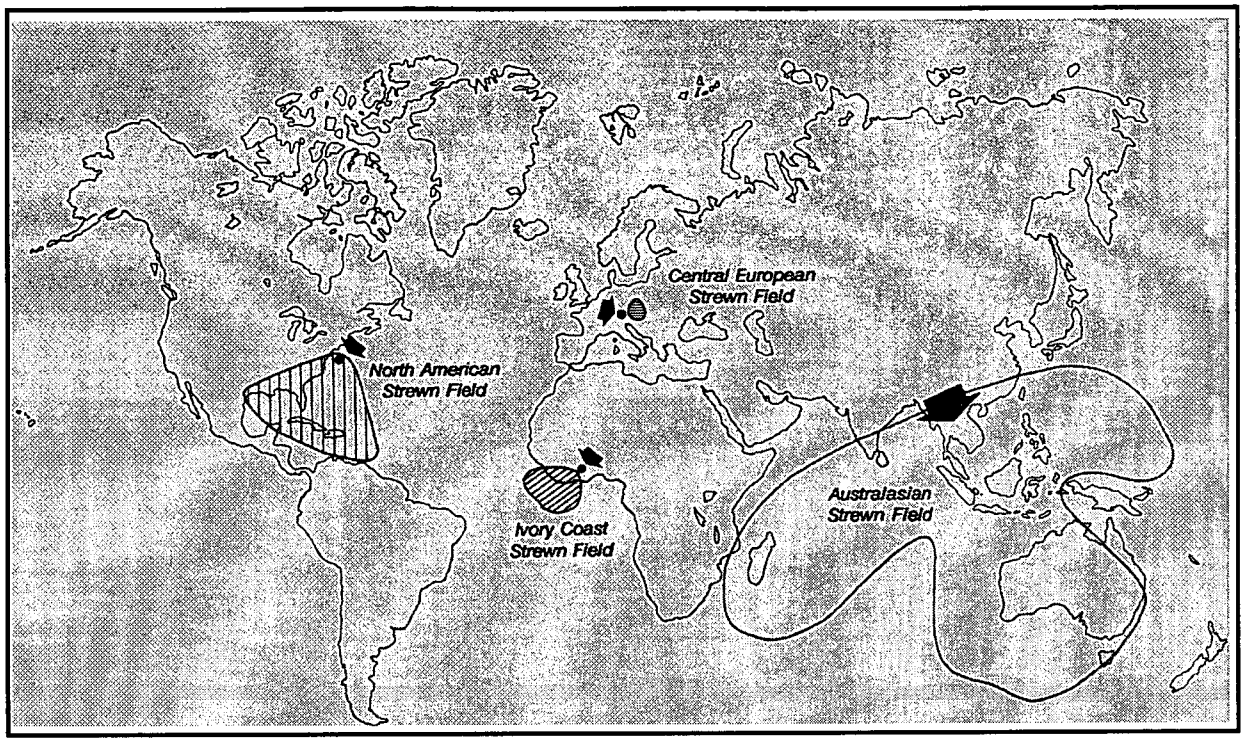

Figure 1.8 Location and currently known extents of the four tektite strewn fields on Eartth. Arrows show the approximate or suspected location of the source craters. From Koeberl (1994, Fig.1).

Figure 1.9A Splashform tektites.
From SE Asia
(scale bar = 5cm).
Microtektites are <2mm in size
and have similar shapes.

Figure 1.9B Small layered tektite fragments. Collected in Thailand
(scale bar =2.5cm).

Figure 1.9C The largest known layered tekites (24kg).
Photographed at House of Gems, Bangkok.

Tektite formation is poorly understood, as are the factors that control the efficiency of melt production, as described above. However, major and trace element chemical compositions (Taylor & Kaye 1969; Koeberl 1992, 1994), and isotopic signatures (Shaw & Wasserburg 1982; Pal et al. 1982; Blum et al. 1992; Chaussidon & Koeberl 1995) indicate that tektites, when formed, are produced by impact induced melting of upper crustal continental sedimentary materials. Why only 4 of the 160 known impacts on Earth, or 4 of the 60 known impacts in the last 40Ma are known to have produced tektite-strewn fields is unknown. This rarity of tektite forming impact events (impact glasses are more commonly found) suggests that there is some critical controlling mechanism(s) during the impact, or conditions in the target stratigraphy, or projectile type that are currently unknown. The critical feature of tektite formation that must be explained is the wide distribution of these glasses in their strewn fields.

The currently preferred mechanism for tektite formation sees a plume of molten and vaporized target rock and projectile material ejected from the impact site first during the very earliest stages of excavation of the transient crater (Melosh 1989; Melosh 1998; Koeberl 1994). This hot plume is highly pressurised (many GPa) and jets in a powerful wave that readily pushes away the ambient atmosphere in its path. In impact events that release at least 150 megatons of energy into the atmosphere the vapor plume is able to push the entire distance through the Earth atmosphere and expand out into the vacuum of space – atmospheric blowout has occurred (Melosh 1989, Fig. 1.10). This is the mechanism cited for dispersing tektites to extreme distances from the source crater, because as the vapor plume extends to a height greater than the atmosphere ejected glasses can then follow long ballistic trajectories above the atmosphere before re-entry and deposition far from the source crater (Melosh 1989; Melosh 1998; Koeberl 1994). Impact glasses are typically found close to the source crater and have apparently not undergone extended transport promoted by atmospheric blowout (Koeberl 1994, French 1998). This tendency for impact glasses to be proximally and continuously distributed around the source crater is one of the distinguishing features between impact glasses and tektites *stricto senso* (table 1.3). Tektites are chemically homogenous relative to impact glasses and typically also have lower volatile contents (Koeberl 1994). It is tempting to suggest that this classification scheme is an arbitrary division along a continuum that purely reflects the energy of the impact event. However, most very large craters are not associated with tektites. Clearly, the mechanism(s) that promotes, or the controlling feature(s) of the target material that allows for, jetting and tektite formation to take place, remains poorly defined.

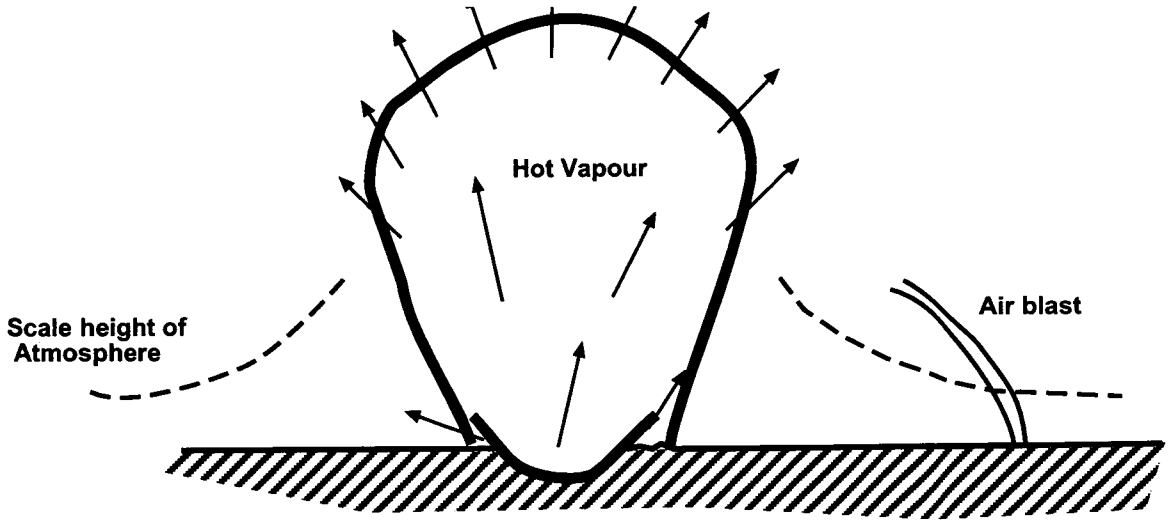

Figure 1.10 Atmospheric blow out during tekite formation. In impacts that release >150MT of energy, the explosion vapour plume may puncture the Earth s atmosphere and extend into space. This allows ejected melt to be transported along ballistic trajectories to very far from the impact site. From Melosh (1989).

	Tektites	Impact Glasses
Occurrence in strewn field	Yes	No
Source crater known	Yes/no	Yes
Occurrence directly at crater	No	Yes
Target rocks	Surface rocks	Deeper lithologies
Chemical homogeneity	Large-scale homogeneity (100mm-mm)	Usually inhomogeneous
Water content (wt%)	0.002-0.02	0.02-0.07
Mineral inclusions (includes partially digested quartz)	Rare	Abundant
Shape	Mostly regular, spherically symmetric	Mostly irregular
Ablation shapes	Yes	No
Meteoritic component (abundance wt%)	<0.02	0.02-0.5
Heavy Noble gas content (Ar, Kr, Xe)	Low	High

Table 1.3 Tektites vs. Impact glasses. The wide distribution of tektites relative to impact glasses, and the large-scale chemical homogeneity across tektite strewn fields, are the most critical differences that require explanation. From Koeberl (1994).

1.3 Darwin Glass

Darwin glass is a siliceous impact glass found in western Tasmania, Australia. The glass is predominantly green to black in colour, and fragments vary in shape from highly irregular contorted chunks to small droplets, spheroids and elongate rods (e.g. Fig. 1.11). The size of the glass fragments varies from mm-sized droplets to large masses weighing close to 1kg. Tasmanian Aborigines discovered the glass more than 20 000 years ago and are its traditional owners. Europeans discovered the glass shortly after the turn of the 20th century in about 1905. Darwin glass is named after Mt Darwin, a prominent peak in the area where it was first found, although in fact it is comparatively rare at the mountain itself. It should be noted that Charles Darwin, who's name is honoured by Mt Darwin, was not involved in its discovery or early investigation.

1.3.1 Previous works

Since it discovery, the glass has been subjected to a significant amount of scientific scrutiny, particularly in the early part of the 20th century. Significant works and previous ideas on the origin of the glass are summarised below.

Suess (1914) was the first to describe the glass and he likened it to both tektites and obsidian. Loftus-Hills (1915) described and analysed the glasses, and also likened them to tektites, particularly the moldavites (now known to be from Ries Crater, Germany). Spencer (1933) was the first to suggest that Darwin glass (and in the same letter to Nature, tektites) was formed by the fusion and ejection of terrestrial crust during the impact of a meteorite, and this paper remains the first description of the current leading hypothesis of tektite origin. The presence of coesite in Darwin glass, and therefore direct evidence for an impact origin, was confirmed by Reid & Cohen (1962). The first major geochemical analyses of Darwin glass, and rocks from near Ten Mile Hill where the glass was found to be abundant, were by Taylor & Solomon (1964) who found that: 1) Darwin glass was not produced by endogenic igneous processes; 2) the major and trace element composition of the glass shows an affinity with upper crustal sedimentary rocks; 3) Ni abundances are high and Cr/Ni, Ni/Co and Fe/Ni ratios are anomalous in some specimens of glass relative to upper crustal sedimentary rocks; 4) two chemical groups can be distinguished on the basis of trace elements data; 5) the glass is chemically distinct from australite tektites, who's distribution overlaps that of Darwin glass; and 6) the glass

Figure 1.11 Darwin glass. Collected near to Mt McCall in 2002. Scale bar = 5cm.

composition is consistent with an origin by fusion of terrestrial sediments in a meteorite impact.

By far the majority of the work that has been conducted on Darwin glass was by the late Ramsay J. Ford. Ford collected many thousands of glass fragments from across the strewn field. Most importantly, when searching aerial photographs and topographic maps he located a circular structure, subsequently named Darwin Crater, that he suggested was the source of the glass (Ford 1972). Ford's field investigation of the site was an incredible achievement given the densely vegetated nature of the terrain. Ford was responsible for construction of an access track into the suspected crater and for the commissioning of two drilling projects at the site. His observations, notes and some samples, particularly country rock samples collected during track constructions, have formed an invaluable resource in this investigation. Where possible, I have tried to compare my observations to Ford's. The drill cores were never described before Ford's untimely passing and form the basis for a significant portion of this investigation. Fudali & Ford (1979) conducted a geophysical survey of the structure that demonstrated that it was an almost circular sediment-filled basin with a slight asymmetry that sees the deepest point displaced SW of the centre. These were the last significant investigations at the structure, prior to this study, and the site is currently not officially recognised as an impact crater.

As for the major and trace element geochemistry, the $^{18}O/^{16}O$ values in Darwin glass are also consistent with terrestrial sandstones, shales or arkoses as the precursor materials from which to form Darwin glass. The $^{18}O/^{16}O$ values in Darwin glass are also distinct from australites, further ruling out a common origin. Matsuda & Yajima (1989) showed that Darwin glass has excess Ne relative the present atmosphere and interpret this to reflect diffusion of Ne from the atmosphere into the glass.

The age of Darwin glass was first determined by the K/Ar method as 0.73±0.04 Ma by Gentner et al. (1973). It was quickly recognised that Darwin glass has a very close temporal association with Australasian tektites and, using the fission track method, Störzer & Wagner (1980b) reported ages of 0.81±0.04 for Darwin glass and 0.82±0.05 Ma for an Australite. Three glass fragments dated using $^{40}Ar/^{39}Ar$ single grain laser fusion technique yielded isochron ages of 796-815ka with an overall weighted mean of 816±7ka (Lo et al. 2002). These data are statistically indistinguishable from the most recent ages reported for Australasian tektites (761-

816 ka, mean weighted age of 803±3 ka. However, the compositional differences and disparity in the suspected impact locations between Australasian tektites and Darwin glasses provide no evidence to suggest that this temporal association is not purely coincidental (Lo et al. 2002).

Meisel et al. (1990) conducted further chemical analyses of 18 glass pieces and 'target rocks'. The stratigraphic control in this investigation was very limited, and by 'target rocks' they refer to rocks collected from within the strewn field only, rather than samples from drill-core or cropping out immediately around the crater. Being the most recent and detailed investigation previously conducted into the origin of Darwin glass, the conclusions of Meisel et al. (1990) are listed below:

1) major and trace elements in the glass are consistent with fusion of terrestrial sediments in an impact;

2) statistical analyses identify 2 closely related compositional groups (A: average Darwin glass, low Fe, Al, and B: High Fe, Al) along with a third group (C) with elevated Mg, Na and enrichments in Cr, Ni and Co;

3) 'target rock' compositional mixtures can reproduce the composition of Group A and B Darwin glass relatively well for most major and trace elements, with best results for a mix of 30% quartzite, 60% shale A, and 10% shale B. Errors remain for Si, Al, and Fe in models of Group A and B glass compositions and these are greater for models of Group C glass composition that also have anomalous Cr, Ni and Co enrichments;

4) there is evidence for the loss of volatile elements Ga, Zn, F and B during the impact, explainable by selective volatilisation of these elements from the impact melt;

5) Na, K, Rb and Cs show lower abundances in the glass than 'target rocks' and this is evidence also for selective volatilisation;

6) Ni and Co abundances and Ni/Co, Cr/Ni ratios in group C glasses can not be explained by contributions from the 'target', or any normal sedimentary target rocks.

As for Taylor & Solomon (1964), Meisel et al. (1990), were unable to reproduce the composition of the transition metal enriched glasses using additions of any putative ultrabasic or meteoritic material, and they concluded with the motivating statement that "*Further investigations are clearly necessary to obtain conclusive chemical data to identify the projectile*" (Meisel et. al 1990, p.1473).

1.4 Methods of study

1.4.1 Field methods

The fieldwork was designed to recover glass fragments from throughout the strewn field, thereby serving to delineate the outer limits of glass distribution. Study sites where detailed petrographic classifications and chemical analyses of recovered glasses were performed were selected so as to define an arc around the suspected source crater. Most of the strewn field has been investigated by 4WD, or by foot streambed traverses to access remote button grass moors and dense forests. An 11-day rafting expedition down the Collingwood-Franklin-Gordon Rivers provided the only access to sites east of the suspected source crater.

The geology surrounding the crater was mapped by aerial photographic interpretation, and ground traverses off the Darwin Crater access track. The area is densely forested and outcrop is often limited to tree root rip-ups and failed slopes.

1.4.2 Analytical methods

Major and some trace elements in Darwin glass were determined by Scanning Electron Microprobe (SEM). Trace elements in Darwin glass were determined by Laser Ablation Inductively Coupled Plasma Mass Spectrometry (LA-ICPMS). X-Ray Fluorescence (XRF) techniques were used for whole rock analyses of major and selected trace elements in target rock samples and some glass specimens. Trace elements in target rocks and a few glass samples were determined by solution ICP-MS, and this technique was also used for Sr and Nd isotopic determinations in glasses and target rocks. Clay minerals and quartz grains in target rocks and some glass samples were characterised using an Environmental Scanning Electron Microscope (ESEM). X-Ray diffraction (XRD) was used for quantitative determination of clay mineralogy. Detailed specifics of the analytical techniques, including a discussion of such issues as sample preparation and selection of standards, are provided in the relevant chapters herein.

1.5 Location and access

The Darwin glass strewn field is located on the central western coast of Tasmania and commences at the northern most edge of the southwest World Heritage Area (WHA) that includes most of the southwest of Tasmania (Fig. 1.12). Darwin Crater lies in the catchment of the Franklin-Gordon Rivers inside of the Wild Rivers National Park and the WHA at 42°18.39's, 145° 39.41'E. The strewn field is accessed from Queenstown by travelling south along the Mt Jukes Road to the Darwin Dam on Lake Burbury; a 54km^2 impoundment that forms a part of the King River Power Scheme. From here, the road becomes the Kelley Basin Track and is unsealed. A four-wheel drive vehicle is desirable; in a two-wheel drive vehicle the track can be followed as far as the junction to Kelley Basin and the Bird River in fine weather only. From this point the Mt McCall Road, or Franklin Track, continues southward into the wilds until the Franklin River is reached some 20 km away (4WD only). A key is needed for vehicles to enter the boom gate that marks the start of the WHA and this is obtained, after prior warning is given and a permit sought, from Parks and Wildlife Tasmania's office in Queenstown. The overgrown access track to the crater, though once having provided vehicular access, is now strictly a walking track. The track exits the Mt McCall road to the east, some 2 km past the boom gate, and is almost always wet and muddy.

Topography, access roads and walking tracks in the strewn field and around the crater are covered by the 1:100 000 scale Franklin (Tasmanian Government 1997), and 1: 25 000 scale Engineer (Tasmanian Government 1995), map sheets. Much of the strewn field is either largely inaccessible, or accessible only by difficult to negotiate 4WD tracks or by foot using walking tracks, or along trackless riverbeds and through dense scrub and forest. In poor weather, investigations in the strewn field are effectively impossible except for in rafts that were used to access sites along rivers to the east of the strewn field.

Collection of glass (or any other natural material) from inside of the park boundaries is prohibited except where a permit has been given by Parks and Wildlife Tasmania. Outside of the park boundaries the material can legally be fossicked for. However, the glass is traditionally owned by Tasmanian Aborigines who discourage its collection, but with the exception for several caves in the region, lack the required sovereignty over their traditional lands to enforce these wishes. Visitors to the strewn field are asked to respect the regions Aboriginal history.

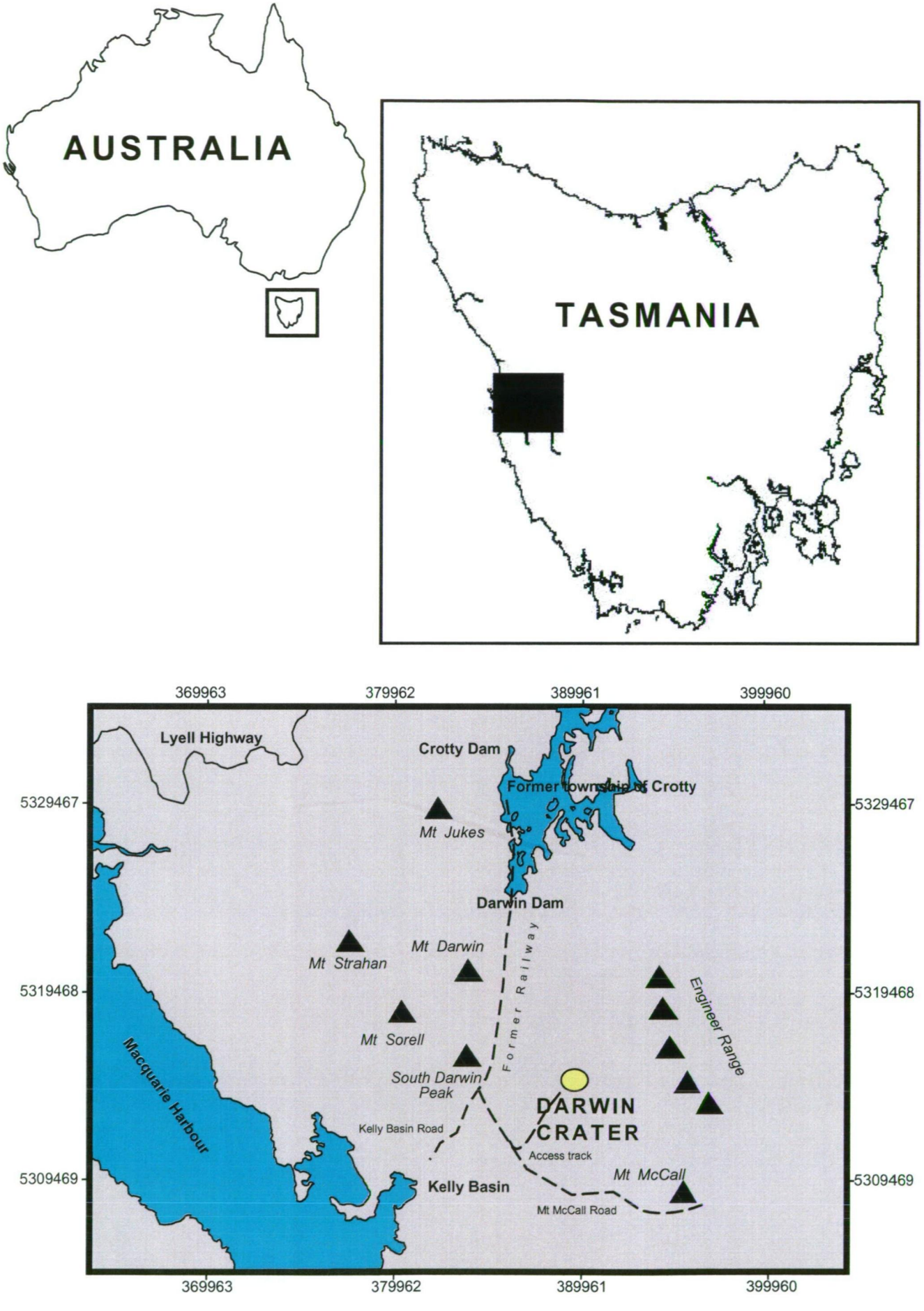

Figure 1.12 Locality maps. Historically glass was found in construction of the railway track to Kelly Basin.

1.6 Geomorphology, climate and vegetation

The strewn field and study region ranges in altitude from sea level to above 1000m (Mt Sorell), with most investigations taking place between 200 and 500m. The study region and southwest Tasmania is characterised by sharply contrasting relief with rugged mountain ranges, deeply incised valleys and flat to gently undulating plains. Rivers in the study region are permanent, carrying huge volumes of water and are often in flood, particularly in winter (e.g. the Franklin River).

The interaction between prevailing westerly winds blowing off the ocean, and topography is the dominant factor controlling rainfall in Tasmania. As such, annual rainfall varies dramatically across the state to average less than 600mm in the Midlands up to ~3,500mm in the mountainous west (Bureau of Meteorology 2004). The highest rainfall occurs in remote unpopulated areas within the WHA, where data are sparse, but average annual totals may be greater than 4000mm (Bureau of Meteorology 2004). The Kelley Basin region is renowned as an area of persistent high rainfall. The highest precipitation typically occurs in the winter months of July and August, but flash flooding can take place in any month of the year.

Throughout most of the study region are areas of potential natural temperate rainforest. However, high fire frequencies in combination with poor soils and often incredibly poor drainage have reduced the vegetation in extensive tracts of land to areas of dense mixed forest, wet sclerophyll forest, scrub and heath (Colhoun & Van de Geer 1988). Trees in areas of temperate rainforest are dominated by Myrtle-beech (*Nothofagus cunninghamii*); Sassafras (*Atherosperma moschatum*); Leatherwood (*Eucryphia lucida*); Celery Top Pine (*Phyllocladus aspleniifolius*); Huon Pine (*Lagarostrobos franklinii*); King Billy Pine (*Athrotaxis selaginoides*) and Pencil Pine (*Athrotaxis cupressoides*) (Department of Primary Industries Water and Environment [DPIWE] 2004). Along with smaller understorey species such as Native laurel (*Anopterus glandulosus*); Horizontal (*Anodopetalum biglandulosum*); Whitey wood (*Acradenia frankliniae*), Lancewood (*Phebalium squameum*); and Native plum (*Cenarrhenes nitida*) (Department of Primary Industries Water and Environment 2004).

Mixed forest refers to a community dominated by rainforest species such as Myrtle and Sassafras along with an understorey dominated by younger eucalypts (Department of Primary Industries Water and Environment 2004). Wet Sclerophyll forests tend to have an understorey dominated by shrubs such as musk (*Olearia*

argophylla), blanket leaf (*Bedfordia salicina*) and wattles (*Acacia* sp.) (DPIWE 2004). Eucalypts dominate the canopy and the species present depends largely on the soil nutrient availability; on moderate to fertile soils Ash species dominate (e.g. *E. delegatensis*) (DPIWE 2004). In the strewn field, the nutrient poor quartzite soils mean that *E. nitina* is the dominant species.

The most common of the vegetation communities in the strewn field are button grass (*Gymnoschoenus sphaerocephalus*) moors (DPIWE 2004). Other species that are commonly found on the moorlands in the study region are *Lepidosperma filiforme*, *Empodisma minus*, *Leptocarpus tenax*, *Sprengelia incarnate* (sprengelia), *Leptospermum nitidum* (shiny tea-tree) *Leptospermum scoparium* (manuka), *Melaleuca squamea* (swamp paper bark), *Melaleuca squarrose* (scented paper bark) and *Banksia Marginate* (banksia, honey suckle) (DPIWE 2004).

Figures 1.13A-D illustrates the dense rainforest and open button grass moors that are the dominant vegetation assemblages across the strewn field and study region.

1.7 Pre-impact environment at ca.800ka

As continues to the present day, westerly air streams and orographic rainfall have dominated the climatic regime of western Tasmania throughout the Quaternary. The Pleistocene climate of southeast Australia was characterised by cycles of rapid glacial advance and retreat (interglacials) (Williams et al. 1993). In Tasmania this has involved the progressive replacement of closed canopy rainforest by drier and more open "dry" rainforest, schlerophyll forest through to herb-dominated communities (Macphail et al. 1993). This progression is interpreted to be controlled by precipitation (e.g. Trusswell & Harris 1982; Kershaw, 1988; Macphail & Trusswell 1989). High-resolution climate reconstructions suggest that at the time of impact (816±7ka) southeast Australia was leaving an interglacial period, and about to plunge into a glacial period that peaked at ca.800ka (Howard et al. 2001). It is estimated that in the last glacial maximum at 18ka precipitation to the southern hemisphere was perhaps 40-50% less than that measured today, and as a result the proliferation of rainforest communities appears to have been significantly restricted in Tasmania (McPhail et al. 1993). At older glacial maxima, rainforest communities appear to have been far more developed in Tasmania (McPhail et al. 1993), and it

Figure 1.13 The Darwin Glass strewn field.

A)The densely vegetated mountains that surround Darwin crater. Dawn in winter, looking east towards Frenchmans cap. Photo: P.Haines.

B) Start of the crater access track. The track commences in rainforest and mixed wet forest typical of that found across the strewn field.

Figure 1.13 The Darwin Glass strewn field.

C) Dense, wet understorey on the crater access track. Re-growth after 20 years, in non-disturbed forest access is even more challenging. This is typical of the forested crater surrounds.

D) Heath and Buttongrass near the crater. The ground surface is a muddy swamp.

can be inferred that these older glacial maxima were, therefore, significantly wetter than at 18ka.

The genetic characteristics of modern Tasmanian rainforest indicate that valleys such as the Andrew River valley and the valley that hosts the crater have always been refugia for rainforest communities, indicating that wet conditions have predominated at low altitudes throughout the Pleistocene (Kirkpatrick & Fowler 1998). As the time of impact was during a transitional period, precipitation is likely to have significantly exceeded the glacial maximum values, and it is suggested that the area received perhaps 60-80% of the current annual rainfall at the time of the impact (ie. at least around 2-2.5 metres per year). As with today, the majority of this rainfall is likely to have fallen in winter. Therefore, the impact was to strike an environment with a similar but somewhat cooler and drier (but still generally wet) climate than at present. As such, the impact event would have destroyed rainforest and associated floristic communities very similar to those that can be found throughout southwest Tasmania today. Further evidence as to the past vegetation immediately surrounding the crater, and the hydrologic setting of the pre-impact environment, is presented later during detailed discussions of the *Origin of Darwin glass*.

Chapter 2

Physical properties, distribution, and abundance of Darwin glass

During the period 2000 – 2003 thousands of fragments of Darwin glass were collected from sites across the strewn field (Fig. 2.1). The glass was recovered in a series of controlled and uncontrolled excavations as described below, and samples held in the collection at the University of Tasmania were also examined. The objectives of this chapter are to describe: 1) the physical appearance of these specimens, and a series of populations are defined that encompass the shape and colour variations observed; 2) the nature and distribution of the field occurrences of Darwin glass (ie. the geography of the strewn field); and 3) variations in the abundance of the glass across the strewn field. Spatial variations in the physical properties and abundance of glass will provide a framework for later discussion of the *origin of Darwin glass.*

2.1 Sample collection: controlled vs. uncontrolled excavations.

A controlled excavation refers to an archaeological style dig where a known volume of material is sieved and searched for glass. At 11 sites a volume of 0.03m^3 of glass-bearing sediment was sieved through 1 and 0.5 cm mesh sieves. Where possible the sediment was excavated from a standard sized area usually around 1m^2 however, dense vegetation with complex root systems and steep rugged terrain often prevented this control. All glass was recovered from the sieves and a ground sheet placed below sieving operations was searched for fine glass fragments. Uncontrolled excavation involves simple fossicking for the glass without consideration of the volume of material or area searched and may or may not include digging and sieving. Uncontrolled excavations were used in areas of low glass abundance where sieving of 0.03m^3 of gravel would be unlikely to recover glass, or in areas of rugged terrain or dense vegetation, thus allowing investigations over the full extent of the strewn field.

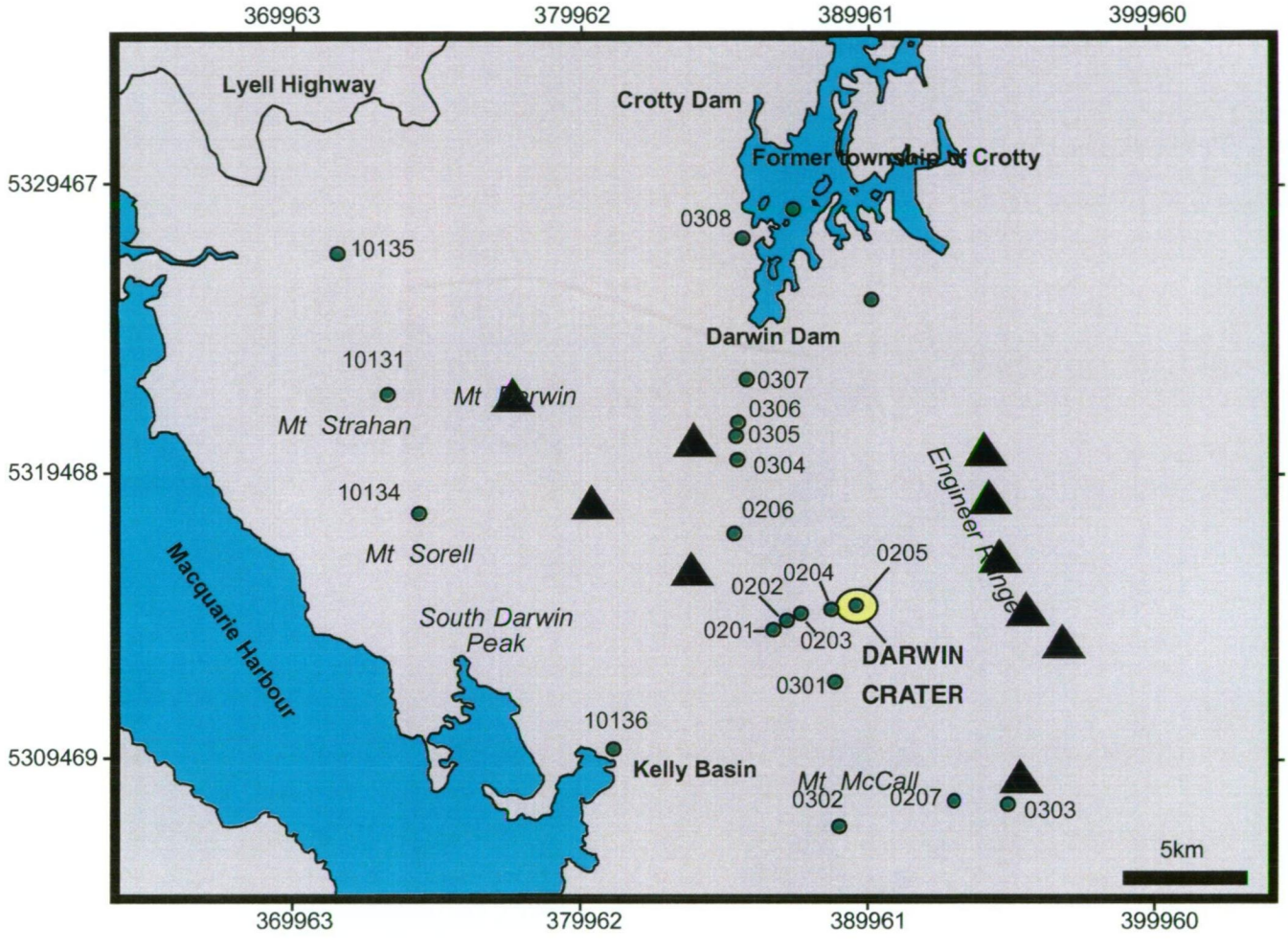

Figure 2.1 Darwin Crater and Darwin glass strewn field.
Showing significant glass collection sites referred to in text (solid green circles).
Solid black triangles are major mountain peaks in the strewn field.
Between sites 0301 and 0206 glass is almost always recovered.

2.2 Description and classification

The glass has a dull to vitreous lustre, and may be compact or frothy in appearance. It has a hardness just less than that of quartz, and breaks with conchoidal fractures. The glass ranges from clear/white to black in colour and from irregular and contorted to spheroid or droplet in shape. Recovered glasses display a wide range in both colour and shape (Fig. 2.2A-D). Because of the presence of vesicles, the apparent specific gravity measured for Darwin glass varies considerably from about 1.7 to 2.3. Superficially some samples of Darwin glass resemble other natural glasses such as obsidian and fulgurites, or show a strong resemblance to slag produced in mining operations. The latter is important to recognise given the historic mining activities within the strewn field. However, the wide distribution and abundance of glass is inconsistent with fulgurites that tend to form localised deposits. Three important features of the glass evident in thin section distinguish Darwin glass from volcanic glass, and are diagnostic of an impact origin, these are: 1) the presence of flow structure (schlieren) accompanied by strain birefringence; 2) the presence of siliceous (lechatelierite) inclusions; and 3) the absence of microlites or phenocrysts (Fig. 2.3A,B).

2.2.1 Darwin glass shape classes

Five shape classes have been recognised that encompass the range of variation in Darwin glass. These shape classes are

- Spheroid
- Droplet
- Elongate
- Ropy
- Irregular

Each shape class is defined below before discussion of statistical analyses.

Figure 2.2 Assorted Darwin Glass **A)** Irregular and ropy glass fragments (scale bar = 5cm) size); **B)** Irregular white glass fragments (scale bar = 1cm); **C)** Splashform Darwin glass (scale bar = 2.5cm); **D)** Splashform mini-glasses (scale bar = 5mm).

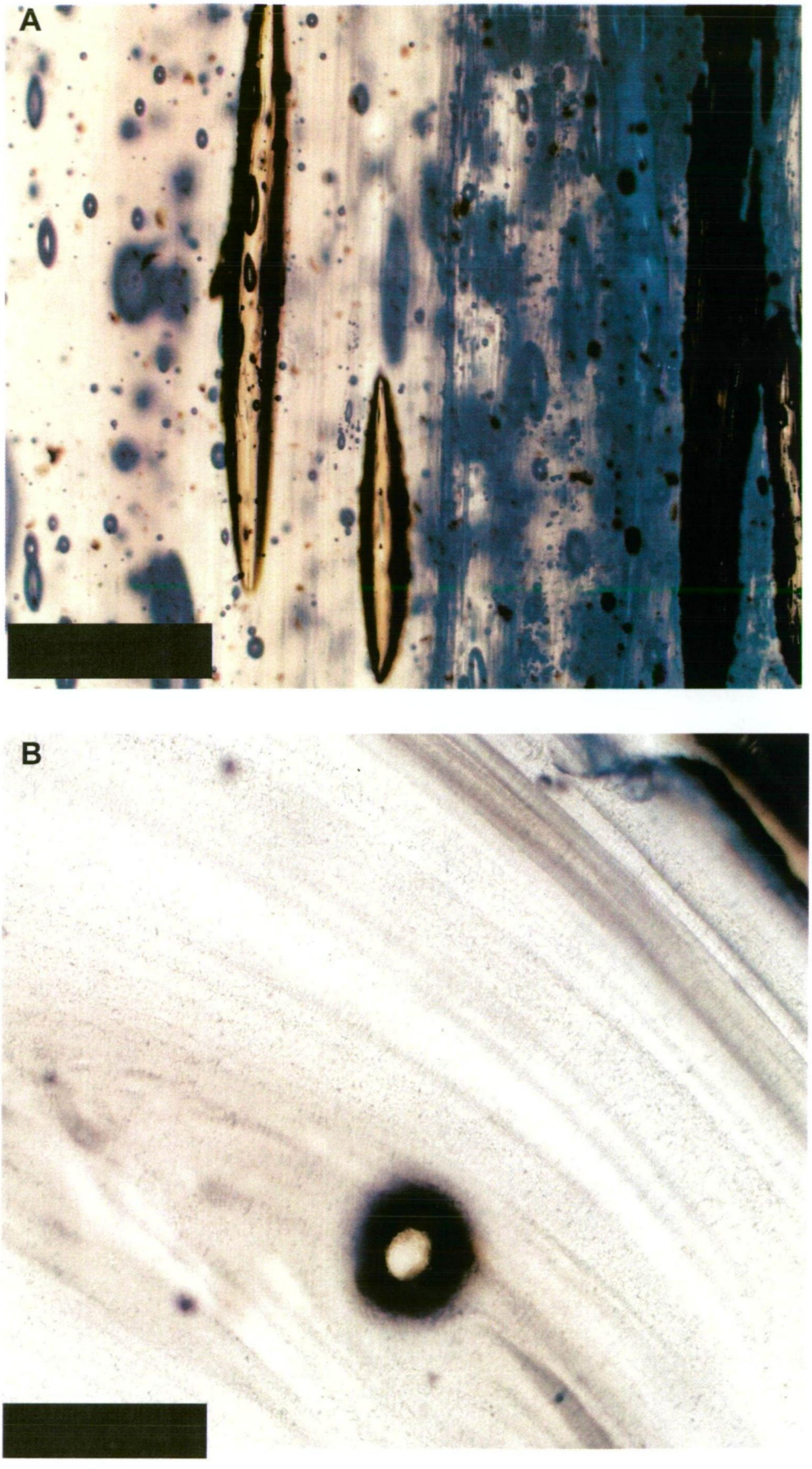

Figure 2.3 Internal features in Darwin glass A) Large elongate inclusions are lechatelierite. The small circular and stretched circular features are vesicles or smaller lechatelierite inclusions. The stretched shaped of the vesicles is indicative of viscous flow (Scale bar is 100µm, PPL); **B)** Flow structure (schlieren) typical of impact glasses (Scale bar is 100µm, PPL). Note the complete absence of phenocrysts or crystallites in both thin sections.

2.2.1a Irregular glass

Irregular shaped Darwin glass ranges in size from fragments of a few millimetres diameter to chunky masses up to 15 * 8cm in size. These glasses have rough contorted shapes and are the most varied in appearance (Fig. 2.4A-H). They may, or may not, show pronounced layering and flow structure in hand specimen (compare Fig. 2.4H,C). Such layering is present at all scales from distinct topographic ridges on hand samples, to the microscopic *schlieren* features observed in thin sections of all Darwin glass samples. In some samples this layering is defined by an obvious colour banding in the glass. Colour changes between adjacent layers may be abrupt, or expressed as a gradual colour transition. The layering tends to be parallel and in places the layers may form closed loops. This is most pronounced in thin sections of irregular glasses where a cavity or zone of optically distinct glass may be enclosed within flow layering (Fig. 2.5A-D). Where flow layering is present, it rarely extends throughout the sample.

2.2.1b Ropy glass

Ropy samples of Darwin glass are rod-like and vary up to 100mm in length, with typical length/width ratios of around 5:1 (Fig. 2.6A-F). The ropy texture is defined by parallel longitudinal ridges that are generally twisted along the length of the sample. The ends of the ropy glass samples are almost always broken to reveal a vitreous fracture surface. There is often a change in colour observed along the longitudinal ridge and between individual ridges. In hand specimen large vesicles are rarely found on the surface of ropy shaped glasses. Ropy glasses generally have a lower specific gravity than the irregular glasses, and some of the ropy rods have a hollow straw-like core. The rarity of vesicles on some ropy glass samples ensures that these samples are extremely vitreous, translucent and 'gem' like. The ropy shapes are apparently due to stretching while in a viscous state.

2.2.1c Elongate shapes

Predominantly rod-like, the elongate shaped glasses are between 10 and 40mm in length and up to 10mm in diameter (Fig. 2.7A-G). Some elongate samples are bent and have bulbous ends (e.g. Fig. 2.7D,E) – referred to as "phallic by Suess (1914) in his description of the glass. Vesicles are rare on the surface of elongate shaped glasses. Internal colour variation is also rare in such shapes. Flow layering is very

fine and any pronounced topographic expression of the layering is rare. The layering is parallel to the long axis.

2.2.1d Droplet shapes

Droplet shapes are between 5 and 50 mm in length. The small droplets are often highly vitreous and may be translucent (Fig. 2.8C-H). Some droplets have pitted surfaces and the interior of these pits may have a polished surface suggesting that these are vesicles. The droplets are typically asymmetrical with bent tails and sloping rounded faces (e.g. Fig. 2.8D). They may appear 'squashed' and the tails are almost always broken leaving a vitreous fracture surface. The droplets may show very fine but distinct flow structure that is enhanced by natural surface etching. The flow layering may wrap around to parallel the external morphology of the droplet shapes and this is particularly pronounced on the leading edges of some droplets.

2.2.1e Spheroid shapes

Spheroid shaped glasses are between 1 and 20mm diameter (Fig. 2.8A,B), and vary from perfect spheres through to discs. They generally have a vitreous lustre and some samples may be translucent and shine with a gem like quality in direct light. Larger spheroid shapes are often highly pitted – especially those of light green colour (e.g. Fig. 2.8B). Colour banding is rare. Disc shaped specimens may show pronounced concentric flow layering. A feature of the small (<5mm) diameter spherical glasses is that they may be found adhering other glass shapes (e.g. Fig. 2.7E). The contact of such spheres with larger glass fragments sometimes involves a thin tail and in such cases the sphere approaches droplet in shape.

2.2.1f Vesicles, pits and fracture surfaces in Darwin glass

Pits and cavities exist in all Darwin glass samples but are more abundant in the irregular shapes compared to the elongate, spheroid or droplet shapes. Most pits are interpreted as vesicles (e.g. Fig. 2.4F) and may be sub-spherical due to stretching. The vesicles interrupt the continuity of layering in the glasses and are therefore interpreted as later features. In a single sample, vesicles and pits may be found only on some surfaces. Rare crescent shaped pits on the surfaces of some irregular glasses may be from collision with other particles during formation and if so are tiny impact structures. Some large cavities in irregular shaped Darwin glasses have a vitreous polished lustre, as do the fresh fractured edges of the fragments.

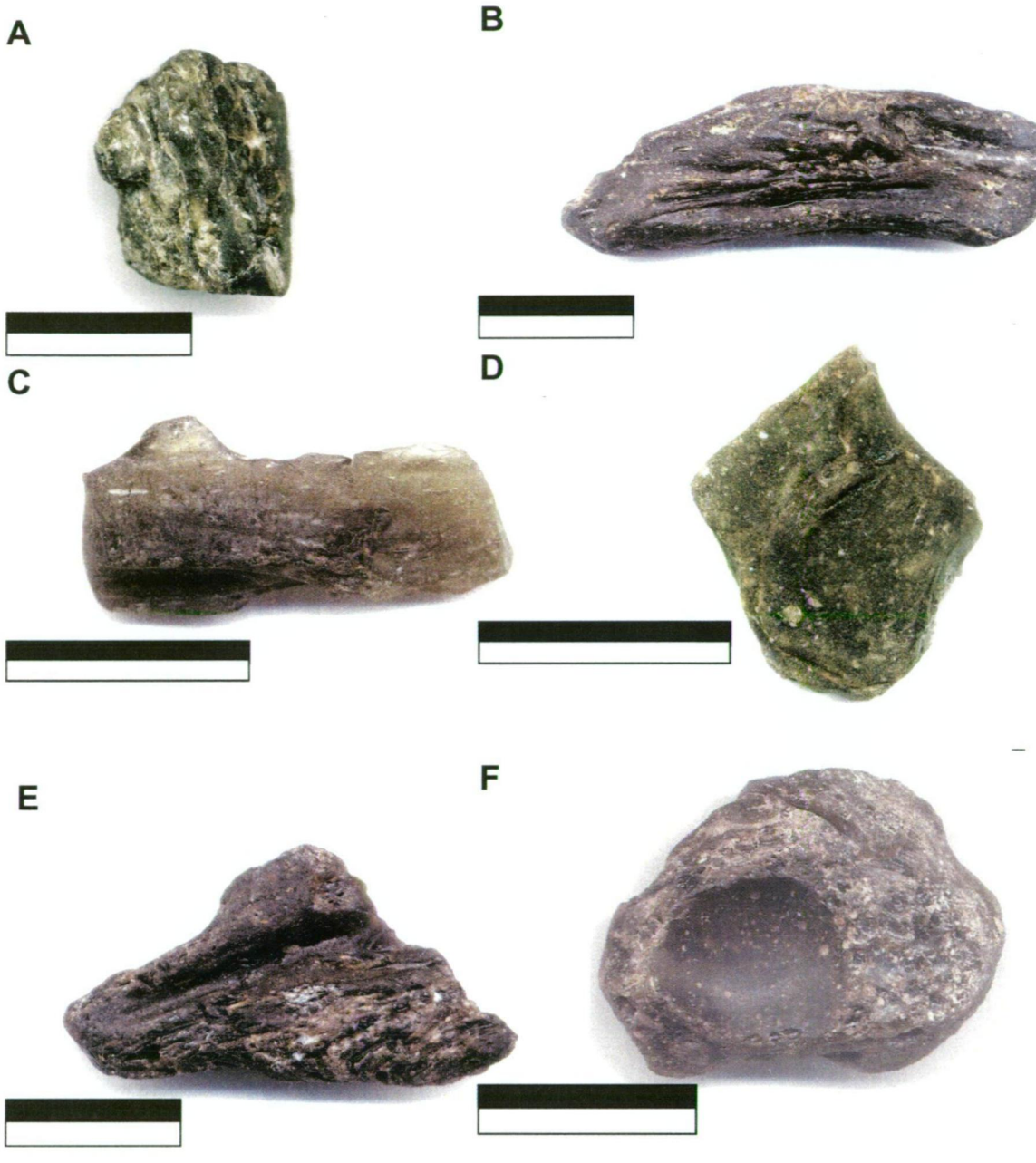

Figure 2.4 Irregular Darwin glass A-F) scale bars = 2cm. Note the parallel layering that is predominantly planar and the common presence of vesicles best illustrated in Fig. 2.4B. These specimens have a superficial resemblance to layered tektites of the Australasian strewn field, particularly Fig. 2.4B,E.

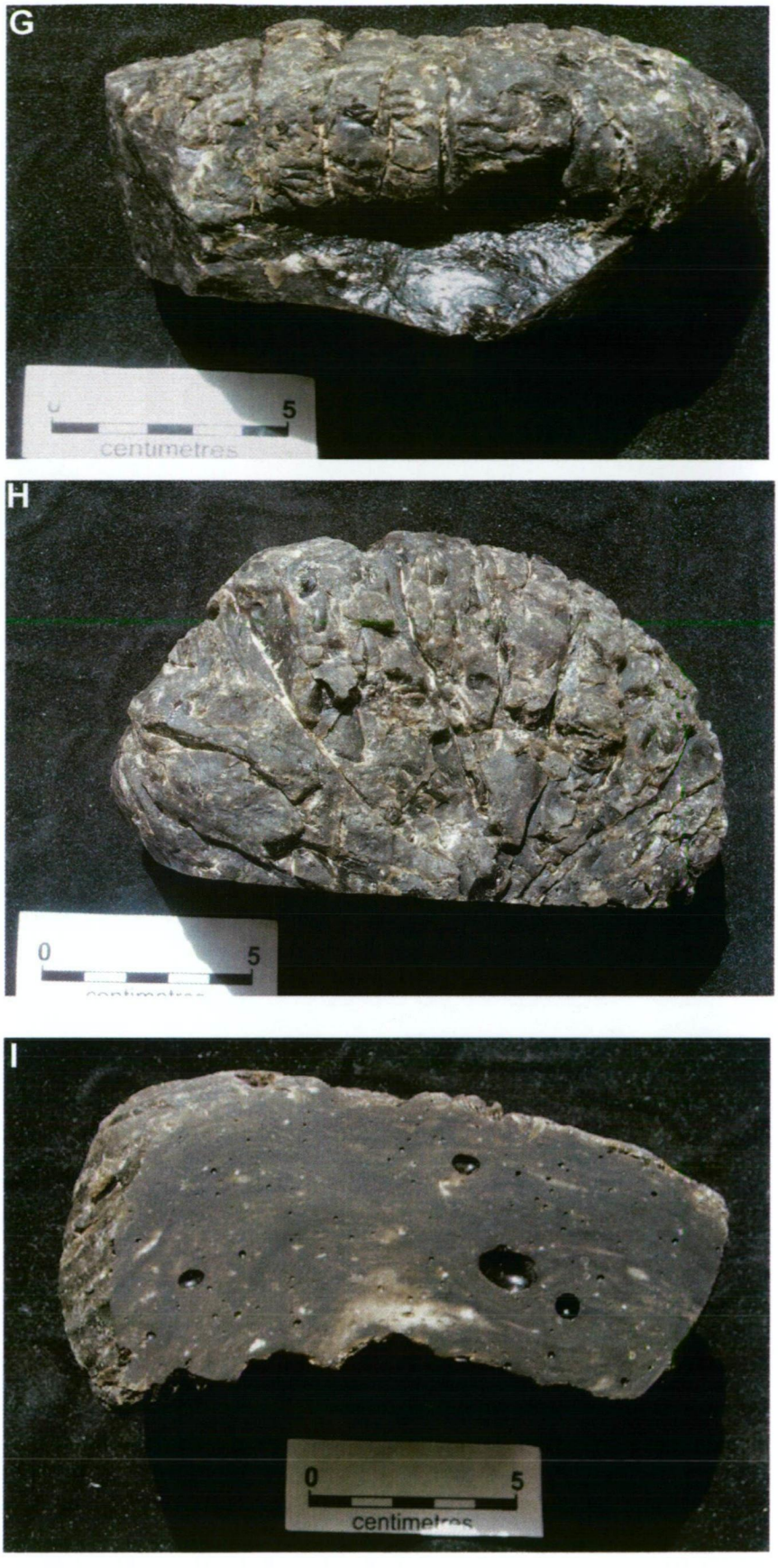

Figure 2.4 Irregular Darwin Glass G-I) The largest known fragment of Darwin glass that weighs 946g after a slice has been removed for sectioning. The fragment was collected by R.J. Ford. This specimen also has a superficial resemblance to layered tektites of the Australasian strewn field.

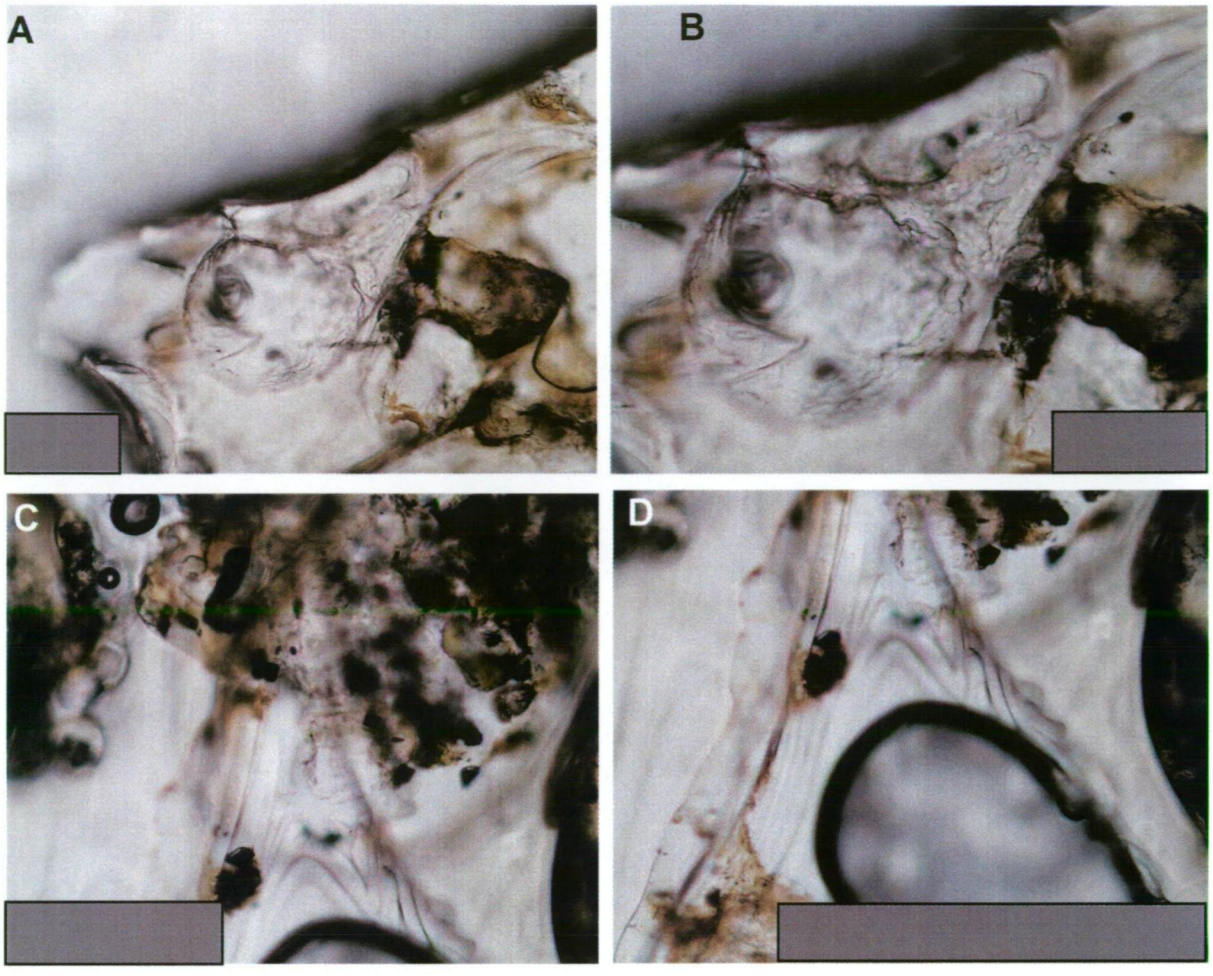

Figure 2.5 Internal features in Darwin glass A) Schlieren defining a wave or droplet shape (Scale bar is 100μm); **B)** Close up of A (Scale bar = 100μm). These features reflect turbulent circulation in the melt jet . **C)** Tail of another droplet shaped feature (Scale bar is 100μm); **D)** Close up of C (Scale bar is 100μm).

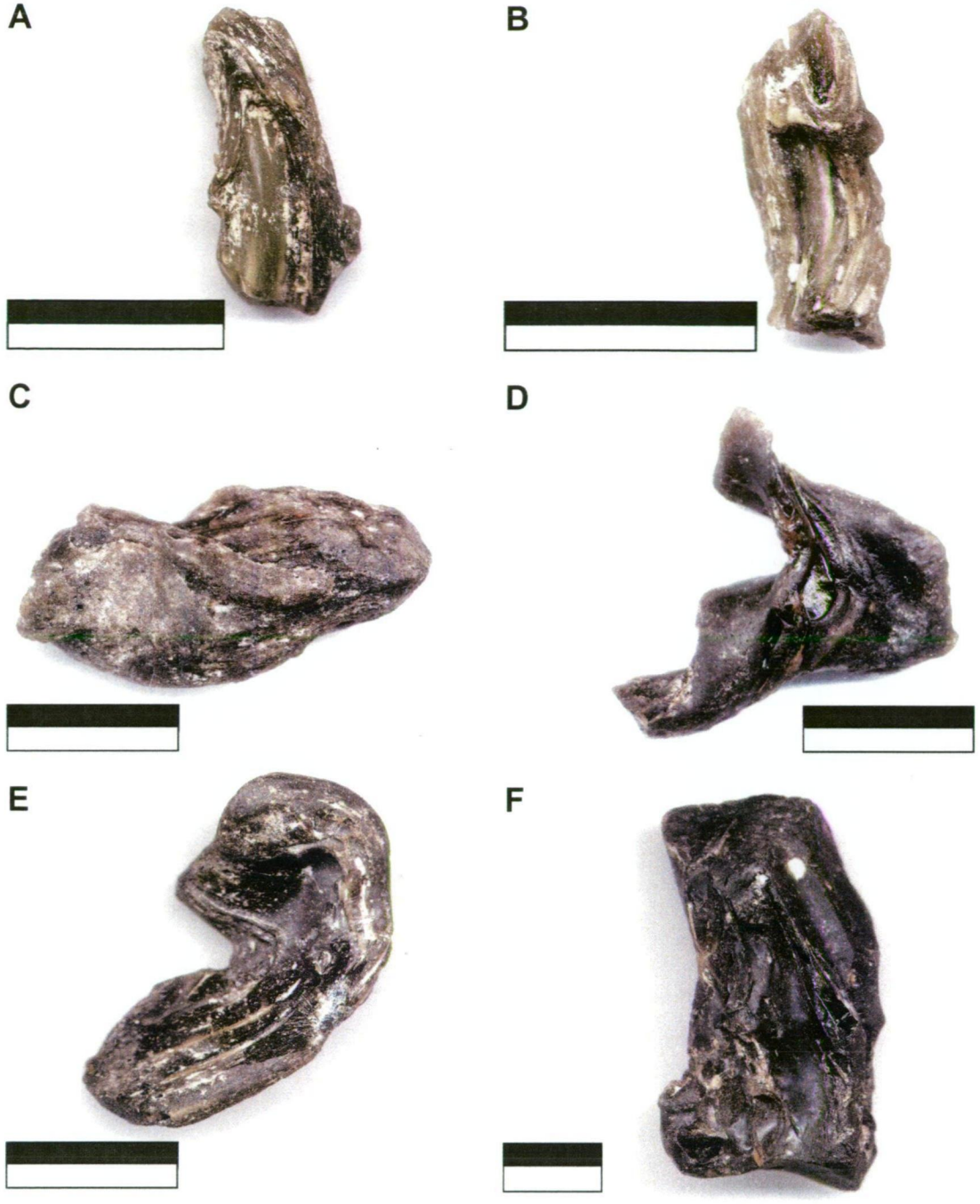

Figure 2.6 Ropy Darwin glass. A-F) scale bars = 2cm.
The twisted ropy texture relfects the extreme topographic expression of the the parallel layering characteristic of the irregular glasses. This texture reflects quenching from a rapidly stretching viscous melt.

Figure 2.7 Elongate Darwin glass **A)** scale bar = 1cm; **B)** scale bar = 2cm; **C)** scale bar = 2cm; **D)** scale bar = 1cm; **E)** scale bar = 1cm; **F)** scale bar = 1cm; **G)** scale bar = 2cm. These are usually planar and rod-like but samples with bulbous ends are also found along with very rare and usually poorly developed dumb-bells. Such elongate samples almost always have broken ends.

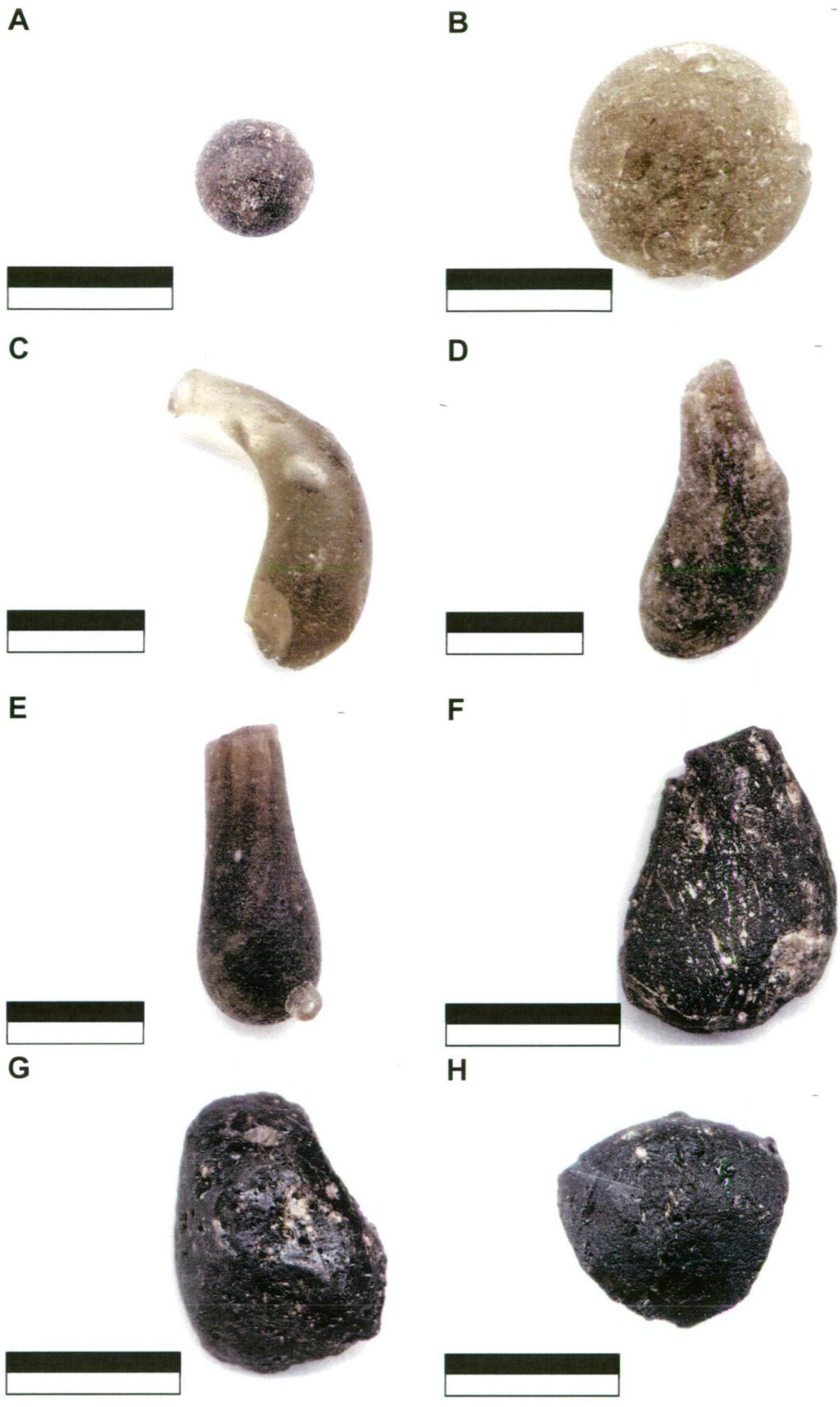

Figure 2.8 Spheroid and droplet shaped Darwin glass A) scale bar = 1cm; **B)** scale bar = 1cm; **C)** scale bar = 0.5cm; **D)** scale bar =0.5cm; **E)** scale bar = 1cm; **F)** scale bar = 2cm; **G)** scale bar = 2cm; **H)** scale bar = 2cm. The spherical glasses appear to have the most highly pitted surfaces of all of the glass shapes (e.g. B). The droplets are almost always aysymetric and typically have broken tails. Examples like F,G and H bear a very strong resemblance to splashform tektites of the Australasian strewn field, particularly Thailandites.

Older fracture surfaces on the glasses reveal very fine stretched layering and this may reflect selective etching and attack of layers of slightly differing compositions. Fracture surfaces showing this selective etching may be interpreted to represent breaks that happened during transport in the atmosphere by impact with other ejected fragments, or as a result of internal forces during contraction and cooling. However, ancient fracture surfaces formed by normal geologic processes may also have undergone selective etching, and care must be excersised in interpreting the origin of fractures in Darwin glass.

2.2.1g Interpretation

Irregular and ropy glasses with parallel flow layering are interpreted to have formed from the most viscous melt that was being stretched and twisted, while rapidly cooling as it was ejected from the crater, probably along with unmelted ejecta. During transport fluid fragments detached from the bulk melt, that was probably a rapidly moving plume, and travelled through the atmosphere as isolated non-rotating fragments before landing fully solidified on the land surface. The most fluid of these fragments continued to change in shape after leaving the bulk melt plume. However, the lack of significant rotation and rapid cooling did not allow significant shape alteration, leading to the most irregular contorted shapes. Generally, irregular and ropy glass shapes are considered typical of proximal impact glass found within 5 crater radii (French 1998), and have a superficial resemblance to some layered tektites that are also considered to be relatively proximal to the source crater (Koeberl 1994).

Relative to the irregular and ropy shapes, the elongate, spheroid and droplet glasses are generally interpreted to have formed from lower viscosity melt. Such elongate, spheroid, and droplet shapes bear superficial resemblance to the splash form tektites that are generally acknowledged to have the form of bodies of revolution and a size controlled by surface tension. To understand the formation of these shapes, empirical models developed to explain the range and distribution of shapes observed in the Australasian tektites (Baker 1958; Ford 1988; see McNamara & Bevan 2001 for a review), and experimental work by Elkins-Tanton et al. (2003), are useful. These shapes are related to the motion of small, very hot, low viscosity molten glass fragments passing through the atmosphere in free transport, rather than in a continuos bulk melt plume. The control on the variation in shape is the degree of rotation or spinning when in transport as a molten fragment (Fig. 2.9). Spheroidal glasses do not spin, or at least do not spin on a preferred axis. As the

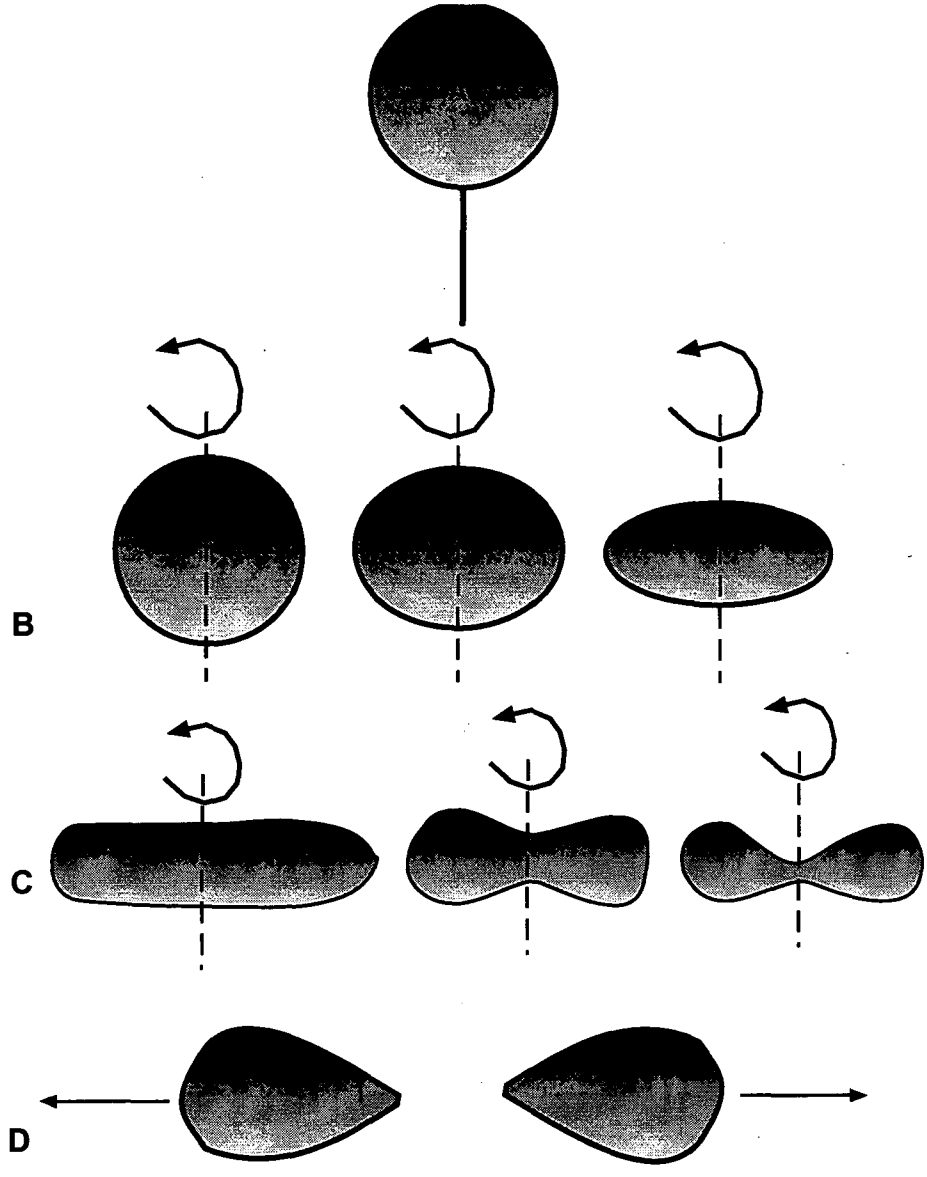

Figure 2.9 Development of splashform shapes. **A)** Spheres are formed from non-rotating blobs. **B)** Lobate spheroids to flattened discs are formed by melt blobs undergoing slow to moderate rates of rotation. **C)** Elongate rods and dumb-bells are formed progressively under rapid rates of rotation as the axial region pinchesout. **D)** Droplets are formed from separation of the most rapidly rotating dumb-bells (after Baker 1959). Dumb-bells are very rare relative to droplets and it is suggested that they also form by the separation of rapidly stretching, low-viscosity melt fragments. In this model, an elongate form separates from the fragment and surface tensions act equally in an attempt to create a sphere. However, the elongate neck has cooled more rapidly than the main droplet and hence is more viscous, this retards the effect of surface tension, and allows a relic of the neck to be preserved thereby producing droplet shaped glass.

small, low viscosity molten fragments fly through the atmosphere those that begin to spin form elliptical shapes that preferentially flatten with increasing rates of rotation. Elongate or rod-shapes are considered to represent ellipsoids that were further elongated during continued rotation. At the most rapid rates of rotation the rods pinch in at the spin axis such that dumb-bell shapes are formed.

In the models of Baker (1958) and Elkins-Tanton et al. (2003) the droplet shapes formed by separation of the most rapidly spinning dumb-bell shapes into two fragments, after which spinning ceased. However, as dumb-bells are very rare relative to the other splashform shapes, particularly when compared to Australasian tektites, the droplet shapes are also interpreted to have formed by the separation of irregular melt masses. In this model, elongate necks are formed by the separation of the rapidly stretching low-viscosity melt fragments. Surface tensions act equally in an attempt to create a sphere, but the elongate neck has cooled more rapidly than the main droplet and hence is more viscous, thus retarding the effect of surface tension and allowing a relic of the neck to be preserved in a droplet shape. This model would seem consistent with the general asymmetric form of the Darwin glass droplets and the small scale of the impact event relative to the Australasian tektite-producing event. It is significant to note that tear-drop shaped Australasian tektites are usually symmetrical as is consistent with formation from separation of a molten dumb-bell shape. In the case of Darwin glass, melt ejection is likely to have been ballistic and splash like, in the presence of an atmosphere, and with continuous deposition of glass from the source crater outwards. In contrast, tektites are likely to be dispersed after removal of the atmosphere in an expanding plume over great distances with increased opportunity for high velocity rotations and progressive formation of dumb-bell shapes by elongation of spheres, and symmetrical tear-drops by separation of the dumb-bells.

The range of shapes is similar to that observed in tektites from the Australasian field, except for the absence of flanged button shapes, which reflects the fact that in the Darwin impact material was not ejected above the atmosphere and did not undergo ablation on re-entry. Unlike is obvious in some Australasian tektites, all Darwin glasses are considered to have cooled sufficiently to prevent plastic deformation on impacting the ground surface. The broad similarity in the range of glass shapes described from the Darwin glass strewn field and Australasian tektite strewn field was noted by Ford (1988) and will be discussed in detail later when the

range of observed glass shapes are discussed in terms of their position relative to the suspected source, Darwin Crater

2.3 Shape distribution in Darwin glasses

All studied glass specimens were placed into one of the 5 recognised shape classes: spheroid; droplet; elongate; ropy; and irregular. The frequency of samples belonging to each class was tabulated and expressed as a percentage of the total sample at each collection site (table 2.1). These data are expressed as histograms in Fig. 2.10A-O. The ranges in the proportion of samples in each shape class at different sites are: spheroid (0 – 7.14 %); droplet (0 – 28.19 %); elongate (0 - 11.11 %); ropy (0 – 32.05 %); and irregular (54.51 – 100 %). These site data are combined to determine the shape distribution in the entire population (Fig. 2.11). Based on 4223 specimens, the Darwin glass strewn field consists of: 0.47% spheroid; 6.01% droplet; 0.68% elongate; 24.74% ropy; and 68.07% irregular shaped fragments of glass.

2.4 Darwin glass colour classes

Four colour classes have been recognised to encompass the range of variation observed in Darwin glass. These colour classes are

- White
- Light green
- Dark green and
- Black

Representative samples of each colour class are shown in Fig. 2.12. The classification is subjective because the colour variation observed is a true continuum and the defined cut off between classes is arbitrary. However, in all cases care was taken to not allow specimen size/thickness to influence the perceived colour, so light green glass is not simply thin flakes of more massive dark green samples. The colour classes are later explained geochemically, but here the purpose of classification is to allow statistical analysis of the entire sample in order to allow for later investigations as to any potential trends in the colour distribution of recovered glasses relative to the suspected crater.

Site		Spheroid		Droplet		Elongate		Ropy		Irregular	
	n =	f	%	f	%	f	%	f	%	f	%
201	17			1	5.9					16	94.1
202	85	1	1.2	3	3.5			9	10.6	72	84.7
203	3126	4	0.1	125	4.0	13	0.4	858	27.4	2126	68.0
204	365	0	0.0	4	1.1	1	0.3	117	32.1	243	66.6
205	3									3	100.0
206	13			2	14.3			1	7.1	10	71.4
207	266	8	3.0	75	28.2	9	3.4	29	10.9	145	54.5
301	80	2	2.5	11	13.8	3	3.8	12	15.0	52	65.0
302	9					1	11.1			8	88.9
303	14	1	7.1	1	7.1			1	7.1	11	78.6
304	33	0	0.0	7	21.2			4	12.1	22	66.7
305	15									15	100.0
306	145	1	0.7	21	14.5	1	0.7	10	6.9	112	77.2
307	10							1	10.0	9	90.0
308	42	3	7.1	4	9.5	1	2.4	3	7.1	31	73.8
All sites	4223	20	0.5	254	6.0	29	0.7	809	19.2	3111	73.7

Table 2.1 Shape distribution in Darwin glass. These fragments were recovered *in situ* from across the strewn field.

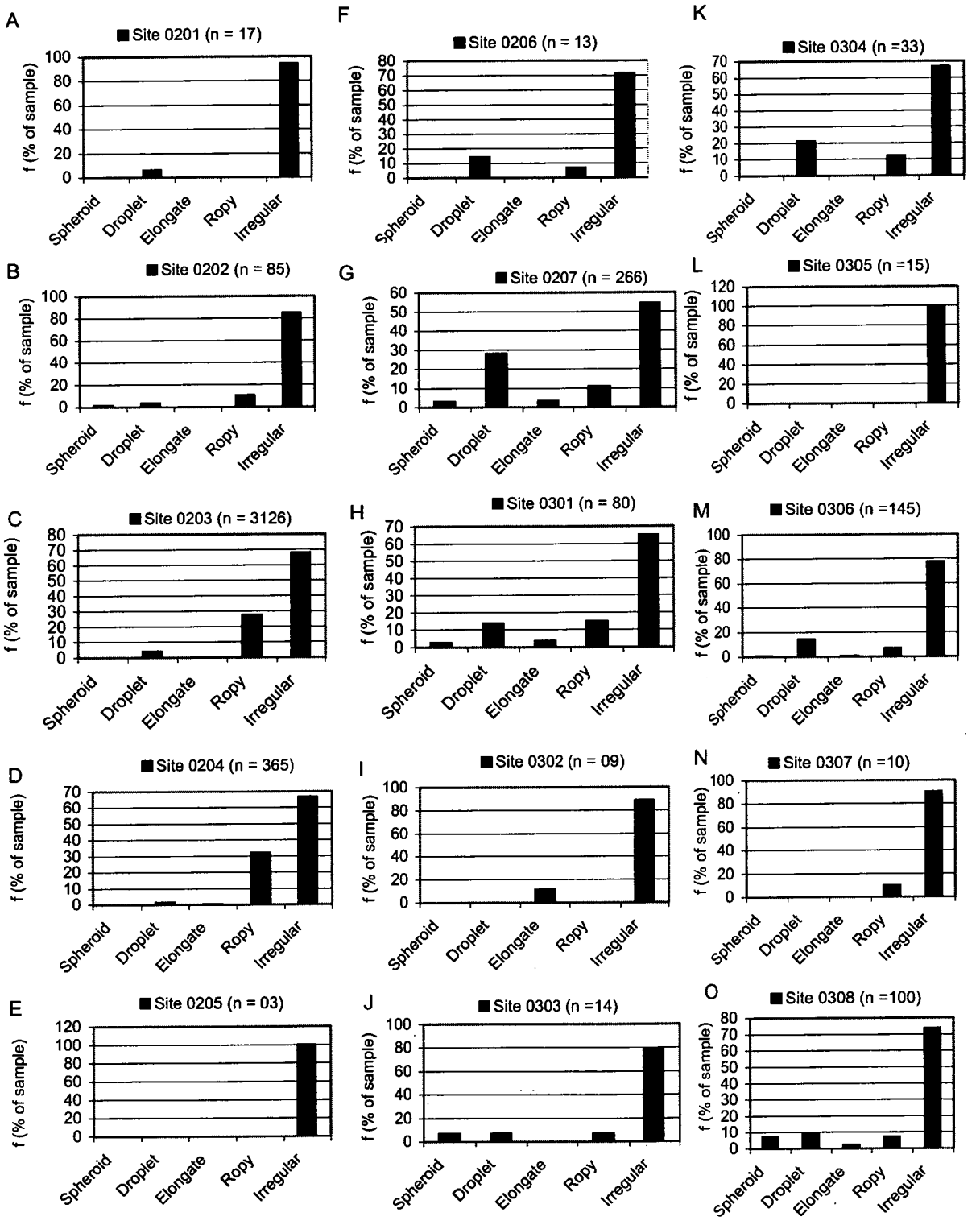

Figure 2.10A-O Shape distribution in *in situ* recovered glass from sites across the strewn field.

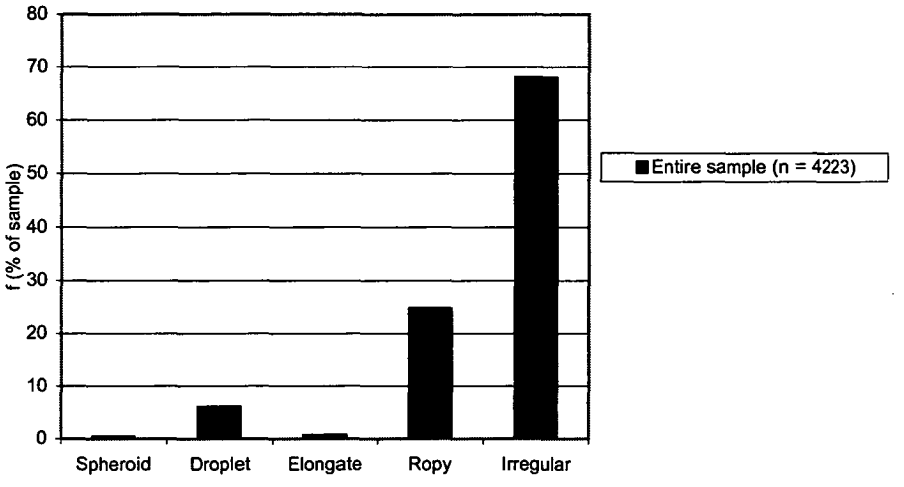

Figure 2.11 Shape distribution across entire sample (all sites combined).

Figure 2.12 Colour variation in Darwin glass A) typical white glass (scale bar = 1cm); **B)** typical light green glass (scale bar = 2cm); **C)** typical dark green glass (scale bar = 2cm); **D)** typical black glass (scale bar = 2cm).

2.5 Colour distribution in Darwin glass

Darwin glass samples were assigned to one of the 4 colour groupings: white; light green; dark green; and black. For each site, the frequency of specimens falling into each class was tabulated and calculated as a percentage the total sample (table 2.2). These data are expressed as histograms in Fig. 2.13A-O. The ranges in the proportions of each colour class across all sites are: white (0 – 7.94 %); light green (0 – 41.17 %); dark green (13.33 – 66.66 %); and black (0- 86.66 %). Data for individual sites are combined to describe the average colour distribution within the entire glass sample (table 2.2, Fig. 2.14). Based on 4223 specimens, the Darwin glass strewn field consists of: 4.78% white, 31.33% light green, 52.66% dark green, and 11.1% black glass fragments.

2.6 Colour vs. Shape distribution in Darwin glass

A matrix combining observations of both the colour and shape at 15 sites was created. The percentage of each colour class represented in each shape class was calculated. These data have been tabulated (table 2.3) and a histogram (Fig. 2.15) created to compare the colour distribution in each of the respective shape classes. These data show that for all colours of Darwin glass an irregular morphology is most common. The proportions of light green, dark green and black glass with irregular morphologies is relatively consistent and varies between 67.48% (black) and 72.26% (light green). However, white glass is almost exclusively (94.44%) irregular in shape. Ropy morphologies are most common in the dark green (27.92%) and light green (23.37%) glasses. Spheroid, droplet and elongate shapes comprise only 7.28% of the total sample, however, 44.24% of the recovered black glasses have either spheroid (2.68%), droplet (20.78%) or elongate (3.17%) shapes. In contrast, 3.7% of light green glasses and 3.07% of dark green glasses have droplet shapes. Elongate shapes are confined to 0.62% of dark green and 0.21% of light green glasses. Spheroid shapes comprise less than 0.5% of light green and dark green glasses. Spheroid, droplet and elongate shapes each comprise 1.1% of white glasses but this percentage represents only 1 single observation of each shape. Similarly ropy shapes were observed in only 2 samples of white glass or 2.2% of the class.

	n =	White		Light green		Dark green		Black	
		f	%	f	%	f	%	f	%
Site 0201	17	0	0.0	7	41.2	9	52.9	1	5.9
Site 0202	85	0	0.0	28	32.9	48	56.5	9	10.6
Site 0203	3126	164	5.2	1121	35.9	1702	54.4	139	4.4
Site 0204	365	29	7.9	112	30.7	191	52.3	33	9.0
Site 0205	3	0	0.0	1	33.3	2	66.7	0	0.0
Site 0206	13	0	0.0	5	38.5	6	46.2	2	15.4
Site 0207	266	6	2.3	32	12.0	134	50.4	94	35.3
Site 0301	80	2	2.5	10	12.5	47	58.8	21	26.3
Site 0302	9	0	0.0	0	0.0	6	66.7	3	33.3
Site 0303	14	0	0.0	0	0.0	2	14.3	12	85.7
Site 0304	33	1	3.0	2	6.1	9	27.3	21	63.6
Site 0305	15	0	0.0	0	0.0	2	13.3	13	86.7
Site 0306	145	0	0.0	1	0.7	42	29.0	102	70.3
Site 0307	10	0	0.0	0	0.0	1	10.0	9	90.0
Site 0308	42	0	0.0	9	21.4	23	54.8	10	23.8
All sites	4223	202	4.8	1328	31.4	2224	52.7	469	11.1

Table 2.2 Colour distribution in Darwin glass. These fragments were recovered *in situ* from across the strewn field.

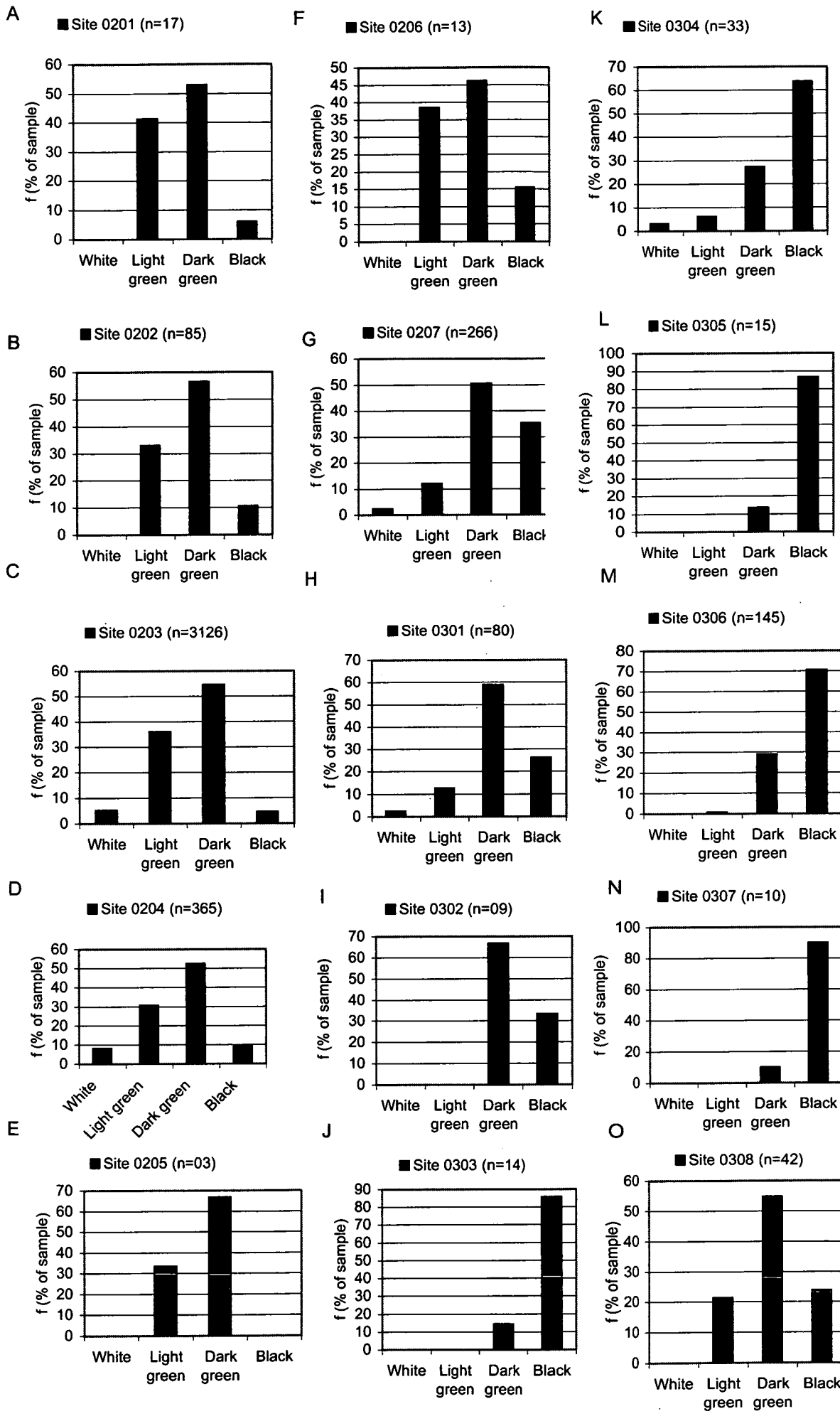

Figure 2.13A-O Colour distribution in *in situ* recovered glass from sites across the strewn field.

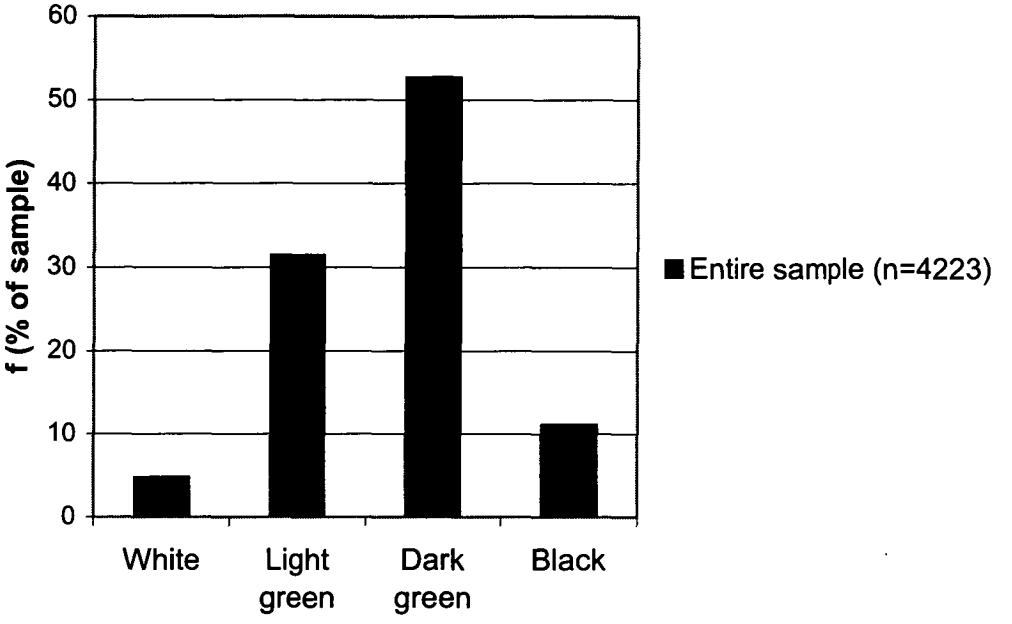

Figure 2.14 Colour distribution across entire sample (all sites combined).

Colour vs. shape (frequency of observations)

	Spheroid	Droplet	Elongate	Ropy	Irregular	Sum
White	1	1	1	2	85	90
Light green	4	35	2	220	680	941
Dark green	3	44	9	399	974	1429
Black	11	85	13	24	276	409
Sum	19	165	25	645	2015	2869

Colour vs. shape (% of total class)

	Spheroid	Droplet	Elongate	Ropy	Irregular
White	1.1	1.1	1.1	2.2	94.4
Light green	0.4	3.7	0.2	23.4	72.3
Dark green	0.2	3.1	0.6	27.9	68.2
Black	2.7	20.8	3.2	5.9	67.5

Table 2.3 Colour vs. Shape in Darwin glass.

Irregular shapes are dominant. Droplet shapes are preferentially black in colour.

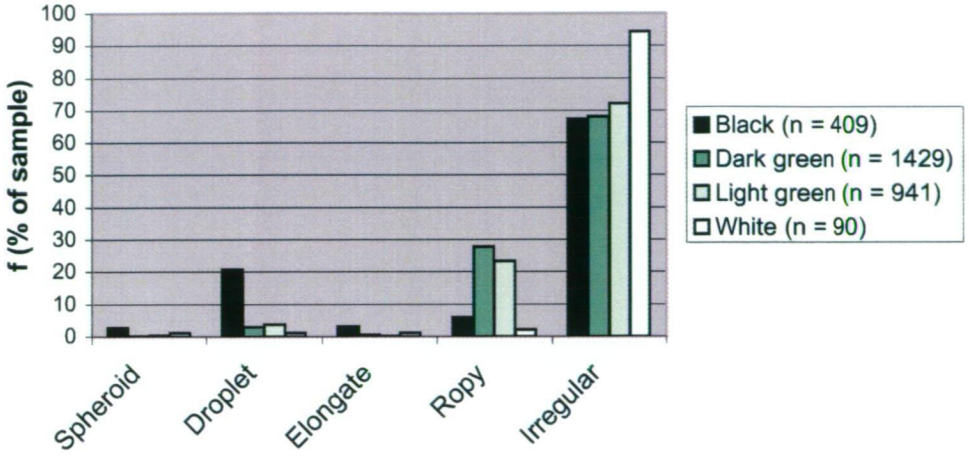

Figure 2.15 Colour vs. Shape in entire glass sample. Dark and light green irregular shapes dominate finds. White shapes are almost exclusively irregular in form. Droplet and spheroid shapes are preferentially black in colour.

2.7 Size distribution in Darwin glass

The largest piece of Darwin glass discovered measures 15 * 8 * 5 cm (Fig. 2.4G-I) and the remainder weighs 946g after one edge was removed for sectioning, the weight of the removed portion is unknown and missing. R.J. Ford collected the sample between sites 0203 and 0204 as a dozer cut the access track to Darwin crater. This sample is many times larger than all recovered glass fragments in this study. There are anecdotal reports of similarly large finds by fossickers, but these have not been confirmed, and as it is prohibited to collect or possess the glass from inside the World Heritage Area without a permit, many finds are kept secret. The sample collected by Ford is dark green to black in colour. One surface of the glass is a young break perhaps from the dozer. The remaining uncut faces are vesicular and of identical lustre to the bulk of the glass suggesting that these faces are primary breaks probably formed while the glass was hot. These faces show fine flow layering, which parallels the concaved base of the sample. At one edge of the concaved face a ropy texture is observed. The upper surface of the specimen shows pervasive radial fractures that diverge from a common point. These radial fractures are interpreted as cooling joints that formed on top of the glass when it was on the ground surface. The apical point at which the radial fractures would converge is not found on this glass fragment and this suggests the fragment was considerably larger and was broken after cooling along the surface that has now had several centimetres cut off it. On this cut surface the flow layering is very pronounced and the surface is densely covered in spherical and elongate vesicles up to 10mm across that display vitreous interior surfaces. The smallest recovered Darwin glass specimens are spheres of less than 1mm diameter and these are found throughout the strewn field after surface material has been finely sieved and searched under binocular microscope.

At 10 sites across the strewn field uncontrolled excavations were conducted with the aim of collecting all visible glass fragments, thus providing representative samples from which the average size distribution in Darwin glass could be estimated. The size was determined by weighing each individual glass fragment. Variations in SG between samples will occur, but were not considered significant enough to make weight an inappropriate proxy of glass size. Weight data for each site are presented in table 2.4. These data were placed in 0.5g bins and are displayed as histograms showing frequency and cumulative frequency (%) of glass fragments falling within

each bin at each site (Fig. 2.16A-K). In these histograms the log of the weight classes is used for ease of presentation.

These data are log – normally distributed and skewed towards outlying heavy glass fragments at all sites except 0305. However, no fragments as large as Ford's almost 1kg sample were found. Excluding the tiny (<1mm) spheres, the range in weights for the recovered glasses from all sites is 0.03 – 26.08 g (table 2.4). The mean recovered glass weights range from 0.56 to 3.2 g. The median recovered glass weight ranges from 0.192 to 2.48 g. The mode in recovered glass weights from all sites ranges from 0.25 to 2.75 g. Data from all sites are combined to illustrate the size distribution across the entire sample (Fig. 2.17). Based on 799 specimens the average fragment of Darwin glass weighs 1.41 g. The median weight of Darwin glass fragments is 0.8 g and the mode 0.25g.

2.8 Field observations of Darwin glass distribution

Since its first discovery in 'soils' near Mt Darwin the glass has been reported across an area of about 400km^2 by Ford (1972). Across much of this area the glass distribution appears to be patchy and remains poorly defined. Historically the glass has consistently been found along the abandoned railway route between the former town of Crotty and the slopes below the South Darwin Peak (Fig. 2.1). This study encompassed this narrow belt and extended outwards to focus in most detail on the region extending south from Darwin Dam to Mt McCall and East from Mt Darwin to the Engineer Range

2.8.1 Stratigraphy of Darwin glass deposits

As most previous studied samples of Darwin glass were collected during road construction, and later from road base, the stratigraphy of the glass occurrence was poorly defined. Early visitors to the Ten-Mile Hill type locality for Darwin glass noted its association with a gravel horizon dominated by angular quartz fragments. Within the currently defined limits of the strewn field gravels exist on top of a wide variety of rocks including PreCambrian metaquartzites, Cambrian volcanics (Mt Read Volcanics), Cambrian to Ordovician terrestrial and marine sediments (Denison Group), Ordovician carbonates (Gordon Group), and Silurian shallow marine sediments (Eldon Group) (Fig. 2.18).

Site	Average weight (g)	% weight <2 g	Max. weight (g)
0204	0.98	96	18.9
0203	1.03	91.08	29.8
0207	1.59	75	9.99
0301	2.15	71.6	26.08
0302	3.26	55.5	8.07
0303	0.56	93.3	4.5
0304	1.31	85.29	7.17
0305	1.58	66	2.87
0306	2.25	68.75	20.96
0307	2.09	60	5.97
0308	0.78	95	4.07
All sites	1.6	78.0	12.6

Table 2.4 Size data for recovered glass fragments (n=1063). The SG of the glass does vary but not significantly enough to prevent fragment weight being used as a proxy for fragment size.

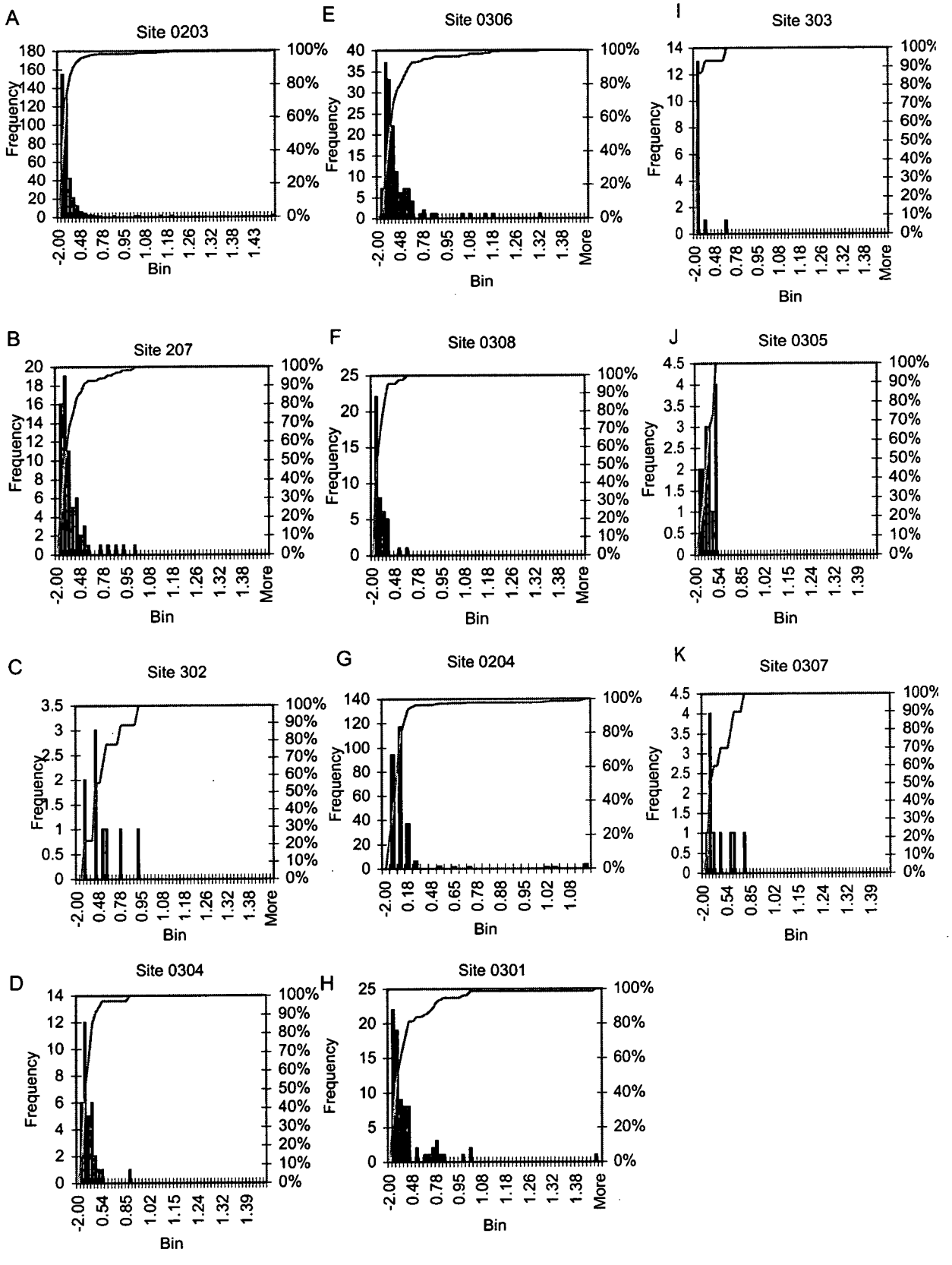

Figure 2.16A-K Size distribution in recovered glass fragments.
The x axis is the log of recovered glass weights (g) placed into 0.5g bins.

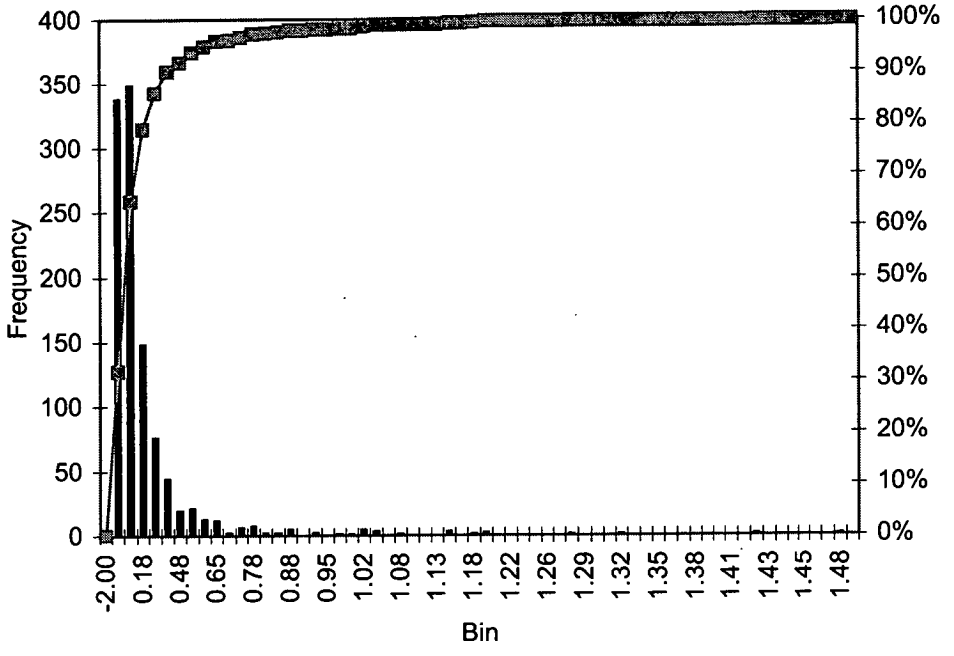

Figure 2.17 Size distribution across entire glass sample (n=1063).
The x axis is the log of recovered glass weights (g) placed into 0.5g bins.
The sample is always skewed towards outlying large fragments.
None of the specimens recovered in controlled excavations in this study are even close in size to the almost 1kg fragment that R.J. Ford found along the access track to the crater.

These gravels are either the residual products of *in situ* weathering, primary or re-worked glacial deposits, or slope derived talus. As such the nature and stratigraphy of the gravel horizons is expected to be strongly influenced by elevation and topography. In order to explain the stratigraphic setting of Darwin glass the stratigraphy of the glass bearing gravel horizons from a range of topographic settings and altitudes is described below. Discussion will then focus on defining the geographic extent of the glass bearing gravels and the strewn field.

2.8.1a Slopes and flat ground between ~230 – ~500 MASL

On steep and gentle slopes and flat lying ground between approximately 230 and 500 m elevation the glass-bearing quartz gravel lies beneath a layer of soil and peat (Fig. 2.19A,B). Immediately below the peat are the largest quartz fragments and glass in a matrix of fine quartz sand that extends to the contact of the highly weathered bedrock. Glass is rare in the fine sand below the larger quartz fragments. The peat layer varies in thickness but is typically around 20 cm thick and free of glass fragments. Below the peat the thickness of the glass bearing gravel horizon ranges from a few centimetres to several metres. On low and mid slopes the gravel horizon is consistently around 30 cm thick. The thickest gravel horizons tend to be on gently sloping and flat lying ground at lower altitudes.

2.8.1b Hilltops and mountaintops > 500 MASL

Peat is absent on hills and on mountain summits in the strewn field and the gravel horizon is also either absent, or confined to isolated free quartz fragments and rare Darwin glass sitting directly on weathered bedrock (Fig. 2.19C). Previous workers assumed that early Holocene ice accumulation and transport had removed Darwin glass from slopes above 500 m

2.8.1c Valley floors < 220 MASL

On valley floors in the strewn field the gravel horizon and Darwin glass are not exposed because of burial under peat and valley filling sediments, or have been incorporated in extensive deposits of re-worked glacial moraine. Fragments of glass have been found sitting atop of valley fill sediments on the crater floor and these have presumable been moved down slope from the surrounding hills.

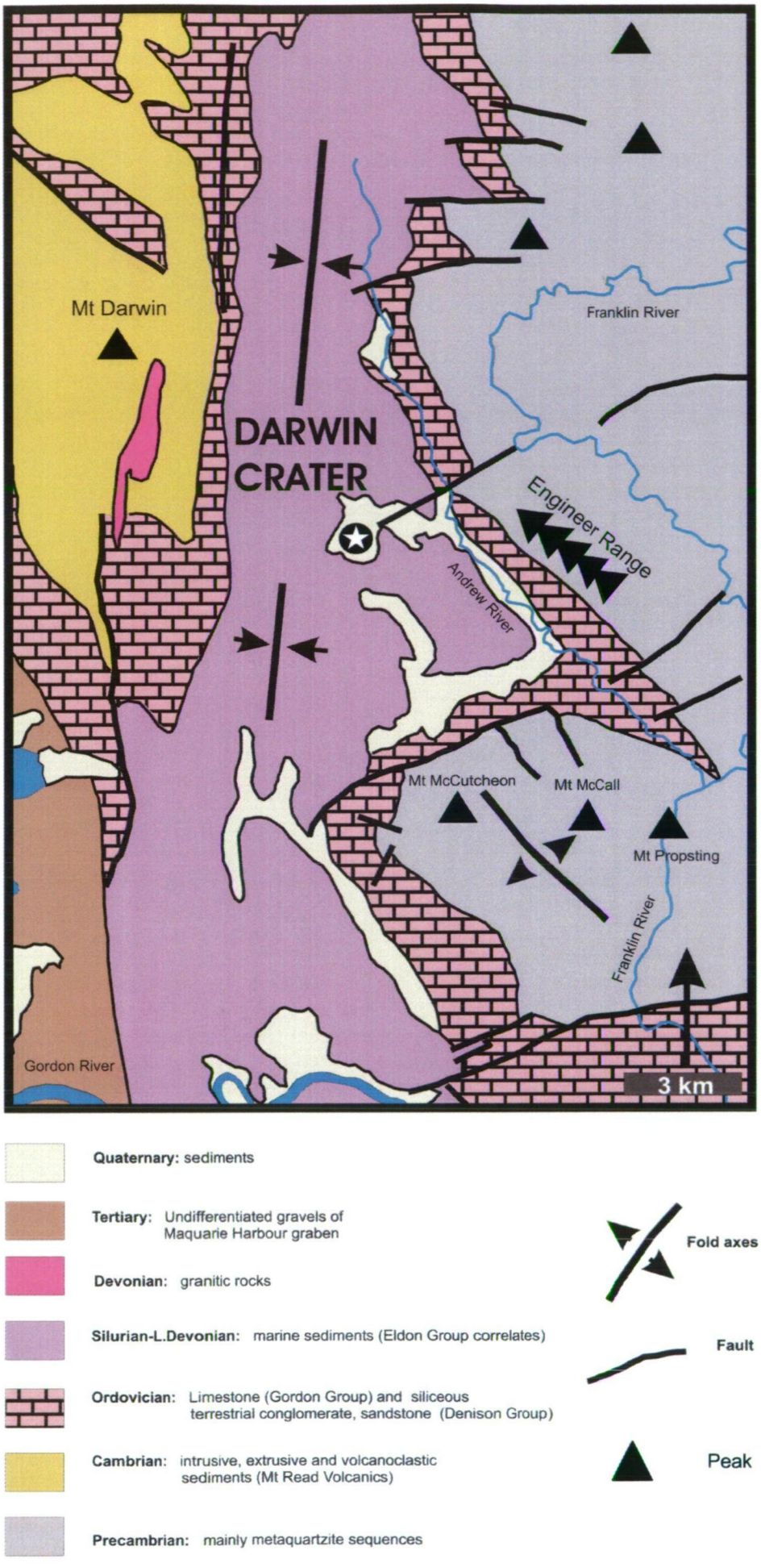

Figure 2.18 Geology of the Darwin glass strewn field.

Based on Corbett & Brown (1975) and Corbett et al. (1993).

Figure 2.19 Field photographs.

A) Exposed residual gravel deposit after peat cover has been removed. Note peat and organic matter at edges of photograph. Hammer is 30cm long. **B)** Close-up of residual gravel deposit in A. Hand lens is 3cm in diameter. **C)** On mountain peaks, the peat and most gravel has been removed by ice action and glass is scarce. Shrubs are approximately 50cm in height.

2.8.1d Interpretation

The angular and blocky nature of quartz fragments in the gravel indicates a local provenance. Quartz veins pervade country rocks across the strewn field and cropping out veins are actively weathering to release free quartz fragments. This suggests that these gravels are residual deposits produced by *in situ* weathering. Transport of the quartz fragments, especially on flat areas, is likely to have largely been vertical and hence the thickest gravel deposits are found on flat ground. Winnowing of fine material and down slope transport has been confined to the hilltops where ice has removed peat and quartz fragments. The process has not been completely efficient because fine fragments of glass (and quartz) are still found on hilltops. On mid and low slopes winnowing is likely to have been very limited given the abundance of small glass fragments. Glass found above the valley fill deposits at site 0305 has been transported down slope from mountain tops or mid slopes after a disturbance such as a landslide removed the peat cover and released the glass fragments for transport.

The fine surface features observed on glass fragments recovered from the residual quartz deposits suggest that the glasses have not been significantly transported laterally by high-energy processes such as floods. An experiment was conducted to simulate the transport of glass fragments as traction load in a fluvial setting. Glass fragments showing fine surface features were placed in a loosely packed drum with hydraulically equivalent quartz pebbles and water for tumbling at low speed. Over the eight-hour duration of tumbling the glass fragments were examined and photographed after 1; 2; 4; 6; and 8 hours. These observations are recorded in table 2.5 and the tumbled fragments are shown before and after 8 hours of simulated transport in Fig. 2.20.

The observed changes in appearance of Darwin glass fragments under crudely simulated conditions of fluvial transport are interpreted to strongly support the suggestion that the glass fragments recovered from the quartz gravels, many of which show fine surface decorations, have not been significantly transported since formation. Based on the topographic settings of the deposits, the size and angularity of quartz fragments and the well preserved fine surface features on Darwin glass fragments, the glass bearing quartz gravels are therefore interpreted to be residual deposits.

Sample	DG1	DG2	DG3
time		**Observation**	
1 hour	Lustre dulled	Lustre dulled	Lustre dulled
2 hours	Surface etching smoothed	Pointy edges eroded	Ropy texture smoothed
4 hours	Ridges defined by layering smoothed	Lighter coloured bands are selectively removed from the bulk fragment	"
6 hours	Bridge joining tails of droplet broken	"	"
8 hours	Adhering droplet detached from fragment	Y (a) axis snapped	Tip of X axis snapped

Table 2.5 Observed changes in glass fragments during simulated fluvial transport. Note that the lustre and delicate surface features of samples are rapidly degraded.

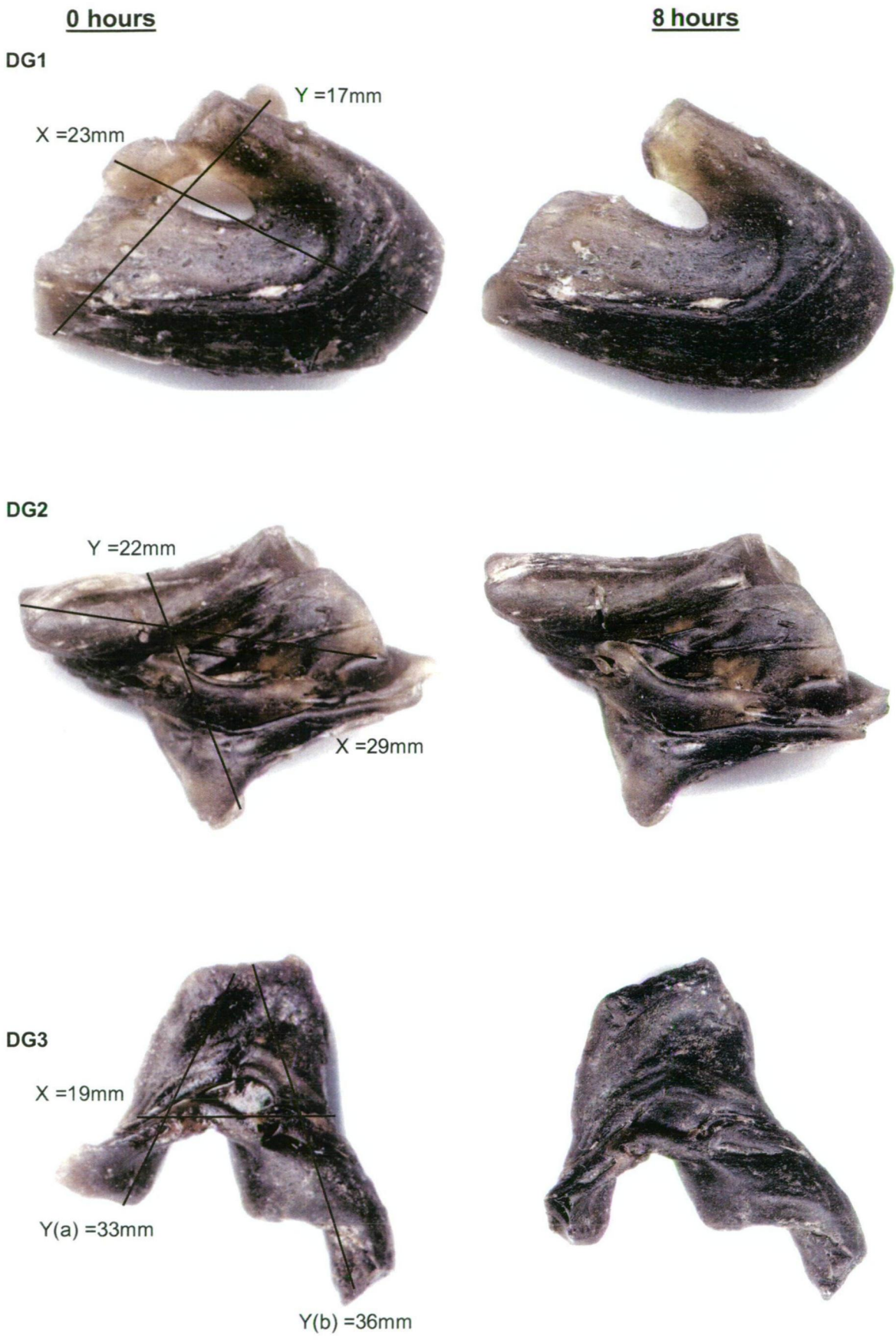

Figure 2.20 Glass abrasion by simulated fluvial transport. Here the glasses are pictured before and after 8 hours tumbling with quartzite gravels. Delicate surface features have been abraded or damaged and progressive observations are described in table 2.5.

2.9 The geography of Darwin glass deposits

Figure 2.21 shows all sites where *in situ* Darwin glass has been found. The map is a composite of sites discovered and/or studied here and those reported in previous works. Verified anecdotal reports of glass finds are also included. In the following description of the distribution of Darwin glass, attention is focused on delineating the outer limits of glass occurrences in all directions to define the size and shape of the strewn field.

2.9.1 Southern extent of glass distribution

This is the first study to report glass from the southern reaches of the McCall Track near Mts McCutcheon and McCall. At around 700m, sites on the Mt McCall plateau are the highest elevations at which Darwin glass has been found. At these locations the gravel residual is thin and sitting directly on weathered Precambrian metaquartzites. To the southeast of site 0303, some glass was found in transported road base but none was found in residual gravel deposits despite several excellent exposures of the horizon.

2.9.2 Western extent of glass distribution

Darwin glass has been found approximately as far west as 145°25' E at location 10135 west of Mt Strahan and south of the King River (145° 25'E, 42 13S). Here the glass is found in residual gravels atop Silurian sedimentary rocks of the Eldon Group. A previously reported find over 10km further west at Liberty Point on the shores of Macquarie Harbour and catalogued in the University of Tasmania collection has been discounted after examination of the specimens revealed that they are fragments of chert. A subsequent visit to the site in 2001 failed to find any glass fragments. West-northwest of location 10135, residual gravels overlying the Eldon Group, accessible from the Lyell Highway, were searched without the recovery of any glass fragments. At sites 10134 and 10131, east – southeast of 10135, glass is found in gravels overlying Cambrian turbidite sequences (Dundas Group). No glass has been found over heavily incised Tertiary terrace and Quaternary alluvial deposits that blanket the Cambrian sequences and extend to the shores of Macquarie Harbour. Quaternary dune fields blanket the coast west of Macquarie Harbour and along much of the West Coast. No *in situ* glass has been recovered in the dune deposits, however fragments of glass worked by Tasmanian

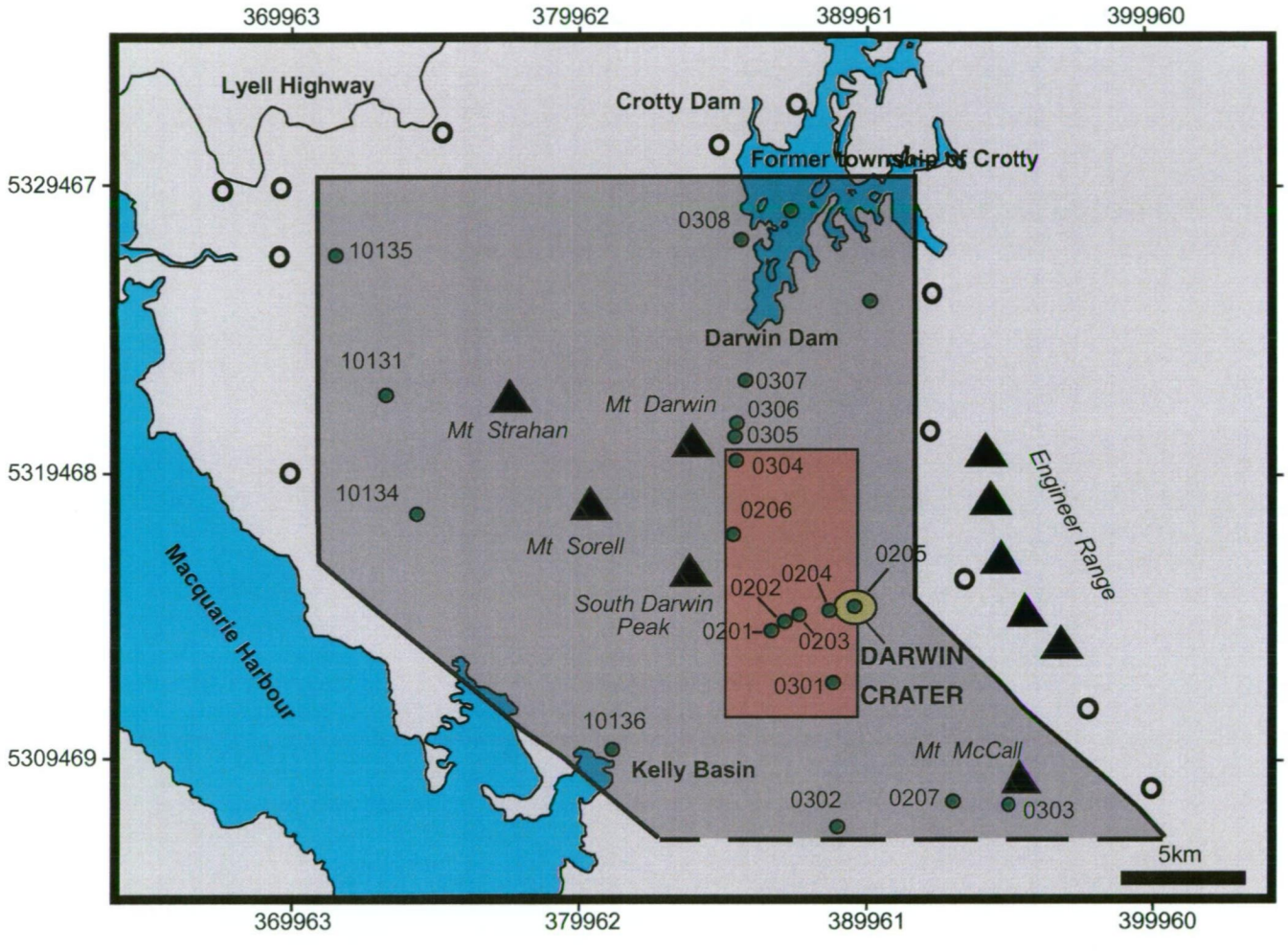

Figure 2.21 The Darwin glass strewn field. Closed green circles are significant glass collection sites referred to in text. The magenta shaded area is where controlled excavations aimed at estimating the abundance of glass were conducted. Open circles are sites where residual gravels have been searched and found to be free of glass and these define the outer limits of the known strewn field as indicated by the black line. The southern boundary of the field is poorly defined (dashed black line). Solid black triangles are major mountain peaks in the strewn field. Darwin Crater lies at the eastern limit of the strewn field, but this apparent asymmetry in glass distribution is considered to be an artefact of preservation.

Aborigines have been found in middens in dunes at several locations along the coast (McNiven 1994).

2.9.3 Northern extent of glass distribution

Darwin glass is found as far north as 42° 10'S in gravel below peat and exposed on the surface of rounded hilltops. Below the peaks of Mt Jukes on the shores of Lake Burbury abundant quartz talus deposits rich in quartz, quartzite and sandstone clasts are actively forming from the erosion of the Owen Conglomerate. No residual deposits are observed but rare pieces of Darwin glass are found in this talus around the shores of the lake. No glass has been found north of site 0308.

2.9.4 Eastern extent

Darwin glass has not been found east of 145° 44'E. No glass has been found on the mountains of the Engineer Range. The Engineer Range forms a sharp divide between the Andrew River on the west and the Franklin River on the east. No glass has been found in gravel deposits along the Franklin River or in gravels from the Andrew River that were searched during an 11-day rafting expedition down the Collingwood-Franklin-Gordon rivers in December 2001. Worked pieces of Darwin glass – sculpted by Tasmanian Aborigines – have been found in caves on the Franklin and Andrew Rivers (McNiven 1994).

2.9.5 Interpretation

The southern limit of the strewn field is defined by the transition from glass-bearing to barren residual quartz deposits. However, this boundary is poorly defined because at some of the southern most sites, such as 0302, glass remains quite common, and it is possible that the glass remains patchily distributed considerably further to the south but access is restricted to the McCall track. The exact limits of the strewn fields' western extent are difficult to define because of the low glass abundance at, and difficulty of access to, sites west of Mts Strahan and Darwin. It seems likely that the northwestern boundary of the strewn field lies somewhere between site 10135 and the Lyell highway, because the limited sites with residual deposits that were accessible and searched along the highway were found to be free of glass. Any glass deposited west–southwest of site 10135 on Tertiary or Quaternary deposits is likely to have been transported and deposited amongst gravels, or into Macquarie Harbour. Such gravel deposits coincide with the apparent western edge to the strewn field parallel to the shores of Macquarie Harbour. The

northern limit of the strewn field is also difficult to define because of the absence of easily identifiable residual gravel deposits on slopes above and around Lake Burbury north of site 0308. Glass at site 0308 is generally small in size and no glass has been found north of this site despite ease of access and heavy historical exploration. It seems likely that site 0308 is close to the northern limits of the strewn field. The eastern limits of the strewn field are controlled by the topography of the region, but accurate definition is affected by poor access. Any glass originally deposited along the Engineer Range has subsequently been re-deposited in valley fill or transported away by floodwaters of the Andrew and Franklin Rivers. Based only on sites with *in situ* glass finds the strewn field has a trapezoidal shape with an area of approximately 410km^2 (Fig. 2.21). This is considered to be a minimum figure for the real strewn field because of difficulties in defining the southern boundary.

2.10 The abundance of Darwin glass

At 9 sites within a 10*5 km area surrounding the suspected crater (Fig. 2.21) controlled excavations (described earlier in section 2.11) were conducted in order to estimate the abundance of glass present. At each site 0.03 m^3 (10 standard prospectors' pans) of glass bearing gravel was sieved through 1 and 0.5 cm mesh sieves. All visible glass was recovered from the sieves and a ground sheet placed below sieving operations searched for fine glass fragments. Recovered glass fragments were weighed and results normalised to kg/m^3. The determined glass abundance ranges from 0.17 to 47 kg/m^3 across the study area (table 2.6). The maximum value is reached in a thick residual gravel deposit at site 0203, approximately 2 km west of the suspected source crater. At the remaining sites measured abundances are more consistent and there is a general trend of decreasing glass abundance away from the crater. Outside of the 50 km^2 study area the abundance of glass in gravels is too low, or distribution too patchy, or access too poor for glass to be recovered in controlled conditions. At such sites, glass is only recovered by fossicking without consideration of the volume of material or area searched and thus the abundance of glass is difficult to quantify.

Site	Recovered glass weight (g/ 30000cm^3)	g/cm^3	kg/m^3
Site 0201	22.3	0.00074	0.7
Site 0202	104.0	0.00347	3.5
Site 0203	1421.6	0.04739	47.4
Site 0204	506.4	0.01688	16.9
Site 0205	5.2	0.00017	0.2
Site 0206	13.3	0.00044	0.4
Site 0301	44.3	0.00148	1.5
Site 0207	7.7	0.00026	0.3
Site 0304	23.4	0.00078	0.8
Average (all sites)	238.7	0.00796	8.0
Average (no Site 0203)	90.8	0.00303	3.0

Table 2.6 Recovered glass abundances.

Specimens were recovered in archaeological style controlled excavations of a known volume of the host residual quartz gravels. The excavation sites were within a 50km^2 area surrounding the crater. In calculating the glass abundance in this area, the more conservative average abundance (excluding Site 0203) was used.

2.10.1 Melt Volume

By estimating the average thickness of the gravel deposits across the 50 km^2 study area the volume of ejected melt can be approximated. The glass bearing gravel ranges in thickness from several meters to less than 1cm on peaks. After accounting for thin gravel cover on peaks, a conservative estimate of the average thickness of the glass bearing gravel horizon in the study area is taken to be 15 cm. Excluding the most abundant site (47 kg/m^3) the average abundance of glass in the gravel deposits across the survey region is 3 kg/m^3. Therefore, in the 50 km^2 area it can be estimated that there is approximately 22 500 tonnes of glass. Assuming a SG of 2 this represents a melt volume of ~11250 m^3 or ~0.00001 km^3. Errors in estimating the average thickness of the glass-bearing gravel horizon, and the abundance of glass in the horizon, strongly influence melt volume determinations, and it should be noted that the estimates given are considered to be conservative. As the survey area represents only $1/8^{th}$ of the known strewn field area, the true melt volume is assumed to be greater.

2.10.2 Comparison with theoretical expectations and observations of melt volumes at other terrestrial craters

At 1.2 km in diameter, Darwin Crater is at the lower limit of scaling equations that model melt production. Based on the equation of Grieve & Cintala (1992) approximately 0.0012 km^3 of melt can be expected to be produced during excavation of a 1.2 km diameter crater. Of this around 1% - 3% of fully melted material (~0.00001 km^3 or 12000 m^3) is expected to be ejected to within a few crater radii (Grieve & Cintala 1992; French 1998; Orphal et al. 1980). This agrees well with the measured minimum estimate of the volume of glass in the study area (0.00001 km^3). If the remaining >350 km^2 of the known strewn field is considered, modelled estimates of ejected melt volume are significantly too small. For other studied craters, and especially those in sedimentary rocks, modelled melt volumes generally far exceed measured volumes (Grieve & Cintala 1992, Kieffer & Simonds 1980). This indicates that relative to the size of the suspected source crater, this is the most abundant ejected impact glass on Earth! In fact the volume of ejected melt at Darwin Crater is more abundant than has been observed at much larger complex craters. Zhamanshin Crater (13 km diameter) is more than 10 times larger in diameter than Darwin, but here it is estimated by Florensky (1976) and Masaitis et al. (1984) that there is less than 100 tonnes of ejected glass – orders of magnitude less than is observed in the Darwin glass strewn field and importantly both glasses

are of almost the same age. At similar sized simple craters, such as Barringer Crater, far less glass has been found and all of this has come from closer to the crater than at Darwin (Kieffer & Simonds 1980, Osinski et al. 2003a). In small crater fields like at Henbury, glass finds are very rare. This is despite the fact that these craters are situated on easily searched flat desert planes, in strong contrast to the mountainous rainforest of the Darwin glass strewn field. As such, the high abundance of Darwin glass seems unlikely to relate to preservation alone, but rather is interpreted to reflect more greater melt ejection efficiency than expected from modelling. The distribution of the glass to more than 20 crater radii also exceeds modeled expectations and field observations at other impact sites (French 1998). When expressed in terms of crater radii, this range is typical of the distribution of tektites from large impact events, but the bulk of Darwin glass has a morphological and chemical character more commonly associated with proximal impact glasses. The relationship between the glass and the suspected source crater will be further examined later in this study. The possible crater lies in weakly metamorphosed sedimentary rocks, and if confirmed as the source of the glass, these data may support the notion that the potential high volatile content of sedimentary rocks may result in the unusually wide dispersion of melt (Kieffer & Simonds 1980).

2. 11 Conclusion

Darwin glass is a predominantly dark to light green irregular impact glass, most commonly with irregular and contorted shapes. It is characterised by abundant layering that is most common in specimens with a ropy shape. Such an irregular morphological character is typical of proximal impact glasses. Some Darwin glass also bares a superficial resemblance to layered tektites in the Australasian strewn field. The irregular and ropy shapes are interpreted to have detached from a high-viscosity, turbulent stretching and rapidly quenching continuos melt plume. They solidified quickly without significant further transport or rotations while still in a molten state. Some other glass samples have elongate, droplet and spheroid shapes that have a superficial resemblance to splashform tektites. These are interpreted to have formed from less viscous melt as surface tension acted on the surface of a hot molten fragment when in free transport. Shape variations are controlled by the degree of rotation or spinning, and on the preferred axial direction of spin relative to the direction of propagation. The splashform Darwin glasses are preferentially black in colour relative to the irregular shapes.

The glass is found effectively *in situ* within residual gravels in a trapezoidal shaped strewn field covering approximately 410km^2. The suspected source crater is situated at the eastern limit of the field, but this apparent asymmetry is considered to be an artefact of glass preservation. The fact that no glass is found to the east of the suspected crater reflects both access difficulties and the presence of steep slopes along the Engineer Range from which glass has been eroded and transported away by the Franklin and Andrew Rivers. Hence, the observed asymmetry in glass distribution does not reflect primary asymmetry in the ejection of the melt that is distributed to relatively equal distances to the north, south and west of the suspected source crater.

It is conservatively estimated that there is at least 11 250m^3 of glass in the strewn field. This minimum calculation is based only on excavations in the immediate 50km^2 surrounding the crater. Relative to the size of the suspected source crater, Darwin glass the most abundant impact glass on Earth, and is anomalously widely distributed out to up to 20-crater radii from the suspected source. Such a distribution is much more typical of tektites, but the bulk of the glass has a morphological character considered to be typical of proximal impact glasses.

Chapter 3

Darwin glass geochemistry

This chapter describes the major and trace element geochemistry of Darwin glass. To create a framework for later discussion of the origin of Darwin glass the composition of the glass will be compared to a series of other impact glasses and tektites. In the description, attention will focus on identifying end member compositions in the glass geochemistry, and identifying any sub-populations in the glass using multivariate statistical tests. The end-member glasses will be compared to a series of average rock types to provide insights into the expected target rocks involved in the formation of Darwin glass. This will provide a basis for later discussion of the geochemistry of rocks collected from outcrop and drill core at Darwin Crater and their potential relationship to the glass. Regional trends in the glass geochemistry will also be discussed later in evaluation of the relationship between Darwin glass and Darwin Crater.

3.1 Scanning Electron Microprobe (SEM) analyses

Small pieces of Darwin glass were carefully chipped from larger fragments and placed in an ultrasonic bath in distilled water for cleaning. The detached pieces ranged in size from 2 to 10mm in diameter and these were mounted in 25mm diameter epoxy discs. The specimens included material collected during the course of this study, and previously collected and catalogued at the University of Tasmania by R.J. Ford and others. Ten glass fragments were analysed from each of nine widely spaced sites and the remaining 16 fragments that were analysed come from Site 0203 (106 fragments in total, Fig. 3.1). In sample selection, care was taken to ensure consistency in the colours and morphologies of analysed glass fragments between sites. In addition 26 glass fragments, less than 5mm in size and showing

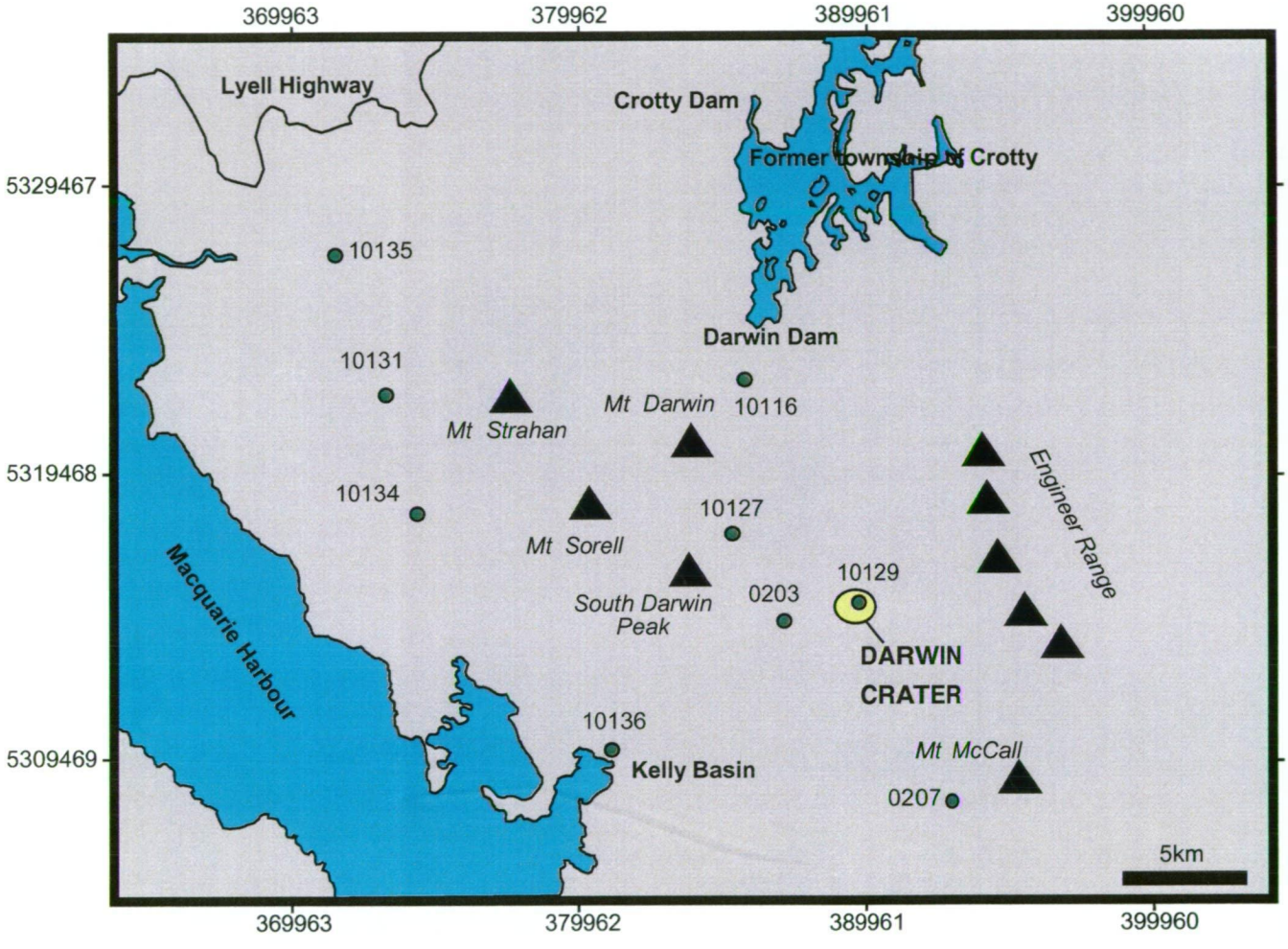

Figure 3.1 Darwin Crater and Darwin glass strewn field. Showing collection sites for the glass specimens chemically analysed in this study (solid green circles). Solid black triangles are major mountain peaks in the strewn field.

splashform (droplet, spheroid and elongate) shapes (see Fig. 2.2D) were collected from across the strewn field and cleaned and mounted intact in 25mm epoxy discs. These 'mini-glass' grains were polished carefully to expose a fresh interior surface for analysis. Discs containing pieces of 5 fragments of white, light green, dark green and black glass pieces from across the strewn field were also prepared.

Major elements were determined using a CAMECA SX50 scanning electron microprobe at the Central Science Laboratory (CSL), University of Tasmania. The regulated electron beam current was operated at 25 nA at an accelerating voltage of 15 kV. A nominal incident beam size of 8μm diameter was used in order to minimise alkali migration and consequent elevation of Si and Al counts. Eight major elements (Si, Al, Fe, Mg, Ti, K, Ca, Na) were analysed using the mineral standards and calibrations provided by Dr D.A. Steele. Detection limits range between 0.05 and 0.1 wt %. Sodium was analysed first to reduce the effect of volatilisation on the analysis.

3.1.1 Major Elements in Darwin Glass

Two different spots were analysed on each of the glass chips from the regional survey sites. Two spots were also analysed on each of the white, light green, dark green and black glass grains. For the <5mm mini-glasses, three spots were analysed on each grain. In each case the beam was positioned manually to ensure that the analysis was taken from a well-polished surface free of irregularities (e.g. vesicles, lechatelierite inclusions, dirt). The ranges in composition for the major elements in the analysed macro Darwin glasses are; SiO_2 (76.5 – 93.9%), Al_2O_3 (3.1 – 11.4%), TiO_2 (0.2 – 0.8%), FeO (0.8 – 5.9%), MgO (0.25 – 4.0%), K_2O (0.7 – 2.7%), CaO (<0.01 – 0.3%), Na_2O (<.01 – 0.2%). For the analysed mini-glasses the ranges in major element composition are; SiO2 (75.24 – 93.18%), Al2O3 (1.98 – 10.68%), TiO_2 (0.13 – 0.7%), FeO (0.74 – 6.8%), MgO (0.19 – 3.67%), K_2O (0.61 – 2.4%), CaO (<0.01 – 0.22%), Na_2O (<.01 – 0.19%). A summary of the mean and range in the major element composition of Darwin glass is presented in table 3.1. Complete analyses are listed in Appendix 1. Macro and mini Darwin glasses have overlapping ranges in major element compositions and very similar average compositions, however relative to average macro Darwin glass, the average mini-glass is slightly enriched in MgO (+ 0.46%) and FeO (+ 0.27%) and depleted in K_2O (- 0.2%) (Fig. 3.2). This variation is insufficient to define the mini-glasses as geochemically distinct from the macro glasses. On the basis of major element geochemistry the mini- and

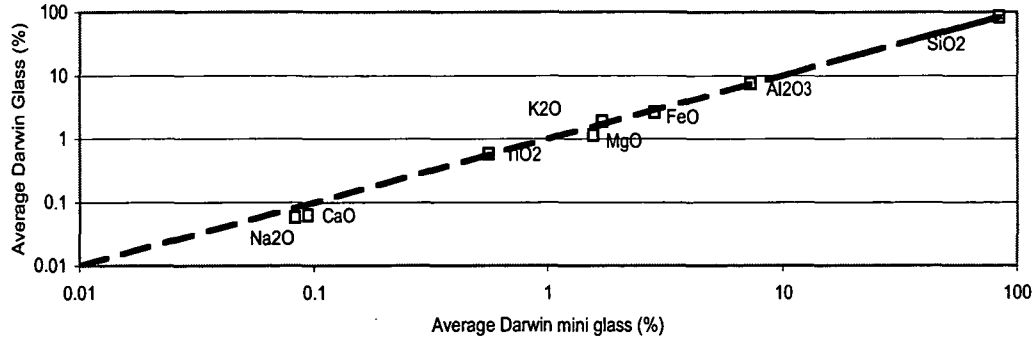

Figure 3.2 Major element composition of macro Darwin glass chips compared to splashform (spheroid, droplet, elongate) shaped mini-glasses (D=<5mm).

	Site	SiO_2	Al_2O3	TiO_2	FeO	MgO	CaO	K_2O	Na_2O	n =
Macro-glasses	10129	82.75 - 93.85	3.14 - 8.46	0.51 - 0.74	0.85 - 3.63	0.24 - 2.05	0.02 - 0.13	1.22 - 2.33	0 - 0.09	20
	10131	79.40 - 92.1	3.83 - 9.84	0.33 - 0.74	1.29 - 4.52	0.25 - 1.93	0.01 - 0.13	1.13 - 2.47	0.03 - 0.21	20
	10115	76.47 - 86.30	6.33 - 10.39	0.49 - 0.76	1.62 - 4.52	0.55 - 2.42	0 - 0.18	1.69 - 2.71	0 - 0.11	20
	10135	83.21 - 89.51	5.8 - 8.4	0.46 - 0.64	0.96 - 2.94	0.55 - 2.36	0.01 - 0.14	1.61 - 2.01	0.02 - 0.12	20
	10134	79.28 - 87.68	6.24 - 11.45	0.49 - 0.8	1.41 - 3.8	0.60 - 2.28	0 - 0.16	1.53 - 2.57	0.01 - 0.14	20
	10127	82.0 - 88.54	5.7 - 9.25	0.42 - 0.72	1.13 - 3.91	0.41 - 1.03	0 - 0.08	1.56 - 2.34	0.01 - 0.17	20
	10136	79.83 - 86.41	6.24 - 9.0	0.50 - 0.70	1.92 - 4.05	0.65 - 3.40	0 - 0.07	1.49 - 2.16	0.02 - 0.18	20
	0203	78.04 - 88.52	6.88 - 10.38	0.52 - 0.68	1.02 - 5.23	0.47 - 2.45	0 - 0.16	1.62 - 2.54	0.03 - 0.11	16
	0207	80.99 - 90.83	4.93 - 9.48	0.36 -0.72	1.01 - 3.74	0.69 - 1.81	0 - 0.12	1.46 - 1.87	0 - 0.08	20
	White	83.76 - 92.07	3.40 - 8.16	0.22 - 0.64	0.89 - 2.19	0.44 - 1.2	0.01 - 0.15	0.74 - 2.09	0.01 - 0.06	10
	Light green	84.02 - 89.1	6.52 - 8.12	0.54 - 0.65	0.87 - 2.50	0.70 - 1.13	0.01 - 0.08	1.7 - 1.95	0 - 0.08	10
	Dark green	82.36 - 86.9	5.5 - 8.09	0.34 - 0.59	1.97 - 3.92	0.37 - 1.18	0.01 - 0.08	1.51 - 2.10	0.01 - 0.06	10
	Black	76.89 - 82.49	6.46 - 9.16	0.49 - 0.62	3.65 - 5.87	0.76 - 4	0.01 - 0.25	1.47 - 2.33	0.02 - 0.15	10
	All sites	76.47 - 93.85	3.14 - 11.45	0.22 - 0.8	0.84 - 5.87	0.24 - 4	0.02 - 0.25	0.75 - 2.71	0 - 0.21	216
	Average	84.6	7.52	0.58	2.55	1.13	0.06	1.87	0.1	216
Mini-glasses	All sites	75.24 - 93.18	1.98 - 10.68	0.13 - 0.7	0.74 - 6.2	0.19 - 3.67	0 - 0.22	0.61 - 2.4	0.02 - 0.19	26
	Average	84.41	7.37	0.56	2.87	1.56	0.09	1.71	0.08	26
Meisel et al. (1990)	Unknown	84 - 89.3	6.75 - 8.20	0.52 - 0.62	1.08 - 3.78	0.61 - 1.13	0.03 - 0.18	1.51 - 2.93	0.02 - 0.06	18
Taylor and Solomon (1962)	Unknown	84.1 - 87.1	5.8 - 7.44	0.56 - 0.62	1.44 - 2.98	0.66 - 1.36	0.05 - 0.19	1.66 - 1.98	0.03 - 0.07	10

Table 3.1 Major element composition of Darwin glass. Chips of macro-glass fragments collected from 10 sites across the strewn field were analysed along with 26 splashform shaped mini-glasses (<5mm). This study significantly extends the ranges in composition for all major elements. Analyses by SEM, detection limits are between 0.05-0.1 wt%.

macro-glasses are considered to be parts of the same population. Colour variation in the glasses appears to be controlled by FeO and MgO abundances (Fig. 3.3). These mean results are similar to previously published analyses of Darwin glass for most elements (e.g. Meisel et al.1990). Average Darwin glass in this study is depleted in SiO_2 and enriched in MgO relative to previous studies. This study significantly extends the ranges in composition of Darwin glass for all analysed major elements.

The major elements in Darwin glass are correlated in a systematic manner. When viewed in X-Y coordinate space, all major elements are inversely correlated with SiO_2. This is because of the high SiO_2 content of Darwin glass and the constraint that major element oxide totals must equal 100% - 'silica closure' (table 3.2). Except for CaO and Na_2O, MgO displays a wider relative range in abundance than the other major elements and this is used as a reference oxide in plots that attempt to illustrate major element compositional variation in the Darwin glass (Fig. 3.4A-G). These plots show a strong positive correlation of FeO, CaO, and Na_2O with MgO, although the abundance of CaO and Na_2O are commonly at or below their detection limits. The triangular data array produced in the Al_2O_3 vs. MgO plot suggests that distinct end members may have been involved in the formation of the glass; one low in MgO and relatively high in Al_2O_3, another low in both MgO and Al_2O_3 and a third relatively rich in MgO. TiO_2 and K_2O vary by only a small amount relative to MgO (or FeO) and subsequently these plots are characterised by flat to gently sloping data arrays. With the exception of Na_2O and CaO (excluded because of very low abundances relative to the other major elements) these data were centered – log ratio transformed (after Aitchison 1977) and an Uncentered Covariance Matrix created in MVSP (Multi-variate Statistical Package; Kovach 1993) Version 2.2 (Table 3.3). The matrix shows positive covariance between MgO, FeO, K_2O and TiO_2 that are inversely related to SiO_2. Al_2O_3 shows little variation in centred-log ration space.

3.1.1a Comparison with Australasian Tektites, selected impact glasses and crustal rocks.

Major element compositions of Australasian tektites were compiled along with data for other high silica impact glasses, in this case Zhamanshinite and Irghizite glass, and Libyan Desert glass (LDG) (Table 3.4). Zhamanshinite and Irghizite glasses are from the Zhamanshin Crater in Russia. LDG is found across the Great Sand Sea in western Egypt and is derived from an as yet unknown source. LDG is selected for

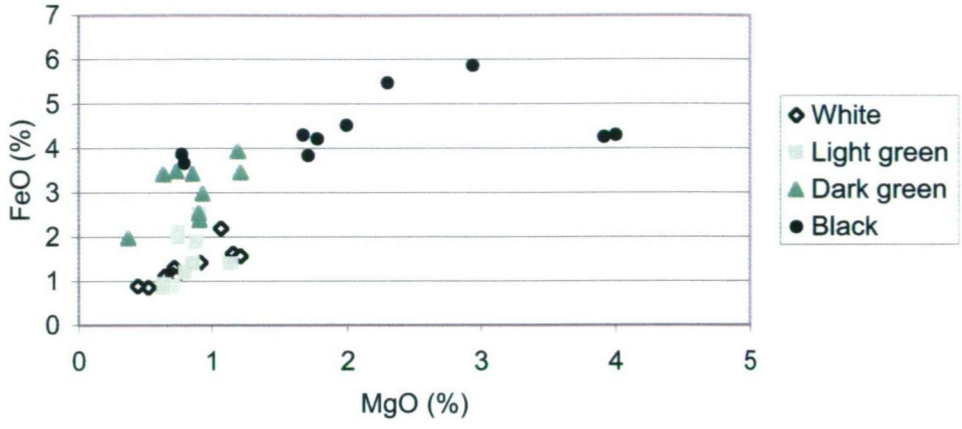

Figure 3.3 MgO vs. FeO in Darwin glass. The observed colour variation in the glass is predominantly controlled by FeO and MgO content.

	Na_2O	MgO	Al_2O3	SiO_2	K_2O	CaO	TiO_2	FeO
Na_2O	1.00							
MgO	0.46	1.00						
Al_2O_3	0.17	0.23	1.00					
SiO_2	-0.38	-0.59	-0.79	1.00				
K_2O	0.14	0.04	0.80	-0.60	1.00			
CaO	0.46	0.88	0.08	-0.44	-0.10	1.00		
TiO_2	0.05	0.06	0.62	-0.43	0.49	-0.05	1.00	
FeO	0.33	0.53	0.52	-0.83	0.39	0.42	0.22	1.00

Table 3.2 Correlation coefficients (r^2) for major elements in Darwin glass (all analyses). The coefficient is considered statistically significant at the 95% confidence level when the calculated r^2 value is greater than 0.36. The r^2 value must be greater than 0.49 to be considered statistically significant at the 99% confidence level. In x-y space, all major elements are inversely correlated with SiO_2 because of the high SiO_2 content of the glass and the constraint that major element oxide totals must equal 100% - 'closure problem'.

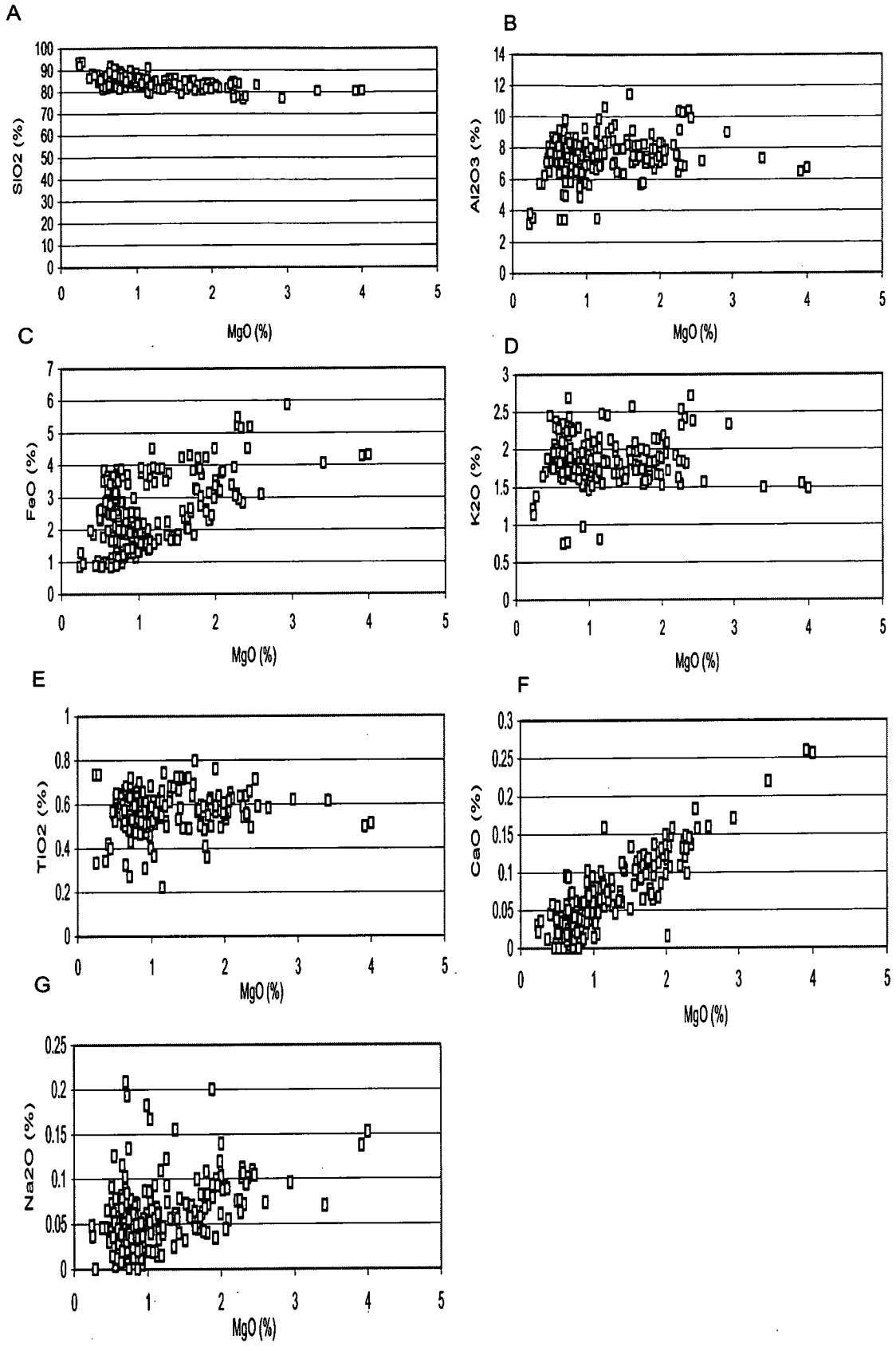

Figure 3.4A-G Major oxides vs. MgO in Darwin glass (all analyses).

	MgO	Al_2O_3	SiO_2	K_2O	TiO_2	FeO
MgO	5.83					
Al_2O_3	0.81	0.14				
SiO_2	-4.98	-0.71				
K_2O	4.09	0.62	-3.62			
TiO_2	6.88	1.01	-6.10	5.07		
FeO	3.66	0.54	-3.19	2.64	4.41	2.48

Table 3.3 Uncentered Covariance Matrix for major elements in Darwin glass (all analyses). Showing positive covariance between MgO, FeO, K_2O and TiO_2 that are inversely related to SiO_2. Al_2O_3 shows little variation in centered log ratio space.

comparisons because this is the only reported impact glass with an abundance of SiO_2 comparable to Darwin glass. The Australasian tektites were selected for comparison because they share overlapping strewn fields and ages, but more importantly because they show a continuum in morphologies from large irregular layered tektites to splash forms (disc, dumb-bell, droplet, button) similar to that seen in Darwin glass but over a far greater distance. Irghizite and Zhamanshinites are also of the same age as Darwin glass; comparisons are made with Darwin glass, Australasian tektites, and LDG in order to describe any systematic trends in impact glass chemistry that may be useful in understanding the origin of Darwin glass. No genetic relationship to a common event is implied by the selection of glasses of similar age or chemistry, as will be shown.

The average major element composition of these select glasses is compared to Darwin glass in a series of correlation plots (Fig. 3.5A-F). Relative to the average Australite and Australasian layered tektite, Darwin glass is depleted in all elements except for SiO_2, which is relatively enriched in average Darwin glass. Compared to Australasian microtektites, Darwin glass is depleted in all elements except TiO_2, K_2O and SiO_2 that have similar values. Low SiO_2 samples of Darwin glass overlap in composition with the high SiO_2 end members of the Australasian tektites. Except for CaO, the large range in major element abundance in Darwin glass also produces compositional overlap with the remaining major elements in the Australasian tektites. In comparison to the average high Si Zhamanshinite, Darwin glass is depleted in all elements except MgO and SiO_2. K_2O, CaO and Na_2O abundances in Darwin glass are outside of the lower limit of the range observed in the high Si Zhamanshinites, while the remaining major element compositions overlap. The average Irghizite is enriched in all elements except SiO_2 relative to Darwin glass. The ranges in SiO_2 abundances in the Irghizites are outside of the lower limit for SiO_2 analysed in Darwin glass. Ranges in CaO and Na_2O abundances in Irghizites are outside of the upper limit for Darwin glass, but the remaining major element abundances overlap. Compared to average LDG, Darwin glass is enriched in all elements except for SiO_2. All analyses of FeO, MgO and K_2O abundances in Darwin glass are outside of the upper limit of abundances for these elements in LDG. High SiO_2 samples of Darwin glass approach the lower limit of the range in SiO_2 in LDG, and as for LDG the high SiO_2 Darwin glass analyses are completely lacking in CaO and Na_2O (below detection). As may be expected given its relatively consistent abundance in upper

	SiO_2	$Al2O_3$	TiO_2	FeO	MgO	CaO	K_2O	Na_2O	n =
Australite tektites[1]	66.9 - 79.7	9.3 - 12.5	0.08 - 0.93	3.11 - 5.3	1.21 - 4.19	1.37 - 5.62	1.25 - 2.81	0.74 - 1.78	6(
Australasian layered tektites[2]	68.2 - 82.57	8.2 - 14.82	0.22 - 0.98	3.09 - 7.95	1.13 - 2.43	0.73 -9.23	2.23 - 2.79	0.77 -1.8	4:
Australasian microtektites[3]	48.1 - 77.0	7.5 - 23.4	0.5 - 1.2	3.0 - 9.6	1.9 - 27.3	1.0 - 5.8	0.1 - 3.7	0.1 - 2.8	7:
High Si Zhamanshinite tektites[4]	71.46 - 77.8	13.25 - 15.55	0.58 - 0.81	4.05 - 5.5	0.71 - 1.11	0.55 - 1.81	2.7 - 2.99	0.88 - 1.85	:
Irghizite tektites[5]	70.0 - 74.12	10.19 - 13.6	0.69 - 1.09	4.68 - 8.15	1.82 - 3.23	6.68 - 9.07	1.22 - 1.85	3.24 - 4.55	3
Libyan Desert Glass[6]	92.9 - 100.0	0.65 - 2.27	0.07 - 0.22	0.06 - 0.19	0.001 - .02	0.001	0.07 - 0.22	0.001	
Darwin glass	76.47- 93.85	3.14 - 11.45	0.22 - 0.8	0.84 - 5.87	0.24 – 4.0	0.02 - 0.25	0.75 - 2.71	0 - 0.21	21(
Darwin mini-glass	75.24- 93.18	1.98 - 10.68	0.13 - 0.7	0.74 - 6.2	0.19 - 3.67	0 - 0.22	0.61 - 2.4	0.02 - 0.19	2(

[1]Data from: Taylor (1962); Taylor (1966); Chapman & Scheiber (1969); Taylor & Epstein (1969); Taylor & McLennan (1979); and Glass et al. (1996)

[2]Data from: Chapman & Scheiber (1969); Taylor & Epstein (1969); Glass & Koeberl (1989); Wasson (1991); Koeberl (1992) ; and Chaussidon & Koeberl (1995)

[3]Data from: Cassidy et al. (1969) ; and Prasad & Sudhakar (1999)

[4]Data from: Bouska et al. (1981)

[5]Data from: Bouska et al. (1981)

[6]Data from: Barrat et al. (1997)

[7] This stud

Table 3.4 Major element composition of Darwin glass (this study) and selected impact glasses and tektites.

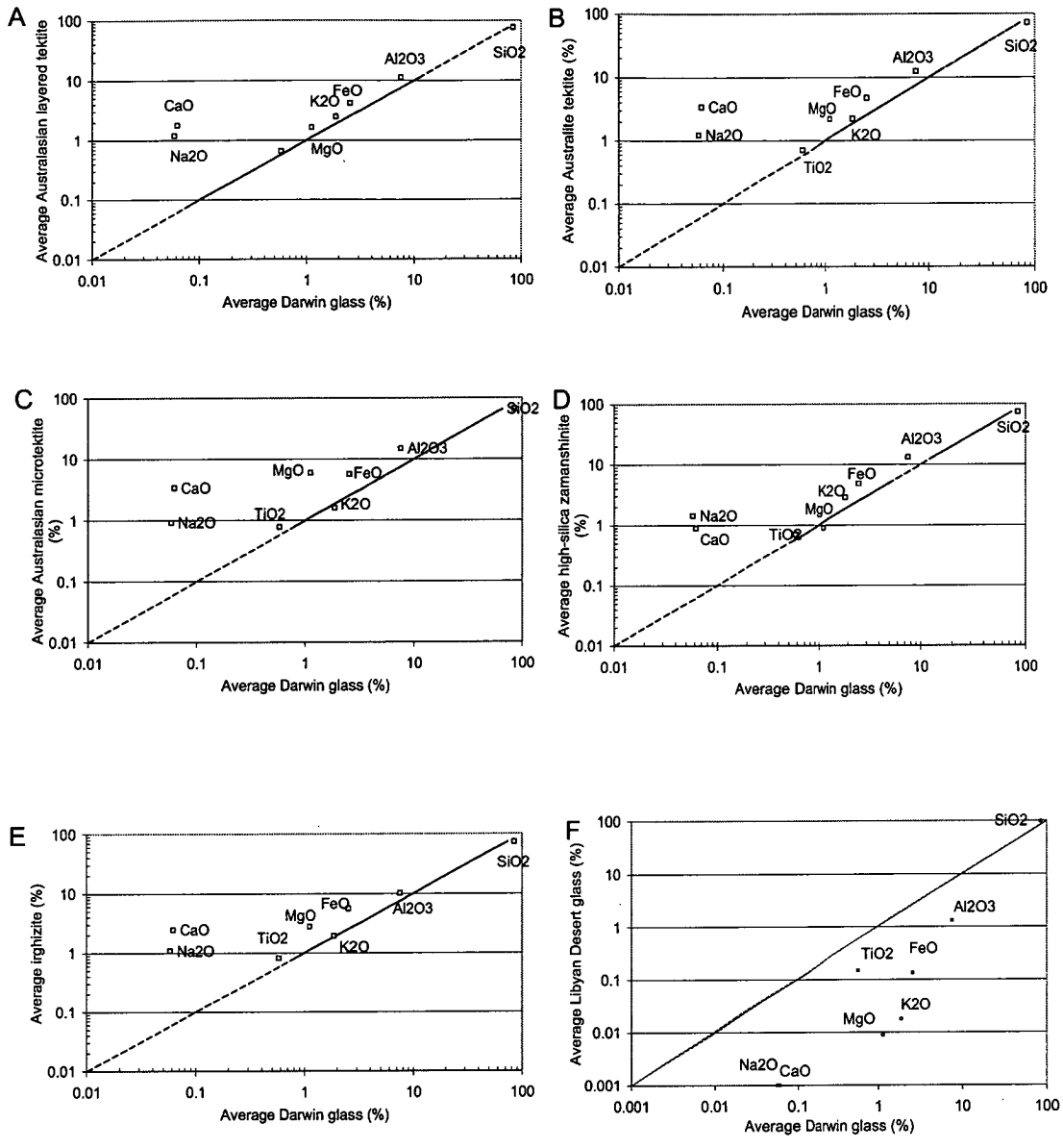

Figure 3.5A-F A series of plots comparing the major element geochemistry of Darwin glass with that of selected types tektites and impact glasses.

crustal sediments, TiO_2 is the major oxide that is most consistent in abundance across the impact glass groups compared here.

Major element data for the 'average' crust and typical sedimentary rocks were compiled (table 3.5) and these are compared to Darwin glass in a series of correlation plots (Fig. 3.6A-G). Darwin glass major element composition is generally unlike any of the average crust estimates. Compared to bulk continental crust, Darwin glass is highly depleted in all major elements except TiO_2, K_2O and SiO_2. TiO_2 is only slightly depleted in Darwin glass relative to bulk continental crust, K_2O abundance is well matched, and as expected SiO_2 contents are far higher in Darwin glass. Except for the volatile K_2O, Darwin glass major element composition is closer to the average upper continental crust. However, Darwin glass remains strongly depleted in all elements except TiO_2 and SiO_2, even when compared to upper continental crust.

The high SiO_2 contents of Darwin glass necessitate comparisons with lithologies rich in quartz. Darwin glass is compared to 5 such lithologies -, quartz arenite, greywacke, post Archaean shale (PAS), loess and average granite - in correlation plots. When compared to the composition of an average quartz arenite, Darwin glass is enriched in all major elements except for CaO, Na_2O and SiO_2; compared to greywacke Darwin glass is strongly depleted in Na_2O and CaO and slightly depleted in Al_2O_3; compared to PAS the glasses are depleted in all major elements except SiO_2 that is enriched in the glasses. Compared to loess the glasses are strongly depleted in CaO and Na_2O, and slightly depleted in K_2O, FeO and Al_2O_3, while MgO is slightly enriched and SiO_2 is strongly enriched in the glass relative to loess. Compared to average granite, Darwin glass is strongly depleted in Na_2O and CaO, and depleted in all elements, except TiO_2 that is of similar concentration, and SiO_2 that is relatively enriched in Darwin glass.

Except for SiO_2, CaO and Na_2O that are more similar to a quartz arenite, greywacke provides the best match to the major element composition of Darwin glass. The SiO_2 abundances in quartz arenite (92.7%) and PAS (62.8%) bracket the upper and lower limits for SiO_2 abundances in Darwin glass. Except for Na_2O that remains slightly depleted in the glasses relative to average quartz arenite, the variation in the remaining major elements between average quartz arenite and PAS overlap those in

	SiO_2	Al_2O_3	TiO_2	FeO	MgO	CaO	K_2O	Na_2O
Bulk Continental Crust[1]	59.1	15.8	0.7	6.6	4.4	6.4	1.9	3.2
Upper Continental Crust[1]	66.0	15.5	0.5	4.5	2.2	4.2	3.4	3.9
Quartz Arenite[2]	92.7	4.2	0.44	0.11	0.42	0.06	1.15	0.1
Greywacke[3]	81.1	10	0.62	2.76	1.44	0.26	1.93	1.69
Post Archaen Shale[3]	62.8	18.9	1	6.5	2.2	1.3	3.7	1.2
Loess[4]	72.7	15.8	0.57	2.97	0.95	1.54	2.39	3.27
Granite – S Type[3]	70.5	14.6	0.56	3.97	1.86	2.54	3.7	2.24
Average Darwin glass	84.6	7.52	0.58	2.55	1.13	0.06	1.87	0.1
Average Darwin mini-glass	84.41	7.37	0.56	2.87	1.56	0.09	1.71	0.08

[1] Rudnick & Fountain (1995); [2]Meisel et al. (1990); [3]Taylor & McLennan (1985); [4]Taylor et al. (1983)

Table 3.5 Major element composition of Darwin glass, 'average' crust and typical sedimentary rock types.

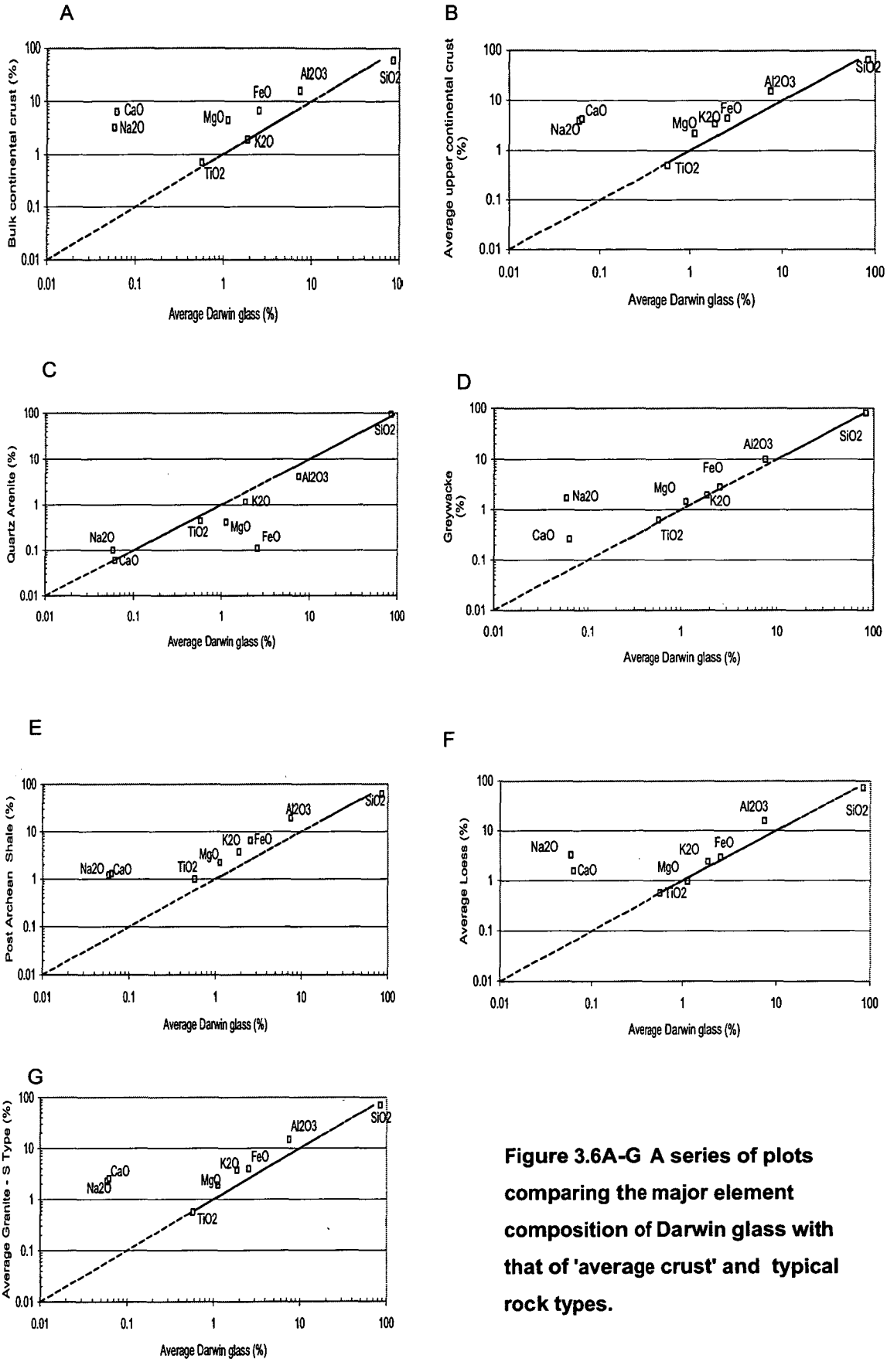

Figure 3.6A-G A series of plots comparing the major element composition of Darwin glass with that of 'average crust' and typical rock types.

Darwin glass. Given the natural variability of sedimentary rock types it is clear that some mixture of average quartz arenite and PAS could reproduce the major element composition of Darwin glass for all elements except Na_2O that remains depleted in the glass. The Na_2O and CaO abundances in Darwin glass suggest that the parent material(s) lacked plagioclase feldspar. The low Na_2O and CaO abundance in Darwin glass also suggests that significant contributions from both granite and average loess are unlikely in the formation of Darwin glass. This high SiO_2, low Na_2O and CaO requirement may suggest that a very clean quartzite was involved in the formation of Darwin glass

3.2 Laser ablation inductively coupled plasma mass spectrometry (LA-ICPMS)

Darwin glass fragments were placed under a low energy focused laser beam that was used to ablate small portions of the glass before a nebulizer gas of high purity Ar sweeps the ablated glass into argon plasma. Here the ablated glass, supported by a stream of argon gas, is disassociated into positively charged ions that are accelerated through a quadruple mass spectrometer to an electron multiplier detector. The magnitude of the resulting current from the detector is proportional to the abundance of specific elements in the sample. The School of Earth Sciences at the University of Tasmania uses an Merchantek 266nm laser operated at 10 HZ and 3-6 J/cm^2 per pulse and the Agilent HP 4500 ICP-MS.

The same 25mm-epoxy discs containing Darwin glass fragments that were analysed by SEM were analysed for trace element compositions using LA-ICPMS. 23 elements were determined during each analysis and these were: Cs, Rb, U, Th, Ba, La, Ce, Nb, Pr, Sr, Nd, Zr, Sm, Eu, Gd, Ho, Yb, Y, Lu, Sc, Cr, Co and Ni. A nominal beam size of 120μm was used throughout all analyses. Relative element sensitivities were calibrated against the glass standard NIST 612, and the well-known standard BCR-2 was analysed as an unknown. During the analyses, 2 analyses of both NIST 612 and BCR-2 were made before 10 analyses of Darwin glass, followed by 2 more analyses each of NIST 612 and BCR-2. As an internal standard the measured intensity of ^{49}Ti during each analysis was normalised to the TiO_2 content of each glass determined previously by SEM. Throughout the course of the study detection

limits were between 0.1 and 0.001 ppm. Analyses spectra for data presented here are flat and smooth with little deviation in counts per second throughout the 60-second duration of each analysis. This is generally the case in analyses of tektites and impact glasses that are well suited to the LA-ICPMS technique, especially for determination of refractory elements (REE, Sr).

The mean composition, standard and relative standard deviations for analyses of NIST 612 are presented along with the published reference values in table 3.6. Repeat analyses of BCR-2, analysed as an unknown during the study, indicate precision of 2-7% and accuracy relative to calibration values of < 2%.

3.2.1 Trace elements in Darwin glass

Glass fragments from sites 1-10 were analysed at 2 points each. The 5 pieces of white, light green, dark green and black glasses were also analysed at 2 points each. Darwin mini-glasses were analysed at 4 points each. A summary of the mean and range of trace element abundances in macro and mini Darwin glasses is presented in table 3.7. Macro and mini Darwin glasses have overlapping compositional ranges and very close average compositions for all elements except Cr, Co and Ni that are enriched in the mini-glasses. With the exception of Ni (enriched by >30%), my results are within 20% of previously published analyses (e.g. Meisel et al. 1990). The range in trace element abundances in Darwin glass by far exceeds analytical uncertainty for all elements. The range in composition in Darwin macro glasses (98% for Nb to 567% for Ni) is greater than in the mini-glasses (74% for Ba to 327% for Ni).

The trace elements are grouped into six classes on the basis of geochemical behaviour: alkali metals (Cs and Rb), alkaline earths (Sr and Ba), rare earth elements (REE) and the REE-like Y, transition metals (Sc, Cr, Co, Ni), high field strength elements (HFSE: Zr and Nb) and the actinide elements (Th and U).

The variation in trace element compositions in Darwin glass is strongly effected by SiO_2 closure. This artefact produces a statistically significant negative correlation between SiO_2 and all trace elements (table 3.8). Subsequently, most trace elements show significant positive correlation with Al_2O_3, K_2O and TiO_2. As a result of these closure effects all trace elements except for Cr, Co and Ni correlate positively with

	Nist 612 Reference	Nist 612 Average analysis (this study, n = 88)	Standard Deviation	Relative Standard Deviation
Sc	41.050	41.0	0.2	0.5%
Cr	39.880	39.9	0.1	0.3%
Co	35.260	35.3	0.3	0.9%
Ni	38.440	38.4	0.7	1.8%
Cu	36.710	36.7	0.1	0.2%
Cu	36.710	36.7	0.2	0.6%
Zn	37.920	37.9	0.5	1.2%
Rb	31.630	31.4	0.8	2.6%
Sr	76.150	76.1	0.1	0.1%
Y	38.250	38.2	0.4	1.1%
Zr	35.990	36.0	0.6	1.8%
Nb	38.060	38.1	0.7	1.8%
Cs	41.640	41.6	0.5	1.1%
Ba	37.740	37.7	0.2	0.7%
La	35.770	35.8	0.3	0.9%
Ce	38.350	38.3	0.6	1.5%
Pr	37.160	37.2	0.3	0.9%
Nd	35.240	35.2	0.4	1.1%
Sm	36.720	36.7	0.3	0.9%
Eu	34.440	34.4	0.7	2.0%
Eu	34.440	34.4	0.3	0.8%
Gd	36.950	36.9	0.5	1.4%
Dy	35.970	36.0	0.4	1.2%
Ho	37.870	37.9	0.7	1.9%
Yb	39.950	39.9	0.2	0.5%
Lu	37.710	37.7	0.2	0.7%
Hf	34.770	34.8	0.4	1.1%
Ta	39.770	39.8	0.7	1.8%
Pb	38.960	39.0	0.4	1.1%
Th	37.230	37.2	0.3	0.8%
U	37.150	37.1	0.4	1.1%

Table 3.6 Nist 612 Reference composition and average analyses in this study.

	Macro- glasses															Mini -glasses		Meisel et al. (1990)	Taylor & Solomon (1962)
Site	10129	10131	10115	10135	10134	10127	10136	0203	0207	White	Light Green	Dark Green	Black	All sites	Average	All sites	Average	Unknown	Unknown
Cs	3.0 – 4.9	1.5 – 4.5	3.3 – 5.5	3.1 – 5.5	2.6 – 5.8	2.5 – 5.4	2.5 – 5.6	2.5 – 5.4	1.6 – 5.4	1.8 – 5.6	2.8 – 4.5	2.1 – 3.9	2.4 – 4.7	1.5 – 5.8	**3.8**	1.6 – 6.7	**3.3**	2.5 – 4.5	3.2 – 4.3
Rb	60.6– 91.3	33.3 – 88.6	69.0– 105.9	60.6– 100.3	51.2– 109.3	51.1– 98.4	52.2 –109.3	56.2 –105.3	34.6– 104.7	34.0 –107.8	62.3 –89.8	50.0 –84.8	58.9– 99.7	33.3 –109.3	**75.3**	35.5 -118.1	**67.7**	71.0 – 137.0	61.0 – 110.0
U	1.3 – 2.9	0.7 – 2.7	0.8 – 2.9	1.5 – 2.8	1.1 – 4.0	1.6 – 3.3	1.0 – 3.0	0.9 – 2.7	0.9 – 2.1	0.9 – 3.4	1.0 – 2.4	1.3 – 2.0	0.6 – 2.4	0.6 – 4.0	**1.9**	0.4 – 3.6	**1.5**	1.5 – 5.4	.
Th	10.8– 18.6	9.3 – 17.6	9.7 – 22.8	8.5 – 19.2	11.7– 19.8	10.6– 18.7	12.4 –19.0	11.1 –15.0	9.1 – 19.5	4.5 – 18.1	11.4 –16.7	8.2 – 15.3	11.6– 13.1	4.5 – 22.8	**14**	6.6 – 18.8	**13.9**	12.0 – 19.0	.
Ba	247.6 – 443.7	186.3 – 382.9	280.2 – 426.9	220.1 – 363.0	235.1 – 427.4	223.2 – 404.4	268.8 – 457.2	240.7 – 424.1	204.9 – 433.4	116.7 – 320.5	249.0 – 372.9	204.6 – 329.9	210.7 – 377.3	116.7 –457.2	**304.9**	166.8 - 384.7	**293.5**	182.0 – 450.0	290.0 – 360.0
La	25.1– 45.2	23.3 – 46.4	32.5– 47.1	21.4– 45.8	31.4– 48.9	25.7– 45.7	30.8 –46.8	28.2 –41.7	22.7– 48.3	11.3– 43.8	33.1 –45.3	22.8 –43.9	31.4– 38.1	48.9 – 11.3	**36.2**	17.1 – 45.5	**35.1**	35.0 – 46.5	.
Ce	58.0– 100.9	49.0 – 99.1	74.1– 110.3	49.8– 104.9	69.1– 110.1	54.9– 100.3	68.9 –99.7	58.5 –89.8	50.6– 106.0	26.9– 108.9	70.3– 92.4	46.8 –101.9	62.5– 80.0	26.9 – 110.3	**79.4**	41.2 – 105.2	**78.3**	70.0 – 97.8	.
Nb	9.6 – 14.6	6.6 – 14.4	9.4 – 14.6	8.4 – 15.5	9.6 – 16.0	8.5 – 14.6	9.4 – 14.0	10.6 – 14.0	7.0 – 14.6	4.6 – 13.6	9.9 – 13.7	7.0 – 12.0	10.0– 12.7	4.6 – 16.0	**11.6**	6.0 – 14.6	**11.2**	.	.
Pr	6.3 – 11.1	5.7 – 11.4	7.8 – 12.5	5.0 – 11.5	7.7 – 12.1	6.2 – 10.5	7.4 – 11.1	6.7 – 9.9	5.7 – 11.6	2.7 – 10.5	7.5 – 10.5	5.3 – 10.3	7.1 – 8.9	2.7 – 12.5	**8.7**	4.4 – 11.3	**8.5**	.	.
Sr	11.9– 20.5	9.2 –2 1.6	14.1– 24.9	8.3 – 21.2	13.6– 23.1	11.1 –21.4	12.9 –19.4	11.2 –27.8	9.1 – 23.3	4.9 – 19.0	6.2 – 8.9	4.8 – 8.6	12.2– 15.7	4.9 – 27.8	**15.6**	7.9 – 24.3	**14.8**	.	13.0 – 16.0
Nd	23.8– 42.1	21.4– 43.0	29.1– 48.2	18.8– 42.4	29.1– 43.8	22.5 –39.9	28.2 –42.4	27.4 –40.5	21.4– 47.6	10.7– 41.1	30.5– 41.0	21.3 –40.3	28.3– 35.5	10.7 – 48.2	**33.4**	16.1 – 43.4	**32.2**	29.0 – 42.0	.
Zr	323.9 – 591.8	314.4 –562.8	269.0 – 553.1	279.7– 547.2	364.8 – 706.0	320.1 – 600.4	383.8 – 658.3	268.6 – 564.3	169.2 – 750.9	54.1 – 537.1	445.9 – 623.5	255.0 – 477.4	295.4 – 462.4	54.1 – 50.9	**433.2**	180.6 – 919.6	**416.7**	254.0 – 547.0	220.0 – 490.0
Sm	5.1 – 8.9	4.4 – 8.5	5.9 – 10.7	4.1 – 8.8	6.0 – 9.2	5.0 – 8.4	5.7 – 8.5	5.5 – 8.6	4.3 – 9.3	2.1 – 9.9	6.2 – 8.4	4.4 – 8.2	5.8 – 7.5	2.1 –10.7	**6.9**	3.4 – 8.6	**6.7**	6.6 – 9.0	.
Eu	0.9 – 1.6	0.8 – 1.6	1.1 – 1.8	0.7 – 1.7	1.1 – 1.8	0.9 – 1.6	1.1 – 1.5	1.0 – 1.8	0.8 – 1.8	0.4 – 1.9	1.2 – 1.7	0.8 – 1.6	1.1 – 1.5	0.4 – 1.9	**1.3**	0.7 – 1.8	**1.3**	0.9 – 1.5	.
Gd	4.9 – 8.4	4.1 – 8.2	5.9 – 11.1	3.7 – 8.5	5.5 – 9.2	4.9 – 8.8	5.8 – 8.2	4.5 – 7.8	4.3 – 9.2	1.9 – 9.7	6.2 – 7.7	4.2 – 7.9	5.3 – 7.4	1.9 – 11.1	**6.6**	3.3 – 8.2	**6.2**	.	.
Ho	0.9 – 1.6	0.8 – 1.5	1.0 – 2.0	0.6 – 1.5	1.0 – 1.8	0.9 – 1.8	1.1 – 1.5	0.8 – 1.6	0.8 – 1.7	0.3 – 1.8	1.1 – 1.5	0.8 – 1.5	1.0 – 1.5	0.3 – 2.0	**1.2**	0.6 – 1.7	**1.2**	.	.
Yb	2.6 – 4.7	2.1 – 4.3	2.3 – 4.7	1.7 – 4.1	2.6 – 4.9	2.7 – 4.9	2.0 – 4.4	3.0 – 4.7	2.0 – 4.9	0.8 – 4.1	3.0 – 4.2	2.3 – 3.8	2.7 – 4.1	0.8 – 4.9	**3.3**	1.3 – 4.4	**3.1**	2.7 – 4.5	.
Y	25.3– 44.1	21.7– 41.4	26.5– 53.4	18.3– 42.0	29.7– 45.2	26.2 –46.1	30.3 –40.5	26.3 –49.0	21.9– 47.6	7.4 – 49.0	30.2– 40.2	21.6– 40.0	26.8– 39.6	7.4 – 53.4	**34.1**	14.2 – 45.4	**31.9**	.	18.0 – 44.0
Lu	0.4 – 0.7	0.3 – 0.6	0.3 – 0.7	0.3 – 0.6	0.4 – 0.7	0.4 – 0.8	0.5 – 0.7	0.3 – 0.6	0.3 – 0.8	0.1 – 0.6	0.5 – 0.6	0.2 – 0.6	0.3 – 0.6	0.1 – 0.8	**0.5**	0.2 – 0.6	**0.5**	0.4 – 0.8	.
Sc	5.8 – 9.2	4.3 – 8.7	7.3 – 10.8	5.5 – 8.6	5.8 – 10.0	5.3 – 9.1	6.0 – 8.9	5.3 – 10.6	4.5 – 8.9	3.5 – 8.8	6.2 – 8.9	4.8 – 8.6	7.5 – 10.1	3.5 – 10.8	**7.3**	3.9 – 9.8	**6.8**	6.0 – 8.2	2.5 – 5.2
Cr	35.7– 170.6	35.0– 196.8	41.6– 223.7	44.8– 204.7	47.4– 221.4	30.3– 106.2	27.0 –157.7	47.9 –505.2	25.3– 148.1	19.5– 145.3	38.3– 82.0	31.3– 78.6	52.6– 211.3	19.5 – 505.2	**89.9**	39.4 – 371.7	**120.2**	48.0 – 522.0	69.0 – 205.0
Co	2.1 – 26.2	1.9– 23.4	3.1 – 39.5	3.0 – 34.0	5.2 – 31.4	2.1 – 15.2	2.7 – 36.5	2.4 – 41.7	2.6 – 32.3	0.3 – 19.4	3.1 – 13.0	2.5 – 12.3	6.0 – 56.7	0.3 – 56.7	**12.7**	4.2 – 59.7	**20.4**	4.6 – 39.0	<3.0 – 27.0
Ni	19.9– 302.1	18.5 –342.7	18.9– 572.1	34.7– 492.9	39.4– 367.6	12.2 –187.7	23.3 –375.8	27.0 –607.0	19.9– 410.2	3.0– 343.9	35.1– 170.5	27.1 – 161	52.6– 917.7	3.0 –917.7	**161.3**	34.7 – 841.8	**246.2**	30.0 – 536.0	82.0 – 205.0

Table 3.7 Trace element composition of Darwin glass. Chips of macro-glass fragments collected from 10 sites across the strewn field were analysed along with 26 splashform shaped mini-glasses (<5mm). This study significantly extends the ranges in composition for all trace elements. Analyses by LA-ICPMS, detection limits between 0.1 and 0.0001 ppm.

	Na^2O	MgO	Al^2O^3	SiO^2	K^2O	CaO	TiO^2	FeO	Sc	Cr	Co	Ni	Rb	Sr	Y	Zr	Nb	Cs	Ba	La	Ce	Pr	Nd	Sm	Eu	Gd	Ho	Yb	Lu	Th	U
Na^2O	1.00																														
MgO	0.46	1.00																													
Al^2O^3	0.17	0.23	1.00																												
SiO^2	-0.38	-0.59	-0.79	1.00																											
K^2O	0.14	0.04	0.80	-0.60	1.00																										
CaO	0.46	0.88	0.08	-0.44	-0.10	1.00																									
TiO^2	0.05	0.06	0.62	-0.43	0.49	-0.05	1.00																								
FeO	0.33	0.53	0.52	-0.83	0.39	0.42	0.22	1.00																							
Sc	0.19	0.30	0.54	-0.60	0.47	0.20	0.73	0.50	1.00																						
Cr	0.32	0.59	0.20	-0.33	0.17	0.54	0.07	0.23	0.30	1.00																					
Co	0.43	0.78	0.23	-0.53	0.15	0.71	0.06	0.50	0.41	0.76	1.00																				
Ni	0.44	0.77	0.21	-0.48	0.16	0.73	0.01	0.42	0.34	0.78	0.94	1.00																			
Rb	0.05	0.03	0.58	-0.46	0.65	-0.06	0.70	0.30	0.73	0.16	0.11	0.12	1.00																		
Sr	-0.01	-0.10	0.18	-0.02	0.09	-0.11	0.57	-0.15	0.37	-0.01	-0.11	-0.13	0.36	1.00																	
Y	0.02	-0.05	0.38	-0.31	0.32	-0.12	0.74	0.20	0.72	0.01	0.02	-0.05	0.55	0.62	1.00																
Zr	-0.02	-0.05	0.16	-0.06	-0.02	-0.09	0.61	-0.15	0.29	-0.09	-0.11	-0.15	0.14	0.68	0.60	1.00															
Nb	0.02	0.00	0.60	-0.40	0.49	-0.10	0.92	0.19	0.75	0.11	0.03	0.00	0.76	0.59	0.78	0.59	1.00														
Cs	0.06	0.04	0.57	-0.41	0.66	-0.04	0.65	0.24	0.62	0.18	0.09	0.12	0.95	0.30	0.48	0.09	0.71	1.00													
Ba	0.01	-0.05	0.54	-0.42	0.49	-0.16	0.77	0.38	0.72	-0.04	0.01	-0.10	0.71	0.49	0.73	0.32	0.82	0.65	1.00												
La	0.05	-0.01	0.38	-0.29	0.30	-0.07	0.77	0.13	0.72	0.05	0.02	-0.03	0.57	0.72	0.86	0.67	0.81	0.51	0.72	1.00											
Ce	0.01	-0.07	0.32	-0.20	0.23	-0.10	0.73	0.00	0.65	0.07	-0.02	-0.06	0.54	0.75	0.84	0.66	0.77	0.49	0.64	0.95	1.00										
Pr	0.07	0.00	0.37	-0.29	0.28	-0.05	0.76	0.12	0.70	0.08	0.04	-0.02	0.55	0.73	0.86	0.66	0.80	0.50	0.72	0.98	0.96	1.00									
Nd	0.03	0.00	0.37	-0.28	0.26	-0.05	0.76	0.10	0.68	0.06	0.02	-0.03	0.53	0.75	0.87	0.68	0.80	0.47	0.69	0.98	0.96	0.97	1.00								
Sm	0.03	-0.02	0.33	-0.25	0.24	-0.07	0.74	0.08	0.69	0.06	0.03	-0.02	0.53	0.75	0.90	0.67	0.78	0.46	0.67	0.96	0.95	0.96	0.97	1.00							
Eu	0.01	-0.04	0.31	-0.22	0.24	-0.08	0.68	0.06	0.67	0.04	0.01	-0.04	0.52	0.75	0.90	0.61	0.73	0.44	0.63	0.90	0.91	0.90	0.92	0.95	1.00						
Gd	0.01	-0.07	0.24	-0.21	0.18	-0.10	0.65	0.06	0.64	-0.01	-0.02	-0.08	0.48	0.71	0.91	0.67	0.70	0.39	0.61	0.90	0.90	0.90	0.92	0.94	0.93	1.00					
Ho	0.01	-0.08	0.26	-0.26	0.19	-0.13	0.64	0.16	0.66	-0.07	-0.02	-0.10	0.48	0.63	0.95	0.61	0.69	0.37	0.66	0.84	0.82	0.84	0.85	0.88	0.90	0.95	1.00				
Yb	0.02	-0.09	0.34	-0.33	0.29	-0.16	0.67	0.30	0.70	-0.11	-0.02	-0.12	0.53	0.51	0.93	0.52	0.70	0.42	0.77	0.79	0.73	0.78	0.78	0.80	0.81	0.85	0.93	1.00			
Lu	0.03	-0.09	0.32	-0.33	0.26	-0.16	0.66	0.33	0.69	-0.11	-0.02	-0.13	0.51	0.49	0.90	0.51	0.69	0.40	0.77	0.78	0.72	0.76	0.77	0.78	0.78	0.84	0.92	0.97	1.00		
Th	0.06	-0.04	0.30	-0.24	0.20	-0.09	0.69	0.10	0.65	0.01	-0.02	-0.07	0.46	0.58	0.86	0.62	0.74	0.43	0.65	0.88	0.88	0.90	0.88	0.88	0.83	0.88	0.86	0.81	0.81	1.00	
U	-0.11	-0.29	0.39	-0.18	0.49	-0.35	0.48	0.07	0.40	-0.13	-0.30	-0.28	0.68	0.16	0.43	0.06	0.55	0.72	0.58	0.42	0.42	0.42	0.37	0.37	0.35	0.35	0.37	0.44	0.43	0.44	1.00

Table 3.8 Correlation coefficients (r^2) for major and trace elements in Darwin glass (all analyses). The coefficient is considered statistically significant at the 95% confidence level when the calculated r^2 value is greater than 0.36. The r^2 value must be greater than 0.49 to be considered statistically significant at the 99% confidence level. In X-Y space, all major and trace elements are inversely correlated with SiO_2 because of the high SiO_2 content of the glass and the constraint that major element oxide totals must equal 100% - 'closure problem'. Subsequently, most trace elements show positive correlation with Al_2O_3, K_2O and TiO_2. As a result of the closure-problem all trace elements except for Ni, Co and Cr correlate positively with each other.

each other. Cr, Co and Ni tend to correlate positively only with each other and Sc, and show no significant correlation with the remaining trace elements.

As for the major elements, trace elements from each class are plotted against the most variable major element MgO in an attempt to illustrate the variation in trace element abundances in Darwin glass (Fig. 3.7A-F). Under the influence of SiO_2 closure effects, the transition metals tend to correlate positively with MgO, while the remaining trace elements show little correlation with MgO. The transition metals also correlate positively with FeO, Na_2O and CaO and again the remaining trace elements show little correlation with these major elements, or with each other. As for the major elements, data for the trace elements were centered – log ratio transformed after Atchinson (1977) and an Uncentered Covariance Matrix created in MVSP 2.2 (table 3.9). The matrix shows positive covariance between MgO, K_2O, TiO_2, FeO, Al_2O_3 and Sc, Cs, U and heavy rare earth elements (HREE) Sm-Lu. Positive covariance also exists between SiO_2 and Zr, Ba, Rb and the light rare earth elements (LREE)La-Nd. Among the transition metals, Co shows relatively little variation compared to Ni and Cr that all show strong covariance. Ni and Cr are very strongly correlated and show positive covariance with Si, Zr, Ba and the LREE, but little systematic covariance with Sc.

A Principal Components Analysis (PCA) was performed on the major (Na_2O; MgO; Al_2O_3; SiO_2; K_2O; CaO; TiO_2; FeO) and trace elements (Sc; Cr; Co; Ni; Rb; Sr; Zr; and Ba) data matrix in MVSP 2.2. The PCA shows that 97.5% of the total variation across the entire sample can be explained on a single axis. This observation suggests that the geochemical variation in Darwin glass can largely be explained as mixing between two end-member compositions. The PCA component scores for axis 1 were used to identify the elements used in ratio plots that illustrate the variation between end-member compositions in Darwin glass. The plots of SiO_2/MgO vs FeO/Al_2O_3 and FeO/K_2O show variation between high SiO_2, low MgO end members and high FeO and MgO end members (Fig. 3.8A-C). These plots also provide a suggestion of a second silica rich end member with slightly less Al_2O_3 relative to FeO. The plot of Zr/Co vs. MgO/TiO_2 shows end members with high Zr and low MgO and end members with high MgO and Co. MgO and the transition metals (Ni, Cr and Co) drive the remaining geochemical variation revealed on axis 2 of the PCA. This suggests a third and distinct end member source contributes to these elements in the glass.

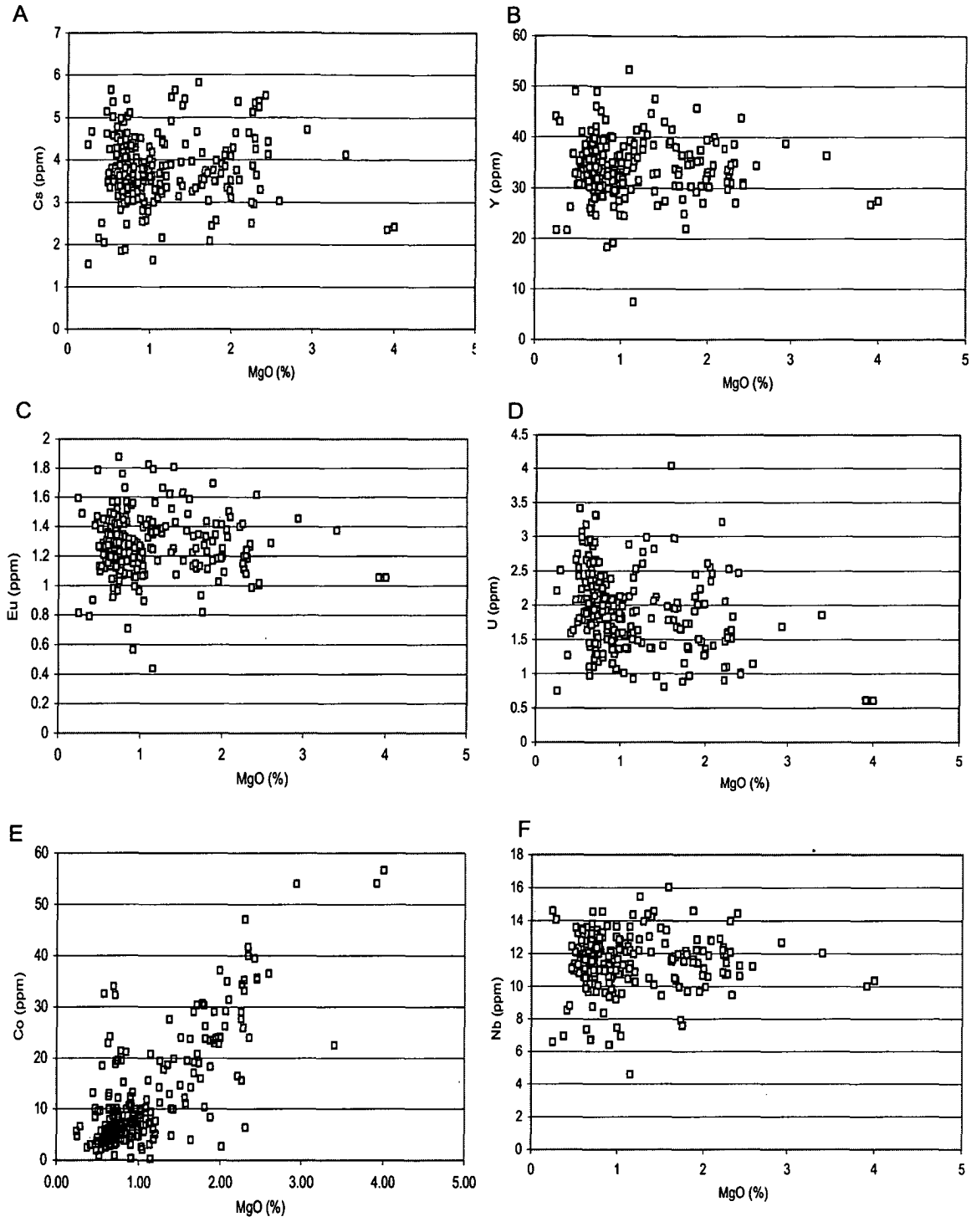

Figure 3.7A-F Selected trace elements vs. MgO in Darwin glass (all analyses).

	MgO	Al_2O_3	SiO_2	K_2O	TiO_2	FeO	Sc	Cr	Co	Ni	Rb	Sr	Y	Zr	Nb	Cs	Ba	La	Ce	Pr	Nd	Sm	Eu	Gd	Ho	Yb	Lu	Th	U
MgO	5.83																												
Al_2O_3	0.81	0.14																											
SiO_2	-4.98	-0.71	4.44																										
K_2O	4.09	0.62	-3.62	3.04																									
TiO_2	6.88	1.01	-6.10	5.07	8.51																								
FeO	3.66	0.54	-3.19	2.64	4.41	2.48																							
Sc	0.85	0.13	-0.76	0.64	1.07	0.56	0.14																						
Cr	-4.67	-0.71	4.19	-3.52	-5.90	-3.07	-0.75	4.24																					
Co	0.53	-0.01	-0.41	0.20	0.38	0.27	0.02	-0.05	0.61																				
Ni	-5.24	-0.86	4.74	-4.06	-6.79	-3.49	-0.89	4.96	0.29	6.09																			
Rb	-4.68	-0.66	4.13	-3.39	-5.71	-2.98	-0.71	3.93	-0.37	4.44	3.88																		
Sr	-0.94	-0.13	0.81	-0.66	-1.11	-0.61	-0.14	0.73	-0.13	0.80	0.76	0.18																	
Y	-2.81	-0.40	2.46	-2.03	-3.41	-1.79	-0.42	2.32	-0.24	2.62	2.31	0.46	1.39																
Zr	-8.81	-1.27	7.77	-6.43	-10.78	-5.65	-1.35	7.41	-0.63	8.45	7.27	1.44	4.35	13.77															
Nb	-0.25	-0.02	0.21	-0.15	-0.26	-0.15	-0.03	0.16	-0.09	0.14	0.20	0.05	0.12	0.36	0.02														
Cs	2.43	0.37	-2.17	1.82	3.04	1.57	0.39	-2.12	0.08	-2.47	-2.01	-0.39	-1.21	-3.86	-0.09	1.11													
Ba	-8.01	-1.15	7.07	-5.83	-9.80	-5.09	-1.22	6.73	-0.59	7.64	6.62	1.30	3.95	12.47	0.33	-3.48	11.35												
La	-2.96	-0.42	2.60	-2.14	-3.59	-1.89	-0.45	2.45	-0.25	2.77	2.43	0.49	1.46	4.59	0.12	-1.28	4.16	1.54											
Ce	-4.82	-0.69	4.25	-3.50	-5.88	-3.09	-0.73	4.04	-0.38	4.58	3.97	0.79	2.38	7.50	0.20	-2.09	6.81	2.51	4.10										
Pr	0.43	0.07	-0.40	0.34	0.58	0.28	0.07	-0.43	-0.03	-0.52	-0.38	-0.06	-0.22	-0.71	-0.01	0.21	-0.65	-0.23	-0.38	0.05									
Nd	-2.76	-0.40	2.43	-2.00	-3.36	-1.77	-0.42	2.29	-0.24	2.59	2.27	0.46	1.36	4.29	0.12	-1.20	3.89	1.44	2.34	-0.21	1.34								
Sm	0.97	0.15	-0.88	0.74	1.24	0.62	0.16	-0.89	0.01	-1.04	-0.83	-0.15	-0.49	-1.56	-0.03	0.44	-1.42	-0.51	-0.85	0.09	-0.48	0.19							
Eu	4.99	0.73	-4.44	3.68	6.18	3.19	0.78	-4.30	0.26	-4.95	-4.16	-0.80	-2.47	-7.84	-0.19	2.20	-7.13	-2.61	-4.27	0.42	-2.43	0.91	4.51						
Gd	1.08	0.16	-0.98	0.82	1.38	0.70	0.18	-0.99	0.01	-1.16	-0.93	-0.17	-0.54	-1.74	-0.04	0.49	-1.59	-0.57	-0.94	0.10	-0.53	0.21	1.02	0.24					
Ho	5.10	0.74	-4.55	3.77	6.33	3.27	0.80	-4.42	0.26	-5.08	-4.26	-0.82	-2.53	-8.03	-0.20	2.26	-7.30	-2.67	-4.38	0.43	-2.49	0.93	4.61	1.04	4.73				
Yb	2.71	0.40	-2.43	2.02	3.40	1.76	0.43	-2.39	0.10	-2.78	-2.28	-0.44	-1.35	-4.30	-0.10	1.21	-3.90	-1.43	-2.34	0.24	-1.33	0.51	2.48	0.57	2.55	1.38			
Lu	7.21	1.05	-6.42	5.32	8.93	4.64	1.12	-6.22	0.40	-7.15	-6.01	-1.16	-3.57	-11.33	-0.28	3.18	-10.30	-3.77	-6.18	0.61	-3.52	1.31	6.50	1.46	6.67	3.59	9.41		
Th	-0.70	-0.10	0.60	-0.49	-0.81	-0.44	-0.10	0.53	-0.11	0.57	0.56	0.12	0.34	1.06	0.03	-0.29	0.96	0.36	0.58	-0.04	0.34	-0.11	-0.59	-0.12	-0.60	-0.31	-0.85	0.10	
U	4.06	0.62	-3.64	3.05	5.10	2.63	0.65	-3.58	0.10	-4.19	-3.39	-0.66	-2.03	-6.46	-0.14	1.85	-5.84	-2.14	-3.51	0.35	-2.00	0.75	3.71	0.84	3.80	2.05	5.36	-0.47	3.14

Table 3.9 Uncentered Covariance Matrix for major and trace elements in Darwin glass (all analyses). Showing positive covariance between MgO, K_2O, TiO_2 FeO, Al_2O_3 and Sc, Cs, U and HREE. Positive covariance also exists between SiO_2, Zr, Ba, Rb and LREE. In the transition metals, Ni, Cr and Co are very strongly correlated with each other but not with Sc. Co shows little variation relative to Ni and Cr that show positive covariance with Si, Zr, Ba and the LREE.

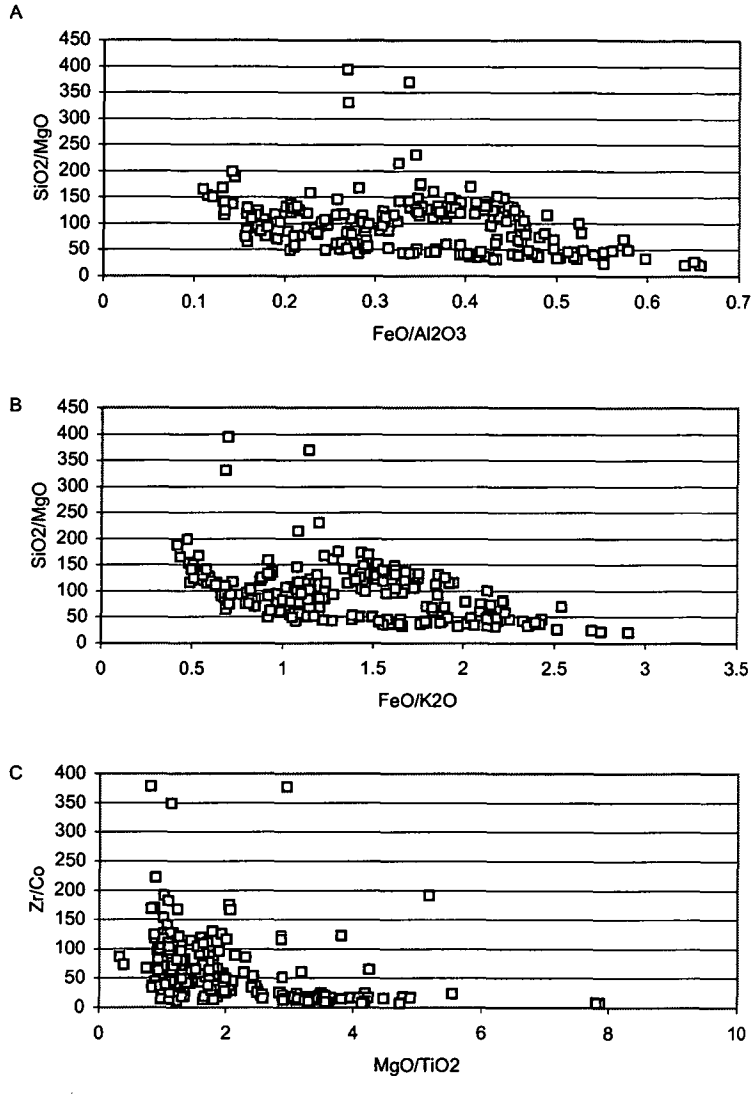

Figure 3.8A-C Principal Components Analysis (PCA) derived ration plots showing end-member compositions in Darwin glass.

A cluster analysis performed on the following major and trace element data: Na_2O; MgO; Al_2O_3; SiO_2; K_2O; CaO; TiO_2; FeO; Sc; Cr; Co; Ni; Rb; Sr; Zr; and Ba results in a dendrogram with 2 main compositional groups (table 3.10). Group 1 includes 80% of the sample and is characterised by large variations in major element compositions. In hand samples and thin sections, glasses belonging to Group 1 are predominantly white to dark green and sometimes black in colour. The range in major element composition in Group 1 glass is: SiO_2 (80.62 – 93.9%), Al_2O_3 (3.14 – 10.6%), TiO_2 (0.2 – 0.76%), FeO (0.8 – 4.23%), MgO (0.25 – 2.31%) and K_2O (0.7 – 2.7%). The average composition of Group 1 glass is close to that of bulk average Darwin glass. The sub-populations in Group 1 glass are defined on the basis of Ni, Cr and Co abundances that are depleted in group 1b glass relative to group 1a and bulk average Darwin glass. Visually, there is no obvious difference between Group 1a and 1b glass. The second population identified in the cluster analysis is characterised by a narrower range in, and lower average abundance of SiO_2 (76.5 to 84.1 %, with an average of 81.2 %). In hand samples and thin sections, Group 2 glass is almost always black. The average MgO (2.2%) and FeO (3.8%) compositions of Group 2 are significantly higher than those of Group 1 glass or average Darwin glass, and Al_2O_3 is also slightly enriched. As such, black Group 2 glass is expected to have a lesser viscosity than Group 1 glass (at equivalent temperature), particularly when compared to the light green and white glass specimens. The average Cr (162 ppm), Co (31ppm) and Ni (416 ppm) content of Group 2 glass is also significantly enriched relative to Group 1 glass or average Darwin glass, with the remaining trace elements being of very similar abundance in both groups and average Darwin glass. These relationships have important implications in the identification of the target rocks and process involved in the origin of Darwin glass.

3.2.1a Comparison with trace elements in Australasian Tektites, selected impact glasses and crustal rocks.

Previously, for the major elements it was shown that Darwin glass has compositions similar to some high silica sediments and impact glasses. Here trace element abundances in Darwin glass are compared with the same estimates of average crust, and typical sedimentary rock types, and impact glasses that were used in description of the major elements. The exceptions are average granite and average loess that have largely been excluded from discussion on the basis of incompatible major

Group		Na_2O	MgO	Al_2O_3	SiO_2	K_2O	CaO	TiO_2	FeO	Sc	Cr	Co	Ni	Rb	Sr	Zr	Ba	Count	%
Group 1	**a**	0.1	1.0	7.2	85.3	1.8	0.1	0.6	2.2	7.2	95.2	12.6	165.2	74.1	16.2	439.0	295.0	95	43.9
	b	0.0	0.8	7.5	85.1	1.9	0.0	0.7	2.4	7.2	51.3	4.5	44.7	75.4	15.4	436.0	315.0	83	38.4
Average Group 1		0.05	0.9	7.3	85.2	1.8	0.05	0.05	2.2	7.2	74.5	8.7	108.4	74.6	15.8	438.9	304.3		
Range		0.0-0.2	0.2-2.3	3.1-10.6	80.62-93.9	0.75-2.6	0.0-0.1	0.2-0.7	0.8-4.23	3.4-10.1	19.5-204.6	0.0-33.9	3.0-492.8	33.2-109.2	4.9-27.8	54.1-750.9	116.7-457.1		
Average Group 2		0.1	2.2	8.2	81.6	2.0	0.1	0.6	3.8	8.1	162.7	31.6	416.6	78.1	14.3	439.0	294.0	38	17.5
Range		0.0-0.2	1.1-4.0	6.4-11.5	76.4-84.5	1.4-2.7	0.06-0.2	0.5-0.80	1.8-5.8	6.3-10.7	67.6-260.4	19.4-56.5	117.4-917.7	56.6-109.2	10.9-20.4	286.6-553.1	210.7-427.3		
Bulk Average Darwin glass		0.1	1.1	7.5	84.6	1.9	0.1	0.6	2.6	7.3	89.9	12.7	161.3	75.3	15.6	433.2	304.9	216	

Table 3.10 Compiled cluster analysis results. The cluster analysis results in a dendrogram with 2 main compositional groups. Group 1 is characterised by a wide range in SiO_2 abundance and a large degree of heterogeneity. Average Group 1 glass is close in composition to bulk average Darwin glass. The cluster analysis based distinction between Group 1a and 1b is based on transition metal concentrations. Group 2 glass has a more limited compositional range and a lower average SiO_2 abundance with significantly higher FeO and MgO contents. Group 2 is also enriched in Ni, Co and Cr relative to Group 1 and bulk average glass.

element geochemistry. As the LA-ICPMS technique is especially well suited to the analysis of rare earth element (REE), these are discussed first.

Average REE abundance for Australasian tektites, Zhamanshinite and Irghizite glass and LDG have been complied along with average Darwin macro- and mini-glasses in table 3.11. These data are normalised to a C1 chondrite composition (Sun and McDonough 1989) and plotted in Fig. 3.9. All of the glasses are relatively LREE enriched (chondrite normalised La/Lu = 5.8 – 8.87) and show small negative Eu anomalies (Eu/Eu* = 0.48-0.66). Darwin glasses have slightly larger negative Eu anomalies than the other glasses. Macro Darwin glass (La/Lu = 6.2) is less enriched in LREE than all of the other glasses except Australasian layered tektites. Mini Darwin glasses (La/Lu = 6.9) show greater LREE enrichment than the macro Darwin glasses and are more LREE enriched than Australasian layered tektites, and Zhamanshinite and Irghizite glasses.

The relative and absolute abundances of REE in Darwin glass, Australites and Australasian microtektites compare well with each other, with the exception of Pr and Nd that are relatively enriched in Australites and La and Ce that are relatively enriched in the Australasian microtektites. With the exception of Pr in the high silica Zhamanhsinites, Darwin glass has a greater relative and absolute abundance of all REE than the other remaining impact glasses and tektites compared here.

REE in Darwin glass are compared to various estimates of average crustal composition and selected rock types previously used for the major elements (table 3.12, Fig. 3.10). The absolute abundances of REE are broadly similar to estimates of the average crustal composition and typical sedimentary rock types. However, bulk continental crust has a smaller Eu anomaly than either Darwin glass or the other rock types. Average upper crust has a similar size negative Eu anomaly to Darwin glass, but has lower REE abundances. None of the typical sediments (greywacke; PAS; or quartz arenite) provide a match with REE abundances in Darwin glass. However, the sediments are all relatively LREE enriched and have small negative Eu anomalies. Because of the natural variability in sedimentary rock compositions, it is likely that some upper crustal sedimentary rocks (or a mixture of such rocks) have REE patterns identical to Darwin glass.

	La	Ce	Pr	Nd	Sm	Eu	Gd	Ho	Yb	Lu
Australite tektites[1]	36.9	78.6	9	35	6.1	1.17	5.34	0.97	2.8	0.44
Australasian layered tektites[2]	28.2	60.7		29.1	4.85	1.01	4.3		2.71	0.42
Australasian microtektites[3]	40	93			7.1	1.37			2.2	0.45
High Si Zhamanshinite[4]	21.6	47	8.98	24.3	5.8	1.15	6.4	0.81	2.36	0.33
Irghizite glass[5]	19.7	44.2	4.53	18.7	3.78	0.8	3.46	0.67	1.9	0.26
Libyan Desert Glass[6]	11.84	25.2	2.66	9.3	1.67	0.297	1.21	0.188	0.579	0.11
Average Darwin glass	36.2	79.4	8.7	33.4	6.9	1.3	6.6	1.2	3.3	0.5
Average Darwin mini-glass	35.1	78.3	8.5	32.2	6.7	1.3	6.2	1.2	3.1	0.5

[1]Data from: Taylor (1966); Taylor & McLennan (1979)

[2]Data from: Glass & Koeberl (1989); Koeberl (1992)

[3]Data from: Frey (1977)

[4]Data from: Taylor & McLennan (1979)

[5]Data from: Bouska et al. (1981)

[6]Data from: Barrat et a (1997)

Table 3.11 Rare earth element (REE) composition of Darwin glass (this study) and selected impact glasses and tektites.

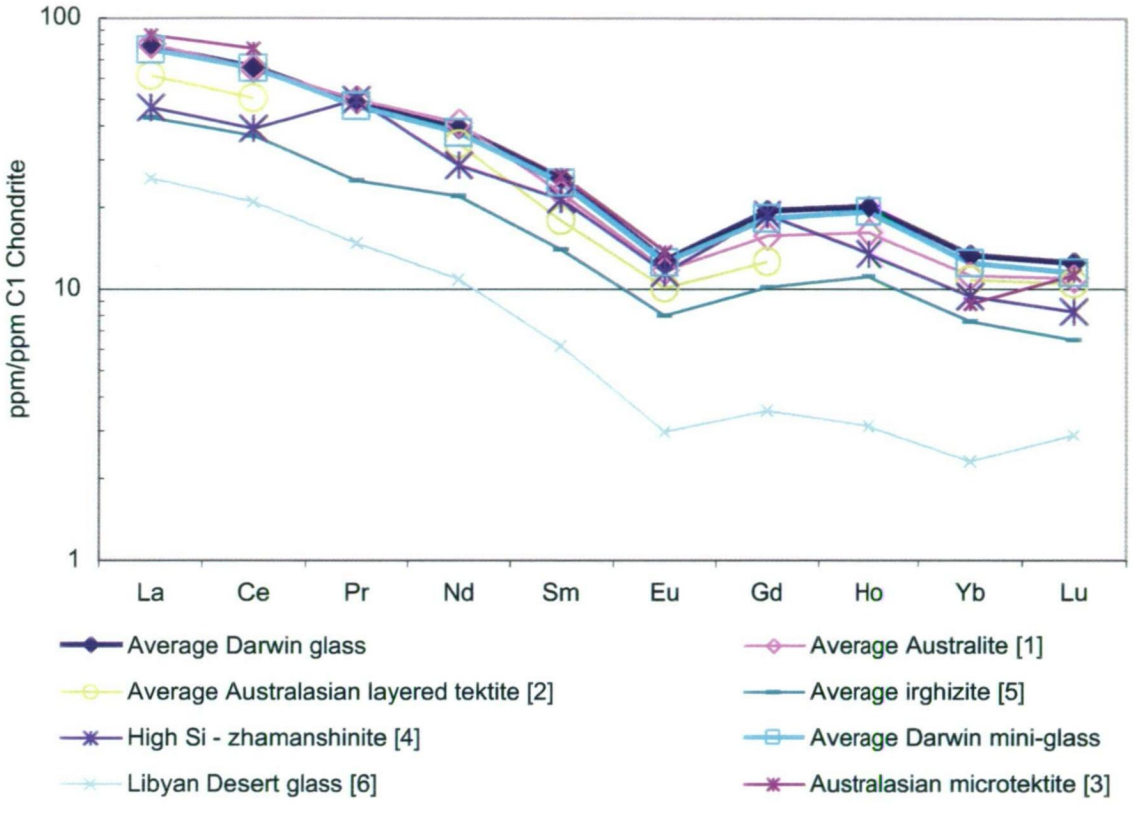

Figure 3.9 Chondrite normalised rare earth element (REE) composition of Darwin glass and selected tektites and impact glasses.

Data from: [1] Taylor (1966); Taylor & McLennan (1979); [2] Koeberl (1992); [3] Frey (1977); [4] Taylor & McLennan (1979); [5] Bouska et al. (1981); [6] Barrat et al. (1997).

	La	Ce	Pr	Nd	Sm	Eu	Gd	Ho	Yb	Lu
Bulk continental crust[1]	18	42	5	20	3.9	1.2	3.6	0.76	2	0.33
Upper continental crust[1]	30	64	7.1	26	4.5	0.9	3.8	0.8	2.2	0.32
Average quartz arenite[2]	17	25.7		9.8	2	0.4			2.2	0.4
Average greywacke[3]	43	83	12	42	7.1	1	5.6	1	2.9	
Average post archaen shale[3]	38	80	8.9	32	5.6	1.1	4.7	1	2.8	0.43
Average loess[4]	34	77	7.14	31.7	5.89	0.95	4	0.77	2.17	
Average granite S-Type[3]	31	69		25						
Average Darwin glass	36.2	79.4	8.7	33.4	6.9	1.3	6.6	1.2	3.3	0.5
Average Darwin mini-glass	35.1	78.3	8.5	32.2	6.7	1.3	6.2	1.2	3.1	0.5

[1] Rudnick & Fountain (1995); [2] Meisel et al. (1990); [3] Taylor & McLennan (1985) ; [4] Taylor et al. (1983)

Table 3.12 Rare earth element (REE) composition of Darwin glass, 'average' crust and typical sedimentary rock types.

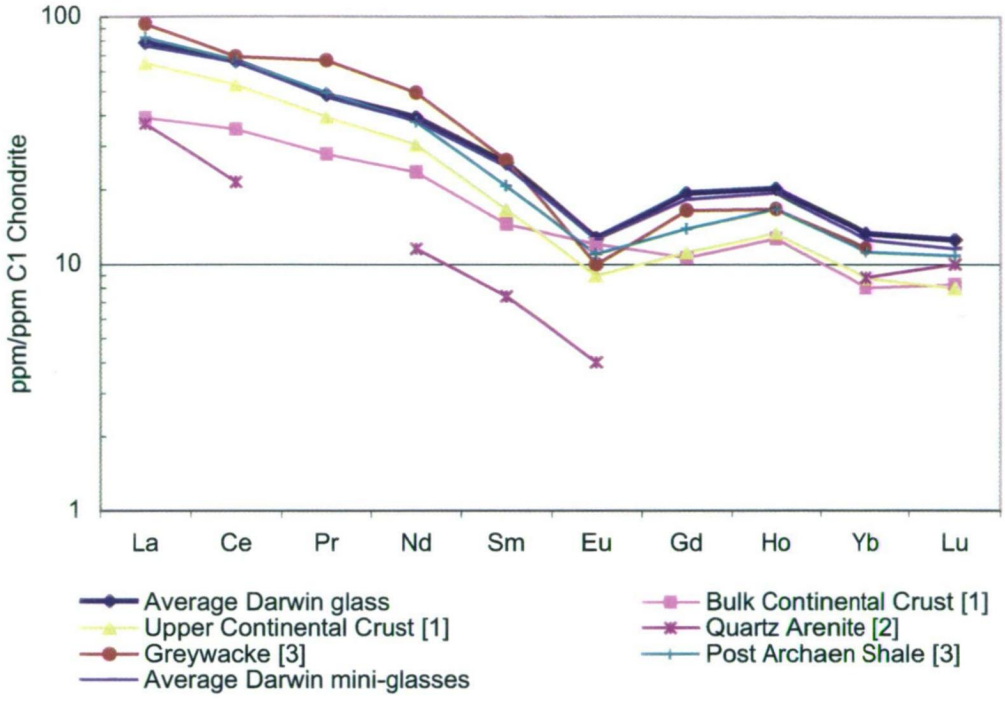

Figure 3.10 Chondrite normalised rare earth element (REE) composition of Darwin glass, 'average' crust and typical rock types.

Data from: [1] Rudnick & Fountain (1995); [2] Meisel et al. (1990); [3] Taylor & McLennan (1985); and [4] Taylor et al. (1983).

All of the trace element compositions determined for Darwin glass and the same tektites and impact glasses discussed above were compiled in table 3.13. These data were normalized to bulk continental crust and plotted in Fig. 3.11. Resultant curves for each glass show strikingly similar trends. Darwin glass and all other plotted glasses, with the exception of the high-Si zamanshinite glasses, are strongly depleted in Sr relative to bulk continental crust. The depletion in Sr is most pronounced in Darwin glass and this will have clear implications in the later identification of the target rocks involved in the glass formation. The actinide and REE elements are enriched relative to bulk continental crust in Darwin glass and all considered glasses except Libyan Desert glass (depleted in all REE) and Irghizite tektites (enriched in LREE but depleted in HREE). Compared to bulk continental crust, the HFSE Zr is strongly enriched in Darwin glass and all of the other glasses. In contrast to Zr, the HFSE Ba is depleted in Darwin glass and all glasses except the Australite tektites and irghizite glass relative to bulk continental crust. In comparison to bulk continental crust, the transition metals Sc, Cr and Co are depleted in all glasses except the for the irghizite tektites. Ni is enriched in Darwin glasses, Australite and Irighizite tektites relative to bulk continental crust, and Ni abundance in Darwin glass is higher than all other glasses except the Irghizite. Enrichment or depletion in any element relative to bulk continental crust appears more pronounced in Darwin glass than in any of the other glasses compared here.

All trace elements determined in this study were compiled and compared with estimates of average crust and typical sedimentary rock types (table 3.14). These are normalized to bulk continental crust and plotted along with Darwin glass in Fig. 3.12. The affinity of Darwin glasses with upper crustal sediments revealed by major and REE elements is evident in the plots that show almost identical trends in relative enrichment and depletion of trace elements compared to bulk continental crust. The exception to this trend is Ba that is enriched in loess relative to Darwin glass and the other rock types. A feature of Darwin glass is the large depletion in Sr relative to bulk continental crust, and the high abundances of Ni and Co in the glass relative to other sedimentary rock types. Ni abundances in some Darwin glass samples are outside of the range of the upper limit for Ni generally reported in sedimentary rocks.

To further define the likely type of target rocks involved in the formation of Darwin glass, data for the typical sedimentary rock types are added to ratio plots that define

	Cs	Rb	U	Th	Ba	La	Ce	Nb	Pr	Sr	Nd	Zr	Sm	Eu	Gd	Ho	Yb	Y	Lu	Sc	Cr	Co	
Australite tektites[1]	5.7	80	2.1	13.7	356	36.9	78.6	18.7	9	200	35	264	6.1	1.17	5.34	0.97	2.8	31	0.44	13	72	25	
Australasian layered tektites[2]	5.09	109.8	2.48	11.1	341	28.2	60.7			135	29.1	280	4.85	1.01	4.3		2.71		0.42	7.7	60.6	12.6	
Australasian microtektites[3]	2.3	66		14.5	530	40	93				36		7.1	1.37	5.4		2.2		0.45	11.9	81	9.9	
High Si Zhamanshinite[4]	7.8	118	2.97	10.3	347	34	83.6			630	34.1	272	6.95	1.56	6.47	1.12	3.4	33.8	0.35	15	92	16	
Irghizite glass[5]	2.6	38	1.02	5.98	527	19.7	44.2				18.7	351	3.78	0.8	3.46	0.67	1.9	17.5	0.26	8.8	170	73	
Libyan Desert Glass[6]	0	0.25	1.04	4.4	24	11.84	25.2		2.66	22.11	9.3	299	1.67	0.297	1.21	0.188	0.579	6.3	0.116			0	
Average Darwin glass	3.8	75.3	1.9	14.0	304.9	36.2	79.4	11.6	8.7	15.6	33.4	433.2	6.9	1.3	6.6	1.2	3.3	34.1	0.5	7.3	89.9	12.7	1
Average Darwin mini-glass	3.32	67.70	1.52	13.88	293.48	35.15	78.27	11.22	8.50	14.76	32.25	416.69	6.68	1.26	6.20	1.16	3.13	31.92	0.46	7.013	120.18	20.41	24

[1]Data from: Taylor (1966); Taylor & McLennan (1979)

[2]Data from: Glass & Koeberl (1989); and Koeberl (1992)

[3]Data from: Frey (1977)

[4]Data from: Taylor & McLennan (1979)

[5]Data from: Bouska et al. (1981); and Taylor & McLennan (1979)

[6]Data from: Barrat et al. (19

Table 3.13 Trace element composition of Darwin glass (this study) and selected impact glasses and tektites.

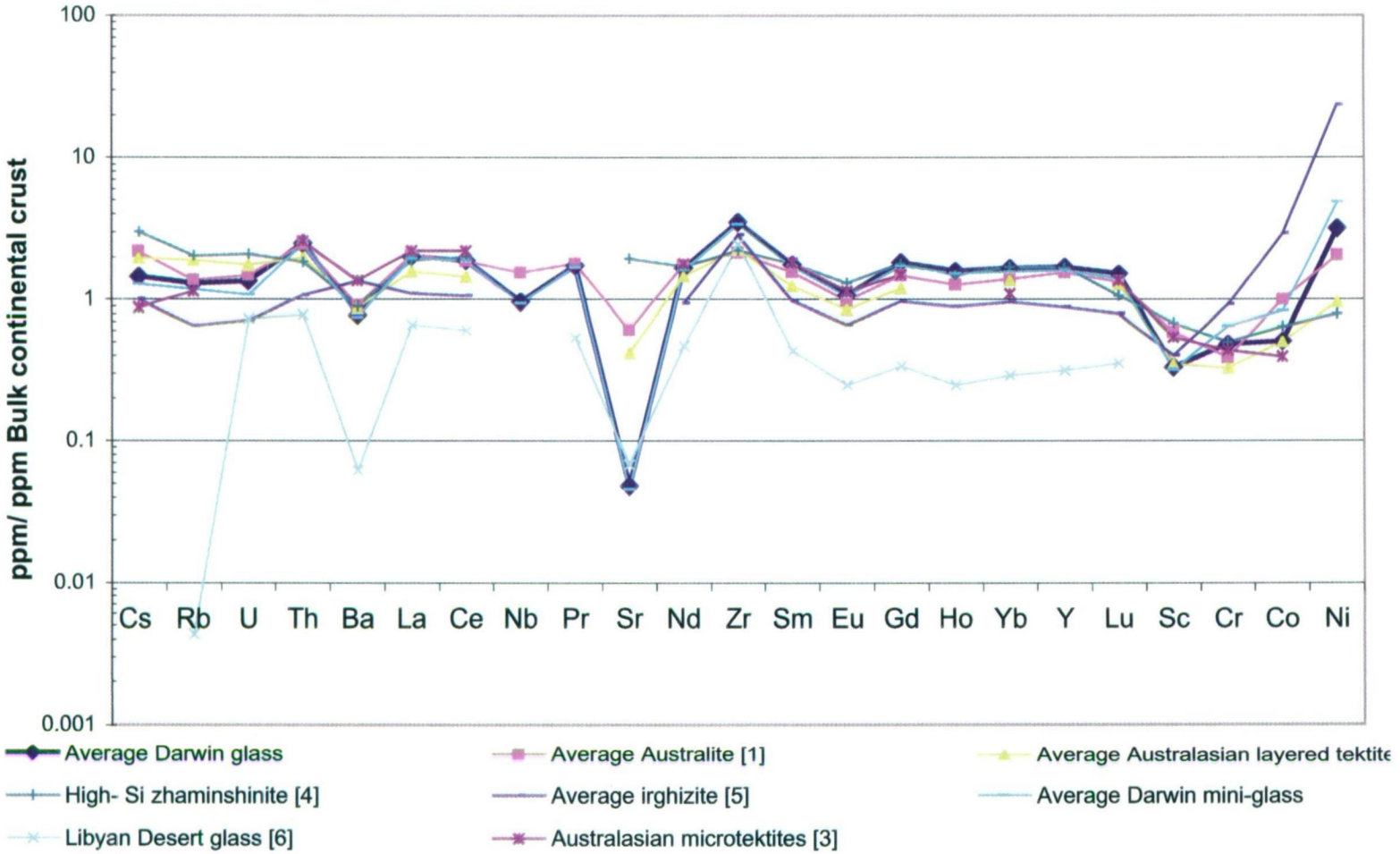

Figure 3.11 Trace element composition normalised to Bulk Continental Crust (Rudnick & Fountain 1995) for Darwin glass and selected tektites and impact glasses.

Data from: [1] Taylor (1966); Taylor & McLennan (1979); [2] Koeberl (1992); [3] Frey (1977); [4] Taylor & McLennan (1979); [5] Bouska et al. (1981); and [6] Barrat et al. (1997).

	Cs	Rb	U	Th	Ba	La	Ce	Nb	Pr	Sr	Nd	Zr	Sm	Eu	Gd	Ho	Yb	Y	Lu	Sc	Cr	Co
[1]Bulk continental crust	2.6	58	1.42	5.6	390	18	42	12	5	325	20	123	3.9	1.2	3.6	0.76	2	20	0.33	22	185	25
[1]Upper continental crust	5.6	112	2.8	10.7	550	30	64	25	7.1	350	26	190	4.5	0.9	3.8	0.8	2.2	22	0.32	11		10
[2]Average quartz arenite	1.4	67	2.5	6.2	133	17	25.7				9.8	634	2	0.4			2.2		0.4	3.1		1.1
[3]Average greywacke		91	3.42	16.4	400	43	83	11	12	44	42	384	7.1	1	5.6	1	2.9	32		10		13
[3]Average post archaen shale	15	160	3.1	14.6	650	38	80	19	8.9	200	32	210	5.6	1.1	4.7	1	2.8	27	0.43	16		23
[4]Average loess	3	74.2	2.24	8.32	635	34	77	16	7.14	187	31.7	400	5.89	0.95	4	0.77	2.17	22		5.7		5
[3]Average granite S-Type		180			480	31	69	11		139	25	170						32		14		13
Average Darwin glass	3.8	75.3	1.9	14.0	304.9	36.2	79.4	11.6	8.7	15.6	33.4	433.2	6.9	1.3	6.6	1.2	3.3	34.1	0.5	7.3	89.9	12.7
Average Darwin mini-glass	3.32	67.70	1.52	13.88	293.48	35.15	78.27	11.22	8.50	14.76	32.25	416.69	6.68	1.26	6.20	1.16	3.13	31.92	0.46	7.013	120.18	20.41

[1] Rudnick & Fountain (1995); [2]Meisel et al .1990); [3]Taylor & McLennan (1985); [4] Taylor et al. (1983)

Table 3.14 Trace element composition of Darwin glass, 'average' crust and typical sedimentary rock types.

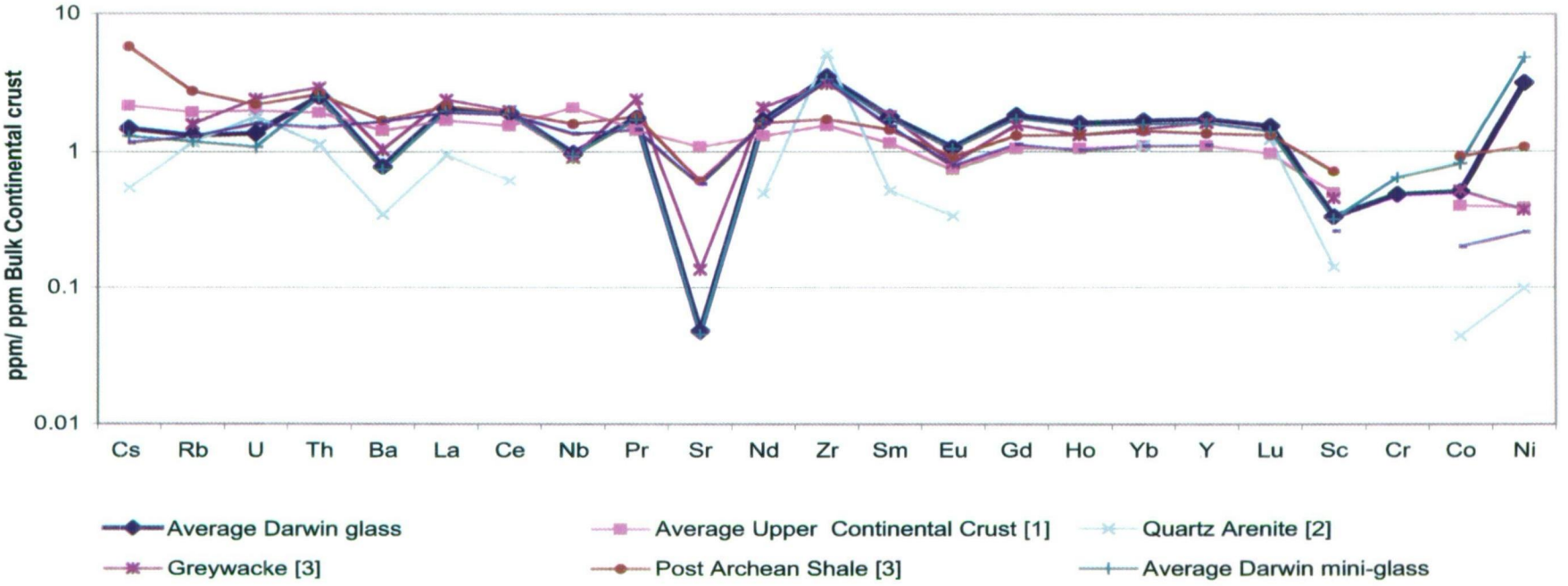

Figure 3.12 Trace element composition normalised to Bulk Continental Crust (Rudnick & Fountain 1995) for Darwin glass, 'average crust' and typical rock types.

Data from: [1] Rudnick & Fountain (1995); [2] Meisel et al. (1990); and [3] Taylor & McLennan (1985).

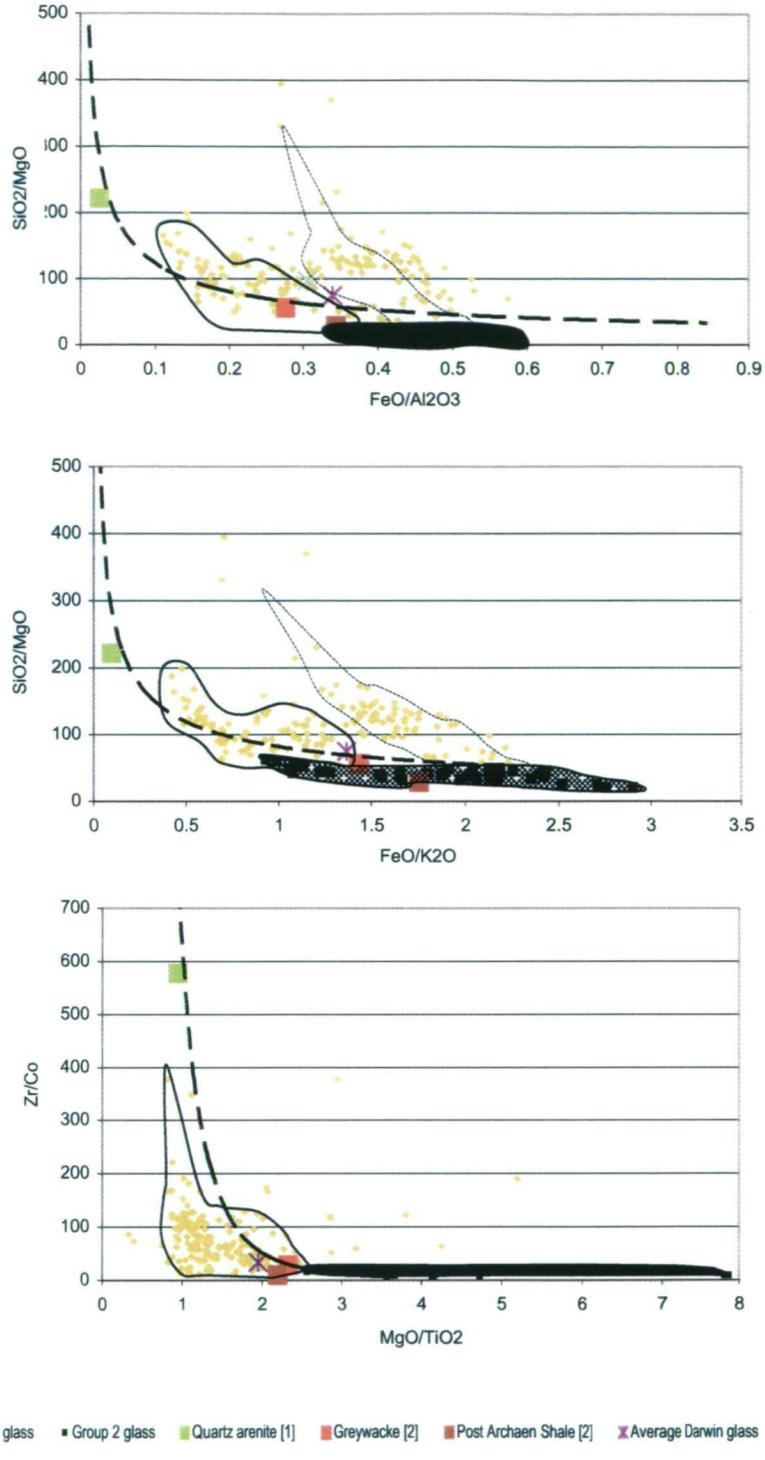

Figure 3.13A-C Principal Components Analysis (PCA) derived ration plots that compare end-member compositions in Darwin glass to average typical rock types.

Data from: [1] Meisel et al. (1990); and [2] Taylor & McLennan (1985).

the end member compositions in Darwin glass (Fig. 3.13A-C). Average Darwin glass is plotted, as are individual analyses that have been placed into the 2 compositional groups defined earlier by the cluster analysis. Average values only are plotted for the rock types. The plots of SiO_2/MgO vs. FeO/Al_2O_3, SiO_2/MgO vs. FeO/K_2O and MgO/TiO_2 vs. Zr/Co show that average Darwin glass plots close to a mixing line created between Average quartz arenite and PAS. Variation in Group 1 glass is predominantly away from the mixing line toward high SiO_2 samples with less Al_2O_3 relative to FeO. Group 2 glass plots outside of the range of PAS and requires a parent material more enriched in FeO, MgO and Co than PAS. This is consistent with the PCA result that suggested a third discrete source of MgO, Cr, Co and Ni. The remaining trace element – especially the REE – data provide no suggestion of a non-sedimentary component in the glass to contribute these elements and this will be discussed in detail later in conjunction with analytical data for western Tasmanian rocks. Average granite and loess lie within the range of Darwin glass in these plots, but fall well outside this range in plots featuring CaO or Na_2O.

3.3 Microscale internal variation in Darwin glass composition

Across the regional survey area the variation in the major element geochemistry of Darwin glass is very large. A large variation in the trace element geochemistry and especially the abundance of the transition metals across the strewn field is also a feature of Darwin glass geochemistry. This variation has resulted in the identification of two populations of glass within the strewn field. In order to test the internal homogeneity of Darwin glass, and the robustness of the group classification, a series of SEM grid traverses were conducted on green, black and white glass fragments. The grids were placed across a 500 * 500 μm area and 11 lines traversed the grid with 8μm spot analyses every 35-40μm. This results in a total of 120 spot analyses across the $2.5mm^2$ area. For the major elements (SiO_2, Al_2O_3, TiO_2, FeO, MgO, K_2O, CaO, Na_2O) 3 grids were analysed on green glass, 2 on black glass and 1 on white glass. The analyses were performed under identical conditions to those previously described. The trace elements Zr and Ni were analysed separately by SEM across a single 500 * 500μm grid on green, black and white glasses. For determination of the trace elements, a nominal 8μm beam was used and the regulated electron beam

current was operated at 50nA. Analytical time for each element was 120 seconds (Ni on LiF-SP3, Zr on TAP-SP4) and detection limits are Ni: 115 ppm and Zr: 75 ppm.

3.3.1 Major element internal variation

The range in major element composition for the grid analyses has been tabulated (table 3.15). For the major elements the compositional ranges in the green, black and white glasses are essentially overlapping and this largely reflects the presence of almost pure silica in each of the different colored glasses. Low silica analyses of black glasses are outside of the lower limit for SiO_2 in green and white glasses. The average compositions for each grid show the low SiO_2, high FeO content of the black glasses. In these grids Al_2O_3 is also elevated in black glasses relative to green and white. Significantly, the average MgO content in the black glasses is not greater than that of the green glasses despite increased FeO.

The standard deviation in the analytical results for each grid provides a measure of the internal heterogeneity of the glasses. For all elements the standard deviation in analytical results is greater in the green glasses than black glasses. Generally the internal heterogeneity is greatest in green followed by white and black glasses. The exception is green grid 1 where Al_2O_3 and TiO_2 analyses show greater standard deviations than in the white grid. K_2O also varies more in white glass than in green glass grid 1 or black glass (table 3.16), but this may be patchy due to volatility. In order to depict the internal variation in the glass geochemistry these data were contoured in Surfer 6.04 using a grid spacing of 1/3 and the Krieging technique (Figs. 3.14-3.19). The salient features of the internal variation in each of the different coloured glasses are described below.

3.3.1a Major element internal variation in Green glass

The grided plots show that the green glasses are characterised by zones of almost pure silica that may stretch across many analytical points and cover areas of over 200μm^2 (Figs. 3.14-3.16A). Away from these pure silica regions the variation in SiO_2 content continues to exceed analytical uncertainty and defines compositional layers and pods between which SiO_2 may vary by several percent. Away from the high silica zones Al_2O_3, K_2O and TiO_2 (Figs. 3.14–3.16A,E,K) vary comparatively little but

Grid	n =	SiO_2	Al_2O_3	TiO_2	FeO	MgO	CaO	K_2O	Na_2O
White 1	121	80.92 - 99.88 **(86.63)**	0.06 - 12.81 **(8.03)**	0.01 -1.01 **(0.59)**	0.09 - 1.35 **(0.86)**	0.03 - 0.91 **(0.53)**	0 - 0.04 **(0.01)**	0.05 - 2.96 **(2.32)**	0 - 0.07 **(0.03)**
Green 1	121	81.81 - 99.55 **(85.4)**	0.04 - 9.25 **(6.9)**	0.01 - 0.8 **(0.56)**	0.08 - 3.09 **(2.18)**	0.03 - 2.60 **(1.79)**	0 - 0.18 **(0.1)**	0.04 - 2.12 **(1.75)**	0 - 0.13 **(0.08)**
Green 2	121	79.33 - 100 **(86.15)**	0.09 - 12.62 **(6.53)**	0 - 1.18 **(0.53)**	0.02 - 3.67 **(2.15)**	0.01 - 2.97 **(1.63)**	0 - 0.21 **(0.1)**	0.04 - 2.59 **(1.66)**	0.01 - 0.20 **(0.11)**
Green 3	121	79.92 - 99.43 **(86.10)**	0.03 - 12.01 **(6.66)**	0.01 - 1.08 **(0.55)**	0 - 3.93 **(2.03)**	0 - 3.11 **(1.60)**	0 - 0.21 **(0.1)**	0.07 - 2.69 **(1.74)**	0 - 0.2 **(0.09)**
Black 1	121	80.99 - 97.82 **(82.20)**	0.70 - 9.23 **(8.53)**	0.02 - 0.81**(0.61)**	0.28 - 3.87 **(3.39)**	0.06 - 1.44 **(1.27)**	0 - 0.12 **(0.06)**	0.39 - 2.38 **(2.19)**	0.02 - 0.09 **(0.06)**
Black 2	121	79.80 - 84.57 **(82.03)**	7.17 - 9.14 **(8.33)**	0.51 - 0.71 **(0.60)**	3.25 - 4.84 **(3.77)**	0.5 - 1.86 **(0.67)**	0 - 0.06 **(0.02)**	2.02 - 2.42 **(2.26)**	0.0 - 0.07 **(0.03)**
Average Darwin glass		**84.6**	**7.52**	**0.58**	**2.55**	**1.13**	**0.06**	**1.87**	**0.1**

Table 3.15 Range and average major element composition of black, green and white Darwin glass fragments. Determined by SEM grid surveys across a 500 * 500 μm grid, 11 lines were traversed with 8μm spot analyses every 35-40μm (total of 121 analyses each grid). The black glass has a low average SiO_2 composition relative to the green and white glass along with elevated FeO and MgO. With the exception of a single high SiO_2 analysis, the black glass also has a far more limited compositional range than the green or white glass.

Grid	n =	SiO_2	Al_2O_3	TiO_2	FeO	MgO	CaO	K_2O	Na_2O
White 1	121	2.61 **(86.63)**	1.73 **(8.03)**	0.13 **(0.59)**	0.19 **(0.86)**	0.13 **(0.53)**	0.01 **(0.01)**	0.38 **(2.32)**	0.01 **(0.03)**
Green 1	121	2.84 **(85.4)**	1.39 **(6.9)**	0.12 **(0.56)**	0.53 **(2.18)**	0.51 **(1.79)**	0.04 **(0.1)**	0.29 **(1.75)**	0.02 **(0.08)**
Green 2	121	3.43 **(86.15)**	1.78 **(6.53)**	0.17 **(0.53)**	0.65 **(2.15)**	0.62 **(1.63)**	0.4 **(0.1)**	0.34 **(1.66)**	0.03 **(0.11)**
Green 3	121	4.29 **(86.10)**	2.12 **(6.66)**	0.19 **(0.55)**	0.85 **(2.03)**	0.75 **(1.60)**	0.05 **(0.1)**	0.49 **(1.74)**	0.03 **(0.09)**
Black 1	121	1.95 **(82.20)**	0.94 **(8.53)**	0.08 **(0.61)**	0.45 **(3.39)**	0.17 **(1.27)**	0.02 **(0.06)**	0.2 **(2.19)**	0.02 **(0.06)**
Black 2	121	0.64 **(82.03)**	0.33 **(8.33)**	0.04 **(0.60)**	0.25 **(3.77)**	0.17 **(0.67)**	0.02 **(0.02)**	0.07 **(2.26)**	0.02 **(0.03)**

Table 3.16 Average major element composition and standard deviation in analyses for black, green and white glass fragments. Data determined by SEM grid surveys previously described. The lesser standard deviations in analytical results for the low SiO_2 black glass indicate that the black glass is more homogenous than the green or white glass. This supports the existence of a low SiO_2, relatively homogenous, glass population as suggested by the cluster analysis (Group 2).

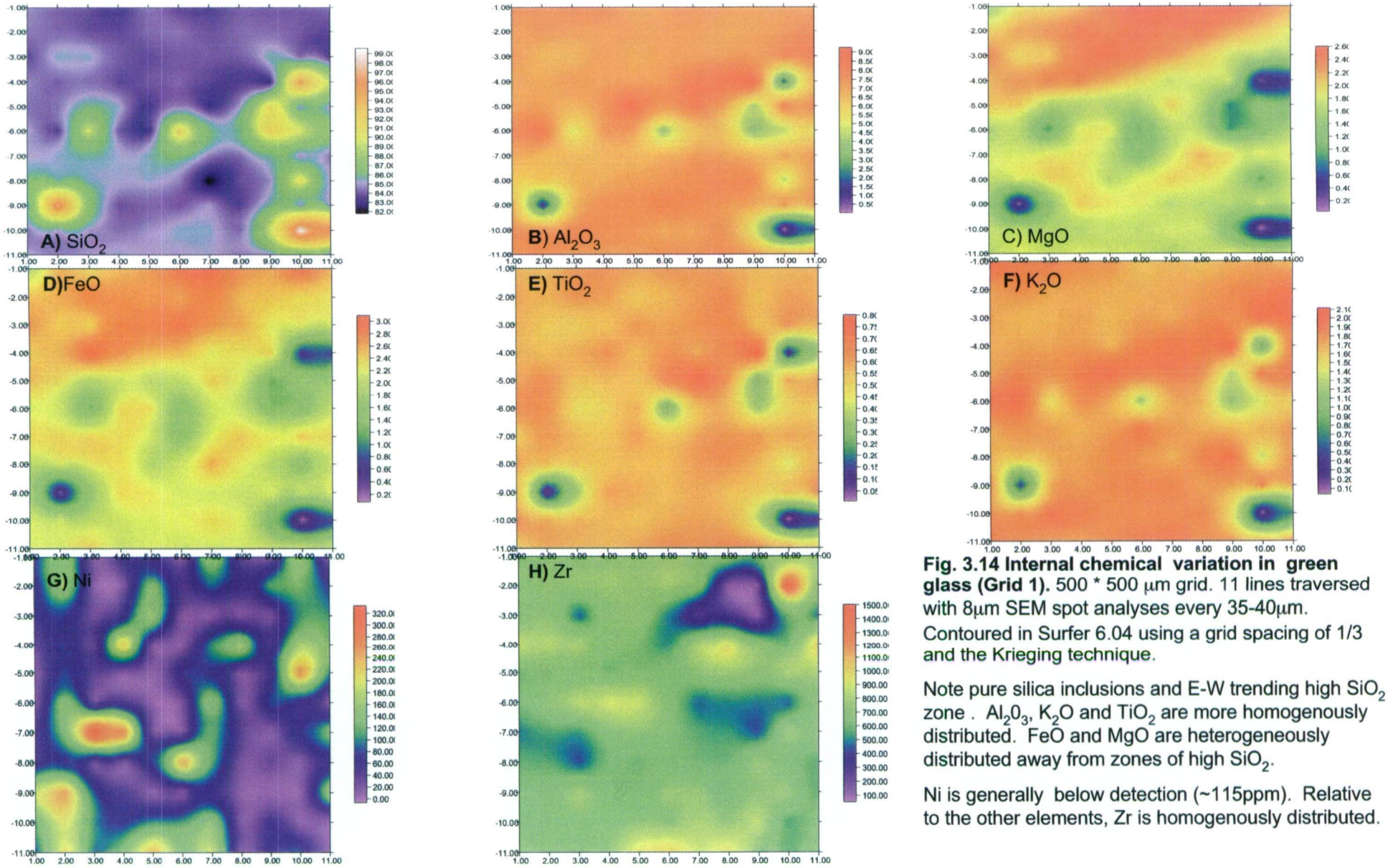

Fig. 3.14 Internal chemical variation in green glass (Grid 1). 500 * 500 μm grid. 11 lines traversed with 8μm SEM spot analyses every 35-40μm. Contoured in Surfer 6.04 using a grid spacing of 1/3 and the Krieging technique.

Note pure silica inclusions and E-W trending high SiO_2 zone . Al_2O_3, K_2O and TiO_2 are more homogenously distributed. FeO and MgO are heterogeneously distributed away from zones of high SiO_2.

Ni is generally below detection (~115ppm). Relative to the other elements, Zr is homogenously distributed.

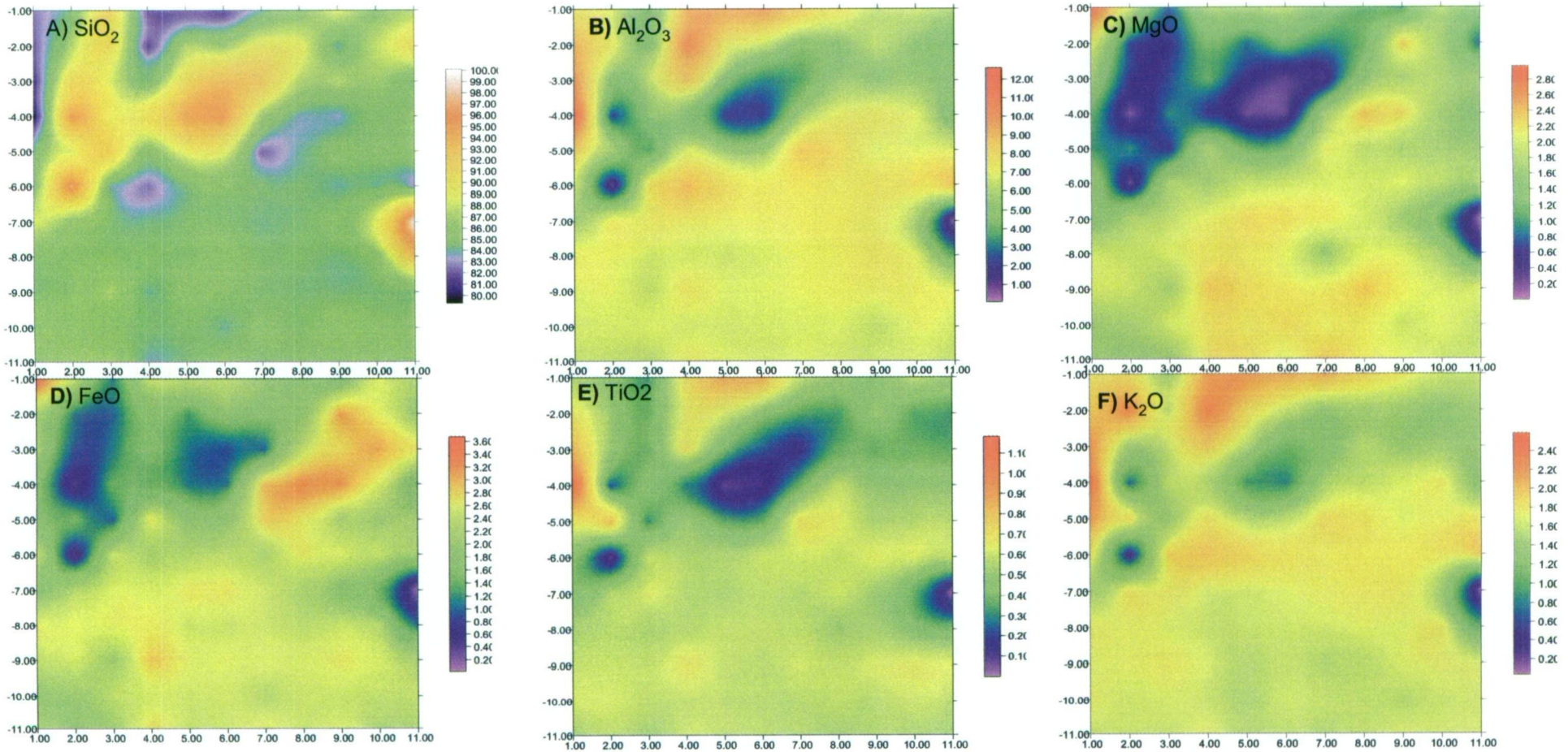

Fig. 3.15 Internal chemical variation in green glass (Grid 2). 500 * 500 μm grid. 11 lines traversed with 8μm SEM spot analyses every 35-40μm.

Contoured in Surfer 6.04 using a grid spacing of 1/3 and the Krieging technique.

Note lenticular shaped high SiO_2 zone. This grid shows a more homogenous distribution of the remaining major elements that appear inversely related to SiO_2 abundance.

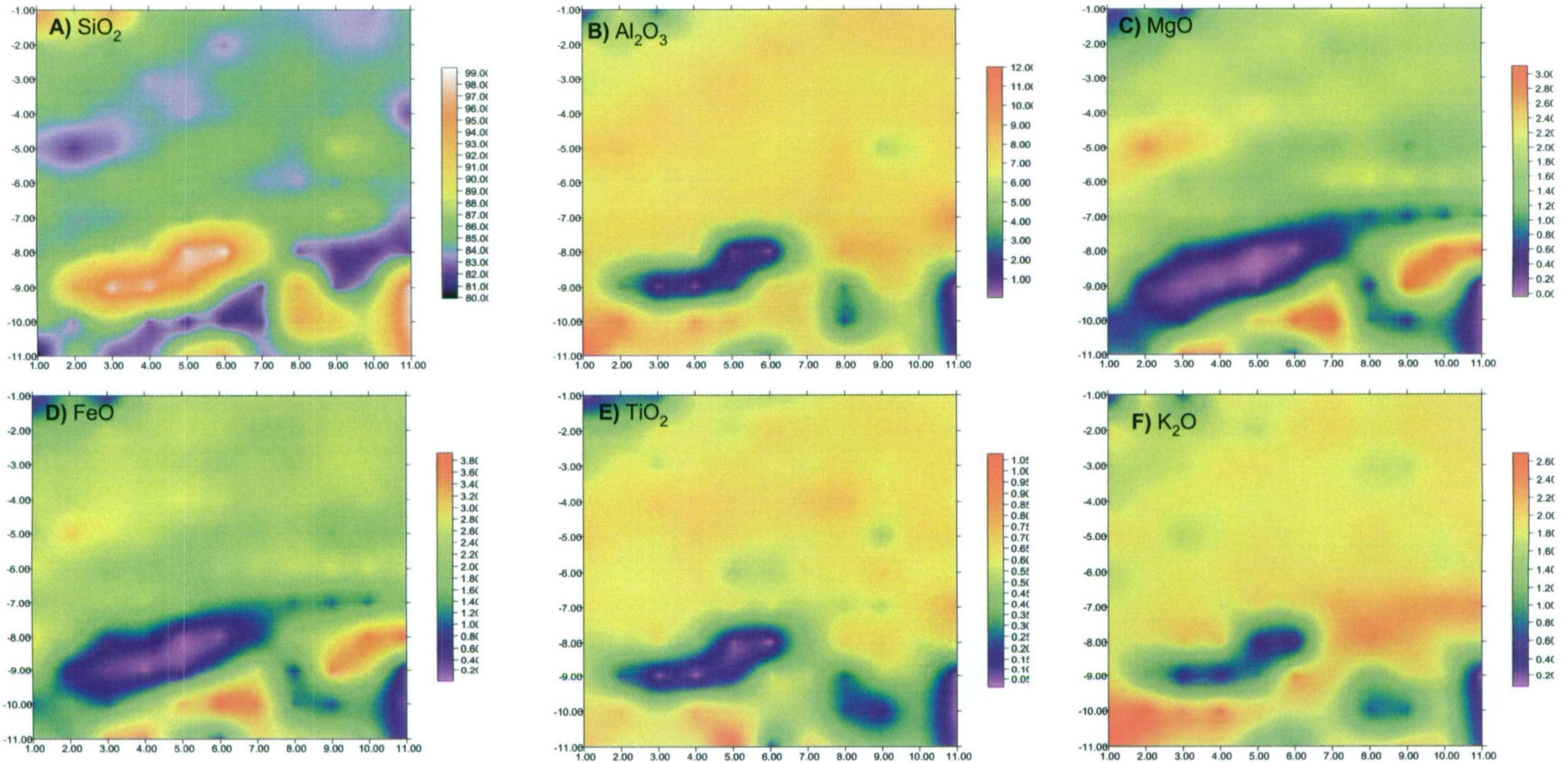

Fig. 3.16 Internal chemical variation in green glass (Grid 3). 500 * 500 μm grid. 11 lines traversed with 8μm SEM spot analyses every 35-40μm.

Contoured in Surfer 6.04 using a grid spacing of 1/3 and the Krieging technique.

Note lenticular shaped high SiO_2 zone, along with E-W trending zones of lower SiO_2 . These low SiO_2 zones correspond to highest FeO, and MgO abundances. Al_2O_3, K_2O and TiO_2 are relatively homogenously distributed away from the high SiO_2 zones.

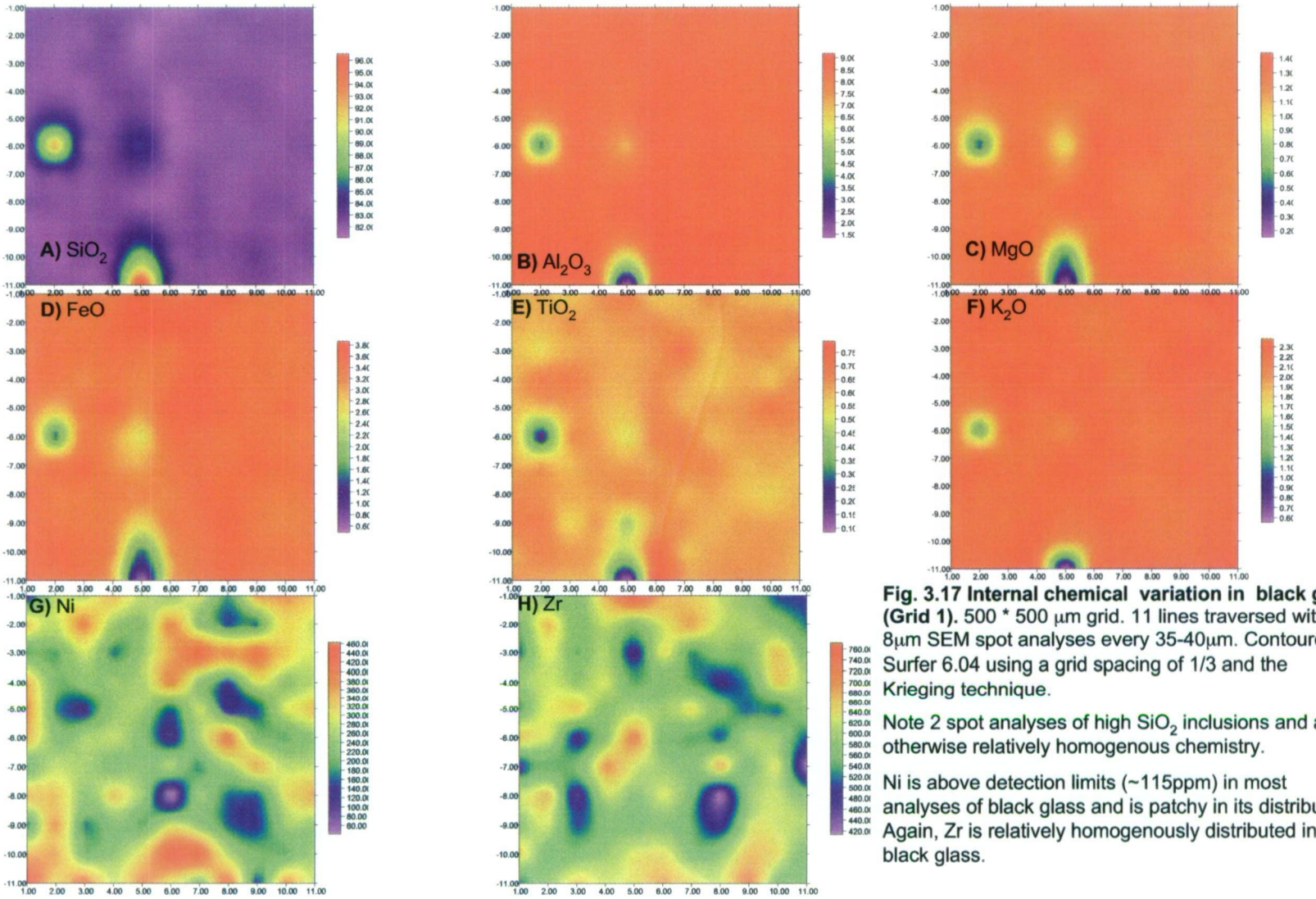

Fig. 3.17 Internal chemical variation in black glass (Grid 1). 500 * 500 μm grid. 11 lines traversed with 8μm SEM spot analyses every 35-40μm. Contoured in Surfer 6.04 using a grid spacing of 1/3 and the Krieging technique.

Note 2 spot analyses of high SiO_2 inclusions and an otherwise relatively homogenous chemistry.

Ni is above detection limits (~115ppm) in most analyses of black glass and is patchy in its distribution. Again, Zr is relatively homogenously distributed in black glass.

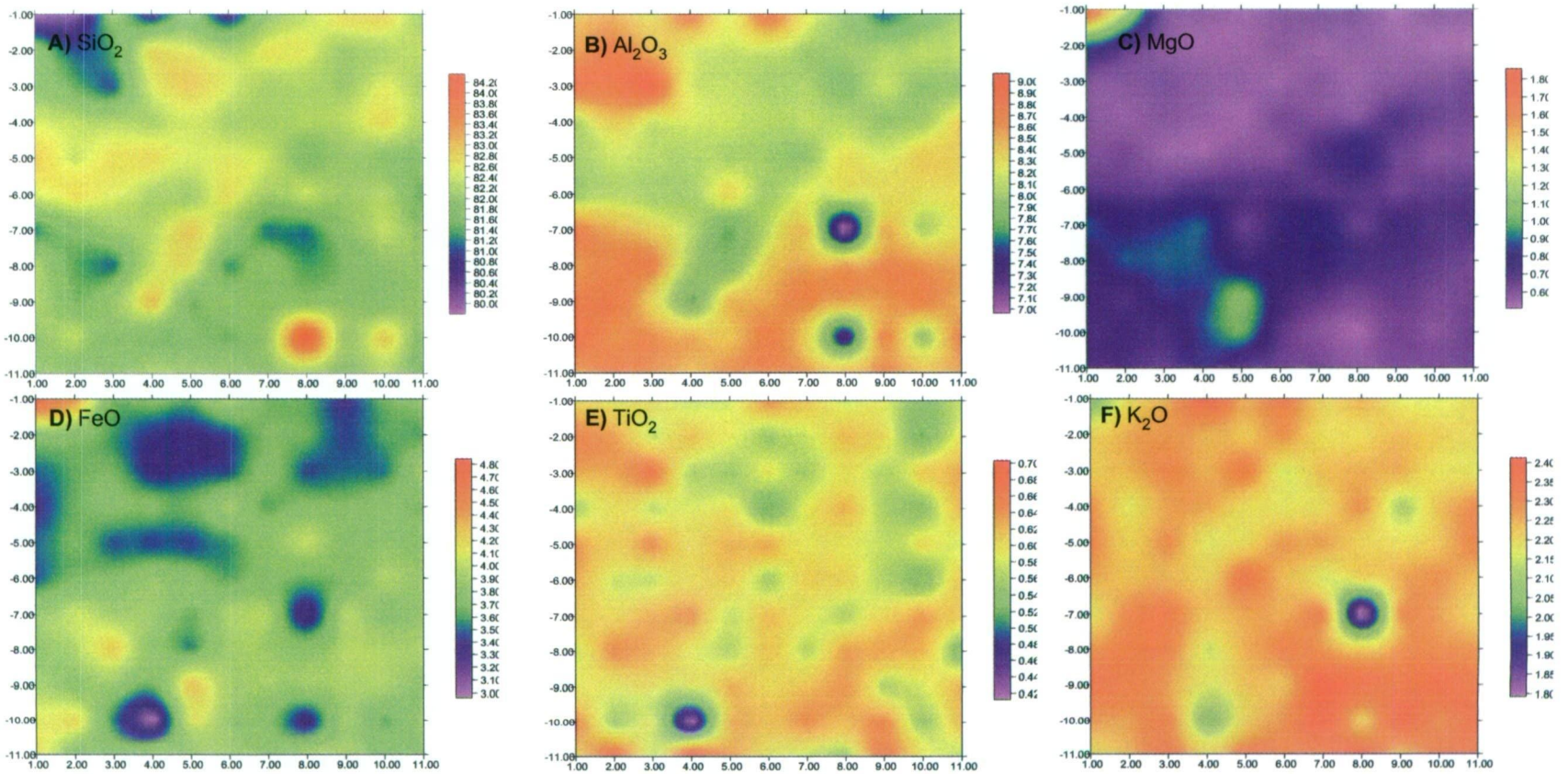

Fig. 3.18 Internal chemical variation in black glass (Grid 2). 500 * 500 μm grid. 11 lines traversed with 8μm SEM spot analyses every 35-40μm. Contoured in Surfer 6.04 using a grid spacing of 1/3 and the Krieging technique.

Note isolated analyses of a pure silica inclusion and SW-NE trending zone of slightly increased SiO_2. The remaining major elements are least abundant along this high SiO_2 zone but are otherwise relatively homogenously distributed when compared to green or white glass.

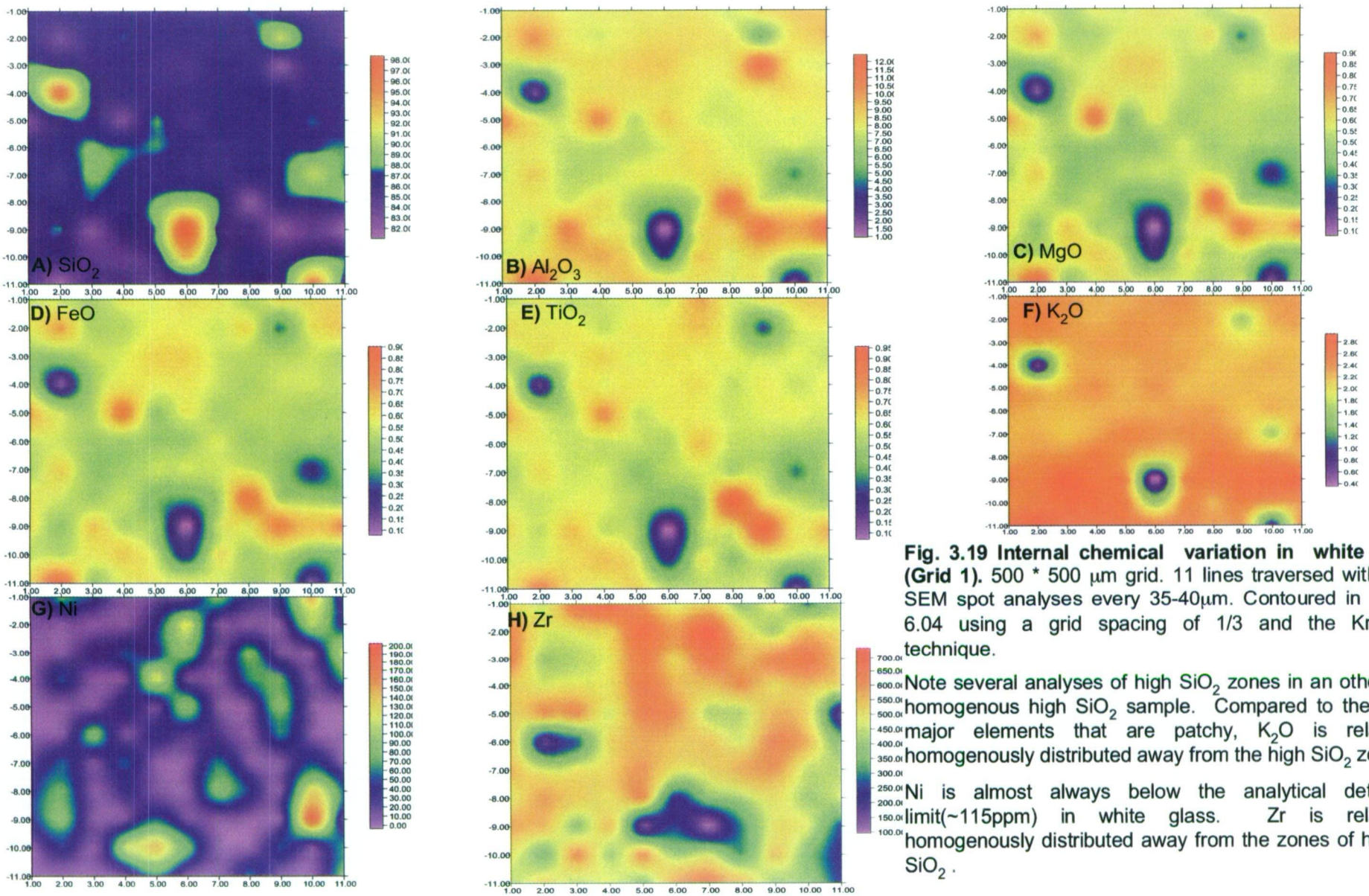

Fig. 3.19 Internal chemical variation in white glass (Grid 1). 500 * 500 μm grid. 11 lines traversed with 8μm SEM spot analyses every 35-40μm. Contoured in Surfer 6.04 using a grid spacing of 1/3 and the Krieging technique.

Note several analyses of high SiO_2 zones in an otherwise homogenous high SiO_2 sample. Compared to the other major elements that are patchy, K_2O is relatively homogenously distributed away from the high SiO_2 zones.

Ni is almost always below the analytical detection limit(~115ppm) in white glass. Zr is relatively homogenously distributed away from the zones of highest SiO_2.

again the variation defines distinct zones or layers of 1-2 percent variation that are outside of that expected due to analytical uncertainty. FeO (Figs. 3.14-3.16D) and MgO (Figs. 3.14-3.16C) in green glasses show large compositional variation away from the zones of almost pure silica. This variation defines irregular non-layered zones of high FeO and MgO across areas up to 250μm across.

3.3.1b Major element internal variation in Black glass

In the black glasses the very high silica zones are confined to 2 single analytical points on grid 1 (Fig. 3.17A). Away from the almost pure silica inclusions the SiO_2 is homogeneously distributed across grid 1. Black grid 2 shows compositional zoning and heterogeneity in SiO_2 in the form of layered bands and pods, however this variation totals less than 5 percent (Fig. 3.18A). The remaining major elements show little variation in black grid 1 (Figs 3.17B-F). In black grid 2, a distinct band of lower Al_2O_3 is evident (Fig. 3.18b). FeO is patchily distributed across black grid 2 (Fig 3.18D), while MgO, K_2O, and TiO_2 show little variation (Fig. 3.18C,E,F)

3.3.1c Major element internal variation in White glass

The white glass grid shows several inclusions of almost pure silica, in a relatively homogenous high silica background averaging around 86% SiO_2 (Fig. 3.19A). Away from the high silica zones K_2O is evenly distributed across the white grid (Fig. 3.19F). The remaining major elements appear patchily distributed across the grid and define small regions of around 100μm across in which the range in major element concentrations may vary by between 1 and 4 percent of the mean.

3.3.2 Trace element internal variation

The range in Ni and Zr compositions across the grids analysed on green, black and white glasses are presented in table 3.17. Ni is present at below the limits of detection for most analyses on green and white glass, and the average Ni values are highest in black glass (269 ppm). The range in analysed Ni abundance is up to 614, 466 and 175 % of the mean in white, green and black glasses, respectively.

Grid	n =	Ni	Ni Sd	Zr	Zr Sd
White 1	121	1 - 210 (34)	44	70 - 753 (492)	132
Green 1	121	1 - 358 (76)	79	58 - 1550 (671)	188
Black 1	121	1 - 473 (269)	93	393 - 784 (588)	67
Average Darwin glass		161		433	

Table 3.17 Range and average trace element composition for white, green and black glass fragments. Showing standard deviation (Sd) in analyses. Data determined by SEM grid surveys previously described. Standard deviations for Ni analyses in green and white glass are lower than for black glass but this is a statistical artefact that reflects the fact that most analyses in white and green glass are below detection (115ppm). The lesser standard deviations in Zr analytical results for the low SiO_2, high Ni, black glass indicates that the black glass is more homogenous than the green or white glass. This further supports the existence of a low SiO_2, relatively homogenous, glass population as suggested by the cluster analysis (Group 2).

Analysed Zr also shows large variation across the analysed grids and varies by 238, 138, and 66 % of the mean in green, white and black glass respectively. Again this indicates that the black glass is less heterogeneous than the green or white glass. The nature of the heterogeneity in internal Ni and Zr abundance revealed by the grid traverses is shown in grided plots described below (Figs. 3.14G,H; 3.17G,H; 3.19G,H).

3.3.2a Internal variation in nickel abundance in green, black and white glass

In all grids (Figs. 3.14G; 3.17G; 3.19G) nickel is patchily distributed and the transition between higher than average and lower than average Ni abundance is sharp. In the black glass Ni is distributed in lenticular shaped areas across several hundred microns. In green and white glass, high or above detection limit Ni abundance is confined to smaller areas and usually represents single spots only. Standard deviations for Ni analyses in green and white glass are lower than for black glass, but this is a statistical artefact that simply reflects the fact that most analyses in white and green glass are below detection.

3.3.2b Internal variation in zirconium abundance in green, black and white glass

Zirconium is comparatively homogeneously distributed across the green (Fig. 3.14H) and white grids (Fig. 3.19H) with the exception of regions of very low Zr that must be the site of almost pure silica inclusions as these spots are also very low in Ni abundance. In the black glass (Fig. 3.18H) Zr is patchy in distribution and occurs in irregular lenses up to approximately 100μm across. The greater homogeneity of black glass relative to green and white glass is reflected in standard deviations for Zr analyses, which equal 132, 138, and 67 in white, green and black glass, respectively.

3.3.3 Spatial relationships in internal trace element variation

The zones of highest Zr abundance are not the zones of lowest Ni content. In the black glass grid the regions of highest Ni and Zr abundance largely overlap. In the grid traverses on green and white glass the spatial relationship between the Ni and Zr distribution is less clear but there are zones where these elements are

simultaneously high in abundance. This is likely to reflect the influence of very high silica regions in the glass and suggests that incomplete mixing rather than selective solidification controls the distribution of Ni and Zr and presumably the remaining trace elements.

3.3.4 Implications of internal geochemical heterogeneity on group classification

The grid surveys confirm the existence of a very heterogeneous, high silica population of glasses (Group 1) that are predominantly dark to light green. The cluster analysis subdivision of Group 1 glass into Groups 1a and 1b, on the basis of Ni, Co and Cr abundances, reflects only the heterogeneity of the distribution of these transition elements (as indicated by Ni) in the glass. Hence, Group 1a and 1b glasses are geochemically identical and there is no need for subdivision of Group 1 glass. The grid traverse on the black glass fragments support the cluster analysis based definition of a more homogenous, low silica, slightly greater Al_2O_3, high FeO, Ni, Co and Cr population in the Darwin glass strewn field. The grid surveys do not show the same MgO enrichment in these glasses, and this may reflect the heterogeneity of MgO composition across the glass sample. The FeO has a more dominant control on colour variation in the glass. As such, the heterogenous distribution of FeO is consistent with the petrographic observations of dark and light layers in the glass (Chapter 2). The low silica glass assigned to Group 2 is almost always black.

3.3.5 Implications of internal geochemical heterogeneity on the identification of systematic geographical variations in glass chemistry.

The large degree of internal compositional heterogeneity typical of the Darwin glass fragments analysed in this study prevents the identification of systematic chemical variations relative to distance from the suspected source crater at this stage and with the current number of analyses. The internal heterogeneity results in all sites having large and overlapping compositional ranges (tables 3.1, 3.7). Mean values for the determined elements are similar between all sites and show random variations only across the strewn field (tables 3.1, 3.7). However, Group 2 glass is predominantly black; such physical characteristics of recovered glass fragments will be related to distance and direction from the crater later in Chapter 6.

3.4 Conclusion

The average major element composition of Darwin glass is: SiO_2 (84.57%), Al_2O_3 (7.52%), TiO_2 (0.57%), FeO (2.55%), MgO (1.12%), K_2O (1.87%), CaO (0.06%), and Na_2O (0.05%). The glass is heterogeneous in major element composition. SiO_2 is particularly variable and may range between 80 to 94% in a single sample. Inclusions of almost pure silica (lechateliertie) are also commonly found in the glass. In green glasses, these lechatelierite inclusions may be several hundred microns long and form elongate lenses and layers. In the black glasses they form more isolated inclusions. FeO content predominantly controls the colour variation in the glass. On the basis of major element composition the white and green glass is more heterogeneous than black glass samples. The trace element composition of Darwin glass is also highly variable and particularly the transition elements Ni, Co and Cr. The <5mm splashform shaped mini-glasses have almost identical major element composition to the larger, irregular glass fragments. However, the average mini-glass is enriched in Cr, Co and Ni relative to larger glass fragments and shows more pronounced LREE enrichment.

Despite the compositional heterogeneity across the Darwin glass sample, two populations can be defined. Group 1 is close to average Darwin glass. The range in major element composition of Group 1 glass is: SiO_2 (80.62 – 93.9%), Al_2O_3 (3.14 – 10.6%), TiO_2 (0.2 – 0.76%), FeO (0.8 – 4.23%), MgO (0.25 – 2.31%) and K_2O (0.7 – 2.7%). Group 2 glass is lower in average SiO_2 (81.16%) and less variable in the range in SiO_2 composition (76.47 – 84.42%). Average Al_2O_3 (8.2%) in Group 2 glass is also greater than in Group 1 glass. Group 2 glasses are significantly enriched in FeO (+ 1.53 %), MgO (+ 1.31 %) and Ni, Co and Cr relative to average Darwin glass.

The trace element data for all Darwin glass samples show affinity with upper crustal sediments, including pronounced negative Eu anomalies ($Eu/Eu^* = 0.48 – 0.66$) and LREE enrichment (chondrite normalised La/Lu = 5.8 – 8.87). A PCA performed on the entire glass sample indicates that over 97% of the entire compositional variation in Darwin glass can be explained on a single axis or as being between two compositional end members. Plots of SiO_2/MgO vs. FeO/Al_2O_3, SiO_2/MgO vs.

FeO/K_2O and MgO/TiO_2 vs. Zr/Co show the variation on axis 1 (Fig. 3.13A-C). The end-member compositions are close to average quartz arenite and PAS.

The composition of Group 2 glass requires a source higher in FeO, MgO and Co than average shale (PAS). Group 2 glass is also enriched in Ni and Cr. The PCA analysis suggests this enrichment may be related a third end-member involved in the formation of the glass. The very high Ni requirements of this end-member are unlike those typical of sedimentary rocks, and this will be an important consideration in discussion of potential target rocks in western Tasmania. The other significant features revealed by the glass analyses that are expected in the target rocks are the absence of plagioclase feldspar and the very low abundance of Sr. These relationships will form the basis for discussion of the relationship between Darwin glass and suspected targets rocks from Darwin Crater in Chapter 5.

Chapter 4

Darwin Crater

While searching topographic maps and air photos for an impact crater that produced Darwin glass, R.J. Ford (University of Tasmania) noticed a circular depression at 42°18.39's, 145° 39.41'E (Ford 1972; Fig. 4.1). The depression lies close to the apparent southeast edge of the strewn field and was subsequently called Darwin Crater. It has become the assumed source of Darwin glass despite the lack of conclusive evidence for an impact origin. The objectives of this chapter are to 1) describe the local geologic setting and outcrop scale geology at Darwin crater; 2) describe and interpret the sub-surface geology at the crater from recovered drill core; 3) describe and interpret the geochemical characteristics of a suite of rocks cropping out around the crater and sampled from drill core; 4) explain the petrographic and geochemical relationships between the surface and sub-surface geology at the crater and 5) explore potential origins for the structure, based on data presented in this chapter and including discussion of the evidence for diagnostic impact induced shock metamorphism.

4.1 Previous work

After identification of the structure, Ford investigated the geology at Darwin Crater using a combination of aerial photographs and field mapping (Ford 1972, Fudali & Ford 1979). Particularly important information was gained during construction of an access track to the crater that ripped up and exposed fresh bedrock in an otherwise densely vegetated terrain. I have accessed catalogued samples and field notes from Ford's extensive work and have attempted to corroborate his observations during my own field investigations.

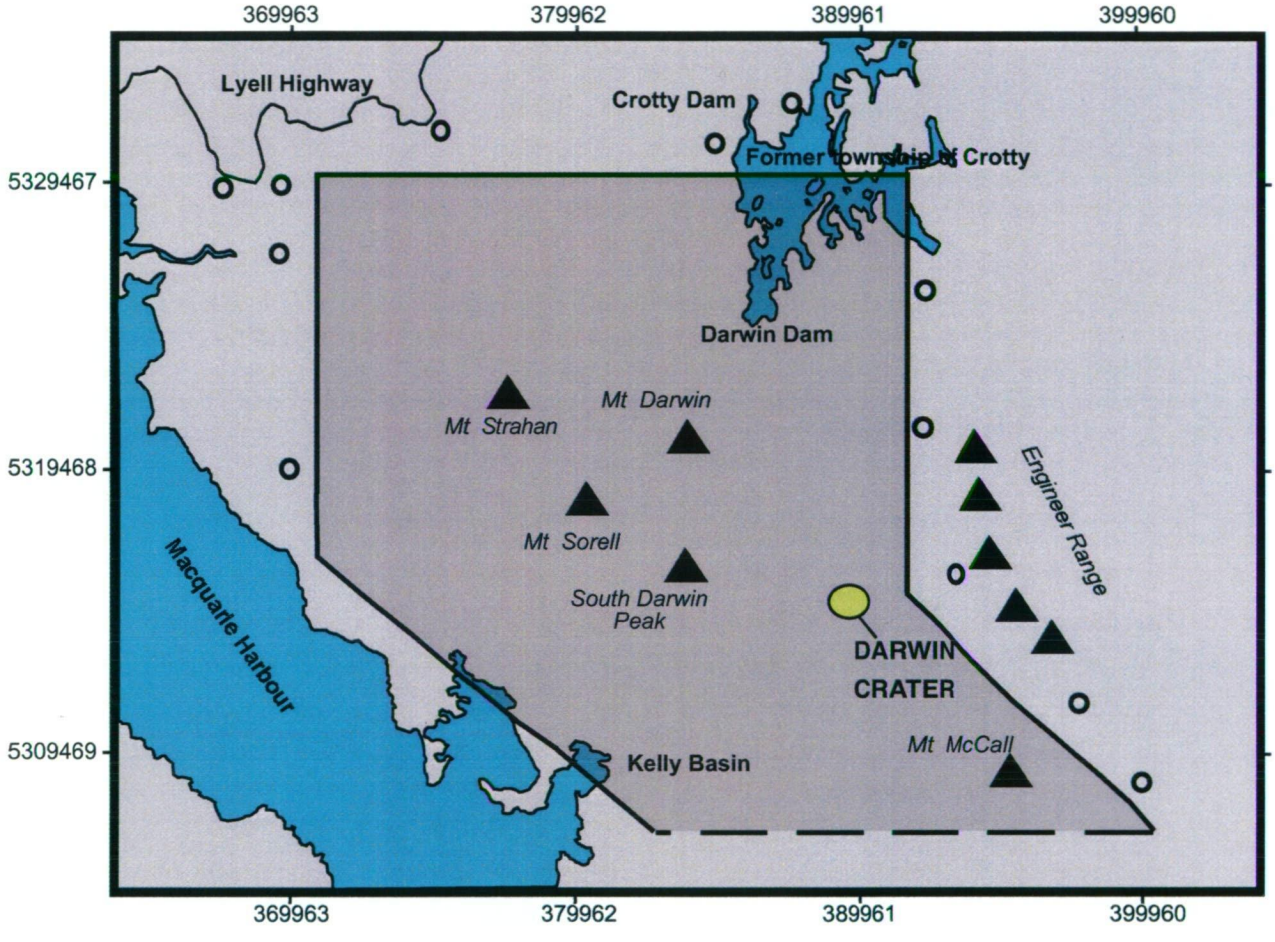

Figure 4.1 Darwin Crater and Darwin glass strewn field. The limits of the field are denoted by the dark shaded area bounded by the black line. Open circles are where residual gravels have been searched and glass is absent. For regional locality see chapter 1.

Since its discovery, a combination of geophysical techniques have been used to describe the subterranean morphology of the structure. Fudali & Ford (1979) conducted a gravity survey and Richardson (1984) combined a gravity survey with magnetic and seismic refraction techniques. Magnetic profiles across the crater show no variation. Bouger anomaly profiles show a low of close to –4 mgal near to the crater centre (Richardson 1984). The modelled gravity data show an asymmetric basin with a maximum depth of 230m to the southwest and a depth to centre of 210m (Richardson 1984).

The seismic refraction survey was conducted along two lines across the crater at right angles to each other. Data for the seismic refraction survey show a range in velocities from 900 m/sec in the upper 20m of the sub-surface geology to 3000 m/sec at depth (Richardson 1984). Travel-time plots for the seismic data are irregular and this suggests a faulted basin and a heterogeneous stratigraphy. The E-W seismic line provides the most regular travel-time plot and these data suggest a depth at the crater centre of around 180m (Richardson 1984).

In an attempt to understand the nature of the sub-surface geology, the crater structure was drilled in 1975 (DDH1) and again in 1983 (DDH2). In DDH1 bottom of hole was at only 100m, but the later DDH2 penetrated to a depth of 230m. The Hydro Electric Commission conducted the drilling operations during the early stages of the Tasmanian Power Scheme. This scheme proposed to impound the Franklin River and would have flooded the structure to the 220m ASL contour level. In both cases diamond drill holes were sited as close to the centre of the crater as possible and inclined at 15° from the vertical towards the southwest. It is assumed that the rationale behind this inclination was based on the geophysical evidence that shows the basin deepens towards the southwest. Both drill cores penetrated finely laminated, reduced lacustrine sediments to a depth of around 60m and, down to this depth, the holes were cased and recovery was complete. All of these lake sediments are normally magnetised and contain abundant Quaternary pollen. Potentially these lake sediment cores provide a continuous palynological record for much of the Pleistocene, but this remains to be described. The oldest spores and pollen assemblages from the top 20 metres of the lake sediments are dominated by *Largostrobus franklinni* (Huon Pine) and there are also short phases where *Casuarina* and *Eucalyptus* both become important (Colhoun et al. 1988). This indicates that the floral assemblages around Darwin Crater had affinity to modern

temperate rainforest and wet sclerophyll forest when the lake sediments were being deposited.

Below the lake sediments, Fudali & Ford (1979) described 40m of mixed clay, sand and rock fragments from DDH1. At a depth of 100m in DDH1 Ford (1972) found sand-sized pieces of Darwin glass. Ford (1972) suggested that the presence of clay layers amongst the sand and rock fragments indicated that these had been washed into the crater after its formation.

4.2 Local Geology

Darwin Crater is situated on the Queenstown 1: 250 000 scale geological map sheet (Corbett & Brown 1975, Fig. 4.2), which shows significant geological complexity across the area of the strewn field. The general geologic structure of the region surrounding the crater is that of a southeast plunging faulted syncline in Ordovician and Silurian-L. Devonian age rocks overlying Proterozoic orthoquartzites of the Engineer Range to the northeast, and Cambrian volcanic and volcaniclastic rocks to the west. The syncline forms a steep sided, N-S trending, elongate basin that is strongly faulted by a series of cross-cutting normal faults trending NW-SE and SW-NE. Three of the major NE trending faults have cut the Engineer Range and can be observed in outcrop from the Franklin River. One of these faults crosses and predates the crater, and is responsible for the topographic development of the small valley that hosts the crater on the eastern margin of the syncline.

4.3 Stratigraphy

The valley where Darwin Crater lies is a tributary to the larger Andrew River valley. The Andrew River valley has been eroded into Ordovician limestone (Gordon Group). Siliceous conglomerate (Denison Group), unconformably dipping off Proterozoic quartzite of the Engineer Range, forms the east side of the valley, and Silurian quartzite the west. Rocks at the crater are correlates of the Eldon Group; a

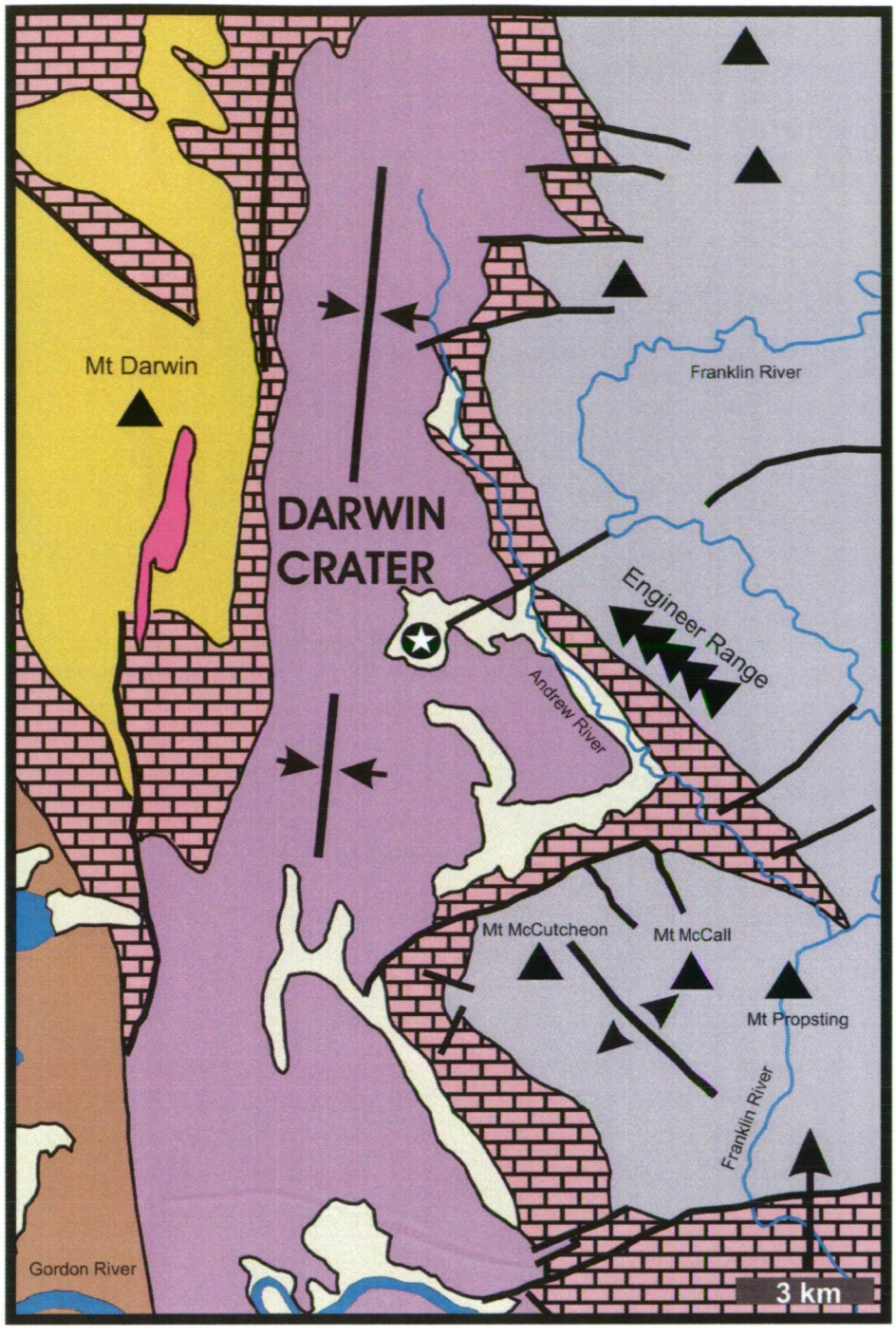

Quaternary: sediments

Tertiary: Undifferentiated gravels of Maquarie Harbour graben

Devonian: granitic rocks

Silurian-L.Devonian: marine sediments (Eldon Group correlates)

Ordovician: Limestone (Gordon Group) and siliceous terrestrial conglomerate, sandstone (Denison Group)

Cambrian: intrusive, extrusive and volcanoclastic sediments (Mt Read Volcanics)

Precambrian: mainly metaquartzite sequences

Fold axes

Fault

Peak

Figure 4.2 Geology of the Darwin glass strewn field.

Based on Corbett & Brown (1975) and Corbett et al. (1993).

succession of low-grade metasedimentary rocks consisting of quartzites and slates. Gould (1866) first named these rocks the 'Eldon Beds' and defined them as the rocks overlying the main limestone succession (Gordon Group) near the mouth of the Gordon and along the Eldon Rivers. Gill & Banks (1950) formally defined the Eldon Group in the Zeehan area and the following formations are recognised: (top) Bell Shale; Florence Sandstone; Keel Quartzite; Amber Slate and Crotty Quartzite (bottom). The Keel Quartzite was initially defined as approximately 250 thick; however, a 60m thick pelite unit was removed from the top of that formation and renamed the Austral Creek Siltstone by Blissett (1962). Interbedded silt is typical of sandstones in the Eldon Group. The laminated siltstones that dominate the Amber Slate are locally associated with thin interbedded calcareous members. Figure 4.3 shows summary stratigraphic columns through the Eldon Group based on Gill & Banks (1950), Blissett (1962), and Banks (1962). To place the crater region in context, Gee et al. (1969) described the transition between the Florence Sandstone and Bell Shale at Horseshoe bend on the Gordon River some 20km south of the crater and the Amber, Florence and Crotty formations outcrop immediately north of the crater.

The metamorphic grade of the rocks is lower greenschist, with the development of aligned micas that define the foliation cleavage of the slate units. In some samples, minor (<2%) chlorite alteration is also observed. This metamorphism is related to widespread deformation during the Devonian that is correlated with the Tabberabberan Orogeny of eastern Australia. In Tasmania this orogeny involved two phases of deformation during the Silurian prior to the intrusion of extensive granitoids during the Devonian. The first phase of movements resulted in folds being developed in closure zones between converging blocks of rock and the distribution of these blocks defined the fold trends (Williams 1989). The second pre-granitoid phase of deformation resulted in a series of northwest and north trending folds (Williams 1989)- including the syncline that Darwin Crater lies in. During the Devonian, intrusive bodies resulted in regional metamorphism of the country rocks. In the Eldon and Gordon Groups conodont Colour Alteration Index (CAI) values average 5, indicating prolonged regional temperatures of 300 - 480°C (Burrett 1992). The Eldon Group is not associated with known economic mineralization, but abundant quartz veining indicates hydrothermal activity during metamorphism.

The nature of the terrain surrounding Darwin Crater, including the limited outcrop offered amongst dense rainforest, prevents the definition of a detailed stratigraphic column through the Eldon Group in this area. In discussing the stratigraphic relations between rocks at the crater, the columns defined by Gill & Banks (1950); Blissett (1962); and Banks (1962), from near Zeehan, north of the crater, are used (Fig. 4.3). Brown (1986) demonstrates the regional applicability of these stratigraphic columns across 1000km^2 of the Dundas Trough, but notes marked fault controlled variability in the thickness of represented formations. The distribution of Eldon Group rocks around Darwin Crater has been determined using a combination of field observations (including Ford's), aerial photographs and published geological maps (Fig. 4.4A,B). The Keel Quartzite, Amber Slate and Crotty Quartzite crop out immediately around the crater and are commonly faulted. These are texturally mature marine sediments lacking feldspars, which is likely to be both a primary depositional feature of these rocks, but may also reflect the metamorphic effects of the Devonian Tabberabberan Orogeny in which micas are expected to have replaced any detrital feldspar originally present. The limited bedrock exposure prevents conclusive determination as to the possible presence of the Austral Creek Siltstone at the top of the Keel Quartzite as for the Eldon Group stratigraphy defined by Blissett (1962) and Blissett & Banks (1962). As such, this formation is only tentatively indicated on the cross section (Fig.4.4B); evidence for the impact melting of an upper pelitic unit (cf. Austral Creek Siltstone) in the Keel Quartzite will be discussed later. Rocks and gravels from around the crater are described below. In total, 29 thin-sections of Eldon Group samples, and 10 grain-mount thin-sections of quartz grains from the glass-bearing gravels, were studied. The petrography of Eldon Group rocks is summarised in tables 4.1A,B. To further characterize the Eldon Group and gravels and to allow for later discussion, fractures in quartz grains were counted and results summarised table 4.2.

4.3.1 Silurian rocks

4.3.1a Crotty Quartzite

A typical sample of Crotty Quartzite is dominantly composed (85%) of clear quartz grains that are typically between 200 and 500 μm in size. Interlocking quartz grains are orientated along poorly developed bedding planes that are defined by interstitial muscovite (10%). Rare (<1%) constituents include fragments of quartzite, zircon and

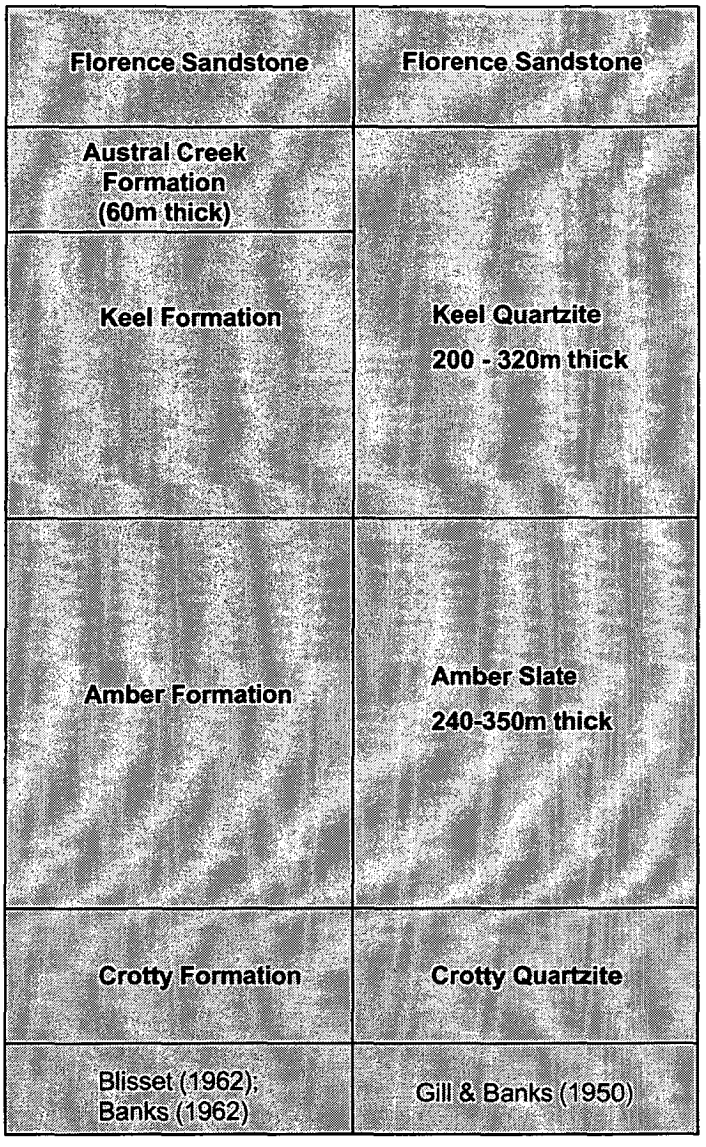

Figure 4.3 Eldon Group stratigraphy. Based on the type section near Zeehan. The dense terrain and limited outcrop around Darwin Crater prevents definition of a locally constrained column.

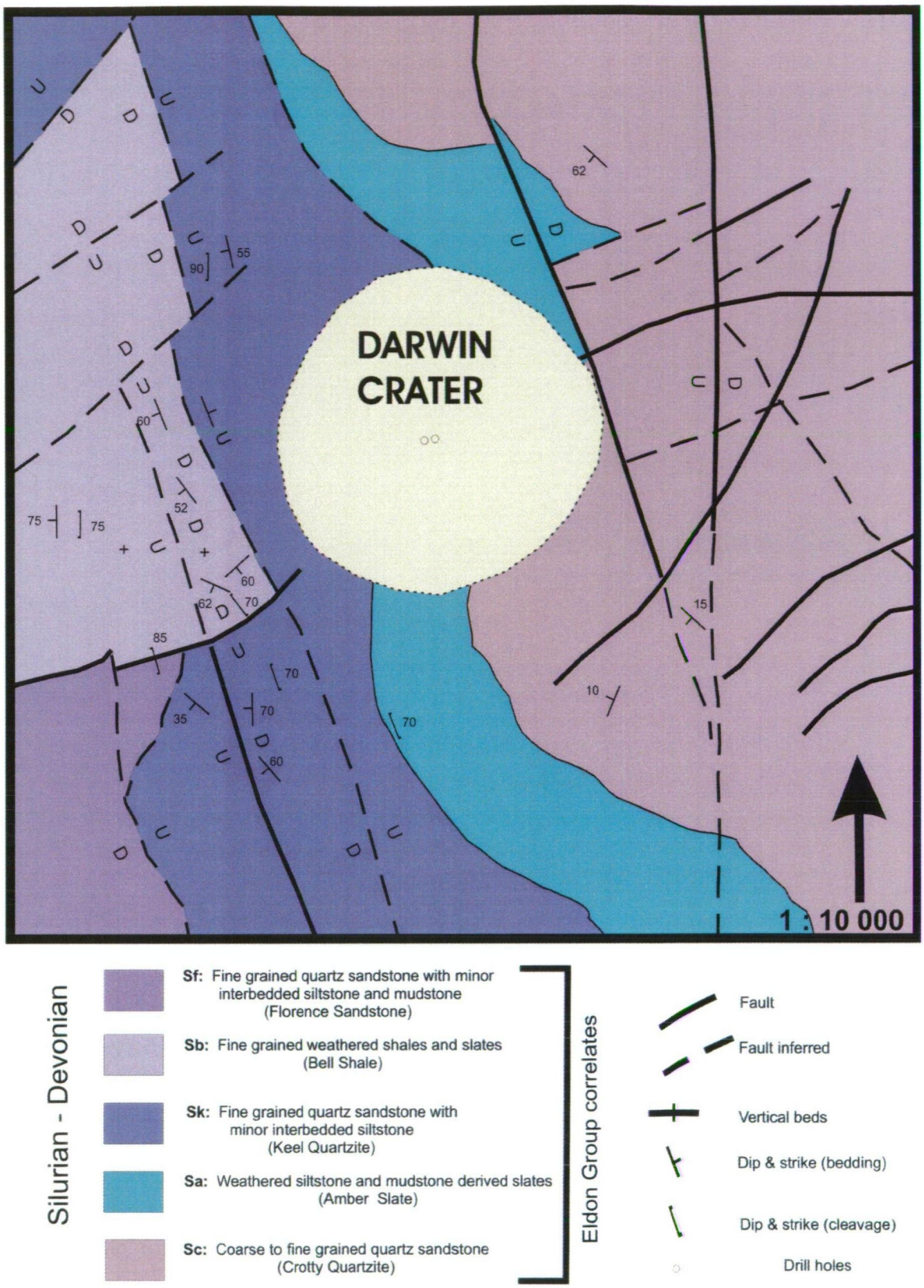

Figure 4.4A Darwin Crater geology. Based on field mapping in this study and by R.J. Ford; 1:25 000 scale aerial photographs; Corbett & Brown (1975); and Corbett et al. (1993).

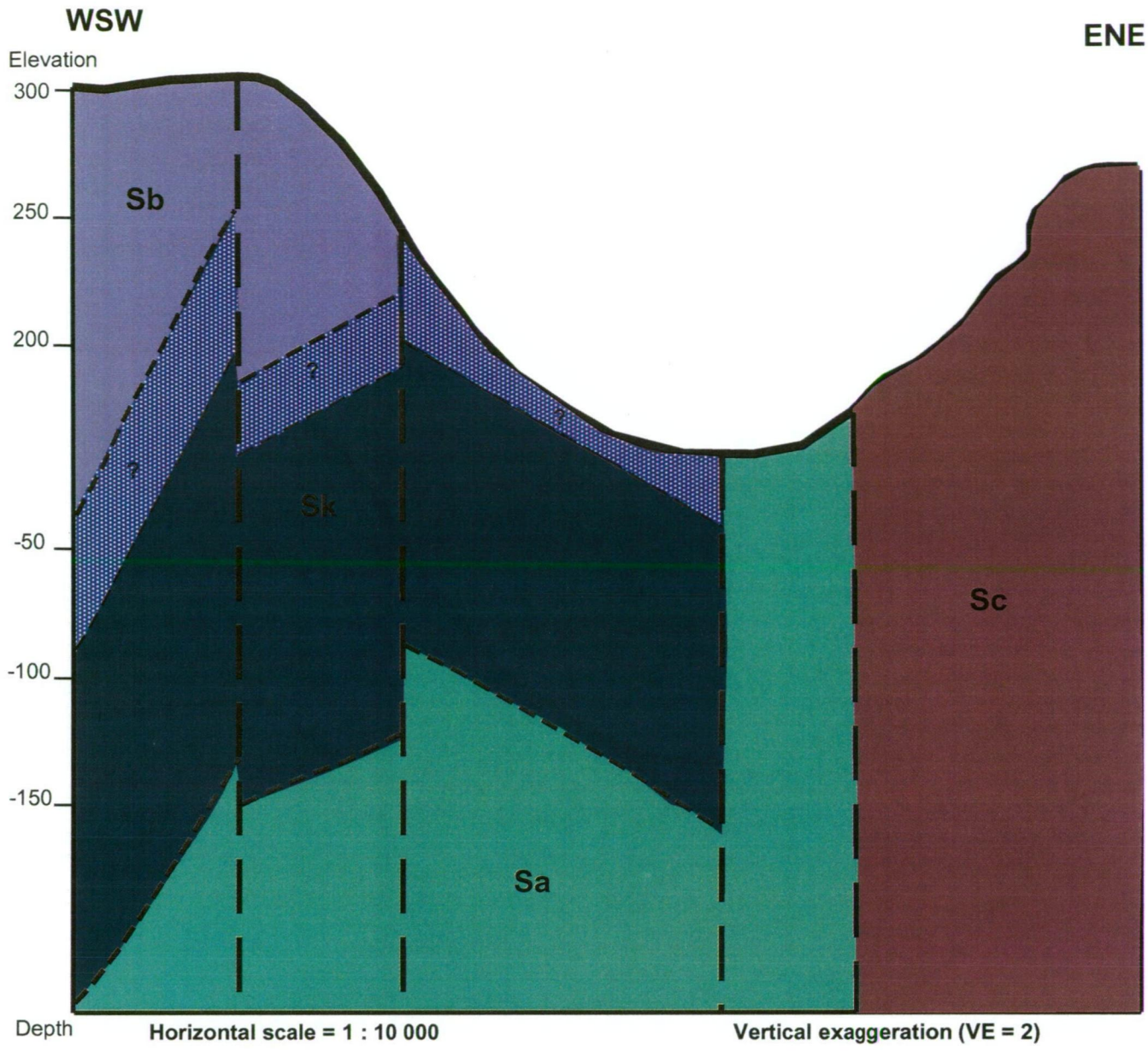

Silurian-Devonian - Eldon Group correlates

Sb: Fine grained weathered shales and slates (Bell Shale)

Sk: Fine grained quartz sandstone with interbedded siltstone (Keel Quartzite). Shaded fill represents siltstone unit that was re-classified as Austral Creek Siltstone by Blisset (1962)

Lithological boundary inferred

Sa: Weathered siltstone and mudstone derived slates (Amber Slate)

Sc: Coarse to fine grained quartz sandstone (Crotty quartzite)

Fault inferred

Figure 4.4B Simplified cross-section across the valley that hosts Darwin Crater. Quaternary cover has been removed and the section is based on surface outcrops and strike trends in the Eldon Group rocks. This simplified section represents the pre-impact or target rock stratigraphy.

tourmaline grains with matrix materials comprising the remaining 4% of typical samples. Approximately 33% of the quartz grains in samples collected from outcrop at and away from the crater show undulose extinction. Of the total quartz grains studied in thin section, around 4% have weakly developed single fractures – these are coarse and non-planar indicating a tectonic origin. Matrix material is composed predominantly of quartz (80%) and mica (15%) up to 20μm in size. The formation also contains minor granule and pebble conglomerate beds. In outcrop cross bedding can be seen in the sandier units of the formation. Fig. 4.5A,B shows the Crotty Quartzite in thin section.

4.3.1b Amber Slate

Originally dominated by laminated quartz silt, this rock has been sufficiently metamorphosed to produce a slatey cleavage and is now a pelite. Typical samples are composed of monocrystalline quartz grains (~55%) and minor muscovite (4%) with very rare opaques (<<1%) in a fine matrix (40%). The quartz grains are typically clear, less than 40μm in diameter and slightly angular in shape. In the studied samples, around 26% of the quartz grains show undulose extinction and around 10% contain single, widely spaced fractures. The remaining quartz grains are monocrystalline, non-undulose and free of fractures. The matrix is composed of aligned micas (60%) and quartz (30%) up to 20μm in size, minor Fe-clays (5%) and chlorite (3%). Associated thin units of calcareous siltstones are not seen in outcrop at Darwin Crater but may be present at depth. Amber Slate can be seen in thin section in Fig. 4.5C-D.

4.3.1c Keel Quartzite

Most of the formation was originally a quartz arenite that is now recrystallised to a quartz rich psammite. Typical samples are predominantly composed of rounded and interlocking quartz grains (~80%) usually less than 125μm in diameter. Muscovite comprises around 20% of grains in the studied thin sections and typically exists in discontinuous bands that suggest some deformation. Magnetite, zircon and tourmaline are all very minor (0.5%) constituent. The quartz grains are clear and around 26% of those studied show undulose extinction. Approximately 10% of quartz grains contain a single, generally irregular fracture. The remaining grains are

	Amber Slate				Keel Quartzite				Crotty Quartzite		
Sample	66024	66015	66014	**Average**	66031	66030	66013	**Average**	66027	2002	**Average**
Clast composition (vol%)											
Monocrystalline Quartz											
Non-undulatory	49.8	46.1	48.1	**48.0**	55.0	36.5	52.2	**47.9**	52.2	47.5	**49.8**
undulatory	0.6	0.6	3.8	**1.7**	19.9	28.9	18.0	**22.3**	23.8	33.3	**28.5**
1 fracture	3.5	2.5	3.5	**3.2**	4.0	12.0	8.0	**8.0**	6.3	1.9	**4.1**
2 fractures		0.0	0.0	**0.0**	0.0	1.0	0.6	**0.5**	0.3	0.2	**0.3**
3 or more fractures	0.0	0.0	0.0	**0.0**	0.0	0.3	0.0	**0.1**	0.0	0.0	**0.0**
Polycrystalline quartz					1.0	0.7	0.3	0.6	0.9	4.3	2.6
Total quartz	**54.0**	**49.2**	**55.4**	**52.9**	**79.8**	**79.4**	**79.1**	**79.4**	**83.4**	**87.2**	**85.3**
Other minerals											
Muscovite	3.2	3.8	4.8	3.9	18.7	17.6	11.6	16.0	11.3	8.7	10.0
Opaques		0.6	0.6	0.6	0.3	0.7	0.3	0.4	0.3	0.2	0.3
Matrix	43.0	44.8	37.9	41.9	0.3	0.3	0.3	0.3	0.9	3.9	2.4

Table 4.1A Clast composition in Eldon Group rocks from Darwin Crater. For each sample, one thin section considered representative of the lithology was selected for detailed point counting. For each analysed thin section, 300 grains were counted in 3 passes (900 grains in total).

	Amber Slate				Keel Quartzite				Crotty Quartzite		
Sample	66024	66015	66014	**Average**	66031	66030	66013	**Average**	66027	2002	**Average**
Matrix composition (vol%)											
Mica	60.0	60.0	60.0	**60.0**	10.0		10.0	**10.0**		10.0	**10.0**
Quartz	30.0	30.0	30.0	**30.0**	80.0		80.0	**80.0**		80.0	**80.0**
Fe-Clays	5.0	5.0	5.0	**5.0**	trace	trace	trace		trace	trace	**trace**
Kaolinite											
Chlorite	3.0	3.0	3.0	**3.0**	trace	trace	trace		trace	trace	**trace**

Table 4.1B Matrix composition in Eldon Group rocks from Darwin Crater. Matrix composition determined by X-Ray Diffraction (XRD) at Mineral Resources Tasmania, by Mr Ralph Bottril.

		Monocrystalline quartz				
				No. of fractures		
		Non-undulatory	Undulatory	1	2	3 or more
	Sample	(%)	(%)	(%)	(%)	(%)
	66024	92.3	1.2	6.5	0.0	0.0
Amber Slate	66015	93.6	1.3	5.1	0.0	0.0
	66014	86.8	6.9	6.3	0.0	0.0
	Average	**90.9**	**3.1**	**6.0**	**0.0**	**0.0**
	66031	68.9	24.9	5.5	0.0	0.0
Keel Quartzite	66030	46.0	36.4	15.1	1.3	0.4
	66013	66.8	22.8	10.2	0.8	0.0
	Average	**61.7**	**26.0**	**10.1**	**0.7**	**0.1**
	66027	62.5	28.5	7.5	0.4	0.0
Crotty Quartzite	2002	54.4	38.1	2.2	0.3	0.0
	Average	**58.5**	**33.3**	**4.9**	**0.3**	**0.0**

Table 4.2 Petrography of monocrystalline quartz in Eldon Group samples from Darwin Crater.

Determined by point counting. Here the observations of quartz grains with, for example, one fracture is expressed as a percentage of the total number of monocrystalline quartz grains. The majority of quartz grains show no evidence for any deformation beyond the level the regional metamorphic grade expected in Eldon Group rocks across western Tasmania.

monocrystalline and apparently non-deformed. The matrix is composed of aligned quartz (80%) and mica up to 20μm in size. The Keel Quartzite surrounding the crater is associated with thin, interbedded finer grained beds that petrographically are indistinguishable from the quartzose pelites of the Amber Slate. Ford (unpublished notes) described a thin sulphide vein in a ripped up sample of the Keel Quartzite uncovered on the access track to the structure. Figure 4.5E-H shows the Keel Quartzite in thin section.

4.3.2 Quaternary sediments

4.3.2a Blocky talus

Mass wasting derived talus exists on and below hills to the southwest of the crater. This talus consists of loose quartzite blocks up to 1m across that can be seen to be detaching actively from cropping out bedrock on the flanks and tops of steep hills. Thin sections of these blocks show non-deformed interlocking quartz crystals.

4.3.2b Glass-bearing angular quartz gravels

Extensive gravel deposits are present on the western side of the crater, typically below peat. These gravels are very poorly sorted and consist of abundant angular quartz pebbles and minor quartzite and slate fragments. In places quartz fragments can be seen to be actively weathering out from veins in the adjacent country rock as described in Chapter 2. Glass is abundant in these gravels, especially the small, aerially shaped mini glasses that are rarely found in the residual gravels away from the crater. After sieving to remove the clay fraction, grain mount thin sections of quartz grains between 250 and > 64 μm size were prepared. The thin sections reveal that many of the quartz grains are highly fractured and deformed. More than 50% of the quartz grains have 2 or more fractures including over 40% with 3 or more. These fractures are generally irregular to sub-parallel, with fractures tending to cut the entire grain and contacts between the fractures are sharp.

An average of around 6% of quartz grains in the studied 64-250μm sub-sample show extreme deformation that has produced sharp, closely spaced (<5μm) fractures.

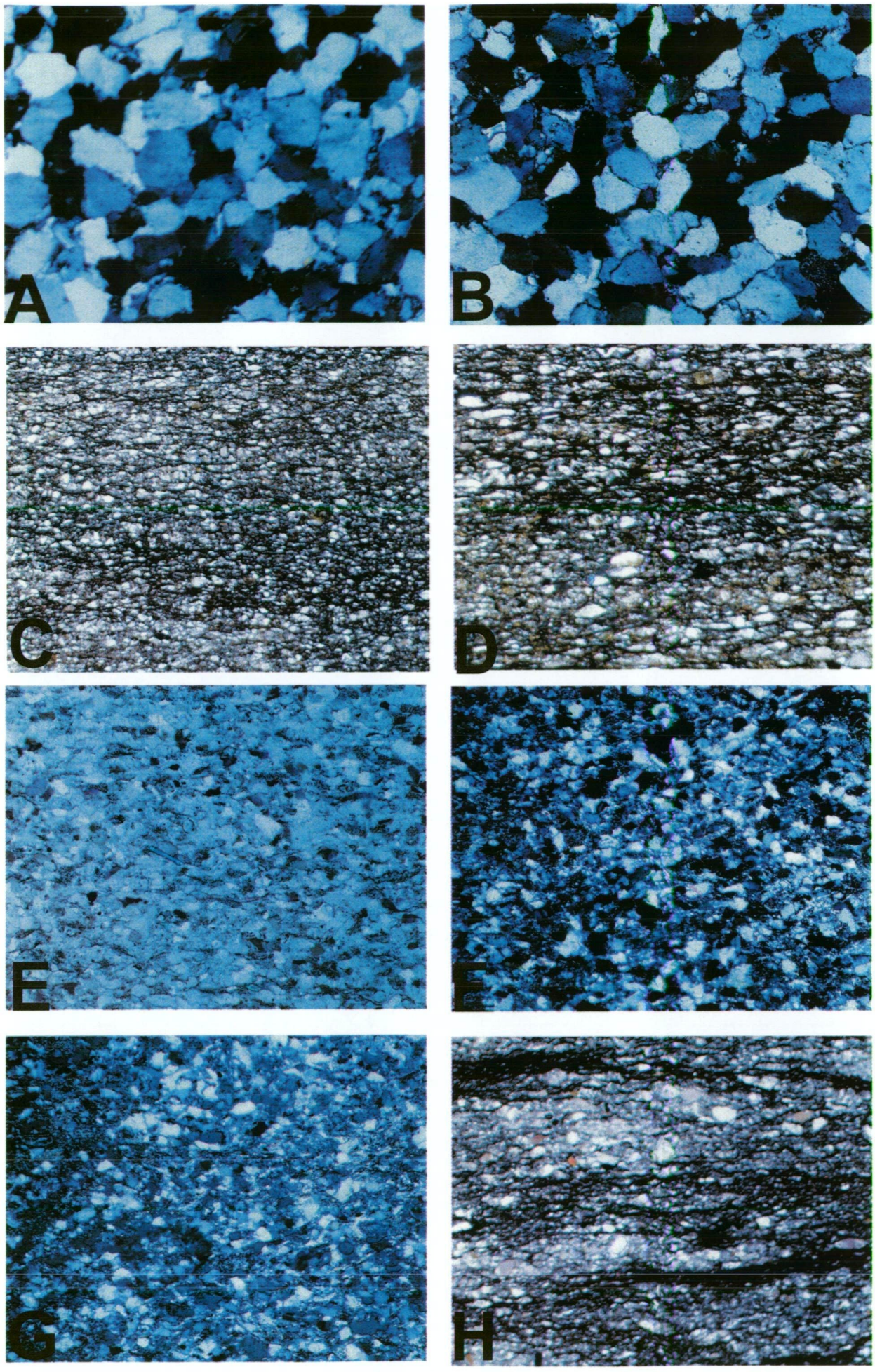

Figure 4.5A-H Outcrop samples of Eldon Group [suspected target] rocks

A) Crotty Quartzite, XPL. FOV=2.2mm; B) Crotty Quartzite, XPL. FOV = 2.2mm;
C)Amber Slate PPL. FOV = 2.2mm; D) Amber Slate XPL. FOV = 2.2mm;
E) Keel Quartzite, PPL. FOV = 2.2mm; F) Keel Quartzite, XPL. FOV = 2.2mm;
G) Keel Quartzite, XPL. FOV = 2.2mm; H) Peletic sample of Keel Quartzite, PPL. FOV = 2.2mm.

These fractures are parallel but not planar, rather the fractures tend to define curved arcs and the fractures almost always pervade the entire quartz grain. Under cross-polarized light these fracture planes separate alternating domains of different extinction. The alternating black-white zones appear superficially as twinning, and for the purposes of discussion grains showing this distinct extinction pattern are referred to as 'twinned' quartz. In rare grains the fracture planes have 2 distinct orientations with high angle inersections. Larger quartzite blocks from the same location are composed of interlocking and fracture free quartz grains. The representative varieties of fractures in quartz grains from these glass-bearing gravels are shown in Fig. 4.6A-Z.

4.4 Crater surface morphology

The surface expression of the crater is initially confusing when visited. As the western edge of the depression is reached it appears as if one is walking down the crater rim to its floor. From the crater floor it initially appears that the crater walls are preserved and outcropping. However, these ramparts are fault controlled and unrelated to the depression. Rather it is only the flat, approximately 1.2km wide, circular floor of the valley that is the surface expression of the crater. This morphology derives from the filling in of a circular depression that is apparently almost exactly as wide as the valley it is contained in and represents an almost closed basin of deposition. Digital elevation models of the surface form of the depression and surrounding rocks are presented in Fig. 4.7A,B.

4.5 Drill core stratigraphy

Core DDH2 has been logged in detail from a depth of 60m (immediately below the laminated lake sediments) to total depth at ~230m. DDH1 has also been re-logged in detail from 60m to total depth at ~100m. In DDH1, the sample recovery throughout the 40m of mixed clay, sands and rock fragments was typically <20%. Recovery was

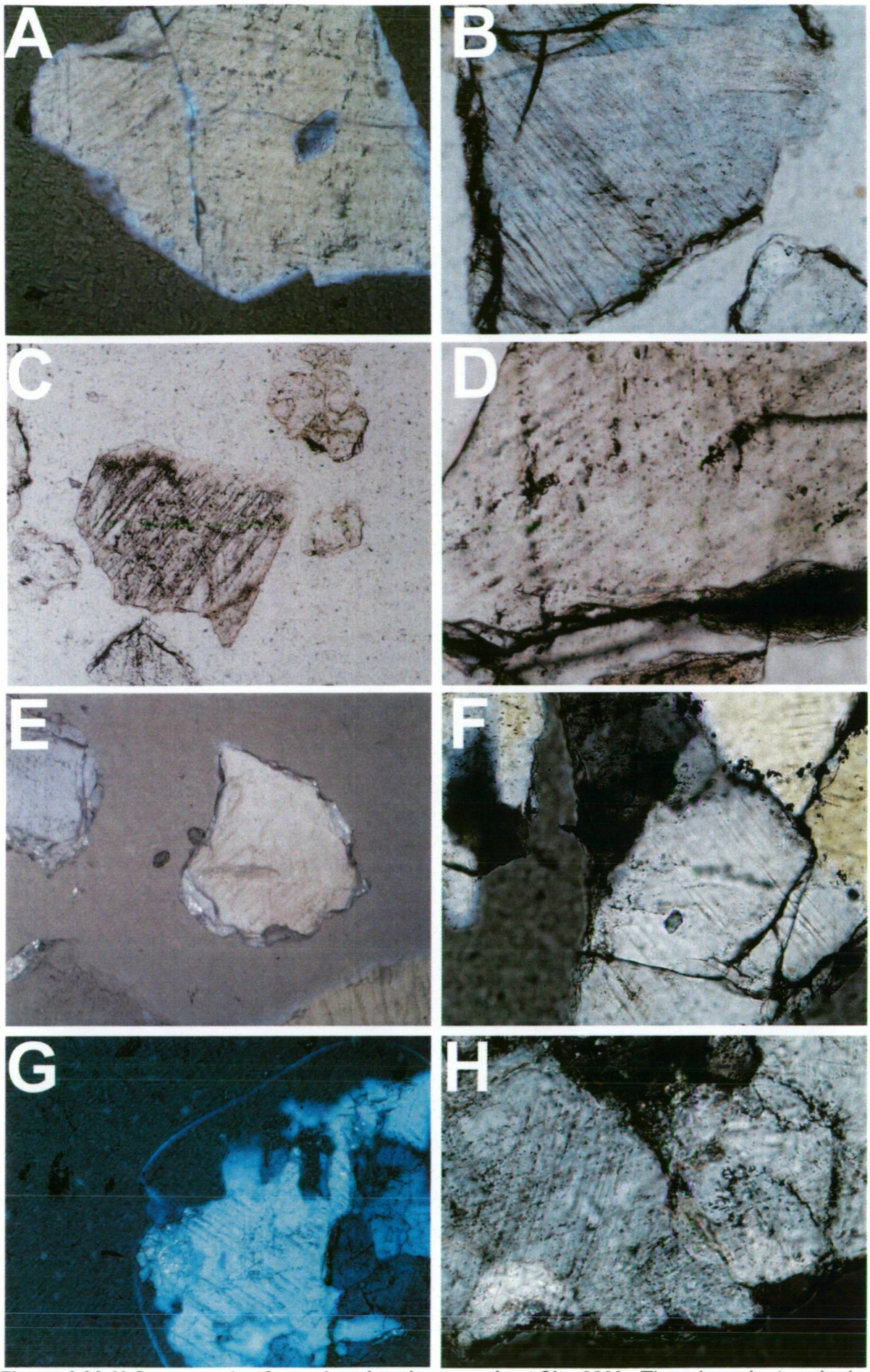

Figure 4.6A-H Quartz grains from glass bearing gravels at Site 0203. These irregular to sub-planar fractures are not diagnostic of impact shock.

A)XPL. FOV = 1.1mm. Sub-planar fractures; B) XPL. FOV = 0.55mm. Sub-planar fractures; C) PPL. FOV = 2.2mm. NE-SW trending Sub-planar fractures; D) PPL. FOV = 0.55mm Close up of grain in C; E) PPL. FOV = 2.2mm. Grain showing fractures at SW edge;F) XPL. FOV = 0.55mm. Grain with sub-planar fractures trending NW-SE. Note also the Limited development of E-W trending fractures in the top right of image; G) XPL. FOV = 1.1mm. Widely spaced sub-planar fractures; H) XPL. FOV = 0.55mm. Grain showing limited evidence for intersecting sets of fractures. With one set of NNE-SSE trending sub-planar fractures and a weakly developed E-W set of irregular fractures.

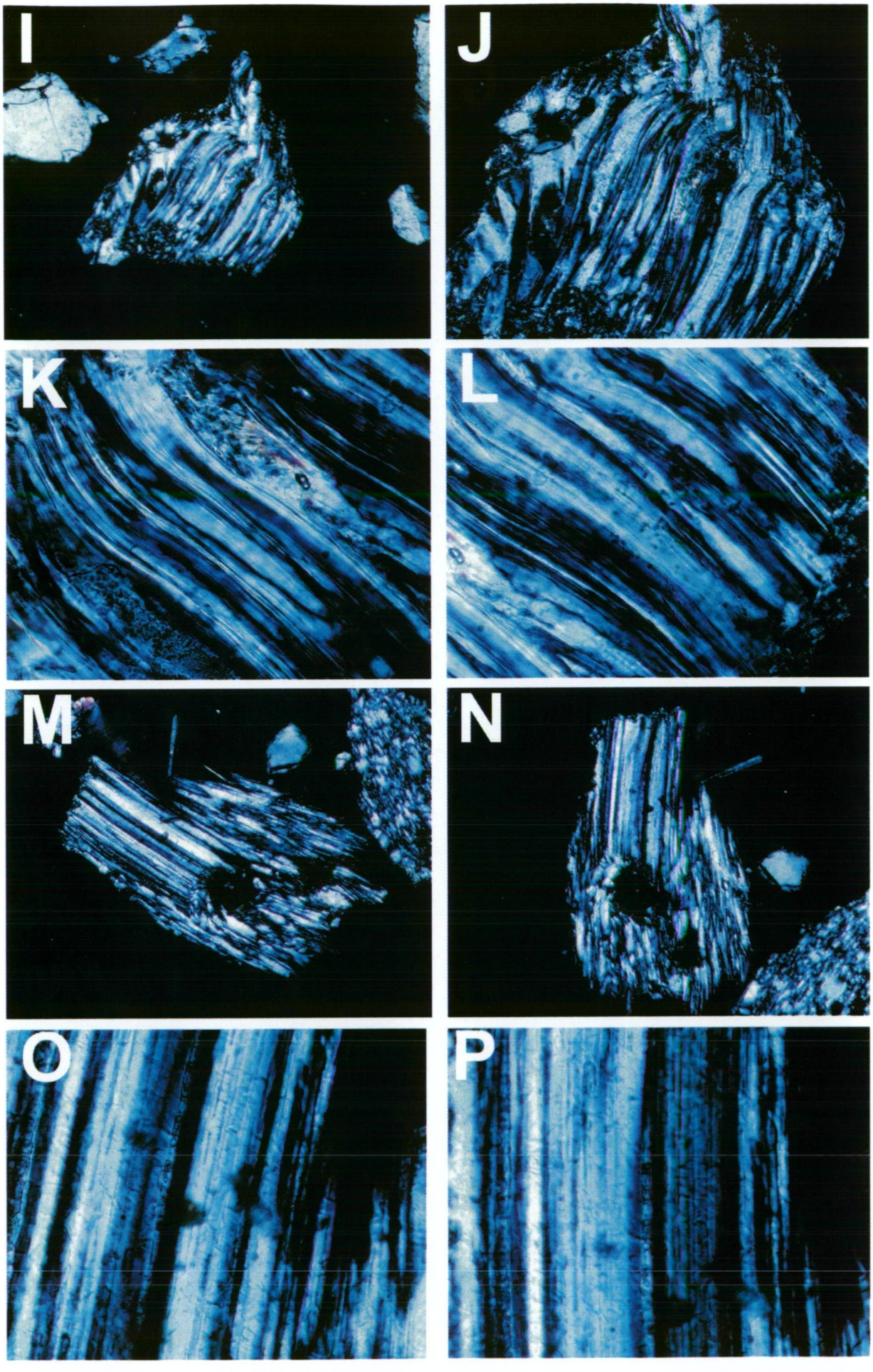

Fig. 4.6I-P Quartz grains from glass bearing gravels at Site 0203. Showing sub-planar fractures that separate domains of different extinction. These are referred to as twinned quartz in discussion.

I)XPL. FOV = 1.1mm; J) XPL. FOV = 0.55mm; K) PPL. FOV = 0.28mm; L) XPL. FOV = 0.28mm; M)XPL. FOV = 1.1mm; N) XPL. FOV = 1.1mm; O) XPL. FOV = 0.28mm; P) XPL. FOV = 0.28mm.

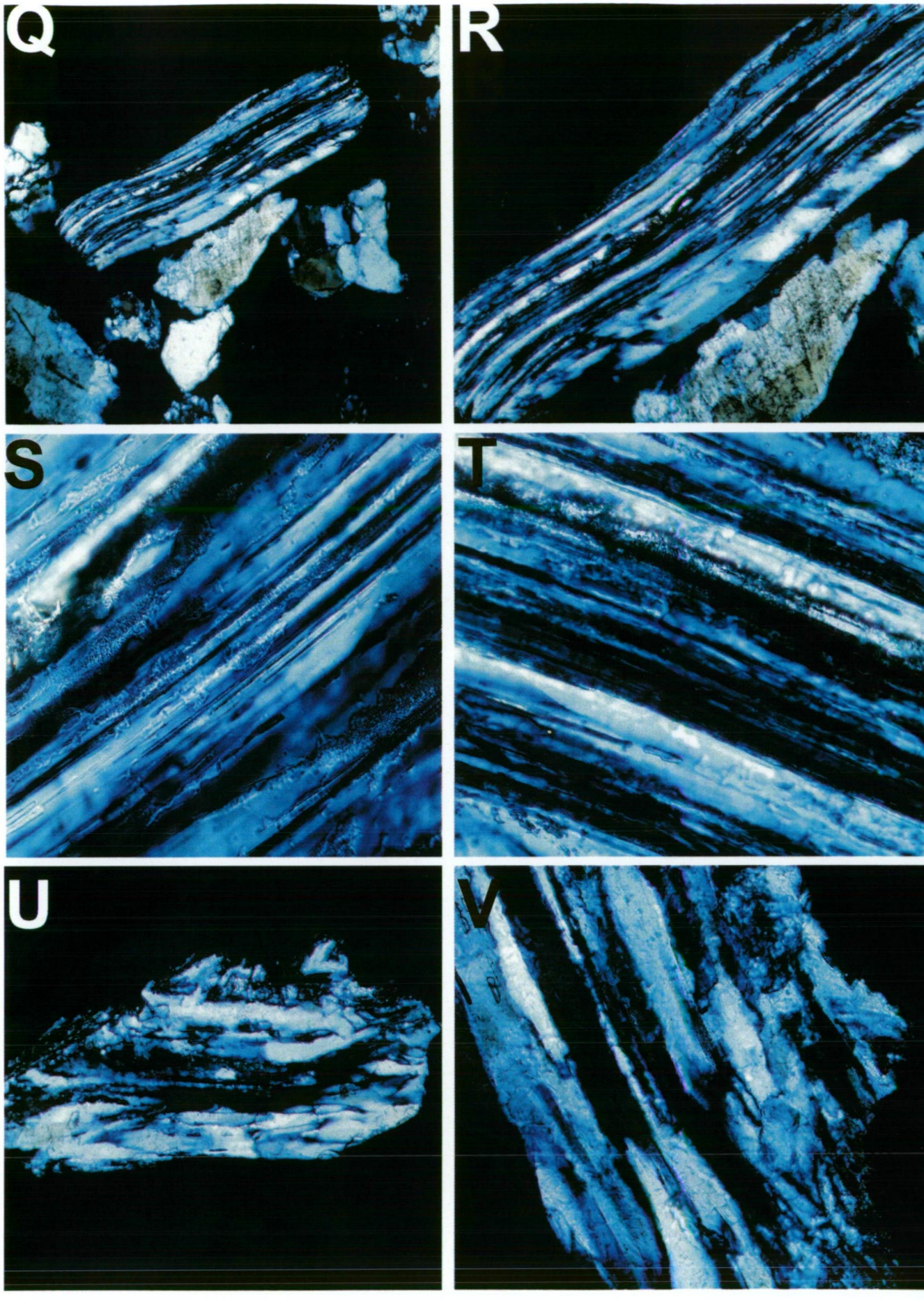

Figure 4.6 Quartz grains from glass-bearing gravels at Site 0203. Showing sub-planar fractures and irregular fractures that separate domains of different extinction.

Q)XPL. FOV = 2.2mm; R) XPL. FOV = 1.1mm; S) XPL. FOV = 0.28mm; T) XPL. FOV = 0.28mm; U)XPL. FOV = 1.1mm; V) XPL. FOV = 0.55mm.

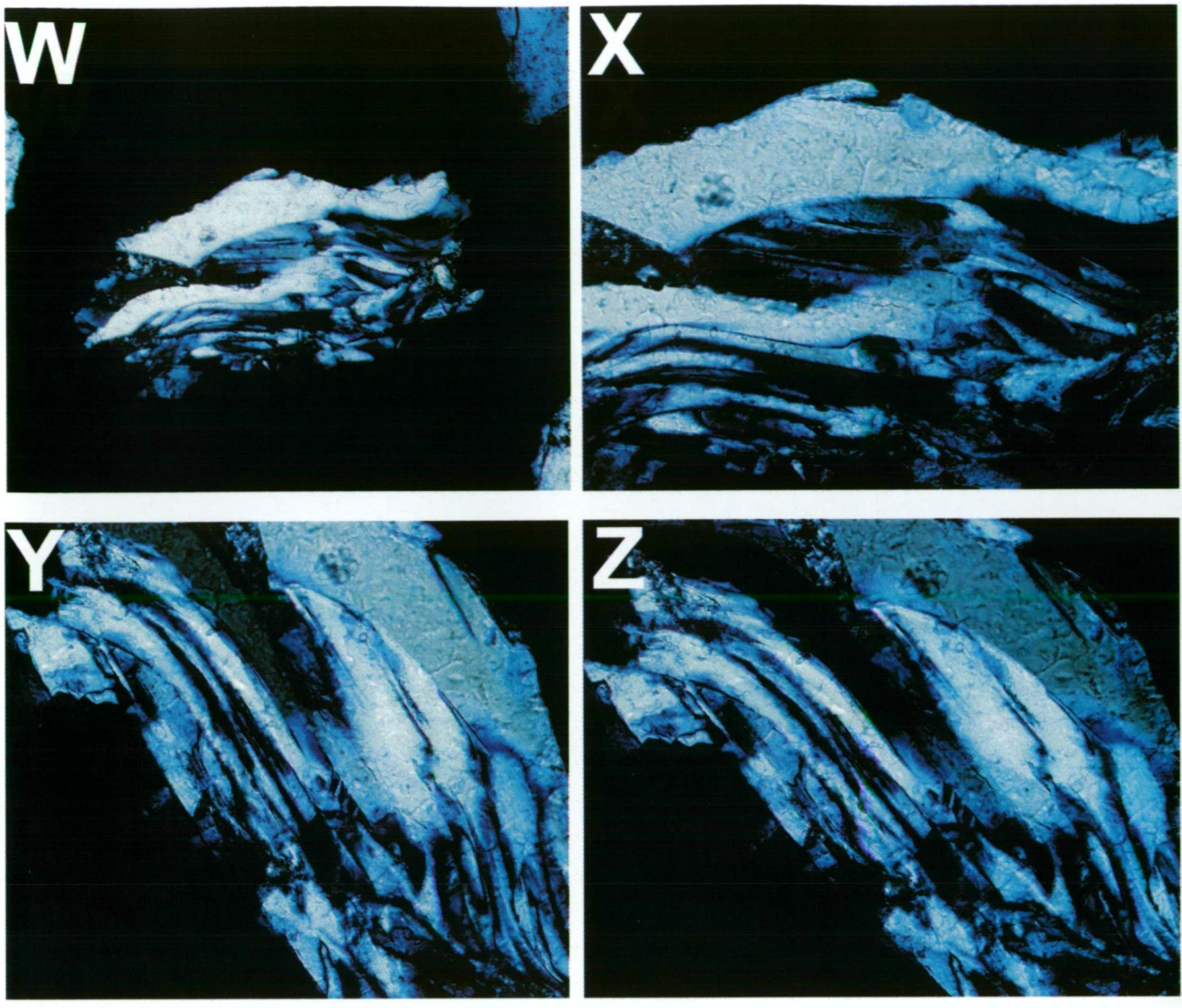

Fig. 4.6W-Z Quartz grains from glass bearing gravels at Site 0203 Showing sharp fractures that separate domains of different extinction.

W)XPL. FOV = 2.2mm; X) XPL. FOV = 1.1mm; Y) XPL. FOV = 0.55mm; Z) XPL. FOV = 0.55mm.

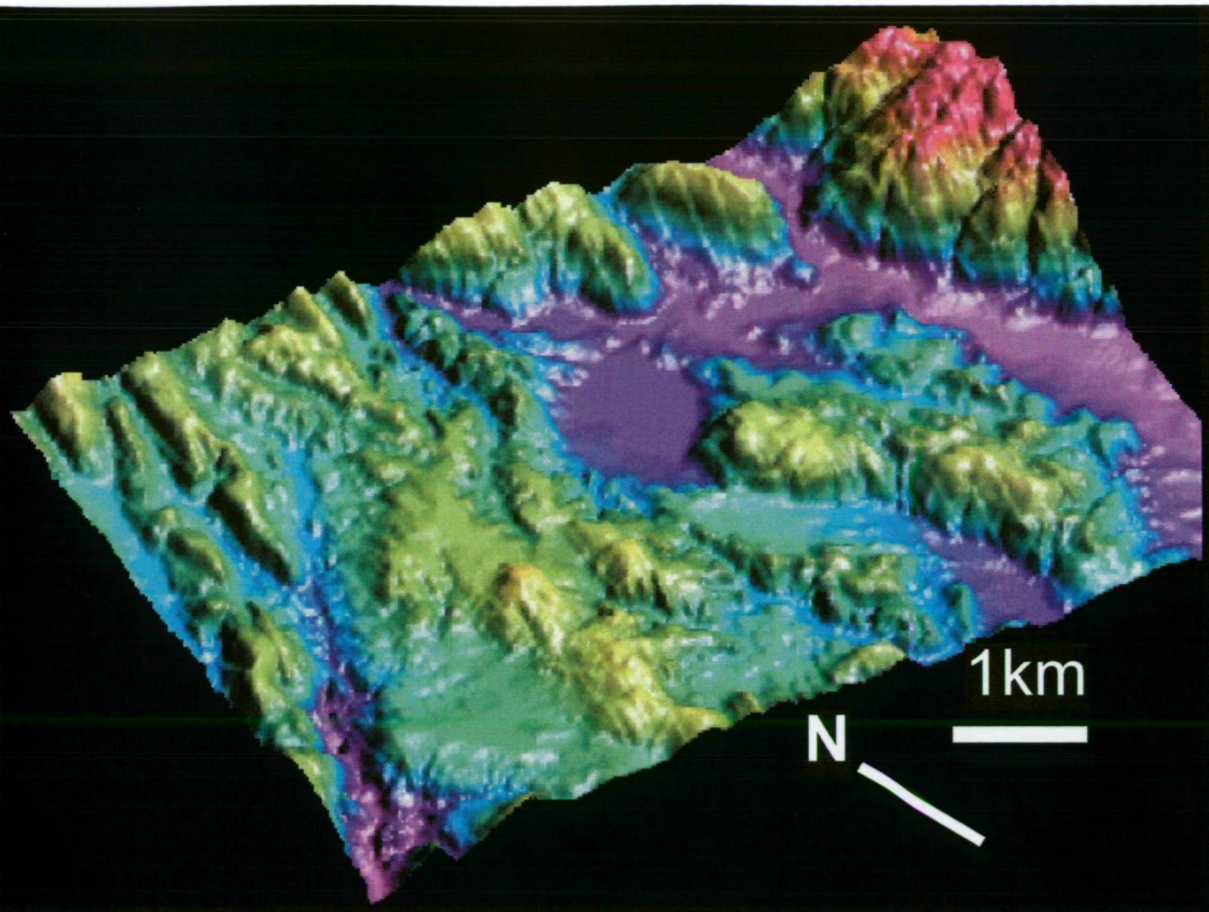

Figure 4.7 A) Digitial Elevation Model 1: 25 000. The flat valley floor derives from the filling in of the circular depression. As can be seen the ramparts represent continuations of the topography and are unrelated to the buried strucutre. The depression is almost as wide as the valley it sits in and an almost closed basin of deposition has been formed. Flat areas such as to the west of the crater preserve the most extenisve residual gravels and glass in highest abundances.

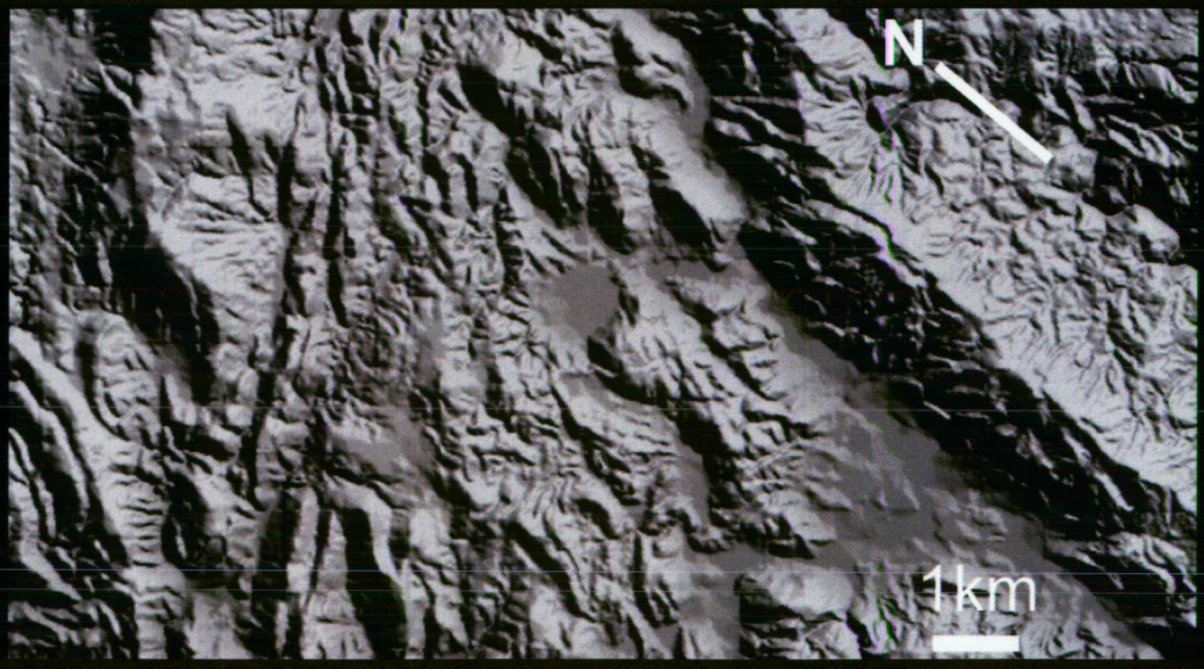

Figure 4.7 B) Digitial Elevation Model -plan view, 1: 100 000. This view highlights the rugged topography of the strewn field in contrast to the flat, circular crater floor.

also poor in DDH2 and averaged <30%. More than 30 thin-sections of the crater-fill facies have been examined in this study. Resulting logs are presented in Fig. 4.8; given the limited recovery, indicated depths should be viewed as approximate only. These logs show that beneath the finely laminated lake sediments is a complicated sequence of loosely consolidated material, and coherent, fractured and plastically deformed slates and minor quartzites. The upper part of the interval comprises unconsolidated sands, while the lower bulk of the stratigraphy consists of deformed quartzite and deformed slate. The slate and quartzite intersected ranges from massive blocks to angular pebble size fragments. In the mid levels of the stratigraphy the large blocks are recognisable in the drill core by abrupt breaks in bedding and cleavage direction as well as variations in oxide clay colours. Distinct facies and fabrics that can be observed throughout the core stratigraphy are described below. The location of samples described and analysed are indicated on Fig. 4.8. The petrography of the described crater-fill facies is summarised in tables 4.3A,B. Fractures in quartz grains were also counted in the crater-fill samples and tabulated (table 4.4). After description, the rocks throughout the crater stratigraphy were classified according to the scheme outlined in French (1998). Thissimplified classification scheme attempts to rely on objective features of a rock type that are observed in outcrop, hand sample and thin section and uses standard geologic terms (table 4.5). This is particularly desirable in the description of rocks from crater features of uncertain origin – such as Darwin Crater - as the scheme avoids genetic connotations in description. In the interpretation of the observed stratigraphy, several key works were used (e.g. Grieve et al. 1977; Grieve 1987; French 1998), these works, and the 'ideal' stratigraphy expected in simple craters were briefly described in Chapter 1.

4.5.1 Crater-fill Facies A

This massive, extremely poorly sorted facies is polymict and composed of clasts of randomly aligned and angular crystalline quartz (57%), slate (10%) quartzite (5%), mica (2%), and opaques (2%), with matrix materials comprising the remaining ~25% of a typical sample. Examples of Crater-fill Facies A are shown in Fig. 4.9A-P. Clasts in thin section are up to 1cm in diameter and larger pebble size, angular, slate, quartzite and carbonate fragments were recovered from the core. The quartzite

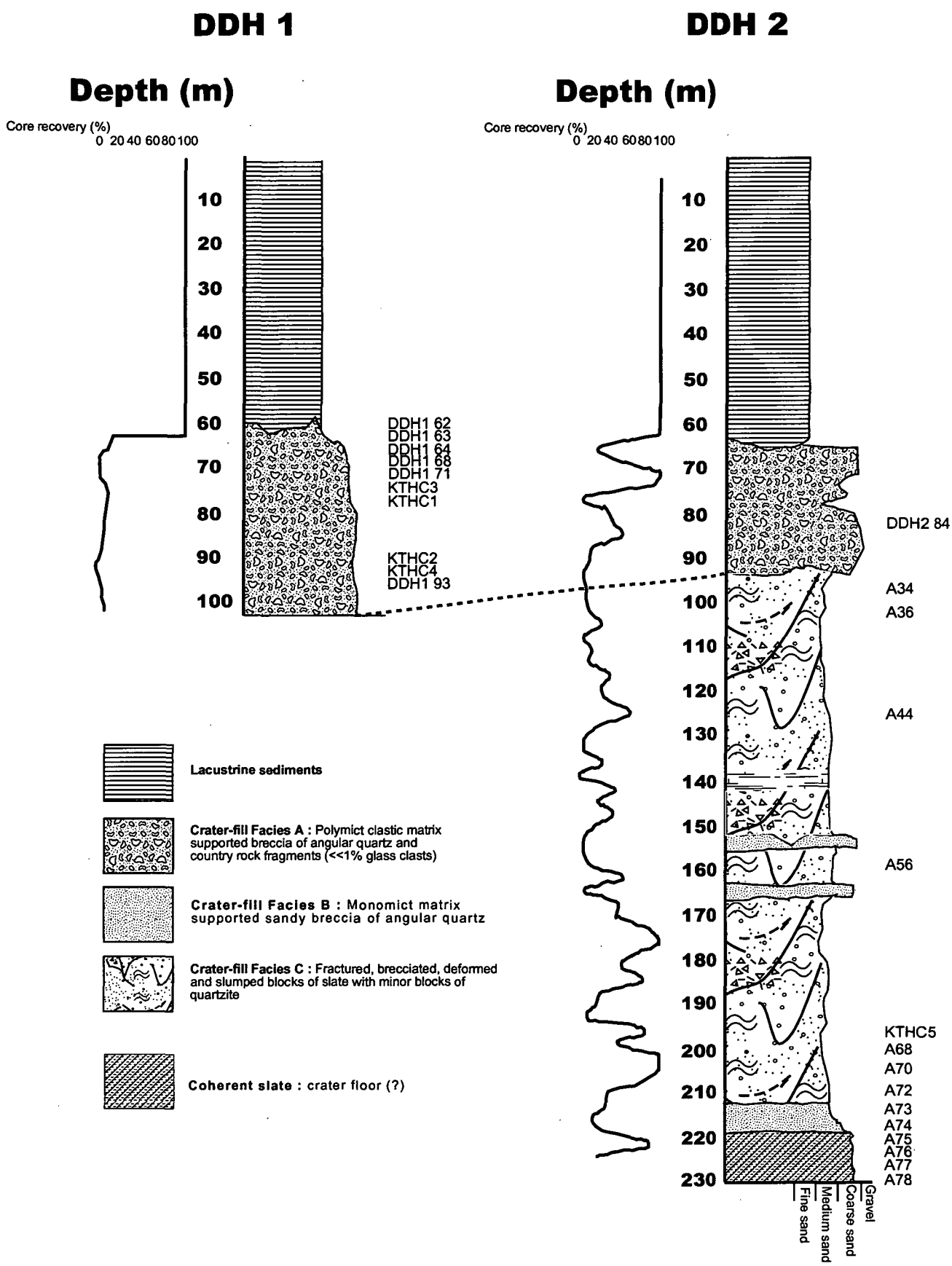

Figure 4.8 Stratigraphy of Darwin Crater. The section also depicts the variation in core recovery with depth. Areas of 0% recovery are interpreted to represent intersections of the monomict sandy breccias formed by shattering of quartzite. These intervals are commonly associated with the arrival at the surface of loose sands according to the drillers log; and the arrival at the surface of loose sands is commonly mentioned in drillers logs. The approximate location of samples from which thin sections were prepared and that are described in text are indicated. In some cases, several thin sections were prepared from an indicated sample depth. Drillers: Hydro Electric Commision (HEC).

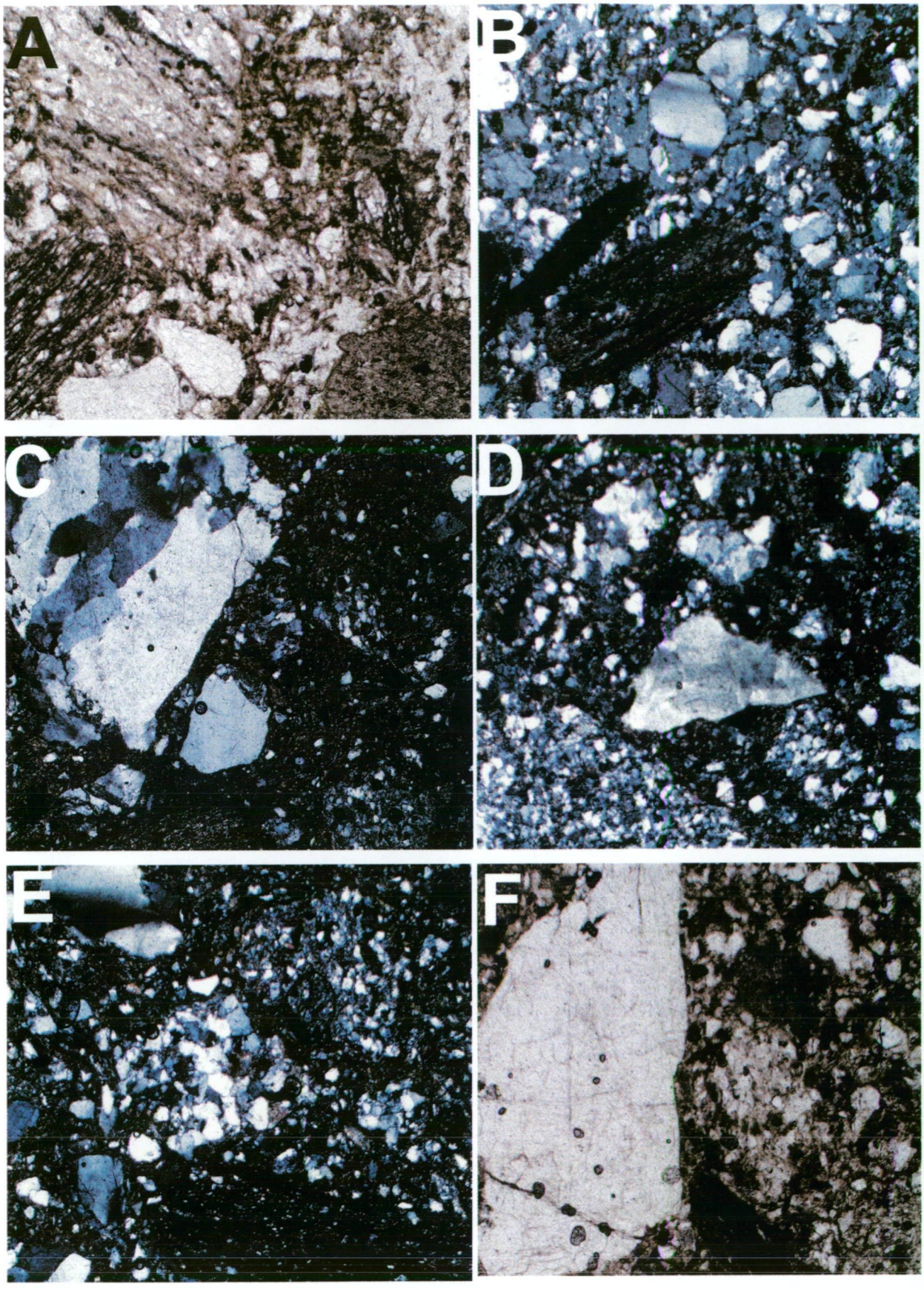

Figure 4.9A-F Crater-fill Facies A (Polymict breccia). A)PPL. FOV = 2.2mm. Angular quartz and slate clasts in fine matrix; B) XPL. FOV = 2.2mm. Slate clasts and angular quartz in fine matrix, note the undulose extinction of the quartz grains; C) PPL. FOV = 2.2mm. Angular quartz in fine matrix,showing the poor sorting in this facies; D) XPL. FOV = 2.2mm. Quartzite and angular quartz in fine matrix; E)XPL. FOV = 2.2mm. Quartzite and angular quartz in fine matrix; F) PPL. FOV = 2.2mm. Quartz and slate in abundant matrix.

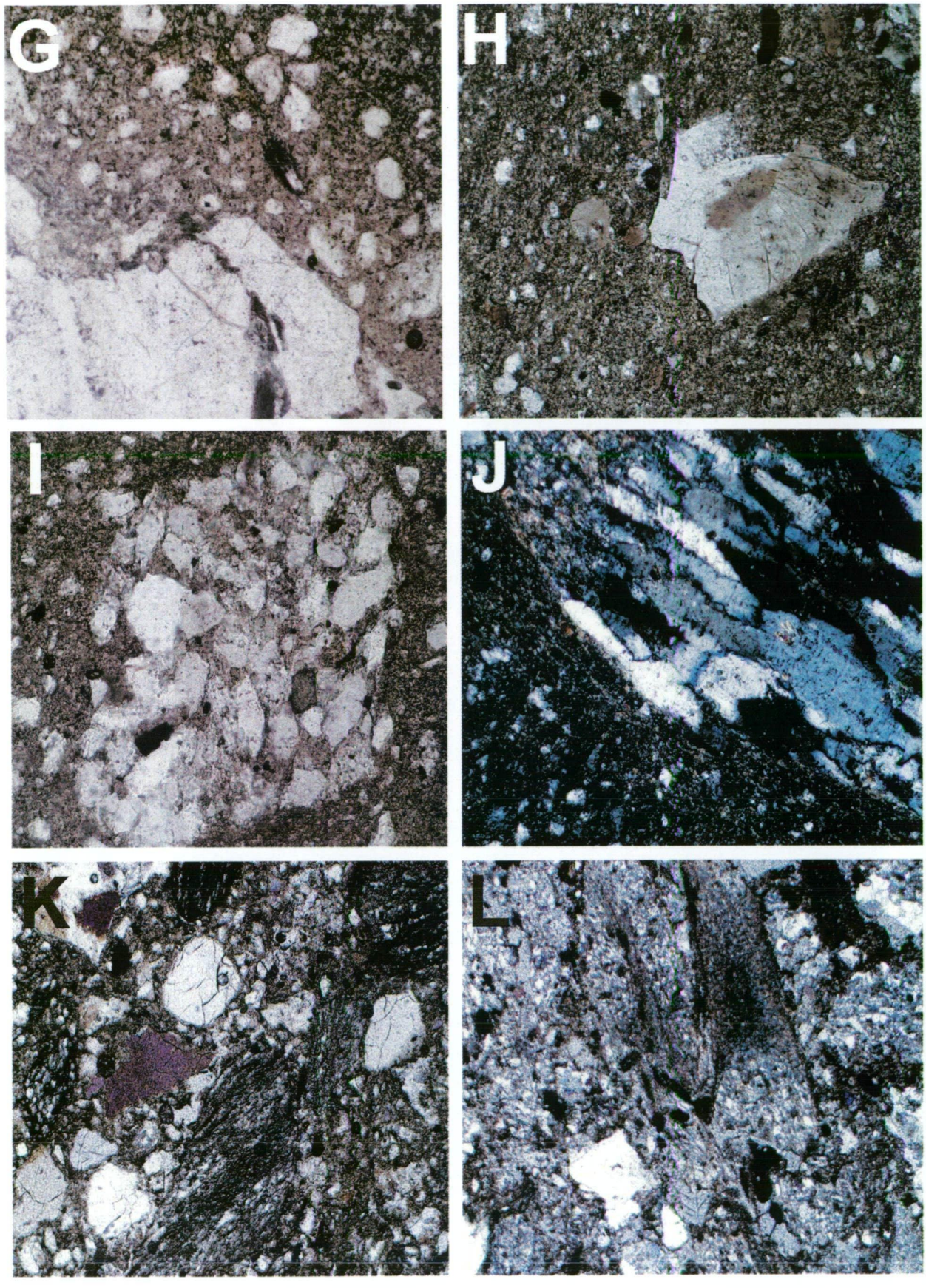

Figure 4.9G-L Crater-fill Facies A (Polymict breccia). G)PPL. FOV = 2.2mm. Angular quartz in matrix, note chlorite growth from matrix across grain boundary of large quartz crystal. H) PPL. FOV = 2.2mm. Note radial fractures on angular quartz in abundant matrix; I) PPL. FOV = 1.1mm. Quartzite clast with angular quartz in matrix; J) XPL. FOV = 1.1mm. Quartz grain showing highly undulose extinction; K)PPL. FOV = 2.2mm. Angular quartz and sheared slate, matrix poor sample; L) XPL. FOV = 1.1mm. Sheared slate clast and angular quartz in matrix.

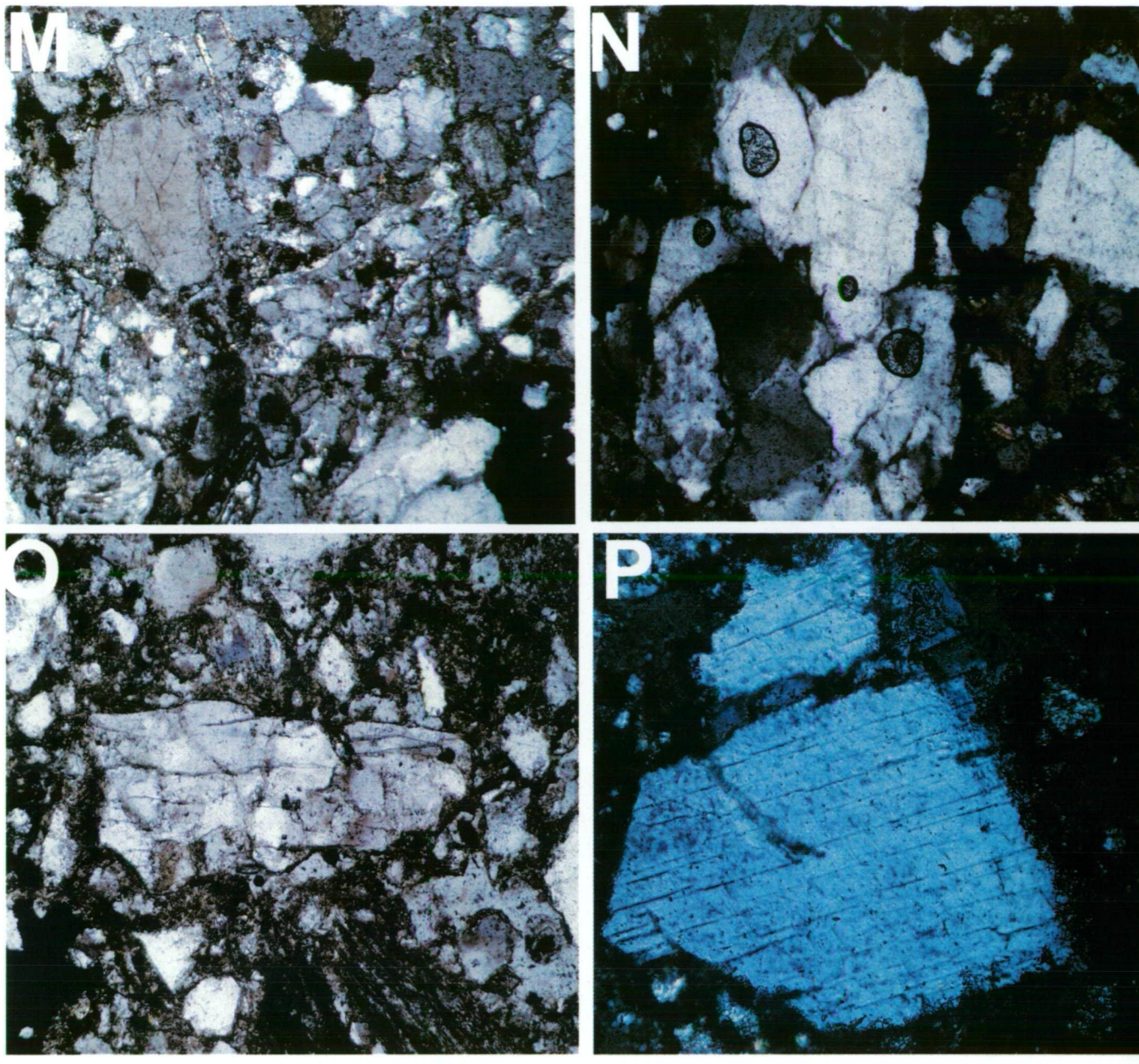

Figure 4.9M-P Crater-fill Facies A (Polymict breccia). M)XPL. FOV = 2.2mm. Matrix poor sample, comprised of interlocking angular quartz and rare slate; N) XPL. FOV = 1.1mm. Undulose quartz;O) XPL. FOV = 2.2mm. Angular quartz showing irregular, widely spaced fractures; P) XPL. FOV = 0.55mm quartz with sub-planar fractures.

clasts are comprised of interlocking quartz grains between 200 and 500 μm in size (Fig. 4.9E). The slate clasts are comprised of angular quartz grains less than 40μm in diameter and these are surrounded by a matrix of mica and finer grained quartz (Fig. 4.9A,B). Fragments of slate tend to be elongate with some rare bladed fragments. Often these slate fragments are deformed and disrupted by a series of fractures and microfaults and bedding or foliations are commonly sheared (Fig. 4.9K,L). The carbonate clasts are comprised of deformed biosparite with minor amounts of quartz, and contain a Silurian age rugose coral. Silurian conodont elements (C.F. Burrett, Personal Communication in 2004) have also been recovered from these pebbles, and these are predominantly matt black in colour. The edges of some elements show limited development of clear colouration.

Of the monocrystalline quartz grains, ~17% show undulose extinction. Up to ~30% of quartz grains in rocks from this facies contain 2 or more fractures and averaged over all samples this includes ~20% of grains with 3 or more fractures. The fractures are predominantly coarsely spaced (>20μm) and anastomosing in form. Rare quartz grains (<1%) show closer spaced (10μm) planar fractures that appear to be annealed and are now filled by pleochroic green chlorite. Isolated quartz grains only, show limited evidence for intersecting sets of such fractures. Equally rare (<1%) are highly deformed quartz grains cross cut by closely spaced (<5μm) parallel, but non-planar fractures that define twins in cross polarised light; these are identical in appearance to those described in the glass-bearing angular quartz gravels to the west of the crater (see section 4.3.2) and are further described later. Very rare fragments of Darwin glass were recovered from disaggregated samples of the polymict breccia after prolonged searching with a binocular microscope, but have not been observed in thin section and must represent very much less than 1% of the breccia clasts. The presence of up to cm-size glass fragments from sands at 100m depth in DDH 1, reported by Ford, has not been confirmed in this study, and it is likely that these samples have been lost.

In typical samples, the matrix is composed of quartz grains (57%) and mica (20%) up to 20μm in size as well as kaolinite (10%) and minor chlorite clays (3%) less than 2μm in size with minor Fe-oxihydroxides of goethite (2%), and significant (up to 5%) amounts of tourmaline and rutile in some samples. In places the matrix shows a radiating fabric of variable birefringence and this reflects the *in situ* growth of the clay

and goethite. Samples from immediately below the lake sediments contain minor pyrite in the matrix, along with the secondary mineral rozenite ($Fe^{2+}SO_4.4H_2O$) that tends to grow on the site of weathering pyrite. Gypsum is also present in the matrix of samples from immediately below the lake sediments. Figure 4.10A-F shows the random alignment of clasts and matrix materials visible in ESEM images.

4.5.1a Crater-fill Facies A associations

This facies exists immediately below the lake sediments and is currently at least 40m thick. Clasts in the breccias have a petrographic affinity with the quartzites and slates of the Eldon Group. However, multiple fractures in quartz grains in this facies are more common than in surface samples of the Eldon Group with ~30% of quartz grains in Crater-fill Facies A showing 2 or more fractures as opposed to <1% of quartz grains in Eldon Group rocks outside the crater. Slate clasts in the breccia also show greater deformation than is observed in corresponding rocks surrounding the crater. Limestone pebbles in the crater contain Silurian fossils typical of carbonates in the Eldon Group. The matt black colour of the conodonts is consistent with the regional Conodont Alteration Index (CAI) for the Eldon Group rocks and indicates temperatures up to 480°C (Epstein et al. 1977). The development of clear colouration suggests exposure to higher temperatures of greater than 600°C, or reflects structural control in colour development as is suggested when only the thin teeth of a conodont element displays the clear colouration (Epstein et al. 1977). The latter is the case at Darwin Crater and as such the indicated CAI values are well within the expected range of Tasmanian Palaeozoic carbonates. Such carbonates do not outcrop around the crater but, based on defined stratigraphy of the Eldon Group, may be interbedded at depth in the shale units. The polymict breccia is associated with a very minor component that contains rare Darwin glass clasts. The poor recovery of this facies prevents accurate determination of glass abundance.

4.5.1b Crater-fill Facies A Interpretation

Crater-fill Facies A is classified as a polymict, clastic, matrix supported breccia of angular quartz and country rock fragments. Darwin glass fragments have not been recovered in sufficient abundance for the facies to be classified as a true melt-bearing breccia according the scheme of French (1998).

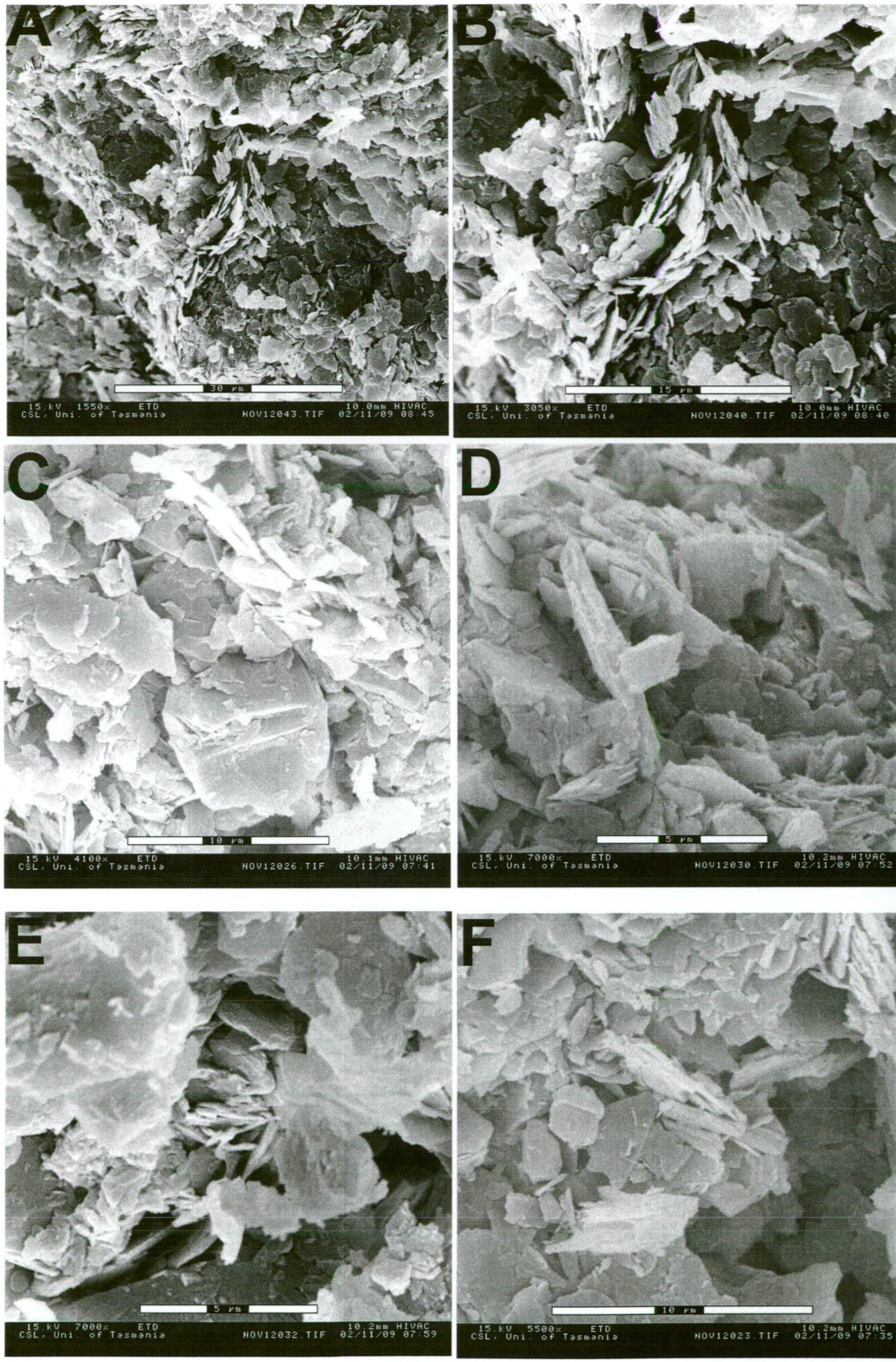

Figure 4.10A-F ESEM images of matrix in Crater-fill Facies A (Polymict breccia). A) Random alignment of quartz grains; B) Enlargement of central part of image A showing widely varied grain orientations; C) Quartz grain surrounded by fine matrix including randomly aligned kaolin laths; D) Close up of small region to NE of the central quartz grain pictured in C; E) Radiating matrix kaolin; F) Randomly alligned kaolin and quartz grains.

The polymict fabric of this breccia suggests it is unlikely to be the product of simple collapse of the crater walls or surrounding hills, as this would be expected to produce mononomict breccias at a local scale. Clasts derived from landslides on hills surrounding the crater would also be expected to be non-deformed. Rather, the mixed assemblage of non-orientated slate and quartzite fragments indicates that this breccia sourced deformed material from across a wide area that was mixed (and further deformed?) during deposition. The observed deformation in these rocks is consistent with shock pressures of <5 GPa or shock stage 1 (Stöffler & Langenhorst 1994, French 1998). Deposition is interpreted to have been very rapid (catastrophic?). This is indicated by the complete absence of pollen or spores in the breccia that would be expected to be abundant had the almost closed basin been gradually filled in, as is the case in the laminated lake sediments. The random alignment of matrix material in this facies would also not be expected if these fragments had gradually washed into the basin. In short, sediments formed by the gradual infilling of the basin should show much more in common with the upper lake sediments.

This breccia facies is not considered to have washed into the crater and, as such, the associated fragments of Darwin glass are also not considered to have washed into the crater. If these glasses had landed in the depression from a distal source some degree of stratigraphic sorting would be expected but rather the very rare glass fragments are randomly distributed. Hence the glass and breccia are either contemporaneous, or during the formation of the breccia, glass fragments that may have previously defined a distinct horizon were reworked. These possibilities will be discussed in more detail later.

4.5.2 Crater-fill Facies B

This poorly sorted sandy breccia is present at varying scales in the crater stratigraphy, from massive units that offered poor recovery during drilling, to fine domains and shear zones in the more pelitic facies that are visible at thin section scale. Typical examples of this facies are monomict and composed of angular quartz grains (~50%) up to 500μm in size in a fine matrix (~50%). Up to ~25% of quartz grains in studied thin sections have 2 or more fractures including on average more than 15% with 3 or more; these fractures are usually irregular and anastomosing. Photomicrographs of samples of Crater-fill Facies B are shown in Fig. 4.11A-N. Rare

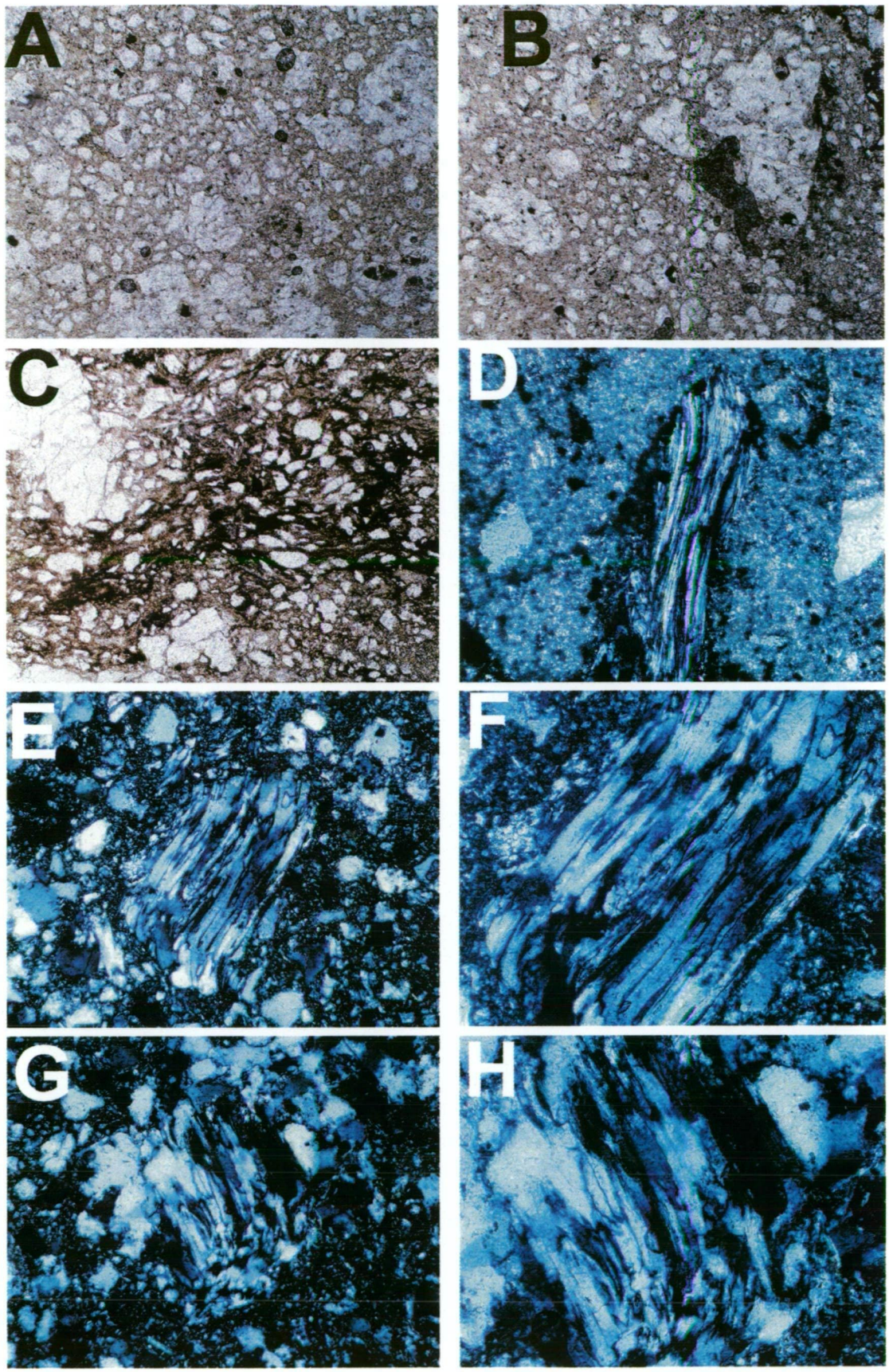

Figure 4.11A-H Crater-fill Facies B (Monomict breccia). A) PPL. FOV = 2.2mm. Angular quartz in matrix of quartz and mica; B) PPL. FOV = 2.2mm. Angular quartz in matrix of quartz and mica. Note goethite (dark) in top right of slide; C) PPL. FOV = 1.1mm. Angular quartz in goethite matrix; D) XPL. FOV = 0.55mm. Quartz grain with sub-planar fractures that define zones of alternating extinction (twinned quartz); E) XPL. FOV = 1.1mm. Twinned quartz ; F) XPL. FOV = 0.28mm. Close up of grain in F; G) XPL. FOV = 1.1mm. Fractured quartz showing disrupted extinction approaching grain mosaicism; H) XPL. FOV = 0.28mm. Close up of grain in G.

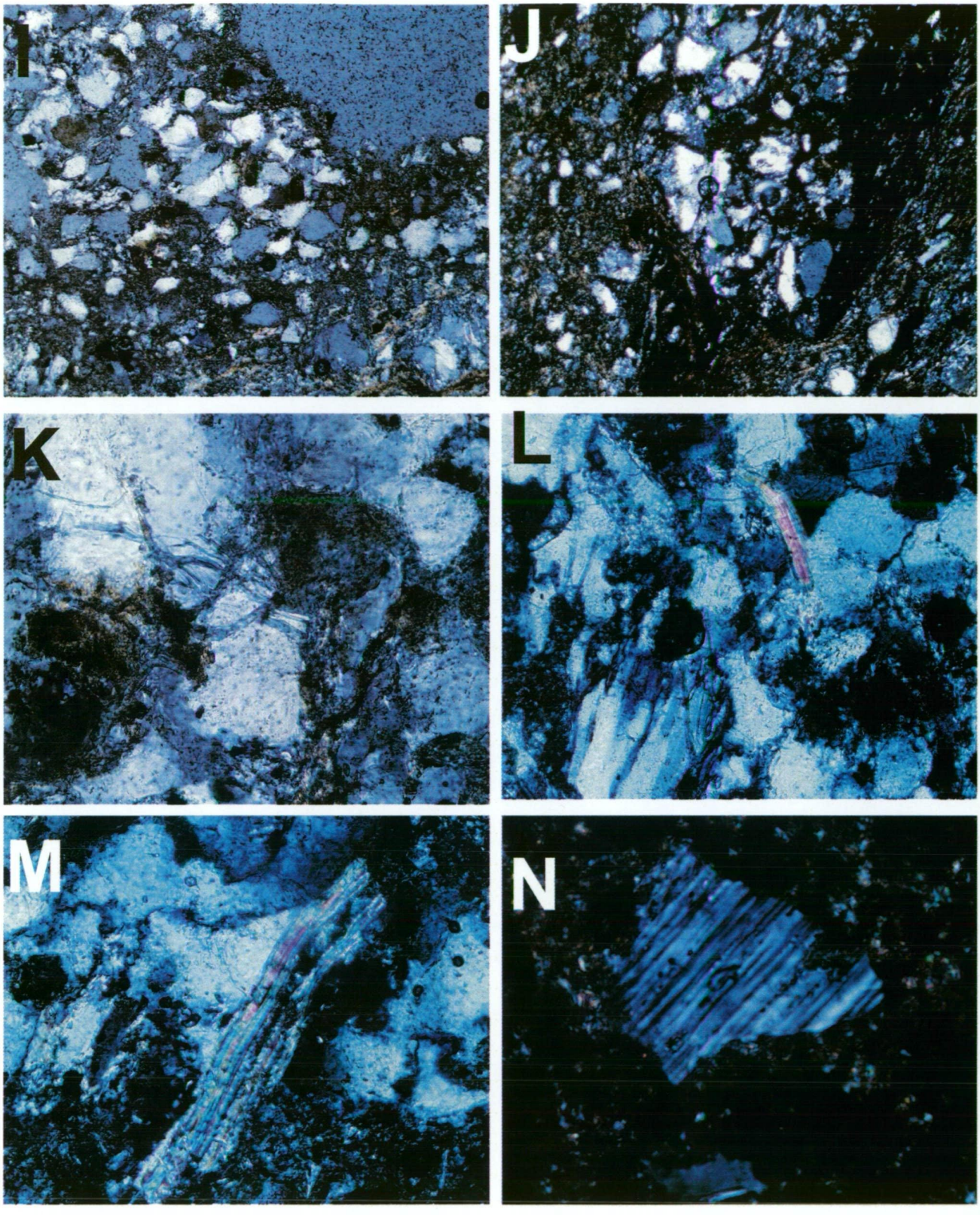

Figure 4.11I-N Crater-fill Facies B (Monomict breccia). I)XPL. FOV = 2.2mm. Relatively coherent deformed quartzite; J) XPL. FOV = 2.2mm. Deformed quartzite, note goethite (dark) along fracture; K) XPL. FOV = 0.55mm. Percussion fractures in quartz; L) XPL. FOV = 0.55mm. Angular quartz and kinked mica; M)XPL. FOV = 0.55mm. Kinked mica; N) XPL. FOV = 0.28mm. Quartz with sub-planar fractures.

grains of the 'twinned' quartz have been found in samples from 165m depth (Fig. 4.11D-F). In this sample, the alternating extinction can also approach grain mosaicism (Fig. 4.11G,H). In the more coherent deformed quartzite, quartz grains have collided to produce and interlocking fabric that approaches what has been called 'jigsaw texture' by Kieffer (1971) in her description of rocks from Barringer Crater (Fig. 4.11I,J). At the contacts of quartz grains that have been compressed into the matrix, percussion fractures can be observed that result from the violent collision of the quartz grains during deformation (Fig. 4.11K). Disassociated hand samples viewed under binocular microscope reveal that the angularity of the quartz grains is associated with conchoidal fracture surfaces. Some of the quartz grains have a milky appearance.

Matrix comprises 50% of typical Crater-fill Facies B samples with quartz (50%) and mica (15%) the dominant matrix minerals distinguishable in thin section. In the more coherent, deformed, quartzites these micas are sometimes kinked to define two, and sometimes three segment orientations (Fig. 4.11L,M). These matrix minerals exist within Fe-oxyhydroxides of goethite and kaolinite clays. XRD on sample A44 indicates equal amounts of Fe-oxyhydroxides (15%) and kaolinite (15%) are present in this sample, but these proportions are highly variable as is obvious in thin sections. Complicated matrix layering is defined by colour variations through yellow, brown and red. This layering forms curved arcs, is generally parallel but discontinuous and highly variable even within a single thin section. There is no evidence of melting or recrystallisation, and the boundaries of the contacts between the different coloured layers are diffuse whereby a transition in colour is observed over tens of μm. This suggests that the colour variation relates to oxidized fluids travelling along structurally controlled pathways such as fractures and bedding planes to produce this colour variation during the formation of the oxyhydroxide goethite.

4.5.2a Crater-fill Facies B associations

These monomict, matrix supported breccias are associated with slumped blocks of brecciated, severely deformed and more coherent slates as described below. Deformed quartz grains characterize the fabric of this breccia along with kinked micas in a clay-dominated matrix as distinct from the more coherent surface examples of Eldon Group quartzites that are composed of interlocking quartz grains, and only very minor matrix material.

4.5.2b Crater-fill Facies B Interpretation

This facies is the product of progressive deformation of quartzite. The quartz grains compressed into the matrix, percussion fractures, multiple fractured quartz grains, and kinked mica are interpreted to be the products of brittle to plastic deformation at pressures <5 GPa. This has produced deformed and brecciated blocks of rock and sandy breccias interpreted to represent the complete shattering of quartzite. The deformation is interpreted to have been essentially *in situ* where shear zones, kinked micas, quartz domains, percussion and multiple fractures and 'twinned' quartz were produced. The shattered quartzite blocks have slumped into the excavated crater cavity leading to the production of the unconsolidated sands that have moved along fractures and infiltrated spaces between collapsed and rotated blocks of rock within the excavated cavity. Some of the fractures filled with these monomict quartz breccias may have formed under high-pressure flow as 'sedimentary dykes' during the deformation, but this is difficult to determine conclusively given the limited core recovery. Hence, this facies and the entire recovered package of slumped and deformed blocks of rock, are considered allogenic. The milky colour of the quartz grains is interpreted to reflect optical distortion produced by disruption of the quartz lattice during deformation. The monomict breccia fabric suggests derivation from a localised area and the mineralogy is consistent with quartzite in the Eldon Group. The non–deformed character of rocks outcropping immediately around the crater indicates that this deformation was very localised and this is difficult to reconcile with normal tectonic processes.

4.5.3 Crater-fill Facies C

This facies is represented by a package of rocks ranging from large blocks at least several metres thick to angular pebble sized clasts. At a depth of 139-142m, DDH2 intersected a pelitic block containing minor carbonate that shows deformed sparite and contains fossils of the early Silurian rugose coral *Stereoxylodes* cf. *multicarinatus* McLean (identified by Dr. M.R Banks). Samples of rocks from this facies preserve to varying extent a recognisable shale/slate fabric and are dominantly comprised of angular quartz grains (53%) less than 40μm in diameter. Photomicrographs of Crater-fill Facies C are shown in Fig. 4.12A-L.

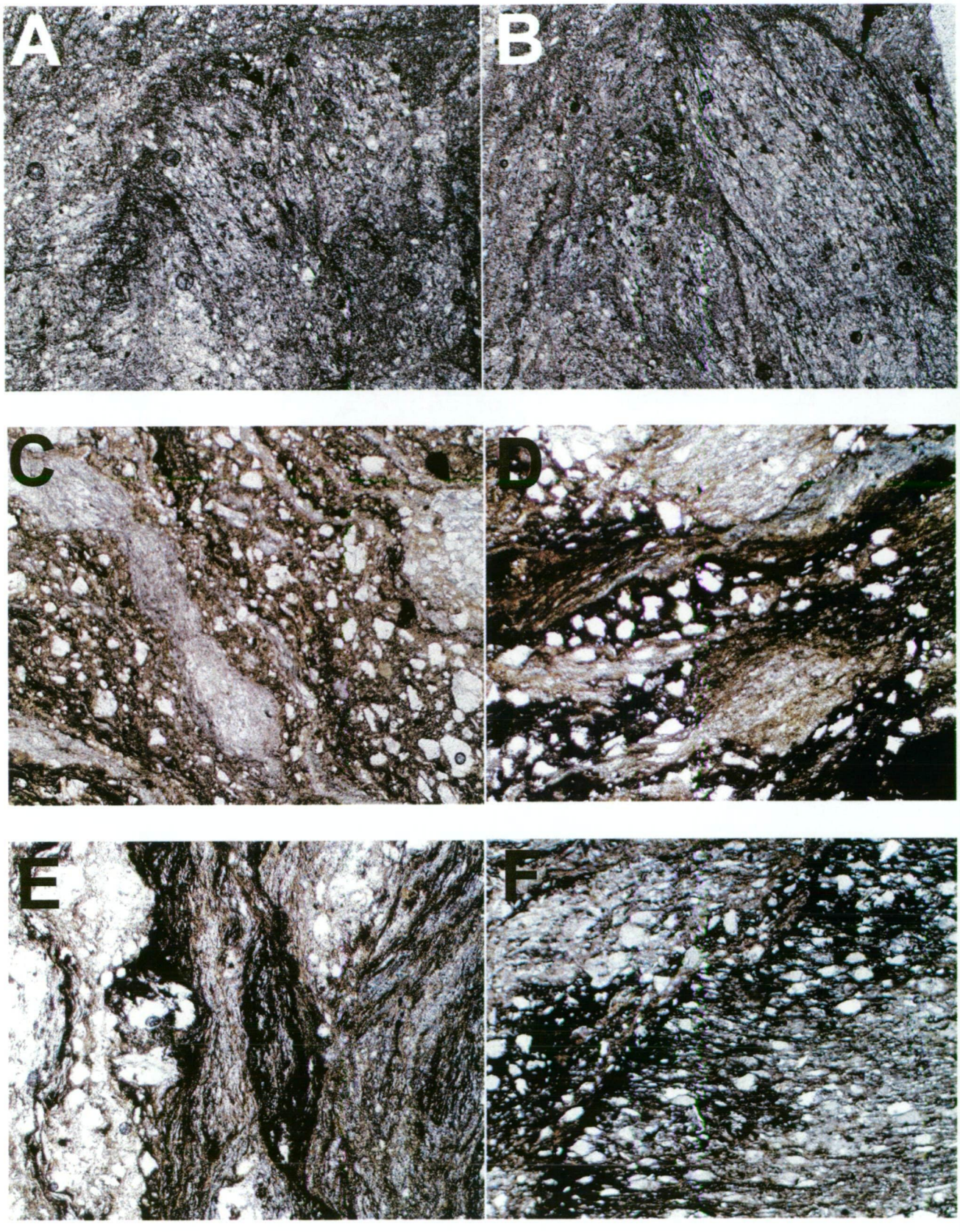

Figure 4.12A-F Crater-fill Facies C (Deformed slates). A) PPL. FOV =2.2mm. Slate showing disrupted foliation fabric; B) PPL. FOV=2.2mm. Slate showing disrupted foliation fabric; C) PPL. FOV=2.2mm. Slate with angular quartz grains;D) PPL. FOV =2.2mm. Fractured slate with goethite matrix. E) PPL. FOV =2.2mm. Slate with disrupted foliation fabric and goethite along fracture zones. F) PPL. FOV=2.2mm. Sheared slate with angular quartz compressed into matrix along shear zone.

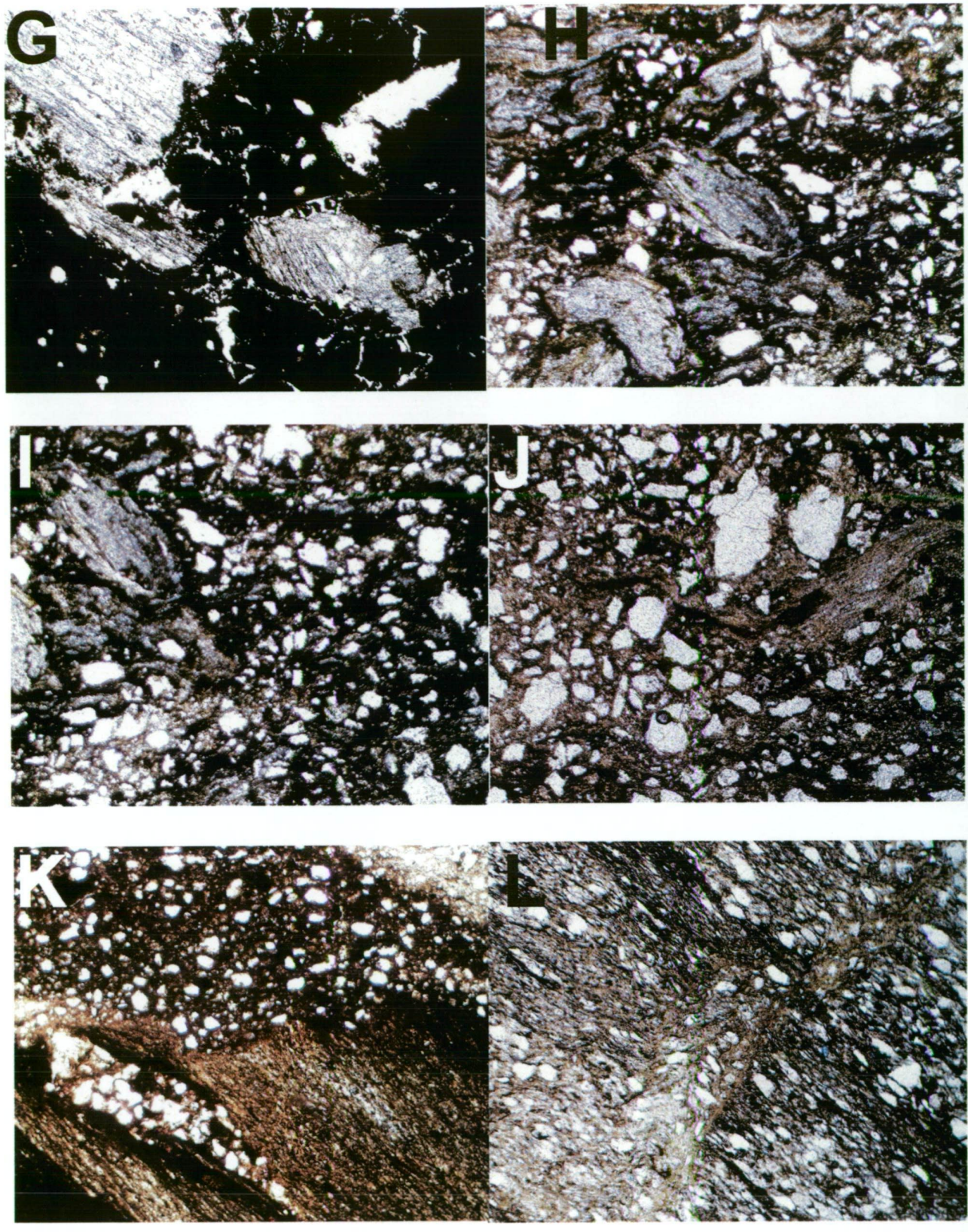

Figure 4.12G-L Crater-fill Facies C (Deformed slates). G) PPL. FOV =2.2mm. Pervasive goethite in a fracture zone; H) PPL. FOV=2.22mm. Slate with disrupted foliation fabric and goethite matrix; I) PPL. FOV = 2.2mm Domain of angular quartz in goethite matrix; J) PPL. FOV=2.2mm. Angular quartz and disrupted foliation fabric; K) PPL.. FOV=2.2mm. Quartz concentrated along shear zones in slate; L) PPL. FOV = 2.2mm. Disrupted slate with goethite filling shear zone.

Studied thin sections indicate that up to 17% of quartz grains display more than two fractures, which are generally coarsely spaced (>20μm). Planar features in quartz grains are very rare. A single grain of quartz with the previously described sharp fracture planes that define alternating zones of extinction (cf. twinning) was found within this facies at a depth of 130m. In most samples, the rock fabric is highly disrupted and may show abundant micro-scale faults (Fig. 4.12A,B). In hand samples of core, broken and dislocated bedding and detached rock fragments can be observed on a cm-scale. Foliation textures produced by aligned mica may be sheared. These foliations and bedding are commonly rotated and highly variable orientations may be observed in a single thin section (Fig. 4.12H). The rotated micas may be kinked. Deformation has produced domains or clusters of fractured detached quartz grains that have collapsed into the matrix material and particularly in shear zones (Fig. 4.12K,L). These domains of quartz may approach the texture of the monomict matrix supported breccias (Crater-fill Facies B).

Matrix material accounts for (on average) 42% of the studied thin sections. Within this matrix, the visible minerals are dominated by quartz (37%) and mica (22%). Here the alignment of these minerals is often disrupted to produce a distinct flow like fabric and rare kinked micas are observed. The remaining matrix material is composed of goethite (22.5%) and randomly aligned kaolinite clays (12.5%). In this facies, the clay and goethite are also most abundant along fractures and between fractured clasts and blocks. This indicates the critical role of infiltrating water in the decomposition of the components, and in the growth of matrix clay and goethite.

4.5.3a Crater-fill Facies C associations

Crater-fill Facies C commences immediately below the polymict breccia of Crater-fill Facies A and is interbedded with Crater-fill Facies B. The petrography of Crater-fill Facies C indicates a clear affinity with the Eldon Group rocks cropping out around the crater. However, the degree of deformation in the rocks from the drill core is significantly greater than that observed in the equivalent lithologies surrounding the crater – even at the site of tectonic faults. Up to of 28% of quartz grains in studied samples of Crater-fll Facies B, and 16% in Crater-fill Facies C, exhibit two or more fractures. This includes up to 16% and 12% of quartz grains with three or more fractures in Crater-fill Facies B and C respectively. In contrast less than 1% of quartz grains in studied samples of outcropping Eldon Group rocks have more than 1

fracture. To further highlight the extreme degree of deformation in quartz grains from Crater-fill Facies A and B, these facies are compared to sample 66030 of Keel Quartzite from a fault zone. In this sample 1% of quartz grains exhibit two fractures and only 0.3% show evidence for three or more fractures. The disrupted bedding fabric in Crater-fill rock samples is also clearly distinct from the coherent regular bedding of the outcropping slates and quartzites. Micas in surface Eldon Group samples are aligned to define the foliation textures of these rocks and there is no evidence for kink deformation. The matrix composition of samples from the drill core has also been significantly altered relative to surface samples by the growth of Fe-oxyhydroxides and clay minerals.

The degree of deformation as represented by fractures in quartz in Crater-fill Facies C is not as great as in polymict breccia Crater-fill Facies A. Beneath the loosely consolidated polymict breccias, in Crater-fill Facies B and C, the degree of deformation observed reflects the competency of the rock types with greatest fracturing and deformation in the more quartz dominated beds. Evidence of such deformation appears to return to the low level seen in surface samples at a depth of around 230m in DDH2 where non-deformed quartzose shale and interbedded psammitic units were encountered. However, as this is where DDH2 was terminated it is impossible to determine if this represents a non-deformed block or the true base of the crater as will be discussed later.

4.5.3b Crater-fill Facies C Interpretation

The highly disrupted rock fabric that features deformed bedding, kinked micas and domains of fractured quartz produced by the collapse of the matrix, are consistent with the expected features of brittle to plastic deformation at pressures <5 GPa. This deformation is interpreted to have initially been *in situ* prior to the collapse of the cavity walls causing the large and small blocks of fractured bedrock to slump into the excavated cavity, possibly undergoing further deformation during this movement. As such, the whole of Crater-fill Facies C represents an allogenic breccia. Evidence for slumping comes from the random and varied bedding that is encountered in the core, and the easily recognized juxtaposition of distinct blocks of rock. This is aided by slight differences in the colour of oxide staining, reflecting the unique fluid pathways present in the fractured and slumped blocks. The fact that the degree of deformation in these rocks from the drill core is far greater than that observed in the equivalent

	Crater-fill Facies A (Polymict breccia)					Crater-fill Facies B (Deformed quartzite)							Crater-fill Facies B (Deformed slate)			
Sample	DDH1 63m	DDH1 64m	DDH1 68m	DDH1 61m	**Average**	A36 2	A44	A72 bot	A75	**Average**	A36 1	A56	A72 top	A77	A78	**Average**
Clast composition (vol%)																
Monocrystalline quartz																
Non-undulatory	21.2	21.5	35.3	21.7	**24.9**	28.6	24.8	38.4	31.3	**30.8**	39.7	41.0	35.5	39.6	40.0	**39.2**
Undulatory	9.6	10.9	6.1	13.3	**10.0**	7.1	1.9	7.2	10.7	**6.7**	8.9	8.1	6.4	9.4	5.2	**7.6**
1 fracture	3.2	0.7	0.0	0.3	**1.1**	0.0	0.3	1.3	0.0	**0.4**	0.0	1.0	0.0	0.8	1.0	**0.6**
2 fracture	7.4	7.9	5.1	1.9	**5.6**	4.3	3.9	1.0	5.2	**3.6**	2.4	2.6	0.0	2.1	0.3	**1.5**
3 or more fractures	12.2	9.9	4.8	16.5	**10.9**	5.7	6.1	6.5	11.7	**7.5**	5.7	7.5	3.4	5.4	0.0	**4.4**
Polycrystalline quartz	5.8	7.9	2.2	3.9	**5.0**				0.7	**0.7**						
Total quartz	59.5	58.9	53.5	57.6	**57.4**	45.7	37.1	54.4	59.6	**49.2**	56.7	60.3	45.3	57.3	46.5	**53.2**
Other minerals																
Muscovite	2.6	4.6	0.3	0.3	**2.0**	2.9	4.5	0.7	0.3	**2.1**	3.6	2.3	3.1		0.6	**2.4**
Opaques	1.0	3.3	1.6		**2.0**			0.6	1.0	**0.8**						
Rock Fragments																
Quartzite	5.8	7.9	2.2	3.9	**5.0**											
Slate	12.3	12.9	13.6	4.8	**10.9**											
Matrix	18.1	12.5	28.7	34.3	**23.4**	51.4	58.4	44.0	35.5	**47.3**	39.7	36.8	48.9	35.5	51.9	**42.6**

Table 4.3A Clast composition in samples of crater-fill facies from Darwin Crater. For each sample, one thin section considered representative of the lithology was selected for detailed point counting. For each analysed thin section, 300 grains were counted in 3 passes (900 grains in total).

	Crater-fill Facies A (Polymict breccia)					Crater-fill Facies B (Deformed quartzite)				Crater-fill Facies C		
Sample	DDH1 63m	DDH1 68m	A27	A29	**Average**	A44		A36 1	A77	**Average**		
Matrix composition (vol%)												
Mica	10.0	20.0	30.0	20.0	**20.0**	15.0		20.0	25.0	**22.5**		
Quartz	75.0	65.0	40.0	50.0	**57.5**	50.0		50.0	25.0	**37.5**		
Goethite	2.0	trace	trace	2.0	**2.0**	15.0		10.0	35.0	**22.5**		
Kaolinite	2.0	10.0	20.0	10.0	**10.5**	15.0		15.0	10.0	**12.5**		
Chlorite	2.0	2.0		5.0	**3.0**							
Rutile			5	5	**5.0**	2		trace				
Pyrite	5.0		trace		**5.0**							
Jarosite	2			2	**2.0**	trace		2		**<2**		
Rozenite	2				**2.0**	trace						
Tourmaline			2	5	**3.5**							
Gypsum	trace											

Table 4.3B Matrix composition in crater-fill facies from Darwin Crater. Matrix composition determined by X-Ray Diffraction (XRD) at Mineral Resources Tasmania by Mr Ralph Bottril.

		Monocrystalline quartz					
				No. of fractures			
	Sample	Non-undulatory (%)	Undulatory (%)	1 (%)	2 (%)	3 or more (%)	"Twinned" quartz
Crater-fill Facies A (Polymict breccia)	DDH1 61m	37.6	23.0	0.6	3.4	28.7	<1
	DDH1 63m	35.7	16.2	5.4	12.4	20.5	<1
	DDH1 64m	36.5	18.5	1.1	13.5	16.9	<1
	DDH1 68m	65.9	11.4	0.0	9.6	9.0	<1
	Average	**43.9**	**17.3**	**1.8**	**9.7**	**18.8**	<1
Crater-fill Facies B (Deformed quartzites)	A36 2	62.5	15.6	0.0	9.4	12.5	<<1
	A44	67.0	5.2	0.9	10.4	16.5	<<1
	A72 bot	70.7	13.2	2.4	1.8	12.0	<<1
	A75	52.5	18.0	0.0	8.7	19.7	<<1
	Average	**63.1**	**13.0**	**0.8**	**7.6**	**15.2**	<<1
Crater-fill Facies C (Deformed slates)	A36 1	70.0	15.7	0.0	4.3	10.0	<<1
	A56	68.1	13.5	1.6	4.3	12.4	<<1
	A72 top	78.4	14.2	0.0	0.0	7.4	<<1
	A77	69.1	16.4	1.4	3.7	9.4	<<1
	A78	86.1	11.1	2.1	0.7	0.0	<<1
	Average	74.3	14.2	1.0	2.6	7.9	<<1
	02031	4.6	11.6	1.7	12.1	51.4	4.6
	02032	10.0	16.7	5.6	10.0	37.8	6.1
	02033	5.2	15.5	4.7	7.8	40.4	7.3
	Average	**6.6**	**14.6**	**4.0**	**10.0**	**43.2**	**6.0**

Table 4.4 Petrography of monocrystalline quartz in surface Eldon Group samples from around Darwin Crater and in crater-fill samples. Determined by point counting. Here the observations of quartz grains with, for example one fracture, is expressed as a percentage of the total number of of monocrystalline quartz grains. Quartz grains in the crater-fill samples and glass-bearing gravels around the crater have experienced a far greater degree of deformation and fracturing than such grains from in surface Eldon Group samples cropping out around the crater (table 4.2).

1. Location with respect to crater (Rc = crater radius)

Crater Floor and Subcrater	Within Crater	Crater Rim and Near-Surface
Parautochtonous rocks: target rocks (coherent) lithic breccias	**Allogenic** rocks **Crater-fill deposits** (=crater-fill breccias) (="breccia lens")	Allogenic rocks **Ejecta:** proximal (<5Rc) distal (>5Rc)
Allogenic rocks (cross-cutting) breccia dykes **impact melt** dykes	**lithic breccias** melt-bearing breccias **suevites**	
Pseudotachylite	**Impact melt breccias** (=melt-matrix breccias) **impact melt rocks**	

2. Sources of component materials

Parautochtonous rocks:	**Allogenic rocks**
Approximately in place (local). Original stratigraphy and structure largely preserved.	Derived from single or multiple sources elsewhere

3. Breccia characteristics

A. Fragment character	**Lithic breccia** Rock/mineral fragments only	**Suevite** breccia Melt/glass fragments present Rock/mineral fragments
B.Fragment lithology	**Monomict** breccia Single rock type	**Polymict** breccia Multiple rock types
C. Matrix character	**Clastic-matrix** breccia Discrete fragements	**Impact melt breccia** (=melt matrix breccia) Coherent melt (glassy or crystalline)

4. Melt rock character (standard geological terms)

Holohyaline (glassy)
Hypocrystalline (mixed glassy/crystalline)
Holocrystalline (completely crystalline)

For grain-size, texture, etc., use other standard igneous rock discriminators e.g. **microcrsytalline**

Table 4.5 Criteria for the classification of impact related rock types. From French (1998).

rocks surrounding the crater is interpreted to indicate that a very localised process was responsible for the deformation. The block of rocks containing deformed carbonate are petrographically identical to carbonate pebbles in the upper polymict breccia and this would require a degree of excavation during the formation of the structure; this will be discussed later.

4.6 Geochemistry of surface and crater-fill samples

Rocks recovered from the drill core show petrographic affinity with Eldon Group slates and quartzites that surround the crater. To further define the relationship between the sub-surface lithologies in the crater-fill and the local surface geology, the major and trace element composition of a suite of samples was determined. These samples come from the drill core and the area immediately surrounding the crater - unlike previous studies that did not access samples from the drill core, but involved only potential 'target rocks' sampled from poorly defined locations across the local area. Later, these analyses will provide the first opportunity for accurate evaluation of the relationship between Darwin glass and its suspected target rocks. Prior to this, the chemical relationship between crater-fill samples and Eldon Group rocks outcropping at the surface surrounding the structure is examined.

4.6.1 Sample selection and preparation

In total, 33 samples that encompass the range of rocks found around the crater and throughout the drill cores were selected for analysis. Ford collected most of the analysed surface samples along a W-E traverse from the access track, to the eastern rim of the crater. The position of analysed core samples are depicted in Fig. 4.13. Outcropping suspected target rock samples were carefully selected to avoid analyses of highly weathered samples although this is obviously difficult when sampling rocks in western Tasmania. The petrography of analysed samples is described in tables 4.3A,B. These hand sized specimens were split into ~10mm chips and weathered material discarded. The chips were further crushed using a hydraulic crusher and cleaned of dust with an airhose. In analyses that exclude Co, around 40g of the crushed material was ground in the tungsten carbide ring mill. For most

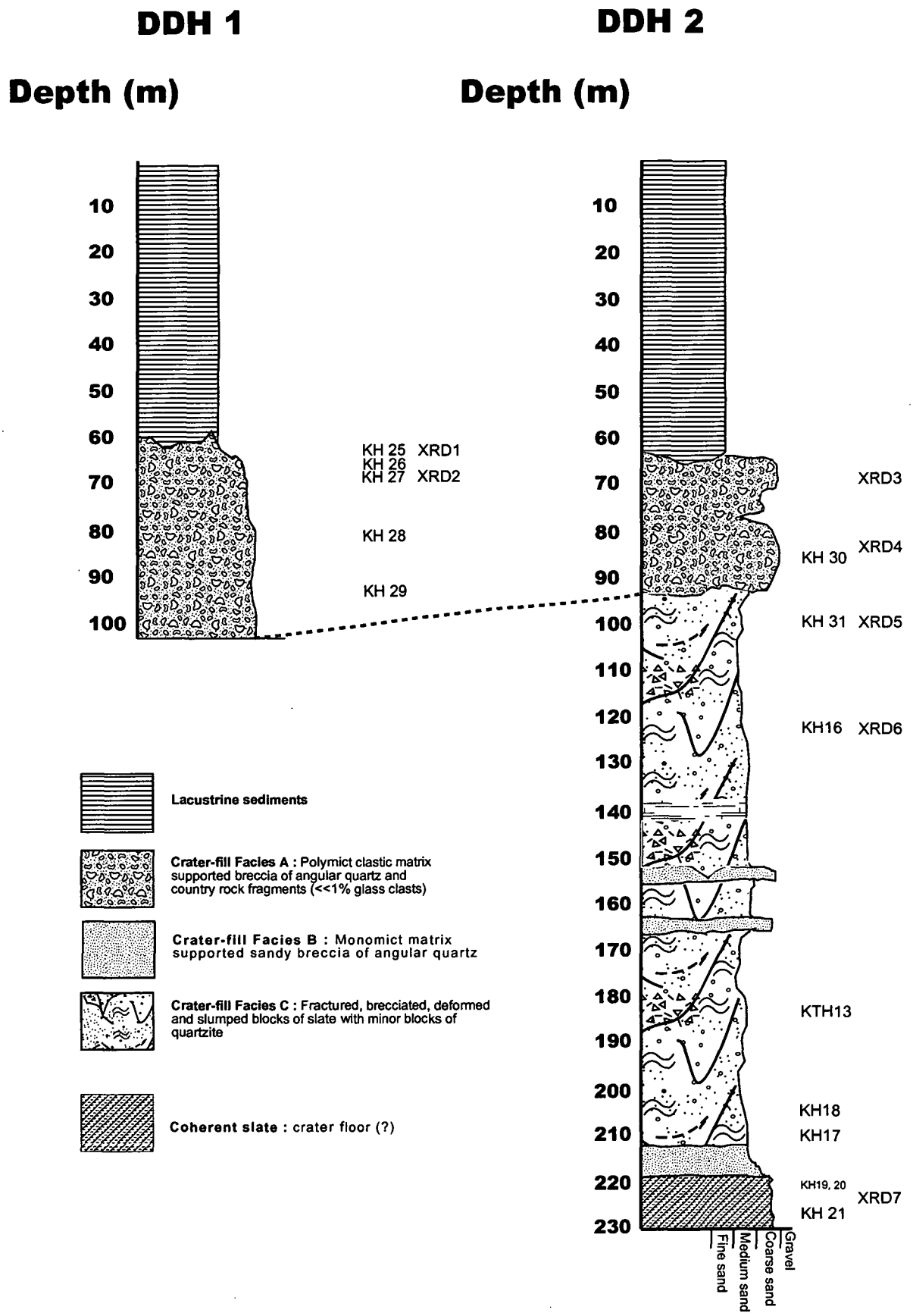

Figure 4.13 Stratigraphy of Darwin Crater showing location of geochemical and XRD samples.
Geochemical samples have preffix KH or KTH.

analyses that include Co, the crushed material was further pulverized in an agate mortar and pestle before being further crushed to fine powder in an agate ring mill.

4.6.2 Analytical techniques

Fusion discs of the powdered samples were prepared for determination of the major elements (SiO_2, Al_2O_3, TiO_2, MnO, MgO, FeO, K_2O, CaO, Na_2O P_2O_5) by X-Ray Fluorescence (XRF). Pressed pills were used for XRF analysis of the following trace elements: Cr, Co, Ni, Cu, Zn, Ga, Nb, Rb, Sr, Ba, Zr and Y. These analyses were conducted on an automated Phillips PW 1480 XRF spectrometer at the School of Earth Sciences, University of Tasmania. Mr Phillip Robinson provided calibrations.

Portions of samples (KH 1,2,4,6,7,8,12,15,17,18,19) that were analysed by XRF were dissolved using HF and HNO_3 acids and brought to a 1:1000 dilution in 2%HNO_3 to allow analyses using ICP-MS. This technique was chosen primarily to determine the REE geochemistry of the suspected target rocks, but trace elements determined by XRF were also analysed by ICPMS. The following trace elements were determined: Sc, Cr, Co, Ni, Ga, Rb, Sr, Y, Nb, Sb, Cs, La, Ce, Pr, Nd, Sm, Eu, Gd, Tb, Dy, Ho, Er, Yb, Lu, Hf, Ta, Pb, Th, and U. The abundance of the trace elements in these samples was calibrated against the well-known rock standard BHVO-1. Instrument drift was monitored and corrected using Ln and Ti as internal standards.

4.6.3 Major elements in suspected target rocks and crater-fill samples from Darwin Crater

Results for analyses of surface Eldon Group rocks and crater-fill samples from the drill cores are presented in table 4.6. Complete analyses are listed in Appendix 2. The average SiO_2 content is highest in the surface samples of Crotty (94.6%) and Keel (90.09%) Quartzite followed by Amber Slate (75.41%). The analysed limestone pebbles (KH29) are relatively pure carbonate and the absence of CaO in all analyses of surface Amber Slate suggests that even minor interbedded limestone or carbonate cement is unlikely in these rocks, as is consistent with the petrography of the analysed samples. The absence of CaO in the remaining crater-fill samples suggests that any limestone is stratigraphically confined to thin beds at depth such as is observed in the sample of

	Keel Quartzite							Amber Slate									Crotty Quartzite				
Sample	KH1	KH2	KH3	KH4	KTH11	KTH12	Average	KH5	KH6	KH7	KH8	KH9	KH10	KTH1	KTH 14	Average	KH11	KH12	KTH 2	KTH 3	Average
SiO_2	85.63	87.68	91.89	90.35	92.38	92.63	90.09	77.27	76.91	79.05	69.46	70.14	77.03	76.54	76.95	75.41	93.64	97.60	93.24	93.91	94.60
Al_2O_3	8.44	6.32	4.53	4.97	4.13	4.18	5.43	11.69	11.83	10.29	14.60	14.45	10.58	10.66	10.58	11.83	3.08	1.11	3.94	3.16	2.82
TiO_2	0.55	0.45	0.56	0.42	0.47	0.50	0.49	0.70	0.86	0.76	0.79	0.78	0.56	0.63	0.63	0.71	0.23	0.14	0.36	0.21	0.24
FeO	0.62	0.44	0.31	0.43	0.38	0.31	0.42	2.01	1.95	1.95	4.43	4.57	3.62	4.00	3.75	3.28	0.51	0.06	0.22	0.59	0.35
MgO	0.51	0.35	0.35	0.35	0.27	0.27	0.35	1.05	1.19	1.06	1.58	1.52	1.25	1.44	1.44	0.01	0.15	0.09	0.17	0.17	0.15
MnO	0.01	0.01	0.01	0.01	0.01	0.01	0.01	0.01	0.01	0.01	0.01	0.01	0.01	0.02	0.01	<0.01	<0.01	<0.01	<0.01	<0.01	<0.01
CaO	0.01	0.29	0.01	0.01	0.09	0.09	0.08	0.01	0.01	0.01	0.01	0.01	0.32	0.16	0.16	0.08	0.13	0.01	0.01	0.15	0.07
K_2O	2.81	2.11	1.56	1.57	1.45	1.44	1.82	3.71	4.04	3.49	3.99	3.95	2.92	2.85	2.84	3.47	1.24	0.38	1.11	1.24	0.99
Na_2O	0.04	0.04	0.03	0.05	0.00	0.04	0.03	0.08	0.11	0.07	0.14	0.13	0.35	0.39	0.42	0.20	0.00	0.04	0.04	0.00	0.02
P_2O_5	0.02	0.30	0.03	0.03	0.01	0.01	0.07	0.11	0.08	0.08	0.10	0.11	0.35	0.17	0.16	0.14	0.12	0.01	0.01	0.13	0.70

	Crate-fill Facies B and C (Deformed slate and quartzite)									Crater-fill Facies A (Polymict breccia)							
Sample	KH16	KH17	KH18	KH20	KH21	KH15	KTH13	KH31	Average	KH25	KH26	KH27	KH28	KH30	Average	KH19	KH29
SiO_2	69.81	90.55	65.46	72.81	69.83	53.38	70.6917	71.81	70.54	73.73	76.91	76.29	75.73	71.1	74.75	37.92	7.03
Al_2O_3	12.68	4.431	11.98	14.25	14.32	9.26	14.3084	9.3	11.32	4.955	8.49	10.93	12.59	10.77	9.55	7.46	1.17
TiO_2	0.758	0.489	0.67	0.75	0.73	0.53	0.8432	0.667	0.68	0.366	0.514	0.653	0.776	0.673	0.6	0.41	0.08
FeO	6.911	1.607	10.75	1.845	3.959	10.25	4.32333	9.828	6.18	6.885	3.568	2.526	2.075	5.0803	4.03	33.52	1
MgO	1.04	0.32	1.17	1.28	1.53	0.71	1.04545	0.68	0.97	0.525	0.915	1.28	1.02	1.04	0.96	0.63	1.04
MnO	0.02	0.04	0.04	<0.01	<0.01	1.01	0.01	0.02	0.19	0.008	0.008	0.118	<.01	0.021	0.03	0.2	0.08
CaO	0.079	0.05	0.1	0.49	0.29	1	0.07916	0.07	0.27	0.06	0.095	0.66	0.04	2.44	0.66	0.55	49.94
K_2O	3.551	1.114	3.685	4.271	4.692	1.913	3.93507	2.399	3.2	1.437	2.487	3.285	3.792	2.933	2.79	2.13	0.3
Na_2O	0.09	<0.03	0.09	0.14	0.09	0.12	0.04941	0.05	0.09	0.07	0.145	0.06	0.08	0.1	0.09	0.09	<0.03
P_2O_5	0.247	0.037	0.467	0.436	0.307	1.411	0.18	0.386	0.19	0.041	0.052	0.158	0.05	0.305	0.12	1.75	0.06

Table 4.6 Major element composition of Eldon Group samples from around Darwin Crater and crater-fill facies. Determined by XRF.

core recovered from a slumped block of deformed rock intersected between 139 – 142m. For most major elements, the deformed rocks from the drill core show obvious affinity with the Amber Slate and Keel Quartzite (KH17) cropping out around the crater. The FeO content increases down hole in the deformed slates of Crater-fill Facies C relative to surface samples and in sample KH19 reaches 33.5% at just 37% SiO_2. A simultaneous increase in P_2O_5 content is observed in Facies C relative to the remaining analysed rocks and in KH19 reaches 1.4%. This sample is taken from a highly fractured and brecciated zone that has been filled by the oxyhydroxide goethite. The polymict, allogenic breccia samples (Crater-fill Facies A) also show strong geochemical affinity with cropping out surface rocks and the deformed shales intersected in the drill cores, except for up to 5% S in samples KH25 and KH26 from the top of this facies. This elevated S content is consistent with petrographic observations and XRD data that indicate pyrite in these samples.

The major elements are correlated in a systematic manner (Fig. 4.14A-H). In all samples there is an inverse relationship between SiO_2 and FeO and a positive relationship between P_2O_5 and FeO that is most pronounced in Crater-fill Facies C. In the surface samples of Eldon Group rocks there is a strong negative correlation between SiO_2 and the remaining major oxides that are correlated positively with each other. In contrast, the drill core samples show positive correlation between SiO_2 and Al_2O_3, TiO_2 and K_2O that are all inversely related to FeO.

The composition of the analysed rocks and the relationship between SiO_2 and the other oxides in surface Eldon Group samples reflect the dilution effects of quartz (Cullers 2000) and is consistent with petrographic observations that show an increase in the proportions of interlocking quartz crystals relative to matrix material from the Amber Shale to the Crotty Quartzite. As such, pelitic zones in the Keel Quartzite are expected to be compositionally, as well as petrographically, very similar to Amber Slate samples and this is important in later discussion of the stratigraphic affinity of the glass. The bulk composition of the crater-fill samples is also controlled by dilution effects of quartz as is evident in the negative correlation between FeO and SiO_2. However, the geochemical variations in the remaining major oxides in the crater-fill samples are strongly influenced by supergene/weathering processes that are preferentially increasing the FeO content. This is also consistent with petrographic observations and XRD data that show abundant goethite has been precipitated in the fracture zones in the core samples. The increased abundance of

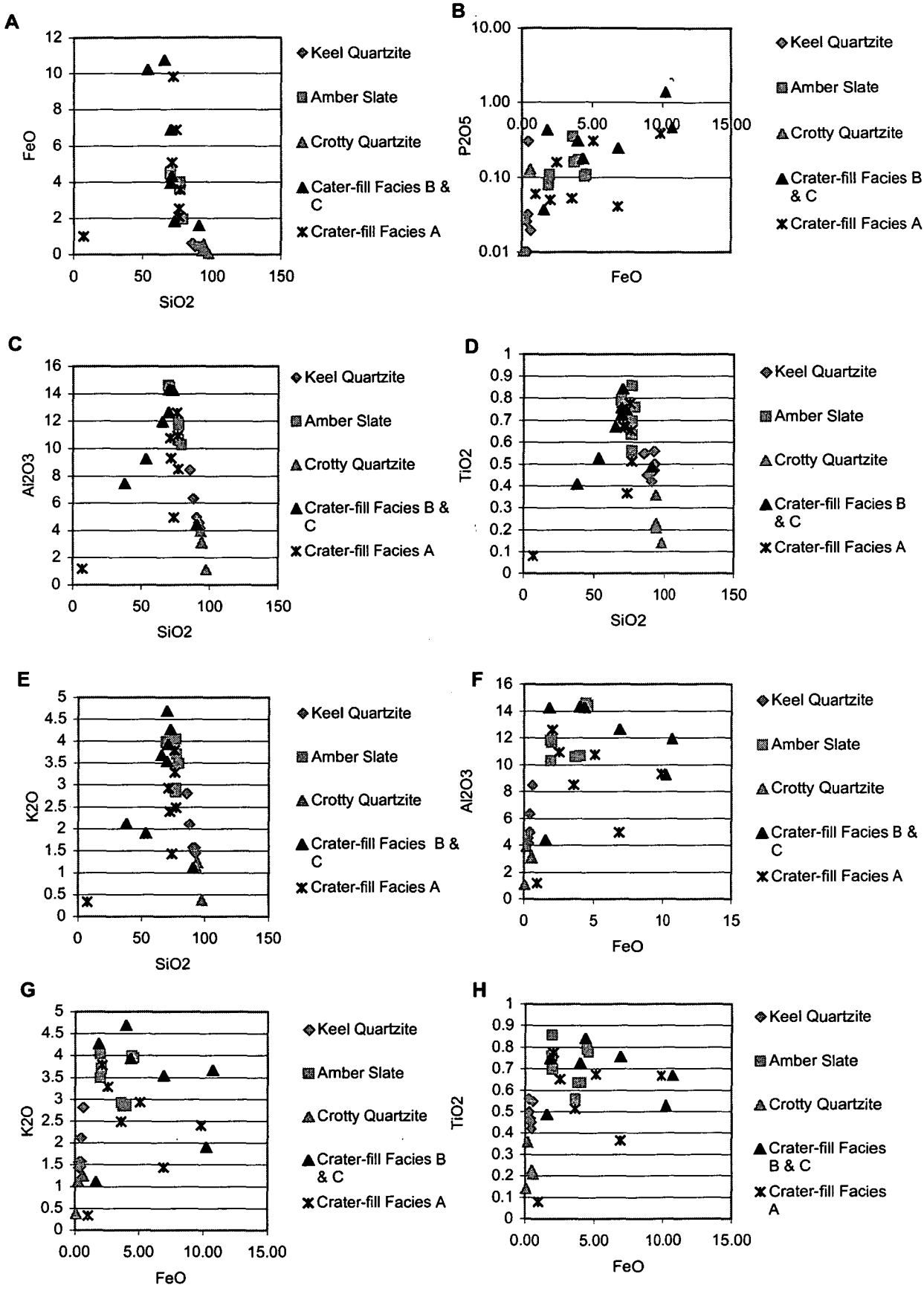

Figures 4.14A-H Major element variations in Eldon Group samples from around Darwin Crater and crater-fill facies.

P_2O_5 in Crater-fill Facies C relative the remaining samples, and the positive correlation between P_2O_5 and FeO is likely to reflect preferential adsorption of P_2O_5 onto the goethite lattice during the mineral's precipitation (Gimsing & Borggaard 2002). The adsorption of P_2O_5 on goethite is favoured relative to kaolinite (Gimsing & Borggaard 2002) and this is consistent with these data that show a lower P_2O_5 content in Crater-fill Facies A where the clay mineralogy is dominated by kaolinite.

A Herron (1988) diagram has been produced in order to chemically classify the Eldon Group rocks, and rocks from the drill core (Fig. 4.15). The diagram supports the petrographic classification of the Eldon Group rocks as varying from shale/slate to quartz arenite and shows the clear affinity of rocks from the drill core with those outcropping around the crater. The high Al_2O_3 content of the samples, especially the Keel Quartzite, causes these to plot towards more 'arkose like' compositions than the petrographic classification suggests, and this reflects the control of muscovite alteration on Al_2O_3 concentration rather than any detrital feldspar component that would be associated with a true arkose.

4.6.4 Trace elements in suspected target rocks and crater-fill samples from Darwin Crater

The range and average abundance of trace elements in surface and crater-fill samples from Darwin Crater are presented in tables 4.7A,B. For most elements the slates show the most limited compositional range. In all analyses the REE – especially the LREE - show the least variation and range from between <2% (e.g. Sm in Amber Slate) and 60 % (e.g. Gd in Keel Quartzite) of mean values. The transition metals Ni and Co and the alkaline earth Sr show the greatest compositional ranges of the determined elements. Sr in analyses of Keel Quartzite may vary by up to 240 % of the mean (8.7ppm) and Ni and Co by 160 and 140 % respectively. This large variation in analytical results – particularly for the transition metals - relates to the dilution effect of quartz and the subsequent very low abundance of these elements in the most quartz-rich samples. The ranges in the abundance of all trace elements in the crater-fill samples fall largely within the total ranges for the analysed Eldon Group rocks from around the crater (Fig. 4.16). The obvious exceptions being enrichments in HREE plus Y, transition metals Ni, Co, Cr and the sulphide metals Zn, As, Cu and Pb in Crater-fill Facies C. This enrichment is most pronounced in those

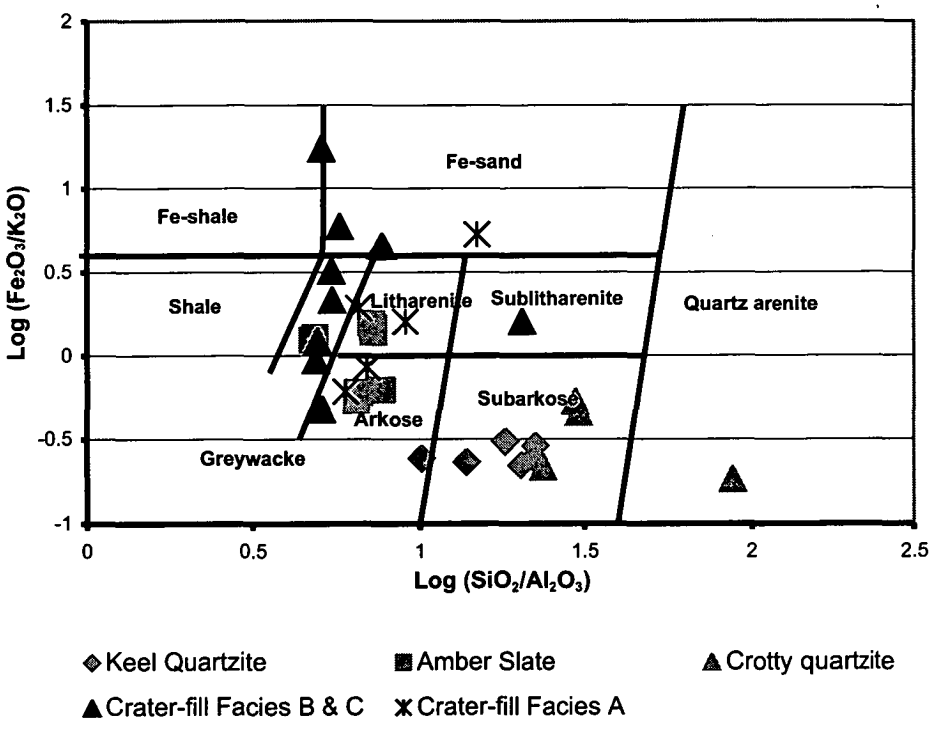

Figure 4.15 Herron (1988) diagram for chemical classification of sedimentary rocks. Note compositional overlap of the surface Eldon Group (suspected target rock) samples and crater-fill facies.

	Keel Quartzite							Amber Slate									Crotty Quartzite					
Sample	KH1	KH2	KH3	KH4	KTH11	KTH12	Average	KH5	KH6	KH7	KH8	KH9	KH10	KTH1	KTH 14	Average	KH11	KH12	KTH 2	KTH 3	Average	
Cs	5.51	4.12		3.18			**4.27**		9.02	7.71	12.35					**9.69**						Cs
Rb	110.50	84.60	62.20	63.00	42.20	14.60	**62.85**	161.60	179.70	157.10	197.70	196.00	138.40	128.20	131.20	**161.24**	42.20	14.60	45.60	42.10	**36.13**	Rb
U	1.75	2.73		2.04			**2.17**		3.24	2.91	3.83					**3.33**						U
Th	7.89	13.37		10.48			**10.58**		17.47	15.54	20.54					**17.85**						Th
Ba	350.50	307.50	253.00	254.30	120.90	108.90	**232.52**	542.10	596.50	507.80	567.30	557.40	707.30	503.70	514.00	**562.01**	120.90	108.90	143.97	124.30	**124.52**	Ba
La	30.01	34.19		29.77			**31.33**		49.44	43.84	46.08					**46.45**						La
Ce	62.15	74.09		61.59			**65.94**		96.00	85.51	91.22					**90.91**						Ce
Nb	12.35	9.81	12.50	9.53	4.70	4.10	**8.83**	15.70	19.83	17.50	18.11	17.60	13.80	14.50	13.80	**16.36**	4.70	4.10	8.10	4.00	**5.23**	Nb
Pr	7.40	8.96		7.19			**7.85**		11.12	9.96	10.85					**10.64**						Pr
Sr	4.74	22.56	4.00	11.05	9.00	1.20	**8.76**	19.60	20.17	18.37	9.00	9.90	22.90	15.05	14.24	**16.15**	9.00	1.20	20.60	9.80	**10.15**	Sr
Nd	27.75	35.35		26.61			**29.90**		39.72	35.66	39.29					**38.22**						Nd
Zr	275.30	385.30	600.30	342.40	142.70	112.90	**309.82**	357.40	404.00	385.00	329.70	312.10	222.60	343.67	339.87	**336.79**	142.70	112.90	305.50	123.85	**171.24**	Zr
Sm	4.96	8.67		5.30			**6.31**		7.63	6.81	7.49					**7.31**						Sm
Eu	0.83	1.64		0.97			**1.14**		1.39	1.18	1.30					**1.29**						Eu
Gd	4.01	8.42		4.50			**5.64**		6.25	5.65	5.99					**5.96**						Gd
Ho	0.87	1.48		0.87			**1.07**		1.25	1.14	1.17					**1.18**						Ho
Yb	2.26	3.91		2.28			**2.82**		3.60	3.23	3.18					**3.34**						Yb
Y	23.44	39.67	27.90	23.96	21.20	9.00	**24.19**	33.70	34.70	30.81	32.69	30.90	35.80	26.20	26.30	**31.39**	21.20	9.00	12.70	19.60	**15.63**	Y
Lu	0.34	0.58		0.34			**0.42**		0.53	0.48	0.47					**0.50**						Lu
Sc	6.96	6.97		4.33			**6.09**		10.99	9.95	12.65					**11.20**						Sc
Cr	57.10	46.70	50.90	37.30	87.10	48.60	**54.52**	77.30	87.60	72.00	100.00	98.70	83.10	81.73	82.71	**85.39**	87.10	78.70	76.70	76.34	**80.83**	Cr
Co	1.00	1.00	1.00	1.00	2.40	2.20	**1.43**	2.50	2.30	1.00	5.30	4.60	6.20			**3.65**	8.10	2.20			**5.15**	Co
Ni	10.60	12.30	7.00	6.00	8.10	0.50	**7.42**	14.20	10.60	9.20	28.60	27.60	24.50	29.10	28.40	**21.53**	2.40	0.50	4.80	9.70	**4.35**	Ni

Table 4.7A Trace element composition of Eldon Group samples from around Darwin Crater. Determined by XRF and solution ICP-MS.

	Crate-fill Facies B and C (Deformed slate and quartzite)									Crater-fill Facies A (Polymict breccia)								
Sample	KH15	KH16	KH17	KH18	KH20	KH21	KH31	KTH13	**Average**	KH25	KH26	KH27	KH28	KH30	**Average**	KH19	KH29	
Cs	10.60		3.98	13.92					**9.50**							9.65		**Cs**
Rb	96.20	163.30	49.70	171.80	197.30	216.10	110.60	177.40	**147.80**	68.90	116.70	142.20	158.70	132.00	**123.70**	83.40	13.80	**Rb**
U	4.11		1.99	3.63					**3.24**							7.94		**U**
Th	15.85		14.61	21.57					**17.34**							21.98		**Th**
Ba	403.20	507.00	181.80	491.40	565.60	627.00	356.60	542.80	**459.43**	248.30	406.20	471.70	578.70	437.50	**428.48**	371.80	56.50	**Ba**
La	39.68		33.91	51.38					**41.66**							87.42		**La**
Ce	82.55		73.22	107.21					**87.66**							161.56		**Ce**
Nb	12.14	16.80	10.55	15.65	20.20	16.10	15.00	18.80	**15.65**	8.20	11.10	15.40	17.80	14.70	**13.44**	10.74	1.50	**Nb**
Pr	9.72		8.57	12.90					**10.40**							22.32		**Pr**
Sr	28.82	10.50	6.65	7.49	18.50	12.60	11.10	8.08	**12.97**	12.10	18.90	23.20	28.70	37.20	**24.02**	16.81	426.60	**Sr**
Nd	37.21		33.95	50.25					**40.47**							106.44		**Nd**
Zr	254.00	306.80	440.80	302.50	285.00	254.80	422.00	294.04	**319.99**	236.10	278.60	345.00	265.80	325.20	**290.14**	265.10	33.40	**Zr**
Sm	8.24		7.87	11.16					**9.09**							36.26		**Sm**
Eu	1.62		1.65	2.19					**1.82**							11.68		**Eu**
Gd	7.65		7.46	10.84					**8.65**							69.06		**Gd**
Ho	1.31		1.24	2.17					**1.57**							24.08		**Ho**
Yb	3.31		3.00	5.86					**4.06**							81.88		**Yb**
Y	35.81	46.20	33.19	65.29	85.80	61.10	41.30	48.70	**52.17**	19.70	28.20	56.50	39.10	63.50	**41.40**	859.83	23.30	**Y**
Lu	0.47		0.44	0.88					**0.60**							13.71		**Lu**
Sc	9.26		4.66	13.42					**9.11**							94.75		**Sc**
Cr	84.80	89.50	44.70	99.90	119.90	114.30	70.40	101.63	**90.64**	55.40	72.50	84.60	80.60	85.50	**75.72**	190.30	8.20	**Cr**
Co	19.10	11.10	1.00	11.50	6.20	10.00	16.50		**10.77**	5.40	20.70	14.10	18.40	14.70	**14.66**	15.31	<2	**Co**
Ni	33.70	40.60	7.60	93.50	22.90	49.10	57.60	37.10	**42.76**	15.60	43.20	29.60	30.50	33.80	**30.54**	153.93	5.70	**Ni**

Table 4.7B Trace element composition of crater-fill facies from Darwin Crater. Determined by XRF and solution ICP-MS.

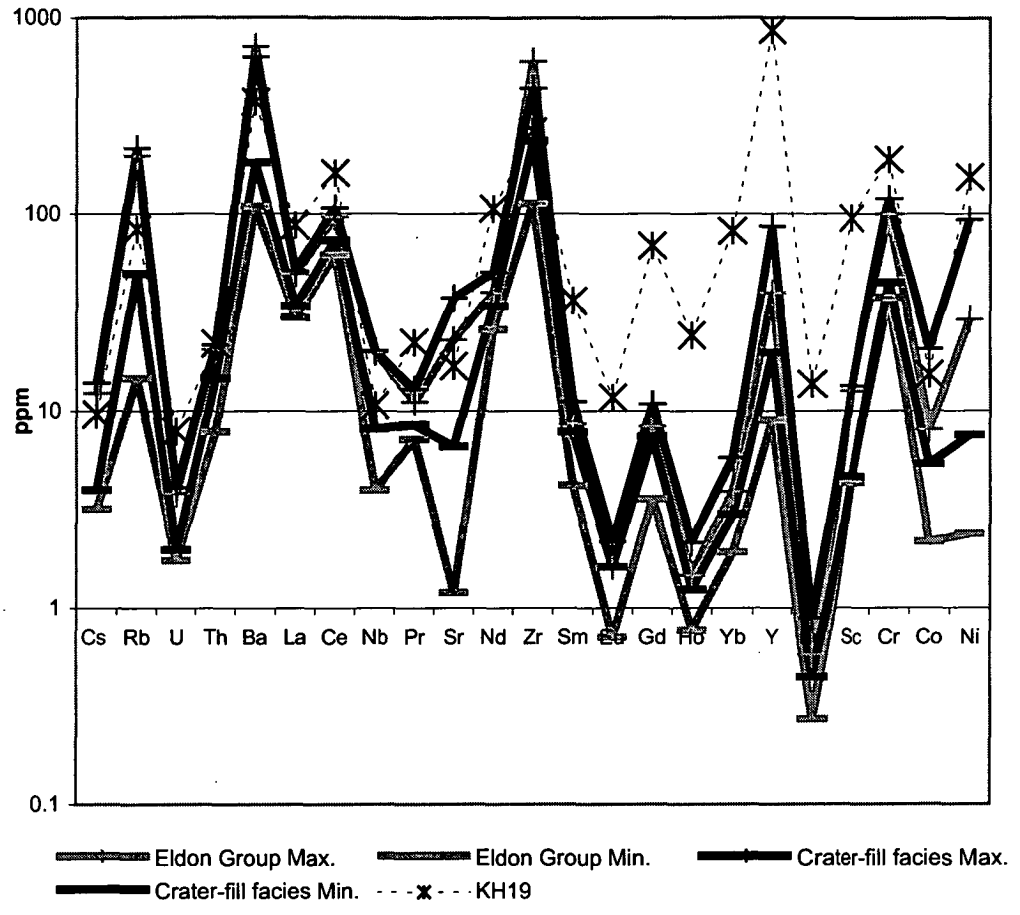

Figxure 4.16 Trace element concentrations in Eldon Group samples from around Darwin Crater and crater-fill facies.

Showing maximum and minimum abundances of each element in Eldon Group samples and crater-fill facies. Note compositional overlap between the Eldon Group samples and crater-fill facies.

analysed samples with the most abundant Fe-oxyhydroxides such as KH19 that has up to 150ppm Ni, 190 ppm Cr and 720ppm Y!

As for the major elements, the trace elements are correlated in a systematic manner and unlike the major elements the variation in trace element geochemistry is generally consistent between surface and drill core samples. All of the trace elements except Zr and Sr correlate positively, and, as may be expected, this correlation is strongest amongst the REE. These interrelated trace elements are inversely related to SiO_2 content and positively correlated with the remaining major oxides (Fig. 4.17A-AM). This reflects both the dilution effects of SiO_2 and primary and weathering-induced concentration of trace elements in the fine, or matrix component of the samples (Nesbitt 1979, Rollinson 1993). As such, the total abundance of trace elements is greatest in the most FeO and Al_2O_3 rich pelites intersected in the drill cores, and least in surface quartzite samples, which is consistent with petrography.

In Crater-fill Facies C where Fe-oxyhydroxides are most abundant, the enriched HREE plus Y, transition (Ni, Co, Cr) and sulphide (Zn, As, Cu, Pb) metals show positive correlations with each other and with P_2O_5 and FeO (Fig. 4.18A-AE). These observed correlations with P_2O_5 and FeO are weakest in Y and strongest amongst the transition elements and sulphides. As such, this enrichment is interpreted to reflect the effects of prolonged deep weathering and incorporation of these elements into the iron oxyhydroxide (goethite) and clay mineral matrix (e.g. Ohlander 2003). This is supported by ESEM analyses that show no evidence of crystalline sulphide minerals indicating that these trace elements were not precipitated from hydrothermal solutions but rather are adhering to the mineral matrix. The ultimate source of the metals is interpreted to be rare sulphide veins in the country rocks as observed by Ford. The correlation between the transition metals, sulphide metals, HREE plus Y, P_2O_5, and FeO, especially given an inverse, or lack of relationship to MgO, rules out the possibility that these elements reflect contamination from the putative projectile. This concentration has taken place preferentially along the abundant fracture controlled pathways in the deformed rocks of crater-fill Facies C. In contrast to the other trace elements, Zr shows positive correlation with SiO_2 and this implies the presence of detrital zircons and again this is consistent with petrographic observations of rare zircon in the Eldon Group quartzites. Sr shows little systematic

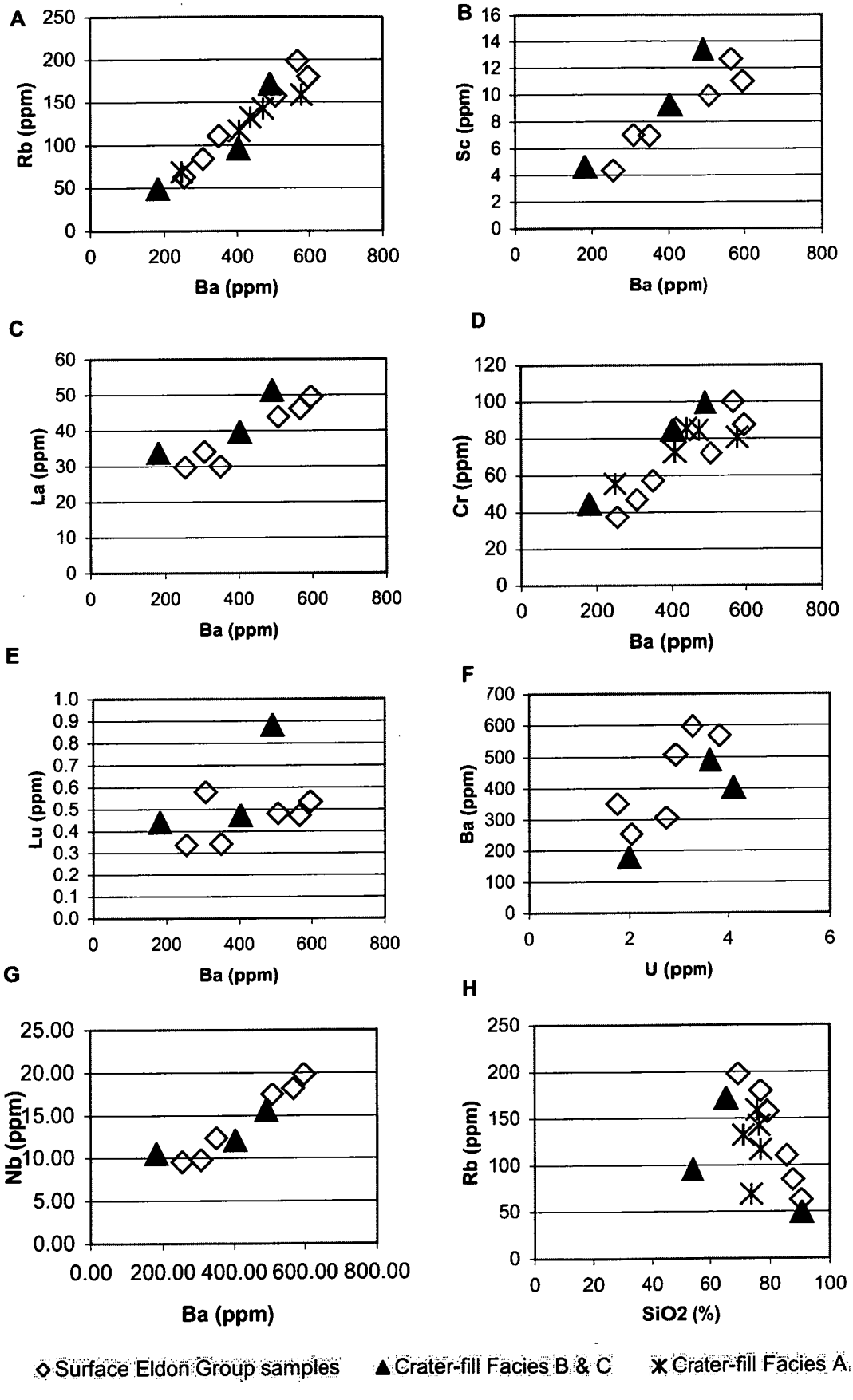

Figure 4.17A-H Trace element variation in Eldon Group samples from around Darwin Crater and crater-fill facies.

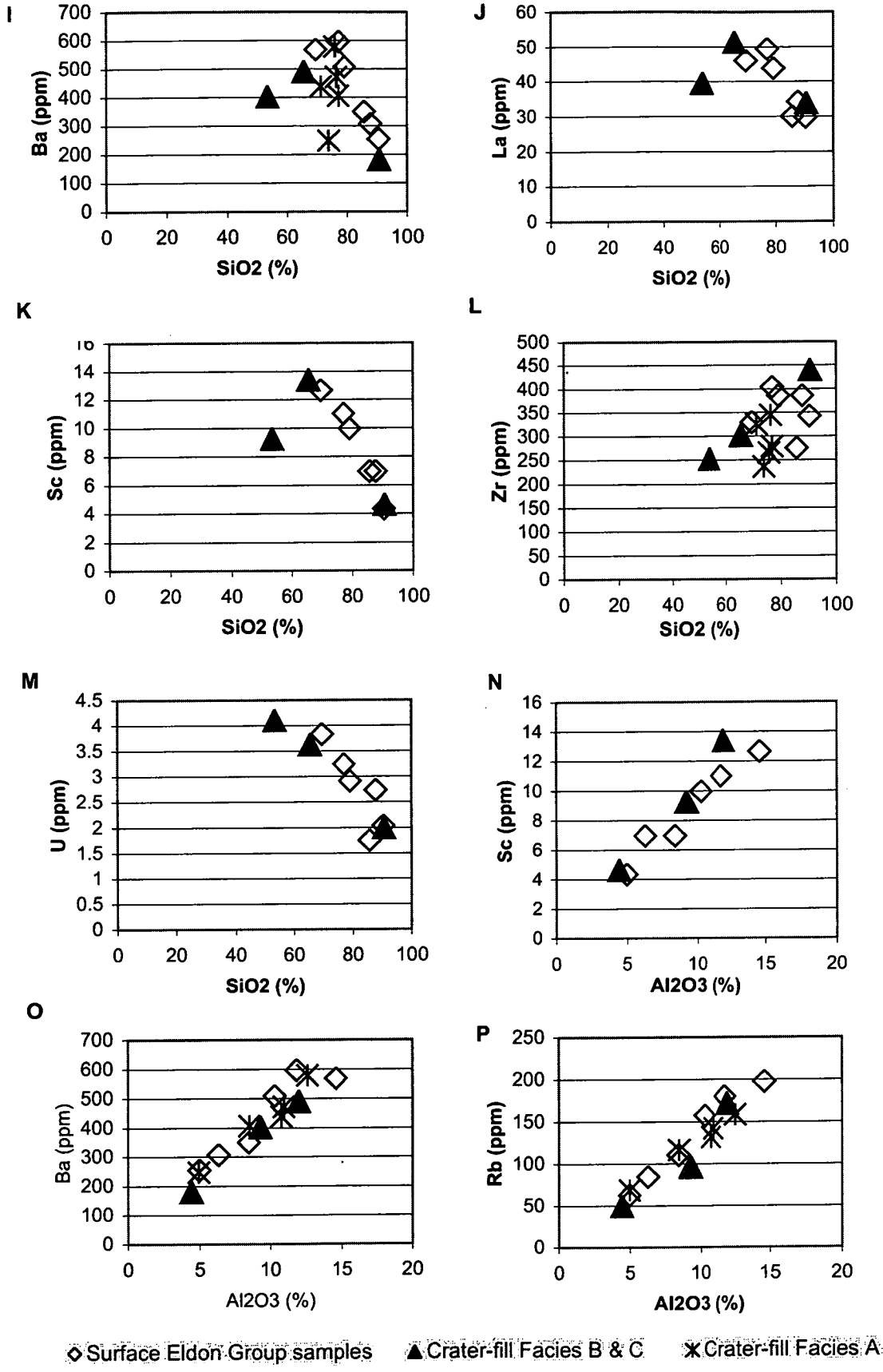

Figure 4.17I-P Trace element variation in Eldon Group samples from around Darwin Crater and crater-fill facies.

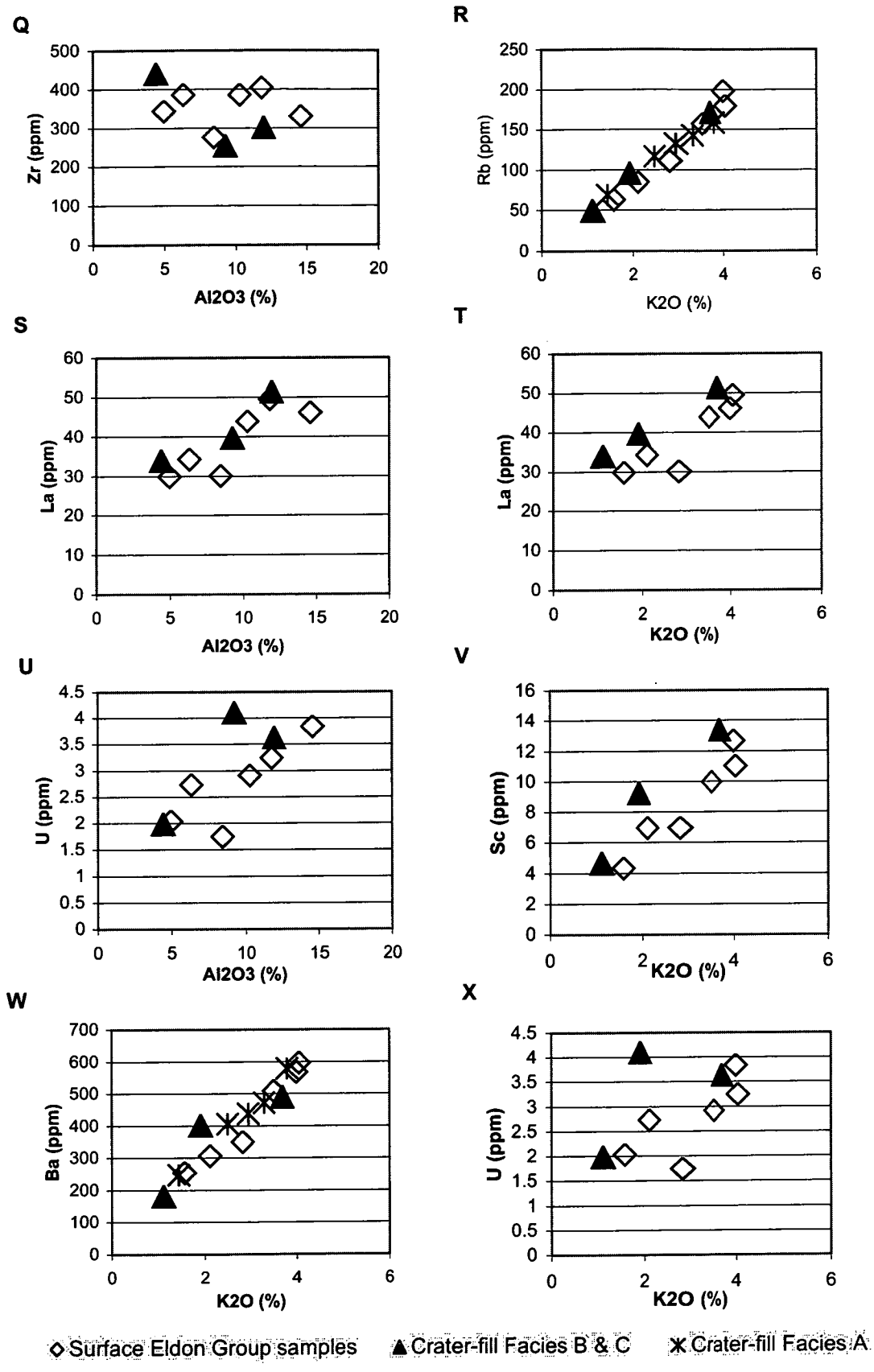

Figure 4.17Q-X Trace element variation in Eldon Group samples from around Darwin Crater and crater-fill facies.

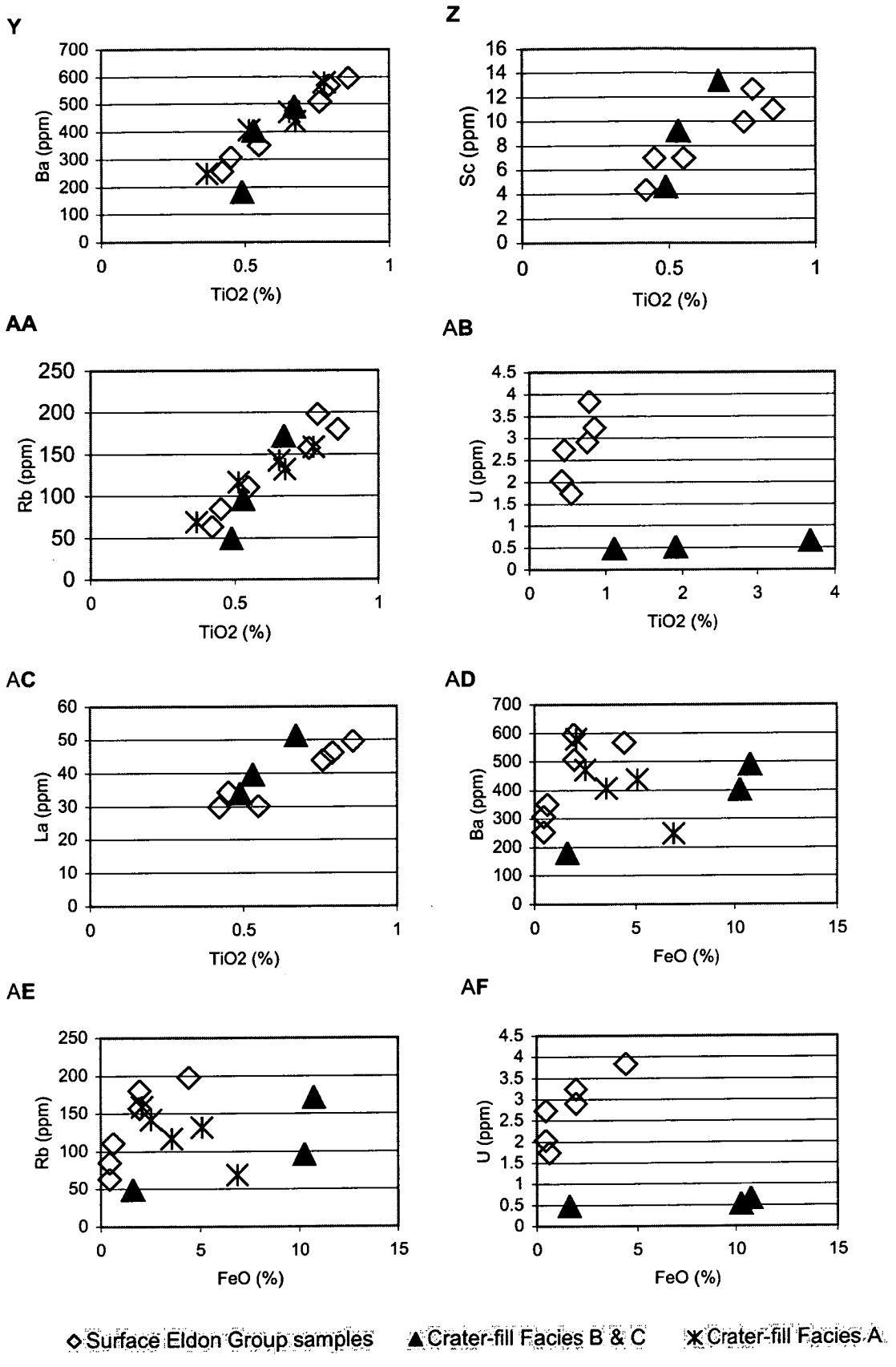

Figure 4.17Y-AF Trace element variation in Eldon Group samples from around Darwin Crater and crater-fill facies.

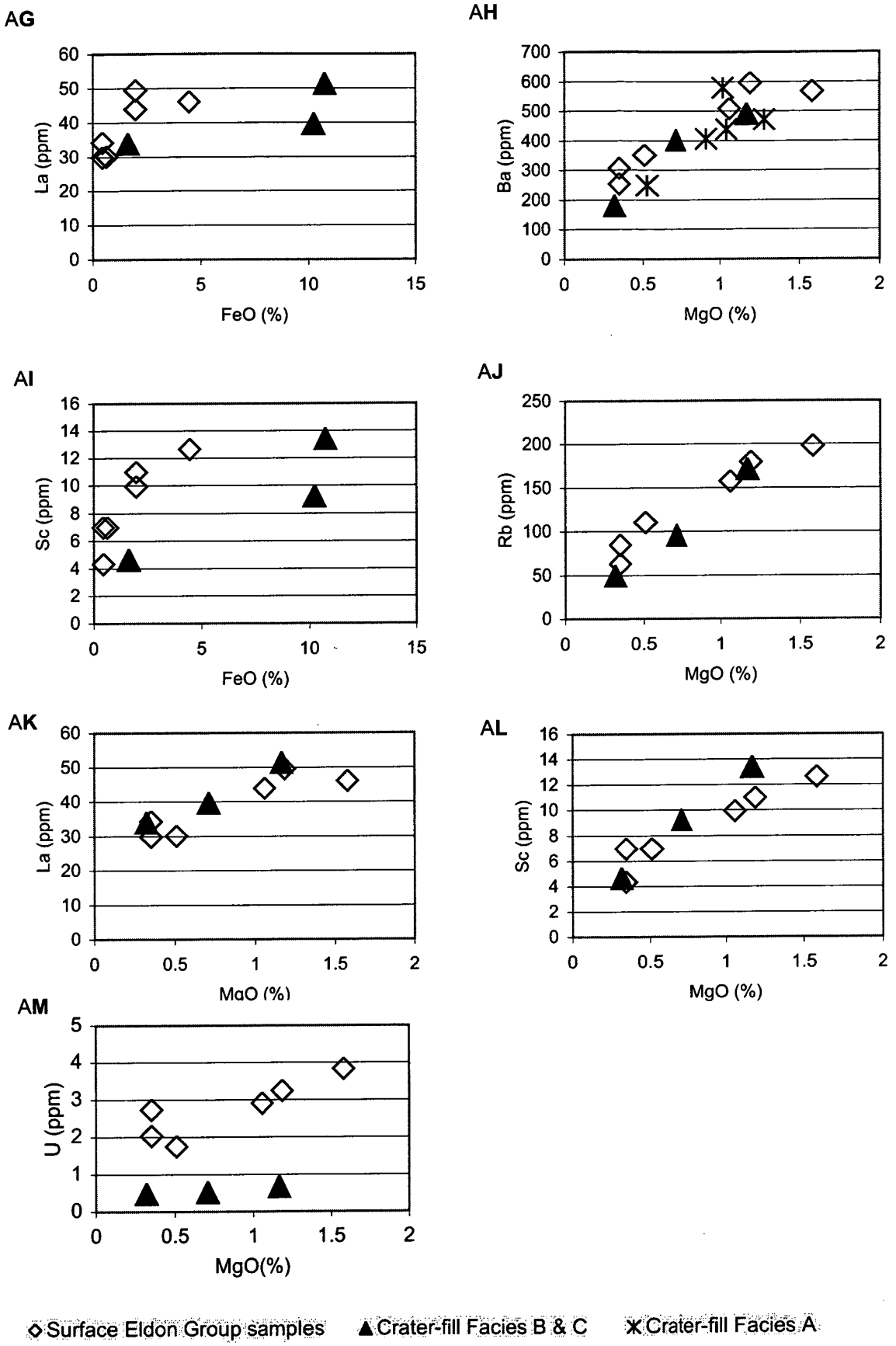

Figure 4.17AG-AM Trace element variation in Eldon Group samples from around Darwin Crater and crater-fill facies.

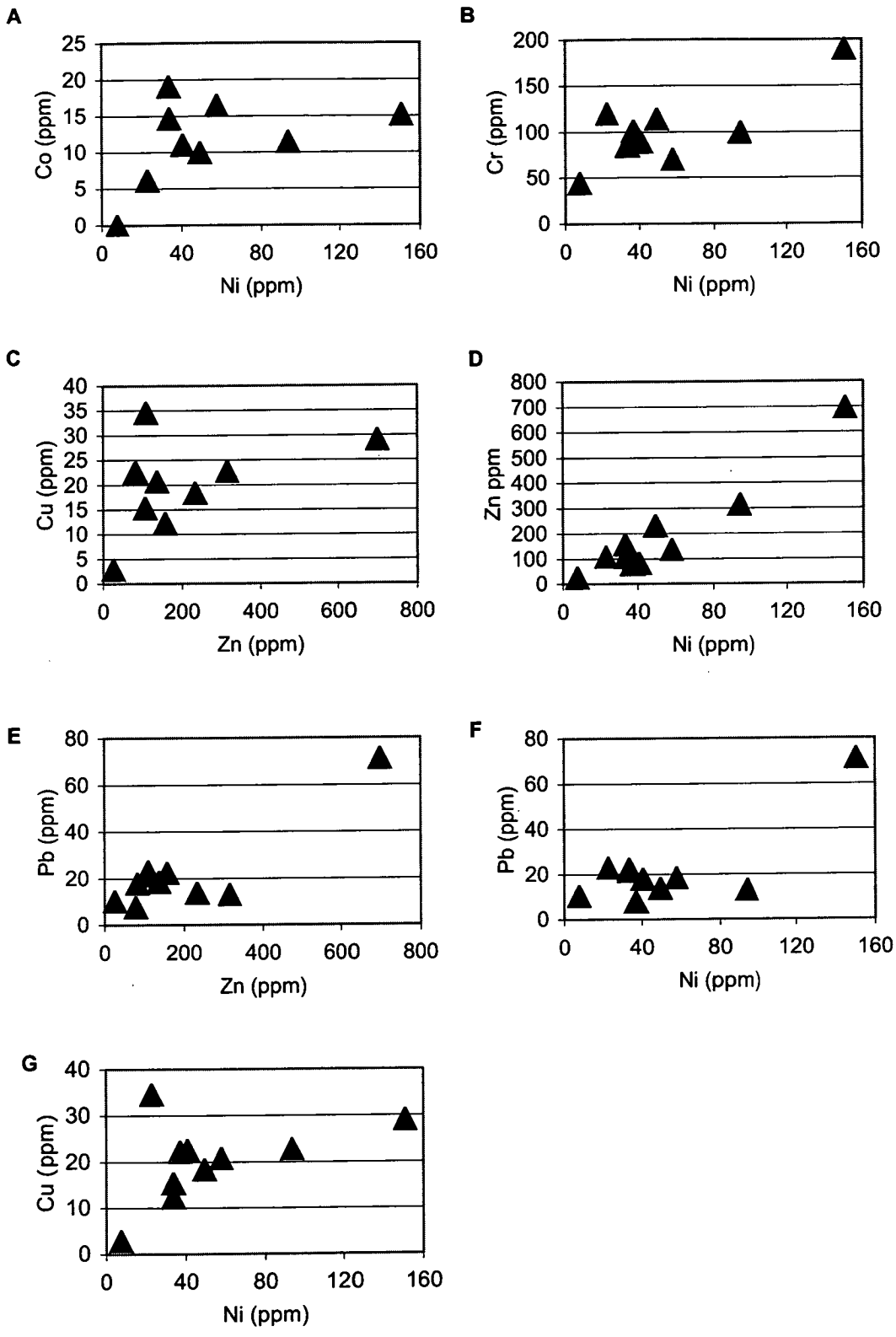

Figure 4.18A-G Variation in selected trace metal abundances in Crater-fill Facies C.

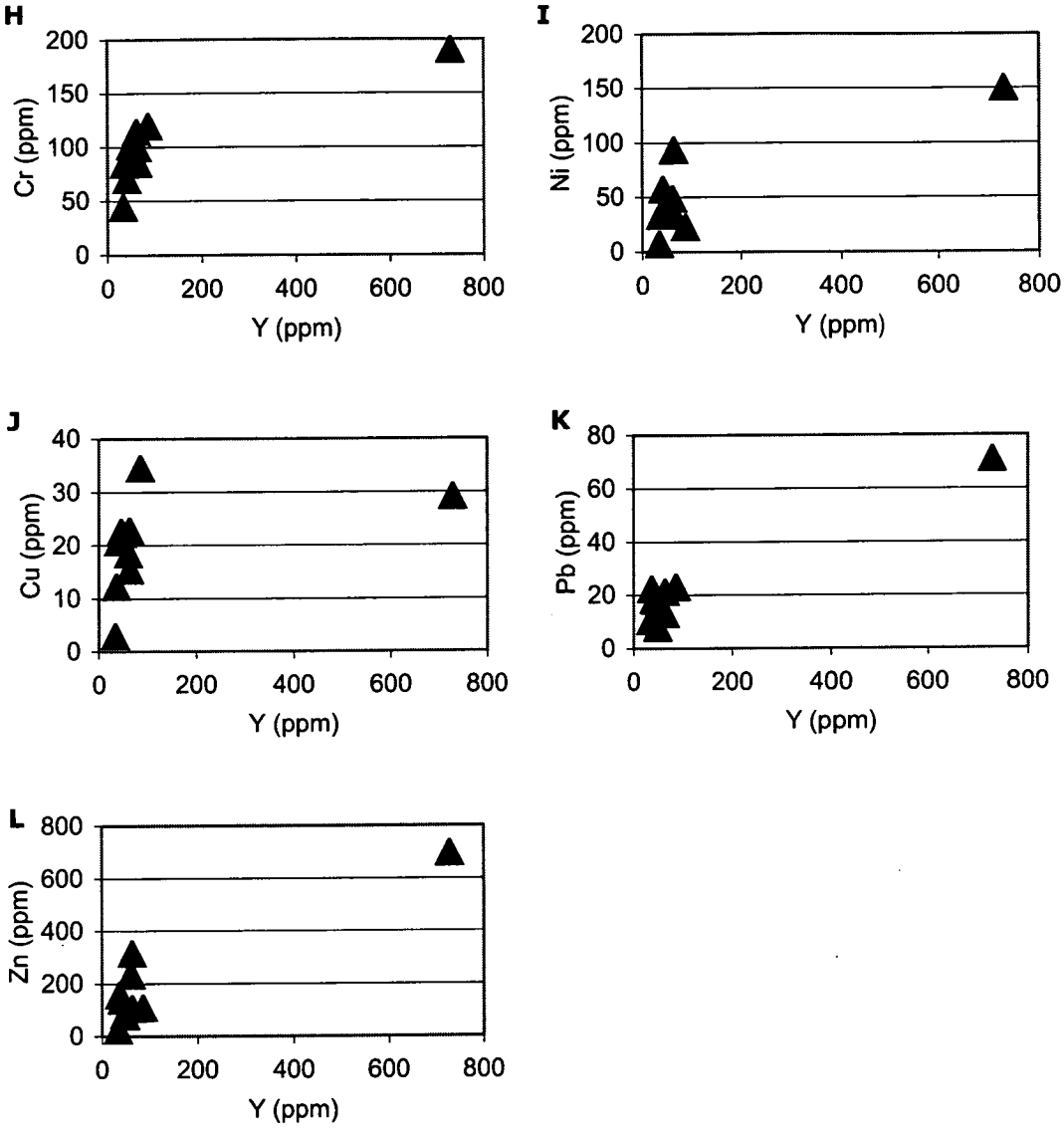

Figure 4.18H-L Variation in selected trace metal abundances, relative to Y, in Crater-fill Facies C.

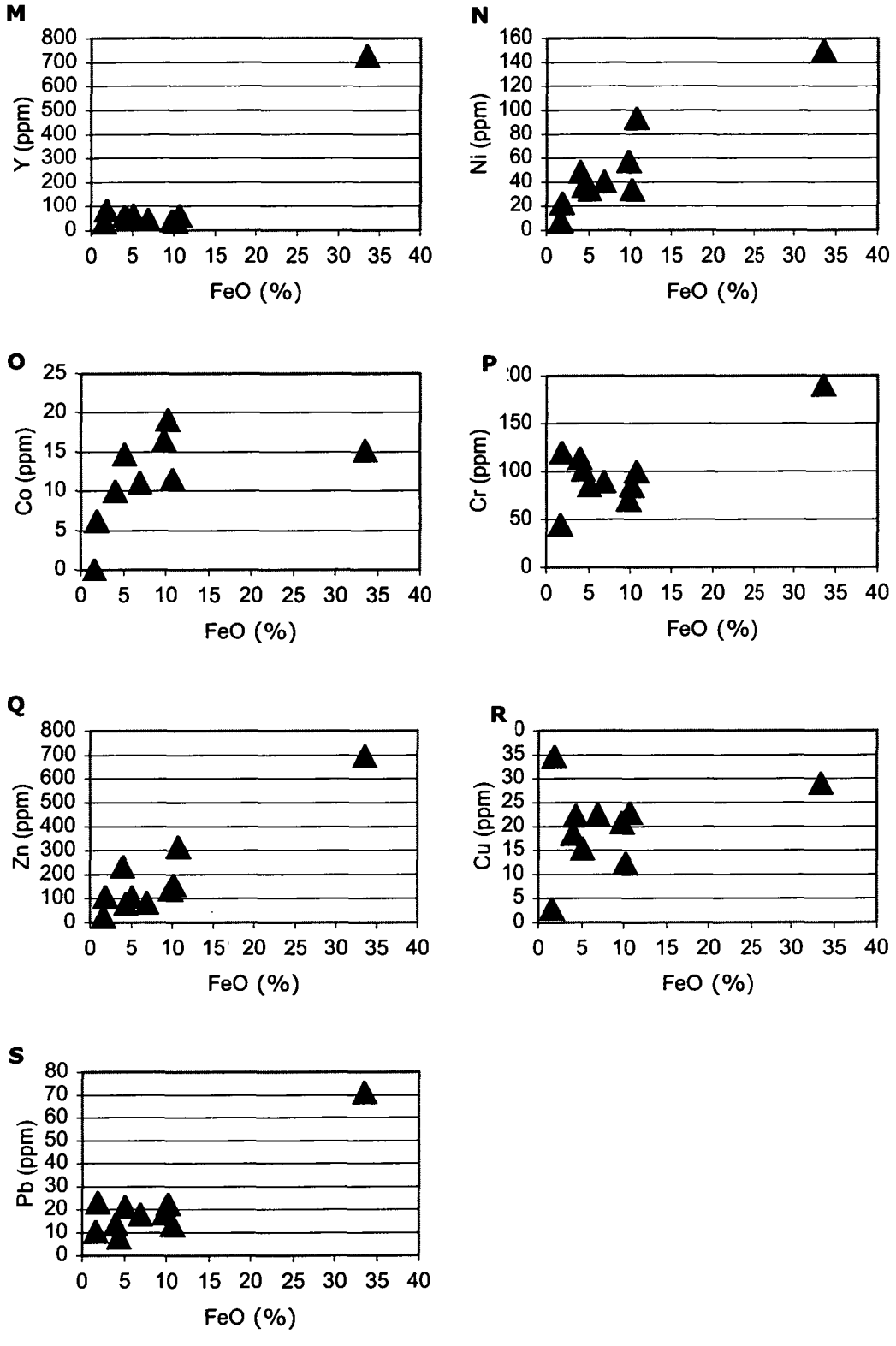

Figure 4.18M-S Variation in selected trace metal abundances, relative to FeO, in Crater-fill Facies C.

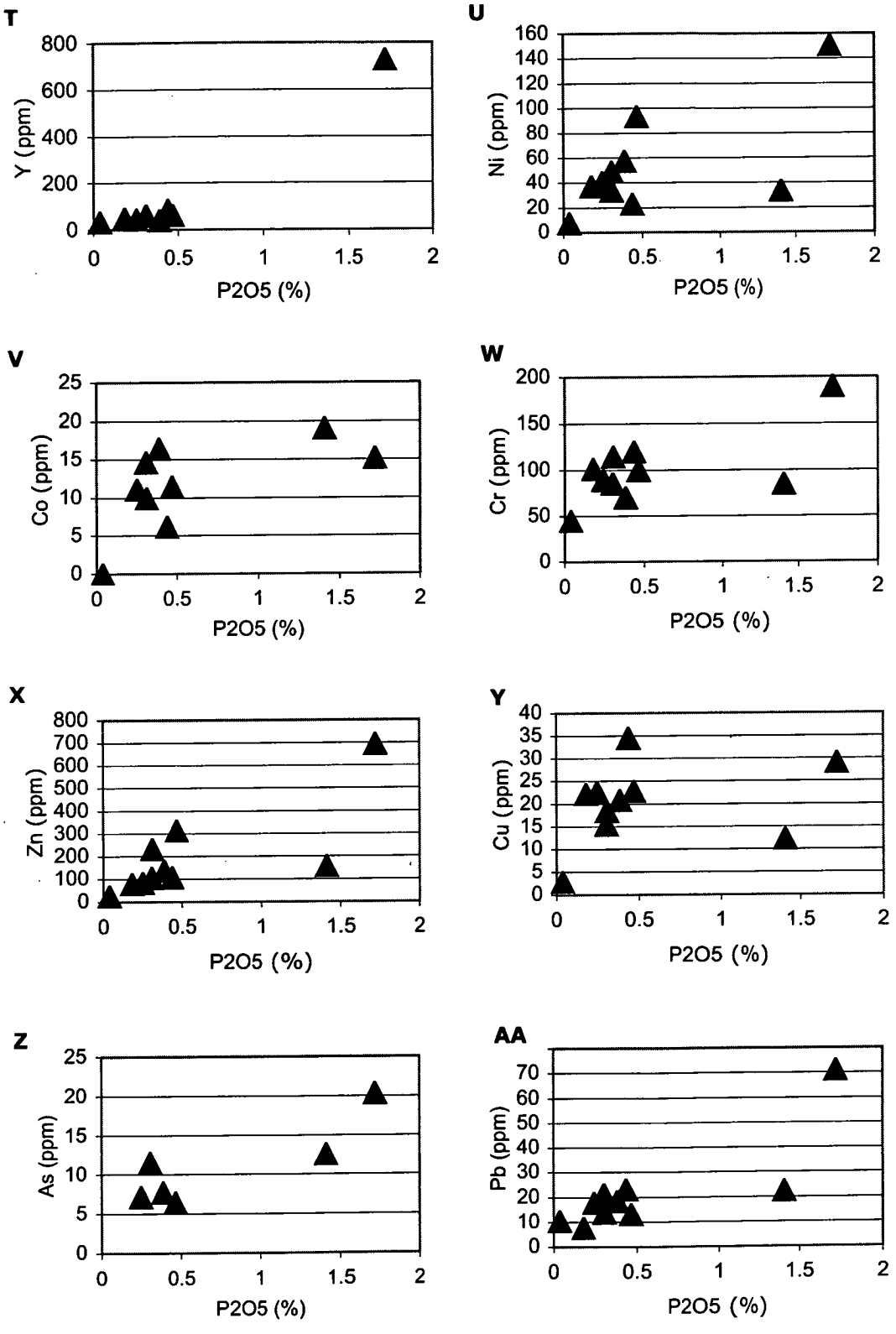

Figure 4.18T-AA Variation in selected trace metal abundances, relative to P_2O_5, in Crater-fill Facies C.

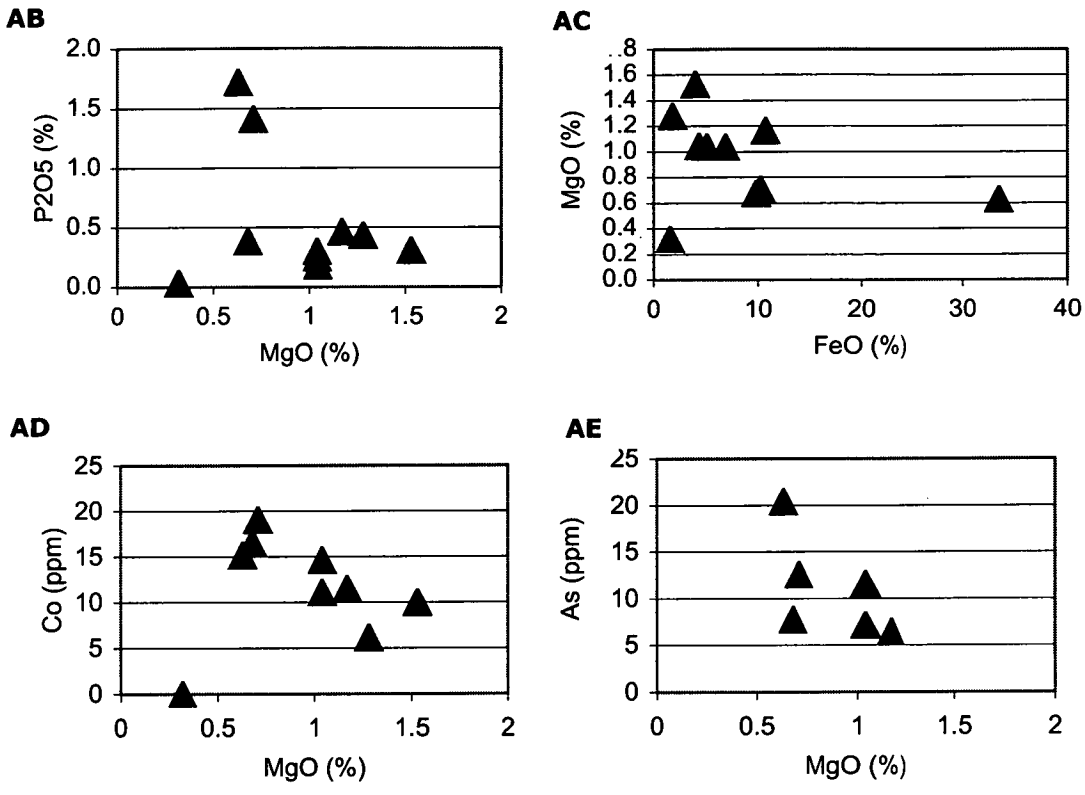

Figure 4.18AB-AE Variation in selected Oxide and trace metal abundances in Crater-fill Facies C.

variation with trace elements or oxides other than CaO and MnO that are present in very low abundance.

Average REE abundances for the Amber Slate, Keel Quartzite and crater-fill samples, normalised to a C1 chondrite, are plotted in Fig. 4.19. All of the rocks show REE patterns generally typical of upper crustal sediments, including relative LREE enrichment (chondrite normalised La/Lu = 7.1 – 10.2), comparatively flat HREE and small negative Eu anomalies (Eu/Eu* = 0.58 – 0.71). The very similar shaped curves and the limited range in Eu/Eu* values between the analysed surface and core rocks are suggestive of a common parent. The flatter REE curve for Crater-fill Facies C reflects the previously discussed concentration of the HREE into goethite during weathering. With the exception of the highly decomposed goethite dominated sample KH19, these data for each rock type show limited and overlapping ranges and similar average values for ratios of La/Sm (3.94 – 6.48) and Gd/Yb (1.73 – 2.49), and this also suggests a common provenance for the surface and crater-fill samples (table 4.8).

All of the trace elements for Eldon Group and crater-fill rocks were normalised to bulk continental crust and plotted in Fig. 4.20. Average analyses for the surface samples and crater-fill rocks show very similar shaped curves with the exception of the previously discussed enrichment in HREE and metals in Crater-fill Facies C. The most striking feature of these curves is the extreme degree of Sr depletion relative to bulk continental crust, and this low Sr abundance is reflected in Rb/Sr ratios that vary between 2.2 and 23.3! (table 4.8). The extreme Sr depletion in some samples is likely to reflect pervasive replacement of feldspar by muscovite during the low-grade metamorphism of these rocks during the Tabberabberan Orogeny. Excluding KH19, elemental ratios critical of the source rock composition (Cullers 2000) are overlapping and limited in range with average values in close agreement e.g. La/Sc (3.6-7.2) and Th/Sc (1.13 – 3.13); these ratios provide further evidence for a limited provenance and a high degree of geochemical affinity between the surface and crater-fill samples (table 4.8). For other ratios useful in comparing the provenance of sedimentary rocks (e.g. Th/Cr, Th/Co, La/Co and Rb/Sr) KH19 shows similar values to other samples (table 4.8).

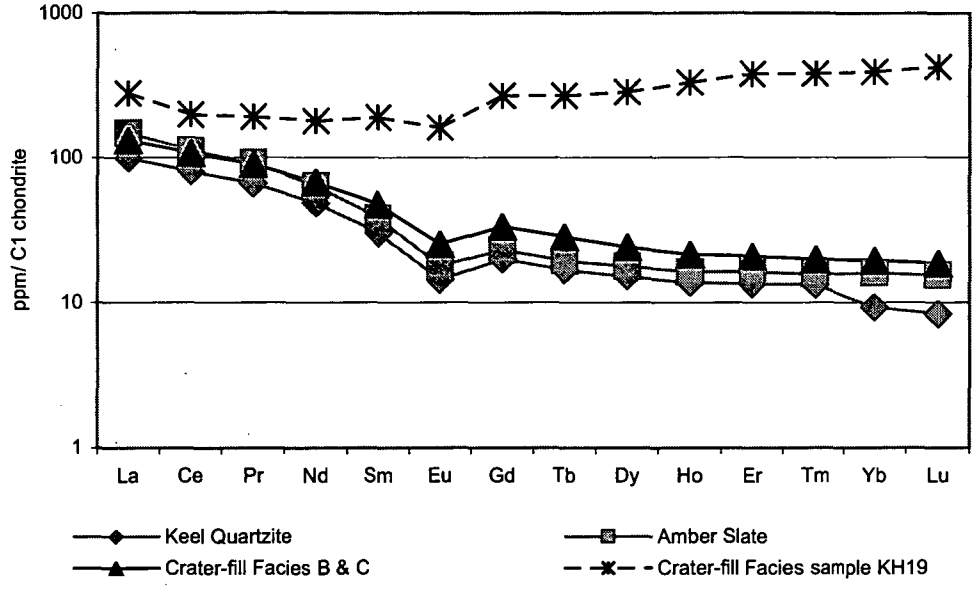

Figure 4.19 Chondrite (Sun & McDonough 1989) **normalised rare earth element (REE) concentrations in Eldon Group samples from around Darwin Crater and crater -fill facies.**

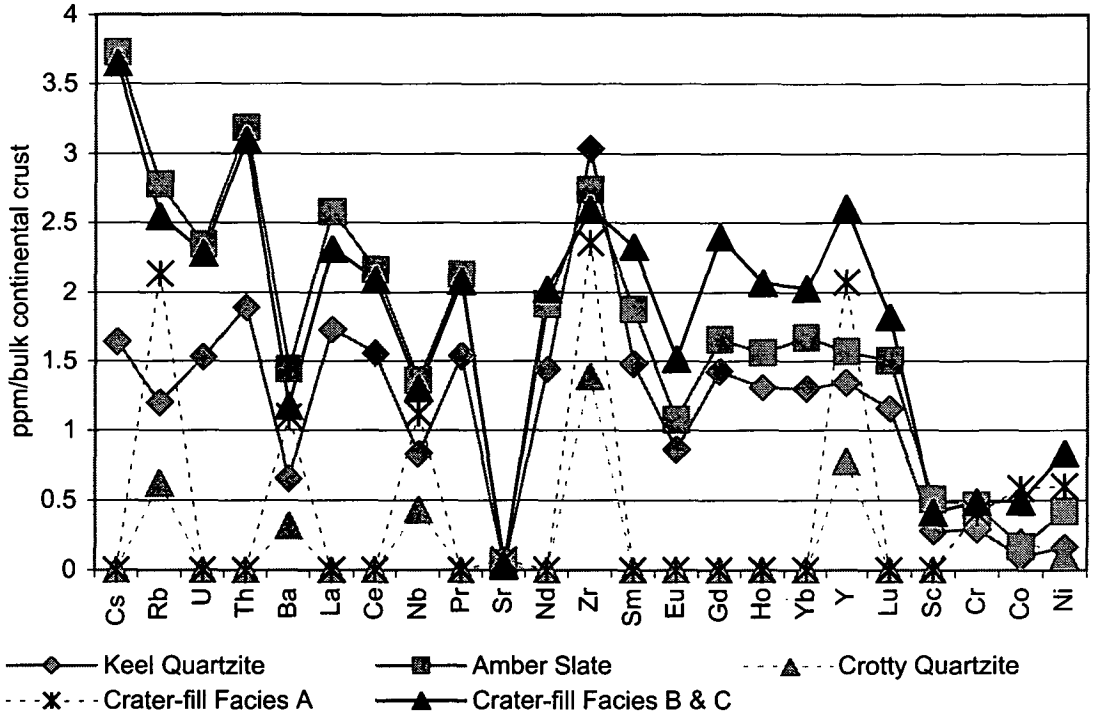

Figure 4.20 Trace element concentrations normalised to bulk continental crust (Rudnick & Fountain 1995) **in Eldon Group samples from around Darwin Crater and crater-fill facies.**

Lithology	Sample	La/Lu	Eu/Eu*	La/Sc	Th/Sc	La/Co	Th/Co	Th/Cr	Gd/Yb	La/Sm	Rb/Sr
	KH1	9.0	0.6	4.3	1.1	62.9	16.5	0.1	1.8	6.1	20.1
	KH2	6.1	0.6	4.9	1.9	47.0	18.4	0.3	2.2	3.9	3.7
Keel Quartzite	KH4	9.1	0.6	6.9	2.4	35.9	12.6	0.3	2.0	5.6	5.6
	KTH12	11.6	0.6	8.5	1.7	na	na	0.1	1.9	7.2	4.7
		8.9	0.6	6.1	1.8	48.6	15.8	0.2	1.9	5.7	8.5
	KH6	9.5	0.6	4.5	1.6	32.6	11.5	0.2	1.7	6.5	8.7
Amber Slate	KH7	9.3	0.6	4.4	1.6	40.5	14.3	0.2	1.7	6.4	8.3
	KH8	10.0	0.6	3.6	1.6	15.7	7.0	0.2	1.9	6.2	19.0
		9.6	0.6	4.2	1.6	29.6	11.0	0.2	1.8	6.4	12.0
Crater –fill Facies B and C (Deformed slate and quartzites)	KH15	8.6	0.6	4.3	1.7	2.3	0.9	0.2	2.3	4.8	3.1
	KH17	7.9	0.7	7.3	3.1	23.6	10.1	0.3	2.5	4.3	7.8
	KH18	6.0	0.6	3.8	1.6	5.3	2.2	0.2	1.8	4.6	18.5
		7.5	0.6	5.1	2.2	10.4	4.4	0.2	2.2	4.6	9.8
Combined	Max.	11.6	0.7	8.5	3.1	62.9	18.4	0.3	2.5	7.2	20.1
	Min	6.0	0.6	3.6	1.1	2.3	0.9	0.1	1.7	3.9	3.1
	Average	8.7	0.6	5.2	1.8	29.5	10.4	0.2	2.0	5.6	9.9
	KH19	6.4	0.2	0.9	0.2	5.7	1.4	0.2	0.8	2.4	10.7

Table 4.8 Selected trace element ratios in Eldon Group samples from around Darwin Crater and crater-fill facies.
*=values normalised to C1 chondrite (Sun & McDonough 1989).

4.6.5 Geochemical evolution of Darwin Crater

Trace gypsum in the upper samples of polymict allogenic breccias (Crater-fill Facies A) revealed by XRD is likely to be evaporitic in origin and this indicates that the breccias were briefly exposed to the atmosphere prior to the deposition of the lake sediments. These geochemical data suggest that, after initial formation of the crater stratigraphy, oxidised surface and groundwater pervasively penetrated the exposed polymict allogenic breccia, and lower fractured and brecciated rocks of Crater-fill Facies B and C that represent a highly permeable aquifer. The deep leaching of K_2O promoted the *in situ* growth of matrix kaolinite clays, and the pervasive decomposition of the country rocks led to extensive development of the Fe-oxyhydroxide goethite. Goethite and clay are both most abundant in fractures but also pervade more coherent lithologies as a result of the high permeability of the crater-fill facies, especially of the polymict breccias (Crater-fill Facies A) where kaolinite is most abundant. The dominance of kaolinite over goethite in Crater-fill Facies A reflects the low abundance of FeO in this quartz dominated breccia and this observation further supports the *in situ* growth origin of these matrix materials. During development of the Fe-oxhydroxides, trace elements including transition metals and sulphides were attenuated and concentrated, especially in the highly fractured and decomposed rocks of Crater-fill Facies C.

As the lake sediments began to gradually fill the basin structure, the high organic component resulted in an anoxic or reduced environment and a boundary between the oxidised allogenic breccias and the reduced lake sediments was created. Across the transition between the upper Crater-fill Facies A and the lake sediments, oxidised fluids carrying dissolved FeO reacted with the anoxic lake sediments to precipitate the pyrite revealed by XRD and petrographic analysis of the uppermost allogenic breccia samples. Today, under a very wet climatic regime, the volume of surface and groundwater flow is very high. These groundwaters are acidic and the extreme deep leaching that is promoted by the highly fractured and blocky crater-fill stratigraphy is continuing the pervasive decomposition, oxidation and clay alteration of the crater stratigraphy.

4.7 Potential endogenic explanations for Darwin Crater

The petrographic and geochemical evidence indicates that the structure is a localised feature developed in the Eldon Group. Local deformation, excavation and mixing of the country rocks during the development of the circular structure has produced a stratigraphy that consists of polymict allogenic breccias, allogenic monomict quartz breccias and slumped and deformed blocks of country rocks. Endogenic origins for a basin filled with brecciated and slumped blocks of rock would necessitate that Darwin Crater be a 1) diatreme; 2) cirque; 3) sink hole; or 4) structurally controlled eroded basin. Each of these possibilities will be addressed individually below.

4.7.1 Diatreme

Diatremes are cone shaped intrusive bodies that result from flow induced by density contrasts (salt domes) or volcanism (e.g. kimberlites). The crater structure is clearly not a salt dome as indicated by the recovered crater-fill samples unless all of the salt has dissolved leaving collapse breccias; however, no thick evaporites are known in the Eldon Group or underlying strata and the geophysical evidence indicates a 'solid' floor. The geophysical evidence does not suggest a cone shaped depression but rather a circular bowl-shaped basin. Volcanic diatremes are characterised by a host of explosively brecciated rock fabrics superficially similar to those observed at Darwin crater. However, the breccias at Darwin Crater are completely lacking in volcanic rock fragments. The crater is not situated in volcanic rocks, and volcanic diatremes are not known in the area, and are rare in the Phanerozoic of Tasmania. Also, most igneous diatremes are strongly magnetic and there is no evidence for a magnetic anomaly over the crater.

4.7.2 Cirque

The area surrounding the structure has been subject to successive glaciations during the Pleistocene, but the permanent ice cover required for cirque formation was restricted to elevations above 500m (Derbyshire 1972), and the crater sits far lower at 220m. If the structure was a cirque, rubble typical of moraine would be expected down slope in the lower Andrew River valley and there is absolutely no evidence for this.

4.7.3 Sink hole

Sinkholes are large solution pits dissolved into carbonate rocks and are common features in regions of karst topography. Rocks at the crater show evidence of only a very minor carbonate component located in an isolated pelitic block at depth and if the structure is related to a sinkhole this must be located at even greater depths. The Gordon Group limestone is present below the Eldon Group rocks at the crater and only the Gordon Group would offer a thick enough package of limestone to accommodate the approximately 200m deep structure. The Gordon Group is exposed in the Andrew River valley west of the Engineer Range and here the low relief topography shows no evidence of limestone dissolution or features typical of karst topography. The Andrew River flows directly over the Gordon Group and remains entirely above ground. This indicates that currently the Gordon Group is largely insoluble in the region of the crater and there is no evidence to relate the structure to a modern sinkhole. Following deposition of the Gordon Group, the Eldon Group sediments are interpreted to have been deposited quickly, thereby limiting the potential for limestone dissolution and karst development. As such, paleokarst features are also not expected at depth.

4.7.4 Structurally controlled erosion of a basin

The main structural control at the site of the crater relates to a major northeast – southwest trending fault that cuts the Engineer Range. The significant down-throw on this fault has been accommodated by several strike-slip faults that trend approximately perpendicular to this and several other major northeast–southwest trending faults. During weathering and erosion, these faults and competency contrasts between the slates and quartzites have produced a geomorphic grain of approximately northwest – southeast trending strike ridges, that when combined with the topographic expression of the faults produces a blocky rectangular surface fabric in the region of the crater. Erosion is actively enhancing this rectangular, blocky topography that is quite distinct from the circular depression that is Darwin crater.

4.8 Evidence for an impact origin

The following paragraphs examine the potential lines of evidence for an impact origin of the structure based on data described herein. This discussion will focus on the physical form of the structure and petrographic features of the studied rocks with a focus on attempts to identify diagnostic evidence for impact-induced shock metamorphism. The geochemical characteristics and relationships between the potential target rocks and crater-fill stratigraphy are interpreted as being entirely consistent with endogenic processes and are not considered here.

4.8.1 Crater morphology

Geophysical modeling provides estimates of depth to crater floor of between 230 m (gravity data) and 180 m (seismic data) (Fudali & Ford 1979, Richardson 1984). In both instances the authors note that the faulted nature of the basement is likely to make recognition of the true crater floor difficult, either from the geophysical data or drill core. From the drill core data it is clear that the structure contains at least 220-230 m of fill. At this level, core DDH2 had reached total depth in coherent slates. From the current drill core data, it is not possible to determine if this is a coherent slumped block in the crater-fill stratigraphy, or if this represents bedrock beneath the true crater floor. The height of the former land surface above the crater-fill, and therefore the true depth of the crater, can also not be determined accurately. However, assuming that the total depth of DDH2 is close to the true crater floor, as the geophysical evidence suggests, the depth to diameter ratio for Darwin Crater (D=1.2km) is taken to be around 1:3-1:4.

According to the theoretical calculations in Grieve (1987) a simple crater with a diameter of 1.2km should have a true depth to floor (dt) of close to 350 m (equation 4.1).

$$dt = 0.29D^{0.93}$$

$$dt = 0.343 \text{ km}$$

Where:

D (Diameter of Darwin crater) = 1.2km

dt = true depth to crater floor

Equation 4.1

Source: Grieve (1987, p.248)

This scaling relationship is based on 9 terrestrial craters, and for examples such as the 1.2km Barringer Crater the relationship agrees well with drill core evidence that shows a depth to floor of around 300 m (depth to diameter ratio of 1:3. Using observations of fresh Lunar craters and modeled observations that describe post explosion crater wall collapse (> diameter to depth ratio) as critical in determination of the final simple crater dimensions, Pike (1980) and Melosh & Ivanov (1999) define depth to diameter ratios of 1:4 - 1:5 for simple craters. These predicted ratios agree well with the depth to crater floor at Darwin estimated by the geophysical data and also for the almost identically sized Tswaing Crater, Pretoria, South Africa, that has a rim to rim diameter of 1.13 km and a depth to crater floor of around 200 m. As such depth to diameter ratios for Darwin Crater (1:3-1:4) appear to be well within the ranges expected in simple craters even if the possible influence of erosion is considered. Erosion has completely removed any raised rim, however the thick and poorly consolidated Crater-fill Facies A would be entirely removed by any prolonged erosional regime. The almost closed basin form of the topography, and high rainfall at Darwin Crater is likely to have created a dominantly depositional setting that allowed for deposition of the lake sediments effectively capping and promoting preservation of the crater-fill stratigraphy.

4.8.2 Shock metamorphic effects

Diagnostic evidence for the impact origin of a crater or eroded impact structure based on petrographic investigations alone requires the identification of a statistically significant sample of quartz grains showing Planar Deformation Features (PDF's) (e.g. French 1998, Chapter 1). Analyses of crater-fill samples have revealed abundant multipley fractured quartz grains. These fractures are generally irregular with contacts at variable angles that pervade the entire quartz grain and are not diagnostic of impact shock. In the deformed and brecciated slates (Crater-fill Facies

C, Fig. 4.12A-K) planar microstructures are largely absent. Only a single isolated example of a 'twinned' quartz grain, with sub-planar fracture planes that define distinct extinctions, has been observed. In the more coherent monomict quartz breccias (Crater-fill Facies B, Fig. 4.11A-N) and deformed quartzites, 'twinned' quartz grains are found in higher but still very low (<1%) abundance but percussion fractures are present. In the polymict breccia samples (Crater-fill Facies A, Fig. 4.9A-R), quartz grains with planar fractures have been identified; these are generally wide (>5μm) coarsely spaced (>15μm) and are sometimes only sub-planar with a bent form. Rare (<1%) 'twinned' quartz grains are also present in the polymict breccia samples. These quartz grains are more common (6%) in the fine sand (64-250μm) fraction of the glass-bearing gravels that are found beyond the western 'rim' of the crater (Fig. 4.6A-Z). Such deformed quartz grains are absent from more distal glass-bearing gravels that contain predominantly fracture free quartz. These are interpreted as residual deposits, and are discussed in detail in Chapter 2. There is no evidence for deformation of quartz grains in bedrock samples below the gravels or in large quartzite blocks found within the gravels. As such, the possibility that the deformed grains are residual is considered unlikely. If Darwin Crater is an impact crater, this suggests that these 'twinned' quartz grains found in the glass-bearing gravels close to the crater represent a component of ejected target material. Non-deformed quartz grains in these gravels may be a combination of both residual grains released from the bedrock during weathering or non-shocked ejected material. The fact that the 'twinned' quartz grains are found in greatest abundance associated with a melt component is consistent with theoretical and field studies of impact craters (French 1998).

Kinked mica grains, as observed in the crater-fill stratigraphy (Fig. 4.11L,M), have been observed at impact structures, but may also be produced by tectonic deformation. Hence their presence is not diagnostic of impact processes. The fact that local surface rocks show no kinked micas does, however, suggest localized deformation and this is interpreted as consistent with impact processes.

4.8.2a ESEM investigations of fractures in quartz grains

To define the deformation in quartz grains from Darwin Crater, grain mount thin sections were examined by Environmental Scanning Electron Microscopy (ESEM).

The ESEM images show progressive deformation in quartz grains from the crater-fill stratigraphy but do not reveal diagnostic evidence for impact-induced shock (Fig. 4.21A-L). Most grains are multipley fractured and regular stepped fracturing is visible. Detached angular fragments of the individual quartz grain have been deposited in the depression produced by wide sub-planar fractures. The ESEM images reveal that the 'twinning' in the quartz grains is defined by domains separated by thin (<2μm), sharp and parallel, generally close (<5μm), but variably spaced fractures that have straight and curved segments. The fractures do not appear to be annealed or filled by glassy material as per impact induced PDF's, and EDS scans show no compositional difference between the fracture voids and the surrounding quartz grain. The fact that these fractures are variably spaced, not filled with glass, only semi-planar and generally curved in form, is more typical of slow strain tectonic deformation. However, this is out of character with the regional metamorphic grade and the 'twinned' quartz grains appear to be localized around the crater.

Samples of the non-'twinned' quartz grains with sub-planar microstructures from the polymict breccia Crater-fill Facies A were etched with HF vapour according to the method of Gratz et al. (1996). Grains were examined after 90, 180, and 300 seconds respectively. Examination of the etched samples by ESEM (Fig. 4.22A-H) shows that the fractures tend to be irregular and non-planar. This demonstrates that although fractures can appear generally planar when viewed under an optical microscope, there is a need for more detailed high-resolution investigations. Generally, the progressive etching produced little change in the observed grains with time because of the absence of any annealing glass to remove (as for impact shocked quartz with PDF's). As such, and the topographic expression of the fractures remained unchanged during exposure to the HF vapour.

The closer spacing and sharper definition of fractures in the 'twinned' quartz grains and the extreme degree of optical distortion present is interpreted to indicate a higher degree of deformation than for the irregular to sub-planar fractures in the non-'twinned' quartz grains. Based on theoretical models (e.g. Melosh 1989, Chapter 1), ejected materials are expected to be products predominantly of deformation of the upper most target rocks. Given the stratigraphy of the Eldon Group rocks surrounding the crater, ejected materials will be mostly from the Keel Quartzite. This faulted formation crops out around the crater and based on aerial photograph interpretation the crater is superimposed on Keel Quartzite. However, this unit was

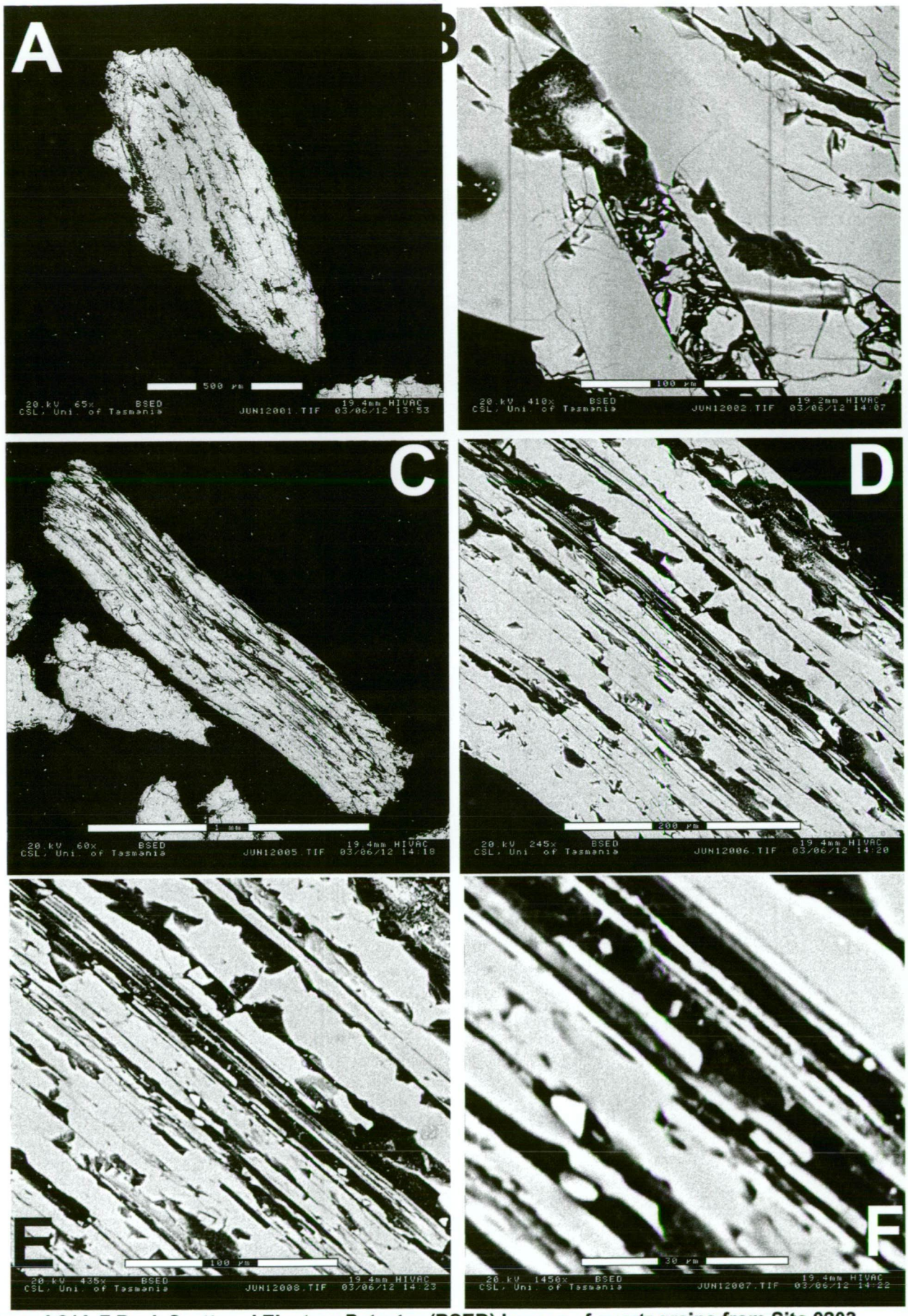

Figure 4.21A-F Back Scattered Electron Detector (BSED) Images of quartz grains from Site 0203. These are the grains with sub-planar fractures that define zones of different extinction in XPL (Fig. 4.5). The sub-planar nature and wide, irregular spacing of these fractures is not diagnostic of impact induced shock.

A) Widely spaced irregular fractures. Scale bar = 500um; B) Close up of fracture in A, showing highly disrupted nature of the grain. Scale bar = 100um; C) Bent sub-planar fractures in quartz. Scale bar= 1mm; D) Close up of fractures in top left of C. Scale bar = 200um; E) Close up of D. Scale Bar = 100um; F) Close up of E. Scale bar = 30um. Note the irregular spacing of the fratctures that are not annealed.

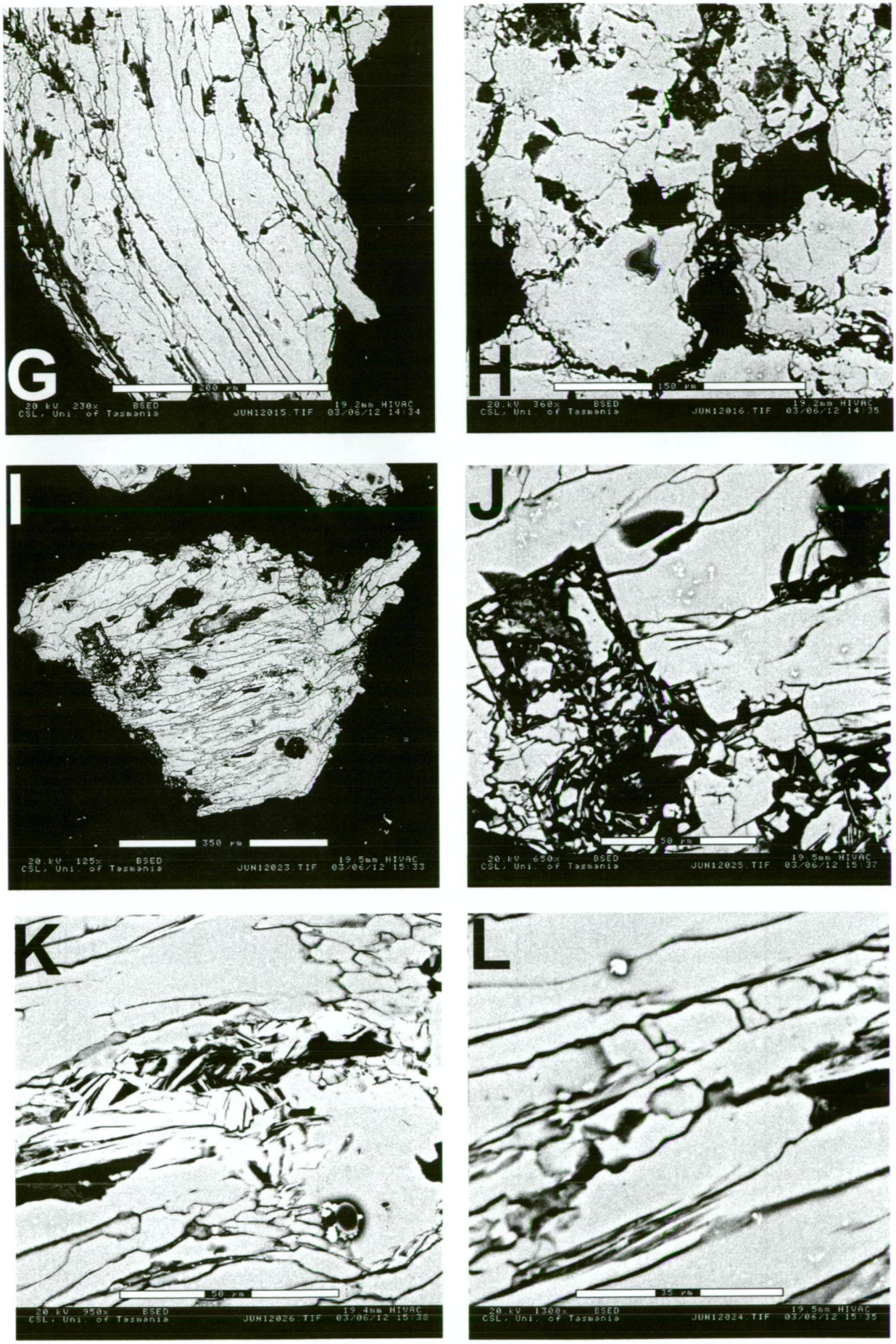

Figure 4.21G-L Back Scattered Electron Detector (BSED) Images of quartz grains from Site 0203. These are the grains with sub-planar fractures that define zones of different extinction in XPL (Fig. 4.5).

G) Irregular fractures. Scale bar = 200um; H) Irregular fractures. Scale bar = 130um; H) Irregular fractures. These appeared far sharper in XPL (Fig. 4.5I-L). Scale bar = 350um; J) Close up of step-like fracture zone in same grain as I. Scale bar = 50um; K) Close up of central zone in grain I showing multiple fractures. Scale bar = 50um; L) Close up of central zone in grain I showing non-planar form of the fractures.

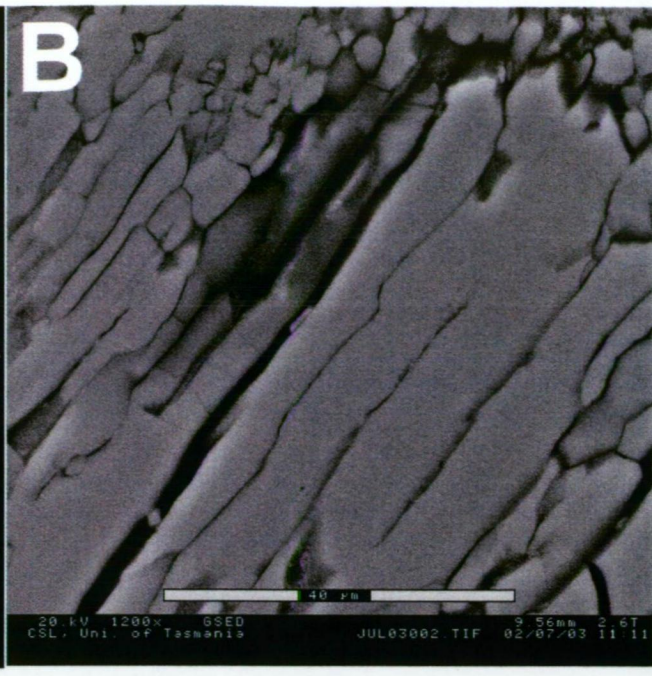

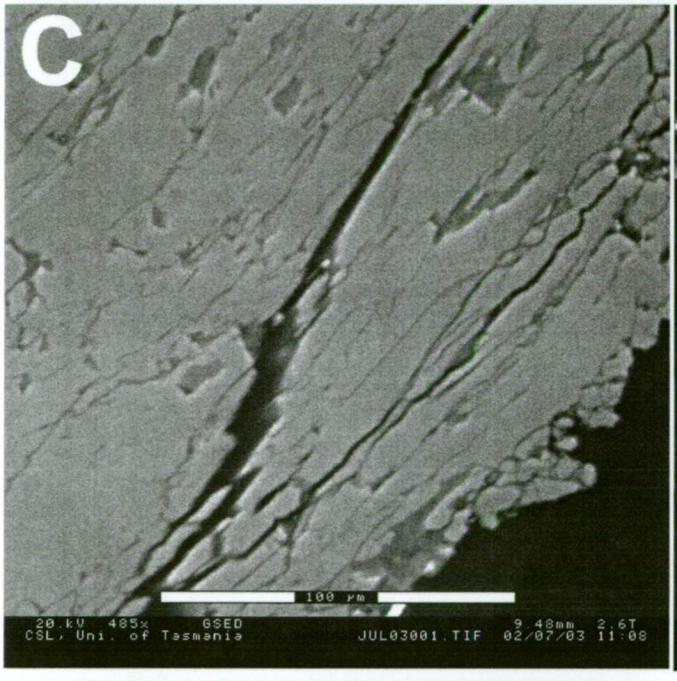

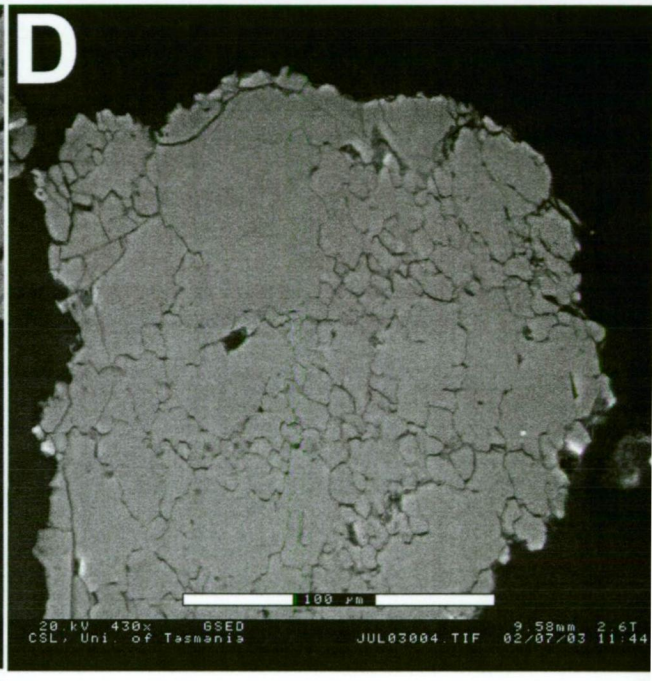

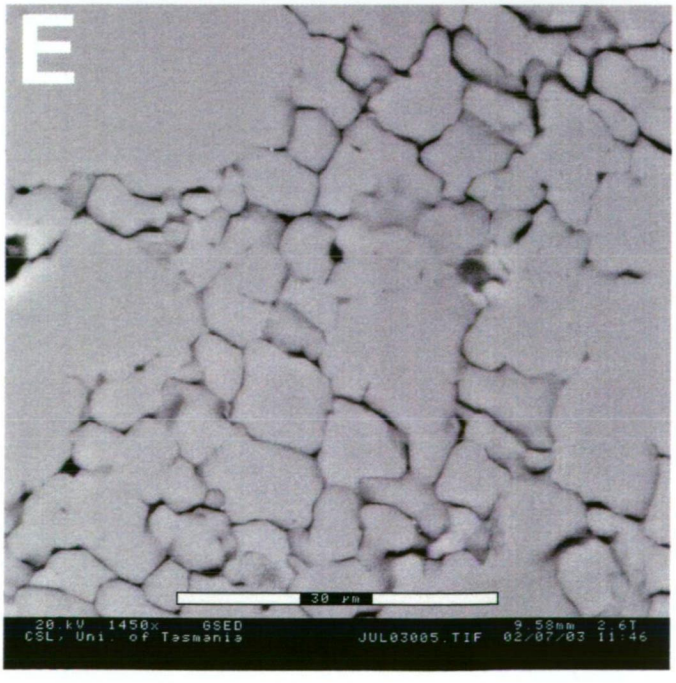

Figure 4.22A-E ESEM images of HF-Etched quartz grains from site 0203.
These are the non-twinned grains such as in Fig. 4.5.

Images taken after 300s HF vapor etching. A) Smooth surface on grain that has sub planar fractures in PPL (Fig. 4.5A). B) Irregular fractures typical of these non-twinned fractured quartz grains. C) More planar fractures in the same grain as B. D) Irregular stepped fractures E) Close up of stepped fractures in D.

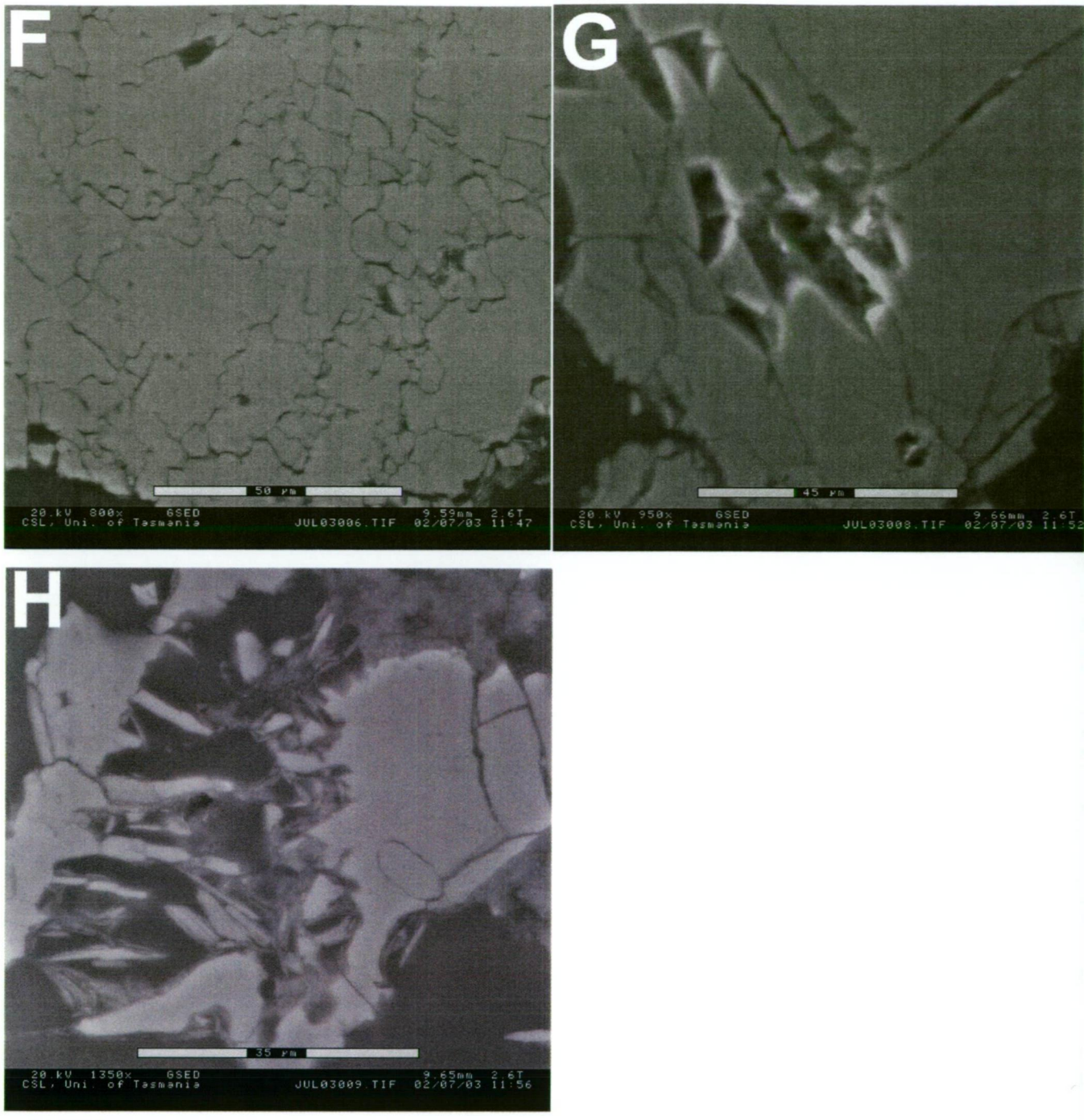

Figure 4.22F-H ESEM images of HF-etched quartz grains from site 0203. These are the non-twinned grains such as in Fig. 4.5.

Images taken after 300 seconds HF vapor etching. F) Irregular stepped fractures; G) Coarsely fractured zone; H) Irregular fractures. Note chlorite filling fractures that has not been removed by etching. This grain was at the edge of the etched region on the thin section.

not intersected in drill core, and beneath the lake sediments the polymict breccias are underlain mainly by deformed Amber Slate. Later, evidence is presented to show that the Keel Quartzite was a part of the suspected pre-impact target stratigraphy that was shock melted and ejected from the central region of the cavity. The non-melted 'twinned' quartz grains found in Crater-fill Facies A and outside of the crater are likely to derive from nearer to the cavity rims in regions of lower shock but from higher levels in the stratigraphy than from where Crater-fill Facies A and B are derived, as will be discussed. It is suggested that the upper Keel Quartzite consumed the bulk of the impact energy prior to compression and brittle to plastic deformation without melting of the lower shales and minor interbedded quartzites (pressures <5 GPa).

4.8.2b Competency contrast controlled deformation in Crater-fill Facies B and C

Crater-fill Facies B and C are intersected in large blocks of rock that were generated by slumping of the crater walls, and as such they are expected to have experienced similar, low levels of shock (<5 GPa). As the entire rock package beneath Crater-fill Facies A has experienced similar degrees of shock, but displays a very wide range of deformed rock fabrics even on a fine scale, it is clear that the formation of a particular rock fabric is also controlled by competency contrasts in the suspected target stratigraphy.

The control of competency on the observed progression of low-energy shock effects observed in Crater-fill Facies B and C at Darwin Crater is summarised in Fig. 4.23 and described below. After the passage of the initial shock wave, the target rocks undergo compression, microfaulting, shearing of bedding, deformation of micas and fracturing of quartz grains. At some point during the deformation event, after the initial *in situ* fracturing of quartz grains (step 2 in Fig. 4.23), the competency contrasts begin to control the resultant rock fabric. This control causes intermixing of quartz grains and matrix material and the development of quartz domains preferentially in the more pelitic units (Crater-fill Facies C) that have a higher compressibility. Fracturing and extreme deformation of quartz grains to produce rare 'twinned' grains and complete shattering to produce monomict breccias is favoured in the more competent quartzites (Crater-fill Facies B). Calibration of individual textures to shock pressure values is not possible as a result of this competency control. This is a general challenge in the study of low-shock pressure effects involving heterogenous target rocks (e.g. Kenkmann 2003).

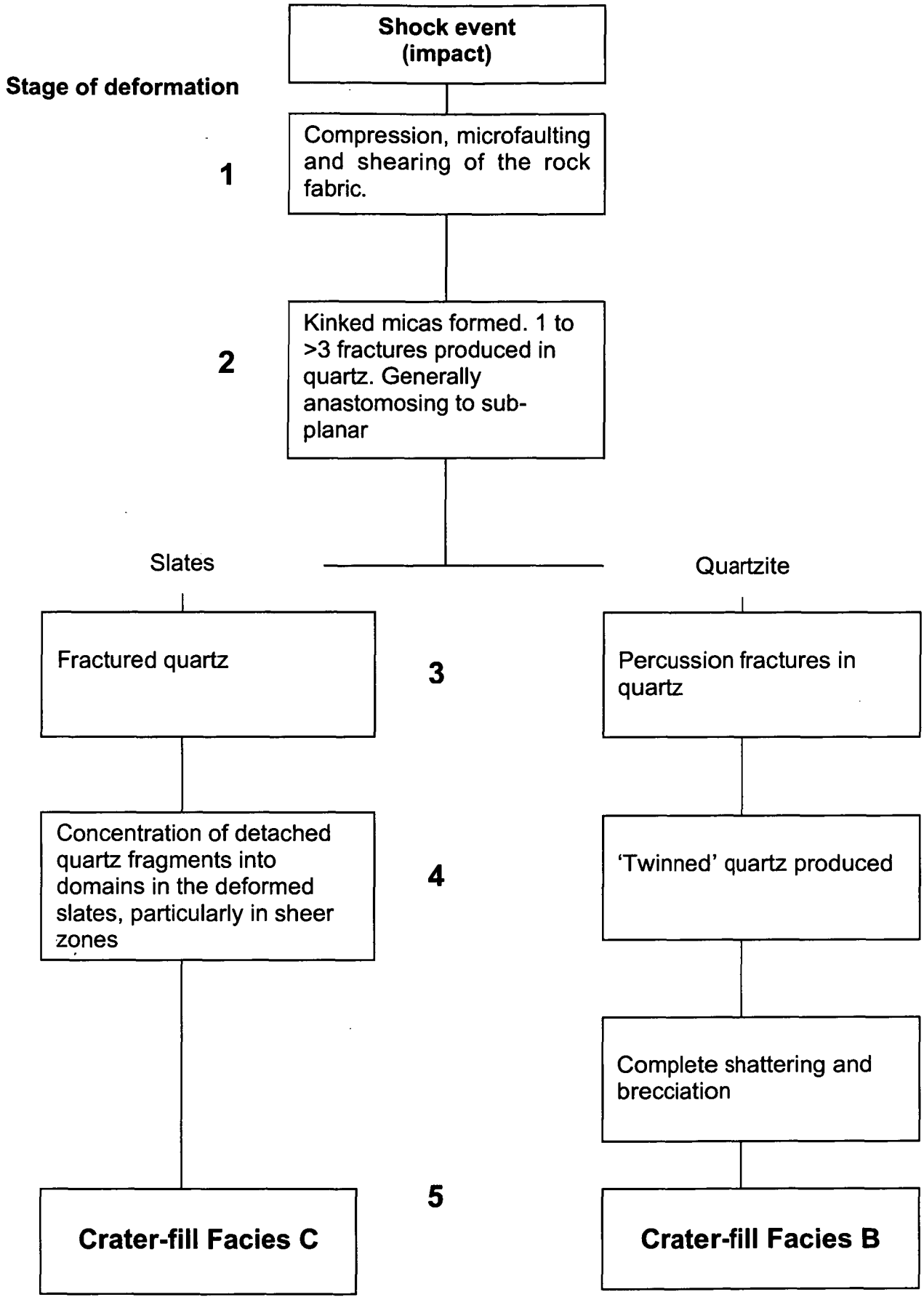

Figure 4.23 Progressive shock metamorphic effects in deformed slates and quartzites from Darwin Crater. This progression and the ultimate rock fabric observed is controlled by competency contrasts between the shales and quartzites. This control is interpreted to commence after the initial compression and fracturing of the target rocks during plastic deformation.

4.8.2c Comparison with deformation features in other simple and complex terrestrial craters

Diagnostic evidence for impact induced shock metamorphic effects have not been observed in quartz grains from the crater-fill samples or in rocks surrounding the crater. At many small simple craters, especially in sedimentary target rocks, there is an absence, or rarity of distinctive shock metamorphic effects. Barringer Crater (D=1.2 km) provides an example of this in the target Coconino Sandstone. Samples of this sandstone from ejected material range from un-shocked through to completely glassy with abundant coesite (indicating shock pressures exceeding 30 GPa), however, PDF's are confined to less than 5% of the studied quartz grains (Kieffer 1971). In crystalline target rocks subjected to equivalent shock energy as those experienced by rocks at Barringer Crater, almost 100% of quartz grains would be expected to show PDF's (Robertson 1980). As at Darwin Crater, most fractures in quartz grains from the Coconino Sandstone are irregular and commonly with more than three cross cutting fractures. Coesite is only present in Darwin glass and has not been observed in any analysed suspected target rocks. Features such as percussion fractures are common in quartz grains at both Barringer and Darwin.

At Tswaing Crater (D=1.12 km) PDF's could not be found in the highly fractured granite blocks that comprise the bulk of the stratigraphy or in basement rocks below the crater floor where shocked rocks are theoretically predicted (Reimold et al. 1992). Hence the coherent rocks encountered at 230m in the Darwin Crater could represent a true crater floor, and not simply a non-deformed slumped block, as is consistent with the gravity data. In studies of Tswaing, PDF's have only been found in quartz grains from the upper sandy polymict breccia facies and not in ejecta outside of the crater despite excellent preservation potential in this desert environment (Reimold et al. 1992). However, some of the shocked quartz grains in the upper sandy polymict breccia facies at Tswaing could be from fallback ejecta. This stratigraphic distribution in the degree of shock is similar to that observed at Darwin Crater where the most abundant and highly deformed quartz grains are found in the upper polymict sandy breccias and suspected ejecta facies. At Darwin Crater, when similar lithologies are compared, a general decrease in the degree of deformation is observed with increasing depth down hole.

At the 4 km diameter Steinheim Crater in Germany (a small complex crater and paired with the Ries Crater), planar microstructures are confined to less than 10% of quartz grains and perhaps 1% or less have true PDF sets (Dr D. Stöffler, Personal Communication in 2003- this has not been confirmed from available literature). Further, no glass is associated with the structure and an impact origin is interpreted from the presence of abundant shatter cones in carbonates. The similar sized Upheavel Dome Crater (D=5km) is another example of an impact crater in sedimentary rocks where PDF's have not been found despite many searches (Kenkmann 2003). Here an impact origin has been confirmed on the basis of cataclastic rock fabrics that have been related to the unique shock conditions associated with impact events (Kenkmann 2003).

The fact that PDF's are developed only rarely in sedimentary rocks at some impact structures is also supported by studies at large complex craters such as Gosses Bluff (D=22km) where planar fractures are far less commonly found in porous sandstones than the heavily silicified units (Milton et al. 1972). At the Ries Crater (D=24km) in Germany also (one of the most studied craters on Earth), PDF's have only been described from the crystalline target rocks and not from the associated sediments, despite the complete range of shock products having been identified in the crystalline rocks (Ostertag & Stöffler 1978, Hörz et al. 1980). Quartz grains from sandstones at the Carswell structure (D=39 km) are un-shocked, yet in the immediately underlying gneissic rocks, quartz grains commonly show PDF sets (Robertson 1980). These observations indicate that the development of PDF's is strongly favored in targets with lower rock compressibility.

When these observations and the suspected target lithologies are considered, shocked quartz grains are expected to be absent, or very rare at Darwin Crater. Most of the shock energy should be rapidly dissipated by compression of the abundant matrix and fine grained slate units and also by melting and vaporization of volatiles. The absence of shock metamorphic effects is especially likely at Darwin Crater because the recovered cores largely intersected slumped pelite blocks from the crater wall. Shock features are generally lacking in crater walls from simple craters, even when formed in crystalline rocks such as granites (Grieve 1987; Melosh 1989; Chapter 1).

4.8.3 Impact melt products (glass)

The presence of breccias containing significant amounts of melt fragments (suevite), or identification of brecciated rocks with a glassy matrix, can be used to provide strong evidence for the impact origin of a crater, and such melt-bearing lithologies are typically associated with the most highly shocked rocks (Grieve 1987; Melosh 1989). At Darwin Crater, the crater-fill stratigraphy does not show any evidence of coherent melt material. Rare glass fragments, recovered from the uppermost disaggregated polymict breccia samples, represent much less than 1% of the volume of clasts in the studied samples. Glass is abundant in gravels surrounding the crater that also contain 'twinned' quartz grains in greatest abundance. As mentioned above, the formation of the glass containing coesite requires shock energies well above the <5 GPA estimated from observed deformation in recovered drill cores and sufficient to produce multiple PDF sets in quartz. Given the expected association between shocked and melted material, and the very poor recovery from drilling, it is possible that highly shocked material with PDF's and melt-bearing units exist in the crater but have not been recovered. The most highly shocked material is expected in the upper crater-fill stratigraphy meaning that erosion may be a explanation for the absence of highly shocked melt-bearing breccias in the cores. Alternatively, and it is suggested more likely, glass and shocked material were always very low in abundance in the crater-fill stratigraphy. This is supported by the currently accessible core samples and observations of most other small impact structures such as Aouelloul, Mauritania (0.39km) and Barringer where glass and partially melted material is found scattered around the crater rim but not in drill core. Significantly, at Aouelloul the crater stratigraphy is also completely free of diagnostic impact shock effects (Koeberl et al. 1998a). If the 1.2km diameter Darwin Crater is the sole source of the glass, the extremely high abundance and widespread distribution of glass in the strewn field indicates that the ejection of the molten target rocks was incredibly efficient. This is a feature of small impact craters that has been both predicted by theoretical studies (e.g. Orphal et al. 1980, Grieve & Cintala 1992) and corroborated by observations at terrestrial craters like Aouelloul (Koeberl et al. 1998a). Later discussion will present models that relate this efficient ejection and wide dispersion of glass to the volatile contents in the suspected pre-impact target stratigraphy.

4.9 Conclusion

Darwin Crater is a circular and almost closed basin developed in a syncline of Silurian age metasedimentary rocks of the Eldon Group. Affinity with the Eldon Group is demonstrated in both petrographic and geochemical data. The structure is filled by a complicated package of slumped, deformed bedrock blocks and sandy breccias that are interpreted to have their origin in a rapid, high energy event involving shattering of quartzite and plastic deformation. These rocks are blanketed by laminar muds interpreted to be lacustrine deposits that subsequently filled in the structure.

The stratigraphy within Darwin Crater is consistent with the products of brittle to plastic deformation during small crater-forming impact events with shock pressures <5 GPa. However, without identification of PDF bearing quartz grains, or abundant melt in the crater-fill stratigraphy, there is little diagnostic evidence of an impact origin for Darwin Crater. This is despite the presence of rare glass in the polymict breccia, kinked micas, and evidence for very localized deformation well beyond that of the surface rocks cropping out around the crater. This is a common paradox in the study of small suspected impact structures where we are faced with the challenge of confirming an impact origin based on the identification of impact products that are observed consistently only at large craters (e.g. shocked quartz, clastic and matrix melt breccias). To counter this problem at Aouelloul crater, Koeberl et al. (1998a) relied not only on elevated Os abundances in the target rocks, but also used the Re-Os isotopic system to define a non-ambiguous mixing relationship between the target rocks, ejected impact glass and an extraterrestrial component from the projectile. The same isotopic system was used to demonstrate the impact origin of Tswaing Crater (Koeberl et al. 1994b) independent of identification and measurement of PDF's in quartz grains from the upper polymict sandy breccia (Reimold et al. 1992).

At young and well-preserved craters, and especially where glass is abundant as at Darwin, it should be possible to identify a range of other geochemical, isotopic and geographic relationships between an impact glass and the source crater. This rationale governs discussions in the following pages that define non-ambiguous trends relating Darwin glass to Darwin Crater and that allow for identification of the projectile involved in the *origin of Darwin glass.* These relationships will highlight the dynamic nature of the interaction between the projectile and target rocks during impact events on Earth.

Chapter 5

Glass vs. Crater Part 1

Geochemistry and Isotope systematics

Chapter 3 explored the geochemical systematics in the Darwin glass and showed that the geochemical variations observed could largely be explained by a mixture of two parent rock types close in composition to average post Archaean shale and quartzite. The exception is in the abundance of transition metals (Ni, Co, Cr), that in some samples are enriched beyond the concentration found in average sedimentary rock types. These transition metal enriched samples belong to the low SiO_2, high FeO+MgO, Group 2 glass, defined by the cluster analysis and scanning electron microprobe (SEM) grid surveys in Chapter 3. A Principal Components Analysis (PCA) suggests this transition metal enrichment is related to a 3rd currently unknown end member that is also rich in MgO and FeO. Chapter 4 described the geology and chemistry of the suspected source (Darwin Crater) and it was shown that the morphology and stratigraphy of the structure is consistent with, but not diagnostic of, an impact origin.

This chapter will attempt to falsify the hypothesis that *"the chemistry and isotopic systematics of Darwin glass match those of mixtures of the Eldon Group (suspected target) rocks in the Darwin Crater area"*. A secondary objective is to explain and identify the source of high Ni, Co and Cr abundances in some specimens. To fulfil this objective, a suite of highly siderophile element (HSE) data, obtained by laser ablation ICPMS (LA-ICPMS) analyses of selected samples, are explored

5.1 Geochemistry

5.1.1 Major Elements

For initial comparisons the range and average major element composition of the suspected target rocks and Group 1 and 2 glasses are compiled in table 5.1. Fig. 5.1A,B are plots of the average suspected target rock compositions normalised to Group 1 and 2 glasses. Major elements in Group 1 Darwin glass are closest to average Keel Quartzite (Sk) but are dramatically enriched in FeO and also enriched in MgO, P_2O_5 and SiO_2 relative to the quartzite. In Group 1 glass, all major elements other than SiO_2 are depleted compared to average Amber Slate (Sa). Group 1 glass is enriched in all elements other than SiO_2, MgO, CaO and P_2O_5 relative to average Crotty Quartzite (Sc). Group 2 glass is most similar in major element composition to Amber Slate (Fig. 5.1A). From these plots it is clear that some mixture of Amber Slate and Keel and/or Crotty Quartzite could closely approximate the major elements composition of Darwin glass and this will be demonstrated later in this chapter.

5.1.2 Trace elements

Average rare earth element (REE) abundances in Group 1 and 2 glasses and suspected target rocks are compiled for comparison in table 5.2. These are normalised to a C1 Chondrite (Sun & McDonough 1989) and plotted in Fig. 5.2. The glasses and suspected target rocks have strikingly similar abundance patterns characterised by negative Eu anomalies typical of upper crustal sediments. The glasses are very slightly depleted in light rare earth element (LREE) relative to average Amber Slate and very slightly enriched in La and Ce relative to average Keel Quartzite. The remaining LREE abundances are effectively identical in both Darwin glass and Keel Quartzite. For the other REE, the glasses and suspected target rocks define identically shaped and overlapping patterns. These glasses have inherited REE compositions that are typical of the suspected target rocks (table 5.2).

Average trace element compositions of glasses and suspected target rocks are compiled for comparison in table 5.3. As for the major elements, the average trace element compositions of Keel Quartzite, Amber Slate and Crotty Quartzite have been normalised to Group 1 and 2 glass (Fig. 5.3A,B). For the alkali metals and the alkali earth Ba, actinide elements and the LREE La-Nd, the compositions of Group 1 and 2 glasses are closest to, but slightly enriched relative to, average Keel Quartzite.

		SiO_2	Al_2O_3	TiO_2	FeO	MgO	MnO	CaO	K_2O	Na_2O	P_2O_5
Keel quartzite	**Average**	90.09	5.43	0.49	0.42	0.35	0.01	0.08	1.82	0.03	0.07
	Range	85.63 - 92.63	4.13 - 8.44	0.42 - 0.56	0.31 - 0.62	0.27 - 0.51	<0.01-0.01	0.01-0.29	1.44 - 2.81	0.03 - 0.05	0.01-0.30
Amber Slate	**Average**	75.41	11.83	0.71	3.28	1.34	<0.01	0.08	3.47	0.2	0.14
	Range	69.49 - 79.05	10.29 - 14.6	0.56 - 0.86	1.88 - 4.57	1.05 - 1.58	<0.01-0.01	0.01-0.32	2.84 - 4.04	0.04 - 0.41	0.08-0.35
Crotty Quartzite	**Average**	94.6	2.82	0.24	0.35	0.15	<0.01	0.07	0.99	0.02	0.07
	Range	93.24 - 97.6	1.11 - 3.94	0.14 - 0.36	0.06 - 0.59	0.09 - 0.17	<.01	0.01-0.13	0.38 - 1.24	0.0 - 0.04	0.01-0.13
Group 1 glass	**Average**	85.2	7.3	0.57	2.2	0.9		0.05	1.8	0.05	<0.01
	Range	80.62-93.9	3.1-10.6	0.2-0.7	0.8-4.23	0.2-2.3	<0.01	<0.01-0.1	0.75-2.6	0.0-0.2	<0.01
Group 2 glass	**Average**	81.6	8.2	0.6	3.8	2.2	<0.01	0.1	2	0.01	<0.01
	Range	76.4–84.5	6.4 – 11.5	0.5-0.80	1.8-5.8	1.1 – 4.0	<0.01	0.06– 0.2	1.4 – 2.7	0.0 – 0.2	<0.01

Table 5.1 Average and range in major element composition of Eldon Group (suspected target rock) samples from around Darwin Crater.

A

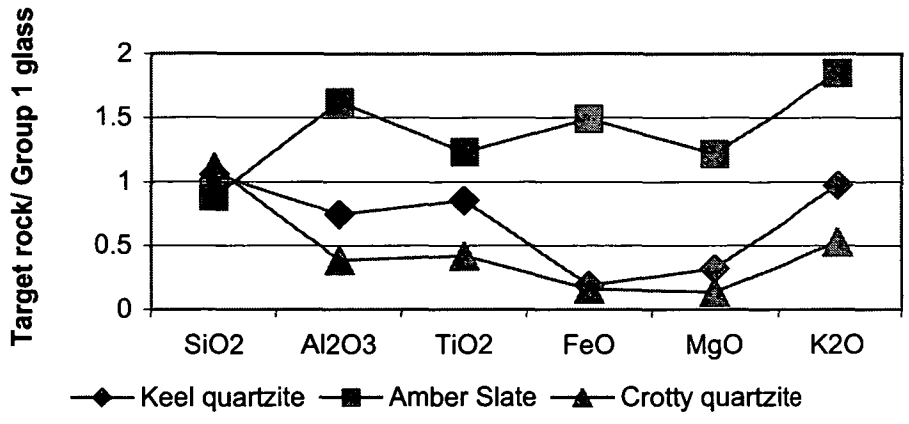

B

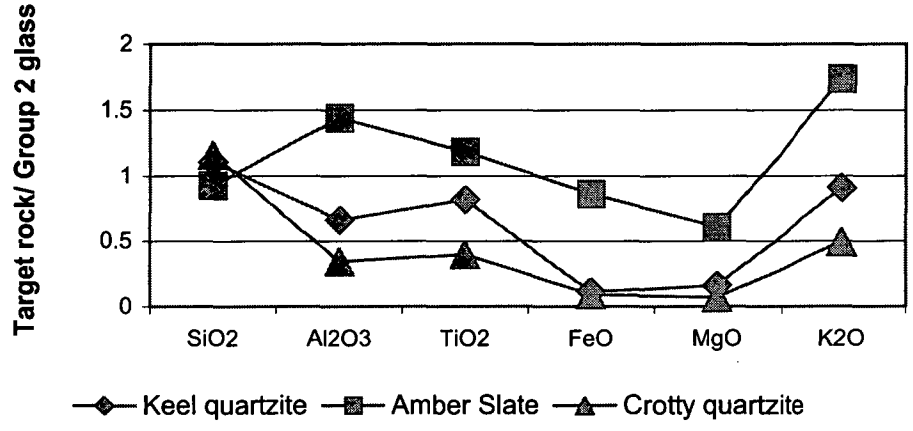

Figure 5.1A-B Average suspected target rock major element compositons normalised to average Group 1 and Group 2 glass.

	La	Ce	Pr	Nd	Sm	Eu	Gd	Tb	Dy	Ho	Er	Tm	Yb	Lu
Keel Quartzite Average	99.4	81.1	67.7	50.1	32.9	15.8	21.8	18.3	16.3	14.7	14.5	13.9	13.6	13.0
Amber Slate Average	147.5	111.8	91.7	64.0	38.1	17.9	23.0	19.4	17.7	16.2	16.2	15.7	16.0	15.4
Group 1 glass Average	36.2	79.4	8.7	33.4	6.9	1.3	6.6	1.1	6.7	1.2	3.9	0.6	3.3	0.5
Group 2 glass Average	34.4	74.4	8.3	31.8	6.6	1.2	6.2			1.1			3.1	0.5

Table 5.2 Average rare earth element (REE) composition of Eldon Group (suspected target rock) samples from around Darwin Crater and Group 1 and 2 glass.

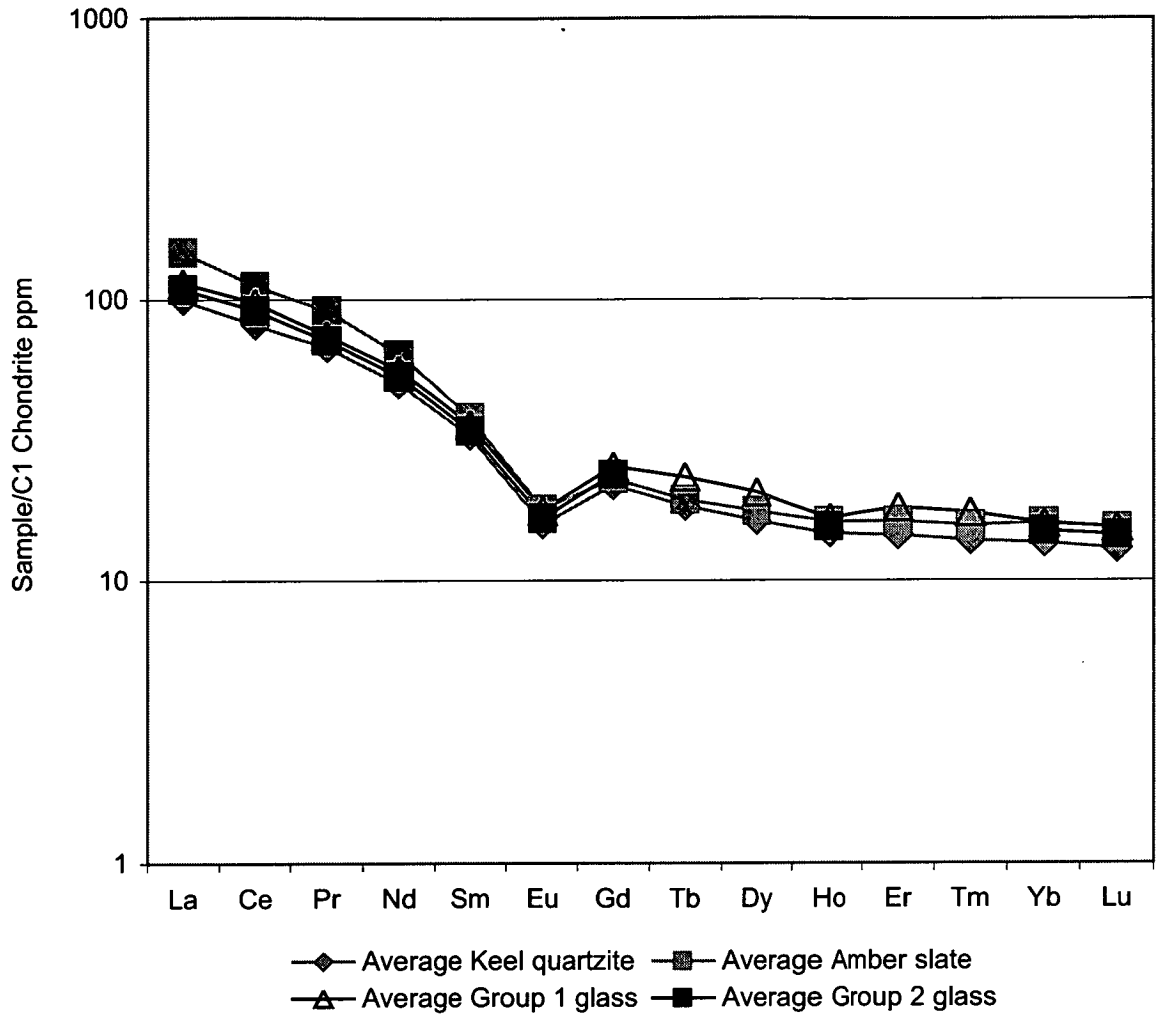

Figure 5.2 Chondrite (Sun & McDonough 1989) **normalised rare earth element (REE) composition of Darwin glass and Eldon Group (suspected target rock) samples from around Darwin Crater.**

Average (ppm)	Keel Quartzite	Amber Slate	Crotty Quartzite	Group 1 glass	Group 2 glass
Cs	4.3	9.7		3.8	3.7
Rb	62.9	161.2	36.1	74.6	78.1
U	2.2	3.3		1.9	1.5
Th	10.6	17.8		14.0	13.2
Ba	232.5	562.0	124.5	304.3	294.0
La	31.3	46.5		36.2	34.4
Ce	65.9	90.9		79.4	74.4
Nb	8.8	16.4	5.2	11.6	11.1
Pr	7.8	10.6		8.7	8.3
Sr	8.8	16.2	10.1	15.6	14.3
Nd	29.9	38.2		33.4	31.8
Zr	309.8	336.8	171.2	438.9	439.0
Sm	6.3	7.3		6.9	6.6
Eu	1.1	1.3		1.3	1.2
Gd	5.6	6.0		6.6	6.2
Ho	1.1	1.2		1.2	1.1
Yb	2.8	3.3		3.3	3.1
Y	24.2	31.4	15.6	34.1	32.3
Lu	0.4	0.5		0.5	0.5
Sc	6.1	11.2		7.3	8.1
Cr	55.0	85.4	80.0	74.5	162.7
Co	1.4	3.7	5.2	8.8	31.6
Ni	7.4	21.5	4.4	108.4	416.6
La/Lu	74.7	93.7		72.4	73.1
Gd/Yb	2.0	1.8		2.0	2.0
La/Sm	5.0	6.4		5.2	5.2

Table 5.3 Average trace element composition of Eldon Group (suspected target rock) samples from around Darwin Crater and Group 1 and 2 glass.

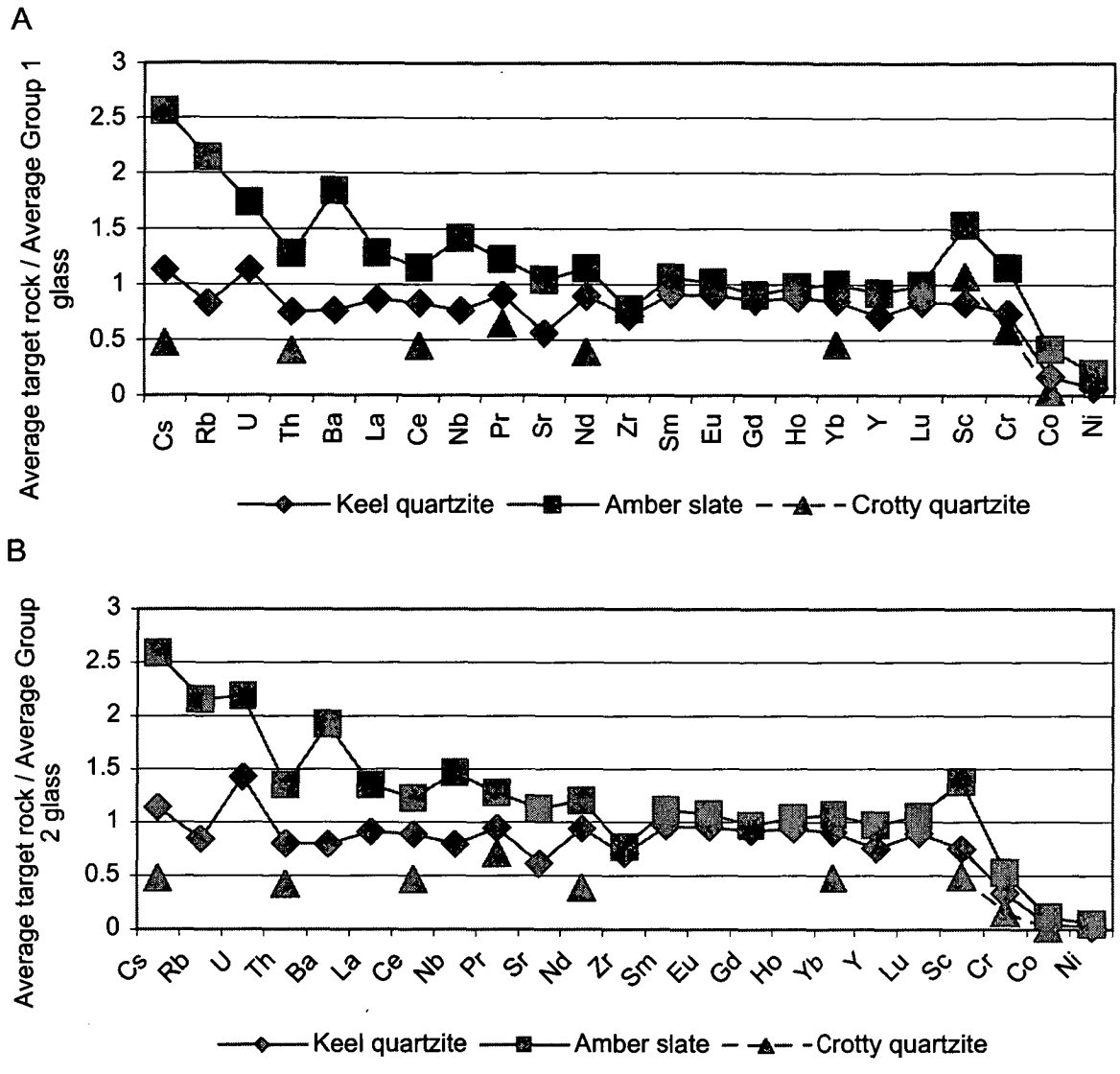

Figure 5.3A-B Average target rock trace element compositons normalised to Group 1 and Group 2 glass.

For Sr and the heavy rare earth elements (HREE) plus Y, the glass composition is closest to average Amber Slate; a near perfect match. Zr is enriched in all glasses relative to the average suspected target rock values but because its concentration is controlled by the abundance of detrital zircons, Zr analyses are typically highly variable in sedimentary rocks and the average suspected target rock values used might be significantly too small. The average Zr abundances in the glass falls within the over all range in Zr abundances of the suspected target rocks. In the transition metals, Sc is depleted in the glass relative to Amber Slate and enriched relative to Keel and Crotty Quartzite. Cr abundances in Group 1 glass are close to average Amber Slate but Group 2 glass is enriched in Cr beyond the range of all of the analysed suspected target rocks. Ni and Co are strongly enriched in all of Group 2 glass and some Group 1 samples relative to all of the analysed suspected target rocks. The upper limits in the abundance of Ni, Co and Cr in Darwin glass are more than 20, 6 and 2 times the average suspected target rock values, respectively. Average Rb/Sr in Group 1 (4.8) and 2 (5.2) glasses falls within the compositional range defined by average Crotty Quartzite (3.55), Keel Quartzite (7.17) and Amber Slate (9.98). The strongly depleted concentration of Sr and high Rb/Sr ratios in both the glass and suspected target rocks, relative to average crustal rocks, is the key feature of the non-transition metal trace element chemistry that links the glass to these proposed target rocks.

5.1.3 End-member compositions in glass and suspected target rocks

In Chapter 3 a Principal Components Analysis was used to derive elemental ratio plots that define the end-member glass compositions. These ratio plots allowed for the constant sum problem to be overcome and the true elemental co-variations to be shown. This chapter is not concerned with deciphering elemental co-variations but rather testing suspected target rock mixtures relative to the glass compositions. As such, 2 element plots provide a better means of comparison than do the ratio plots (Fig. 5.4A-H). On the major element plots, almost all except the most enriched Group 1 glass samples are depleted in SiO_2 relative to Keel and Crotty Quartzite. Some Group 1 and most Group 2 glass specimens are enriched in FeO relative to Average Amber Slate and some Group 1 and all Group 2 glasses plot beyond Average Amber Slate towards higher MgO abundances. Clearly, the bulk of Group 1 glasses plot within the data array defined by the suspected target rocks, and can be explained as a mixture of these rocks. However, Group 2 glass requires an end-member enriched in MgO and FeO beyond the range of these potential target rocks.

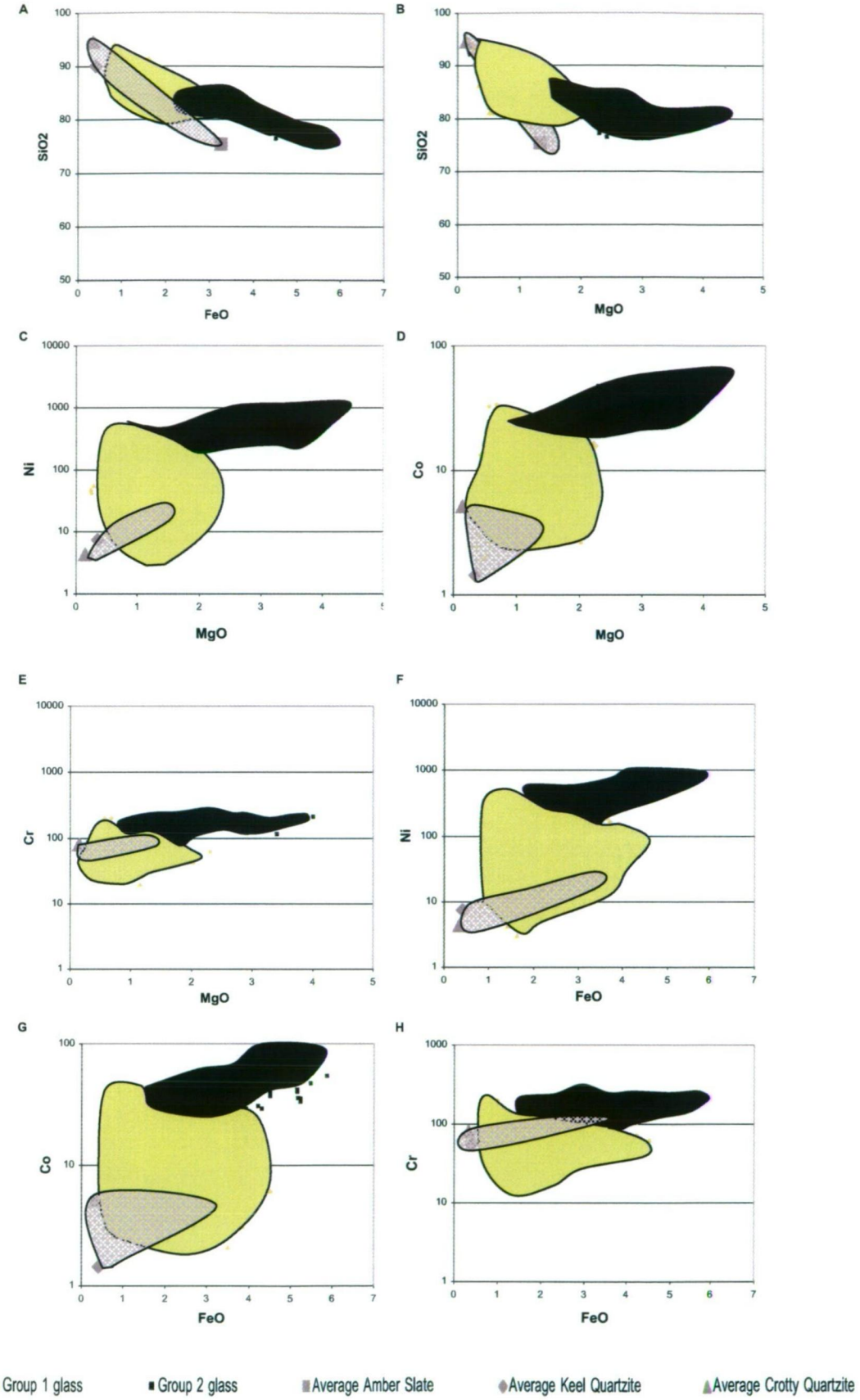

Figure 5.4A-H Plots comparing end-member compositions in Group 1 and 2 glass to average Eldon Group (suspected target rock) samples from around Darwin Crater. Oxides in %, trace elements in ppm.

On the plots of MgO, FeO vs. Ni, Co, Cr the least enriched end-members in Group 1 glass fall within the broad data array defined by the suspected target rocks. However, on these plots high MgO, FeO, ± transition metal samples of Group 1 glass, and all of Group 2 glass, fall outside of the range in the suspected target rocks and require a currently unknown end member rich in FeO, MgO and Ni, Co, Cr, as was predicted by the PCA.

Tektites form from rocks melted at shallow depths within the target stratigraphy (Blum et al. 1992, Koeberl 1994) as is indicated by ^{10}Be concentrations of around 40-200 $*10^6$ atoms/g in Australasian tektites (Tera et al. 1983, Englert et al. 1984). As such, there is always a component of regolith (weathered rock + soil) in the target stratigraphy, and weathering processes in the regolith can concentrate FeO and the transition metals (e.g. Ohlander 2003) that might subsequently have contributed to the glasses. For this reason, analytical data for the most weathered drill core sample (KH19) and soil from the top of DDH1 (K15) has been added to the elemental plots as proxy for highly weathered rock that it might be speculated was impacted (e.g. surface samples) and formed a component of the glasses source material (Fig. 5.5A-H).

The plot of SiO_2 vs. FeO (Fig. 5.5A) shows that all of the glasses are strongly depleted in FeO relative to KH19 and KH15. Respectively, the FeO abundances in KH19 and KH15 are approximately 6 and 2 times higher than in the most FeO rich glasses, thus a small component of such weathered material could contribute FeO to the Group 2 glass. MgO abundances in KH19 and KH15 are within the range of the average target rocks and, as such, some Group 1 and all of Group 2 samples are significantly enriched in MgO relative to KH19 and KH15. Most of the Group 2 glass samples are enriched in Cr relative to KH19 and KH15. The least Cr enriched samples in Group 2 and all of Group 1 glass have similar Cr abundances to KH19. Ni and Co are enriched in KH19 and KH15 compared to the average target rocks, but relative to these samples most Group 1 and all Group 2 glasses remain strongly enriched in Ni and Co. As such, the composition of Group 2 glass is difficult to relate to either weathered material (KH19, KH15) or fresh rocks in the suspected target stratigraphy alone, and the speculated end-member rich FeO, MgO, Ni, Co and Cr remains to be defined by this study.

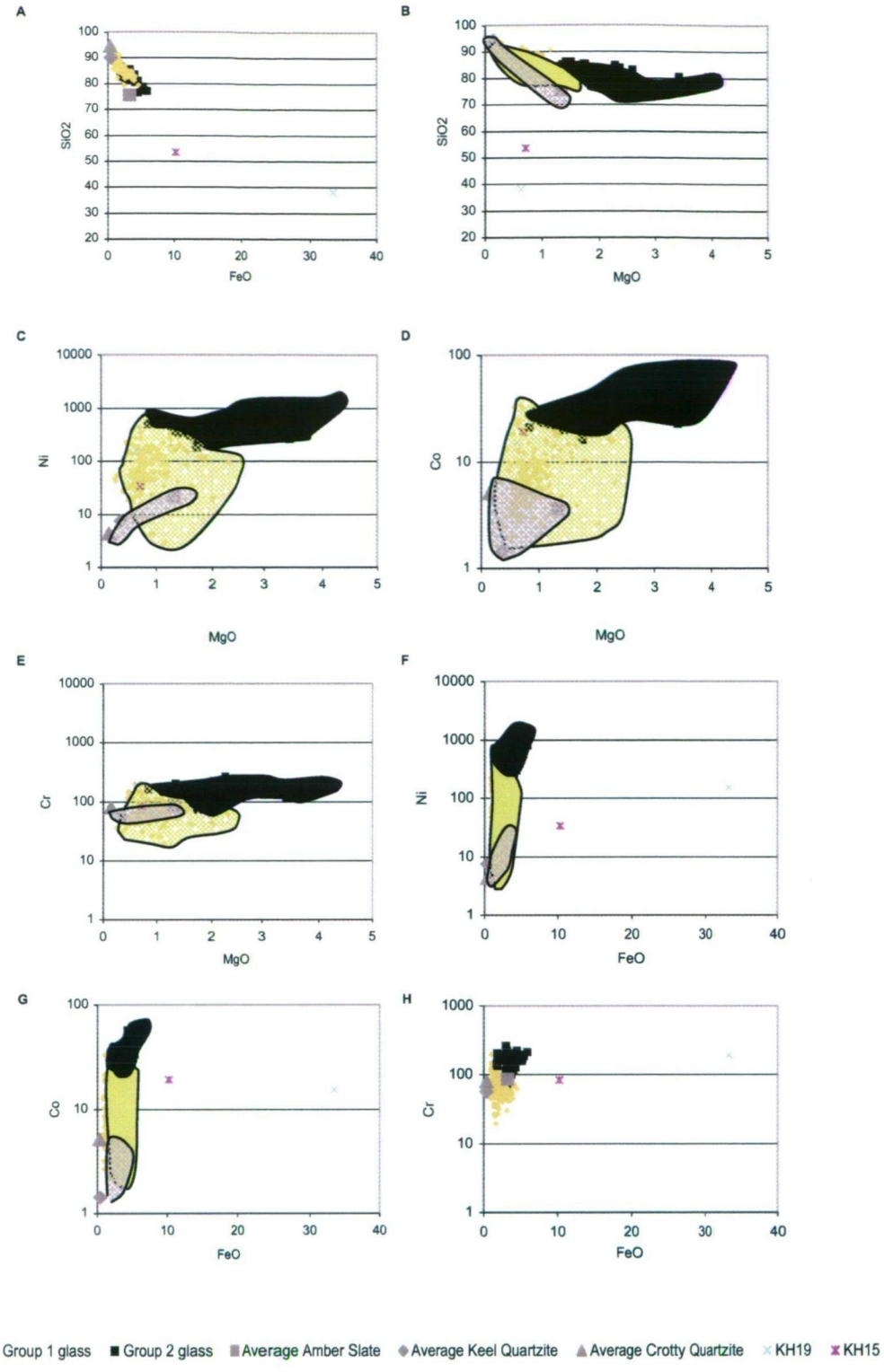

Figure 5.5A-H Plots comparing end-member compositions in Group 1 and 2 glass to average Eldon Group (suspected target rock) samples, highly weathered (KH19) and soil (KH15) samples from around Darwin Crater.
Oxides in %, trace elements in ppm.

5.1.4 Mixing models with average suspected target rocks

To further test the compatibility of the analysed rocks as parent materials of Darwin glass, a least squares regression model was created in Excel. All elements in the individual analyses were normalised to the composition of bulk average (Groups 1 and 2 combined) Darwin glass. The following elements were modelled simultaneously: SiO_2, TiO_2, Al_2O_3, FeO, MgO, K_2O, Cr, Co, Ni, Y, Rb, Zr, Sr and Ba using equation 5.1.

$$\text{Residual error in fit} = (SiO_{2\,Glass} - (\%\,Sa * SiO_{2\,Sa} + \%Sk * SiO_{2Sk} + \%Sc * SiO_{2Sc}))^2$$

Equation 5.1

Least squares regression equation, this example is for a 3-component mixture

Where:

SiO_{2Glass} = Average Glass SiO_2

$SiO_{2Sa,k,c}$ = Average target SiO_2

%Sa,Sk,Sc = proportion of each target rock mixed in model where: Sa = Amber Slate; Sk = Keel Quartzite; and Sc = Crotty Quartzite

Using the Solver function in Excel, the model was used to find the best compositional match for every glass analysis with suspected target rock mixtures. The model was run subject to the constraint that the percentage contributions from each target rock can not be negative. Volatile fractionation was not considered in this interpretation.

The preferred model is a 3-component mixture of average suspected target rock compositions. The parameters and average result for the model of bulk average glass composition (Groups 1 and 2 combined) is presented in table 5.4. Log-residual errors in the model fit are normally distributed suggesting that all the glass samples can be considered to be a part of a single population because the model is not forced to produce widely divergent compositions such as felsic and mafic glasses. Rather, the compositional range of all analysed samples is largely a continuum (Fig. 5.6).

	SiO_2	TiO_2	Al_2O_3	FeO	MgO	K_2O	Cr	Co	Ni	Y	Rb	Zr	Sr	Ba
Target Rock compositions														
Average Amber Slate (Sa)	75.4	0.7	11.8	3.3	1.3	3.5	85.9	3.7	21.5	31.4	161.2	336.8	16.2	562.0
Average Keel quartzite (Sk)	90.1	0.5	5.4	0.4	0.4	1.8	55.8	1.4	7.4	24.3	62.9	309.8	9.0	232.5
Average Crotty quartzite (Sc)	94.6	0.2	2.8	0.3	0.1	1.0	80.0	5.2	4.4	15.6	36.1	171.2	10.2	124.5
Bulk Average glass	**84.6**	**0.6**	**7.5**	**2.5**	**1.1**	**1.9**	**89.7**	**12.6**	**159.3**	**33.9**	**75.5**	**431.1**	**15.6**	**304.9**
Model result (residual error) in normal units	1.0	0.1	0.6	0.9	0.4	0.5	33.8	9.3	148.3	9.2	25.9	156.3	3.5	53.8
Residual error as % of average composition	1.2	10.6	7.9	36.3	39.7	25.9	37.6	72.8	91.9	26.9	34.4	36.1	22.2	17.6

Best model target rock mixtures

Amber Slate (Sa)	Keel Quartzite (Sk)	Crotty Quartzite (Sc)
46.8%	**23.5%**	**29.7%**

Table 5.4 Average suspected target rock compositions used in least-squares regression model of bulk average glass composition, showing the average residual errors in the model result.

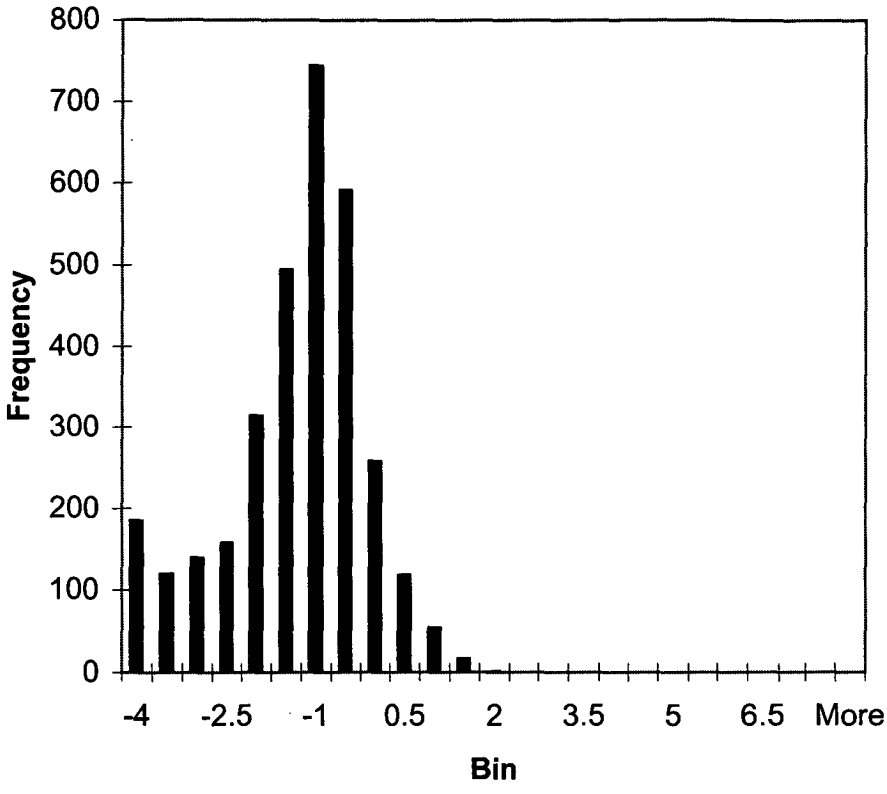

Figure 5.6 Histogram showing log-normal distribution in residual errors from mixing model result.

Average residual errors for each element in the model of bulk average glass composition are plotted in normal units in Fig. 5.7A-B and as a percentage of the bulk average value for each element in Fig. 5.8A-B. Relative to the bulk average abundances the worst model fits are (in order) Ni, Co, MgO, Cr and FeO. For the remaining elements the model produces a good match using an average target rock mixture of 47% Amber Slate (Sa), 24% Keel Quartzite (Sk) and 30% Crotty Quartzite (Sc) (table 5.4).

The average of all individual model results for Group 1 and 2 glasses have been separated and are compiled in table 5.5. As is expected for Group 1 glasses, these results are almost identical as those for the model of bulk composition using an average suspected target rock mixture of 43% Sa, 27% Sk and 30% Sc. In Group 2, the average model result was 66% Sa, 4% Sk and 30% Sc. This mixture results in increased residual errors for (in order) Ni, Co, Rb, MgO Cr, and FeO. The concentrations of the remaining elements are successfully modelled. When soil (e.g. KH15) or weathered samples (e.g. KH19), more enriched in transition metals are added to the mixing models the residual errors in Ni, Co, Cr, MgO and FeO are not improved (table 5.6); even if soil or weathered material is allowed to contribute at an unrealistically large level to the mix.

In the interpretation of model results, it is the Amber Slate proportions that are most significant as the numerical distinction between Keel and Crotty Quartzite is poorly constrained and could easily also be accounted for by SiO_2 variations in either lithology. Given that for many trace elements, the glass compositions are closest to Keel Quartzite, it is suggested that model amounts of Crotty Quartzite are over estimates, better viewed as representing contributions from high SiO_2 components of the Keel Quartzite. Similarly, the slate proportions can also be interpreted as representing contributions from pelitic zones in, and pelitic units (e.g. Austral Creek Siltstone) associated with, the Keel Quartzite. This is because the petrography of pelitic zones in Keel Quartzite samples is almost identical to Amber Slate, as is the composition expected to be, given the fact that in Eldon Group samples the observed composition is controlled by the abundance of quartz (Chapter 4). The anomalous Ni, Co, Cr, MgO and FeO enrichments in Group 2 glasses are discussed in section 5.3.

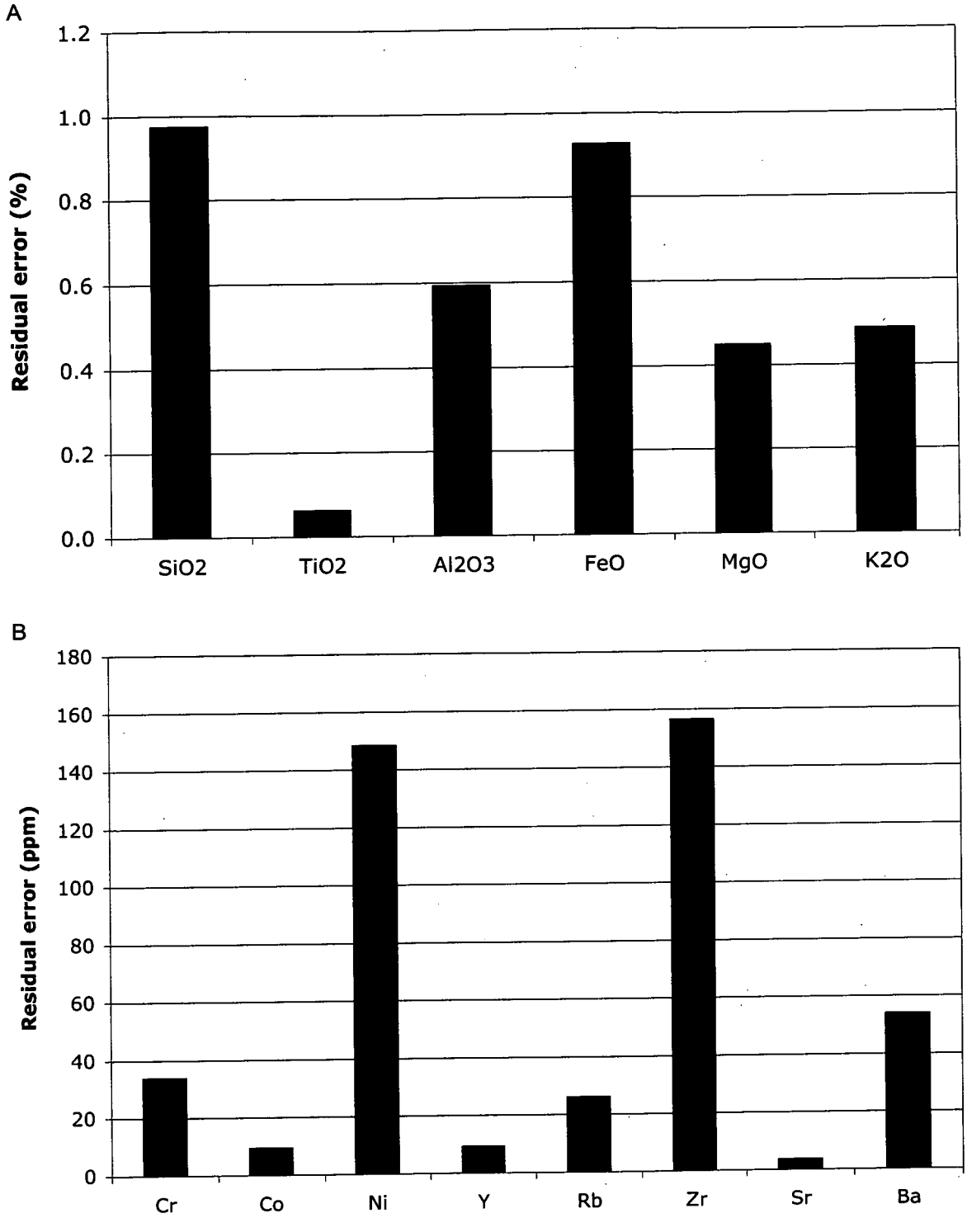

Figure 5.7A-B Average residual errors in mixing model result in normal units (%, ppm).

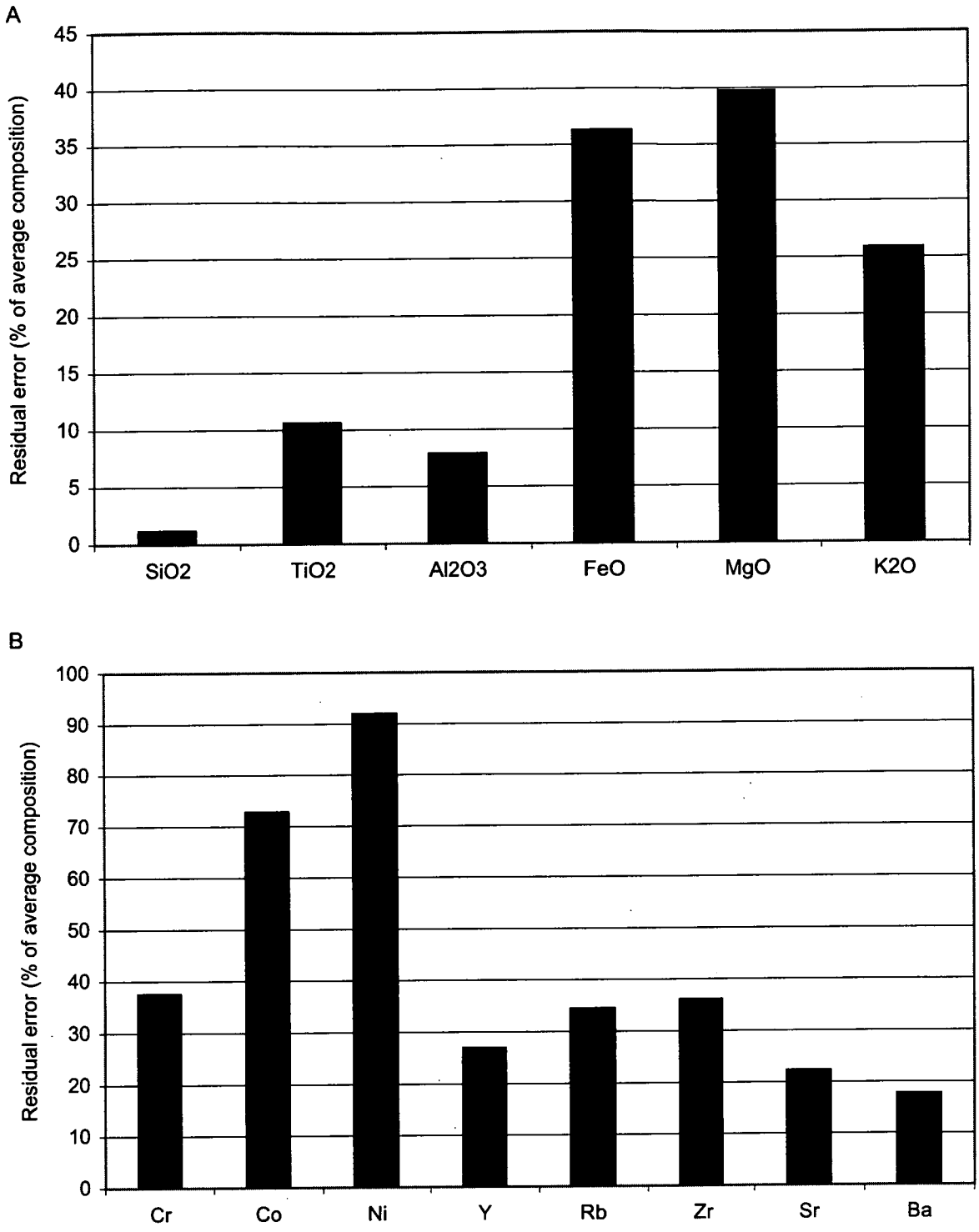

Figure 5.8A-B Average residual errors in mixing model result expressed as a percentage of the bulk average value for each element.

	SiO_2	TiO_2	Al_2O_3	FeO	MgO	K_2O	Cr	Co	Ni	Y	Rb	Zr	Sr	Ba
Target Rock compositions														
Average Amber Slate (Sa)	75.4	0.7	11.8	3.3	1.3	3.5	85.9	3.7	21.5	31.4	161.2	336.8	16.2	562.0
Average Keel quartzite (Sk)	90.1	0.5	5.4	0.4	0.4	1.8	55.8	1.4	7.4	24.3	62.9	309.8	9.0	232.5
Average Crotty quartzite (Sc)	94.6	0.2	2.8	0.3	0.1	1.0	80.0	5.2	4.4	15.6	36.1	171.2	10.2	124.5
Average Group 1 glass	**85.2**	**0.6**	**7.3**	**2.2**	**0.9**	**1.9**	**74.5**	**8.8**	**108.4**	**34.1**	**75.3**	**433.2**	**15.6**	**304.9**
Model result (residual error) in normal units	1.0	0.1	0.5	0.8	0.3	0.4	26.0	5.9	101.2	9.7	22.8	165.0	3.6	42.0
Residual error as % of average composition	1.2	11.4	7.3	37.5	33.6	23.6	35.0	68.0	93.4	28.4	30.2	38.1	23.3	13.8
Average Group 2 glass	**81.6**	**0.6**	**8.2**	**3.8**	**2.2**	**2.0**	**160.7**	**30.4**	**405.9**	**32.3**	**74.8**	**391.9**	**14.3**	**292.6**
Model result (residual error) in normal units	0.9	0.0	0.9	1.5	1.2	0.7	76.2	27.5	393.0	6.3	43.3	108.2	2.5	118.9
Residual error as % of average composition	1.1	6.0	11.2	39.0	56.7	35.9	47.5	90.4	96.8	19.6	57.9	27.6	17.6	40.7

Best model target rock mixtures

Amber Slate (Sa)	Keel Quartzite (Sk)	Crotty Quartzite (Sc)
43.3%	**27.0%**	**29.6%**

Amber Slate (Sa)	Keel Quartzite (Sk)	Crotty Quartzite (Sc)
65.7%	**4.1%**	**30.2%**

Table 5.5 Average target rock compositions used in least-squares regression models of average Group 1 and Group 2 glass composition, showing the average residual errors in the model results.

	SiO_2	TiO_2	Al_2O3	FeO	MgO	K_2O	Cr	Co	Ni	Y	Rb	Zr	Sr	Ba
Target Rock compositions														
Average Amber shale (Sa)	75.4	0.7	11.8	3.3	1.3	3.5	85.9	3.7	21.5	31.4	161.2	336.8	16.2	562.0
Average Keel quartzite (Sk)	90.1	0.5	5.4	0.4	0.4	1.8	55.8	1.4	7.4	24.3	62.9	309.8	9.0	232.5
Average Crotty quartzite (Sc)	94.6	0.2	2.8	0.3	0.1	1.0	80.0	5.2	4.4	15.6	36.1	171.2	10.2	124.5
Soil	53.5	0.5	9.2	10.2	0.7	1.9	84.0	19.1	33.7	36.2	96.2	254.0	30.7	403.2
Bulk Average glass	**84.6**	**0.6**	**7.5**	**2.5**	**1.1**	**1.9**	**89.7**	**12.6**	**159.3**	**33.9**	**75.5**	**431.1**	**15.6**	**304.9**
Model result (residual error) in normal units	**4.9**	**0.1**	**0.6**	**0.7**	**0.5**	**0.3**	**31.4**	**7.1**	**145.7**	**7.4**	**13.7**	**156.2**	**3.4**	**36.4**
Residual error as % of average composition	**5.8**	**12.2**	**7.9**	**25.6**	**48.2**	**13.4**	**34.9**	**55.8**	**90.3**	**21.6**	**18.1**	**36.1**	**21.9**	**11.9**

Best model target rock mixtures

Amber Slate (Sa)	Keel Quartzite (Sk)	Crotty Quartzite (Sc)	Soil
23.7%	38.1%	17.3%	20.9%

Average Amber shale (Sa)	75.4	0.7	11.8	3.3	1.3	3.5	85.9	3.7	21.5	31.4	161.2	336.8	16.2	562.0
Average Keel quartzite (Sk)	90.1	0.5	5.4	0.4	0.4	1.8	55.8	1.4	7.4	24.3	62.9	309.8	9.0	232.5
Average Crotty quartzite (Sc)	94.6	0.2	2.8	0.3	0.1	1.0	80.0	5.2	4.4	15.6	36.1	171.2	10.2	124.5
KH19	37.9	0.4	7.5	33.5	0.6	2.1	190.3	15.2	150.6	729.6	83.4	265.1	21.7	371.8
Bulk Average glass	**84.6**	**0.6**	**7.5**	**2.5**	**1.1**	**1.9**	**89.7**	**12.6**	**159.3**	**33.9**	**75.5**	**431.1**	**15.6**	**304.9**
Model result (residual error) in normal units	**2.4**	**0.1**	**0.6**	**0.6**	**0.5**	**0.4**	**30.6**	**9.4**	**146.4**	**7.6**	**17.9**	**146.5**	**3.9**	**38.3**
Residual error as % of average composition	**2.8**	**10.7**	**8.4**	**25.0**	**43.9**	**20.6**	**34.1**	**74.7**	**91.9**	**22.4**	**23.7**	**34.0**	**25.1**	**12.6**

Best model target rock mixtures

Amber Slate (Sa)	Keel Quartzite (Sk)	Crotty Quartzite (Sc)	KH19
35.4%	40.7%	22.9%	2.2%

Average Amber Slate (Sa)	75.4	0.7	11.8	3.3	1.3	3.5	85.9	3.7	21.5	31.4	161.2	336.8	16.2	562.0
Average Keel Quartzite (Sk)	90.1	0.5	5.4	0.4	0.4	1.8	55.8	1.4	7.4	24.3	62.9	309.8	9.0	232.5
Average Crotty quartzite (Sc)	94.6	0.2	2.8	0.3	0.1	1.0	80.0	5.2	4.4	15.6	36.1	171.2	10.2	124.5
KH19	37.9	0.4	7.5	33.5	0.6	2.1	190.3	15.2	150.6	729.6	83.4	265.1	21.7	371.8
Soil	53.5	0.5	9.2	10.2	0.7	1.9	84.0	19.1	33.7	36.2	96.2	254.0	30.7	403.2
Bulk Average glass	**84.6**	**0.6**	**7.5**	**2.5**	**1.1**	**1.9**	**89.7**	**12.6**	**159.3**	**33.9**	**75.5**	**431.1**	**15.6**	**304.9**
Model result (residual error) in normal units	**0.3**	**0.1**	**0.6**	**0.6**	**0.5**	**0.4**	**31.1**	**9.5**	**146.3**	**9.7**	**17.2**	**149.9**	**4.1**	**37.1**
Residual error as % of average composition	**0.3**	**12.0**	**8.5**	**22.8**	**44.1**	**19.5**	**34.6**	**75.2**	**91.8**	**28.5**	**22.8**	**34.8**	**26.3**	**12.2**

Best model target rock mixtures

Amber Slate (Sa)	Keel Quartzite (Sk)	Crotty Quartzite (Sc)	KH19	Soil
34.9%	40.3%	22.2%	2.4%	0.2%

Table 5.6 Average suspected target rock, weathered suspected target rock (KH19) and soil compositions used in least-squares regression models of bulk average composition, showing the average residual errors in the model results.

5.2 Sm-Nd, Rb-Sr Isotope Systematics

5.2.1 Use of Sm-Nd and Rb-Sr isotopes in impact studies

Numerous authors have used Rb-Sr and Sm-Nd isotopic analyses of tektites and impact glasses to determine the age and provenance of the target materials that were melted during impact to form these glasses (e.g. Shaw & Wasserburg 1982; Koeberl et al. 1998b; Whitehead et al. 2000; Schaaf & Müller-Sohnius 2002). In the case of the Nd system, resultant $^{143}Nd/^{144}Nd$ values are referenced to present chondritic values that form the model Nd reservoir (that is equivalent to a model primitive mantle on the Earth). Reference $^{87}Sr/^{86}Sr$ values in this system correspond to the model of an undifferentiated mantle source.

Provided the assumptions that a sample was derived from a reservoir with the isotopic characteristics of the model reservoir and that the isotopic system has remained undisturbed since that time are met, model Sr and Nd ages can be calculated (Rollinson 1993). These ages are derived from regression lines of their respective isotopic evolution plots ($^{87}Rb/^{86}Sr$ vs. $^{87}Sr/^{86}Sr$, $^{147}Sm/^{144}Nd$ vs. $^{143}Nd/^{144}Nd$). Model isotope ages reflect the last time the sample separated from the model reservoirs and underwent major fractionation of parent and daughter species (Shaw & Wasserburg 1982). If the assumptions are met, then Sr and Nd model ages are concordant, and if not, fractionation has taken place. Post-reservoir fractionation most often occurs in the Sr isotopic system where weathering may increase Rb abundance as clays develop (Rollinson 1993).

The deviation in isotopic ratios from values for the model reservoirs provides a means of characterising a sample. Isotopic evolution plots define distinct and limited arrays between lithologies of different age, provenance and history. Impact glasses and tektites inherit the isotopic and geochemical signals of their source rocks. As such, Rb-Sr and Sm-Nd analyses of these glasses allow for direct comparison with potential target lithologies. This technique has successfully linked Late Eocene impact ejecta with the Popigai Crater in Siberia (Whitehead et al. 2000). It has also been used to characterise the target materials involved in the formation of Australasian tektites (Shaw & Wasserburg 1982); although the impact site has not yet been identified. Nd model ages were also use to link Georgiaite tektites with an Appalachian source, later tracked to the Chesapeake Bay Crater (Shaw & Wasserburg 1982).

Schaff & Müller Sohnius (2002) studied Rb-Sr and Sm-Nd isotope systematics in Libyan Desert Glass (LDG) and the, then suspected, target sandstones cropping out within the strewn field. LDG is a siliceous impact glass in many ways similar to Darwin glass (see Chapter 3), but yields consistent fission track ages of around 29Ma (Gentner et al. 1969). The sandstones they analysed belong to the former "Nubian Sandstone" – an imprecise term now avoided- and are of upper Cretaceous, probably Coniacian (88.5-86.6 Ma) age (Schaff & Müller Sohnius 2002). The sandstones contain impact diagnostic shock metamorphic effects in the form of PDF bearing shocked quartz (Kleinman et al. 2001). The relative abundance of major and most trace elements in the sandstones is also also considered to be compatible with these rocks being target rocks for LDG (Koeberl 1997).

However, Schaff & Müller Sohnius (2002) demonstrated that the Rb-Sr, Sm-Nd isotopic signals in LDG are in fact consistent with an inherited Pan-African age of 540Ma, far removed from signature of the Cretaceous sandstones. Rather, it was suggested that the glasses had an inherited isotopic composition consistent with derivation from Precambrian granitoid rocks found in northeast Africa, west of the Nile. This single data set rules out the Cretaceous rocks as the target rocks for LDG despite the spatial association, a compatible major and trace element composition and the presence of impact shock effects. While I suspect at least some dune sands in the LDG strewn field might preserve Pan-African isotopic signals, this study highlights the power of Sr and Nd isotopes in testing the relationship between a glass and suspected target rocks.

5.2.2 Methodology

In order to test the demonstrated major and trace element compatibility of the suspected target rocks from Darwin crater as the pre-cursors of Darwin glass, the Sr and Nd isotope compositions of 12 samples have been determined: 3 slates, 3 quartzites, 3 crater-fill samples and 3 pieces of glass. The analysed suspected target rock powders were sub-sampled from those prepared and analysed in Chapter 4. Glass samples were wrapped in clean cloth and crushed under a hydraulic press before being ground to a fine powder suitable for fused disc production for XRF, and digestion for solution ICP-MS analyses of major and trace elements. These analyses were conducted following an identical methodology and in the same analytical run as for target rock analyses in Chapter 4. Rb, Sr, Sm and Nd concentrations and isotope compositions were re-determined by Dr Karin Barovich at the University of Adelaide.

Sr, and Nd isotopic compositions were measured in static mode on a Finnigan MAT 262 Thermal Ionisation Mass Spectrometer. The average $^{87}Sr/^{86}Sr$ ratio for standard SRM987 during the course of the study was 0.710264 ± 28 (2σ) on 12 runs. The full procedural blanks for Sr are better than 1ng. Whole rock powders were dissolved and split before spiking with ^{84}Sr and ^{85}Rb. Samples for the Sm-Nd analyses were spiked with a mixed ^{149}Sm-^{150}Nd spike. The Nd isotopic ratios were monitored by measuring the standard J & M specpure Nd_2O_3 that yielded a $^{143}Nd/^{144}Nd$ ratio of 0.511696 ± 8 (2σ) on 18 runs. The value for standard Lajolla gave a $^{143}Nd/^{144}Nd$ ratio of 0.511848 ± 8 (2σ). The procedural blanks for Nd are less than 300pg and for Sm less than 150pg.

5.2.3 Results

The Rb, Sr, Sm and Nd concentrations in the analysed samples have been compiled in table 5.7 along with selected major and trace elements for reference. Sm has a very limited compositional range in the glass (6.74- 7.12ppm) and suspected target rocks including crater-fill samples (4.59-9.32ppm). Nd concentrations have a very limited range in the glasses (34.82-35.45ppm) and a larger range in the suspected target rocks and crater-fill samples (25.8-48.16ppm). The highest Nd concentrations are in KH18, followed by Amber Slate and Keel Quartzite. Rb and Sr have limited compositional ranges in the glass (Rb: 74.9–82.9ppm; Sr: 12.6-17.6ppm). In the suspected target rocks and crater-fill samples, Rb and Sr show greater variation (Rb: 49.7-148ppm; Sr: 4.74-24.08 ppm).

Figure 5.9A,B shows plots of Sm vs. Nd and Rb vs. Sr. The plot of Sm vs. Nd defines a vaguely linear array with the glasses tightly clustered in the centre of the suspected target rock and crater-fill samples and showing greatest similarity to Amber Slate samples. The plot of Rb vs. Sr defines a far broader data array featuring no obvious trends. Again, the glasses are clustered in the centre of the suspected target rock and drill core samples, this time showing greatest similarity to two of the Keel Quartzite samples. The wide range in Rb concentrations probably reflects variations in the mineralogy of samples with Rb concentrated in muscovite and Sr in feldspar, carbonate and apatite.

Sample	Lithology	ppm Rb	Sr	Sm	Nd	% SiO_2	Al_2O_3	K_2O	TiO_2	FeO	ppm Cs	Y	Zr	Ba
KH1	Keel Quartzite (Sk)	110.5	4.7	4.6	27.6	85.6	8.4	2.8	0.5	0.6	5.5	23.4	275.3	350.5
KH2	Keel Quartzite (Sk)	84.6	22.6	8.4	35.6	87.7	6.3	2.1	0.5	0.4	4.1	39.7	385.3	307.5
KH4	Keel Quartzite (Sk)	63.0	11.0	4.9	25.8	90.4	5.0	1.6	0.4	0.4	3.2	24.0	342.4	254.3
KH6	Amber Slate (Sa)	179.7	20.2	7.1	40.2	76.9	11.8	4.0	0.9	1.9	9.0	34.7	404.0	596.5
KH7	Amber Slate (Sa)	157.1	18.4	6.2	34.7	79.1	10.3	3.5	0.8	2.0	7.7	30.8	385.0	507.8
KH8	Amber Slate (Sa)	197.7	9.0	6.6	40.5	69.5	14.6	4.0	0.8	4.4	12.3	32.7	329.7	567.3
KH15	DDH1 52	96.2	28.8	7.6	36.3	53.4	9.3	1.9	0.5	10.2	10.6	35.8	254.0	403.2
KH17	DDH 2 A44	49.7	6.7	7.6	33.9	90.6	4.4	1.1	0.5	1.6	4.0	33.2	440.8	181.8
KH18	DDH2 A74	171.8	7.5	9.3	48.2	65.5	12.0	3.7	0.7	10.8	13.9	65.3	302.5	491.4
KH22	Light green glass	74.9	12.6	7.0	34.9	86.9	7.2	1.8	0.5	2.0	4.10	34.8	420.1	317.9
KH23	Dark green glass	82.6	17.2	7.1	35.5	87.3	7.4	1.9	0.5	1.8	4.60	33.5	418.5	306.8
KH24	Black glass	82.9	17.6	6.7	34.8	86.2	7.7	1.9	0.6	2.9	4.59	35.9	406.0	357.2

Table 5.7 Rb-Sr and Sm-Nd elemental abundances in Eldon Group (suspected target rock) samples from around Darwin Crater, crater-fill samples and Darwin glass, along with other selected major and trace elements.

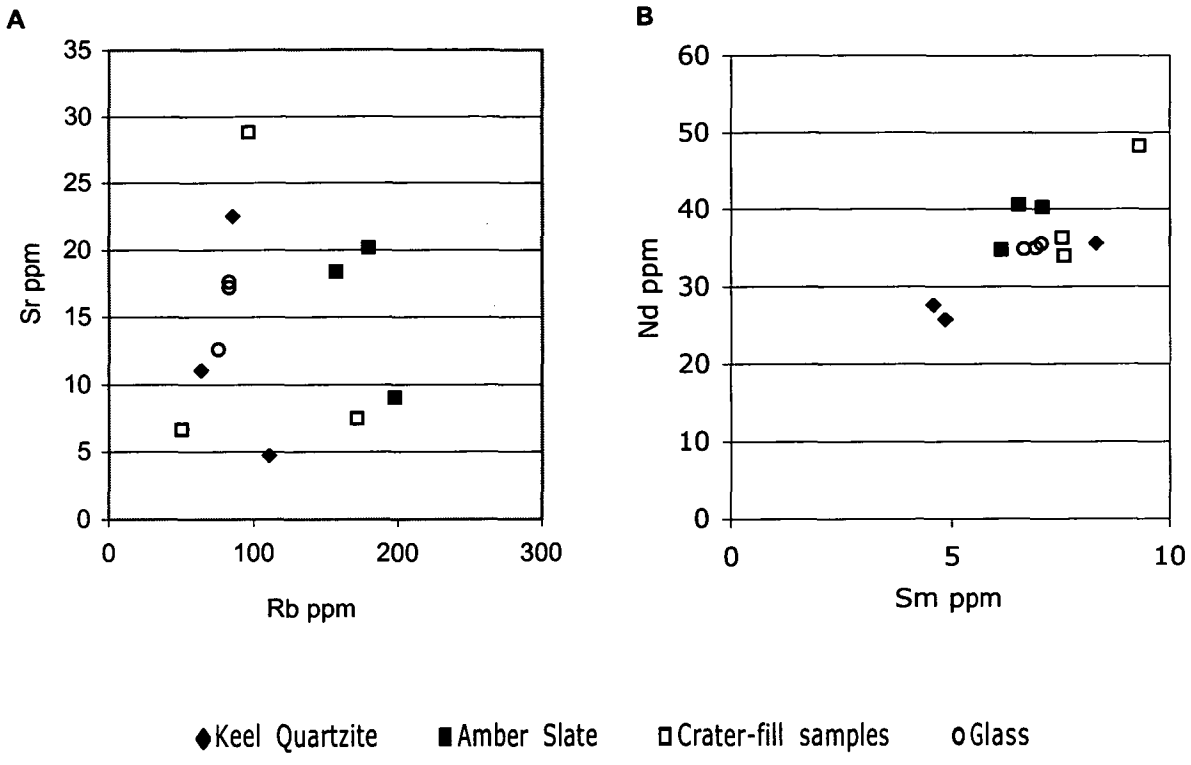

Figure 5.9A-B Sm vs. Nd and Rb vs. Sr in glass, Eldon Group (suspected target) samples from around Darwin Crater and crater-fill samples.

In table 5.8 the isotopic results have been compiled along with elemental concentrations. In 2 analyses (KH8, KH18) Sr isotopes were not detected in sufficient abundance. The $^{87}Sr/^{86}Sr$ ratios show a limited range in the glasses (0.80778-0.81605) with the black glass being most radiogenic. These $^{87}Sr/^{86}Sr$ ratios for the glasses fall within the very large range (0.76481-1.1212) defined by all suspected target rocks and crater fill samples. Significant to note is that the quartzite KH1 is significantly more radiogenic ($^{87}Sr/^{86}Sr$ =1.1212) than the other suspected target rock and crater fill samples that define a more limited range ($^{87}Sr/^{86}Sr$=0.76481-0.88216) clustered around the glasses. Large errors in KH1 are likely to be related to the very low concentration of Sr in the sample.

In the Sm-Nd isotopic system the glass, suspected target rock and crater-fill samples have homogeneous ε-Nd results ranging from -13.57- -15.86 with the glasses falling close to the middle of this compositional range (-14.54 - -15.11, Fig. 5.10). Nd model ages for all analysed samples range from 1.2 – 1.9 Ga using a reference chondritic mantle reservoir (CHUR) and again the glasses (1.2-1.5 Ga) fall within the range defined by the suspected target and crater-fill samples and that expected in Tasmanian Palaeozoic sediments (table 5.8).

These data are plotted in isochron diagrams (Fig. 5.11A,B). The glass, suspected target rock and crater-fill samples define clear linear trends with glasses falling near to the centre of the data array in plots of both of $^{143}Nd/^{144}Nd$ vs. $^{147}Sm/^{144}Nd$ and $^{87}Sr/^{86}Sr$ vs. $^{87}Rb/^{86}Sr$. These results are consistent with the interpretation that the samples all belong to the same isotopic system and that Darwin glass can be formed from the suspected target rocks analysed in this study. A Rb-Sr regression line through all of the analysed samples yields an age of 411 ± 42 Ma (2σ) and an initial $^{87}Sr/^{86}Sr$ value of 0.725 ± 0.016 (2σ). In the Sm-Nd system, the intial $^{143}Nd/^{144}Nd$ ratio is 0.51153 ± 0.00011 (2σ) and the regression yields an age of 451 ± 140 Ma (2σ). These age estimates overlap and are consistent with each other within the error limits of these data.

Sample	Lithology	Rb (ppm)	Sr (ppm)	$^{87}Rb/^{86}Sr$	error	$^{87}Sr/^{86}Sr$	error	Sm (ppm)	Nd (ppm)	$^{147}Sm/^{144}Nd$	error	$^{143}Nd/^{144}Nd$	error	ε - Nd	tCHUR (ma)
KH1	KQ	110.5	4.7	68.3	2.73	1.12	0.0000670	4.59	27.63	0.10	0.00001	0.51183	0.00009	-15.70	1273.14
KH2	KQ	84.6	22.6	10.6	0.43	0.78	0.0000130	8.35	35.57	0.14	0.00000	0.51194	0.00001	-13.58	1932.72
KH4	KQ	63.0	11.0	16.2	0.65	0.82	0.0000380	4.86	25.80	0.11	0.00001	0.51186	0.00001	-15.17	1430.54
KH6	AS1	179.7	20.2	25.5	1.02	0.88	0.0000150	7.13	40.24	0.11	0.00001	0.51184	0.00001	-15.64	1363.96
KH7	AS2	157.1	18.4	24.5	0.98	0.87	0.0000190	6.23	34.73	0.11	0.00000	0.51183	0.00001	-15.86	1402.00
KH8	AS3	197.7	9.0	.	0.00	.		6.61	40.53	0.10	0.00001	0.51184	0.00001	-15.59	1239.93
KH15	DDH1 52	96.2	28.8	9.5	0.38	0.76	0.0000180	7.58	36.29	0.13	0.00000	0.51190	0.00001	-14.35	1586.81
KH17	DDH2 A44	49.7	6.7	21.3	0.85	0.85	0.0000550	7.63	33.92	0.14	0.00002	0.51194	0.00001	-13.57	1744.19
KH18	DDH2 A74	171.8	7.5	.	0.00	.		9.32	48.16	0.12	0.00001	0.51191	0.00001	-14.16	1386.29
KH22	Light green glass	74.9	12.6	16.9	0.68	0.81	0.0000170	7.00	34.91	0.12	0.00000	0.51188	0.00001	-14.83	1533.57
KH23	Dark green glass	82.6	17.2	13.7	0.55	0.81	0.0000170	7.12	35.45	0.12	0.00000	0.51189	0.00001	-14.54	1504.93
KH24	Black glass	82.9	17.6	13.4	0.54	0.82	0.0000180	6.74	34.82	0.12	0.00007	0.51186	0.00001	-15.11	1478.66

Table 5.8 Rb-Sr and Sm-Nd elemental concentrations, isotope ratios and Nd model ages for Eldon Group (suspected target rock) samples from around Darwin Crater, crater-fill samples and Darwin glass.

Regression calculated in Excel using Isoplot. Errors are 2 σ (4%). The average $^{87}Sr/^{86}Sr$ ratio for SRM987 during the course of the study was 0.710264 ± 28 (2σ) on 12 runs. The Nd isotopic ratios were monitored by measuring the J & M specpure Nd_2O_3 that yielded a 143Nd/144Nd ratio of 0.511696 ± 8 (2σ) on 18 runs. The value for Lajolla gave a 143Nd/144Nd ratio of 0.511848 143 ± 8 (2σ).

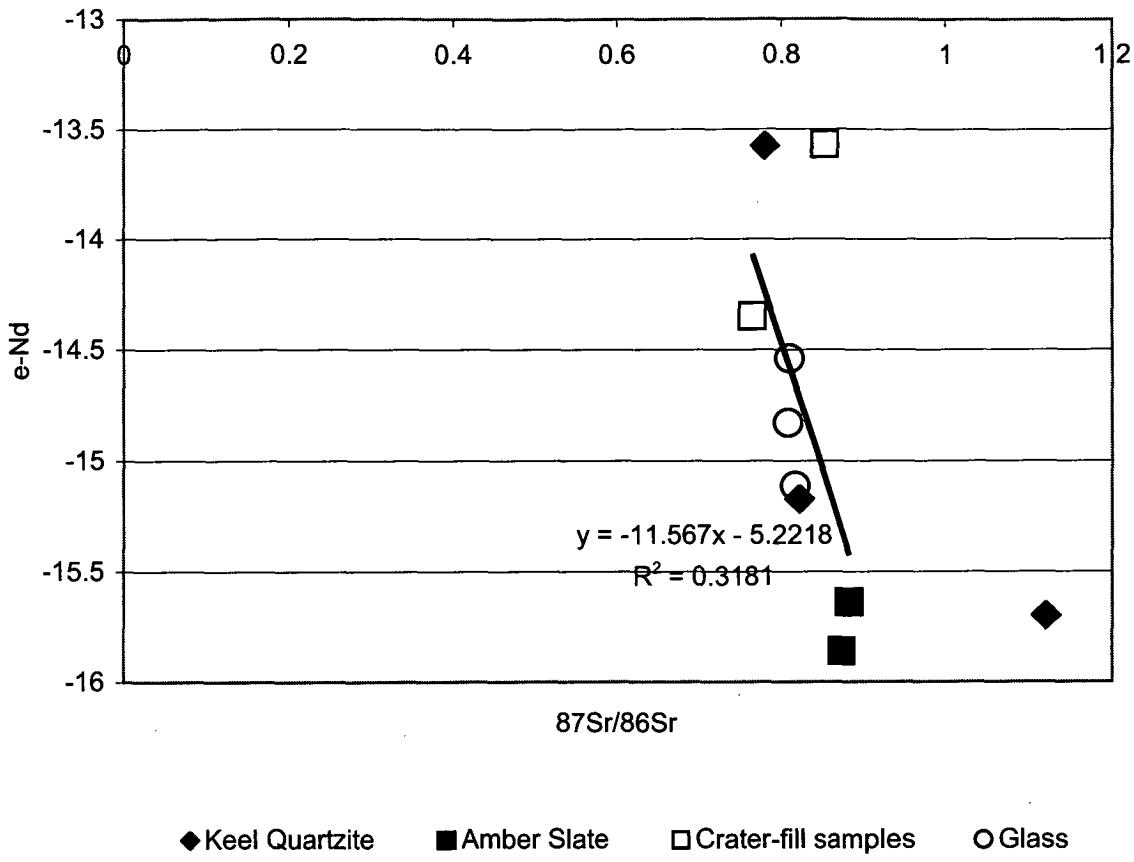

Figure 5.10 e-Nd vs. $^{87}Sr/^{86}Sr$ in glass, Eldon Group (suspected target) samples from around Darwin Crater and crater-fill samples.

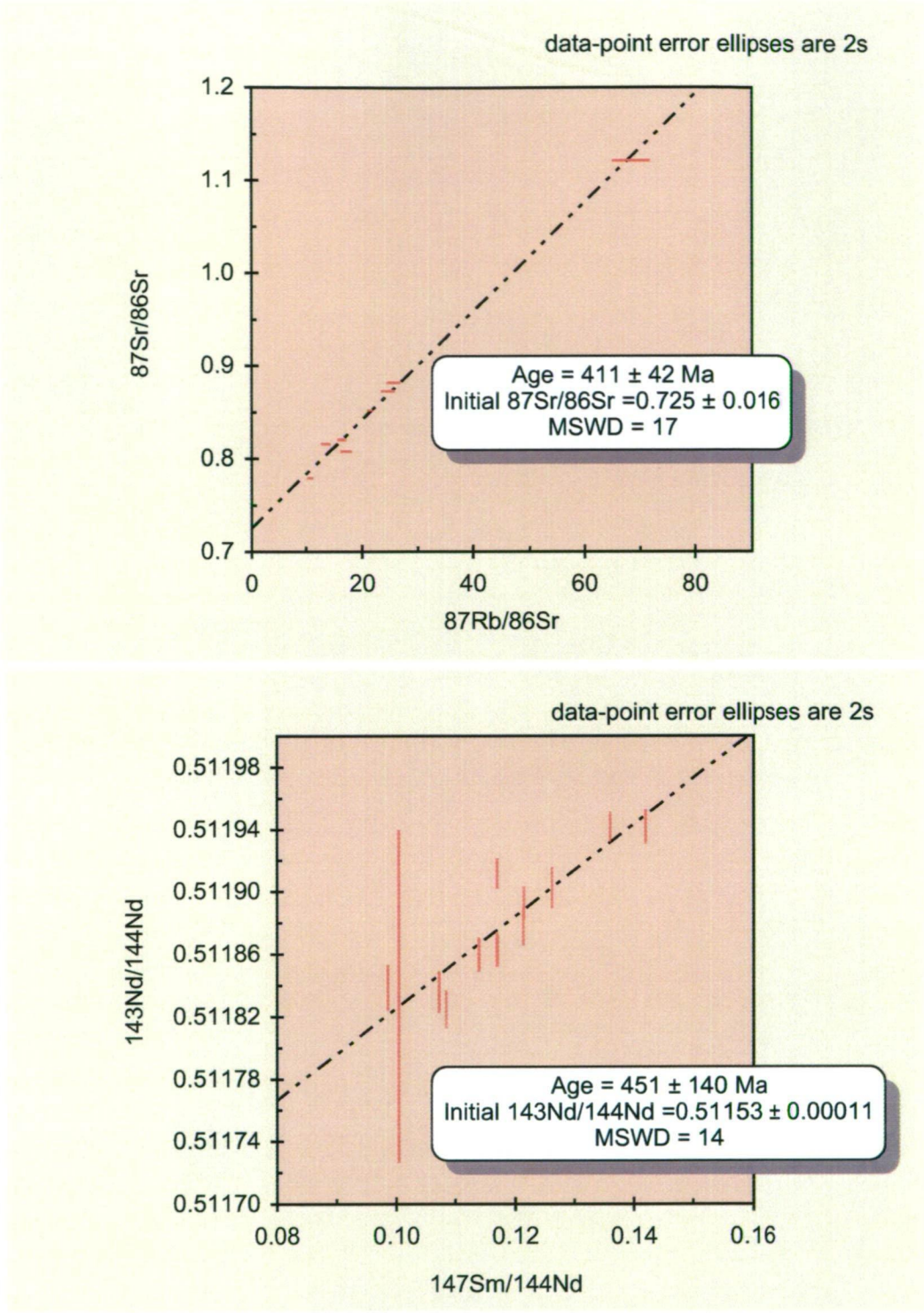

Figure 5.11 A) Rb-Sr isotopic evolution diagram for glass, Eldon Group (suspected target) samples from around Darwin Crater and crater-fill samples B) Sm-Nd isotopic evolution diagram for identical samples as in A.

5.2.4 Interpretation

In the case of the Rb-Sr system, the initial Sr ratio (0.725 ± 0.016 [2σ]) resulting from the regression is close to within error of the estimated value for Silurian seawater (0.70875) and is also close to the value for modern seawater. The regression age might be considered to reflect the depositional age of the sediments. 411 Ma is very close to the Siluro-Devonian boundary and would offer a good average depositional age for the Eldon Group consistent with the stratigraphic and palaeontological evidence. However, given the analytical errors, the Rb-Sr regression age is also within error of the age of the Tabberabberan Orogeny that commenced at around 395 Ma (Williams 1989) and this may have reset the system. The isotopic composition and regression ages in the samples may reflect a combination of a depositional age signal and the effects of the Tabberabberan Orogeny as is consistent with the wide scatter and large errors in the data points. However, this interpretation assumes that the Sm-Nd and Rb-Sr fractionation, as measured in the impact glasses, reflects processes that occurred during deposition or later digenesis and deformation of the target rocks. Given the previous evidence that the glass compositions reflect mixing, the isotopes are unlikely to have true age significance.

These isotopic data support derivation of the glass from Eldon Group target rocks. However, as there is possible evidence for resetting of the isotopic system by regional metamorphism, the question then becomes *"how diagnostic of a genetic relationship between the suspected target rocks and glass are these data?"* Volcanic and igneous rocks in the strewn field can be ruled out as potential targets on the basis of glass major and trace element geochemistry that indicates a sedimentary origin. Isotope data for the Mt Read Volcanics (MRV) in the centre of the strewn field also show distinctly different εNd values than the glass or Eldon Group that range between +1 to –2 in basalts and andesites and > +5 in tholeiitic dykes (Whitford et al. 1990). Initial Sr ratios in the MRV (<0.7 to >0.72) are similar to the Eldon Group and glass reflecting the effects of regional metamorphism in the Devonian (Whitford et al. 1990).

Data for other sedimentary rocks in the region are scarce. Raheim & Compston (1977) report Rb-Sr isotope data for a suite of Precambrian metasediments from near Strathgordon and the Collingwood River. These rocks are correlates of the Precambrian quartzites in the south of the strewn field. The initial Sr ratios in these rocks (average 0.72678 ± 0.00207) are within the range of the Eldon Group and glass, but regressions yield divergent data arrays and distinctly older model ages

(Raheim & Compston 1977). The other significant sedimentary rocks in the strewn field belong to the Ordovician Denison Group. These siliceous conglomerates contain mostly Precambrian clasts and are expected to have significantly older Rb-Sr model ages than the suspected Eldon Group target rocks but data are lacking. The Denison Group is not associated with any suspected impact structure and geochemical data suggest these conglomerates are too siliceous to be the dominant target rocks involved in the formation of Darwin glass.

Given these isotopic and major and trace element data, all geochemical tests to exclude the hypothesis that the 'suspected target rocks' match the glass chemistry have failed. At this stage the suspected Eldon Group target rocks in the Darwin Crater area are highly likely to be the source of the glass.

5.3 Explaining Ni, Co, Cr , MgO and FeO abundances in Darwin glass.

The chemical and isotopic compositions of Darwin glass have been modelled as a mixture of Eldon Group rocks. In mixing models for Group 2 glass compositions the worst fits are for Ni, Co, Cr, MgO and FeO. This is consistent with the principal components analysis (PCA) of glass compositions that suggests the existence of a 3rd end-member rich in these elements that was involved in the formation of the glass. In table 5.9 analytical results for the most anomalous glass compositions have been compiled. Fig. 5.12A,C are plots of Co and Cr vs. Ni showing excellent correlation in Group 1 and 2 glass. Sc does not correlate with the Ni, Co or Cr, it is present in concentrations equal to the suspected target rocks and is therefore considered unrelated to the 3rd end-member (Fig. 5.12B,D,F). Figure 5.13A-F shows plots of MgO and FeO versus Ni/Co, Ni/Cr and Cr/Co in Group 1 and 2 glass along with average suspected target rocks. The poorest modelled glass compositions have distinct elemental ratios in Ni/Co (avg. 15.4), Ni/Cr (avg. 3.4) and Cr/Co (4.7) compared to average glass, that cannot be related to any mixture of the analysed suspected target rocks, and that must therefore be related to an additional source component.

The Ni abundances in the most anomalous glasses are beyond the published ranges for Ni in sedimentary rocks. If terrestrial in origin, the Ni and Co abundances in the most anomalous glasses suggest a mafic or ultramafic volcanic rock as the source of these elements. The remaining trace elements and isotopic data show no evidence for a mafic or ultramafic signature, but volumetrically a contribution from such a

Sample	SiO_2	TiO_2	Al_2O_3	FeO	MgO	K_2O	Cr	Co	Ni	Ni/Co	Ni/Cr	Cr/Co
	%						ppm					
1011513	76.5	0.7	10.4	4.5	2.4	3	224	39	572	14.5	2.6	5.7
Site020315	84.0	0.5	7.5	3.0	2.3	2	260	34	551	16.0	2.1	7.6
Site020321	78.6	0.6	10.4	5.2	2.3	3	175	33	569	17.1	3.2	5.3
Site020322	78.6	0.6	10.4	5.2	2.3	3	168	35	563	15.9	3.4	4.7
Site020323	78.0	0.6	9.9	5.2	2.5	2	160	36	543	15.2	3.4	4.5
Site020324	78.0	0.6	9.9	5.2	2.5	2	155	35	535	15.1	3.5	4.4
Site020329	78.1	0.7	10.3	5.2	2.3	2	193	42	607	14.6	3.1	4.6
Site020330	78.1	0.7	10.3	5.2	2.3	2	177	40	562	14.0	3.2	4.4
Black03	80.5	0.5	6.5	4.3	3.9	2	201	54	889	16.4	4.4	3.7
Black04	80.6	0.5	6.7	4.3	4.0	1	209	57	918	16.2	4.4	3.7
Black07	77.2	0.6	9.2	5.5	2.3	2	184	47	722	15.3	3.9	3.9
Black08	76.9	0.6	9.0	5.9	2.9	2	211	54	802	14.9	3.8	3.9
Average	**78.8**	**0.6**	**9.2**	**4.9**	**2.7**	**2.2**	**193.1**	**42.3**	**652.8**	**15.4**	**3.4**	**4.7**
Maximum	84.0	0.7	10.4	5.9	4.0	2.7	260.5	56.7	917.7	17.1	4.4	7.6
Minimum	76.5	0.5	6.5	3.0	2.3	1.5	155.2	33.2	535.4	14.0	2.1	3.7

Table 5.9 Composition of the most transition metal enriched glass samples from Group 2. These are the analyses with the greatest residual errors in the mixing model results.

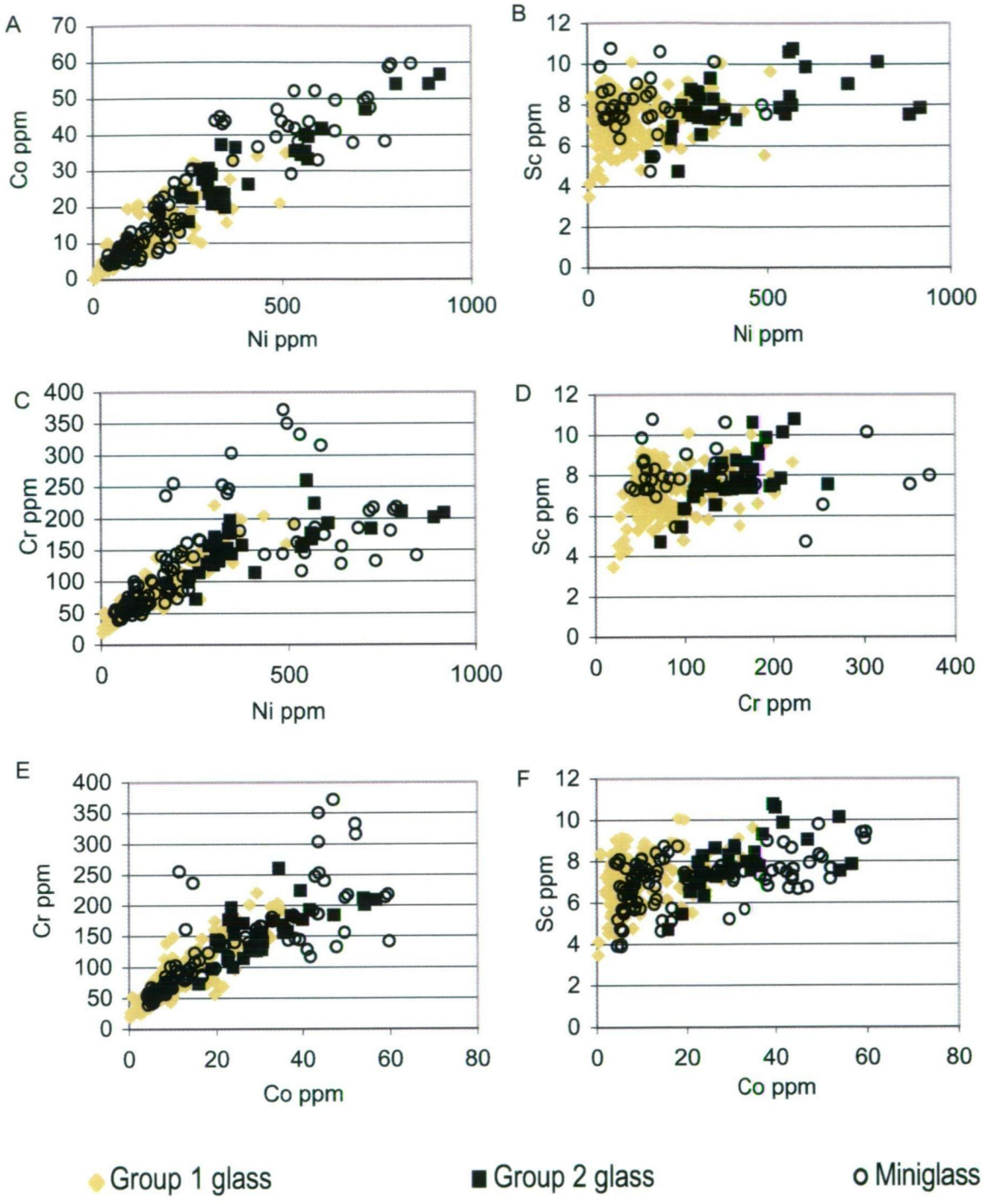

Figure 5.12A-F Plots that show the covariation in transition metal abundances in Darwin glass.

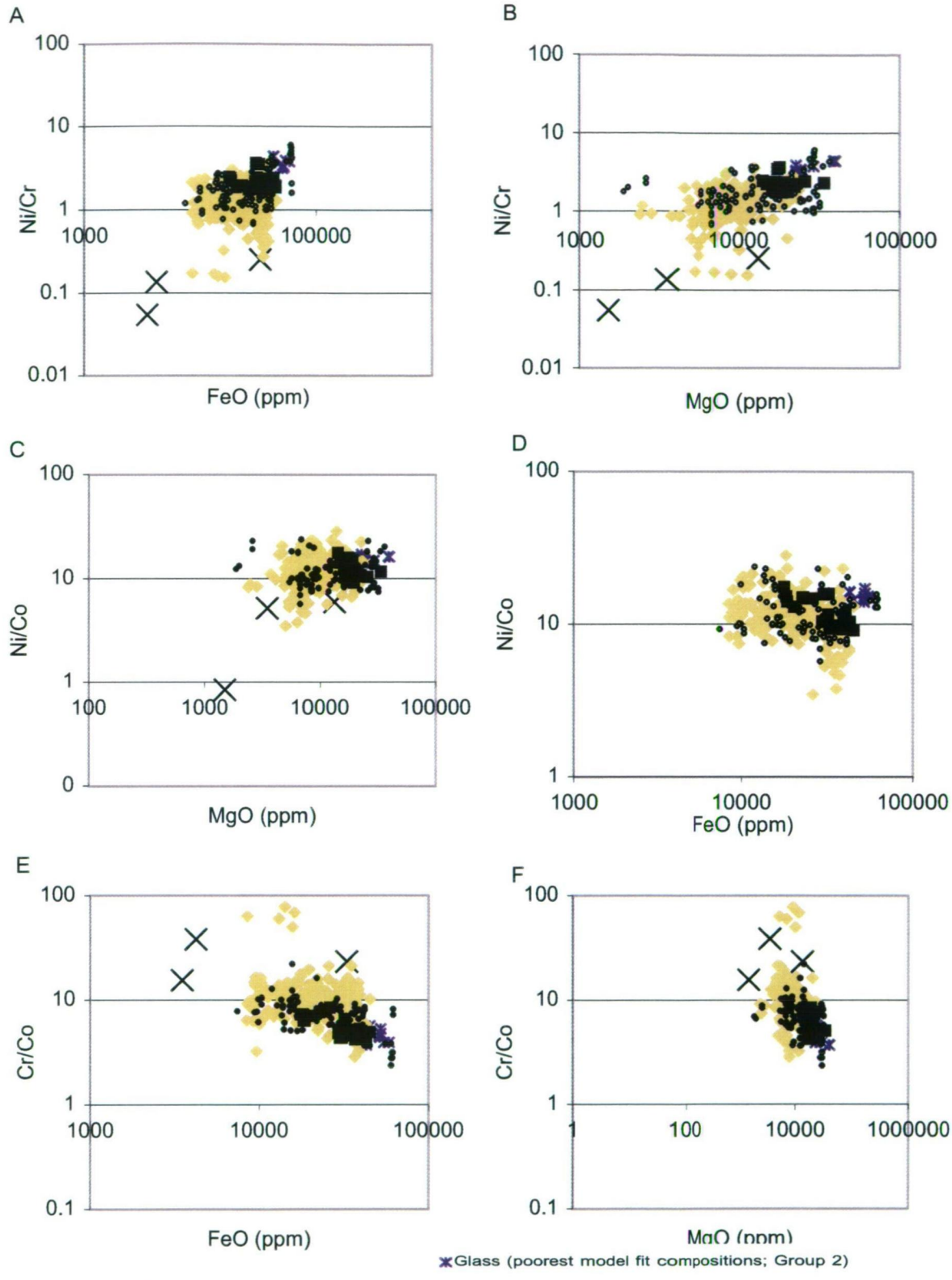

Figure 5.13A-F Plots showing selected transition metal ratios vs. MgO and FeO in Darwin glass and Eldon Group (suspected target rock) samples from around Darwin Crater.

source should have been insufficient to allow its signature to be recognised in elements other than the transition metals.

In the context of the geology of Tasmania, the most common mafic-ultramafic volcanic rocks are Jurassic dolerite (Hergt et al. 1989), Tertiary and Cambrian basalts (Sutherland 1989, Brown 1986), Cambrian ultramafic dunites and pyroxenites (Brown 1986), and (rare) middle-late Devonian (?) lamprophyres (Rock 1991, Baillie & Sutherland 1992). Dolerite intrusions are extensive across central and eastern Tasmania where the exposed dolerite sills cap most mountain tops. Tertiary basalts are most common in the northwest of the state. In the study area, Cambrian basalts and ultramafics crop out in the centre and north of the strewn field. These are unknown in the area surrounding the crater and are not expected within the Eldon Group. Lamprophyres are also unknown amongst the suspected target rock stratigraphy, but are known to exist in southwest Tasmania (Baillie & Sutherland 1992).

As described in Chapter 4, bedrock exposure around the crater is extremely limited and drill core recovery was poor. The early geologic history of western Tasmania is characterised by major thrust faulting and allocthonous emplacement of slices of volcanic rocks (Crawford & Berry 1992). Lamprophyres typically exist as small irregular dykes easily hidden in thick sedimentary packages (Rock 1991). These factors combined mean that it is impossible to rule out completely the existence of a small mafic or ultramafic body, especially a lamprophyre dyke, in the target stratigraphy. While this is considered extremely unlikely, the possibility must be considered because if a terrestrial source can be excluded from consideration these transition metal enrichments can be explored as potential evidence for projectile contamination. Not only is such contamination rarely described in ejected glasses or tektites but if a mafic or ultramafic source can be ruled out, the excellent control on the indigenous contributions of Ni, Co and Cr in this study means that projectile identification may be possible. On the topic of identification of the projectile type involved in an impact event, Morgan et al. (1979, p. 813) stated that this is a "*...rather frustrating exercise*". However, it is only through the difficult task of linking projectile types with impact structures and products that we can understand the true nature of the Earth's cratering history. Additionally, identification of non-terrestrial geochemical signatures in impact glasses can potentially allow us to infer geochemical information about the composition of meteorite parent bodies back through time, and thereby to supplement actual analyses of recovered meteorites.

5.3.1 Mixing with terrestrial ultramafic rocks?

For comparisons, analytical data for representative examples of west coast mafic and ultramafic rocks have been compiled in table 5.10. Average Amber Slate is taken to represent the Ni, Co, and Cr contributed to the glass by the suspected target rocks, and linear mixing lines have been calculated between mixtures of slate and ultramafic rocks for Ni/Co, Ni/Cr and Cr/Co vs. MgO and FeO (Fig. 5.14A-F). From these plots it is clear that at any given MgO or FeO content, Ni/Cr ratios in all of the volcanic rocks are lower than those found in the most enriched glasses. The mixing line with Amber Slate indicates that even a 100% contribution from the most Ni rich rock, average dunite (Ni/Cr=1.2), could not produce Ni/Cr ratios as high as in most Group 2 glasses (average=3.4) and as such the addition of FeO to the average Amber Slate or mixing with highly weathered samples like KH19 does not improve the model fit.

Ni/Co ratios in dunite and Darwin glass show better agreement and in the plot of Ni/Co vs. MgO the mixing line between average Amber Slate and dunite passes through the Group 2 glasses at up to about 10% contribution from dunite. However, these worst modelled glass compositions have excess FeO relative to average dunite at similar Ni/Co ratios. At any given FeO or MgO content Ni/Co ratios in rocks other than the dunite (2.6-7.1) remain lower than for all Group 2 glasses (average 13.4).

The dunite and pyroxenite have excess Cr relative to Co when compared to all of the glasses, and trends toward higher FeO and MgO defined by the mixing lines between these rocks and Amber Slate, are widely divergent from the glass arrays. On the Cr/Co plots, mixing lines between Amber Slate and average basalt, dolerite and ultramafic lamprophyre define trends in the broad direction of the most enriched glasses. However, at the required FeO and MgO abundances, the dolerite, basalt and lamprophyre also have excess Cr relative to Co. Even if allowed to contribute an unrealistically large proportion to the melt, the mixing lines show that 100% contribution from the dolerite, basalt or lamprophyres results in excess FeO and MgO, and Cr/Co ratios would be higher than for all Group 2 glass samples. Significant to note is that based on limited analyses, Tasmanian West Coast lamprophyres (Cr/Co= >15, Baillie & Sutherland 1992) appear to be more differentiated than the plotted average ultramafic lamprophyres (Cr/Co <10, Rock 1991), which can be compared to an average Cr/Co ratio of 4.7 in the most enriched glasses.

	%		ppm					
	FeO*	MgO	Cr	Co	Ni	Ni/Co	Ni/Cr	Cr/Co
Average Tasmanian Jurassic Dolerite [1]	8.8	6.6	108	30	78	2.6	0.7	3.6
Average Tasmanian west coast tholeite [2]	11.9	7.1	261	30	133	4.4	0.5	8.7
Average Tasmanian Lamprophyre [3]	12.2	15.0	480	75	430	5.7	0.9	6.4
West Coast Dunites [4,5]								
Average	6.2	42.0	2084	100	2547	25.5	1.2	20.8
Maximum	7.8	49.5	2630	137	3090			
Minimum	5.5	33.3	1670	78	2072			
85-0135 median dunite	5.8	39.4	2010	100	2470	24.7	1.2	20.1
West Coast Pyroxenite [4,5]								
Average	6.2	31.8	33	4839	70	10.2	0.1	70.9
Maximum	7.4	35.6	36	5770	85	903.0		
Minimum	4.3	21.0	30	3150	50	429.0		
85-0161 median pyroxenite	6.1	30.0	4836	76	540	7.1	0.1	63.6
Average Group 1 glass	2.2	0.9	75	9	108	12.4	1.5	8.5
Average Group 2 glass	3.8	2.2	161	30	406	13.4	2.5	5.3

Table 5.10 Selected major and trace element abundances in Tasmanian west coast dunite and pyroxenite samples.
*=all Iron as FeO. Data from: [1] Hergt et al. (1989); [2] Crawford & Berry (1992); [3] Baillie & Sutherland (1992); [4] Brown (1986); Keays (Personal Communication in 2003).

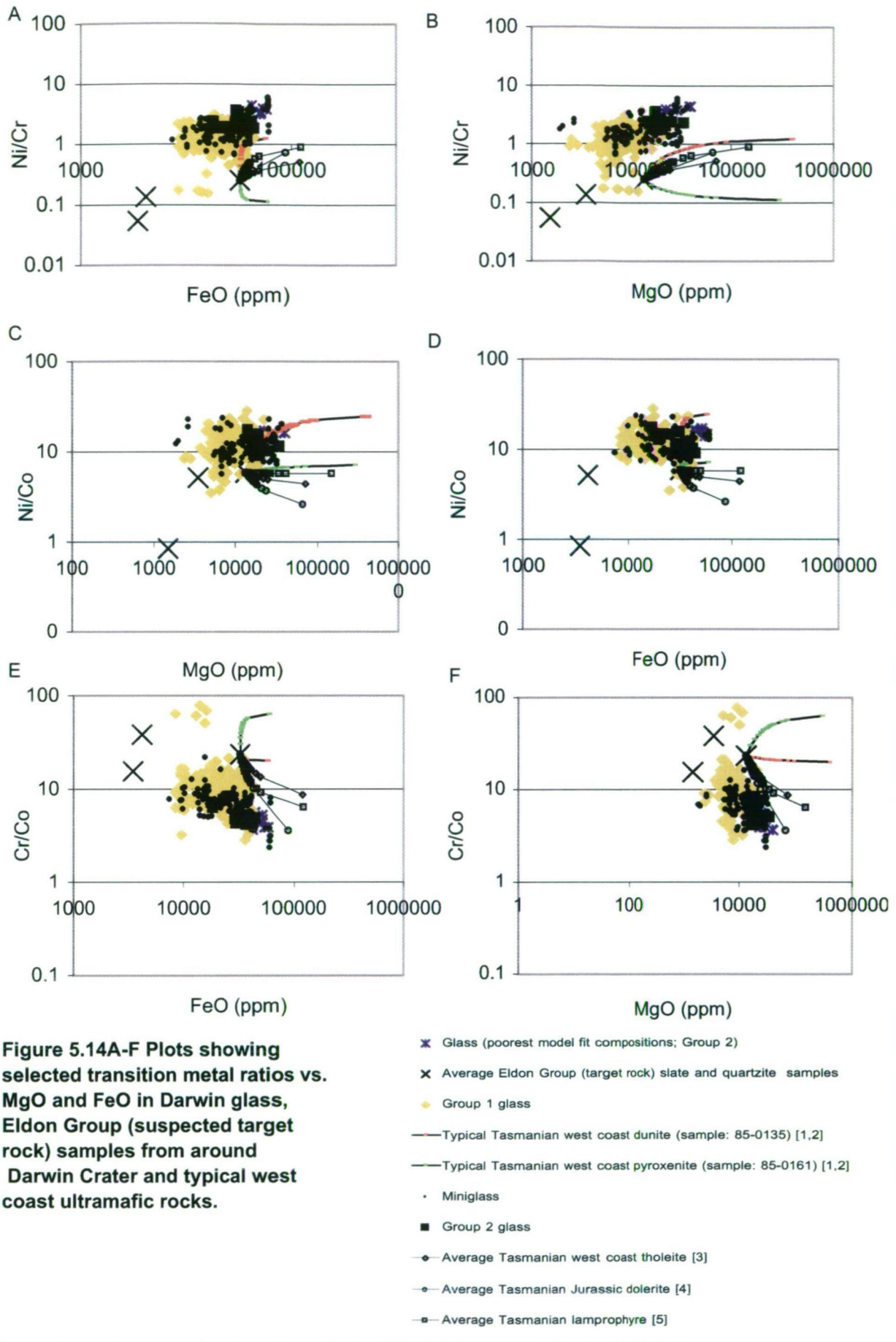

Figure 5.14A-F Plots showing selected transition metal ratios vs. MgO and FeO in Darwin glass, Eldon Group (suspected target rock) samples from around Darwin Crater and typical west coast ultramafic rocks.

In each plot, linear mixing lines have been calculated between Average Amber Slate and the ultramafic rocks in an attempt to model the composition of the most anomalous (high MgO, FeO, Ni, Cr, Co) glasses. The composition of the most transition metal enriched glass can not be explained by a contribution from these ultramafic rocks.

Data from: [1] Brown (1986); [2] Keays (Personal Communication in 2003); [3] Crawford & Berry (1992); [4] Hergt et. al. (1989);[5] Baillie & Sutherland (1992).

This makes any contribution from lamprophyres, that are the most geologically reasonable ultramafic candidates to exist in the target stratigraphy, even less likely.

On the basis of excess Cr relative to Ni and Co it is not possible to mix west coast mafic or ultramafic rocks and Amber Slate, or any other analysed suspected target rock, or multiple combinations thereof, to reproduce the Ni, Co, Cr, MgO, and FeO composition of the anomalous Group 2 glass. Therefore, potential terrestrial sources of the enriched transition metals in these glasses, known from the west coast of Tasmania, can largely be excluded from any further consideration. This leaves contamination from the impacting projectile as the remaining viable mechanism for Ni, Co, Cr, MgO, and FeO enrichment in the glasses and it is here that discussion will now focus.

5.3.2 Projectile contamination?

Compositional data for various meteorite classes have been compiled in table 5.11 and these data are added to the plots of MgO, FeO versus Ni/Co, Ni/Cr and Cr/Co (Fig. 5.15A-F). Mixing lines have also been calculated and plotted between the projectiles and average Amber Slate. Iron meteorites lack Cr relative to Ni and have excess Co relative to Cr compared to the glasses. Ni/Co ratios in iron meteorites are similar to the glasses but at far lower MgO abundances and in all plots the mixing line arrays between iron meteorites and average Amber Slate define trends away from the poorest modelled glass compositions towards lower MgO contents.

Much better fits are obtained with chondrite and some primitive achondrite meteorites. In plots of MgO, FeO versus Ni/Co and Ni/Cr, mixing lines between Amber Shale and Antarctic carbonaceous (ALHA83100 CM2) and L- type chondrites, (ALHA77011 L3) or the primitive achondrite Divnoe, trend directly through Group 2 glasses with most of the poorest model fit samples falling on the mixing lines at around 10% chondrite. The mixing line data array with the chondrites brackets the high MgO, FeO samples at lower Ni/Cr and Ni/Co ratios (<1% chondrite) and variation away from this line is in a broad mixing array towards low FeO, MgO, Ni,Co,Cr target rocks. In plots of Cr/Co, some of the poorest fit analyses appear to have lost Cr relative to Ni compared to chondrites, and plot slightly away from the mixing lines. Again in Cr/Co plots the mixing line with chondrites brackets the high MgO, FeO samples and variation away from the line is a broad mixing array towards the quartzite compositions. Cr loss relative to Ni is less pronounced, but also evident in some glass samples.

Projectile	Class	MgO	FeO*	Cr	Co	Ni
		ppm				
Sikhote-Alin [1]	Iron	500	933200	3	4800	57100
Yamato 791694 [1]	Iron	500	650000	5.67	5670	342000
chondrite: ALHA77011 [2]	L chondrite	238900	200700	3903	600	10200
ALHA83100 [2]	C chondrite	189200	107000	2805	600	11000
Divnoe [3]	Primitive Achondrite	290100	164100	3352	610	8200

Table 5.11 Selected major and trace element abundances in various meteorite classes.
*All Iron as FeO. Data from: [1] Wasson et al. (1989); [2] Jarosewich (1990); [3] Petaev et al. (1994).

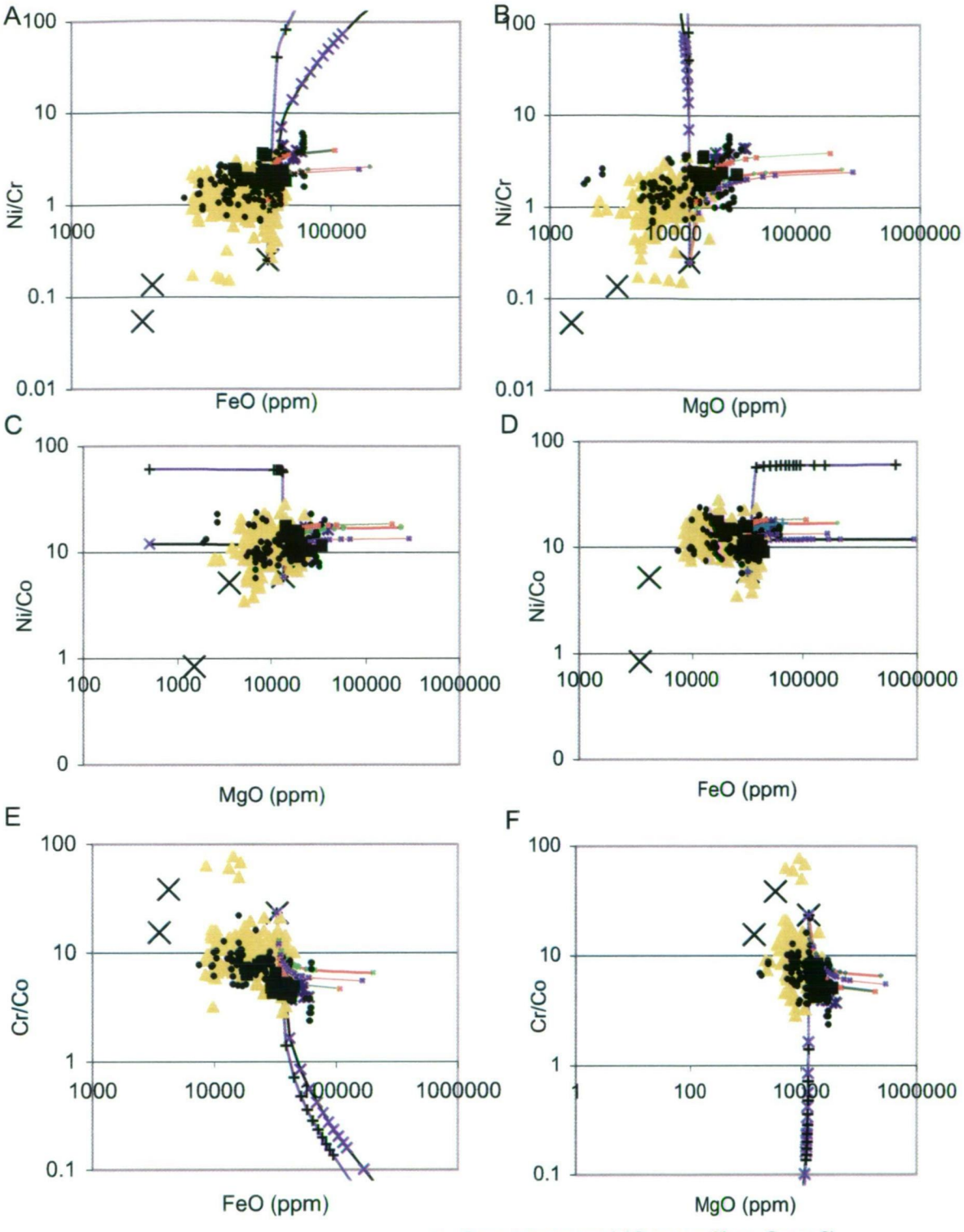

Figure 5.15A-F Plots showing selected transition metal ratios vs. MgO and FeO in Darwin glass, Eldon Group (suspected target rock) samples from around Darwin Crater and selected meteorites.

In each plot, linear mixing lines have been calculated between Average Amber Slate and the meteorite types in an attempt to model the composition of the most anomalous (high MgO, FeO, Ni, Cr, Co) glasses. The composition of the most transition metal enriched glass is best modelled by contribution from a chondrite or primitive achondrite like projectile. Data from: [1] Wasson et al. (1989);[2] Jarosewich (1990); [3] Petaev (1994).

Therefore, on the basis of these data, the enrichments of Ni, Co, Cr, MgO and FeO in some black Group 2 Darwin glasses, that cannot be related to the suspected target rocks or any speculated ultramafic rock, can be explained as projectile contamination from a chondrite or primitive achondrite. Based on Ni and Co data, the most anomalous glasses require a chondritic contribution of between 5-9%. This is consistant with estimates based on MgO that require a chondritic contribution of between 6-10%. Cr enrichments are less pronounced and require a chondritic contribution of between 3-5%; reflecting the Cr loss relative to Ni and Co described above and discussed in more detail in section 5.4.3a. Estimating the level of FeO enrichment from the projectile in the anomalous glasses is difficult because of uncertainties in the estimated indigenous contribution of FeO. We have seen that a small volume of highly weathered FeO rich material may have contributed to the glasses thereby producing a huge range in the potential FeO composition of the target stratigraphy, thus confusing any attempts to identify possible FeO inputs from the projectile. The amount of contribution from the projectile being invoked here is greater than generally expected, but projectile contamination at the 10% level has been shown by Attrep et al. (1991) in Australian impactites from Wolfe Creek and Henbury Craters. If the composition of the Ni rich glasses does reflect such a high level of contribution from a chondrite or primitive achondrite, and assuming no fractionation of other highly-siderophile elements (HSE) such as the platinum-group elements (PGE), relative to transition metals, these glasses should contain HSE in above crustal abundances and at chondritic elemental ratios as for Ni, Co and Cr.

5.3.3 Laser ablation ICPMS (LA-ICPMS) analyses of HSE in Darwin glass

To further define the source of Ni, Co and Cr enrichments, samples of Darwin glass were analysed for a suite of HSE by LA-ICPMS at the Research School of Earth Sciences, Australian National University (ANU), Canberra. These analyses were conducted using and ArF excimer with a wavelength of 193nm and an Agilent 7500 quadrupole ICPMS. A full description of the ICPMS instrumentation and general operating conditions is given by Eggins et al. (1998). Ablation was done under a helium + hydrogen atmosphere in a custom-built sample cell before being mixed with argon and transported to the ICPM for analyses. Six samples of black irregular glass and 4 mini-glasses (<5mm aerially shaped, defined in Chapter 2) were selected to study. The following HSE were determined: W; Re; Os; Ir; Pt and Au along with Ni. The number of analyses per sample was controlled by the size of the sample, in total 23 spots were analysed on the macro glasses and 7 spots on the mini-glasses. HSE

element concentrations were expected to be low in the glass, and to promote sufficient ablation yields for abundance determinations, analyses were conducted using a 300μm diameter beam size at 50Hz and 80mJ/cm^2. Relative element sensitivities and interferences were calibrated against several standards including NIST 612, iron meteorite Lombard, and a Mud Tank zircon. As an internal standard the measured intensity of ^{61}Ni was normalised to the Ni content of each glass previously determined by ICP-MS.

Iron meteorite Lombard was selected for use as an analytical standard because this has high HSE and transition metal abundances, a well-known composition and no expected interferences during the analyses that relate to oxide production from lithophile elements like Hf and the HREE. Conversely, the Mud Tank zircon was also selected for use as an analytical standard because this has a high abundance of lithophile elements and it is assumed no HSE. Therefore, when analysing the Zr all the HSE signals observed are interpreted to be interferences from lithophile elements (eg ^{180}Hf^{16}O on ^{196}Pt). The ratio of the observed Hf, Yb and Lu oxide masses/oxide abundances measured for the standard zircon were calculated to arrive at an oxide production factor. This factor is applied to the other isotopes measured and the residual count rates after correction for oxide production are assumed to reflect the primary HSE signal. The residual count rates for each isotope were examined to see if they were present in the correct proportions for the siderophile element in question as a further check on the quality of these data.

5.3.3a Results

Analytical results for macro- and mini-glasses are contained in table 5.12, along with detection limits and literature data for the representative chondrites and primitive achondrites that it has been shown provide the best compositional models for the Ni, Co and Cr abundances in the glasses. Complete analyses are listed in Appendix 3. These HSE abundances in Darwin glass show no evidence for enrichments above the range of crustal average values. In macro and miniglass, W is the most abundant HSE followed by Pt, Re and Au. Oxide corrections leave insufficient residual counts for determination of Os and Ir implying these elements are present in abundances less than the detection limits that are easily good enough to allow measurement of these PGE if present in concentrations significantly above crustal average values. In the case of Ir, the oxide corrections removed the entire ^{191}Ir signal and left only a very small residual count rate on ^{193}Ir preventing abundance determinations.

The HSE are correlated together (Fig. 5.16A-C); however, in plots of HSE versus Ni little co-variation exists suggesting these derive from distinct sources (Fig. 5.17A-D). Figure 5.18A-D shows plots of HSE ratios to Ni versus MgO in the glass, also plotted are average crustal values and data for selected projectiles, which will be discussed. The glasses plot in a distinct array compared to average crust and all projectile types with excess Ni relative to all HSE reflecting the fact that Ni is present in chondritic abundances while HSE are present only at crustal values in the glass. Mixing relationships between average crust and any of the projectile types fail to model the composition of the glasses because the models all predict much higher abundances of HSE than are observed in the glass.

5.3.3b Interpretation

In an attempt to reconcile the observed transition metal enrichments with the absence of any simultaneous HSE enrichments, without invoking complex processes of fractionation during the glasses formation, HSE depleted chondrite-like projectiles must be considered. The most HSE poor chondrite-like impactors are bodies that have undergone partial differentiation during heating either from internal parent body magmatism, or during planetesimal collision events. Here partial melts are produced with potential for fractionation of silicate and metallic phases. Examples are the Lodran-like primitive achondrites that probably represent a suite of partial melt residues in which both the silicate and metal-sulphide melts migrated out of the source region of the parent body (McCoy 1994; Miyamato & Takeda 1994; Takeda et al. 1994). One such sample, MAC 88117,37 is a coarse-grained granular rock composed of 90% volume silicate material dominated by orthopyroxene and olivine (Mittlefehldt et al. 1996). Mittlefehldt et al. (1996) suggest this sample is likely to have formed from localised heating in a region of the parent body, where, under the influence of gravity, the metallic melt drained away from the buoyant silicate melt to leave an almost purely olivine-pyroxene dominated melt region. This melt is depleted in HSE that are expected to be concentrated in the metallic phases. Another example is the Chico L-Chondrite that is a highly shocked impact melt breccia produced in a massive collision between the L-Chondrite parent and another asteroid at 500Ma (Nakamura et al 1990; Bogard et al 1995; Haack et. al, 1996.) The sample is crosscut by a fine-grained dyke of clast poor melt, and coarse FeNi metal + sulphide globules are concentrated along the axis of the dyke (Norman & Mittlefehldt 2002). Analyses of the Chico melt dyke show evidence for loss of PGE relative to the host chondrite and metals (Norman & Mittlefehldt 2002). As such, it may be

Analyses	Sample	ppm MgO	Ni	ppb W	Pt	Re	Os	Ir	Au
ju21b06	DG-B2	39567	281	1120	0.71	0.34	.	.	0.55
ju21b07	DG-B2	39567	360	1240	0.57	0.31	.	.	
ju21b08	DG-B2	39567	354	1380	0.58	0.21	.	.	
ju21b09	DG-B3	7766	203	1810	0.79	0.33	.	.	0.23
ju21b10	DG-B3	7766	223	1770	0.92	0.23	.	.	0.17
ju21b11	DG-B3	7766	233	1780	0.92	0.39	.	.	0.2
ju21b12	DG-B3	7766	271	2030	1.09	0.26	.	.	0.27
ju21b13	DG-B3	7766	395	259	0.4	0.15	.	.	
ju21b14	DG-B4	26160	478	316	0.41	0.25	.	.	
ju21b15	DG-B4	26160	594	413	0.47	0.29	.	.	0.11
ju21b16	DG-B5	18503	77	2070	0.34	0.26	.	.	0.26
ju21c05	DG-B5	18503	46	2700	.	.	.	.	0.38
ju21c06	DG-B5	18503	390	1240	0.68	.	.	.	0.19
ju21c07	DG-B5	18503	326	1410	0.46	.	.	.	0.34
ju21c08	DG-B6	21842	294	1220	0.64	.	.	.	0.21
ju21c09	DG-B6	21842	262	1380	0.55	.	.	.	0.3
ju21c10	DG-B6	21842	257	1610	0.55	.	.	.	0.42
ju21c11	DG-B1	17215	652	1590	0.77	.	.	.	0.44
ju21c12	DG-B1	17215	616	1960	0.94	.	.	.	0.34
ju21c13	DG-B1	17215	647	1720	0.91	.	.	.	0.33
ju21c14	DG-B2	39567	397	1570	0.78	.	.	.	0.41
ju21c15	DG-B2	7766	290	1590	0.7	.	.	.	0.52
ju21c16	DG-B2	26160	378	1740	0.79	.	.	.	0.46
ju21d05	Mini-glass 26	28329	560	702	0.49	.	.	.	0.25
ju21d06	Mini-glass 25	29551	480	457	1.17	.	.	.	0.28
ju21d07	Mini-glass 25	29784	687	620	0.44	.	.	.	
ju21d08	Mini-glass 24	12514	562	761	0.78	.	.	.	0.22
ju21d09	Mini-glass 23	30913	110	748		.	.	.	0.18
ju21d10	Mini-glass 23	21458	98	657	0.2	.	.	.	0.13
ju21d11	Mini-glass 23	19264	104	745	0.16	.	.	.	0.22
Detection limits					0.13-0.22	0.03-0.01	0.04-0.075	0.04-0.2	0.07-0.19
Chondrite [1]		189200	11000	95	1060	35	510	510	160
Divnoe [2]		290100	8200				113	104	51
Mac88177,33 min seps [3]		310000	8300					36	98
Chico-L Chondrite melt rock [4]			1770					37	24
Dunite [5]		420000	2130		2.88		7.94	0.616	0.126
Crust [6,7]		13300	20	2	0.51	0.5		0.02	1.8

Table 5.12 MgO, Ni and highly siderophile element (HSE) abundances in Darwin glass, selected meteorites and terrestrial rocks.

Data from: [1] Sun & McDonough (1989); [2] Pataev et al. (1994);
[3] Mittlefehldt et al. (1996); [4] Norman & Mittlefehldt (2002); [5] Peck & Keays (1990);
[6] Taylor & McLennan (1985); [7] Peucker-Ehrenbrink & Jahn (2001).

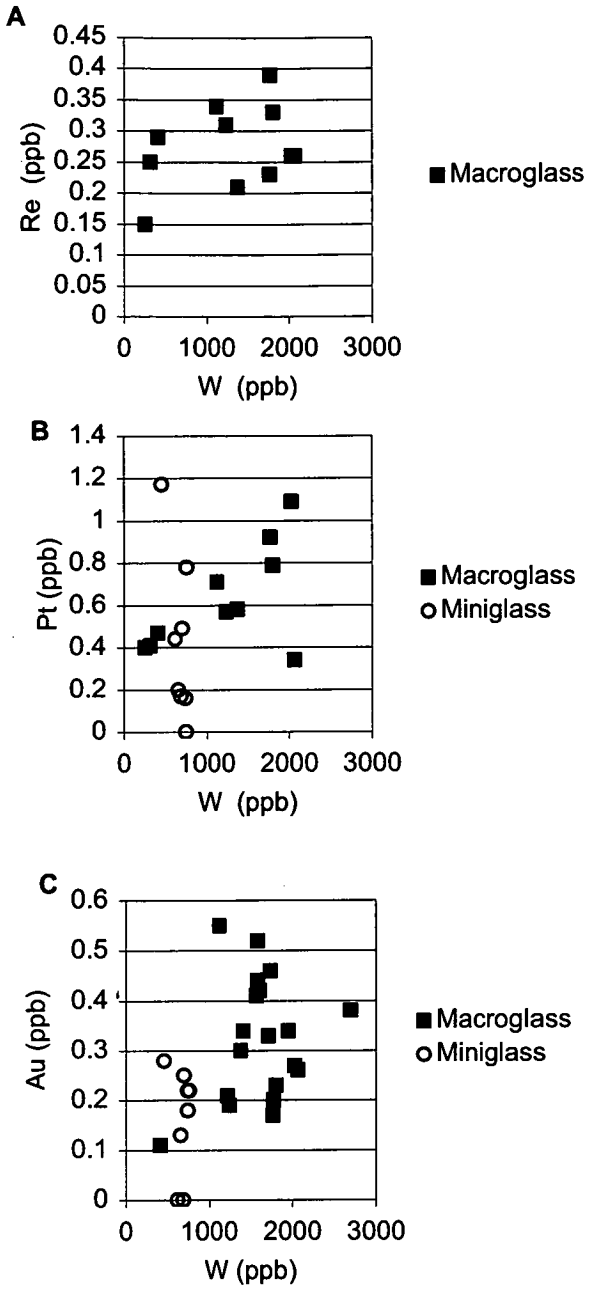

Figure 5.16A-C Plots that show co-variation in HSE concentrations.

In Darwin glass. Re, Pt, W and Au are present at crustal abundances only. The remaining HSE analysed for (Os, Ir)are not present in the glass at concentrations above detection limits.

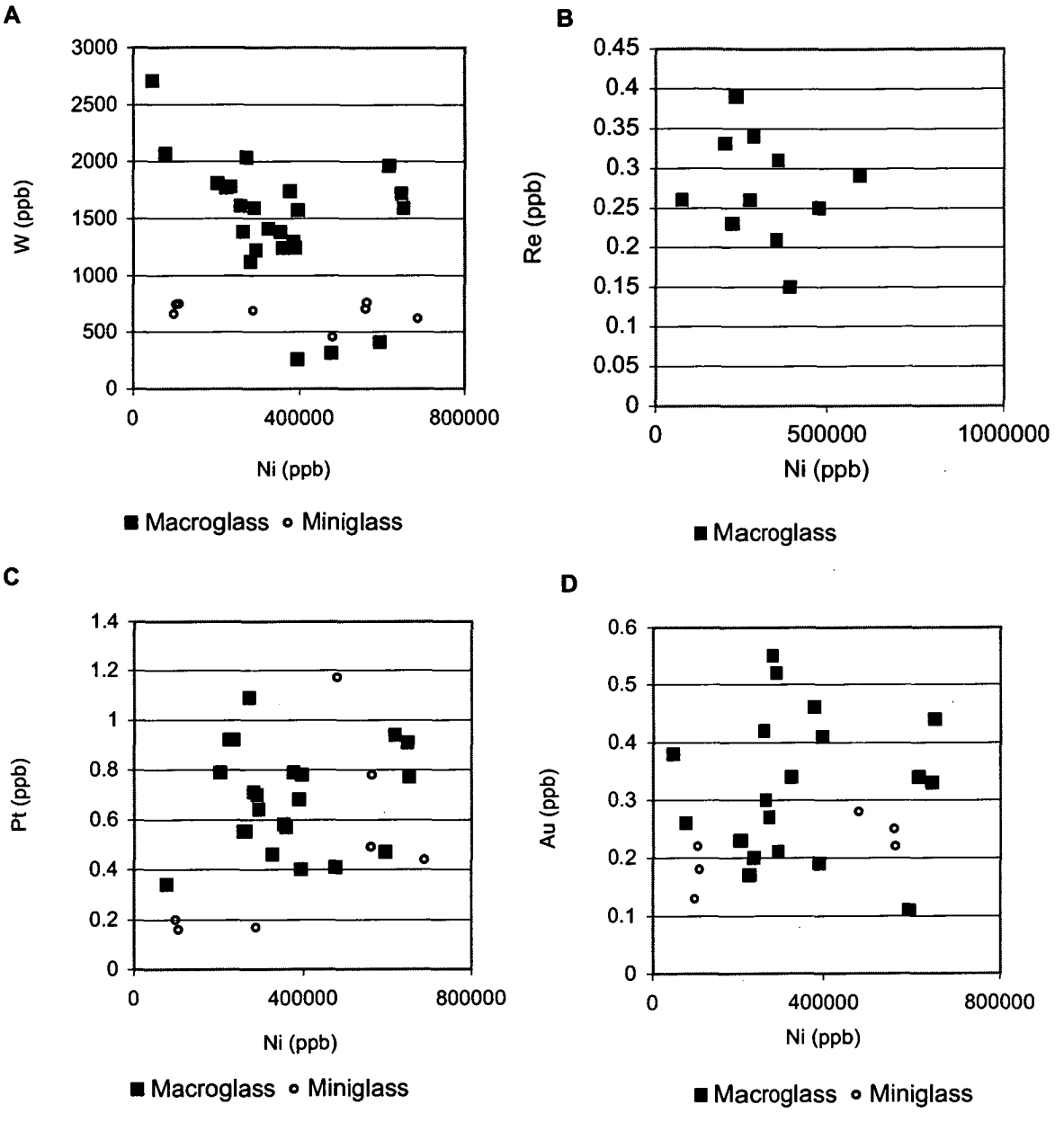

Figure 5.17A-D Ni vs HSE in in Darwin glass.

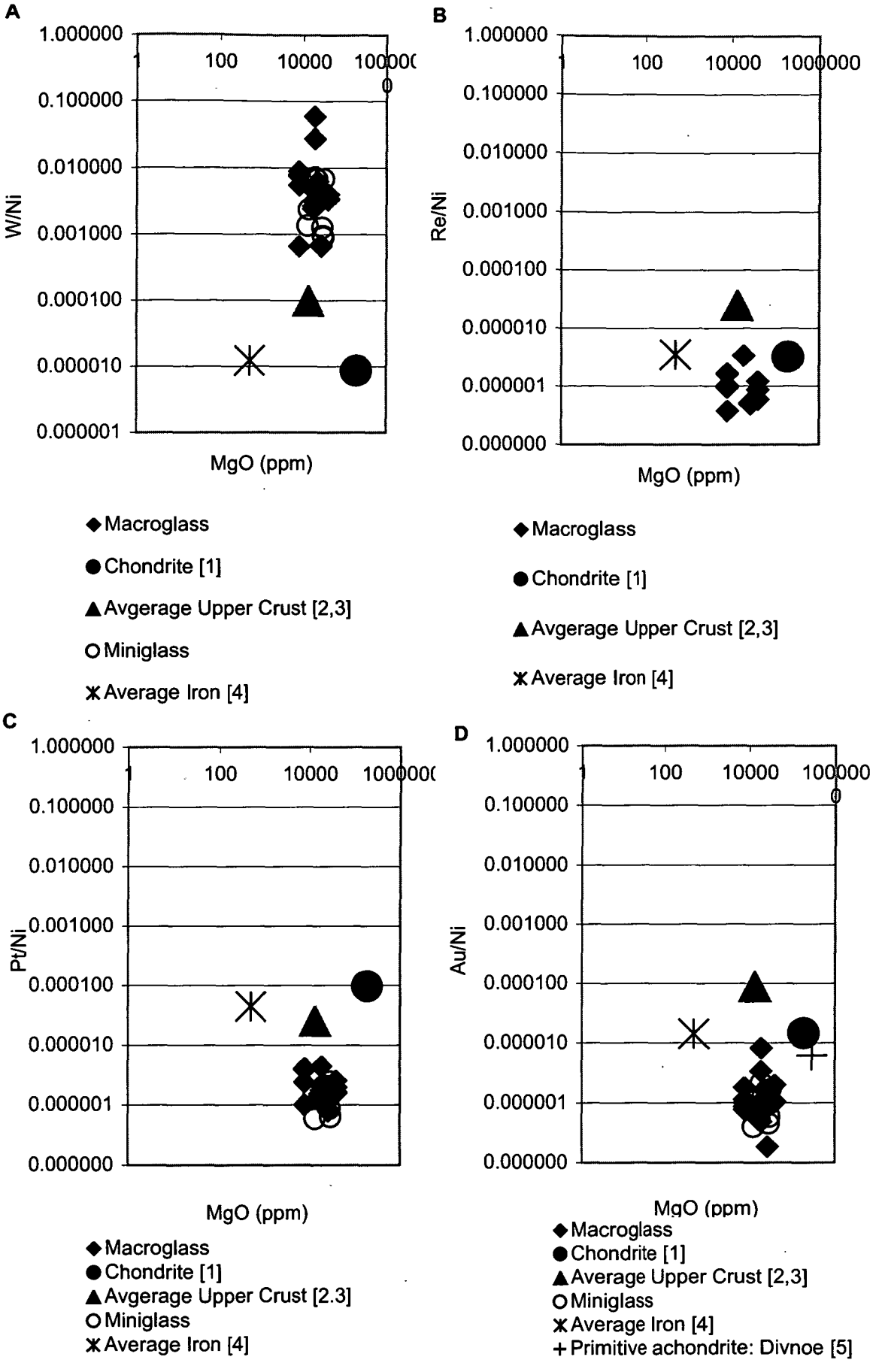

Figure 5.18A-D MgO vs selected HSE/Ni in Darwin glass, Average Upper Crust and selected meteorites.

Data from: [1] Sun & McDonough (1989); [2] Taylor and McLennan (1985); [3] Peucker-Ehrenbrink & Jahn (2001); [4] Wasson et al. (1989); [5] Pataev et al. (1994).

suggested that a partially differentiated asteroid fragment was the projectile involved in the formation of Darwin glass. However, from the compositional data contained in table 5.12, it is clear that even a 1% contribution from the most differentiated and PGE poor silicate dominated phase in the Lodran-like primitive achondrites or L-chondrite Chico would result in Ir concentrations above crustal abundances.

It is tempting to speculate that further differentiation on the parent body produced a large region of melt almost void of HSE that was ejected from the parent body to become the Darwin glass forming impactor. Firstly, this is challenged by volumetric considerations as most recovered chondrite meteorites are heterogenous on a centimetre scale and contain silicate and metallic materials, whereas a pure silicate body 10's of meters in size, at the point of impact, is required and obviously this body would have to have initially been very much larger prior to atmospheric entry and ablation. Secondly, these data from the Chico L-chondrite show that even partial differentiation has fractionated Ni relative to Cr and several analyses yield Ni/Cr ratios <1 (Norman & Mittlefehldt 2002); increased differentiation would further remove Ni and also Co relative to Cr. This is unlike the respective transition metal ratios in Group 2 glasses that are most consistent with a non-differentiated chondrite or primitive achondrite source. Hence a paradox exists in the chemistry of Darwin glass that has a transition metal signature that can best be related to a chondrite-like projectile, but without any evidence for the predicted simultaneous enrichments of the HSE. We will return to speculate on a possible explanation for this shortly.

5.4 Discussion

5.4.1 Volatile fractionation versus mixing controlled geochemical variation

Darwin glass is essentially volatile free as indicated by analytical totals of very close to 100%, and this is a diagnostic geochemical characteristic of impact glasses and tektites. Analytical totals for the target rocks rarely equal 100% and this is most pronounced in average Amber Slate totals of 96%. This is evidence for impact-induced vaporisation of target rock volatiles. Volatile induced fractionation of major and trace elements during target rock melting may also influence melt compositions. Some authors have suggested volatile fractionation, rather than mixing of compositionally distinct targets, offers the dominant control on the geochemical variation observed in an impact glass population (e.g. Walter, 1967, 1989, Walter &

Clayton 1967). These authors generally cite observed inverse correlations between SiO_2 and the other major elements as evidence for differentiation of tektite compositions by vapour fractionation from a single high silica starting composition. Here elements with lower boiling points ("volatile elements") volatilise more readily than the elements with higher boiling points ("refractory elements") leading to the progressive variation in melt compositions by fractionation of major elements from SiO_2. In Chapter 3, it was demonstrated that in Darwin glass these inverse correlations are purely statistical artefacts of the constant sum problem that mask the true elemental co-variations that are better revealed in centred log-normal space.

Rather than volatile fractionation, variable mixing of slate and quartzite is the preferred explanation for the geochemical variation in these glasses. That the trace element composition of the glasses shows affinity with both Keel Quartzite (Ba, actinides, LREE) and Amber Slate (Sr, HREE plus Y) indicates that the glass groups represent mixtures of the shale and quartzite. This is supported by the Rb-Sr, Sm-Nd data arrays where the glasses plot between average Amber Slate and average Keel Quartzite. The correlation of ratios in refractory trace elements, such as Sr/Eu with SiO_2 (Fig. 5.19), is further evidence that is considered to rule out fractionation as an important process in the origin of the glass because volatilisation would not be expected to fractionate these refractory elements. Indeed, the incredible compositional heterogeneity in Darwin glasses, and the lesser, but significant, chemical variation in tektite and impact melt trace element compositions generally, are considered inconsistent with volatile controlled fractionation from a single homogenous target.

Based on data presented in this study the evidence for volatilisation controlled chemical variation is very limited. P_2O_5 is the only element that is depleted in average glasses relative to the target rocks. P is typically considered to be a refractory element so a volatility control on its abundance in the glass would be surprising. Rather, the apparent loss of P_2O_5 in average glass relative to the target rocks is likely to be an artefact that reflects the wide variability in sedimentary rock compositions, and uncertainties in determining the indigenous P_2O_5 contributions. Here, the average P_2O_5 abundances over the bulk rock melted to form the glass, may have been significantly less than the average values determined for the target rocks in this study. Volatility effects are expected in alkali elements such as Na and K. However, the glass and target rocks have overlapping abundances of Na_2O and K_2O and there is no evidence for such volatile losses during the glass formation.

Cooling time is interpreted to have been the limiting factor preventing volatile fractionation of major and trace elements from SiO_2 during the formation of the glass. The duration of high temperatures required for the glass formation is likely to have been very short and cooling very rapid as the glass was ejected from the crater cavity; thereby limiting/removing the opportunity for volatile fractionation to take place. This is supported by the abundant vesicles in the glass, the dominantly contorted and irregular morphology of the glass, the common presence of lechatelierite in the glass, with some inclusions that preserve the original quartz grain morphology, and also the presence of layered, colour variations in the glass that probably reflect incomplete mixing and homogenisation of the molten target rocks.

5.4.2 Stratigraphic affinity of Group 1 and 2 Glass

All available geochemical and isotopic data, as well as field evidence indicates that Darwin glass was formed by the melting of a mix of Amber Slate, and Keel and Crotty Quartzites. Lechatelierite inclusions and the extremely heterogenous trace element compositions of the glass that show affinities to both Keel Quartzite (Ba, actinides, LREE) and Amber Slate (Sr, HREE plus Y), indicate that melting and mixing during the glass formation was incomplete and the glass was quenched before significant homogenisation took place. Group 1 glass shows greatest affinity with Keel Quartzite and Group 2 glass with Amber Slate. Mixing model results reflect the greater affinity of Group 2 glasses with Amber Slate relative to quartzite and vice versa for Group 1 glass. The absence of any volatile controlled chemical variation supports these stratigraphic affinities, as the glass has not undergone any significant selective elemental losses relative to the target rocks. However, Group 2 glass may also be derived from melting of pelitic regions within the Keel Quartzite that are petrographically and chemically indistinguishable from the Amber Slate because the compositional variation between the slate and quartzite is controlled by the abundance of detrital quartz. This is certainly the case for glasses that show incompletely mixed light and dark layers. Significant to note is that Blissett (1962) and Banks (1962), describe a 60m thick pelite unit (Austral Creek Siltstone), that is petrographically almost identical to the Amber Slate, from the top of the Keel Quartzite (Chapter 4). The heterogenous Keel Quartzite is the uppermost formation in the suspected target stratigraphy, and the fact that Darwin glass shows geochemical affinities with this formation (that was not intersected by the drill cores),

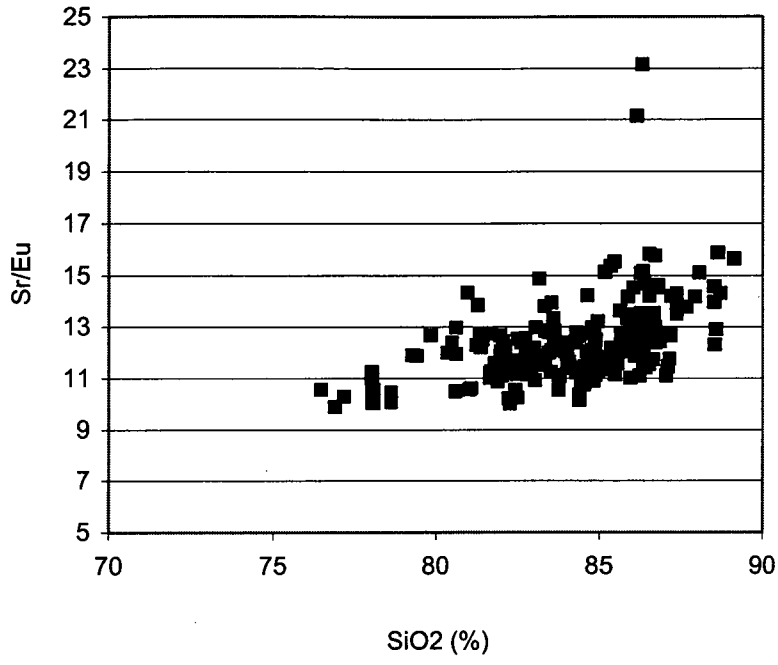

Figure 5.19 Sr/Eu vs. SiO_2 in Darwin glass.

suggests the entire formation was ejected from the crater as incompletely mixed impact melt, or unmelted ejecta. This is the preferred interpretation because all theoretical and geochemical studies demand that ejected glasses are derived from the upper most units during crater formation (Melosh 1989; Chapter 1). Heterogeneity in the target stratigraphy, the rapid quenching of the melt without complete mixing, and the limited number of analyses at each site, prevent identification of systematic chemical variations in recovered glasses relative to distance from the crater (e.g. the proportion of Group 2 glasses vs. distance from crater). However, Group 2 glass is black (Chapter 3) and it will be shown that trends are observed in the physical properties of recovered glasses, such as colour, relative to distance from the crater.

5.4.3 Projectile identification: the transition metal/HSE paradox

The single aspect of the geochemistry of Darwin glass that cannot be explained as a mixture of Eldon Group rocks or any other west coast rock type, including ultramafics, relates to the transition metals (Ni, Co and Cr), and MgO and FeO. At the required MgO and FeO abundances, Ni, Co and Cr enrichments in the most anomalous Group 2 glasses can only be satisfactorily modelled by invoking projectile contamination from a chondrite or primitive achondrite. At up to 9% chondrite (based on Ni and Co) this would represent one of the largest known extraterrestrial contributions to a terrestrial glass (Dressler and Reimold, 2001). This is particularly anomalous because these are widely dispersed ejected glasses (cf. layered tektites), and it is normally only coherent melt samples that show evidence for projectile contamination at percent levels (Dressler & Reimold 2001). However, there are high Mg australites (e.g. Chapman & Scheiber 1969, Taylor & McLennan 1979) and clinopyroxene (CPX) spherules (Glass & Koeberl 1999), in which Ni,Co and Cr abundances exceed crustal average values, but HSE are present in crustal abundances only. The absence of simultaneous HSE enrichments in the glasses is difficult to reconcile with a chondritic transition metal signal and, as discussed, there are no known projectile types with chondritic transition metal abundances that are void of HSE. The existence of such a projectile is fundamentally challenged on geochemical and volumetric grounds as described previously in section 5.3.3b

This absence of HSE enrichments, despite chondritic transition metal enrichments, is suggestive of a heterogenous distribution of impactor contamination. This heterogeneity in the distribution of projectile material in impact melt glasses has been demonstrated at several scales in other impact units (Dressler & Reimold 2001).

Projectile mixing with impact melt is limited and occurs preferentially close to the point of impact and complete vaporisation of the projectile (Melosh 1989, Dressler & Reimold 2001). In complex craters, projectile contamination occurs preferenitally within the more coherent "in crater" melt relative to more clast-rich suevites, or ejected glasses. For example at Lappajarvi crater, only clast-poor samples from the centre of the melt sheet reveal evidence for significant mixing with the inferred C or H chondrite projectile, while suevites show no evidence for projectile contamination (Reimold 1982). The absence of projectile enrichments in ejected tektites has been used as an argument against an origin in hypervelocity jets from the earliest contact with the projectile as described in Chapter 1 (O'Keefe 1976), but it has recently been suggested that this is related to the rapidity of ejection from the crater cavity that prevents mixing of projectile and silicate melt (Artemieva 2003).

Within an individual impact glass sample a heterogeneous distribution of projectile material is also typical (Dressler & Reimold 2001). Generally, this is related to melt immiscibility that sees the partitioning of projectile materials into siderophile non-silicate phases such as sulphides or alloys. Siderophile rich sulphides in impact glasses have been observed or inferred to be present as nuggets or blebs heterogeneously distributed within the silicate melt sheet (e.g. East Clearwater (Palme et al. 1979), and Chixulub (Koeberl et al. 1994b) Craters). These nuggets have also been described in ejected glasses, usually those formed from the impact of iron meteorites (e.g. those at Barringer (Mittlefehldt et al. 1993), Henbury, and Wolfe Creek (Attrep et al. 1991) Craters). In the case of Libyan Desert Glass (LDG) meteoritic contamination is associated with darker immiscible, or incompletely mixed layers in lighter silicate melt (Koeberl 1997). These phases may contain the only evidence for projectile contamination in a silicate impact glass that is otherwise purely a mixture of the target rocks, as for LDG. Alternatively, the silicate melt may show some evidence for projectile contamination and the effect of these nuggets is evident in complex fractionations amongst the siderophile elements that can complicate projectile identification. For example Fe-Ni nugget effects are evident in glasses from Henbury and Wolfe Creek Craters that show evidence for fractionation of some PGE relative to transition metals (Attrep et al. 1991). PGE alloys are known from terrestrial ultramafic rocks (e.g. Spandler et al. 2000) and have been produced experimentally where the formation of PGE alloy nuggets has been used to explain heterogeneous siderophile element distributions in silicate melts (Borisov & Palme 1997).

In other cases, the control on heterogeneity is less clear as an immiscible phase is not obvious. For example, in impact glasses from Bosumtwi and Tswaing Craters there is good evidence for chondritic transition metal enrichments but PGE abundances remain too low by a factor of 2-10 times (Koeberl, 2003). In contrast, Koeberl et al. (1994b) describe K-T boundary melt rocks that preserve close to chondritic PGE ratios without simultaneous enrichments in transition metals. In trying to understand the heterogenous distribution of siderophile elements that cannot be related to an immiscible phase, Koeberl (2003, p. 46) asks, *"Is there some non-equilibrium process going on in the impact vapor plume? "*

5.4.3a Melt-immiscibility-induced siderophile heterogeneity in Darwin glass?

Complex fractionation of PGE's and other HSE from transition metals during the impact process is the only remaining viable explanation for the observed Darwin glass compositions. Post-impact processes of alteration such as weathering are not considered because all analyses are of fresh and un-devitrified glass samples. Given the above observations, the production of HSE-rich nuggets in Darwin glass may be speculated. To produce the observed glass composition, this would require that during mixing of the molten projectile with the silicate melt produced by fusion of the target rocks the transition metals underwent oxidation into the silicate phase (bulk Darwin glass) and the HSE reduction into an insoluble metallic nugget phase in the glass that has not been analysed. Alternatively, the metallic HSE phase was not incorporated into the glass, but was physically segregated from the silicate melt during the impact process.

Evidence for limited transition metal oxidation can be derived from plots of Ni/Cr and Cr/Co that indicate the loss of Cr relative to Ni and Co at high FeO and MgO abundances. In Darwin glass, these Cr losses are interpreted to reflect formation of minor oxide phases such as chromite, that like the speculated HSE rich nuggets, have not been analysed. There is no evidence for any sensible HSE versus transition metal variations in the glass chemistry that may be reconciled with HSE fractionation into a metallic phase. This implies an instantaneous or progressive process that occurred early in the impact event, simultaneously or before production of the silicate melt.

Spencer (1933) and Conder (1934) reported metallic beads in a thin section of Darwin glass. Attempts that were made to locate Spencer and Conder's samples were unsuccessful. During observations of many glasses in thin and thick sections

viewed under transmitted and reflected lights, and ESEM (including BSED), or shattered hand samples viewed under binocular microscope, I have *never* observed a spherical or otherwise shaped metallic phase. Attempts to recover magnetic grains from disaggregated glass have yielded no results. Vesicles that could easily be filled with metallic contaminants to give the impression of *in situ* nuggets are abundant, and it is suggested that Spencer and Conder's observations were not of primary metallic nuggets but introduced contaminants. That early workers had difficulty distinguishing vesicle infilling as a primary or secondary processes, is evident in uncertainty surrounding the interpretation of abundant inclusions of fine rock flour in the glass that are never visible in clean thin sections (samples cleaned in an ultra sonic bath) and are interpreted here as secondary products.

Darker layers that can be observed in Darwin glass are most common in Group 1 samples described in Chapters 2 and 3. These darker layers are zones of higher FeO, MgO ± transition metals also compositionally most like Group 2 glasses. This colour variation is rare in the more homogenous Group 2 glasses that show evidence for projectile contamination. Therefore, these layers that contain no metallic phases may possibly represent a further example of the heterogenous distribution of projectile materials in the bulk melt. However, these colour variations do not aid in explaining the observed fractionation of HSE from transition metals in Group 2 glass. Rather, these darker layers reflect incomplete mixing after transfer of projectile material to a portion of the silicate melt, or simply incomplete mixing of quartzite and more pelitic facies. Probably there is evidence for both processes existing because not all zones enriched in FeO and MgO in the glasses appear to have elevated transition metals (Chapter 3).

Hence in Darwin glass we have found no evidence for the presence of insoluble HSE rich nuggets or immiscible layers that might explain the heterogenous distribution of projectile contaminants. These may exist in impact melt that was retained in the crater, although such a deposit has not been intersected in the drill cores. Further, given that the ejected glasses are enriched in transition metals (indicating exposure to the projectile), any such nuggets should be obvious either in thin section or the time-resolved LA-ICPMS spectra and have not been discovered. However, the presence of tiny, sub-micron sized 'nano-nuggets', that could potentially have a significant effect on the siderophile element budget, cannot be completely ruled out in this study.

5.4.3b Vapour phase transfer of projectile material?

A vapour phase model for the transfer of projectile material to the silicate melt may explain the observed glass chemistry. Condensation of projectile material into the silicate melt is controlled by temperature, pressure and oxidation state (Ebel & Grossman 2000, Alexander 2002). Ebel & Grossman (2000) explore vaporisation and condensation of elements into silicate melt. They show that condensation of systems enriched in dust of chondritic composition can produce abundant molten silicate along with metal and sulphide. Ebel & Grossman (2000) begin with a CaO-MgO-Al_2O_3-SiO_2 (CMAS) liquid at 1930°C and phase diagrams demonstrate progressive temperature controlled condensation. At temperatures of around 1525°C gaseous Mg, Fe and Cr begin to react with liquid to form an Mg-spinel plus minor Cr, Fe and Ti. As temperatures fall Mg and Ti continue to condense into spinel, and Si and Mg to the liquid. The SiO_2 and MgO contents of the liquid increase and the $MgAl_2O_4$ component of spinel dissolve into the liquid. The liquid is now enriched in SiO_2, MgO and olivine that has formed almost exclusively by condensation of Mg and Si from the gas. At 1420°C metallic NiFe + Co, Cr alloy condenses.

Differences in pressure, oxidation states and assumptions as to the behaviour of alkali elements are limiting, but aspects of the Ebel & Grossman (2000) model can be used to understand the observed glass compositions and the HSE/transition metal paradox. The transition metals (Ni, Co, Cr) FeO and MgO have far lower boiling points and condensation temperatures than the other HSE in question (table 5.13). If it is hypothesised that during target rock melting and glass formation, temperatures were sufficient to vaporise transition metals but not HSE, a mechanism exists for preferential condensation of transition metals into silicate melt formed from the target rocks with MgO and FeO. With higher boiling temperatures, the HSE are retained in the bulk projectile/melt. Given higher and more varied indigenous contributions, the MgO and especially FeO contributions from the projectile are difficult to decipher in the glasses. Significant to note is that the Artemieva (2003) model indicates the possibility of gas diffusion of projectile material into silicate melt being an important process. However, in the case of the moldavite tektites that the model is based on, there is no evidence for this diffusion of projectile materials in to the glasses and similarly this study has found little direct evidence for such diffusion in Darwin glass.

Mixing of the silicate melt and projectile vapour is expected to have occurred at the interface between the projectile and target rock surface (Melosh 1989). This can

	Melting Point	Boiling Point
MgO	648	1090
Cu	1083	2567
Cr	1857	2672
Ni	1453	2732
FeO	1535	2750
Au	1064	2807
Co	1495	2870
Pt	1772	3827
Ir	2410	4130
Os	3045	5027
Re	3180	5627
W	3410	5660

Table 5.13 Melting and boiling point of selected elements. Values are in degrees celcius. Data from: Winter (2003).

explain the heterogenous distribution of projectile material that sees preferential enrichment of Ni, Co, Cr, FeO and MgO in glasses derived from the centre of the expanding cavity, closest to the projectile/target interface allowing mixing with molten target as these are blasted out of the expanding cavity. This is consistent with the interpretation that transition metal enriched Group 2 glass is derived from pelitic units in the upper most Keel Quartzite.

If transfer of projectile material had taken place in an expanding vapour plume at the front of the jetting silicate melt, a more widespread mixing of projectile material into the bulk melt as well as more homogenous glass compositions (as for tektites) would be expected. The morphology and extreme compositional heterogeneity of Darwin glass indicates that melting, ejection and quenching was without the large degree of mixing that prolonged transport in turbulent jet or a vapor plume allows. This highlights the differences in small and large cratering events. Tektites require a mechanism such as jetting of superheated melts or an expanding vapour plume to remove the Earth's atmosphere and allow prolonged transport and mixing in order to explain their extremely wide distributions, large distances from source, morphology, and relative to Darwin glass, homogenous chemistry (Melosh 1989; Koeberl 1994; Chapter 1). In contrast, lower energy ballistic processes in the presence of an atmosphere appear to dominate melt ejection and distribution in small impact events. This is further evident in the trends in glass distribution around the crater as discussed in Chapter 6.

The clear implication is that the projectile did not completely disintegrate on impact and projectile fragments may be preserved in the crater stratigraphy or in the surrounding forests as for most small craters on Earth. These fragments have not been recognised and may no longer be recognisable as a result of weathering. Without incorporation of the HSE into the silicate melt, or discovery of projectile fragments, the impactor type cannot be defined beyond a chondrite or primitive achondrite. Excluding Dalgaranga in Western Australia (Smith & Hodge 1996), and with the possible exception of Tswaing, this represents the smallest terrestrial crater to be associated with a projectile other than an iron meteorite. At 1.2km diameter, Darwin crater is close to the 1km threshold defined by Opik (1961), below which size he states terrestrial craters are likely to be formed by iron meteorites only.

5.5 Conclusion

Every attempt to falsify the hypothesis that *"the chemistry and isotopic systematics of Darwin glass match those of mixtures of the Eldon Group (suspected target) rocks in the Darwin Crater area"* has failed. All aspects of the geochemical and isotopic systematics in rocks at Darwin Crater are entirely consistent with these rocks being the source materials melted under impact conditions to produce Darwin glass. Major elements in Group 1 Darwin glass are closest to Keel Quartzite. With a higher FeO content, major elements in Group 2 glasses have concentrations more similar to Amber Slate. The trace element composition of the glasses shows affinity with both Keel Quartzite (Ba, actinides, LREE) and Amber Slate (Sr, HREE plus Y) and this indicates that the glass groups represent mixtures of the shale and quartzite, rather than discrete melting of individual units in the target rock stratigraphy to produce Group 1 and 2 Glasses. This is supported by the Rb-Sr and Sm-Nd data that indicate that the glass and target rocks belong to a single isotopic system, and in all isotopic evolution plots the glasses fall between average Amber Slate and average Keel Quartzite. The huge compositional heterogeneity in Group 1 Darwin glass, and lechatelierite inclusions in all glass samples, indicates that this mixing of molten target rocks was incomplete and that the melt quenched rapidly. There is no evidence for volatile fractionation being an important control on the glass compositions and it is probable that high temperatures were too short-lived owing the rapid and efficient ejection of melt.

Mixing calculations using average target rock compositions successfully model the glass compositions, and support the greater affinity of Group 2 glasses with Amber Slate and Group 1 glasses with Keel Quartzite. Group 2 glass can also be explained as reflecting melting of pelitic zones associated with the upper most target formation, the Keel Quartzite, and this is consistent with the theoretical expectations (Melosh 1989; Koeberl 1994) that ejected glasses are formed from the upper most target rocks. Mixing models result in significant errors only for Ni followed by Co, MgO, Cr and FeO. Such enrichments in Group 2 glasses require an ultramafic contribution. However, mixing models with west coast dunites, pyroxenites or lamprophyres fail to produce the required glass compositions and can be ruled out as a component in the target rock stratigraphy.

The observed bulk composition of Group 2 glass can only be explained by mixing with a chondrite or chondrite-like projectile. The maximum contribution from the projectile is around 9% and this is one of the largest known extraterrestrial

contaminations in a terrestrial material. The distribution of projectile material is extremely heterogenous. Only some of the black Group 2 glass samples, that are interpreted to form from melting at, or very near to the interface between the projectile and target rocks, are enriched in projectile material. In such samples, only the transition metals are enriched with no simultaneous enrichment in the HSE that are present in entirely crustal abundances. This transition metal/HSE paradox can be explained by condensation of transition metals into the silicate melt from a projectile vapor at temperatures insufficient to vaporise and allow condensation of the HSE. These data indicate that Darwin Crater is one of the smallest structures to have its origin in the impact of a projectile other than an iron meteorite. The following chapter will describe physical trends in the distribution of Darwin glass around the crater that will further confirm that Darwin Crater is the source of the glass, and require that the structure be officially recognised as an impact crater.

Chapter 6

Glass vs. Crater Part 2

Abundance and physical properties of Darwin glass relative to distance from the crater

In Chapter 2 the physical properties of more than 4000 glass fragments collected from across the strewn field were described. The glass can generally be characterised by an irregular, contorted morphology and is usually dark green to light green in colour. However, significant variation in the physical properties of the glass is also evident. This variation encompasses a range of shapes that have been subdivided into five main classes: irregular contorted, ropy, elongate, droplet and spheroid. The dominant irregular and ropy glass shapes were interpreted as typical of proximal impact glasses. With parallel flow layering observable in hand-samples and thin sections, these irregular and ropy glasses bear superficial resemblance to layered tektites. The spheroid, elongate and droplet shaped glass is formed by surface tensions during transport. The shape produced depends on the speed and direction of rotation during transport, and viscosity; these samples have a morphological similarity to splashform tektites. The colour variation across the entire sample is from white, to light green, through dark green to black and there is a trend for droplet and spheroid shaped glasses to be preferentially black in colour.

Chapter 2 also described the stratigraphic setting and abundance of glass in the strewn field. This showed that glass is associated with residual gravels and has not undergone significant re-working or lateral transport. Estimates suggest that, relative to the size of the suspected source crater, Darwin glass is the most abundant ejected impact glass on Earth. It is this high-abundance and the young-age of Darwin glass that combine to allow for trends in the physical distribution of the glass relative to distance and direction from the suspected source crater to be explored.

In this chapter discussion will attempt to falsify the hypothesis that "*the observed variations in the physical properties (abundance, size, shape, colour) of glass fragments recovered in situ can be related to distance and direction from the crater*". Any trends from field observations that can be sensibly reconciled by theoretical models of impact cratering are considered non-ambiguous vectors that relate the glass to the structure. Thereby supporting a genetic relationship between these entities. A secondary objective of this chapter is to explain the high abundance and wide distribution of Darwin glass.

6.1 Site selection and methodology

A detailed description of the excavation techniques and important issues in site selection is contained in Chapter 2. To recap, sites were selected from a >180° arc spanning north, west and south from the crater, and extending outwards to the limits of the strewn field. In this site selection, access was the dominant control and most sites are close to the Kelley Basin Track/Mt Mcall Road. Controlled excavations were used to estimate the abundance of glass at 10 sites in a 50km^2 area surrounding the crater. At the other locations uncontrolled excavations collected all glass that could be found. From all sites the characteristics of the recovered glass population were described in terms of the colour and shape classes defined earlier. The sites referred to in the following discussion are shown on the map in Fig. 6.1 and are plotted relative to the crater on a rose diagram in Fig. 6.2. Rose diagrams will be used to display the size, shape and colour distribution of recovered fragments from each site relative to the direction and distance from the crater and provide a means of visually examining any trends in the glass distribution. For a more general depiction of trends in the glass distribution, samples recovered in all directions are combined and also plotted relative to distance from the crater in x-y space.

6.2 Abundance and size distributions

Recovered glass abundances have been normalised to g/cm^3 and compiled in table 6.1. Figure 6.3 is a plot of recovered glass abundance versus distance from the crater. There is a clear trend of decreasing glass abundance with increasing distance from the crater. My own field observations and those of Ford (1972) and

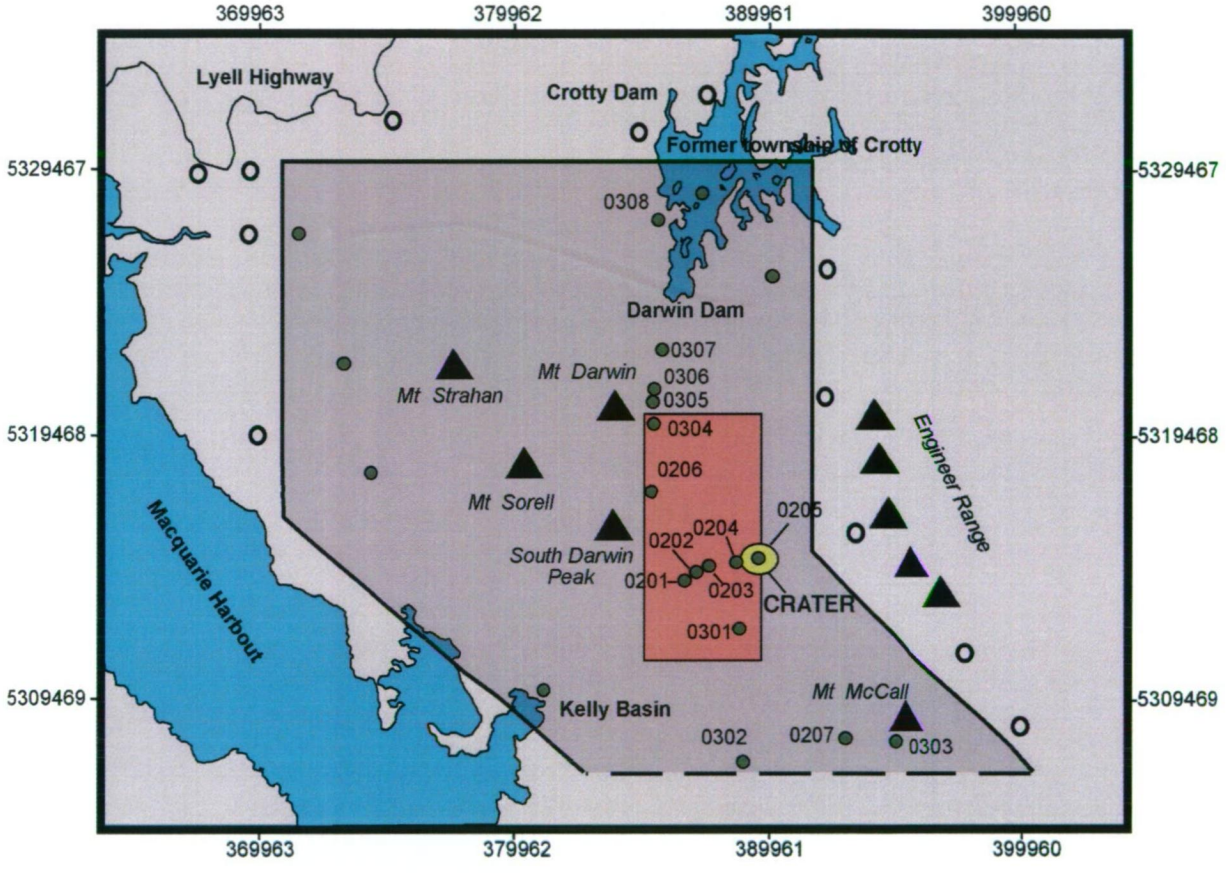

Figure 6.1: Study locations. Closed green circles indicate significant glass find sites. The magenta shading encloses the area where controlled excavations aimed at estimating the abundance of glass were conducted. At the remaining labelled find sites, recovered glasses have been described and classified in detail. Non-labelled find sites are close to the outer limits of the glasses occurrence. Open circles mark sites where residual gravels have been searched, but found to be free of glass, thereby defining the outer limits of the strewn field.

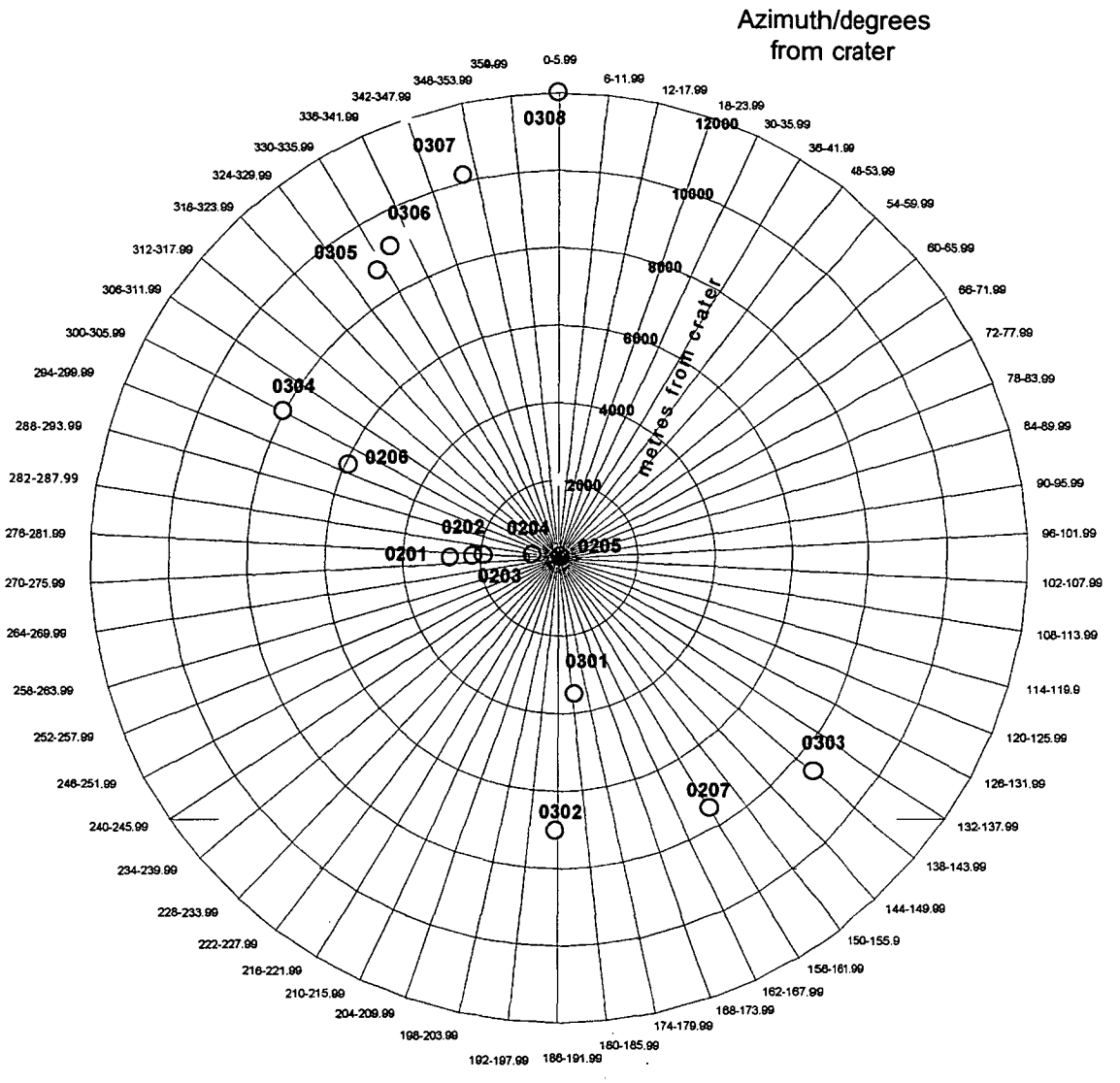

Figure 6.2 Study locations on rose diagram. The crater is located at the centre of the rose diagram and study sites are plotted relative to distance and direction from the crater. In the following discussion, the ranges in proportions of recovered glass falling into the respective colour and shape classes at each site, will be represented by scaled circles on the rose diagram. In these plots, the circles are centred at the above site locations. In some cases the overlap prevents labelling of individual sites, and the reader is asked to refer to the above figure.

Site	Distance from crater (m)	Direction from crater (deg.)	Recovered glass abundance (g/ 30000cm3)	g/cm^3	kg/m3
Site 0201	3000	270	22.3	0.00074	0.7
Site 0202	2500	270	104.0	0.00347	3.5
Site 0203	2000	270	1421.6	0.04739	47.4
Site 0204	500	270	506.4	0.01688	16.9
Site 0205	0	0	5.2	0.00017	0.2
Site 0206	6000	305	13.3	0.00044	0.4
Site 0301	3500	185	44.3	0.00148	1.5
Site 0207	7500	160	7.7	0.00026	0.3
Site 0304	8000	305	23.4	0.00078	0.8
Average (all sites)			238.7	0.00796	8.0
Average (excluding 0203)			90.8	0.00303	3.0

Table 6.1 Recovered glass abundances showing distance and direction from crater. These fragments were recovered in archaeological style controlled excavations of a known volume of the host residual quartz gravels. There is a clear decrease in glass abundance with increasing distance from the crater as noted by Ford (1972) and Fudali & Ford (1979). There is no evidence for any asymmetry in the glass abundance distribution that can not be explained as relating to preservation.

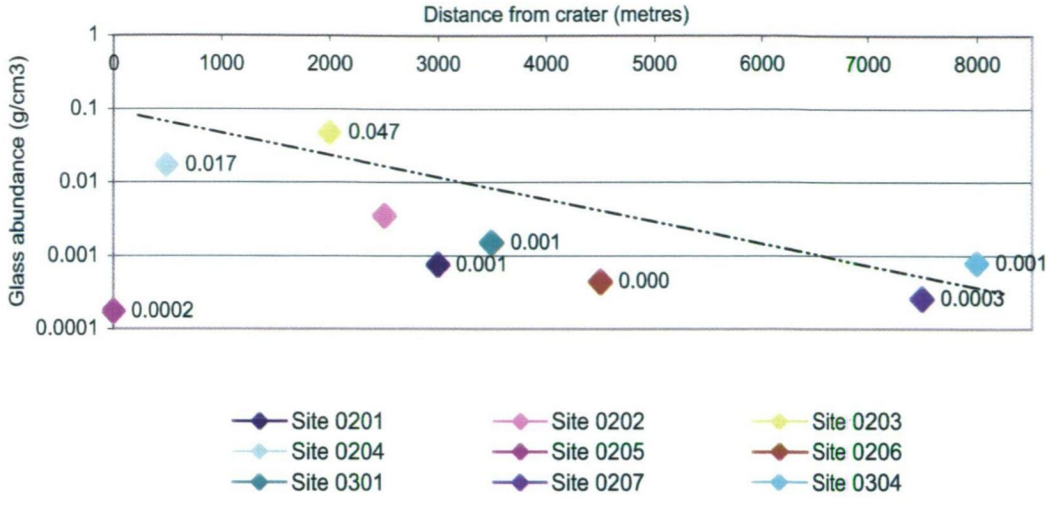

Figure 6.3 Recovered glass abundance (g/cm^3) versus distance from crater (all directions). There is a clear decrease in the abundance of glass recovered from residual gravel deposits with increasing distances from the crater.

Fudali & Ford (1979) support this positive correlation between glass abundance and proximity to the crater. It is also clear in the field that with increasing distance from the crater, particularly at distances beyond around 5000m (e.g. 10 crater radii), the glass distribution and abundance becomes increasingly patchy. For example, in the northwest of the strewn field glass is relatively more abundant at site 0306, compared to site 0305 to the south, and 0307 to the north. When fossicking at these distances from the crater it is typical to encounter local patches of increased glass abundance in a region characterised by low abundance. These patches of elevated glass abundance may also exist closer to the crater, but given the much higher general glass abundances, these are more difficult to recognise.

There does not appear to be any discernable relationship between direction from the crater and the abundance of glass that cannot be explained as relating to preservation. The absence of glass to the east of the crater relates to the steep topography and the Andrew and Franklin Rivers that have combined to erode away any glass that may have been present and access is mostly impossible. Glass is found to the southwest of the crater but difficulty of access prevents detailed studies in this area.

At 11 sites, all observed glass fragments were collected in uncontrolled excavations and recovered finds were weighed individually. Weight is used as a proxy for fragment size and the weight data for recovered fragments are compiled in table 6.2. The average fragment weight recovered, considering all sites, was 1.6g, and at any individual site was less than 3.5g. The ranges in the average weights are plotted on rose diagrams that show distance and direction from the crater and as weight vs. distance in x-y space in Fig. 6.4A,B. These results do not yield strong correlations but there is limited evidence for an increase in the average weight of recovered glass fragments with increasing distance from the crater. This initially unexpected observation is explained in table 6.2 and Fig. 6.5A,B that display the proportion of recovered glass fragments weighing <2g relative to distance from the crater. The proportion of glass fragments of < 2g weight is greatest closest to the crater (producing low values for average weight) and a decrease in the proportion of glass fragments weighing <2g takes place with increasing distance from the crater until the most outlying sites are reached where the glass fragments are almost exclusively <2g. These conclusions have been arrived at only after a prolonged period of investigation. This is because with only limited observations and time in the field, the average size appears to decrease away from the crater because the

Site	Distance from crater (m)	Direction from crater (deg.)	Average weight (g)	% wieight <2 g	Max weight (g)
0204b	500	270	0.98	96	18.9
203	2000	270	1.03	91.08	29.8
207	7500	160	1.59	75	9.99
301	3500	185	2.15	71.6	26.08
302	7000	185	3.26	55.5	8.07
303	8500	140	0.56	93.3	4.5
304	8000	305	1.31	85.29	7.17
305	9000	330	1.58	66	2.87
306	9200	330	2.25	68.75	20.96
307	10500	340	2.09	60	5.97
308	12000	359	0.78	95	4.07
All sites			1.6	78.0	12.6

Table 6.2 Size data for recovered glass fragments showing distance and direction from crater (n=1063). The SG of the glass does vary but not significantly enough to prevent fragment weight being used as proxy for fragment size. The largest glass fragments are found closest to the crater.

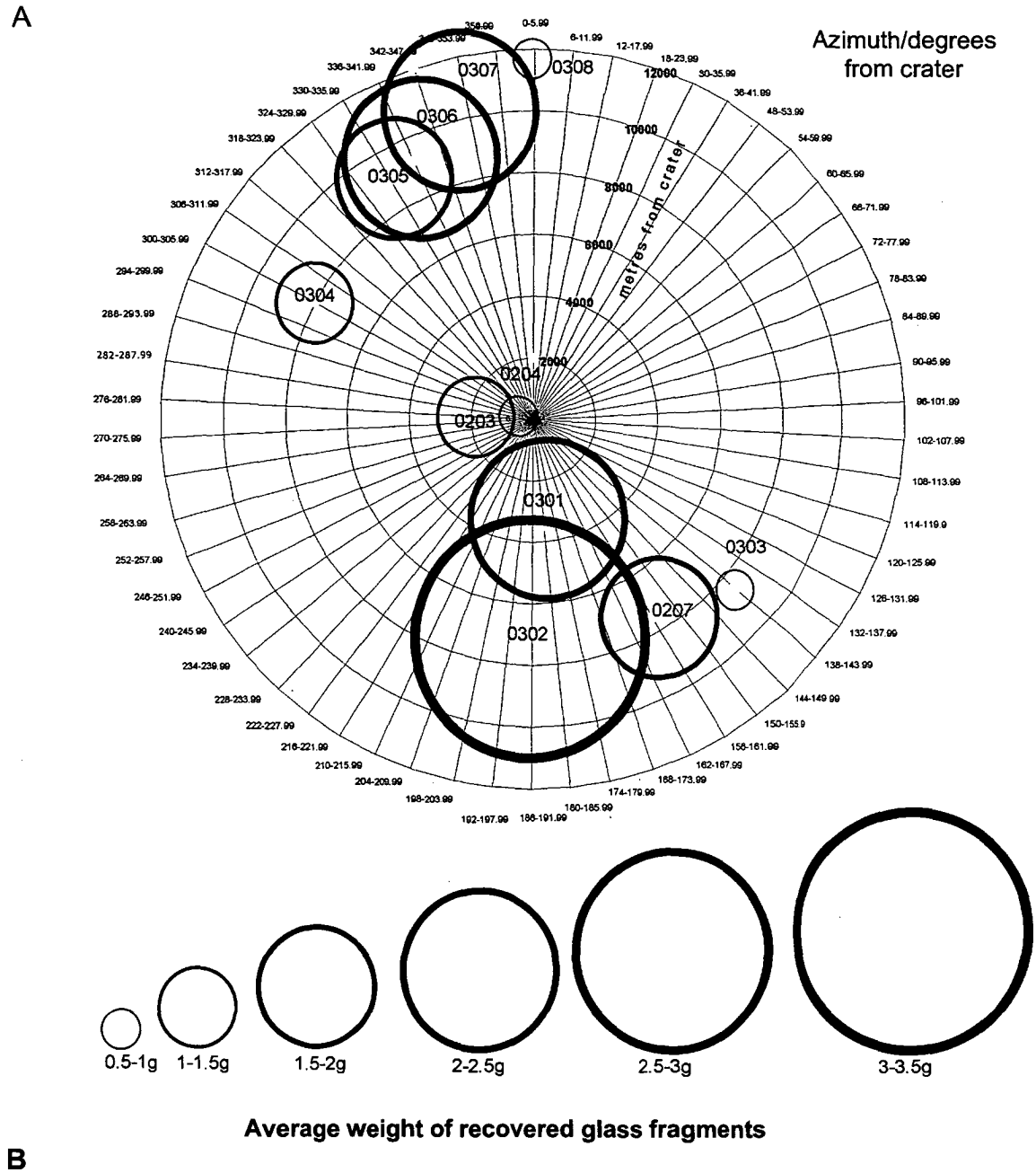

Figure 6.4 Average weight of recovered glass fragments.
A)Average weight vs. distance and direction from crater.
B)Average weight vs. distance from crater.
The apparent increase in average size *away* from the crater is a statistical artifact that reflects the relatively very high abundance of small fragments close to the crater as described below.

A

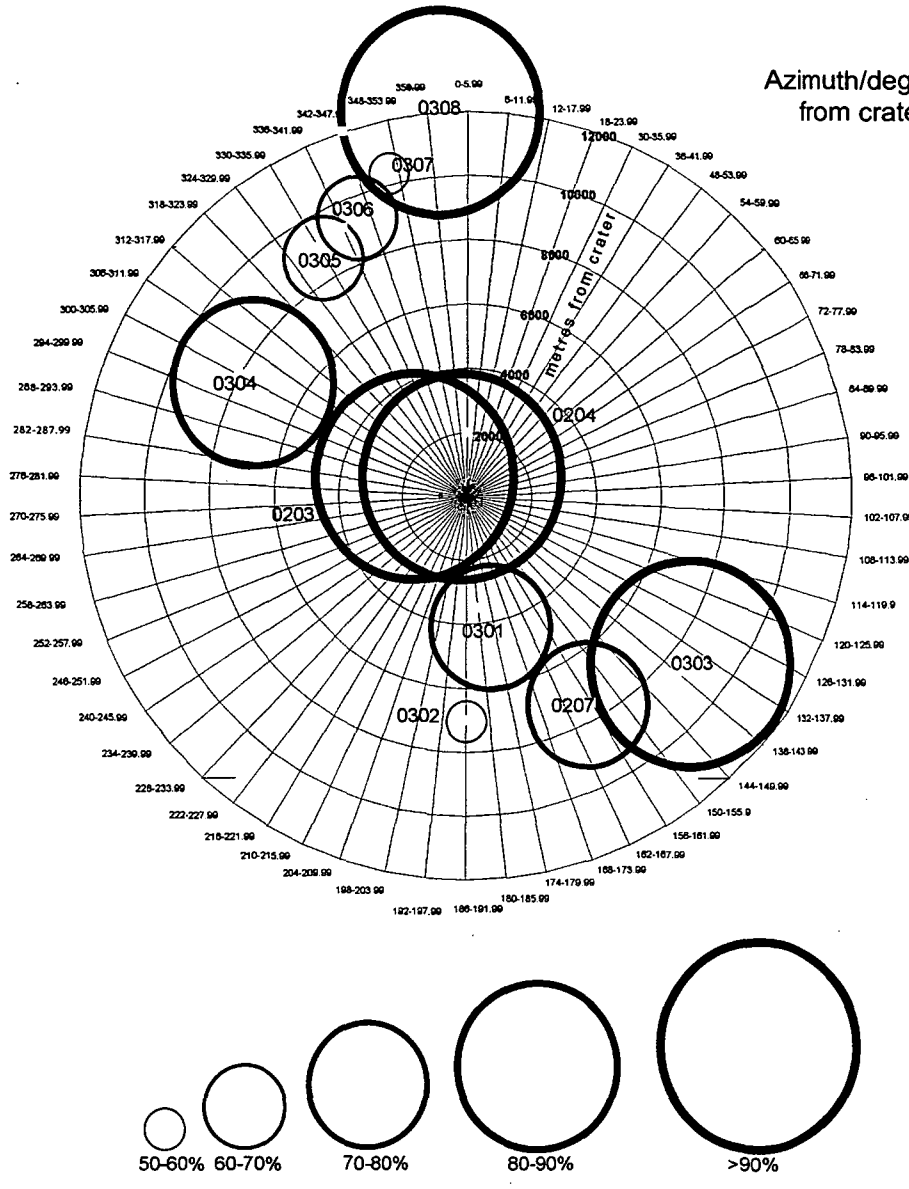

Proportion of recovered glass fragments weighing <2grams

B

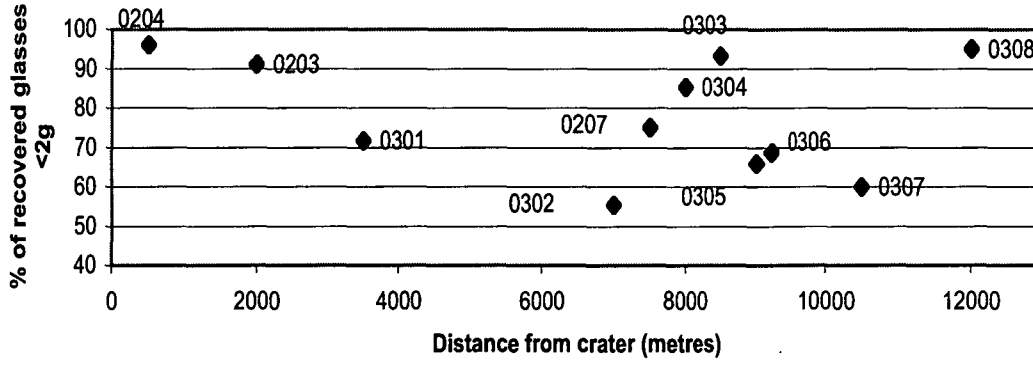

Figure 6.5 Proportion of recovered glass fragments weighing < 2 grams.
A) % weight <2g vs. distance and direction from crater.
B) % weight <2g vs. distance from crater.

There is a very weak trend of a general decrease in the proportion of <2 gram fragments recovered with increasing distances from the crater until the most outlying sites are reached where recovered glasses are almost exclusively <2g.

true abundance of the small glass fragments is only noticeable in controlled excavations, and even then only to the trained eye as small glass fragments are hard to recognise amongst the abundant quartzite pebbles.

The largest fragment of Darwin glass ever collected during scientific investigations was found by Ramsay J. Ford and weighs just less than 1kg after a slice was removed for sectioning. It was found proximal to the crater between sites 0203 and 0204. No fragments even close to this size were discovered in the 3 year course of these investigations and I am aware of only one reported find of a similar sized fragment discovered in the 1980's (Christo Lees, Personal Communication in 2003). In table 6.2 and Fig. 6.6A,B it can be seen that, excluding site 0306, there is clear evidence for a decrease in the maximum recovered glass weight with increasing distance from the crater. Rather than an anomaly, site 0306, is typical of the patchy distribution of the glass at large distances from the crater, described above in abundance estimates, and when fossicking at these distances occasional large fragments are found amongst the predominantly much smaller ones. Again, there does not appear to be any discernable relationship between direction from the crater and the size of recovered glass fragments and the erosional removal of glass to the east of the crater prevents further inferences.

6.2.1 Interpretation

To interpret the trends in glass abundance relative to the crater it is useful to visualise the impact and melt ejection process. The reader is referred to the recent work of Artemieva (2003) that integrates data from the Moldavite strewn field into hydrocode simulations that model the path of melt ejecta from the expanding cavity through the atmosphere. In the interpretation of observed trends, the models of Melosh (1989) provide important constraints, and panels from such models that depict the melt excavation process were described earlier (Chapter 1). The reader is also reminded of the haunting images of above ground nuclear explosions that provide an analogue for small impact events.

That there is no evidence for primary asymmetry in the distribution of glass prevents inferences as to the projectiles trajectory. Without knowing if glass was initially abundant to the east of the crater, an impact from this direction cannot be ruled out. However, an impact from the east would seem inconsistent with the geophysical evidence that shows the crater deepens slightly towards the south-southwest, suggesting an impact from the north-northeast. The lack of primary asymmetry in

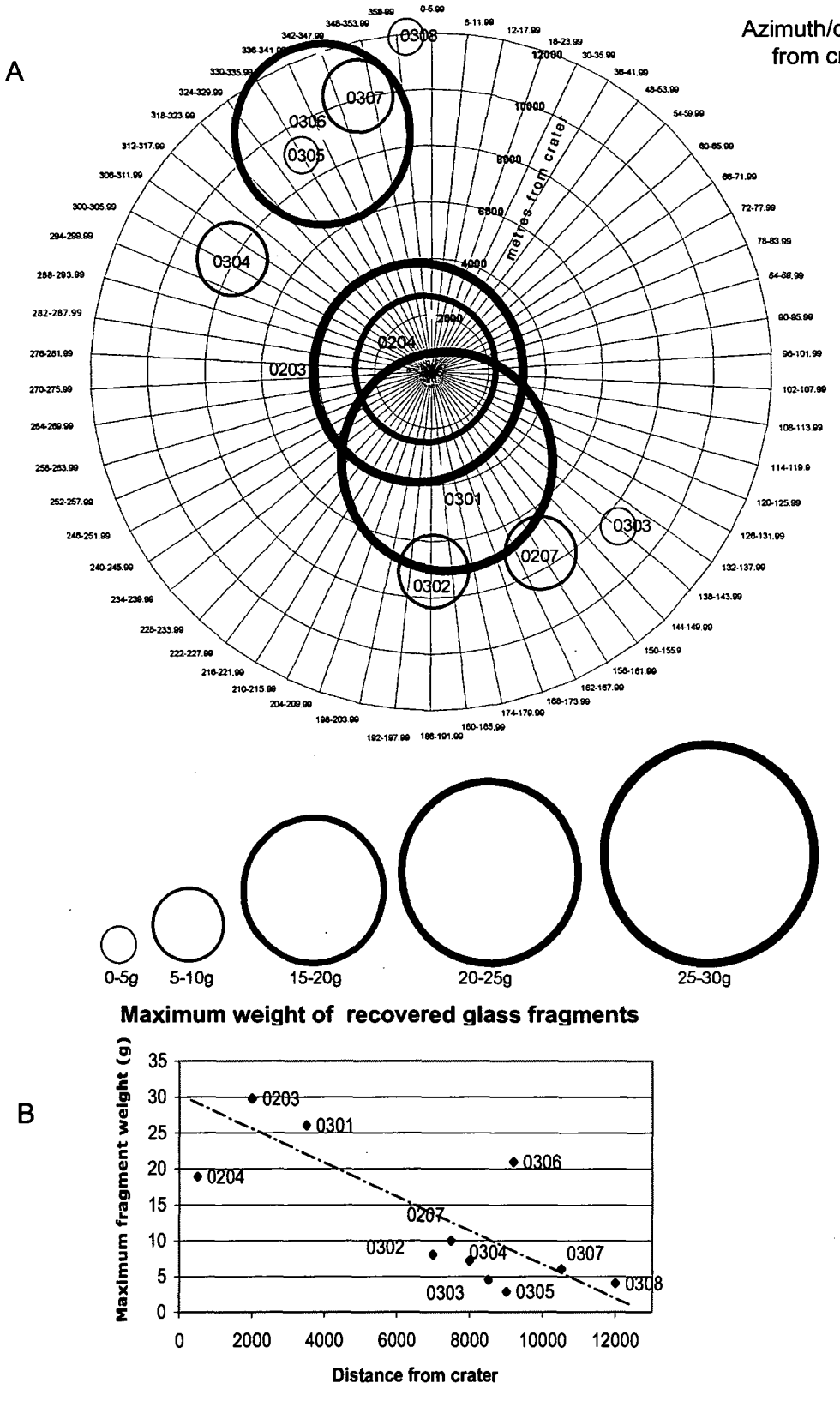

Figure 6.6 Maximum weight of recovered glass fragments.
A) Maximum weight vs. distance and direction from crater.
B) Maximum weight vs. distance from crater.

There is a clear trend showing a decrease in the maximum weight of recovered glass fragments with increasing distance from the crater. Consistent with this trend is the fact that the largest known fragment (just less than 1kg, collected by Ford) was collected between sites 0204 and 0203.

the glass distribution indicates a high angle impact (45° is most likely angle for an impact on Earth).

Observed size distributions of glass fragments in the strewn field are only reconcilable with ballistic fallout following explosive ejection from the crater. The continuous distribution of glass from the crater out to a maximum of around 20km from source does not require removal of the atmosphere by the expanding vapor plume (atmospheric blowout) to explain the observed glass distribution, as for the jetting theory of tektite origin (Melosh 1989). It also rules out any suggestion that the glass condensed from a vapour distal from the impact site. The phenomenon of atmospheric blowout is restricted to impacts that release at least 150MT energy (Melosh 1989, Chapter 1). This is well beyond the scale of the Darwin impact. Equations in Grieve & Cintala (1992) estimate that the amount of explosive energy released during the formation of a crater the size of Darwin (D= 1.2km) will be <20MT. Such an explosion will result from the impact of a projectile of between 20-50m in diameter (Melosh 1989). However, it must be noted that based on observations at other craters, if we had the glass alone and not the suspected crater to consider, it would be possible to use the ejected glass abundance to infer a much larger source than Darwin Crater.

The melt is inferred to have been ejected in a viscous stretching plume in the absence of atmospheric blowout. The internal and external morphologies and the glass chemistry indicate that the melt ejection was highly turbulent and that quenching was rapid. Here the turbulent interaction of the melt with the atmosphere promotes dispersal of melt and the breakdown of the plume (Vickery 1993) resulting in glass deposition, as is illustrated in Fig 6.7 and described below. Initially, the upper target material is molten and rapidly ejected upwards and outwards. The melt sprays upwards and sideways in a turbulent plume and is stretching as it rapidly begins to quench. Turbulence in the plume, promoted by interaction with the atmosphere, and shrinkage and breakage during cooling of the melt, causes its dispersal as small fragments which then rain down on the surface. The turbulence prevents significant size sorting and as the turbulent cells in the plume break down, large and small glass fragments are deposited together as is evident from the fact that recovered glass sizes are always skewed towards outlying large fragments. The presence of turbulent cells in the melt plume, and the subsequent break- down of these plumes, also explains the patchy distribution of glass at large distances from the crater as has been invoked as an explanation for the discontinuous

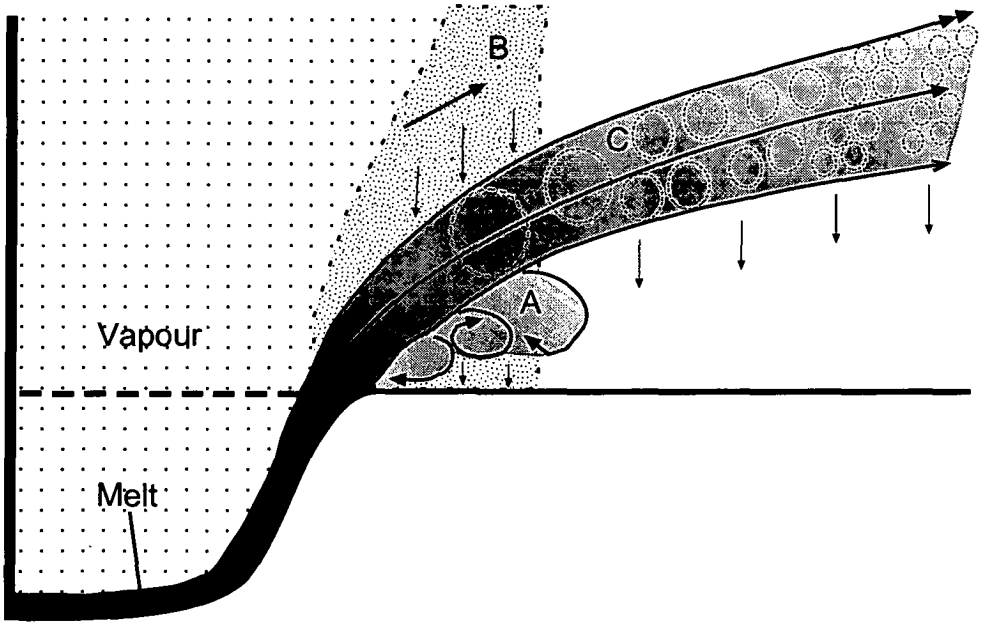

Figure 6.7 Model for Darwin glass ejection. A) As the turbulent melt is blasted from the expanding crater cavity it rapidly quenches and glass rains to the surface depositing the largest fragments, from low in the jetting melt, closest to the structure. **B)** Ejecta curtain of fine, frothy and incompletely molten glass and non-melted materials. The small <2mm glass fragments are blasted upwards and outwards and are rapidly slowed by interaction with the atmosphere to be deposited preferentially close to source. **C)** The rapidly propagating melt jet is highly turbulent. As the turbulent cells break down, large and small quenched glass fragments are deposited together because the turbulence prevents significant size sorting. The breakdown of turbulent transport cells also explains the patchy distribution of glass in the strewn field at large distances from the crater.

distribution of Suevite deposits surrounding the Ries and Chicxulub Craters (Claeys et al. 2003), although such deposits are formed during a later stage of excavation and ejection than impact glasses.The largest glass fragments, from lowest in the ejected plume, represent the deepest target rocks melted and are deposited preferentially close to the crater. The frothy small glass fragments are blasted upwards and outwards, probably along with non-melted material in an "*ejecta curtain*". These small fragments are light and are rapidly slowed upon interaction with the atmosphere, therefore promoting deposition preferentially close to the crater.

6.3 Colour and shape

Glass fragments recovered under controlled and uncontrolled conditions from across the strewn field were classified into the colour (white; light green; dark green; black) and shape (irregular; contorted; ropy; elongate; droplet; spheroid) classes as defined in Chapter 2, these data are presented again in tables 6.3 and 6.4. The proportions of fragments falling into each of the colour and shape classes are plotted relative to distance from the crater in rose diagrams and in x-y space in Figs. 6.8A-D and 6.9A-D, respectively. White glass comprises less than 1% of the entire strewn field and is almost exclusively found closest to the crater where it may comprise up to almost 8% of recovered fragments. White fragments are almost exclusively small (<2g). Light-green glass is most abundant closest to the crater and there is a general decrease in the proportion of light green glass relative to other colours away from the crater. Dark green is the most common overall colour, and there is also a general decrease in the proportion of dark green glass relative to the other colours with increasing distance from the crater. The most pronounced colour trend relative to distance from the crater is in the abundance of black glass. Black glass increases in abundance relative to other colours with increasing distance from the crater; this is most pronounced in the northwest direction at sites 0305, 0306 and 0307.

Irregular glass shapes always dominate the sample at any location in the strewn field. Ropy glass shows a clear decrease in abundance relative to the other shapes with increasing distance from the crater. Conversely, the proportion of droplet, spheroid and elongate shapes is greatest at sites >3000 metres from the crater (e.g. 6 crater radii). If the specimens classified as 'splashform' (spheroid, droplet and elongate shapes) are combined and plotted relative to distance from the crater (Fig. 6.10A,B) a trend is defined that shows the proportion of splashform shapes increasing with increasing distance from the crater.

	Distance from crater (m)	Direction from crater (deg)	n	White		Light green		Dark green		Black	
				f	%	f	%	f	%	f	%
Site 0201	3000	270	17.0	0.0	0.0	7.0	41.2	9.0	52.9	1.0	5.9
Site 0202	2500	270	85.0	0.0	0.0	28.0	32.9	48.0	56.5	9.0	10.6
Site 0203	2000	270	3126.0	164.0	5.2	1121.0	35.9	1702.0	54.4	139.0	4.4
Site 0204	500	270	365.0	29.0	7.9	112.0	30.7	191.0	52.3	33.0	9.0
Site 0205	0	0	3.0	0.0	0.0	1.0	33.3	2.0	66.7	0.0	0.0
Site 0206	6000	305	13.0	0.0	0.0	5.0	38.5	6.0	46.2	2.0	15.4
Site 0207	7500	160	266.0	6.0	2.3	32.0	12.0	134.0	50.4	94.0	35.3
Site 0301	3500	185	80.0	2.0	2.5	10.0	12.5	47.0	58.8	21.0	26.3
Site 0302	7000	185	9.0	0.0	0.0	0.0	0.0	6.0	66.7	3.0	33.3
Site 0303	8500	140	14.0	0.0	0.0	0.0	0.0	2.0	14.3	12.0	85.7
Site 0304	8000	305	33.0	1.0	3.0	2.0	6.1	9.0	27.3	21.0	63.6
Site 0305	9000	330	15.0	0.0	0.0	0.0	0.0	2.0	13.3	13.0	86.7
Site 0306	9200	335	145.0	0.0	0.0	1.0	0.7	42.0	29.0	102.0	70.3
Site 0307	10500	340	10.0	0.0	0.0	0.0	0.0	1.0	10.0	9.0	90.0
Site 0308	12000	359	42.0	0.0	0.0	9.0	21.4	23.0	54.8	10.0	23.8
All sites			4223	202	4.8	1328	31.4	2224.0	52.7	469	11.1

Table 6.3 Colour distribution in Darwin glass showing distance and direction from crater. All fragments were recovered *in situ* from across the strewn field. Dark green glass dominates recovered finds. White glass is found almost exclusively close to the crater. Relative to the other colours, the proportion of black glass recovered increases with increasing distance from the crater. There is no evidence for any asymmetry in the colour distribution of recovered glass relative to the crater.

	Distance from crater (m)	Direction from crater (deg)	n	spherical		droplet		elongate		ropy		irregular	
				f	%	f	%	f	%	f	%	f	%
Site 0201	3000	270	17.0			1.0	5.9					16.0	94.1
Site 0202	2500	270	72.0	1.0	1.2	3.0	3.5			9.0	10.6	72.0	84.7
Site 0203	2000	270	3126.0	4.0	0.1	125.0	4.0	13.0	0.4	858.0	27.4	2126.0	68.0
Site 0204	500	270	365.0	0.0	0.0	4.0	1.1	1.0	0.3	117.0	32.1	243.0	66.6
Site 0205	0	0	3.0									3.0	100.0
Site 0206	6000	305	13.0			2.0	14.3			1.0	7.1	10.0	71.4
Site 0207	7500	160	266.0	8.0	3.0	75.0	28.2	9.0	3.4	29.0	10.9	145.0	54.5
Site 0301	3500	185	80.0	2.0	2.5	11.0	13.8	3.0	3.8	12.0	15.0	52.0	65.0
Site 0302	7000	185	9.0					1.0	11.1			8.0	88.9
Site 0303	8500	140	14.0	1.0	7.1	1.0	7.1			1.0	7.1	11.0	78.6
Site 0304	8000	305	33.0	0.0	0.0	7.0	21.2			4.0	12.1	22.0	66.7
Site 0305	9000	330	15.0									15.0	100.0
Site 0306	9200	335	145.0	1.0	0.7	21.0	14.5	1.0	0.7	10.0	6.9	112.0	77.2
Site 0307	10500	350	10.0							1.0	10.0	9.0	90.0
Site 0308	12000	359	42.0	3.0	7.1	4.0	9.5	1.0	2.4	3.0	7.1	31.0	73.8
All sites			4223	20	0.5	254	6.0	29	0.7	809	19.2	3111	73.67

Table 6.4 Shape distribution in Darwin glass showing distance and direction from crater. All fragments were recovered *in situ* from across the strewn field. Irregular shapes dominate the sample. Relative to the other shapes there is a decrease in the proportion of ropy shapes with increasing distance from the crater. The proportion of splash-form shapes (elongate forms, spheres, droplets) is greatest at sites beyond 3000m (6 crater radii) from the suspected source crater.

A

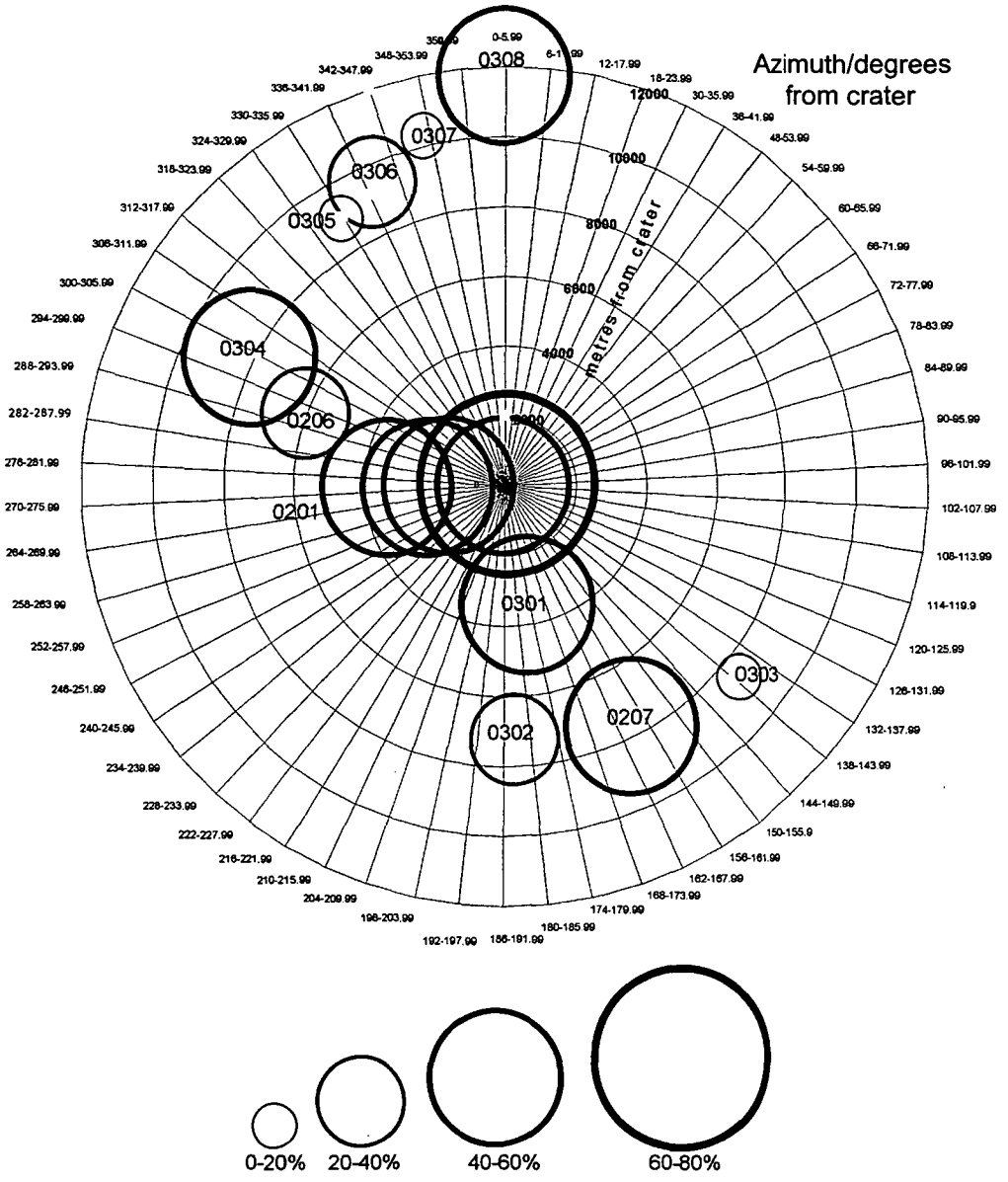

B

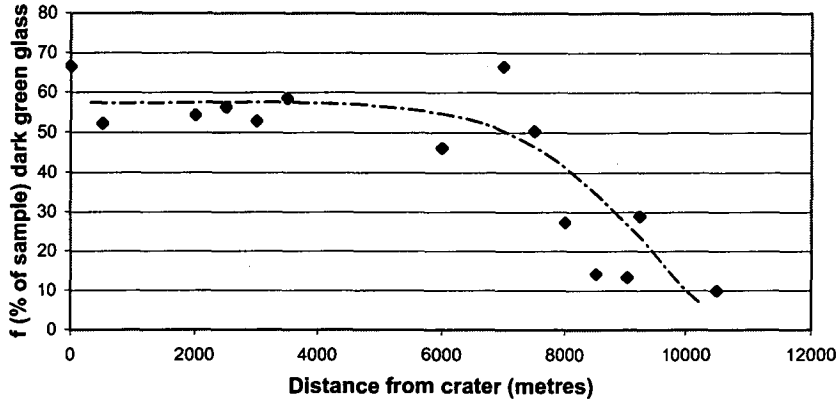

Figure 6.8A Proportion dark green coloured glass fragments.
A) % dark green glass vs. distance and direction from crater.
B) % dark green glass vs distance from crater.

Dark green glass almost always dominates recovered finds. Relative to the other colours there is a general decrease in the proportion of dark green glass recovered with increasing distances from the crater.

A

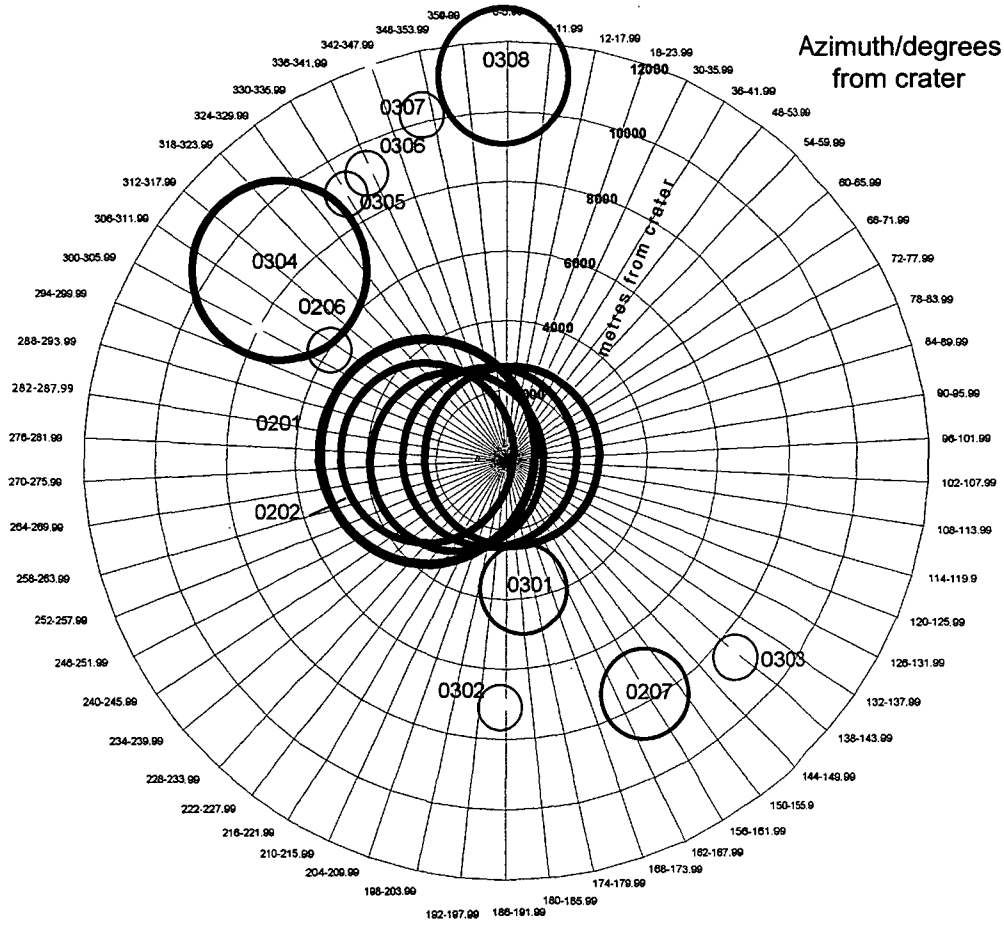

B

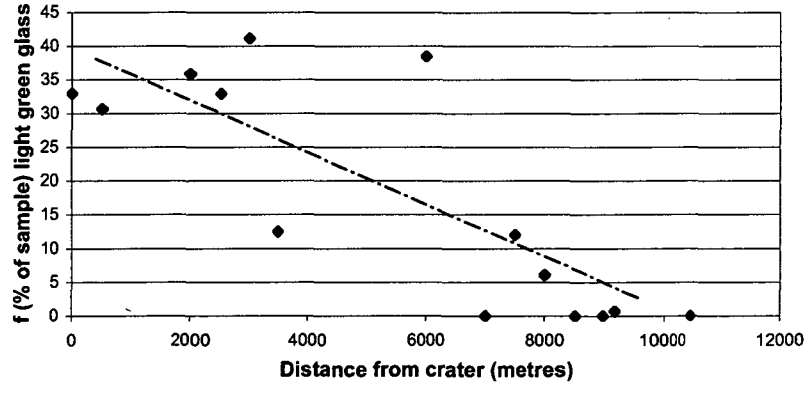

Figure 6.8B Proportion of light green coloured glass fragments.
A) % light green glass vs. distance and direction from crater.
B) % light green glass vs. distance from crater.

Relative to the other colours there is a general decrease in the proportion of light green glass with increasing distances from the crater.

A

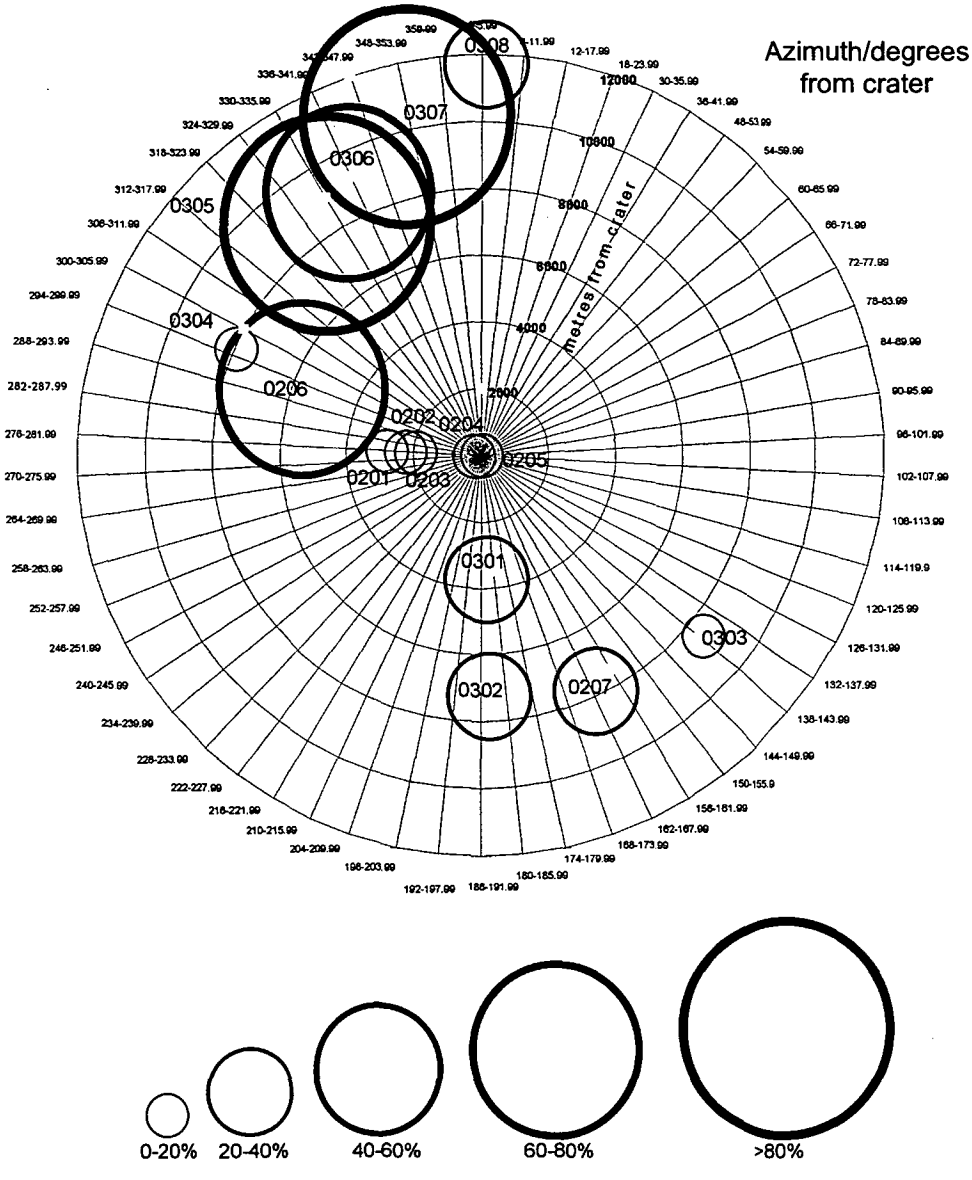

B

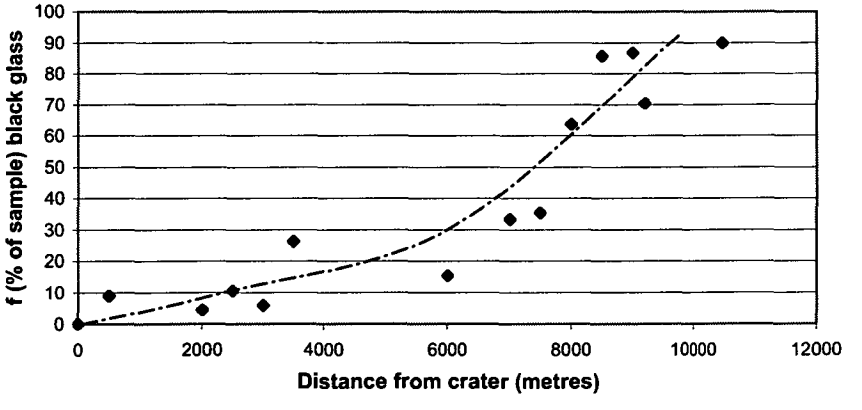

Figure 6.8C Proportion of black coloured glass fragments.
A)% black glass vs. distance and direction from crater.
B) % black glass vs. distance from crater.

Relative to the other colours there is a clear increase in the proportion of black glasses with increasing distances from the crater.

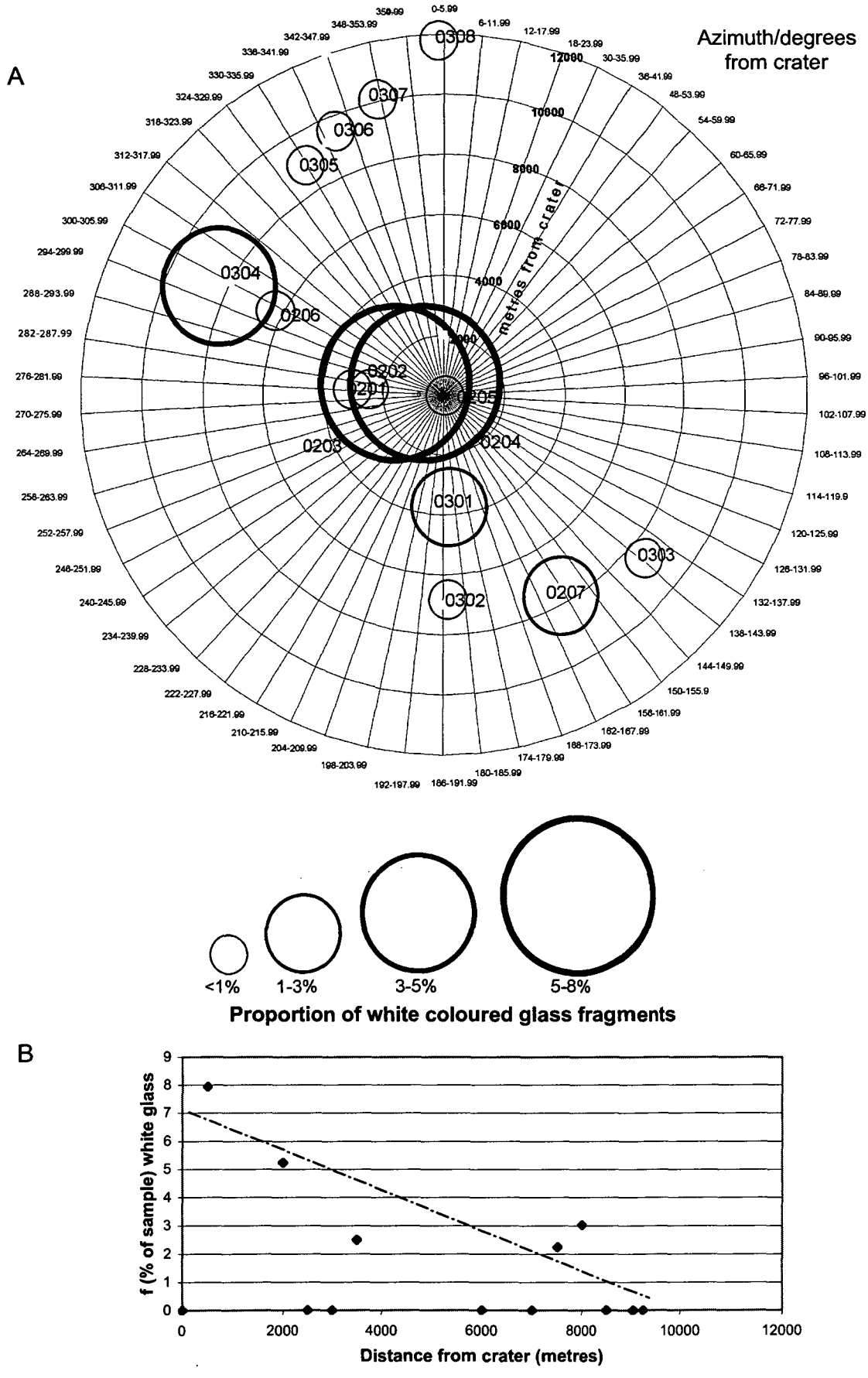

Figure 6.8D Proportion of white coloured glass fragments.
A) % white glass vs. distance and direction from crater.
B) % white glass vs. distance from crater.

Relative to the other colours white glass is very rare and found almost exclusively at sites near to the crater.

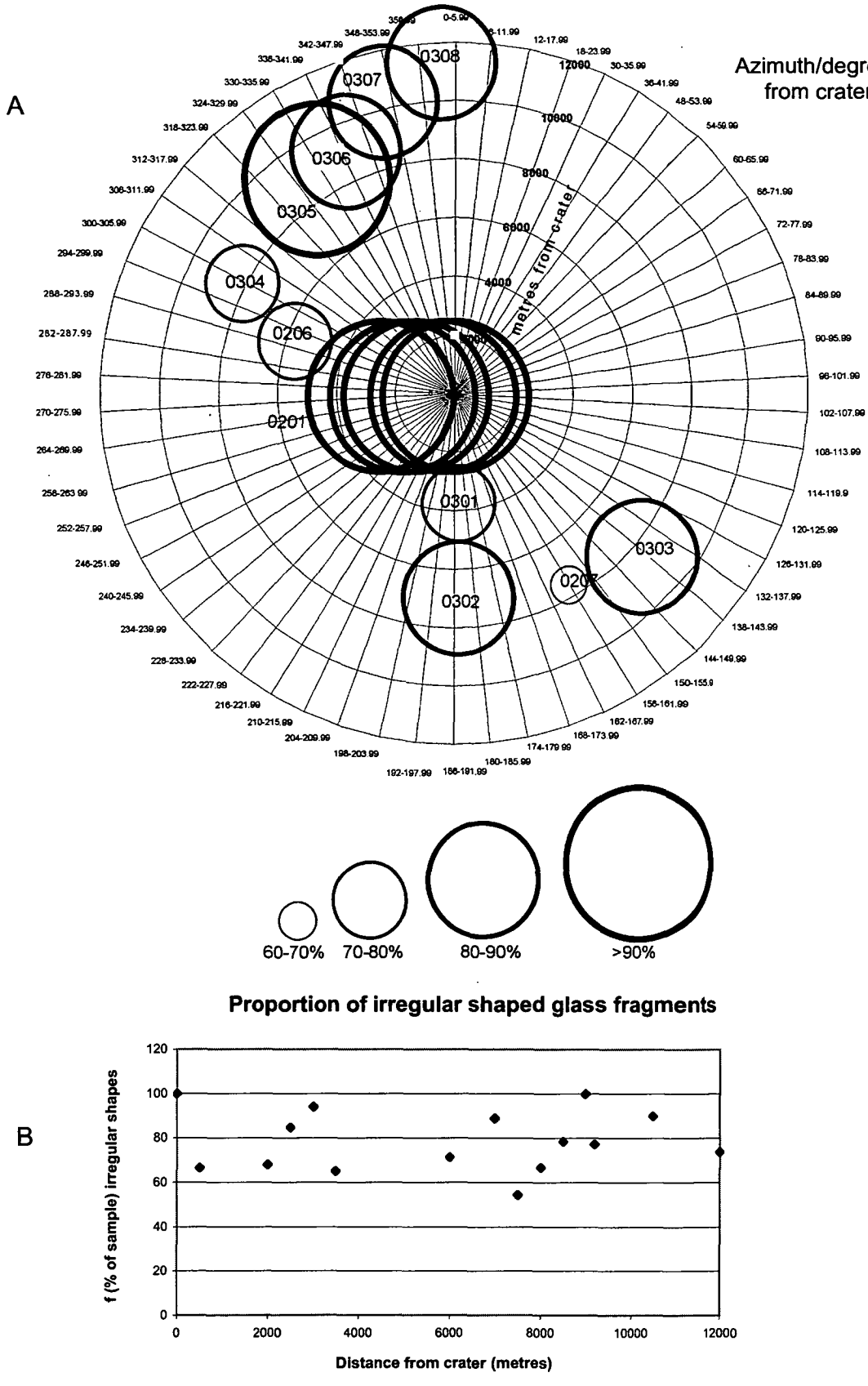

Figure 6.9A Proportion of irregular shaped glass fragments.
A) % Irregular vs. distance and direction from crater.
B) % irregular glass vs. distance from crater.

Irregular shapes always dominate glass finds. These shapes are considered to form from an turbulent expanding melt plume without significant rotations and shaping of the molten fragments by surface tensions when in transport.

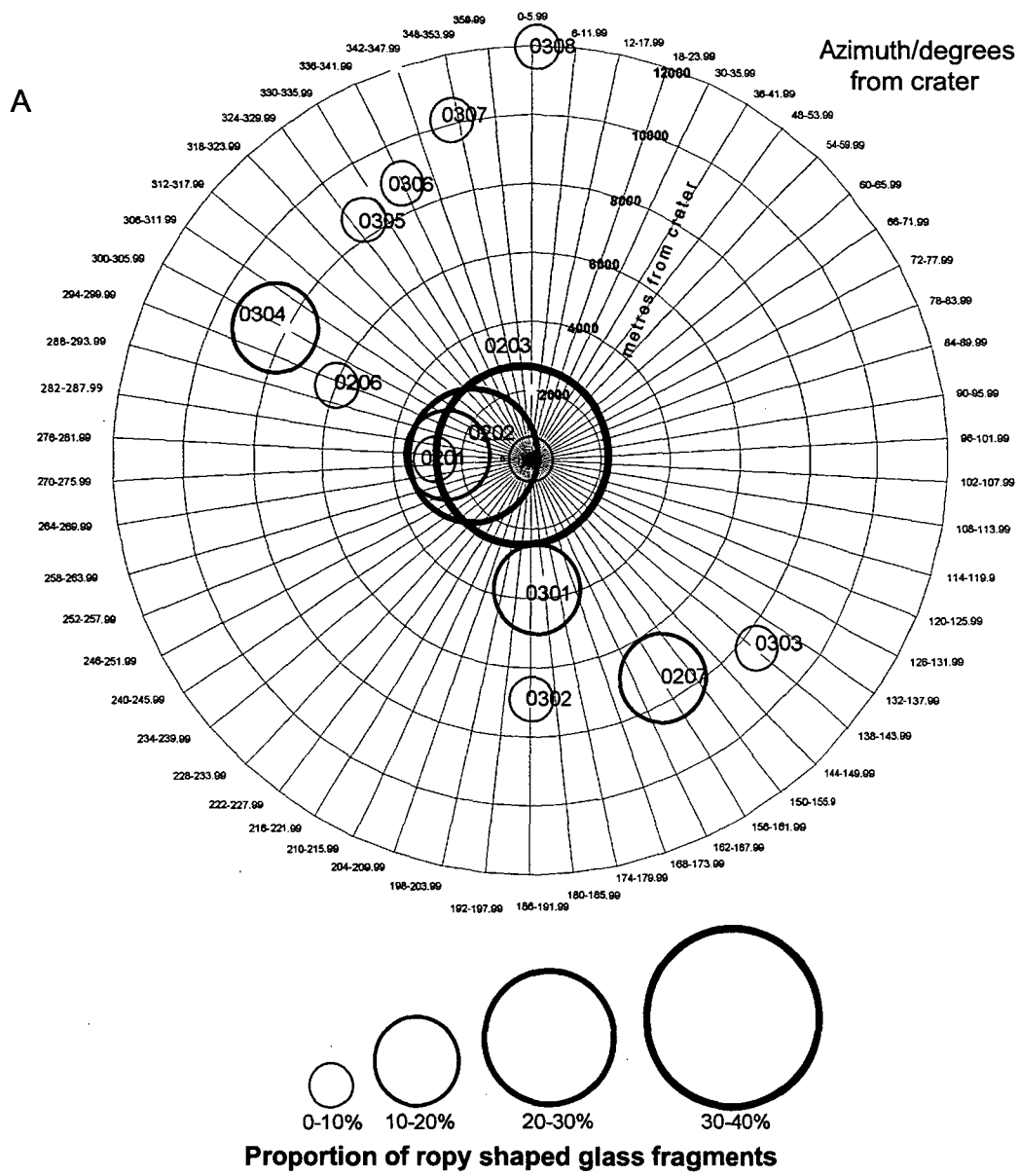

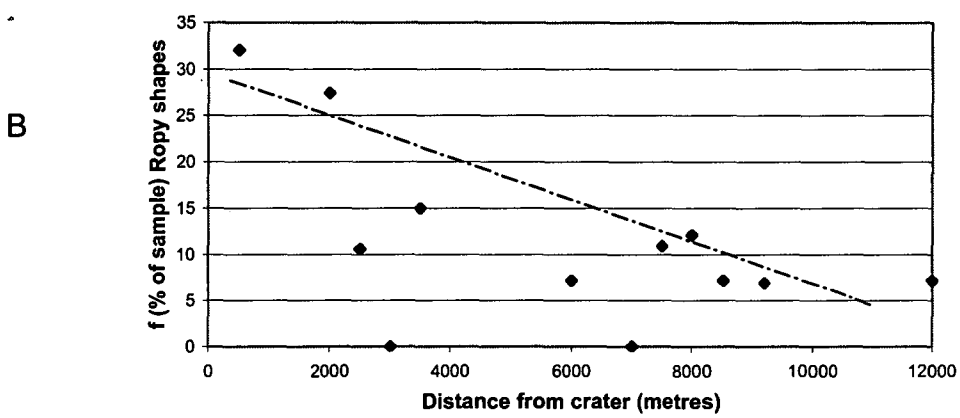

Figure 6.9B Proportion of ropy shaped glass fragments.
A) % ropy shapes vs. distance and direction from crater.
B) % ropy shapes vs. distance from crater.

Relative to the other shapes there is a clear decrease in the proportion of ropy shapes recovered with increasing distances from the crater. Like the more irregular shapes, the ropy samples are also considered to form from a turbulent expanding melt plume without significant rotation and shaping of the molten fragments by surface tensions.

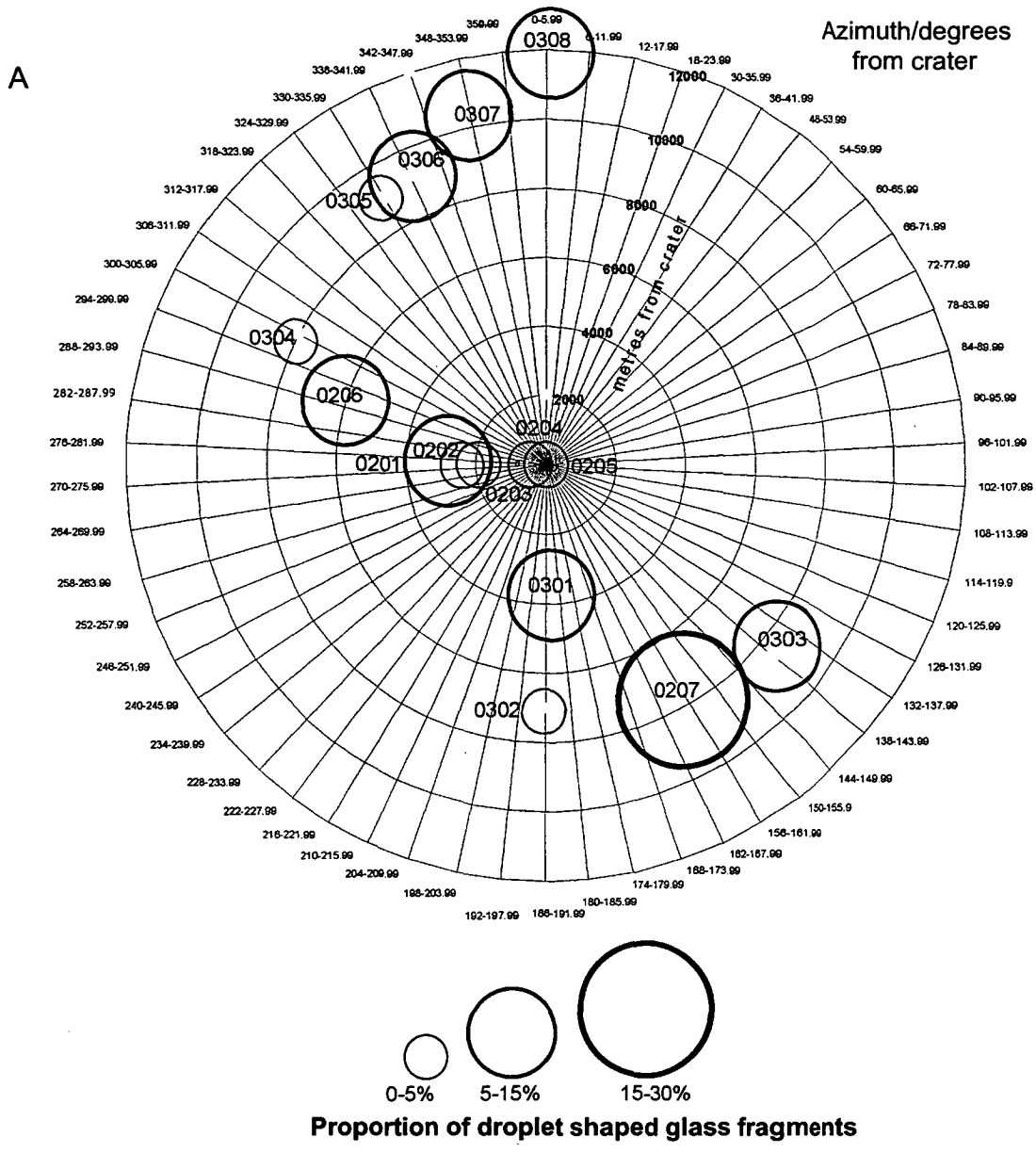

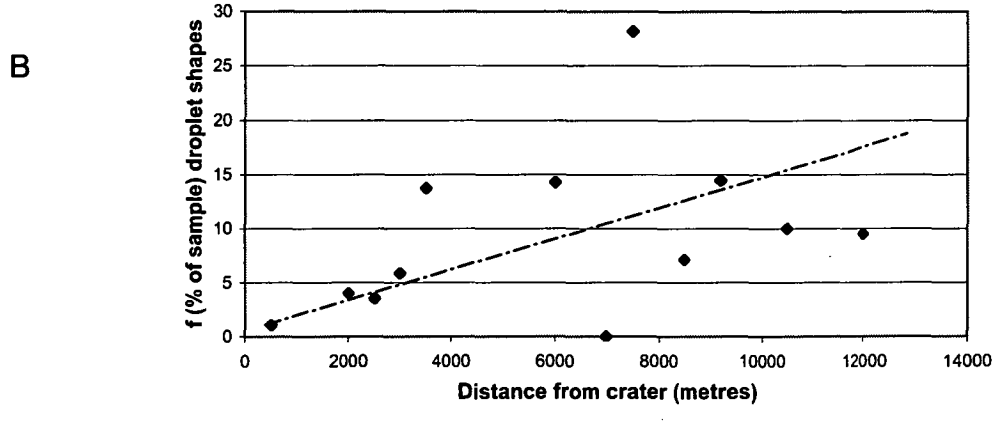

Figure 6.9C Proportion of droplet shaped glass fragments.
A) % droplet shapes vs. distance and direction from crater.
B) % droplet shapes vs. distance from crater.

Relative to the other shapes there is a clear increase in the proportion of droplet shapes recovered with increasing distances from the crater.
Droplet shapes are formed by surface tensions acting on rotating molten fragments.

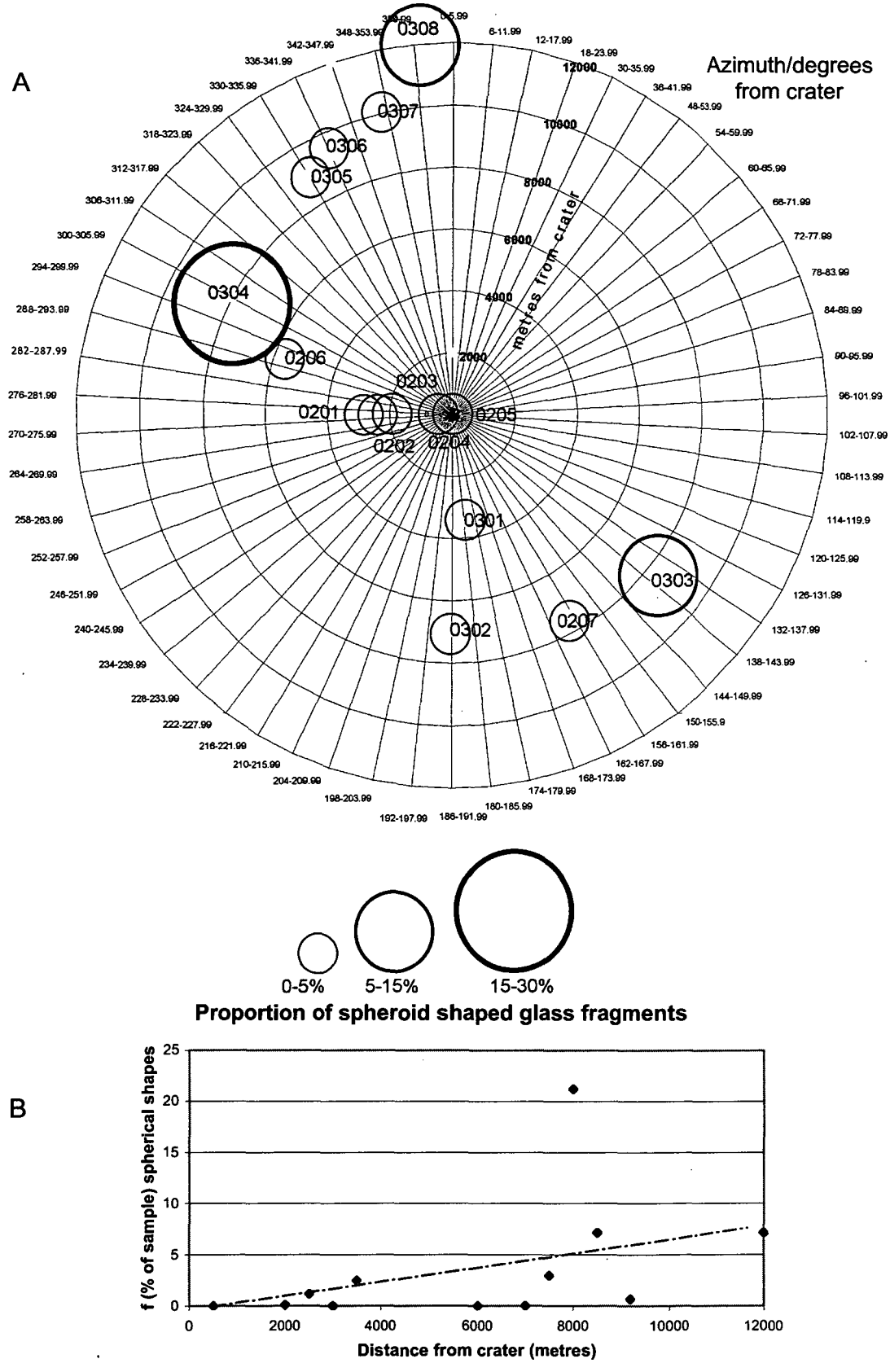

Figure 6.9D Proportion of spheroid shaped glass fragments.
A) % spherical shapes vs. distance and direction from crater.
B) % spherical shapes vs. distance from crater.

Spheroid shapes are rare. Relative to the other shapes there is an increase in the proportion of spheroid shapes with increasing distances from the crater. Spheroid shapes are formed from surface tensions on molten fragments in free transport without significant rotation or at least without spinning on a preferred axis.

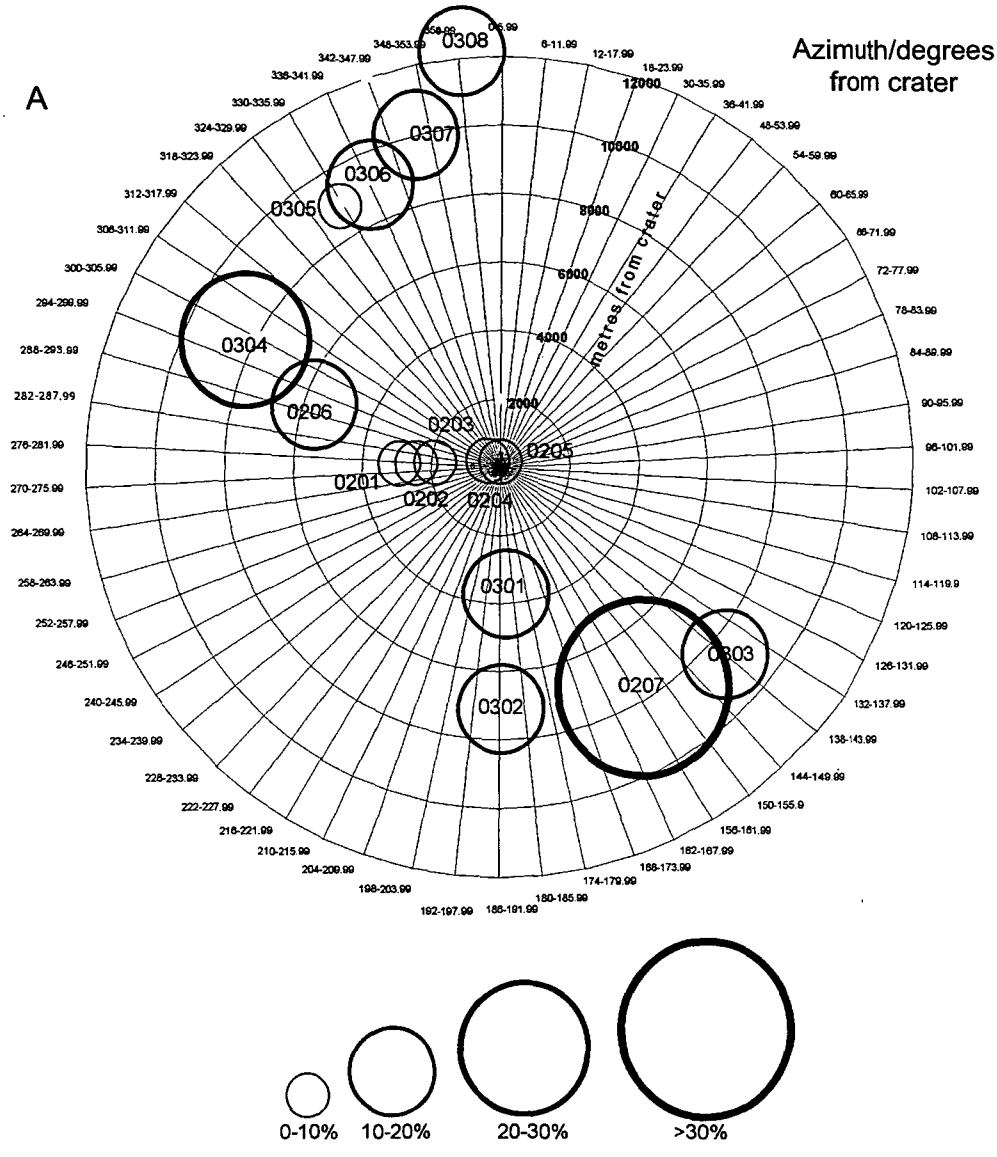

Proportion of splash-form shaped glass fragments

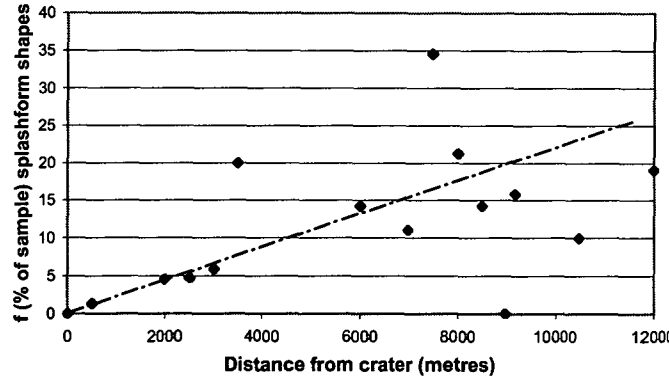

Figure 6.10 Proportion of splashform shaped glass fragments.
A) % splash-form shapes vs. distance and direction from crater.
B) % splashform shapes vs. distance from crater.

The glasses classified as splash-form (spheroidal, elongate and droplet shapes) have been combined. There is a clear increase in the proportion of splashform shapes recovered with increasing distances from the crater. This is because prolonged transport of the molten fragments, in the presence of surface tensions, promotes development of splash-form shapes with the control on the shape being the degree of rotation.

The variation in combined splashform abundance also has significant scatter, and this is consistent with field observations that show that the distribution of splashform shapes across the strewn field is patchier than the distribution of the irregular and ropy shapes. When fossicking along a transect, irregular glass may comprise all finds until, within a small area, splashform shapes become common as at site 0306 and in the surrounding area where large black droplets can be found patchily distributed across the hillside (e.g. Fig. 2.8F-H). The samples from this area show the closest physical resemblances to Australasian splashform tektites of all the glass recovered from the strewn field. Generally splashforms are only found where the glass is abundant, but the rule that the relative abundance of splashforms increases with distance from the crater holds true. That irregular shaped glass is found more than 20 crater radii from the likely source, and has an overlapping distribution with splashform shaped glass is a challenge to the usual observation that contorted irregular and ropy morphologies are restricted to proximal impact glass, as is discussed below.

6.3.1 Interpretation

At all sites the most common recoveries are irregular, light to dark green fragments. The irregular internal and external morphologies, and composition of the glass, is consistent with this material having quenched from a turbulent, stretching and rapidly propagating melt plume. Before more complete mixing and chemical homogenisation could take place, the melt had dispersed and quenched and fragments began to fall to the surface. To allow the formation of splashform shapes requires that fluid fragments be dispersed from the bulk melt plume and transported as 'free' melt blebs being shaped by forces of surface tension (see Chapter 2). Prolonged aerial transport when hot and molten promotes the formation of splashforms and, as such, the increase in the proportion of these shapes with increasing distances from the crater is to be expected. The ejection of melt to form the observed distributions of the irregular, ropy and the splashform shapes is summarised in Fig. 6.11.

Generally, the distance of melt ejection can be directly related to depth of excavation, with the uppermost target stratigraphy being ejected to farthest distances from the crater (Melosh 1989). The Keel Quartzite is the upper most formation in the target stratigraphy, and it is commonly associated with interbedded pelites that are indistinguishable from the Amber Slate. Elsewhere, sections exposed on the west coast show that the top ~60m of the Keel Quartzite is pelitic,

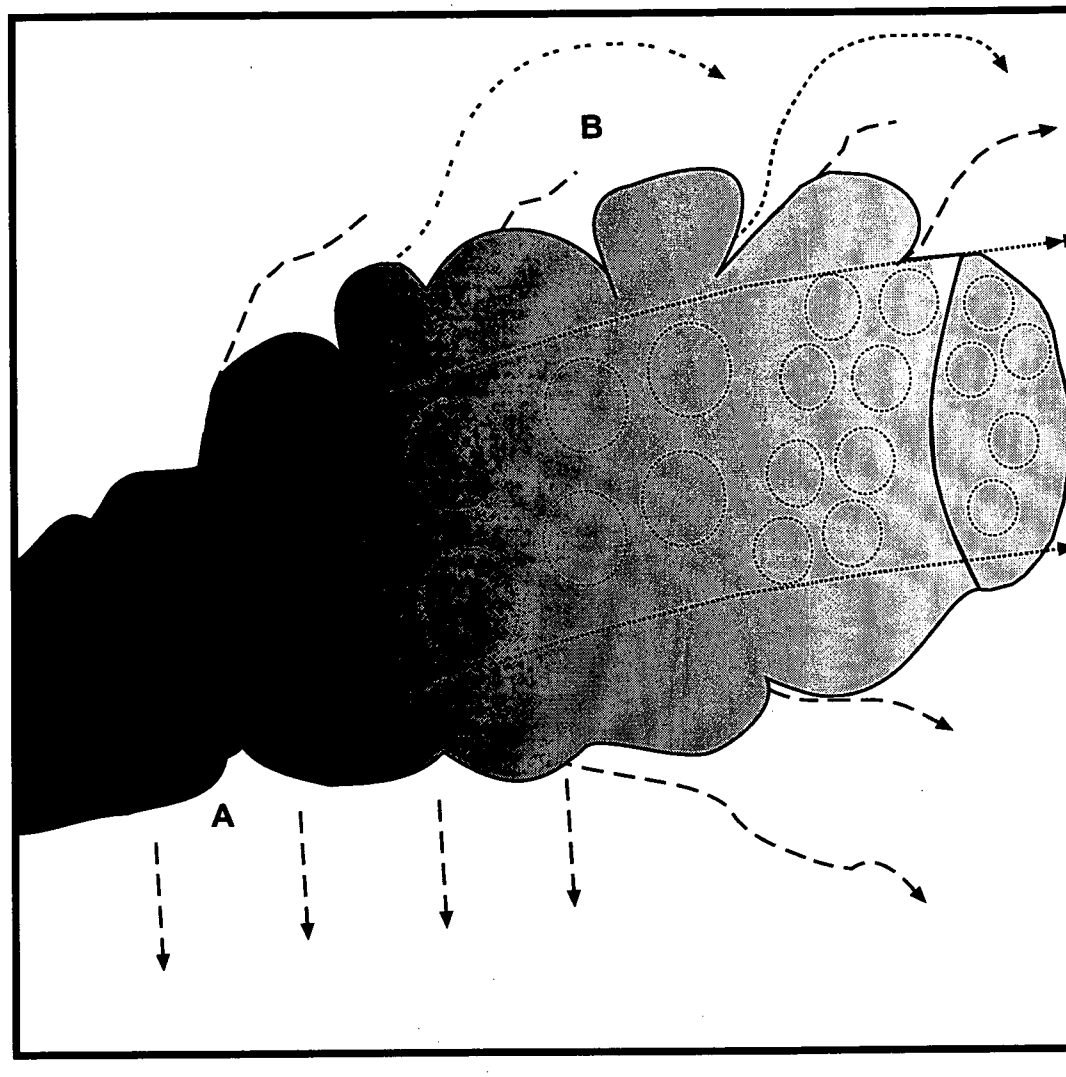

Figure 6.11 Model for observed shape variation in recovered Darwin glass **A)** As the turbulent expanding melt plume propagates outwards, volatile escape and kinetic energies disperse the melt that rapidly quenches and the glass fragments rain down. The irregular and ropy fragments quench rapidly from in the turbulent bulk melt jet. **B)** The least viscous, hot molten fragments are continuing to disperse from the bulk plume. These are transported as free melt blebs and surface tension shapes the fragments before complete cooling and deposition. Which splashform shapes are formed depends on the degree and direction of spinning by the molten glass fragments during transport. Increased time in aerial transport when molten promotes the development of splashform shapes and, as such, there is an increase in the proportion of splashform shapes, relative to irregular or ropy shapes with increasing distance from the crater.

and this unit has been re-classified as the Austral Creek Siltstone by Blissettt (1962, see Fig. 4.4B). The chemistry of the glass is consistent with a mixture of Keel Quartzite and pelite. As such, the observed increase in the proportion of black glass with increasing distance from the crater is interpreted to reflect the depth of excavation from the target stratigraphy. The black glass deposited distal to the crater is interpreted to have been derived from melting of pelitic regions in the Keel Quartzite that is the uppermost formation in the target rock stratigraphy. This is consistent with theoretical and geochemical studies that, as stated above, indicate that the uppermost target stratigraphy is ejected to farthest distances from the crater. This is also consistent with the preferred interpretation as to the stratigraphic affinity of Group 2 glass based on its geochemistry, as discussed during comparisons of glass compositions with potential target rock compositions in section 5.4.2. Deriving black Group 2 glass from melt at the interface of the projectile and target rock surface is also consistent with the evidence for projectile contamination that is preferentially observed in some of these specimens (Melosh 1989, Chapter 5). Under this scenario, the prolonged transport of the black molten fragments, derived from the earliest stages of melting and ejection of the uppermost target rocks, explains the preference for the development of splashform shapes in the black glass. The lower viscosity of black melt is also interpreted to have promoted the development of splashform shapes, in contrast to the higher viscosity white melt that is almost always irregular in shape.

6.4 Summary

All of the observed trends in glass size, shape and colour distribution relative to distance from Darwin Crater have been related to the impact process. The described trends do not provide any inferences as to the projectile trajectory. Although the glass is distributed in a 270° arc around the crater, the absence of observed glass to the east can be related to non-preservation in that area. The ejection of melt is interpreted to have taken the form of a viscous and turbulent melt plume. Interaction of the plume with the atmosphere led to dispersal of melt and breakdown of the plume, leading to glass deposition across the strewn field. The size variation of recovered glass within the strewn field is consistent with ballistic ejection from Darwin Crater. This mechanism can explain how the glass is continuously distributed out to <20km from source with the largest fragments being deposited closest to the crater. Ballistic ejection is also consistent with the

observed decrease in the proportion of small glass fragments with increasing distance from the crater as these small fragments are rapidly slowed and deposited on interaction with the atmosphere. At all sites, size distribution trends show poor sorting and reflect the turbulent nature of melt ejection such that large and small glass fragments are deposited together after the breakdown of turbulent cells in the melt plume.

The most obvious physical trend is an increase in the proportion of black coloured and splashform shaped glass, relative to the other colours and shapes, with increasing distance from the crater. The control on the colour and shape trends observed is interpreted to be the depth of derivation from the target rock stratigraphy. The farthest distributed black glass reflects melting of an upper pelitic unit in the Keel Quartzite, and derivation of this glass from the projectile target interface also aids in explaining the evidence for preferential projectile contamination in some black Group 2 glass specimens. Here the prolonged transport of the black molten fragments explains the preference for the development of splashform shapes in the black glass. The lower viscosity of black melt is also interpreted to aid in the development of splashform shapes, in contrast to the higher viscosity white melt that is almost always irregular in shape.

Therefore, at this stage, attempts to falsify the hypothesis that "*the observed variations in the physical properties (abundance, size, shape, colour) of glass fragments recovered in situ can be related to distance and direction from the crater*" have failed and the crater appears further consistent with being the sole source of the glass.

6.5 Discussion

6.5.1 Explaining the high abundance and wide spread distribution of glass

In Chapter 2, it was shown that, relative to the size of the suspected source crater, Darwin glass is the most abundant and widely distributed ejected impact glass on Earth. It was also shown that the estimated volume of glass across the strewn field exceeds theoretical expectations of ejected melt volumes for a 1.2km crater. This is particularly unusual because at all other studied craters, and especially those in sedimentary rocks, modelled melt volumes based on energy scaling equations related to crater diameters, generally far exceed measured volumes (Grieve &

Cintala 1992, Chapter 1). This study has shown that the crater-fill stratigraphy is largely free of melt, and this would support the findings of Grieve & Cintala (1992) and Orphal et al. (1980) that although in small impacts a smaller volume of in-crater melt is produced, a greater proportion (all?) of this melt is ejected. This is also consistent with field observations at most small craters on Earth, where ejecta may be found around the crater, but large volumes of melt are rarely reported from within the crater-fill stratigraphy. However, at most small craters ejecta is only found scattered close (<5 crater radii) to the source. To validate the interpretations above and further define the relationship between the glass and crater, this anomalously high abundance and wide distribution of ejected glass requires explanation.

The structure is formed entirely in sedimentary rocks and theoretical studies indicate that the volumes of target material shocked to pressures sufficient for melting do not differ significantly between sedimentary and crystalline rocks (Kieffer & Simonds 1980). Huginot curves suggest more melt should be produced by impact onto sedimentary rocks compared to crystalline rocks (Kieffer & Simonds 1980), and this is attributed to the higher porosity of sedimentary rocks, which are predicted to promote melting (Kieffer & Simonds 1980, Melosh 1989). As such, impacts into sedimentary rocks are expected to produce equivalent or greater volumes of melt than impacts into crystalline rocks (Kieffer & Simonds 1980, Osinksi et al. 2003a). However, this is not observed in most field investigations that show craters formed in thick sedimentary cover are associated with less melt than craters in crystalline targets (Kieffer & Simonds 1980, Grieve & Cintala 1992), although this may change with increasing recognition of sedimentary melts within craters (e.g. Osinski et al. 2003b). Kieffer & Simonds (1980) explain this as relating to the increased volatile contents of typical sedimentary, relative to crystalline, rocks that they suggest promotes an unusually wide dispersal of melt, and inhibits the development of coherent in-crater melt bodies.

The reason theoretical predictions of melt generation in sedimentary rocks exceed observed abundances is also likely to reflect the fact that most sedimentary rocks have undergone at least some metamorphism that will greatly reduce porosity even during very low-grade deformation. Such metamorphism will also significantly reduce the volatile contents of the target rocks, thereby removing a potential mechanism for promoting melt dispersal that may have resulted in increased melt ejection efficiency, and a widespread distribution of ejecta from the crater. This is certainly the case at Darwin Crater where the pelites have been subjected to

greenschist facies metamorphism and based on ignition loss totals from XRF analysis contain on average about only 6% volatiles. Quartzite is also typically expected to have a very low porosity due to extensive cementation. As such, the fact that the target stratigraphy is entirely sedimentary does not appear to explain the high abundance and wide distribution of ejected glass because the porosity and volatile contents of these target rocks are both relatively low.

6.5.1a Enhanced target rock volatility induced by interactions with water

The most explosive volcanic eruptions are phreomagmatic; that is those that involve the interaction of ascending magma with ground/sea waters (Fisher & Schmincke 1984). The addition of water to an ascending melt, of any composition, greatly increases volatility and generates far higher energy eruptive explosions in comparison to the eruption of a melt of identical composition in the absence of water (Zimanowski *et al.* 1986; Kurszlaukis et al. 1998). Underground nuclear explosions also indicate a larger cavity excavation in rocks with high water contents (Butkovich 1971). Theoretical studies of large impact events indicate that an impact onto ice can produce an order of magnitude more melt+vapor than for any other terrestrial material considered (Pierazzo et al. 1997). The fact that tektites and impact glasses are effectively 'dry' presents no challenge to the formation of melt from a 'wet' target because water is easily lost from tektite melt under impact conditions (Melosh & Artemieva 2004). The question becomes *"can ground water induced volatility explain the extremely efficient ejection of glass from Darwin Crater?"* To answer this question, the hydrologic setting of the study site at the time of the impact must be understood.

Throughout the Quaternary in Tasmania, westerly air streams have dominated the climatic regime, as is the case today. These wet westerly air streams deliver orographic rainfall preferentially to the west coast creating a distinct rain shadow effect that extends across the midlands and into the east of the state. Today for example, the study site receives around 3500mm of rain per year as compared to Hobart in the east with around 500mm of rain per year. The Pleistocene climate of southeast Australia is characterised by cycles of rapid glacial advance and retreat (interglacials) (Williams et al. 1993). In Tasmania, and in very general terms, this has involved the progressive replacement of closed canopy rainforest that usually includes *Nothofagus,* by drier and more open "dry" rainforest and schlerophyll forest dominated by Casurinaceae and/or Myrtacea through to herb dominated communities (Macphail et al. 1993). This progression is interpreted to be controlled

by precipitation (e.g. Trusswell & Harris 1982; Kershaw 1988; Macphail & Trusswell 1989). High-resolution climate reconstructions suggest that, at the time of impact (816±7ka), southeast Australia was leaving an interglacial period and about to plunge into a glacial that peaked at ca.800ka (Howard et al. 2001). In this study palynomorphs examined in slides of samples recovered from the lowest laminated lake sediments in the crater stratigraphy, from between 55-60m (DDH1), are dominated by tree ferns (*Cyatheaceae sp.*), followed by grasses, daisies (*Asteraceae sp.*) and heath (*Epacridaceae sp.*), along with conifers (e.g. *Nothofagus gunnii; Nothofagus cunninghami, Lastrobus Franklinii*), wattles (*Acacia sp.*), Sheoak (*Casuarina sp.*) and rare Waratah (*Proteaceae sp.*). McPhail et al. (1993) reported similar assemblages from poorly defined sample locations between 50-60 metres depth in the Darwin Crater drill core (DDH1).

The abundant ferns, grasses and daisies are interpreted to best represent the immediate environment surrounding the crater as the less common conifer and shrub pollen may have been transported by aeolian processes. The daisies, acacia, casuarina, waratah and conifers are more consistent with interglacial conditions. The common presence of *Nothofagus sp* in the recovered samples indicates water was abundant and this is a common tree around the crater today. The rare presence of saltbush (*Chenopodiaceae sp.*) is an important indicator of glacial conditions. These palynomorphs suggest that the climate shortly after the time of impact was in transition between interglacial and glacial maxima, with the glacial peaking at ca. 800ka. The high abundance of ferns is consistent with many other studies that show that ferns are the first species to recover following a major disturbance event (e.g. Wolf & Upchurch 1986).

Based on this palynological data and models of Howard et al. (2001), the climate and vegetation at the time of impact is likely to have been similar to, but somewhat cooler and drier than today. It is estimated that during the last glacial maximum at 18ka precipitation in the southern hemisphere was perhaps 40-50% of that measured today, and as a result the proliferation of rainforest communities appears to have been significantly restricted in Tasmania. At older glacial maxima, rainforest communities appear to have been far more pronounced in Tasmania and it can be inferred that these older glacial maxima were significantly wetter than at 18ka. Significantly, the genetic characteristics of modern Tasmanian rainforest flora require that valleys such as the Andrew River valley and the valley that hosts the crater have always been refugia for rainforest communities, indicating wet

conditions have predominated at low altitudes throughout the Pleistocene (Kirkpatrick & Fowler 1998). As the time of impact is considered to have been during a transitional period, precipitation is likely to have significantly exceeded the glacial maximum values and as such it is suggested that at the time of impact the area received perhaps 60-80% of the current annual rainfall (e.g. around 2-2.5 metres per year). As with the modern climate, the majority of this is likely to have fallen in winter.

The particular setting of Darwin Crater, being in a narrow steep valley, encourages a high volume of recharge from surface and infiltrating meteoric waters and at the crater floor and along the valley floor, the current ground surface is a swamp. The common faults that cross cut the crater and its host valley are also likely to aid the infiltration of meteoric waters and also promote recharge. Major examples of such faults are shown on the crater geology map (see Fig. 4.4A). Where outcrop exists, minor faults are observed in all rocks across the strewn field, and the Eldon Group is known to be faulted from exposures across the west coast (Gill & Banks 1950; Blissett 1962; Gee et al. 1969; Brown 1986). The geophysical surveys also indicate a faulted basement stratigraphy (Fudali & Ford 1979, Richardson 1984). Today, especially in winter, but also during prolonged rain periods that occur in all seasons, ground waters aided by fracture and fault pathways have saturated country rocks cropping out along the crater access track and in many cases the groundwater is seeping out at the surface or is inferred to be located at very shallow depths. Even if it is conservatively estimated that only 60% of the current 3600mm annual rainfall (e.g. ~2000mm/year) was received at the crater at the time of the impact, and given the topographic setting, abundant ground water is still expected to be located at shallow depths and easily within the depth of impact excavation and melting. If the impact took place in winter or during/after a rainy period, conditions could be expected to be very similar to those during rainy periods today with seeping groundwater and sheet flow across bedrock.

An independent line of evidence that groundwater was very near to, or at, the ground surface at the time of the impact comes from the intriguing Tasmanian Burrowing Crayfish, *Parastoacides sp.* (Fig. 6.12). *Parastacoides* live in burrows on buttongrass plains and in rainforests across west and southwest Tasmania. The crayfish can only survive in burrows associated with standing water or away from standing water but in contact with the water table. Recent work by Hansen & Smolenski (2002) and Hansen & Richardson (2002) has defined several new

species of *Parastacoides* with very limited geographical ranges scattered across the southwest. Genetic characterisation of the crayfish species indicates that this is only possible if these isolated species have survived throughout the Pleistocene period in southwest and western Tasmania (Hansen & Smolenski 2002, Hansen & Richardson 2002). Also associated with the crayfish are a host of other endemic species of crustaceans that are specialised for living in pools of water in the burrows (Hansen & Richardson 2002). The clear implication of this work is that deep waterlogged soils in contact with the water table have existed continuously throughout the Pleistocene at several locations in the southwest and west of Tasmania (Hansen & Smolenski 2002, Hansen & Richardson 2002). In particular, the area around Darwin Crater is the hot spot of genetic diversity suggesting a particularly long history of waterlogged conditions in this region (Hansen & Richardson 2002).

This abundant surface water is expected to produce a volatile charged target stratigraphy at the time of impact. This volatile enhancement is promoted by infiltration of meteoric fluids along faults and fractures that are common in the Eldon Group (Gill & Banks 1950; Blissett 1962; Gee et al. 1969; Ford & Fudali 1979; Brown 1986; see Fig. 4.4A). The surface swamps are also likely to have been an important source of volatiles because ejected glasses are believed to form from the upper most target rocks impacted. There is also the potential for porous sandstone layers to exist within the Eldon Group and, if present, these are likely to be saturated by H_2O. Based on theoretical studies of impact melt production and cratering (e.g. Kieffer & Simonds 1980, Pierazzo et al. 1997), this extreme volatile enrichment of the target stratigraphy would be expected to promote an increased magnitude explosion and exceptionally efficient dispersal and ejection of melt as the volatiles escape. This volatile enhancement aids the explosion and dispersal and ejection of glass. The water is readily lost from the melt during the impact (Melosh & Artemieva 2004), hence the low H_2O content in the glass. This model of meteoric water infiltration enhanced target rock volatility is the most parsimonious explanation for the high abundance and wide distribution of Darwin glass and highlights the dynamic control of the receiving environment on the nature of the impact process.

Figure 6.12 Tasmanian burrowing crayfish *(Parastacoides tasmanicus tasmanicus)*. Scale bar = 5cm. Photograph: Frutiger (2004).

6.5.2 Classification of Darwin glass

The characteristic features of tektites and impact glasses were described in Chapter 1 and are summarised in table 6.5 of Koeberl (1994). In an attempt to classify Darwin glass, the observed characteristics of the glass across the strewn field are compared to each of the criteria in the table and key observations are described in an additional column.

6.5.2a Interpretation

Darwin glass does not fulfil the requirements to be classified as a tektite *senso stricto*. The characteristics of Darwin glass that preclude its classification as a tektite relate primarily to the large degree of chemical heterogeneity, its relatively high heavy noble gas and H_2O contents, and the large degree of meteoritic enrichment present in some samples. The rarity of mineral inclusions in Darwin glass is more typical of tektites. The wide distribution of splashform shapes relative to the craters size is also more similar to tektites than to impact glasses except for the fact that the glass is present directly at the source crater and the strewn field is generally far smaller than at the four known tektite strewn fields, or the K-T boundary glass/tektite strewn field. The absence of ablated forms and the general predominance of irregular morphologies over splashform shapes is more typical of impact glasses than of tektites, although ablated forms are rare in all but the Australasian strewn field.

Therefore, Darwin glass must be classified as an impact glass that exists in a strewn field. This strewn field is tiny (~410 Km^2) compared to tektite strewn fields, but the Darwin Impact Glass Strewn Field is one of the largest impact glass strewn fields after the Libyan Desert Glass Strewn Field that it is estimated covers up to 6500km^2 (Koeberl et al. 2003). It is worth noting that the observed splashform and irregular morphologies of the Darwin glass fragments, along with the presence of mini-glasses continuously distributed from the crater, is very similar to what is observed in Zhamanshin glass, from the 13km diameter Zhamanshin Crater, Kazakhstan; although here the glass is less abundant and more proximally distributed (Masaitis et. al 1984).

	Tektites	Impact Glasses	Darwin glass
Occurrence in strewn field	Yes	No	Exists in a small strewn field that spans over 410km^2 across West Tasmania. Glass may be found up to 20 crater radii from source.
Source crater known	Yes/no	Yes	All available evidence demands that the 1.2km Darwin Crater is the sole source of glasses in the strewn field.
Occurrence directly at crater	No	Yes	Found at the source crater.
Target rocks	Surface rocks	Deeper lithologies	Formed from the melting and ejection of surface quartzites and shales.
Chemical homogeneity	Large-scale homogeniety (100mm-mm)	Usually inhomogenous	Most samples are incredibly heterogeneous and were classified chemically as Group 1 glass. These have a range in SiO_2 from 80-93% and an average of 84%. Group 2 glass is far more homogenous; these have a lower average SiO_2 composition (81%) and a smaller range 76-84%. Grid surveys on individual samples of Group 2 glass support the greater degree of mm-mm scale homogeneity in these glasses relative to Group 1 glass. However, these remain more heterogenous than is typical of tektites.
Water content (wt%)	0.002-0.02	0.02-0.07	The H_2O content is within the range of 0.01-0.06 wt% (Taylor & Solomon 1962).
Mineral inclusions (includes partially digested quartz)	Rare	Abundant	With the exception of lechatelierite glass, mineral inclusions are very rare and have never been observed in thin section. Inclusions are known only from X-Ray Diffraction analyses and are limited to rare coesite (Reid and Cohen 1962), tourmaline and quartz (Smith and Hey 1965).
Shape	Moslty regular, spherically and radially symmetric	Mostly irregular	Shape is mostly characterised by layered, contorted irregular forms considered typical of proximal impact glasses, except that these are found up to about 20 crater radii from the source. There are also regular more symmetric splash form shapes considered typical of tektites present in the strewn field and these overlap the range in the distribution of the irregular shapes.
Ablation shapes	Yes, but rare outside of Australasian strewn field.	No	There are no known ablated shapes as the impact event was too small to produce the energy required eject glasses out of the Earths atmosphere, thereby preventing ablation shapes forming on atmospheric re-entry. This is typical of impact glasses.
Meteoritic component (abundance wt%)	<0.02	0.02-0.5	The inferred meteoritc component 6-9% in Darwin glass may be up to 9% in some samples; well beyond the range expected in tektites.
Heavy Noble gas content (Ar, Kr, Xe)	Low	High	High noble gas content. For example He in Darwin glass is typically present in concentrations of around to $3*10^{-9}$g/g (Matsuda & Yajima, 1989), compared to around $4.5*10^{-12}$g/g in an Australite tektite.

Table 6.5 Tektites vs. Impact glasses vs. Darwin glass. This table is based on Koeberl (1994) and compares the characteristic features of Darwin glass to the features considered diagnostic of impact glasses and tektites. Darwin glass blurs this distinction, but on the basis of an heterogenous chemistry must be considered an impact glass.

6.5.3 Where are the large masses?

When conducting excavations for glass one of the enduring research questions, and the motivator of many fossickers, remains where are the large glass masses such as that found by Ford? The answer is likely to relate to more than simply the rugged terrain preventing discoveries, as many thousands of hours have been spent fossicking over the last 100 years, which demonstrate that small glass fragments are abundant.

6.5.3a Darwin glass and Tasmanian Aborigines

In the last 20 years Darwin glass flakes have been found in the densely forested limestone valleys of southwest Tasmania (McNiven 1994, Fig. 6.13), well beyond the natural range of the glass distribution as defined in this study. Glass fragments have also been found on button grass plains at Trial Harbour, beyond the northern limit of the field and another find at Lune River is the southern most reported find of Darwin glass (Nigel Ellis, Personal Communication in 2004). Predominantly, the glass appears to have been used to create thumbnail scrapers, and the evidence suggests that the glass was one of the most sought after materials for tool making, along with chert and quartzite (Jones 1990, McNiven 1994). The scrapers were mainly used in woodworking, including cutting branches and other vegetation, and for carving and planing wooden implements (Jones 1990, McNiven 1994). Sometimes the scrapers also appear to have been hafted onto wooden implements greatly increasing the versatility of these scrapers, which were undoubtedly extremely important tools (McNiven 1994). There was a trend for a dramatic increase in the use of Darwin glass, compared to all other materials, for thumb scraper production by Aborigines after the last glacial maximum at ca. 18ka (McNiven 1994).

The process of flaking glass to produce thumbnail scrapers requires an initial or 'core' fragment, typically around 10cm in height and width. This is held in one hand and chipped away at with a larger rock held in the second hand (e.g. Wright 1977). This process is far from trivial and requires a high degree of skill to produce useable scrapers, obviously this would be far easier given a large 'core' fragment such as collected by Ford and more difficult with the smaller fragments collected in this study. It is suggested that local tribes travelled to the crater site and preferentially collected the largest glass masses for use in making thumb scrapers. The explosion

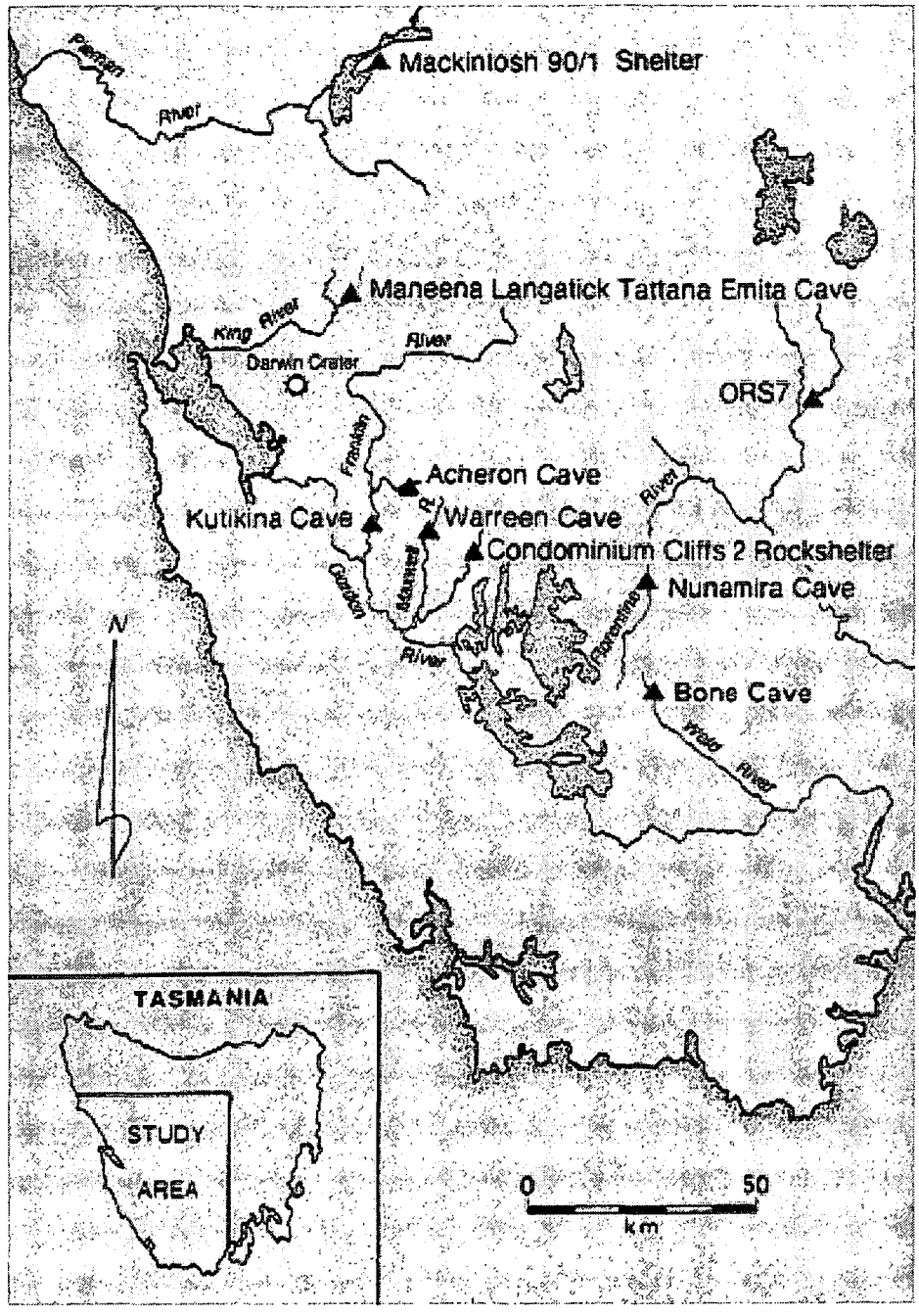

Figure 6.13 Sites where worked Darwin glass flakes have been found

Source: McNiven (1994, p.2).

of Darwin glass tool use after the last glacial maximum at 18ka probably relates to stress on rainforest communities during the glacial maximum that lead to the retreat of rainforest species. This resulted in the opening up of vegetation around the crater thereby allowing for far easier fossicking and an increased discovery rate of large glass masses.

That the glass can be found at locations almost 200km apart, well outside the strewn field, indicates that the glass was transported and was traded between tribes. This leads to discussion of the so-called Mt Macedon glass. In 1920, shortly after fresh excavations to construct a new reservoir at Mt Macedon, Woodend, Victoria, Mr F. H. McKGrant and his son discovered 2 glass fragments exposed on a small area stripped of vegetation. These glass fragments, called Mt Macedon Glass, have a morphology, chemical composition and age that is indistinguishable from samples of Darwin glass (Chapman et al. 1967), and there is no doubt that these are fragments of Darwin glass. No other fragments have ever been found in Victoria or mainland Australia. There is debate as to whether or not these pieces of Darwin glass, catalogued as Mt Macedon glass, were in fact found in the field at Mt Macedon, or if these are simply mislabelled samples of Darwin glass collected from Tasmania. On examining the records of the Melbourne University Museum, George Baker states that:

" The two specimens of glass were among a collection of Macedon-Woodend rock and mineral specimens collected by Mr. F.H. McK. Grant and his son while they lived in Woodend. Grant Sr. was the pharmaceutical chemist in Woodend and a keen collector of the rocks and minerals of the district...His son was employed on the water conservation area for a time, and it was he who collected the specimens of Macedon glass from near the top reservoir. This was confirmed by Grant Sr. who brought his collection to the University and donated it to the geology department with full notations. ***There therefore seems to be no valid reason for doubting the record of where these specimens were found, particularly as all the rest of Grant's collection was accurately labelled."*** (Dr George Baker, Personal Communication in Chapman et al. 1967, pp:1602, emphasis added)

In 1945, twenty five years after the initial discovery by Grant Jr., Baker and his wife returned to the find locality for a follow up search, without success. Baker's observations are critical:

"Only a small area stripped of vegetation was exposed when we visited the site a quarter of a century after the finding in 1920 of the two pieces of natural glass. This area was intensively searched by two people for about two hours. We also closely scrutinized small, scattered bare patches still evident on the reservoir banks, but much of these were vegetation-covered after the 25 years lapse of time.

The whole point is this – other pieces of glass could still be in the area, but dense vegetation and soil cover would mask them completely. Areas on which to search are now very limited compared to the conditions existing when Grant Jr. found the specimens shortly after the time of the construction of the reservoir." (Dr George Baker, Personal Communication in Chapman et al. p. 1602; emphasis added).

In their discussion, Chapman et al. (1967) find no definitive basis for determining if these two specimens of glass represent a separate natural occurrence in Victoria of Darwin glass, or mislabelled pieces of Darwin glass from Tasmania. They discount the possibility that the glass specimens were pieces of Darwin glass "*somehow*" transported to Victoria, However, at the time of writing it was unknown that Darwin glass had been sought after, utilized, transported and traded by Tasmanian Aborigines. If the reported finds in Victoria are accurate, and as Baker stated there seems no reason to doubt this, the possibility that these glass fragments were transported to mainland Australia by Tasmanian Aborigines must be raised.

Here it may be suggested that during the last glacial maximum, tribes crossed Bass Strait via the land bridge that was present at ca. 18ka (Williams et al. 1993, Fig. 6.14), taking with them the glass fragments later found at Mt Macedon some 560km from Darwin Crater. A challenge to this hypothesis is that the recovered fragments do not show any evidence for having being sculpted and the size of the fragments is too small for these to have been 'raw materials'; this would imply that the fragments were not being transported for utilitarian purposes and this is unusual. Similarly, the fragments found on button grass at Trial Harbour and Lune River show no evidence of having been worked or chipped from larger fragments. One possibility is that the glass fragments were transported and traded as a packet (e.g. lots of pieces wrapped in a bark package), and on receipt of the package the new owners sorted through the fragments and discarded the smallest pieces.

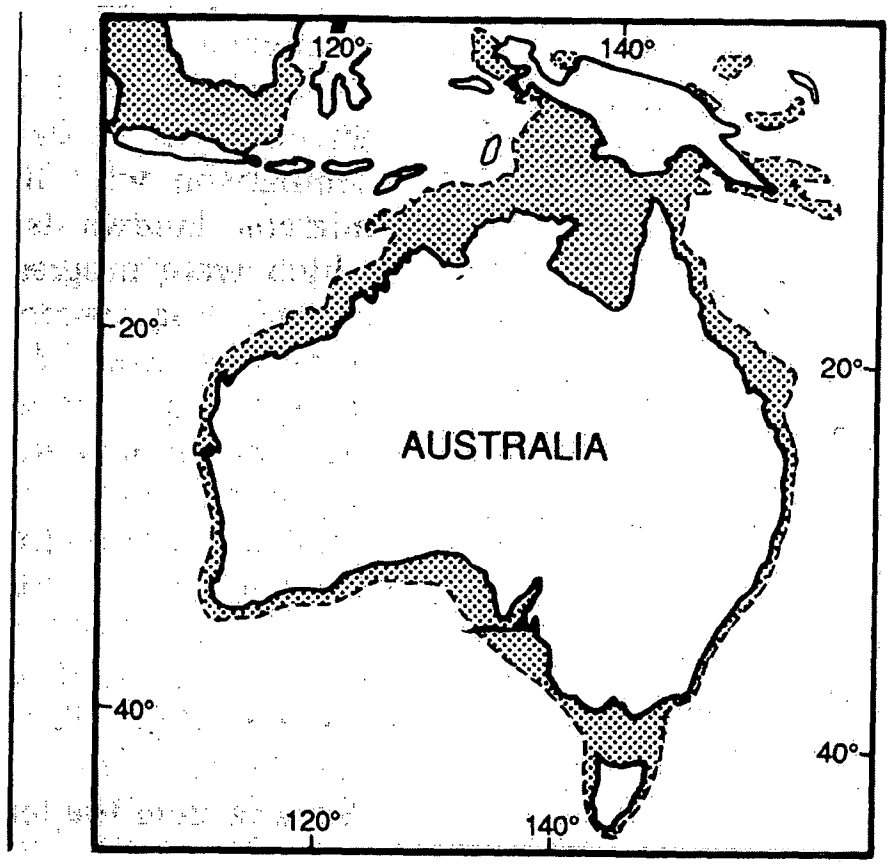

Figure 6.14 Approximate extent of the Australian and Papua New Guinea land bridges at the last glacial maximum (21-17ka).
Source: Williams et al. (1993, p.81).

Perhaps the answer also lies in the perceived 'magical' properties of glass and crystals to indigenous tribes. This is most evident in the status of Australite button tektites amongst some Aboriginal tribes who consider them 'sacred stones' with a variety of perceived positive or deleterious powers. Essentially the linking theme in the spiritual applications of tektites in Australian Aboriginal Culture appears to be an association with telepathic communications -"pointing the bone"*. As such, non-worked fragments of glass may also have been transported for 'spiritual purposes'. The potential implications of this hypothesis are highly significant to the current understanding of early Australian history, as migration across the Bass Strait land bridge from Tasmania to mainland Australia has not been demonstrated elsewhere. To test the hypothesis, collections of stone implements such as those at the Victorian Museum, must be searched for Darwin glass fragments because the cataloguers would not have been familiar with Darwin glass and may have thought that such tools were composed of volcanic glass or molten bottle glass from after European invasion. If Darwin glass is found, the hypothesis will be validated.

6.6 Conclusion

Every attempt to falsify the hypothesis that "*the observed variations in the physical properties (abundance, size, shape, colour) of glass fragments recovered in situ can be related to distance and direction from the crater*" has failed. There is a clear decrease in the abundance of glass with increasing distances from the crater. The size distribution data in recovered glass is consistent with ballistic ejection from the crater. As such the largest recovered fragments are found deposited closest to the source crater. A decrease in the proportion of fine glass fragments away from the crater is also observed because these fragments are rapidly slowed and deposited close to source on interaction with the atmosphere. At all sites, size distribution data for the recovered glass fragments is strongly skewed towards outlying large fragments and this poor sorting indicates that the ballistic ejection of melt from the crater was highly turbulent. On the break down of turbulent cells, large and small glass fragments are deposited together.

---

* I am being necessarily general in this description because as a white scientist I do not feel that it would be either appropriate or accurate for me to attempt describe the significance of these Ceremonies to Aboriginal Culture.

The most obvious physical trend is an increase in the proportion of black coloured and splashform shaped glass, relative to the other colours and shapes, with increasing distance from the crater. The control on the observed colour and shape trends is interpreted to be the depth of excavation depth. The farthest distributed black glass is interpreted to reflect melting of upper pelitic zones in the Keel Quartzite. Derivation of this black glass from the projectile target interface is consistent with the evidence for preferential projectile contamination in some black Group 2 glass specimens. Prolonged transport of the black molten fragments is interpreted to explain the preference for the development of splashform shapes in the black glass. The lower viscosity of black melt is also considered to have aided in the development of splashform shapes, in contrast to the higher viscosity white melt that is almost always irregular in shape.

There is no evidence for any primary asymmetry in the glass distribution. This suggests the impact was not significantly oblique and prevents potential inferences as to the trajectory the projectile.

An outstanding feature of the glass is its extremely wide distribution and high abundance relative to all other known small craters. It is hypothesised that ground water saturation of the country rocks produced a highly volatile target stratigraphy at the time of the impact. As predicted by the theoretical models, this volatile enhancement increases the explosiveness of the impact and the dispersal and ejection of impact melt to form the abundant ejected glass fragments. This interaction between terrestrial processes within the target environment and the projectile highlights the dynamic nature of impact events on Earth.

Given the constraints placed on the dimensions of the strewn field in this study, it is certain that Darwin glass was widely transported by Aborigines across west and south Tasmania. The explosion in the use of Darwin glass after ca. 18ka is explained as relating to climatic stresses at the last glacial maximum reducing the density of vegetation cover at the crater and allowing for increased recovery of large glass masses for use in the production of thumb scrapers. This selective recovery of the large fragments by Aborigines, and the current density of forest cover, explains the absence of large glass finds in this study. There seems no reason at all to doubt the validity of the reported finds of Darwin glass fragments from Mt Macedon in Victoria. With increased recognition of the significance of Darwin glass to Tasmanian Aborigines and given the presence of a land bridge at 18ka, the possibility that the controversial Mt Macedon glass was transported with travelling tribes must be seriously considered.

Chapter 7

Conclusions and implications

The aim of this study was to determine the *origin of Darwin glass*. Investigations to fulfill this aim first involved collection of *in situ* glass fragments from sites across the strewn field. The physical properties of recovered glass fragments were described and sub-populations defined that encompass the range of shape and colour variations observed in the collection. This study has also involved the field occurrences of Darwin glass (e.g. the stratigraphy of glass deposits and the dimensions of the strewn field), and estimated the abundance of glass (Chapter 2). Geochemical systematics in Darwin glass were investigated by SEM, LA-ICPMS, solution ICPMS and XRF. Multivariate statistical analyses were used to define end member compositions and chemical sub-populations in the glass, as well as to explore the co-variations in major and trace element concentrations (Chapter 3). The geology of Darwin Crater was also investigated and, for the first time, the crater-fill stratigraphy described and interpreted from drill core samples (Chapter 4). Geochemical and isotopic analyses (Sr, Nd) were used to test the relationship between Darwin glass and the suspected target rocks, namely the Eldon Group sampled from around Darwin Crater, and from drill core of the crater-fill. High-resolution LA-ICPMS analyses of selected glass samples were used in an attempt to identify the nature of the impactor, and to explore the transition metal and highly-siderophile element (HSE) chemistry of the glass (Chapter 5). Systematic geographic variations in the abundance and physical properties of *in situ* recovered glasses, relative to distance from the crater, have also been described (Chapter 6).

Key features of Darwin glass and crater revealed by this investigation are contained in tables 7.1 and 7.2, respectively. In this concluding chapter, these features are integrated into a summary of the origin of the glass as determined by this study. The implications of these data to our understanding of tektite and impact glass genesis is discussed, along with contentious issues in the understanding of the origin of Darwin glass, and recommendations for future work that is considered necessary in the continued attempt to further understand this enigmatic substance.

Colour	White (4%), Light green (31%), Dark green (52%), Black (11%)
Shape	Irregular (73%), ropy (19%), elongate (0.7%), droplet (6%), spheroid (0.5%)
Abundance	At least 11250m^3 ejected glass (estimate based on a 50km^2 area surrounding the crater). Relative to the size of the crater, this is the most abundant impact glass known on Earth.
Distribution	Exists in a small strewn field that spans over 410km^2 across West Tasmania. Glass may be found out to at least 20 crater radii from source.
Composition (trace elements in ppm)	**Group 1 glass:** SiO_2 (80.62 – 93.9%), Al_2O_3 (3.14 – 10.6%), TiO_2 (0.2 – 0.76%), FeO (0.8 – 4.23%), MgO (0.25 – 2.31%), K_2O (0.7 – 2.7%), Rb (33.2-109.2), Zr (54.1-750.9), Sr (4.9-27.8), Ba (116.7-457.1), Cr (19.5-204.6), Co (0.0-33.9), and Ni (3.0-492.8). **Group 2 glass:** SiO_2 (76.4-84.5%), Al_2O_3 (6.4-11.5%), TiO_2 (0.5-0.80%), FeO (1.8-5.8%), MgO (1.1-4.0%), K_2O (1.4-2.7%), Rb (56.6-109.2), Zr (286.6-553.1), Sr(10.9-20.4), Ba (210.7-427.3), Cr (67.6-260.4), Co (19.4-56.5), and Ni (117.4-917.7)
Target rocks (trace elements in ppm) **Stratigraphic column** Top Keel Quartzite + interbedded pelite Amber Slate Crotty Quartzite	**Siluro-Devonian Eldon Group** quartzite (Keel and Crotty Quartzite) and slate (Amber Slate). **Average Keel Quartzite:** SiO_2 (90.1%), Al_2O_3 (5.4%), TiO_2 (0.5%), FeO (0.4%), MgO (0.3%), K_2O (1.4%), Rb (62.8), Zr (309.8), Sr (8.7), Ba (232.5). Cr (54.5), Co (1.4), and Ni (7.4) **Average Amber Slate:** SiO_2 (75.4%), Al_2O_3 (11.8%), TiO_2 (0.7%), FeO (3.3%), MgO (0.01%), K_2O (3.4%), Rb (161.2), Zr (336.8), Sr(16.2), Ba (562). Cr (85.39), Co (3.6), and Ni (21.5) **Average Crotty Quartzite:** SiO_2 (94.6%), Al_2O_3 (2.8%), TiO_2 (0.2%), FeO (0.3%), MgO (0.1%), K_2O (0.9%), Rb (36.1), Zr (171.2), Sr(10.2), Ba (124.5). Cr (80.8), Co (5.1), and Ni (4.3)
Chemical relationship to target rocks	Mixing models with average target rock composition result only in significant errors for **Ni, Co, MgO, Cr and FeO.** For the remaining elements. the glass composition is successfully modelled using the following mixtures: **Group 1** = 43% Amber Slate, 27% Keel Quartzite, and 30% Crotty Quartzite **Group 2** = 66% Amber Slate, 4% Keel Quartzite, and 30% Crotty Quartzite Slate proportions are most significant as the numerical distinction between Keel and Crotty Quartzite is poorly constrained. Slate proportions are largely interpreted as representing contributions from pelitic units associated with he Keel Quartzite that is the upper most unit in the target rock stratigraphy.
Meteoritic component	Some Group 2 glass has a transition metal composition that can only be explained by mixing with a chondrite or chondrite-like projectile. Based on transition metals, the maximum contribution from the projectile is up to 9%, but there is no detectable meteoritic enrichment in highly siderophile elements (HSE)
Geographic trends in glass distribution relative to crater	With increasing distances from the crater the proportion of black glass increases relative to the other colours. White glass is found almost exclusively at the crater. With increasing distance from the crater the proportion of splashform (elongate, spheroid, droplet) shape glass increases relative to irregular shapes.

Table 7.1 Characteristic features of Darwin glass. These data are for *in situ* glass specimens recovered from across the strewn field and analysed in this study. In total the petrographic characteristics of more than 4000 samples was examined. More than 150 individual glass fragments were chemically analysed for major and trace element concentrations.

Location	42°18.39'S, 145° 39.41'E
Diameter	1.2km
Depth	~220m
Crater-fill stratigraphy	**Facies A:** Polymict clastic matrix supported breccia of angular quartz and country rock fragments (top) **Facies B:** Monomict matrix supported breccia of angular quartz (deformed quartzite) **Facies C:** Fractured, brecciated, deformed slate with minor quartzite
Crater-fill composition	**Average Crater-fill Facies A:** SiO_2 (74.8%), Al_2O_3 (9.6%), TiO_2 (0.6%), FeO (4.0%), MgO (0.96%), K_2O (2.8%), Rb (123.7), Zr (290.1), Sr(24.0), Ba (428.4). Cr (8.2), Co (<2), and Ni (5.7) **Average Crater-fill Facies B and C:** SiO_2 (70.5%), Al_2O_3 (11.3%), TiO_2 (0.68%), FeO (6.2%), MgO (0.97%), K_2O (3.2%), Rb (147.8), Zr (319.9), Sr(12.9), Ba (459.4). Cr (90.6), Co (10.7), and Ni (42.7)
Evidence for shock metamorphism	The degree of deformation observed in crater-fill samples is well beyond the regional metamorphic grade of the target rocks. Quartz grains in the crater-fill samples are angular, and typically contain multiple (>3) fractures. The most deformed quartz grains have sub-planar fractures that define zones of alternating extinction in cross-polarised light (XPL). In contrast, surface Eldon Group (target rock) samples from around the crater are non-deformed. However, diagnostic evidence for impact induced shock metamorphism (eg. PDF bearing shocked quartz) has not been found.
In-crater melt	The evidence for in-crater melt is limited to isolated, small (<1cm) fragments of glass in Crater-fill facies A. As such, melt fragments represent <<1% of clasts and this low abundance prevents the facies from being classified as a true impact melt breccia.

Table 7.2 Characteristic features of Darwin Crater.

7.1 Summary of the impact event: *"the origin of Darwin glass"*

At 816 ± 7ka a meteorite between 20 and 50m in diameter (using scaling relationships in Melosh 1989) penetrated the atmosphere and impacted east of Mt Darwin, W Tasmania, Australia. The site was a synclinal valley within Siluro-Devonian (Eldon Group) slates and quartzite. In seconds, the explosion excavated an almost circular crater, Darwin Crater, up to 230m deep and 1.2km in diameter.

Based on energy scaling equations derived from nuclear explosion craters (Roddy & Shoemaker 1993), the formation of a 1.2km crater will be associated with an explosive release of around 20Mt of energy. This would equate to a ~135kPa (10PSI) blast wave at a radial distance of 20km (Glasstone & Dolan 1977). The effects of blast waves at these pressures are well documented, and at ~135kPa correspond to a short burst of wind over 800km/hr, destroying all forest and most life. Topographic effects, including deflection and channeling of blast winds produce locally variable damage across the receiving environment (Glasstone & Dolan 1977). As such, the blast wave is expected to have been channeled northwards along the host valley towards the peaks of Mt Jukes above modern Lake Burbury, and southwards down the Andrew River valley. In the east and west directions the blast is expected to have been ramped vertically up the narrow valley ramparts, thus the environmental destruction is likely to have been more limited in extent in these directions.

During earliest stages of crater excavation, the upper target rocks were molten before being ejected from the expanding cavity in a turbulent plume. Glass fragments (rarely exceeding 1kg size) rained down over more than 400km^2 of western Tasmania - *the Darwin glass strewn field*. The glass is predominantly dark to light green in colour, irregular and contorted in shape, and parallel flow layering is typical. This irregular morphological character is typical of proximal impact glasses, and some specimens of Darwin glass bear a superficial resemblance to layered tektites in the Australasian field.

Irregular and ropy glasses are interpreted to have formed from the most viscous melt that was being stretched and twisted, while rapidly cooling as it was ejected from the crater, probably along with unmelted ejecta. During transport, fluid fragments detached from the bulk melt, that was probably a rapidly moving plume, and traveled through the atmosphere as isolated non-rotating fragments before landing fully solidified on the land surface. The most fluid of these fragments continued to

change in shape after leaving the bulk melt plume. However, the lack of significant rotation and rapid cooling did not allow significant shape alteration, leading to fragments with the most irregular contorted shapes. Other Darwin glass specimens have elongate, droplet and spheroidal shapes that have a superficial resemblance to splash form tektites. These shapes are related to the motion of small, very hot, low viscosity melt fragments passing through the atmosphere in free transport, rather than in a continuous melt plume. The control on the variation in shape is the degree of rotation or spinning when in transport, and also the viscosity of the molten fragment

The bulk average major element composition of Darwin glass is: SiO_2 (84.57%), Al_2O_3 (7.52%), TiO_2 (0.57%), FeO (2.55%), MgO (1.12%), K_2O (1.87%), CaO (0.06%), and Na_2O (0.05%). The glass is highly heterogeneous in its major element composition. SiO_2 is particularly variable and may range between 80 to 97% in a single sample. Inclusions of almost pure silica (lechatelierite) are also commonly found in the glass. FeO is the major control on the colour variation, and on the basis of major element composition, green glass is more heterogeneous than black glass. The trace element concentrations in Darwin glass are also highly variable, and particularly the transition elements Ni, Co and Cr. The <5mm spheroid, droplet, and elongate shaped miniglasses discovered in this study have an almost identical major element composition to the larger irregular glass fragments.

Despite the compositional heterogeneity across the Darwin glass sample, two populations can be defined. Group 1 is close to bulk average Darwin glass and is highly variable in composition. The ranges in major element composition in Group 1 glass are: SiO_2 (80.62 – 93.9%), Al_2O_3 (3.14 – 10.6%), TiO_2 (0.2 – 0.76%), FeO (0.8 – 4.23%), MgO (0.25 – 2.31%) and K_2O (0.7 – 2.7%). Group 1 glass is predominantly light green to dark green or white in colour. Group 2 glass has a lower average SiO_2 (81.16%) content, and a decreased range in SiO_2 (76.47 – 84.42) concentrations. Average Al_2O_3 (8.2%) in Group 2 glass is also greater than in Group 1 glass. Group 2 glass is significantly enriched in FeO (+ 1.53 %), MgO (+ 1.31 %) and Ni, Co and Cr relative to Group 1 Darwin glass. Group 2 glass is almost always black.

The trace element data for Darwin glass shows affinities with upper crustal sediments, including pronounced negative Eu anomalies ($Eu/Eu^* = 0.48 – 0.66$), and LREE enrichment ($La/Lu^* = 5.8 – 8.87$). In Group 1 glass, the end member compositions are close to average quartz arenite and post Archaean shale (PAS). Group 2 glass requires a source richer in FeO, MgO, Ni, Co and Cr than PAS. The

very high Ni requirements of this end-member are unlike those typical of sedimentary rocks and this was an important consideration in identification of the target rocks in western Tasmania. The other significant feature, revealed by the glass analyses, and demonstrated in the Eldon Group target rocks, is an absence of plagioclase feldspar, and very low Sr abundances.

All of the available geochemical data presented in this thesis are consistent with the Eldon Group rocks at Darwin Crater being the parent materials melted under impact conditions to form Darwin glass. Major elements in Group 1 glass are closest to Keel Quartzite. With a higher FeO content, major elements in Group 2 glass have concentrations more similar to Amber Slate. The trace element composition of the glass has affinities with both the Keel Quartzite (Ba, actinides, LREE) and Amber Slate (Sr, HREE plus Y), and this indicates that the glass groups represent mixtures of the slate and quartzite rather than discrete melting of individual units in the target rock stratigraphy. This is further supported by the Sr and Nd isotopes that indicate that the glass and target rocks belong to a single isotopic system, and in all isotopic evolution plots the glasses fall between average Amber Slate and average Keel Quartzite. The compositional heterogeneity in Darwin glass, and lechatelierite inclusions, indicate that this mixing of molten target rocks was rapid and incomplete. The glass chemistry, the presence of abundant vesicles, and the predominantly irregular shape of fragments, all indicate that the cooling was very rapid. There is no evidence for volatile fractionation being an important control on the glass compositions, and probably high-temperatures were too short-lived to allow this process to dominate, owing to the rapid and efficient ejection of melt.

Mixing calculations using average Eldon Group compositions successfully model the glass compositions and support the greater affinity of Group 2 glass with Amber Slate and Group 1 glass with Keel Quartzite. However, mixing models result in significant errors for Ni, and to lesser extents Co, MgO, Cr and FeO. Enrichments of these elements in Group 2 glass require an ultramafic contribution. However, mixing models involving a component of Tasmanian West Coast dunite, pyroxenite or lamprophyre fails to produce the required glass compositions and can be ruled out as a significant component of the target rock stratigraphy.

The observed composition of Group 2 glass samples can only be explained by mixing with a chondrite or chondrite-like (primitive achondrite) projectile. The maximum contribution from the projectile is up to 9% in some samples, and this is one of the largest known extraterrestrial contaminations reported in a terrestrial

material. The distribution of projectile material is extremely heterogenous. Only some glass samples are enriched in projectile material, the amount of projectile contribution is varied, and only the transition metals are enriched, no simultaneous enrichment in the HSE is detected as these elements are present in entirely crustal abundances. Vapour phase transfer of projectile materials into the silicate melt can possibly explain this apparent transition metal/HSE paradox. It is suggested that the temperatures at which the studied glass specimens formed were sufficient to vaporise, and allow condensation of the transition metals into the silicate melt that subsequently cooled to form the glass. However, the HSE have far higher boiling points than the transition metals (+~1000°C), and as such the temperatures at which the studied glass specimens formed may have been insufficient to vaporise and allow transfer of the HSE to the glass. If the projectile was chondritic, Darwin Crater is one of the smallest structures to be produced by the impact of a projectile other than an iron meteorite.

Trends in the distribution of the glass around Darwin Crater are consistent with the structure being the source of the glass. There is clear decrease in the abundance of glass with increasing distances from the crater. The size distribution data for glass recovered during this study is consistent with ballistic ejection from the crater, hence the largest recovered fragments are found closest to the source crater. A decrease in the proportion of fine glass fragments away from the crater is also observed, this is explained by rapid slowing of fine particles after interaction with the atmosphere, and hence preferential deposition of this material close to source. At all sites, size distribution data for the recovered glass specimens is strongly skewed towards outlying large fragments. This poor sorting indicates that the ballistic ejection of melt from the crater was highly turbulent, as the break down of turbulent cells will tend to cause large and small fragments to be deposited together.

The dominant spatial colour trend is an increase in the proportion of black glass away from the crater. The dominant control on this trend is interpreted to be the depth of excavation. Black glass is interpreted to be derived from pelitic layers which are known to be interbedded within the Keel Quartzite at the top of the target stratigraphy. This interpretation is consistent with the expectation that the upper most ejected target rocks are dispersed to the greatest distances from the source crater (Melosh 1989). Deriving the black glass from the upper most target rocks, close to the interface between the vaporizing projectile and the target rocks, is also consistent

with the evidence for preferential projectile contamination in some Group 2 black glass samples (Melosh 1989).

The dominant trend in the observed shape variation of *in situ* glass, relative to distance from the crater, is an increase in the proportion of splashform (spheroid, droplet, elongate) shapes with increasing distance from the crater. Because these shapes are formed by surface tension during aerial transport as rotating molten fragments, increased ejection distances will allow greater travel time for surface tension to shape the fragments. This is consistent with the preference for black glasses to be splashform because the black melt is distributed the greatest distances from the crater. The lower viscosity of the black melt will also promote the development of splashform shapes, in contrast to the higher viscosity white glass that is almost exclusively irregular in shape.

There is no evidence for any primary asymmetry in the distribution of glass relative to Darwin Crater. This prevents any inferences as to the projectile trajectory. The outstanding feature of the glass is its extremely wide distribution, and high abundance relative to the size of the crater. In a 50km^2 area surrounding the crater it is conservatively estimated that there is at least 11 250m^3 of glass. Outside of this area the glass is patchily distributed, and its abundance is difficult to estimate. However, based only on the estimated melt volume in the 50km^2 area, relative to the size of the source crater, this is the most abundant impact glass known on Earth. The glass is scattered across a strewn field with a known size of at least 410km^2. This wide distribution, and high abundance may be explained by ground water infiltration of the target rocks along abundant fractures and faults, which are typically present in the Eldon Group (Fudali & Ford 1979). Surface swamps have existed in the study area throughout the Pleistocene (Hansen & Smolenski 2002, Hansen & Richardson 2002), and may thus have been an important feature the pre-impact environment. Abundant groundwater would have produced a highly volatile-charged target stratigraphy at the time of the impact. It is suggested that this volatile enhancement increased the explosiveness of the impact and the efficiency of melt dispersal and ejection from the crater.

The crater-fill stratigraphy is a complicated package of slumped, deformed bedrock blocks, and sandy breccias that are interpreted to have been formed by impact shattering of quartzite, and plastic deformation of pelitic units. In the expanding cavity, non-melted angular quartz and country rock fragments were blasted outwards and upward along the cavity floor before collapsing inwards, and mixing to form

polymict matrix supported breccias of angular quartz, and country rock at the top of the crater-fill (Crater-fill Facies A). Rare pieces of Darwin glass have been recovered from this breccia. Beneath the polymict breccia is a complicated package of plastically deformed (<5GPa), brecciated, and more coherent rocks sourced from slumping of the cavity walls (Crater-fill Facies B, C). Kinked micas are present, as are abundant quartz grains with sub-planar to irregular fractures. Under cross-polarized light, some fracture planes in quartz separate alternating domains of different extinction. These alternating black-white zones appear superficially as twinning. These grains are most abundant in glass-bearing gravels to the west of the crater. The degree of deformation observed in these quartz grains and the crater-fill rocks generally, is far beyond the regional metamorphic grade. However, diagnostic evidence for an impact origin of the structure (e.g. PDF bearing quartz grains, abundant melt) has not been discovered in the crater-fill samples. As no diagnostic deformation features have been found in quartz grains from the glass-bearing gravels surrounding the crater, it is not possible to determine if any of the glass-bearing gravels represent true ejecta deposits.

Rocks of the crater-fill stratigraphy are blanketed by laminar muds interpreted to be lacustrine deposits formed during the gradual infilling of the structure. Palynomorphs are recovered in high abundance from these lake sediments and indicate that the crater was a lake until around 30ka (Colhoun & Van de Geer 1988). Throughout the Pleistocene, the vegetation surrounding the lake has had affinity with modern floristic communities found in southwest Tasmania today. This has involved closed canopy rainforest that usually includes *Nothofagus* during interglacial periods, and progressive replacement by open "dry" rainforest, schlerophyll forest dominated by Casurinaceae and/or Myrtacea, through to herb dominated communities as the climate shifts towards glacial conditions (Macphail et al. 1993). These vegetation assemblages and independent evidence from the *Parastacoides sp.* crayfish (Hansen & Smolenski 2002, Hansen & Richardson 2002) indicate that wet, waterlogged, conditions have existed across the study site throughout the entire Pleistocene period. Such a climatic regime is required by the model of volatile enhanced glass ejection, which was invoked to explain the high abundance and wide distribution of ejected glass. This study demonstrates the critical effects of the interaction between terrestrial processes in the target environment and the projectile, and highlights the dynamic nature of impact events on Earth.

7.2 Discussion

In this study, every attempt to falsify the hypothesised existence of a genetic relationship between Darwin glass and Darwin Crater has failed. The geochemical and isotopic compositions of the suspected target rocks from around Darwin Crater are entirely consistent with being the parent materials of Darwin glass. The crater-fill stratigraphy is consistent with theoretical and field studies at other small, simple craters in sedimentary rocks, although diagnostic evidence for an impact origin has not been found. However, when combined with the geographic trends in the abundance and physical properties of glass relative to the crater, these data strongly support the contention that Darwin Crater is of impact origin, and the source of Darwin glass. These conclusions pave the way for Darwin Crater to be officially recognized as an impact structure.

7.2.1 Implications of the origin of Darwin glass to theories of impact melt and tektite genesis

The highly efficient production of ejected melt during the Darwin impact event appears to have been promoted by volatile enhancement of the target rocks. Such volatile enrichment was probably not related to intergranular porosity, but rather to groundwater infiltration along faults and fractures. Waterlogged soils present in the study area throughout the Pleistocene (Hansen & Smolenski 2002, Hansen & Richardson 2002) are also likely to have enhanced the volatility of the surface layers of the pre-impact stratigraphy. As such, Darwin is considered an excellent analogue for impacts onto ice/water that are predicted to produce orders of magnitude more melt than impacts onto any other material (Pierazzo et al. 1997).

These observations may also have implications for our understanding of tektite strewn fields on Earth. The reasons why most impacts on Earth do not produce tektites are unknown. It may be that as well as a chemically and physically suitable target material (e.g. high porosity), a volatile charged target stratigraphy is required to promote efficient ejection, and hence the widespread dispersal of melt that is the defining feature of tektites. The presence of abundant water in the target stratigraphy is one obvious means of providing this volatile enhancement.

The resolution of currently available climate data prevents accurate determination of the climate at the time of formation of the Central European tektites. However, the Moldavites are believed to have formed from thin surface sand deposits present at

the time of impact (Huttner & Schmidt-Kaler 1999, Stöffler et al. 2003). Such surface materials have a high potential to be aquifers, and as such a ground water saturated target stratigraphy cannot be ruled out. The North American tektites derive from the Chesapeake Bay Crater that was situated on the continental shelf (Koeberl et. al 1995, Koeberl et al. 1995), so volatiles were abundant. The tektite-like K/T boundary glass from Chicxulub Crater was also formed in a continental shelf impact (Hildebrand et al. 1994). The Ivory Coast tektites were ejected from the Bosumtwi Crater (Koeberl et al. 1998b), but little is known about the pre-impact environment. Bosumtwi is currently in a wet and tropical climate, and this may also have been the case during the Pleistocene. As such, a wet pre-impact environment cannot be ruled out.

It has been suggested that loess is the perfect parent material for the Australasian tektites (e.g. Wasson & Heins 1993). Loess is considered an ideal tektite forming material because of its high average SiO_2 content, similar to tektites, its tendency to exist in wide spread chemically homogenous deposits, and its relatively uniform grain size and high porosity; all of which are considered to enhance melt production during impact (Melosh 1989; Wasson & Heins 1993; Chapter 1). In their model of tektite origin, Wasson and Heins (1993) suggest an additional feature of loess deposits that they interpret as critical – an absence of water in the pore space. They suggest that a *"...problem associated with melt production in a target having a high water content is that a large fraction of the available energy is absorbed by H_2O"* (Wasson & Heins 1993, p.3047). This argument hinges on energy being too limited in most impacts to vaporize water as well as producing abundant melt. Unaware that the North American tektites were formed in an sub-aqueous impact (Chesepeake Bay structure), and ignoring the K-T boundary glasses of similar origin, they see dry glacial conditions that promote extensive development of dry loess deposits as critical to the formation of tektites, and suggest that it is the requirement of an impact coincident in time with dry glacial conditions that explains the rarity of tektite forming impact events on Earth.

The fossil isotope record for the Australasian microtektites indicate that these were deposited during glacial conditions, and the high ^{10}Be content of the Australasian tektites is also consistent with formation from surface deposits and can not rule out loess (Blum et al. 1992, Koeberl 1994). The high concentrations of B and the range in $\delta^{11}B$ values are also interpreted to suggest fluvial or deltaic sediments, or marine pelagic and neritic sediments were a component of the target rock stratigraphy

(Chaussidon & Koeberl 1995). This isotopic evidence for deltaic and fluvial or marine input calls into question the general hypothesis of Wasson & Heins (1993) that tektites be formed from *dry* loess. It is important to also note that the effectively volatile free, or 'dry' composition of tektites does not require a dry target stratigraphy as water is easily expelled from the tektite melt under impact conditions (Melosh & Artmeteiva 2004). Perhaps, the ideal target material for the Australasian tektites would be loess deposits on an exposed continental shelf being dissected by streams, and flooded by abundant groundwater percolating through the porous medium that would act as an aquifer. This would provide a target stratigraphy consistent with all available chemical and isotopic data. In addition and critically, the abundant water will create a volatile charged target stratigraphy. This provides a mechanism for promoting the efficient ejection, and extremely widespread dispersal of melt from the crater, as is the defining feature of tektites.

7.3 Contentious issues and possible future works required in the study of the origin of Darwin glass

The exact nature of the projectile involved in the impact remains ambiguous because of the apparent lack of meteoritic HSE enrichments in the glass. The HSE are interpreted to have been retained in the projectile melt or an unidentified phase, and the absence of these elements prevents determination of the projectile species beyond chondrite or primitive achondrite. The model to explain the absence of HSE in the glass, despite transition metal enrichments, invokes boiling point controlled vapour phase transfer of the projectile material and is both qualitative and highly speculative at present. Discovery of a HSE bearing phase in the glass (e.g. nano-nuggets) would further define the projectile type, as would the discovery of actual projectile fragments. Bulk amounts of glass should be crushed and subjected to heavy metal separations in an attempt to isolate a potential HSE bearing residue for analysis.

Much information could be gained from new drilling operations into the structure. With complete core recovery it could be conclusively determined if the crater is truly free of melt, and if it contains diagnostic shock metamorphic effects. Such information would further strengthen both the conclusions of this thesis, and the implications of these data and observations to our understanding of small crater genesis and impact melt production. Any proposal to re-drill the structure will need

to be reconciled with the potential ecologic and social impact of the operations.

The upper laminated lake sediments were completely recovered in both the 1975 and 1981 cores and have been housed in plastic wrap since recovery at the University of Tasmania, Department of Geography, and in a storeroom on the University of Tasmania Farm, Richmond. Very limited work has been done on these cores. As the lake formed, and is likely to have began in filling with sediment immediately after impact at 816 ± 7 ka, the cores potentially contain one of the longest continuous Quaternary palynological records in the southern hemisphere. This is a severe oversight that must be reconciled. These cores are under the control of Dr Eric Colhoun, Department of Geography, University of New Castle, NSW, who should be approached for access.

7.4 Final remarks

- Darwin glass was formed by impact melting and ejection of Siluro-Devonian Eldon Group quartzite and slate during the formation of Darwin Crater. This is supported by all available geochemical and isotopic data, and by trends in the abundance and physical properties of glass relative to the crater, although diagnostic evidence for an impact origin of the crater in the form of shocked quartz or abundant within-crater melt, has not been described. The outstanding feature of the ejected glass is its high abundance and widespread distribution that, relative to the size of the source crater, is unrivalled on Earth. This characteristic is intimately related to Pleistocene climate of western Tasmania that, as today, was dominated by high-rainfall resulting from prevailing moist westerly airstreams. Abundant water infiltrated fractures and faults in the target stratigraphy, and the presence of deep waterlogged soils ensured that the projectile struck a volatile charged target stratigraphy capable of ejecting glass across an area of more than 410km^2. This study highlights the effect that a planet's surface geology and environment have on the result of extraterrestrial bombardment. Once again the dynamic nature of impact events has been illuminated in this study on the *Origin of Darwin glass.*

References

Ahrens T. J. and O'Keefe J. D. (1977) Equations of state and impact-induced shock-wave attenuation on the Moon. In Roddy D. J., Pepin R.O., and Merrill R. B. (eds) *Impact and Explosion Cratering: Planetary and Terrestrial Implications.* Pergamon, New York, 639–656.

Aitchison J. (1977) *The Statistical Analysis of Compositional Data.* Chapman and Hall, London, 416pp.

Albin E. (1977) Georgiates: tektite geochemistry and stratigraphic occurrence in east-central Georgia. Ph.D thesis, Univeristy of Georgia, 302pp.

Alexander C.M. O'D. (2002) Application of MELTS to kinetic evaporation models of FeO-bearing silicate melts. *Meteoritics and Planetary Science* **37**, 245-256.

Artemieva N. (2003) Distal ejecta from the Ries Crater – Moldavites and Projectile. *Proceedings International Conference on Large Meteorite Impacts* 3rd, abstract no. 4050.

Attrep M., Orth C.J., and Quntana L.R. (1991) Chemical fractionation of siderophile elements in impactites from Australian meteorite craters. *Proceedings of Lunar and Planetary Science Conference* **22nd**, 39-40.

Baillie P.W., and Sutherland F.L. (1992) Devonian Lamprophyres from Mt Lyell, Western Tasmania. *Papers and Proceedings of the Royal Society of Tasmania* **126**, 19-22.

Baker G. (1958) The role of aerodynamical phenomena in shaping and sculpting Australian tektites. *American Journal of Science* **256**, 369-383.

Banks M. R. (1962) Silurian and Devonian Systems. In Spry A.H., and Banks M.R. (eds) The Geology Of Tasmania. *Journal of the Geologic Society of Australia* **9**, no.2, 177-187.

Barrat J. A., Jahn B. M., Amosse J., Rocchia R., Keller F., Poupeau G. R., and Diemer E. (1997) Geochemistry and origin of Libyan Desert glasses. *Geochimica et Cosmochimica Acta* **61**, 1953-1959.

Blisset A.H. (1962) *One mile geological map series. K/55-5-50. Zeehan.* Geological Survey of Tasmania.

Blum J.D., Papanastassiou D. A., Wasserburg G. J., and Koeberl C. (1992) Neodymium and strontium isotopic study of Australasian tektites - New constraints on the provenance and age of target materials. *Geochimica et Cosmochimica Acta* **56**, 483-492.

Bogard D.D., Garrison D.H., Norman M., Scott E.R.D., and Keil K. (1995) ^{39}Ar-^{40}Ar age and petrology of Chico: Large scale impact melting on the L chondrite parent body. *Geochimica et Cosmochimica Acta* **59**, 1383-1399.

Borisov A., and Palme, H., (1997) Experimental determination of the solubility of platinum in silicate melts. *Geochimica et Cosmochimica Acta* ***61,*** 4349-4357.

Bouska Vl., Povondra P., Florensky P. V., and Randa Z. (1981) Irghizites and zhamanshinites – Zhamanshin crater, USSR. *Meteoritics* **16**, 171-184.

Brown A. V. (1986) Geology of the Dundas-Mt Lindsay-Mt Youngback Region. Tasmania Department of Mines, *Geolocial Survey Bulletin No. 62,* 218pp.

Bureau of Meteorology (BOM) (2004) *Average Annual Rainfall (Tasmania).* Available online @ (URL): http://www.bom.gov.au/cgibin/climate/cgi_bin_scripts/annual_rnfall.cgi

Burrett C. F. (1992) Conodont geothermometry in Palaeozoic carbonate rocks of Tasmania and its economic implications. *Australian Journal of Earth Sciences* **39**, 61-66.

Butkovich T.R. (1971) Influence of Water in Rocks on Effects on Underground Nuclear Explosions. *Journal of Geophysical Research* **76**, no. 8, 1993-2010.

Cassidy W.A., Glass B.P., and Heezen B.C. (1969) Physical and chemical properties of Australian microtektites, *Journal of Geophysical Research* **74**, 1008-10025.

Chapman D.R., and Scheiber L. C. (1969) Chemical investigation of Australasian tektites. *Journal of Geophysical Research* **74**, 6737-76.

Chapman D.R., Keil K., and Annell C. (1967) Comparison of Macedon and Darwin Glass. *Geochimica et Cosmochimica Acta* **31**, 1595-1603.

Chaussidon M., and Koeberl C. (1995) Boron content and isotopic composition of tektites and impact glasses: Constraints on source regions. *Geochimica et Cosmochimica Acta* **59**, no. 3, 613-624.

Claeys P., Heuschkel S., Lounejeva-Baturina E., Sanchez-Rubio G., and Stöffler D. (2003) The suevite of drill hole Yucatàn 6 in the Chicxulub impact crater. *Meteoritics and Planetary Science* **38**, no. 9, 1299-1317.

Colhoun E.A., and Van de Geer G. (1988) Darwin Crater, The King and Linda Valleys. In Colhoun E.A. (ed) (1988) *Cainozoic Vegetation of Tasmania.* Department of Geography, University of Newcastle, NSW, Australia.

Conder H. (1934) Darwin Glass. *Industrial Australian and Mining Standard* **89**, p.329.

Corbett K.D., and Brown A.V. (1975) *Geological Atlas 1:250 000 Series, Queenstown.* Geological Survey of Tasmania, Department of Mines

Corbett K.D., Pemberton J., and Vicary M.J. (1993) *Map 13. Geology of the Mt Jukes-Mt Darwin Area, 1:25 000.* Geological Survey of Tasmania, Department of Mines.

Crawford A.J., and Berry R. F. (1992) Tectonic implications of late Proterozoic-early Palaeozoic igneous rock associations in western Tasmania, *Tectonophysics,* **214**, no. 1-4, 37-56.

Cullers R.L. (2000) The geochemistry of shales, siltstones and sandstones of Pennnsylvanian-Permian age, Colorado, USA: implications for provenance and metamorphic studies. *Lithos* **51**, 181-203.

Department of Primary Industries Water and Environment (DPIWE) (2004) *Native Plants of Tasmania.* Available online @ (URL): http://www.dpiwe.tas.gov.au/inter.nsf/ThemeNodes/BHAN-54746E?open

Derbyshire E. (1972) Pleistocene Glaciation of Tasmania: Review and Speculations. *Australian Geographical Studies* **10**, 79-94.

Dressler B. O., and Reimold W. U. (2001) Terrestrial impact melt rocks and glasses. *Earth Science Reviews* **56**, no. 1-4, 205-284.

Ebel D.S., and Grossman L. (2000) Condensation in dust-enriched systems. *Geochimica et Cosmochimica Acta* **64**, no.2, 339-366.

Eggins S. M., Rudnick R. L., and McDonough W. F. (1998) The composition of peridotites and their minerals: a laser-ablation ICP-MS study. *Earth and Planetary Science Letters* **154**, 53–71.

Elkins-Tanton L.T., Aussillous P., Bico J., Quéré D., and Bush J.W.M. (2003) A laboratory model of splash-form tektites. *Meteoritics and Planetary Science* **38**, no.9, 1331-1340.

Englert So-P., Pal D. K., Tuniz C., Moniot R. K., Savin W., Kruse T. H., and Herzog G. F. (1984) Manganese-53 and beryllium-10 Contents of Tektites . *Proceedings of Lunar and Planetary Science Conference* **15th**, 250-251.

Epstein A.G., Epstein J.B., and Harris, L. D. (1977) Conodont Color Alteration- an Index to Organic Metamorphism. *Geologic Survey Professional Paper 995*, United States of America, Department of The Interior, 27pp.

Faul H. (1966) Tektites are terrestrial. *Nature* **152**, 1341-1344.

Fisher R.V., and Schmincke, H.U., (1984) Pyroclastic Rocks. Springer-Verlag, 540pp.

Florensky P. V. (1976) The First Tektite Deposits in a Meteoritic Crater (Zhamanshin North Aral Region, USSR). In Abstracts of Papers Presented to the Symposium on Planetary Cratering Mechanics. *LPI Contribution no. 259*, Lunar and Planetary Institute, Houston, p.33.

Ford R. J. (1972) A possible impact crater associated with Darwin Glass. *Earth and Planetary Science Letters* **16**, 228–230.

French B.M. (1998) Traces of Catastrophe: A Handbook of Shock-Metamorphic Effects in Terrestrial Meteorite Impact Structures. *LPI Contribution No. 954*, Lunar and Planetary Institute, Houston, 120pp.

Frey F.A. (1977) Microtektites: a chemical comparison of bottle-green microtektites, normal microtekites and tektites. *Earth and Planetary Science Letters* **35**, 43-48.

Frutiger A. (2004) *Land yabbies 9, Parastacoides.* Located @ (URL) http://www.crayfishworld.com/parastacoide.htm

Fudali R. F., and Ford R. J. (1979) Darwin glass and Darwin crater - A progress report. *Meteoritics* **14**, 283-296.

Gault D. E., Quaide W. L., and Oberbeck V. R. (1968) Impact cratering mechanics and structures. In French B.M., and Short N.M. (eds) *Shock Metamorphism of Natural Materials.* Mono Book Corp., Baltimore. 87–99.

Gee R.D., Moore W.R., Pike G.P., and Clarke M.J. (1969). The Geology of the Lower Gordon River, particularly the Devonian sequence. *Geological Survey Record No. 8*, Tasmania Department of Mines, 28pp.

Gentner W., Kirsten T., Storzer D., and Wagner G. A. (1973). K-Ar and fission track dating of Darwin Crater Glass. *Earth and Planetary Science Letters* **20**, no. 2, 204-210.

Gill E.D., and Banks M.R. (1950) Silurian and Devonian Stratigraphy of the Zeehan Area, Tasmania. *Papers and Proceedings of the Royal Society of Tasmania* **1949**, 259-271

Gimsing A.L., and Borggaard O.K. (2002) Competitive adsorption and desorption of glyphosphate and phosphate on clay silicate and oxides. *Clay Minerals* **37**, no. 2, 509-515.

Glass B. P., Chapman D. R., and Prasad M. S. (1996) Ablated tektite from the central Indian Ocean. *Meteoritics and Planetary Science* **31**, 365-369.

Glass B.P., and Koeberl C. (1989) Trace element study of high- and low-refractive index Muong Nong-type tektites from Indochina. *Meteoritics* **24**, 143-146.

Glass B.P., and Koeberl C. (1999) ODP Hole 689B spherules and upper Eocene microtektite and clinopyroxene-bearing spherule strewn fields. *Meteoritics and Planetary Science* **34**, no. 2, 197-208.

Glasstone S., and Dolan P.J. (1977) *The Effects of Nuclear Weapons,* Third Edition. United States Department of Defense, 644pp.

Gould C. (1866) On the position of the Gordon Limestone relative to other Palaeozoic Formations. *Papers and Proceedings of the Royal Society of Tasmania* **1866**, 63-66.

Gratz A.J., Fisler D.K., and Bohor B.F. (1996) Distinguishing shocked from tectonically deformed quartz by the use of the SEM and chemical etching. *Earth and Planetary Science Letters* **142**, 513-521.

Grieve R. A. F. (1987) Terrestrial impact structures. *Annual Reviews of Earth and Planetary Sciences* **15**, 245–270.

Grieve R. A. F., and Cintala M. J. (1992) An analysis of differential impact melt-crater scaling and implications for the terrestrial impact record. *Meteoritics* **27**, 526–538.

Grieve R. A. F., Dence M. R., and Robertson P. B. (1977) Cratering process: As interpreted from the occurrence of impact melts. In Roddy D. J., Pepin R.O., and Merrill R. B. (eds) *Impact and Explosion Cratering: Planetary and Terrestrial Implications,* Pergamon, New York, 791–814.

Haack H., Farinella P., Scott E.R.D., and Keil K. (1996) Meteoritics, asteroidal, and theoretical constraints on the 500 Ma disruption of the L chondrite parent body. *Icarus* **119**, 182-191.

Haines P. W., and Rawlings D. J. (2002) The Foelsche structure, Northern Territory, Australia: An impact crater of probable Neoproterozoic age. *Meteoritics and Planetary Science* **37**, no. 2, 269-280.

Hansen B., and Richardson A.M. (2002) Geographic ranges, sympatry and the influence of environmental factors on the distribution of species of an endemic Tasmanian freshwater crayfish. *Invertebrate Systematics* **16**, 621-629.

Hansen B., and Smolenski A. (2002) A preliminary examination of the molecular relationships of some crayfish species from the genus Parastacoides (Decapoda: Parastacidae). In Whisson G.J., and Knott B. (eds) Freshwater Crayfish 13. *Proceedings of the Thirteenth Symposium of the International Association of Astacology*, 547-554.

Hergt J.M., McDougall I., Banks M.R., and Green D.H. (1989) Igneous Rocks: Jurassic Dolerite. In Burrett C.F. and Martin E.L. (eds) Geology and Mineral Resources of Tasmania. *Special Publication Geological Society of Australia* **15,** 375-409.

Herron M.M. (1988) Geochemical classification of terrigenous sands and shales from core or log data . *Journal of Sedimentary Petrology* **58**, no.5, 820-829.

Hildebrand A. R., Asaro F., Attrep M., Bermúdez-Santana J. C., Bonis S., Cedillo-Pardo E., Claeys P., Gonzalez-Casildo V., Grajales-Nishimura J. M., Grégoire D. C., Ortiz-Aleman C., Pilkington M., Sánchez-Rios M. A., Smit J., and Stansberry J. A. (1994) The Chicxulub Crater and Its Relation to the KT Boundary Ejecta and Impact-Wave Deposits. Abstracts of Papers Presented to " New Developments Regarding the KT Event and Other Catastrophes in Earth History". *Lunar and Planetary Institute Contribution no. 825*, p.49.

Hörz F. (1982) Ejecta of the Ries crater, Germany. In Silver L.T., and Schultz P.H., (eds.) Geological Implications of Impacts of Large Asteroids and Comets on the Earth. *Geological Society of America Special Paper* ***190***, 39–55.

Hörz F., Ostertag R., and Rainey D.A. (1980) Target stratigaphy and its manifestations in continuos crater deposits: the "Bunte Breccia" of the Ries Crater, Germany. *Proceedings of Lunar and Planetary Science Conference* **11th**, 844-46.

Howard W.R., van de Geer G., and Zahn R. (2001) Marine-terrestrial correlations from a million-year record of pollen in the Southwest Pacific. Proceedings of American Geophysical Union (AGU) fall meeting. *Eos* **82**, no.47, supplement, Abstract no, PP51B-06.

Huttner R., and Schmidt-Kaler H. (1999) Erlauterungen zur geologischen Karte des Rieses 1:50000. *Geologica Bavarica* **104**, 7-76.

Jarosewich E. (1990) Chemical analyses of meteorites: A compilation of stony and iron meteorite analyses. *Meteoritics* **25**, 323-337.

Jones R. (1990) From Kakadu to Kutikina: the southern continent at 18000 years ago. In Gamble C., and Soffer O. (eds.) *The world at 18000 BP* 2: *low latitudes*. Unwin Hyman, London, 264-95.

Kenkmann T. (2003) Dike formation, cataclastic Flow, and rock fluidization during impact cratering: an example from the Upheaval Dome Structure, Utah. *Earth and Planetary Science Letters* **214**, 43-58.

Kershaw A.P. (1988) Australasia. In Huntley B., and Webb T. (eds) *Vegetation History*, Kluwer Academic Publishers, 238-306.

Kieffer S. W. (1971) Shock metamorphism of the Coconino Sandstone at Meteor Crater, Arizona. *Journal of Geophysical Research* **76**, 5449–5473.

Kieffer S. W., and Simonds C. H. (1980) The role of volatiles and lithology in the impact cratering process. *Reviews of Geophysics and Space Physics* **18**, 143–181.

Kirkpatrick J.B., and Fowler M. (1998) Locating likely glacial forest refugia in Tasmania using palynological and ecological information to test alternative climate models. *Biological Conservation* **85**, 171-182.

Kleinman B., Horn P., and Langenhorst F. (2001) Evidence for shock metamorphism in sandstones from the Lybian Desert Glass strewn field. *Meteoritics and Planetary Science* **36**, 1277-1282.

Koeberl C., Rampino M. R., Jalufka D. A., and Winiarski D. H (2003) A 2003 Expedition into the Libyan Desert Glass Strewn Field, Great Sand Sea, Western Egypt. *Proceedings of Third International Conference on Large Meteorite Impacts*, abstract no.4079.

Koeberl C. (1992) Geochemistry and origin of Muong-Nong-type tektites. *Geochimica et Cosmochimica Acta* **56**, no. 3, 1033-1064.

Koeberl C. (1994) Tektite origin by hypervelocity asteroidal or cometary impact: Target rocks, source craters, and mechanisms. In Dressler B.O., Grieve R.A.F., and Sharpton V.L., (eds) Large Meteorite Impacts and Planetary Evolution. *Geological Society of America Special Paper 293*, 133-151.

Koeberl C. (1997) Libyan Desert Glass: Geochemical composition and origin. In de Michele V. (ed) *Proceedings of "Silica 96" Meeting on Libyan Desert Glass and Related Events.* Pyramids, Segrate, Italy, 121-131.

Koeberl C. (2003) Using geochemical observation to constrain projectile types in impact cratering. Proceedings of Impact Cratering: Bridging the Gap Between Modeling and Observation. *LPI Contribution No. 1155,* 45-47.

Koeberl C., Reimold U.W., and Shirey S.B. (1994a) Saltpan impact crater, South Africa: Geochemistry of target rocks, breccias, and impact glasses, and osmium isotopic sytematics. *Geochimica et Cosmochimica Acta* **58**, 2893-2910.

Koeberl C., Sharpton V.L., Schuraytz B.C., Shireyy S.B., Blum J.D., and Marin L. (1994b) Evidence for a meteoritic component in impact melt rock from the Chicxulub structure. *Geochimica et Cosmochimica Acta* **58**, no. 6, 1679-1684.

Koeberl C., Reimold W. U., Brandt D., and Poag C. W. (1995) Chesapeake Bay Crater, Virginia: Confirmation of Impact Origin. *Meteoritics* **30**, no. 5, p.528.

Koeberl C., Bottomley R., Glass B. P., and Störzer D. (1997) Geochemistry and age of Ivory Coast tekites and microtektites. *Geochimica et Cosmochimica Acta* **61**, 1745–1772.

Koeberl C., Reimold W. U., and Shirey S. B. (1998a) The Aouelloul crater, Mauritania: On the problem of confirming the impact origin of a small crater. *Meteoritics & Planetary Science* **33**, 513-517.

Koeberl C., Reimold W.U., Blum J.D., and Chamberlain C. P. (1998b) Petrology and geochemistry of target rocks from the Bosumtwi impact structure, Ghana, and comparison with Ivory Coast tektites. *Geochimica et Cosmochimica Acta* **62**, 2179-2196.

Kovach W.L. (1993) *MVSP- a Multivariate Statistical Package for IBM-PC's version 2.1.* Kovach Computing Services, Pantreath, Wales.

Kurszlauskis S., Buttner R., Zimanowski B., and Lorenz V. (1998) On the first experimental phreatomagmatic explosion of a kimberlite melt. *Journal of Volcanology and Geothermal Research* **80**, 323-326.

Laurenzi M. A., Bigazzi G., and Balestrieri M. L., (2001) $^{40}Ar/^{39}Ar$ Chronology of Central Europe Tektites (Moldavites) *Meteoritics and Planetary Science* **36**, supplement, p.A109.

Loftus-Hills C. (1915) Darwin Glass. *Records of the Geologic Survey of Tasmania* **3,** 1-16.

Lo C.H., Howard K.T., Chung S.L., and Meffre S. (2002). Laser fusion argon-40/argon-39 ages of Darwin Impact glass. *Meteoritics and Planetary Science* **37**, 1555-1562.

Macphail M.K., and Truswell E.M. (1989) Palynostratigraphic of the central west Murray Basin. *Bureau of Mineral Resources Journal of Australian Geology and Geophysics* **11**, 301-31.

Macphail M.K., Jordan G. J. and Hill R.S. (1993) Key Periods in the Evolution of the Flora and Vegetation in Western Tasmania I: The early-middle Pleistocene. *Australian Journal of Botany* **41**, 673-707.

Masaitis V. L. (1994) Impactites from Popigai crater. In Dressler B.O., Grieve R.A.F., and Sharpton V.L. (eds) Large Meteorite Impacts and Planetary Evolution. *Geological Society of America Special Paper 293,* 153–162.

Masaitis V. L., Boiko Ya I., and Izokh E. P. (1984) Zhamanshin Impact Crater (western Kazakhstan): Additional Geological Data. *Proceedings of Lunar and Planetary Science Conference* **15th**, 516-15.

Matsuda J., and Yajima H. (1989) Noble Gases in Darwin Glass: Anomalous Neon Enrichment. *Proceedings of Lunar and Planetary Science Conference* **20th**, p. 628.

McCoy T.J. (1994) *Partial melting on the acapulcoite-lodrandite meteorite parent body.* Ph.D dissertation. Univ. Hawaii.

McNamara K., and Bevan A. (2001) *Tektites.* Western Australian Museum, 38pp.

McNiven I.J. (1994) Technological organization and settlement in southwest Tasmania after the glacial maximum. *Antiquity* **68**, 75-82.

Meisel T., Koeberl C., and Ford R.J. (1990) Geochemistry of Darwin impact glass and target rocks. *Geochimica et Cosmochimica Acta* **54**, 1463-1474.

Melosh H. J. (1989) *Impact Cratering: A Geologic Process.* Oxford Univ., New York. 245 pp.

Melosh H. J., and Vickery A. M. (1991) Melt droplet formation in energetic impact events. *Nature* **350**, 494–497.

Melosh H.J. (1998) Impact physics constraints on the origin of tektites. *Meteoritics and Planetary Science* **33**, p. A104.

Melosh H.J. and Ivanov B.A. (1999) Impact Crater Collapse. *Annual Reviews in Earth and Planetary Sciences* **27**, 385-415.

Melosh H. J. and Artemieva N. (2004) How Does Tektite Glass Lose Its Water?. *Proceedings of Lunar and Planetary Science Conference* **35th**, abstract no. 1723.

Milton D.J., Barlow B.C., Brett R., Brown A.R., Glikson A.Y., Manwaring E. A., Moss F.J., Sedmik E.C.E., Van Son J., and Young G.A. (1972) Gosses Bluff Impact Structure, Australia. *Science* **175**, no. 4027, 1199-1207.

Mittlefehldt D.W., See T. H., and Scott E. R. D. (1993) Siderophile element fractionation in meteor crater impact glasses and metallic spherules. *Proceedings of Lunar and Planetary Science Conference* **24th**, 995-996.

Mittlefehldt D.W., Lindstrom M.M., Bogard D.D., Garrison D.H., and Field S.W. (1996) Acapulco-and Lodran-like achondrites: Petrology, geochemistry, chronology and origin. *Geochimica et Cosmochimica Acta* **60**, no.5, 867-882.

Miyamato M., and Takeda H. (1994) Thermal history of Iodrandites Yamato 74357 and MAC 88177 as inferred from the chemical zoning of pyroxene and olivine. *Journal of Geoophysical Research* **99**, 5669-5677.

Morgan J.W., Janssens M.J., Hertogen J., Gros J., and Takahashi H. (1979) Ries impact crater, southern Germany: search for meteoritic material. *Geochimica et Cosmochimica Acta* **43**, 803-815.

Nakamura N., Fujiwar T., and Nohda S. (1990) Young asteroid melting event indicated by Rb-Sr dating of Point of Rocks meteorite. *Nature* **345**, 51-53.

Nesbitt H.W. (1979) Mobility and fractionation of rare earth elements during weathering of a granodiorite. *Nature* **279**, 206-210.

Norman M.D., and Mittlefehldt D.W. (2002) Impact processing of chondritic planetismals: siderophile and volatile element fractionation in the Chico L chondrite. *Meteoritics and Planetary Science* **37**, 329-344.

O'Keefe J. A. (1976) *Tektites and Their Origin.* Elsevier, New York. 254 pp.

O'Keefe J. D., and Ahrens T. J. (1975) Shock effects from a large impact on the Moon. *Proceedings of Lunar Science Conference* **6th**, 2831–2844.

O'Keefe J. D., and Ahrens T. J. (1993) Planetary cratering mechanics. *Journal of Geophysical Research* **98**, 17011–17028.

Ohlander B., Thunberg J., Land M., Hoglund L.O., and Quishang H. (2003) Redistribution of trace metals in a mineralized spodosol due to weathering, Liikavaara, northern Sweden. *Applied Geochemistry* **18**, no. 6, 883-899.

Opik E.J. (1961) Notes on the theory of impact craters. In *Proceedings Geophysics. Laboratory, Lawrence Radiation Laboratory Cratering Symposium,* Rep. UCLR-6438, Vol.2, Paper S, 1-28.

Orphal D. L., Borden W. F., Larson S. A., and Schultz P. H. (1980) Calculations of Impact Melt Generation and Transport. *Proceedings of Lunar and Planetary Science Conference* **11th**, 833-835.

Osinski G. R., Bunch T. E., and Wittke J. (2003a) Evidence for the Shock Melting of Carbonates from Meteor Crater, Arizona. *Meteoritics and Planetary Science* **38**, supplement, abstract no.5070.

Osinski G. R., Spray J. G., and Grieve R. A. F. (2003b) Impact Melting in Sedimentary Target Rocks? Proceedings of Impact Cratering: Bridging the Gap Between Modeling and Observations. *LPI Contribution No. 1155.* Lunar and Planetary Institute, Texas, p.59.

Ostertag R., and Stöffler D. (1978) The Ries Crater Continuous Deposits: Sedimentological Investigations of NASA Drill Cores. *Proceedings of Lunar and Planetary Science Conference* **9th**, 844-846.

Pal D. K., Moniot R. K., Kruse T. H., Herzog G. F., and Tuniz C. (1982) Beryllium-10 in Australasian tektites - Evidence for a sedimentary precursor. *Science* **218**, 787-789.

Palme H., Gobel E., and Grieve R.A.F. (1979) The distribution of volatile and siderophile elements in the impact melt of East Clearwater (Quebec). *Proceedings of Lunar and Planetary Science Conference* ***10th***, 2465-2492.

Peck D. C., and Keays R. R. (1990) Insights into the behaviour of precious metals in primitive, S-undersaturated magmas: Evidence from the Heazlewood River Complex, Tasmania. *Canadian Mineralogist* **28**, 553-577.

Petaev M.I., Barsukova L.D., Lipchutz M.E., Wang M.S., Ariskin A.A., Clayton R.N., and Mayeda T.K. (1994) The Divnoe meteorite: Petrology, chemistry, oxygen isotopes and origin. *Meteoritics* **29**, 182-199.

Peucker-Ehrenbrink B., and Jahn B-M. (2001) Rhenium-osmium isotope systematics and platinum group element concentrations; loess and the upper continental crust . *Geochemistry, Geophysics, Geosystems* **2**, no.10.

Pierazzo E., Vickery A. M., and Melosh H. J. (1997) A Reevaluation of Impact Melt Production. *Icarus* **127**, no. 2, 408-423.

Pike R. J. (1980) Control of crater morphology by gravity and target type - Mars, earth, moon. *Proceedings of Lunar and Planetary Science Conference* **11th**, 2159-2189.

Prasad M. S., and Sudhakar M. (1999) Australasian minitektites discovered in the Indian Ocean. *Meteoritics and Planetary Science* **34**, no. 2, 179-184.

Raheim A., and Compston W. (1977) Correlations between metamorphic events and Rb-Sr ages in metasediments and eclogite from Western Tasmania. *Lithos* **10**, 271-289.

Reid A.M., and Cohen A.J. (1962) Coesite in Darwin Glass. *Journal of Geophysical Research* **67**, p.1654.

Reimold W. U. (1982) The Lappajarvi meteorite crater, Finland - Petrography, Rb-Sr, major and trace element geochemistry of the impact melt and basement rocks. *Geochimica et Cosmochimica Acta* **46**, 1203-1225.

Reimold U.W., Koeberl C., Partridge T.C., and Kerr S.J. (1992) Pretoria Saltpan Crater: Impact origin confirmed. *Geology* **20**, 1079-82.

Reimold W.U, Koeberl C., and Brandt D. (1999) The Origin of the Pretoria Saltpan Crater. In Patridge (ed). *Memoir No. 85: Investigations into the origin, age and palaeoenvironments of the Pretoria Saltpan.* Council for Geoscience. Pretoria, South Africa. 35-54.

Richardson, R.G. (1984) Geophysical surveys of the Darwin Crater. *Report UR1984_06*, Mineral Resources of Tasmania, 2pp.

Robertson P.B. (1980) Anomalous development of planar deformation features in shocked quartz of porous lithologies. *Proceedings of Lunar and Planetary Science Conference* **11th**, 938-940.

Rock N. M. S. (1991) *Lamprophyres*. Blackie, Glasgow, 285pp.

Rollinson H.R. (1993) *Using geochemical data: evaluation, presentation, interpretation.* Longman Scientific, Essex, pp.343.

Rudnick R.L., and Fountain D.M. (1995) Nature and composition of the continental crust: a lower crustal perspective. *Reviews of Geophysics* **33**, 267-309.

Schaaf P., and Müller-Sohnius D. M. (2002) Strontium and neodymium isotopic study of Libyan Desert Glass: Inherited Pan-African age signatures and new evidence for target material. *Meteoritics and Planetary Science* **37**, no. 4, 565-576.

Shaw H. F., and Wasserburg G. J. (1982) Age and provenance of the target materials for tektites and possible impactites as inferred from Sm-Nd and Rb-Sr systematics. *Earth and Planetary Science Letters* **60**, no. 2, 155-177.

Smith T. R. and Hodge P. W. (1996) Microscopic Meteoritic Material at the Dalgaranga, Odessa, and Veevers Meteorite Craters. *Lunar and Planetary Science* **27**, p.1223.

Spandler C.J., Eggins S.M., Arculus R., and Mavrogenes J.A. (2000) Using melt inclusions to determine parent-magma compositions of layered intrusions: Application to the Greenhills Complex (New Zealand), a platinum group minerals-bearing, island-arc intrusion. *Geology* **28**, no.11, 991-994.

Spencer L.J. (1933) Origin of tektites. *Nature* **131**, p.876.

Stöffler D. (1994) Glasses formed by hypervelocity impact. *Journal of Non-Crystalline Solids* **67**, 465–502.

Stöffler D., and Langenhorst F. (1994) Shock metamorphism of quartz in nature and experiment: I. Basic observation and theory. *Meteoritics* **29**, 155–181.

Stöffler D., Knöll H.-D., and Maerz U. (1979) Terrestrial and lunar impact breccias and the classification of lunar highland rocks. *Proceedings of Lunar and Planetary Science. Conference* **10th**, 639–675.

Stöffler D., Artemieva N. A., and Pierazzo E. (2003) Modeling the Ries-Steinham impact event and the formation of the moldavite strewn field. *Meteoritics and Planetary Science* **37**, 1893-1907.

Storzer D., and Wagner G.A. (1980a) Australites older than indochinites-evidence from new fission track plateau dating. *Naturewissenschaften* **67**, 90-91.

Storzer D., and Wagner G.A. (1980b). Two discrete tektite-forming events 140 thousand years apart in the Australian-Southeast Asian area. *Meteoritics* **15**, p. 372.

Suess F. E. (1914) Ruckschau and Neueres uber die tektitfrage. *Geol. Ges. Wien. Mitt*, **7**, 51-121.

Sun S.-S., and McDonough W. F. (1989). Chemical and isotopic systematics of oceanic basalts: implications for mantle composition and processes. In Saunders A. D., and Norry M. J. (eds) *Magmatism in the Ocean Basins*. Geological Society, London, 313–345.

Takeda H., Mori H., Hiroi T., and Saito J. (1994) Mineralogy of new antarctic achondrites with affinity to Lodran and a model of their evolution in an asteroid. *Meteoritics* **29**, 830-842.

Tasmanian Government (1995) *Tasmania 1: 25 000 Topographic Map: Engineer, Sheet 3831, Edition 1.* Land Information Services, Department of Primary Industries, Water and Environment (DPIWE).

Tasmanian Government (1997) *Tasmania 1:100 000 Topographic Map: Franklin, Sheet 8013, Edition 6.* Land Information Services, Department of Primary Industries, Water and Environment (DPIWE).

Taylor S.R. (1962) The chemical composition of australites. *Geochimica et Cosmochimica Acta* **26**, 685-722.

Taylor S.R. (1966) Australites, Henbury impact glass, and subgreywacke: a comparison of the abundances of 51 elements. *Geochimica et Cosmochimica Acta* **30**, 1121-36.

Taylor S. R., and Solomon M. (1962) The geochemistry of Darwin Glass. *Geochimica et Cosmochimica Acta* **28**, no. 4, 471-474.

Taylor S. R., and Kaye, M. (1969) Genetic significance of the chemical composition of tektites: A review . *Geochimica et Cosmochimica Acta* **33**, no. 9, 1083-1100.

Taylor S.R., and Epstein S. (1969) Correlations between $^{18}O/^{16}O$ ratios and chemical compositions of tektites. *Journal of Geophysical Research* **74**, 6834-44.

Taylor S.R., and McLennan S.M. (1979) Chemical relationships among irghizites, zhamanshinites, Australasian tektites, and Henbury impact glasses. *Geochimica et Cosmochimica Acta* **43**, 1551-65.

Taylor S.R., and McLennan S., (1985) *The Continental Crust: Its Composition and Evolution.* Blackwell, Oxford, UK. 312 pp.

Taylor S. R., McLennan S. M., and McCulloch M. T (1983) Geochemistry of loess, continental crustal composition and crustal model ages. *Geochimica et Cosmochimica Acta* **47**, no. 11, 1897-1905.

Tera F., Brown L., Klein J., Middleton R., and Mason B., (1983) Beryllium-10 and Aluminum-26 in Tektites. *Meteoritics* **18**, p.405.

Truswell E.M., and Harris W.K. (1982) The Cainozioc palaeobotanical record in arid Australia: fossil evidence for the origins of an arid-adapted flora. In Barker W.R., and Greenslade P.J.M. (eds) *Evolution of the Flora and Fauna of Arid Australia*, Peacock Publications, Adelaide, 67-76.

Vickery A. M. (1993) The theory of jetting - Application to the origin of tektites. *Icarus*, **105**, 441—453.

von Engelhardt W., Stöffler D., and Schneider W. (1969) Petrologische Untersuchungen im Ries. *Geologica Bavarica* **61**, 229–295.

Walter L.S. (1967) Tektite compositional trends and experimental vapor fractionation of silicates. *Geochimica et Cosmochimica Acta* **31**, 2043-2063.

Walter L.S. (1989) Volatile fractionation and tektites source material. *Geochimica et Cosmochimica Acta* **53**, 2445-2446.

Walter L.S., and Clayton R.N. (1967) Oxygen isotopes: Experimental fractionation and variations in tektites. *Science* **156**, 1357.

Wasson J.T., Ouyang X., Wang J., Jerde E. (1989) Chemical classification of iron meteorites: XI. Multi-element studies of 38 new irons and the high abundance of ungrouped irons from Antarctica. *Geochimica et Cosmochimica Acta* **52**, 735-744.

Wasson J. T. (1991) Layered tektites - A multiple impact origin for the Australasian tektites . *Earth and Planetary Science Letters* **102**, no. 2, 95-109.

Wasson J. T., and Heins W. A. (1993) Tektites and climate. *Journal of Geophysical Research* **98**, no. E2, 3043-3052.

Whitehead J., Papanastassiou D. A., Spray J. G., Grieve R. A. F., Wasserburg G. J. (2000) Late Eocene impact ejecta: geochemical and isotopic connections with the Popigai impact structure. *Earth and Planetary Science Letters* **181**, no. 4, 473-487.

Whitford D.J., Crawford A.J., Korsch M.J., and Craven S.J. (1990) Strontium and neodymium isotopic studies of the Mount Read Volcanics, Tasmania. *Proceedings of Tenth Australian Geologic Convention.* Geologic Society of Australia, 215-16.

Williams M.A.J., Dunkerly D.L., De Deckker P., Kershaw A.P., and Stokes T. (1993) *Quaternary Environments.* Arnold, Sydney, 329pp.

Williams E. A. (1989) Summary and Synthesis. In Burrett C.F. and Martin E.L., (eds) Geology and Mineral Resources of Tasmania. *Special Publication Geological Society of Australia* **15**, 468-515

Winter M. (2003) *Web Elements Periodic Table*. Available online @ (URL): www.webelements.com

Wolf J.A., and Upchurch, G.R. (1986) Vegetation, climatic and floral changes at the Cretaceous-Tertiary boundary. *Nature* **324**, 148-152.

Wright R.V.S. (ed) (1977) *Stone tools as cultural markers: Change, evolution and complexity*. Australian Institute of Aboriginal Studies, Canberra.

Yamei H., Potts R., Baoyin Y., Zhengtang G., Dieno A., Wei W., Clark J., Guangmao X., and Weiwen H. (2000) Mid-Pleistocene Acheulean-like stone technology of the Bose Basin, South China, *Science* **287**, 1622-1626.

Zimanowski B., Lorenz V., and Frohlich G. (1986) Experiments on phreatomagmatic explosions with silicate and carbonatitic melts. *Journal of Volcanology and Geothermal Research* **30**, 149-153.